
รายงานวิจัยฉบับสมบูรณ์

# โครงการ การใช้ฟังก์ชันนัลโคพอลิเมอร์บรัชสำหรับประยุกต์ทางการตรวจวัดทางชีวภาพและชีวการแพทย์

โดย วรวีร์ โฮเว่น และคณะ

มิถุนายน 2559

**สัญญาเลขที่ DBG 5580003**

# รายงานวิจัยฉบับสมบูรณ์

# โครงการ การใช้ฟังก์ชันนัลโคพอลิเมอร์บรัชสำหรับประยุกต์ทางการตรวจวัดทางชีวภาพและชีวการแพทย์


| คณะผู้วิจัย | สังกัด |
|---|---|
| 1. รองศาสตราจารย์ ดร.วรวีร์ โฮเว่น | ภาควิชาเคมี คณะวิทยาศาสตร์ จุฬาลงกรณ์มหาวิทยาลัย |
| 2. นางสาวกีรติ กุศลกรรมบถ | สาขาปิโตรเคมีและวิทยาศาสตร์พอลิเมอร์ คณะวิทยาศาสตร์ จุฬาลงกรณ์มหาวิทยาลัย |
| 3. นางสาวอะรุณี แสงสุวรรณ | สาขาปิโตรเคมีและวิทยาศาสตร์พอลิเมอร์ คณะวิทยาศาสตร์ จุฬาลงกรณ์มหาวิทยาลัย |
| 4. นางสาววิไลพร ไกรสุวรรณ | สาขาปิโตรเคมี คณะวิทยาศาสตร์ จุฬาลงกรณ์มหาวิทยาลัย |
| 5. นางสาวอรพรรณ เวียรชัย | สาขาปิโตรเคมี คณะวิทยาศาสตร์ จุฬาลงกรณ์มหาวิทยาลัย |
| 6. นางสาวพรเพ็ญ แซ่อึ้ง | สาขาวิทยาศาสตร์มหโมเลกุล คณะวิทยาศาสตร์ จุฬาลงกรณ์มหาวิทยาลัย |
| 7. นางสาวเมธาวี บุ่นวรรณา | สาขาปิโตรเคมีและวิทยาศาสตร์พอลิเมอร์ คณะวิทยาศาสตร์ จุฬาลงกรณ์มหาวิทยาลัย |
| 8. นางสาวมาลินี ลี้กระจ่าง | สาขาปิโตรเคมีและวิทยาศาสตร์พอลิเมอร์ คณะวิทยาศาสตร์ จุฬาลงกรณ์มหาวิทยาลัย |



**สนับสนุนโดย**
**สำนักงานกองทุนสนับสนุนการวิจัย**

# EXECUTIVE SUMMARY

Effective functionalization with targeted molecules is certainly important for the development of materials desirable for biotechnology-related applications ranging from biosensor, biomaterials to biomedical devices. Polymer has become increasingly attractive platform for functionalization because a variety of functional groups can conveniently be incorporated and proportionally customized employing a combination of specific monomers in the polymerization step. In particular, once introduced as surface-grafted polymer brushes, a thin film of which the polymer chains have one end tethered to substrate surface by covalent linkage, the polymer offers greater functional group density for binding per surface area in three-dimensional fashion than a conventional and two-dimensional platform based on self-assembled monolayer (SAM). This research features the development of surface-grafted (co)polymers as functional materials for a number of biotechnology-related applications.

**Chapter I** describes the development of polymer-conjugated gold nanoparticles (AuNPs) for protein/peptide identification. An array-based sensing platform for protein detection by chemical nose approach based on fluorescence quenching of tricationic branched phenylene-ethynylene fluorophore by AuNPs can be successfully developed from gold nanoparticles stabilized by thermoresponsive poly(*N*-isopropylacrylamide) (PNIPAM-AuNPs).

Research work explained in **Chapter II** is based on the application of surface-grafted poly(acrylic acid) (PAA) brushes having *in situ* generated gold nanoparticles (AuNPs). The developed substrate is capable of detecting both small (m/z $\leq$ 600) and large (m/z $\geq$ 1000) peptides by surface-assisted laser desorption/ionization mass spectrometry (SALDI-MS) without the interference from matrix signal. The AuNPs can also act as the capture probe for selectively identify thiol-containing peptide from the peptide mixture.

Biomolecular probe immobilization is a key step in the development of biosensor. Since most bioactive molecules (i.e. protein, antibody, enzyme, DNA) contain amino groups, the polymeric platform is therefore designed to have either carboxyl (-COOH), amino (-$NH_2$), or hydroxyl (-OH) groups. However, conjugation with such amino-containing biomolecules usually require an additional activation step using coupling agent to render them more active towards nucleophilic attack by amino functionality. Here in this research, two precursor polymer has been introduced as an alternative functional material that can bind directly with designated

nucleophilic modifier, particularly biomolecules, without having to undergo activation step. Specific interactions with target molecules as opposed to the non-targeted components or the ability to resist non-specific adsorption known as “anti-fouling” property is another key element that determines the fate of the developed materials for biosensing applications, especially under real physiological condition of which numerous types of biological components concurrently exist. Taking this issue into consideration, selected biocompatible and highly hydrophilic polymers have been incorporated along with the designated precursor polymer.

**Chapter III** showcased a precursor copolymer of poly[(propargyl methacrylate)-*ran*-(2-methacryloyloxyethyl phosphorylcholine)] (PPgMAMPC), as a platform for binding with biomolecular probes for biosensing applications. The alkyne moiety of propargyl methacrylate (PgMA) serve as an active site for binding azide-containing molecules via a click reaction, i.e., Cu-catalyzed azide/alkyne cycloaddition (CuAAC), and 2-methacryloyloxyethyl phosphorylcholine (MPC), the hydrophilic monomeric unit, enables the copolymer to suppress non-specific adsorption. After conjugating with azide-containing probes, namely biotin and peptide nucleic acid (PNA) via CuAAC, the surface-attached PPgMAMPC was capable of detecting specific target molecules, i.e., streptavidin (SA) and DNA, as monitored by surface plasmon resonance.

DNA sequence determination is crucially important for clinical diagnosis, forensic identification as well as pathogen detection in food and agricultural products, most of which require advanced instruments and have to be done in well-equipped laboratories. The development of highly sensitive and specific, yet simple and economical test kit/assays without the demand for sophisticated instruments, suitable for point-of-care usages still remains a challenge. Therefore, this research aims to develop a paper-based DNA sensor employing a conformationally rigid pyrrolidinyl PNA derived from D-prolyl-2-aminocyclopentane carboxylic acid (acpc) backbones (acpcPNA) as probes. The filter paper was grafted with another precursor copolymer, poly[glycidyl methacrylate-*co*-poly(ethylene glycol)methacrylate] (P(GMA-*co*-PEGMA). The epoxide group of the GMA unit can act as versatile active site for binding with PNA capture probe via epoxide ring opening without having to use additional coupling agent. The PEGMA unit was incorporated as hydrophilic entity to prevent non-specific adsorption of non-target DNA as well as non-DNA components. Signal amplification used in this research relies on sandwich-hybridization assay employing biotinylated acpcPNA probe (b-PNA) as reporter probe together with horseradish peroxidase streptavidin (SA-HRP) and *o*-

phenylenediamine (OPD) substrate can be visualized by an enzyme-based colorimetric assay. Research in this part was described in **Chapter IV**.

Polymers carrying active pentafluorophenyl ester side chain, pentafluorophenyl (meth)acrylate (PFP(M)A), have been recently recognized as potential and versatile precursor polymers due to their solubility in many common organic solvents and higher hydrolytic stability in water**.** Their ability to undergo tandem post-polymerization modification allows for multiple functionalities to be conveniently and proportionally incorporated into the polymer structure. The last part of research focused on a controlled synthesis of homo- and co-polymers from active ester-containing monomer, pentaflorophenyl acrylate (PFPA) by a controlled radical polymerization based on reversible addition-fragmentation chain transfer (RAFT). Light responsive moieties of *o*-nitrobenzyl (ONB) were introduced to the copolymers of PFPA and *N*-isopropylacrylamide (NIPAM) (P(PFPA-*co*-NIPAM)) via partial post-polymerization modification with ONB-protected diamine. The ONB-containing copolymers could then be self-assembled or fabricated into UV-crosslinkable micelles or electrospun fibers. The crosslinked micelles having residual PFPA moieties in their cores are capable of not only chemically incorporating amino-containing molecule, NBD via post-functionalization but also physically encapsulating hydrophobic molecule, pyrene, suggesting their potential to be used as thermoresponsive cargos for drug delivery. Detailed information is provided in **Chapter V**. Results from *in vitro* cytocompatibility studies demonstrated that the GRGDS-immobilized crosslinked electrospun fibers may serve as thermoresponsive 3D scaffold for cell culture and tissue engineering applications. Studies were reported in **Chapter VI**. On the other hand, thermoresponsive platform for cell sheet fabrication can also be developed from the surface-grafted PPFPA brushes via the “grafting onto” and “grafting from” approaches via sequential post-polymerization modification with isopropylamine and collagen type I, a cell adhesion promoter. The detailed investigation is described in **Chapter VII**.

Basic knowledge gained from this research allow us to explore further the use of surface-grafted polymer brushes as multifunctional polymeric stabilizers for metal nanoparticles, namely gold nanorods (AuNRs), quantum dots (QDs), and magnetic nanoparticles (MNPs). It is our on-going investigation to develop these materials for advanced biotechnological applications such as AuNRs as cancer drug carrier for synergistic photothermal and chemo therapy, QDs for bioimging of targeted cells, and MNPs for separation and detection of bacteria.

# ACKNOWLEDGEMENT

This research was financially supported by a Directed Basic Research Grant by the Thailand Research Fund (DBG5580003), a Distinguished Research Professor Grant by the Thailand Research Fund and Chulalongkorn University (DPG5780002), the Ratchadaphiseksomphot Endowment Fund of Chulalongkorn University (RES560530126-AM), and the Thai Government Stimulus Package 2 (TKK2555), under the Project for Establishment of Comprehensive Center for Innovative Food, Health Products and Agriculture, the Commission on Higher Education, Thailand for the program Strategic Scholarships for Frontier Research Network for the Joint Ph.D. Program Thai Doctoral degree for Miss Wilaiporn Graisuwan, PhD Chulalongkorn University Dutsadiphiphat Scholarships for Miss Oraphan Wiarachai and Miss Pornpen Sae-ung.

# บทคัดย่อ

การดัดแปรหมู่ฟังก์ชันด้วยโมเลกุลเป้าหมายได้อย่างมีประสิทธิภาพมีความสำคัญต่อการพัฒนาวัสดุสำหรับการประยุกต์ทางเทคโนโลยีชีวภาพครอบคลุมตั้งแต่อุปกรณ์รับรู้ทางชีวภาพ วัสดุทางการแพทย์ และอุปกรณ์ทางชีวการแพทย์ พอลิเมอร์เป็นวัสดุที่ได้รับความสนใจเพิ่มมากขึ้นเป็นลำดับเนื่องจากสามารถให้ความหนาแน่นของหมู่ฟังก์ชันในการยึดติดกับสารต่าง ๆต่อหน่วยพื้นที่ในลักษณะสามมิติโดยเฉพาะอย่างยิ่งเมื่ออยู่ในลักษณะพอลิเมอร์บรัชที่กราฟต์บนพื้นผิว เป็นสัดส่วนที่สูงกว่าวิธีการดั่งเดิมที่อาศัยฟิล์มบางของโมเลกุลชั้นเดียวที่ได้จากการประกอบตัวเองบนพื้นผิวซึ่งมีลักษณะเป็นสองมิติ งานวิจัยนี้มีเป้าหมายที่จะพัฒนาการใช้โคพอลิเมอร์บรัชเป็นวัสดุฟังก์ชันนัลสำหรับการประยุกต์ในงานหลายด้านที่เกี่ยวข้องกับเทคโนโลยีชีวภาพ ผู้วิจัยประสบความสำเร็จในการพัฒนาแพล์ทฟอร์มที่เป็นอุปกรณ์รับรู้ในรูปแบบแอเรย์สำหรับการตรวจวัดโปรตีนตามหลักการของ chemical nose approach จากการใช้อนุภาคนาโนทองที่ทำให้เสถียรด้วยพอลิเมอร์ที่ตอบสนองต่ออุณหภูมิ คือพอลิเอ็นไอโซโพรพิลอะคริลาไมด์ (PNIPAM-AuNPs) พอลิแอคริลิกแอซิดบรัชที่ตรึงบนพื้นผิวและมีอนุภาคนาโนทองที่ทำให้เกิดขึ้นภายในสามารถใช้ในการวิเคราะห์เพปไทด์ได้ทั้งขนาดเล็กและใหญ่ รวมทั้งสามารถเลือกจับกับเพปไทด์ที่มีหมู่ไทออลจากของผสมได้ จากการวิเคราะห์ด้วยเทคนิค surface-assisted laser desorption/ionization mass spectrometry (SALDI-MS) พรีเคอร์เซอร์โคพอลิเมอร์สองชนิดได้รับการพัฒนาขึ้นเพื่อเป็นแพล์ทฟอร์มให้การตรึงโพรบที่เป็นสารชีวโมเลกุลสำหรับใช้ในงานทางด้านไบโอเซนเซอร์ ชนิดแรกคือ poly[(propargyl methacrylate)-*ran*-(2-methacryloyloxyethyl phosphorylcholine)] (PPgMAMPC). หลังจากการคอนจูเกตกับโพรบที่มีหมู่เอไซด์ ได้แก่ ไบโอติน และเพปไทด์นิวคลีอิกแอซิด (พีเอ็นเอ) ผ่านปฏิกิริยา Cu-catalyzed azide/alkyne cycloaddition แพล์ทฟอร์มที่เตรียมได้สามารถตรวจวัดโมเลกุลเป้าหมาย ได้แก่ สเตรปทาวิดิน และดีเอ็นเอ ได้จากการติดตามด้วยเทคนิค surface plasmon resonance ชนิดที่สองคือ poly[glycidyl methacrylate-*co*-poly(ethylene glycol)methacrylate] (P(GMA-*co*-PEGMA)). หมู่อิพ็อกไซด์สามารถใช้ในการตรึงพีเอ็นเอโพรบโดยปฏิกิริยาการเปิดวงของอิพ็อกไซด์ enzyme-based and sandwich-hybridization colorimetric assay สำหรับการตรวจวัดดีเอ็นเอได้รับการพัฒนาโดยใช้กระดาษกรองที่กราฟต์ด้วยโคพอลิเมอร์ร่วมกับพีเอ็นเอโพรบ พอลิเมอร์ที่มีหลายหน้าที่ได้รับการพัฒนาขึ้นจากโคพอลิเมอร์ที่สังเคราะห์มาจากมอนอเมอร์ที่มีหมู่แอกทีฟเอสเทอร์ คือ pentaflorophenyl acrylate (PFPA) และ *N*-isopropylacrylamide (NIPAM) (P(PFPA-*co*-NIPAM)) การเติมหมู่ที่ว่องไวต่อแสงของ *o*-nitrobenzyl (ONB) เข้าไปในโคพอลิเมอร์ทำให้ได้ไมเซลล์และเส้นใยที่เชื่อมขวางได้ด้วยยูวี หลังจากการขึ้นรูปด้วยการประกอบตัวเองและอิเล็กโทรสปินนิง ตามลำดับ ไมเซลล์แสดงศักยภาพในการพัฒนาเป็นพาหะในการควบคุมการนำส่งยา ในขณะที่เส้นใยที่ผ่านการเชื่อมขวางและตรึงด้วยเพปไทด์ GRGDS สามารถใช้เป็นโครงพยุงสามมิติที่ตอบสนองต่ออุณหภูมิสำหรับงานทางด้านการเลี้ยงเซลล์และวิศวกรรมเนื้อเยื่อได้ นอกจากนี้แพล์ทฟอร์มที่ตอบสนองต่ออุณหภูมิสำหรับการเตรียมแผ่นเซลล์ยังได้รับการพัฒนามาจากพอลิเมอร์บรัชของ PPFPA ที่เตรียมผ่านการดัดแปรหลังพอลิเมอไรเซชันด้วยการทำปฏิกิริยากับไอโซโพรพิลเอมีนและคอลลาเจน

**คำสำคัญ**: พอลิเมอร์บรัช, พรีเคอร์เซอร์พอลิเมอร์, อุปกรณ์รับรู้ทางชีวภาพ, ตอบสนองต่ออุณหภูมิ, วัสดุทางการแพทย์, อนุภาคนาโนทอง, เพปไทด์, โปรตีน, ดีเอ็นเอ, เส้นใยนาโน, ไมเซลล์

# ABSTRACT

Effective functionalization with targeted molecules is certainly important for the development of materials desirable for biotechnology-related applications ranging from biosensor, biomaterials to biomedical devices. Polymer has become increasingly attractive platform for functionalization particularly when introduced as surface-grafted polymer brushes because it can offer greater functional group density for binding per surface area in three-dimensional fashion than a conventional and two-dimensional platform based on self-assembled monolayer (SAM). This research features the development of surface-grafted (co)polymers as functional materials for a number of biotechnology-related applications. An array-based sensing platform for protein detection by chemical nose approach based on fluorescence quenching of tricationic branched phenylene-ethynylene fluorophore by AuNPs can be successfully developed from gold nanoparticles stabilized by thermoresponsive poly(*N*-isopropylacrylamide) (PNIPAM-AuNPs). Surface-grafted poly(acrylic acid) (PAA) brushes having *in situ* generated gold nanoparticles (AuNPs) was capable of detecting small/large peptide and selectively identify thiol-containing peptide from the peptide mixture by surface-assisted laser desorption/ionization mass spectrometry (SALDI-MS). Two precursor copolymers were successfully developed as platforms for conjugating with biomolecular probes in biosensing applications. One is based on poly[(propargyl methacrylate)-*ran*-(2-methacryloyloxyethyl phosphorylcholine)] (PPgMAMPC). After conjugating with azide-containing probes, namely biotin and peptide nucleic acid (PNA) via Cu-catalyzed azide/alkyne cycloaddition, the surface-attached PPgMAMPC was capable of detecting specific target molecules, i.e., streptavidin and DNA, as monitored by surface plasmon resonance. The other is poly[glycidyl methacrylate-*co*-poly(ethylene glycol)methacrylate] (P(GMA-*co*-PEGMA). The epoxide group of the GMA unit can act as versatile active site for binding with PNA capture probe via epoxide ring opening. Enzyme-based and sandwich-hybridization colorimetric assay for DNA detection can be developed using P(GMA-*co*-PEGMA)-grafted filter paper together with PNA probes. Multifunctional polymers were developed from copolymers synthesized from active ester-containing monomer, pentaflorophenyl acrylate (PFPA) and *N*-isopropylacrylamide (P(PFPA-*co*-NIPAM)). Light responsive moieties of *o*-nitrobenzyl introduced to the copolymers could be self-assembled or electrospun into UV-crosslinkable micelles or fibers. The micelles possess a great potential to be used as thermoresponsive cargos for drug delivery. GRGDS-immobilized crosslinked electrospun fibers may serve as thermoresponsive 3D scaffold for cell culture and tissue engineering applications. On the other hand, thermoresponsive platform for cell sheet fabrication can also be developed from the surface-grafted PPFPA brushes via sequential post-polymerization modification with isopropylamine and collagen type I.

**Keywords**: polymer brush, precursor polymer, biosensor, thermoresponsive, biomaterial, gold nanoparticles, peptide, protein, DNA, nanofibers, micelles

# CONTENTS

# Chapter I

## Poly(*N*-isopropylacrylamide)-stabilized Gold Nanoparticles in Combination with Tricationic Branched Phenylene-ethynylene Fluorophore for Protein Identification

### INTRODUCTION

Gold nanoparticles (AuNPs) have been a focus of considerable interest due to their potential applications for catalysis, diagnosis, and photoelectronic devices. Highly dispersed AuNP solutions exhibit a red color with an absorption band around 520 nm due to the excitation of surface plasmon by incident light. The association of the AuNPs in the dispersed solution induces a color change from red to blue-purple, which can be applied for the development of colloidal sensors.[1-3] Considerable effort has been devoted to synthesis of AuNPs, focusing on control over their size, shape, solubility, stability, and functionality. In general, AuNPs in solution are susceptible to aggregation themselves. To improve their dispersibility and introduce functionality to particle surfaces, the AuNPs may be coated with a water-soluble polymer having a functionality that can interact with gold. It has been reported that some polymers are effective stabilizing agents because they are capable of providing both electrostatic and steric stabilizations to the gold particles.[4, 5]

Intelligent polymers, also known as “stimuli-responsive” or “environmentally sensitive” polymers,[6-9] can undergo relatively large and abrupt, physical or chemical changes in response to small external stimuli in the environmental conditions.[10-13] One of the most recognizable polymer in the class is poly(*N*-isopropylacrylamide) (PNIPAM). PNIPAM dissolves in water assuming a random coil conformation at room temperature, but it separates from the aqueous phase when heated above 31-32 °C, its lower critical solution temperature (LCST).[14-17] Such thermoresponsive behavior is also maintained for PNIPAM grafted on AuNPs(PNIPAM-AuNPs) which can be evidenced from color transition of AuNPs aqueous solution above and below the LCST. The solution would turn from red to

blue upon the collapse of extended brush-like PNIPAM chains above LCST and caused AuNPs aggregation.[18-22]

Recently, it has been reported that protein as a biomarker can be detected by chemical nose approach based on fluorescence quenching of fluorophore by functionalized AuNPs.[23-26] The binding equilibrium between fluorophore and AuNPs would be altered because of competitive binding of protein analyte. Upon an addition of protein analyte, quenched fluorophore adsorbed on the AuNPs surface can be replaced by protein resulting in the recovery of fluorescence signal from the fluorophore. The fluorescence response may be positive or negative depending on the binding affinity of protein towards AuNPs and fluorophore. Although the chemical nose approach relies very much on non-specific interactions between protein and AuNPs, it is selective enough to be used for identifying the type of individual protein based on the variation of quenching ability of AuNPs having different functionality and the binding strength between the functionalized AuNPs and different kind of protein.[26]

Taking advantage of the PNIPAM-AuNPs being capable of undergoing thermoresponsive conformational transition of the surface-grafted PNIPAM between extended brushes to collapsed chains upon heat treatment above or below the LCST, it is anticipated that the distance between the core of AuNPs and fluorophore as well as protein in solution and so the degree of fluorescent quenching/recovery and the binding strength with the protein should be altered upon heat treatment. This would be highly beneficial if these PNIPAM-AuNPs are to be put in an array-based protein detection following chemical nose approach strategy because the other kind of AuNPs can be obtained by simply heating the existing AuNPs. Considering that PNIPAM is a polymer, such distance may also be varied as a function of PNIPAM molecular weight. In particular, reversible addition-fragmentation chain transfer (RAFT) polymerization has been well recognized as an effective controlled radical polymerization process for PNIPAM synthesis. Not only can a precise control over molecular weight and polydispersity of PNIPAM be achieved, but the terminal dithioester group at the PNIPAM chain end can also be converted to thiol group which is readily available for grafting onto the surface of gold.[27-31]

This research aims to combine the thermoresponsive behavior of PNIPAM and the fluorescence quenching properties of AuNPs to create hybrid materials to be used for

protein detection, a mode of biosensing application, to the best of our knowledge, has never been described before. Together with phenylene-ethynylene tribranched fluorophores having tunable charge characteristic, synthetic dyes successfully used for protein discrimination based on chemical nose approach,[32] an array-based chemical nose sensor for protein detection was developed based on the concept of fluorescence quenching schematically described in **Scheme 1.1(a)**.

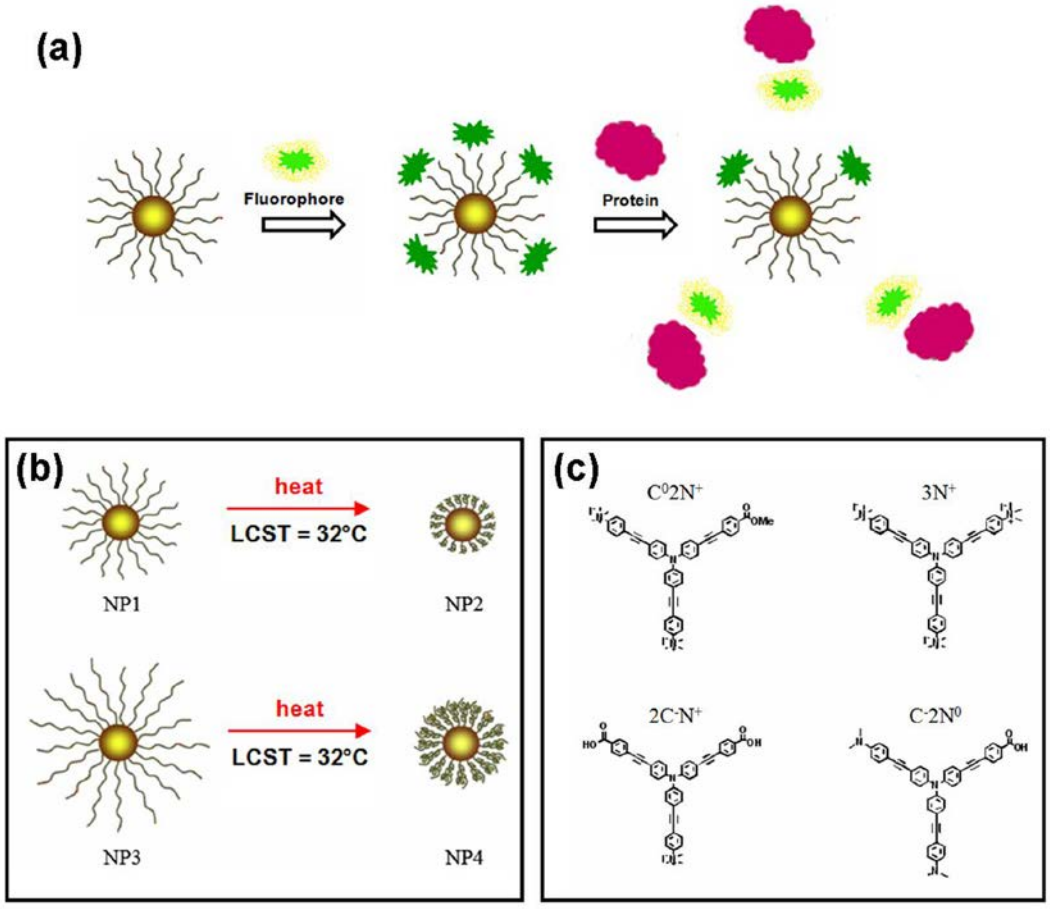


**Scheme 1.1** (a) Concept of sensor based on competitive binding of PNIPAM-AuNPs and protein with fluorophore that has impact on fluorescence quenching, (b) four different types of PNIPAM-AuNPs (NP1-NP4), and (c) chemical structures of four tribranched phenylene-ethynylene fluorophores.

**EXPERIMENTAL SECTION**

**Materials.** Hydrogen tetrachloroaurate ($HAuCl_4.3H_2O$), 4,4'-azobis(4-cyanopentanoic acid) (ACPA), 4-cyano-4-(thiobenzoylthio)pentanoic acid (CPD), tris(2-carboxyethyl)phosphine hydrochloride (TCEP), and *N*-isopropylacrylamide (NIPAM) were obtained from Aldrich (USA). Bovine serum albumin (BSA), lysozyme (Lys), fibrinogen (Fib), concanavalin A (Con A), hemoglobin (Hgb), holo-transferrin human (TF), dialysis bag (cut-off molecular weight of 3,500 g/mol), and phosphate buffered saline pH 7.4 (PBS) were bought from Sigma (USA). 2-Ethanolamine and tri-sodium citrate dihydrate ($Na_3C_6H_5O_7.2H_2O$) were obtained from Fluka (Switzerland). The above chemicals as well as all solvents used (1,4-dioxane, tetrahydrofuran (THF), methanol (MeOH)) were analytical grade and used as received without further purification except NIPAM which was recrystallized in a mixture of benzene and n-hexane (3:7, v/v) prior to use. Four fluorophores($C^0 2N^+$, $3N^+$, $2C^- N^+$ and $C^- 2N^0$) having different charges were synthesized according to a published procedure reported by Niamnont *et al*.[32] All solutions were prepared using ultrapure distilled water that was obtained after purification using a Millipore Milli-Q system (USA) that involves reverse osmosis , ion exchange, and a filtration step (18.2 MΩ cm resistance).

**Characterization.** Molecular weight of the synthesized PNIPAM were analyzed by GPC using Waters 600 controller chromatograph equipped with HR1 and HR4 columns (Waters, MW resolving range = 100-500,000) at 35 °C and refractive index detector (Waters 2414). THF was used as an eluent with the flow rate of 1.0 mL/min. Five polystyrene standards (996-188,000 Da) were used for generating a calibration curve. Fluorescence signals of the fluorophores were recorded by a Perkin Elmer precisely (LS 45) luminescence spectrometer (PerkinElmer Inc., UK) in a scanning wavelength range of 400-700 nm. The presence of the polymer around the AuNPs was confirmed by a Seiko SPA 400 atomic force microscope (SII Nanotechnology Inc., Japan). Measurements were performed in air at ambient temperature using tapping mode and silicon tips with a resonance frequency of 115-190 kHz. Surface plasmon resonance (SPR) measurements used for the determination of PNIPAM coverage on gold surface were conducted using a double channel, AutoLab ESPR (Eco Chemie, Netherlands). The morphology and actual size of AuNPs were analyzed by a JEOL JEM-2010 transmission electron microscopy (Japan) operating at 80 keV. The average diameters of AuNPs were reported from measurements of 30 random

particles for each sample using Semafore software. The zeta-potential ($\zeta$) of AuNPs were determined using Nanosizer Nano-ZS (Malvern Instruments, UK). The analysis was performed at 25ºC using a scattering angle of 173º. The data were calculated using the Helmholtz-Smoluchowski equation.

**Synthesis of Thiol-terminated PNIPAM (PNIPAM-SH).** PNIPAM having two different target degree of polymerization (DP = 40 and 70) were prepared by RAFT polymerization. According to a method modified from that of Yusa *et al*.[19], CPD (17.5 mg, 62.5 μmol) and ACPA (8.8 mg, 31.3 μmol) were added to a NIPAM (565.8 mg, 5.0 mmol) solution in 1,4-dioxane (5 mL). The solution was degassed by purging with nitrogen gas for 30 min, and then heated at 70 °C for 24 h. After being cooled down in an ice bath, the reaction mixture was dialyzed against DI water at 4°C for 3 days, before the PNIPAM was recovered by lyophilization. To remove the terminal dithiobenzoate group, an aqueous solution of PNIPAM was treated with 2-ethanolamine (30 mol equivalent of PNIPAM) and a trace amount (3-5 mg) of tris(2-carboxyethyl)phosphine hydrochloride (TCEP) at 25$^{\circ}$C for 24 h. The solution was dialyzed against DI water at 4$^{\circ}$C for 3 days. The PNIPAM-SH was then obtained after lyophilization. The condition mentioned above was used to prepare PNIPAM with targeted DP=40 (targeted molecular weight = 4805.78 g/mol). To prepare PNIPAM with targeted DP= 70 (targeted molecular weight = 8200.58 g/mol), CPD (11.1 mg, 39.7 μmol) and ACPA (4.5 mg, 15.9 μmol) were used instead.

**Preparation of AuNPs Stabilized by PNIPAM (PNIPAM-AuNPs).** PNIPAM-AuNPs were prepared by surface grafting of PNIPAM-SH onto citrate-stabilized AuNPs. In the first step, citrate-AuNPs were synthesized according to a method modified from that of Hayat et al.[33] An aqueous solution of tri-sodium citrate (1% w/v, 1.75 mL) was added to a boiling aqueous solution of $HAuCl_4$ (0.01% w/v, 50 mL). Then, the mixture was heated for 30 min and cooled down to ambient temperature. At this point, the color of the solution was changed from gray to red. Finally, the synthesized AuNPs were stored at 4 $^{\circ}$C prior to use. It should be noted that all glasswares used for the synthesis of AuNPs were washed with freshly prepared aqua regia solution ($HCl:HNO_3$ = 3:1, v/v) and rinsed thoroughly with

distilled water prior to use. PNIPAM-AuNPs were obtained by grafting to method modified from that of Zhu *et al.*[18] PNIPAM-SH (2.0 μmol) was dissolved in 10 mL of citrate-stabilized AuNPs solution obtained from the first step and kept at 4°C for 48 h. After that, excess PNIPAM-SH was removed from the PNIPAM-AuNPs by twice centrifugation (MIKRO 120, Hettich, Germany) at 14,000 rpm for 15 min interval. After redispersion in Milli-Q water, a red solution of PNIPAM-AuNPs was obtained and kept at 4 $^{\circ}$C.

**Determination of Fluorescence Quenching of Fluorophores by PNIPAM-AuNPs.** Quenching efficiency of four tribranched phenylene-ethynylene fluorophores having different charges of which structures are shown in Scheme 1.1(c) was evaluated with PNIPAM-AuNPs to find the fluorophores that can be highly quenched by AuNPs. The abbreviated names of the fluorophores are assigned according to the number and types of the functional groups on their peripheries in which $C^0$, $C^-$, $N^0$, and $N^+$ stand for carboxylate ester, carboxylic acid (or carboxylate anion in basic condition), amino, and quaternary ammonium groups, respectively. For example, $C^0 2N^+$ possesses one carboxylate ester and two quaternary ammonium groups on its periphery. To determine quenching efficiency, the initial fluorescence signal of fluorophore was determined by diluting the fluorophore stock solution (10.0 μM, 100 μL) in 2.9 mL of PBS solution and measured by a Luminescence Spectrometer. The quenching efficiency of PNIPAM-AuNPs was determined by mixing the fluorophore stock solution (10.0μM, 100 μL) and 500 μL of PNIPAM-AuNPs solution in 2.4 μL of PBS solution in a cuvette. To assure that the equilibrium was attained, the mixture was allowed to stand at ambient temperature for 30 min before the measurement of the emission spectrum.

**Determination of Fluorescence Response of Fluorophore by Proteins.** All of fluorophores were tested with BSA. The selected fluorophore (10.0μM, 100 μL) was first dissolved in 2.9 mL of PBS solution in a cuvette. After the solution was left for 30 min, the initial fluorescence emission of fluorophore was analyzed by Luminescence Spectrometer. BSA (10 μL, 1 mg/mL) was then added to the mixture obtained from the first step. To assure that the equilibrium was attained, the mixture was analyzed by Luminescence Spectrometer after leaving for 30 min. To maximize the fluorescence quenching effect of

the PNIPAM-AuNPs on the fluorophores, the fluorophores showing the least response to proteins were selected for developing a sensor platform based on chemical nose approach.

**Protein Detection Based on Fluorescence Quenching.** The synthesized PNIPAM-AuNPs were put in an array-based sensing platform. Six types of proteins (BSA, Lys, Fib, Con A, Hgb, and TF) were analyzed by using four different types of PNIPAM-AuNPs having varied PNIPAM molecular weight and conformation (induced by thermal treatment) together with the selected phenylene-ethynylene fluorophore. There are four different types of PNIPAM-AuNPs used for this investigation. Two types were obtained from the AuNPs stabilized by 4 kDa of PNIPAM-SH (4k PNIPAM-AuNPs). The first type is 4k PNIPAM-AuNPs at 25 °C (NP1) which was obtained directly from section 2.3. The second type is 4k PNIPAM-AuNPs at 40 °C (NP2) which was obtained by heating NP1 for 15 min and cool it down to 25 °C and leave it for 30 min before conducting further experiment. Another two types were obtained from AuNPs stabilized by 8 kDa of PNIPAM-SH (8k PNIPAM-AuNPs). The third type is 8k PNIPAM-AuNPs at 25°C (NP3) and the forth type is 8k PNIPAM-AuNPs at 40°C (NP4) obtained by a similar heat treatment as mentioned above of NP3. The detection of protein was done as follows. In the first step, 0.5 mL of NP1 was dissolved in 2.4 mL of PBS. After that, $3N^{+}$fluorophore ($1\times10^{-5}$ M, 100 µL) was then added and analyzed by Luminescence Spectrometer after 30 min allowed for the equilibrium time. The second step, BSA (10 µL, 1mg/mL) was added to the previous mixture and analyzed by Luminescence Spectrometer again after the equilibrium time. BSA was subjected to the same analysis with NP2, NP3, and NP4. To generate an array-based sensing platform, other types of proteins were also tested with NP1, NP2, NP3, and NP4.

**Data analysis**. All data analysis program were written in-house using MATLAB version R2011b. The software for Principal Component Analysis (PCA) and Linear Discriminant Analysis (LDA) was programmed using the algorithm described elsewhere.[34] In our case, LDA was not directly performed to the original dataset where the number of variables (wavelengths) exceeds the number of samples as the inverse of the pooled variance-covariance matrix is impossible to be calculated.[34,35] To avoid the problem, the procedure called “PCA-LDA” was used to demonstrate the classification power.[36-38] The approach is to

compress the dimension of the data into a low number of Principal component (PC) using PCA and LDA is then performed on the resulting PC scores to quantify the discriminant ability.

## RESULTS AND DISCUSSION

**Preparation and Characterization of PNIPAM-SH.** Here in this research, PNIPAM was synthesized by RAFT polymerization of which molecular weight and polydispersity can be well controlled by using a chain transfer agent. Besides, the dithioester group at the polymer chain end can be converted to a thiol group that is readily available for grafting onto the gold surface.[39] The chemical structure of the synthesized PNIPAM was verified by $^{1}$H-NMR (**Figure 1.1**). Its characteristic signals were consistent with those reported in the literature.[40,41] As determined by $^{1}$H-NMR data, it was found that the % conversion and the average $M_n$ of PNIPAM were 41% and 4,053 g/mol and 42% and 7,015 g/mol for targeted DP of 40 and 70, respectively.

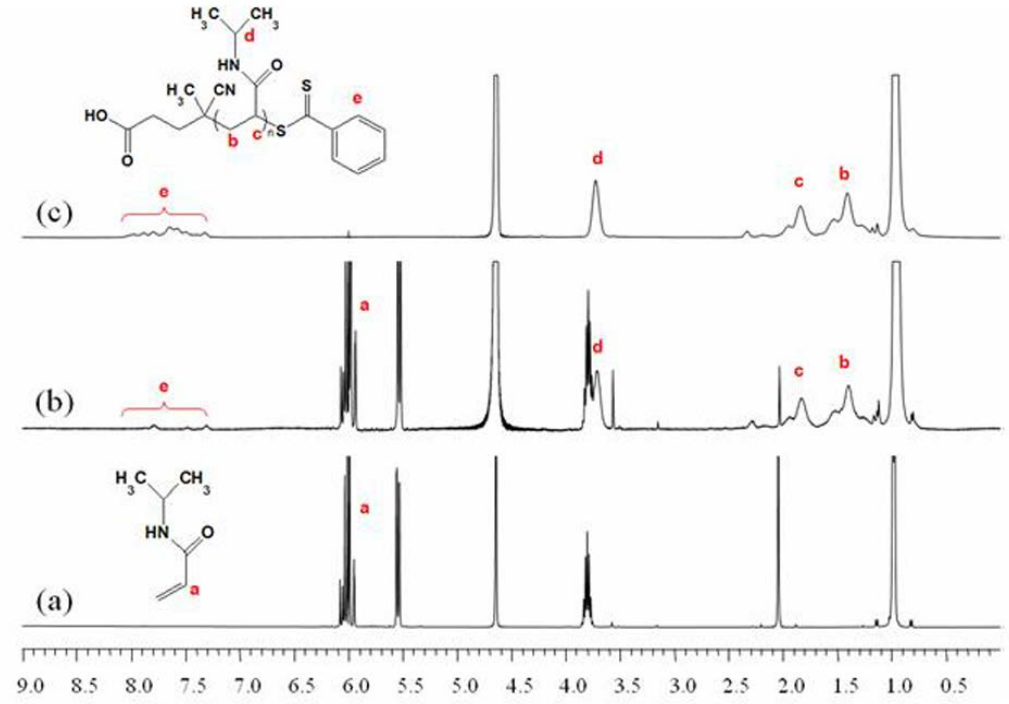


**Figure 1.1** $^{1}$H-NMR spectra of (a) NIPAM monomer, (b) non-purified PNIPAM, and (c) purified PNIPAM in $D_2O$.

Cleavage of the terminal dithiobenzoate group at the PNIPAM chain end was confirmed by UV-Vis analysis. Upon aminolysis by using 2-ethanolamine, the UV absorption band around 300 nm corresponding to the dithiobenzoate group disappeared resulting in the formation of thiol group and yielded PNIPAM-SH (**Figure 1.2**). The success of aminolysis was also confirmed by the appearance of PNIPAM which changed from pink-orange to white as a result of dithiobenzoate group removal. Since the thiol-terminated polymers can easily be oxidized by oxygen, internal disulfide linkage may be formed and possibly yielded an overestimated molecular weight.

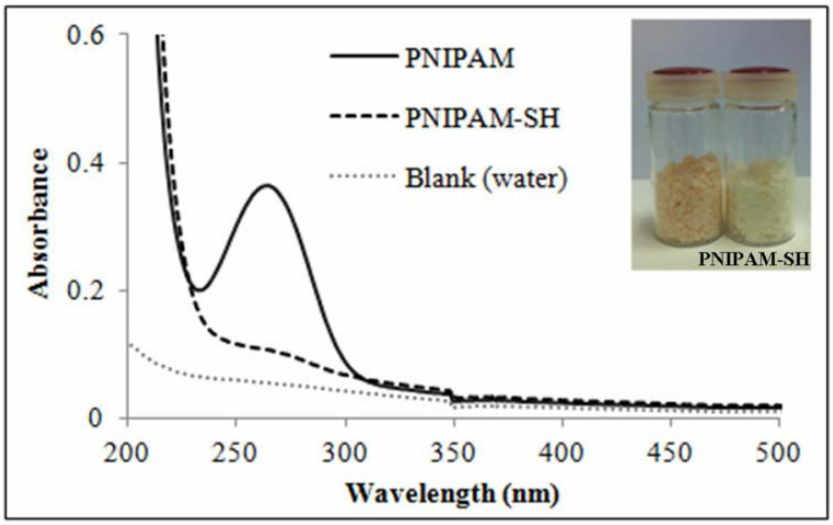


**Figure 1.2** UV-vis absorption spectra of PNIPAM and PNIPAM-SH in water. The inset shows physical appearance of PNIPAM (left) and PNIPAM-SH (right).

To ensure that such incidence did not occur, the molecular weights of PNIPAM-SH were also determined by GPC. The data shown in **Table 1.1** indicated that the $M_n$ and PDI ($M_w/M_n$) values of PNIPAM before aminolysis and those after aminolysis (PNIPAM-SH) were closely resembled implying that the disulfide bond formation was absent.[42] The fact that all PDI values are very close to one verifies that the molecular weight distribution is narrow and that the RAFT polymerization is well-controlled.

**Table 1.1** Molecular weight and polydispersity values of PNIPAM and PNIPAM-SH.

| Polymer | Target | | [M]/[I]/[CTA] | $M_n$ [a] | PDI [a] | $M_n$ [b] |
|---|---|---|---|---|---|---|
| | DP | $M_n$ | (mmol) | | | |
| PNIPAM | 40 | 4,526 | 1.600/0.01/0.020 | 3,816 | 1.09 | 4,053 |
| | 70 | 7,921 | 3.145/0.01/0.025 | 8,552 | 1.13 | 7,015 |
| PNIPAM-SH | 40 | 4,526 | 1.600/0.01/0.020 | 4,180 | 1.11 | n/a |
| | 70 | 7,921 | 3.145/0.01/0.025 | 8,788 | 1.14 | n/a |

[a] determined by GPC analysis using THF as eluent

[b] calculated from $^1$H-NMR data

**Preparation and Characterization of PNIPAM-AuNPs.** PNIPAM-SH obtained from the previous section was directly grafted onto the surface of AuNPs through sulfur-gold interaction. As compared with the FTIR spectrum of PNIPAM **(Figure 1.3a)**, the FTIR spectrum of the PNIPAM-AuNPs **(Figure 1.3b)** has characteristic peaks of N-H stretching from secondary amide at 3,276 $cm^{-1}$ and C-H deformation of isopropyl groups with a 1:1 intensity ratio at 1386 and 1367 $cm^{-1}$ which indicated the success of PNIPAM-SH coating on the surface of AuNPs.

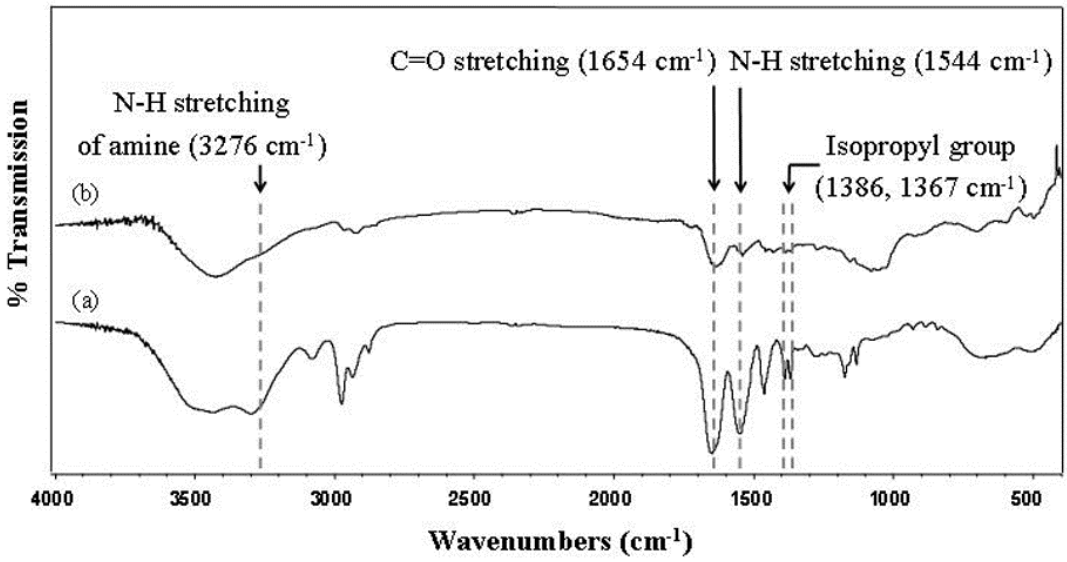


**Figure 1.3** FTIR spectra of (a) PNIPAM and (b) PNIPAM-AuNPs.

The layer of PNIPAM shell surrounding the AuNPs can be visualized from AFM image shown in comparison with that of the uncoated AuNPs stabilized by citrate ions in **Figure 1.4**. In addition, the effects of molecular weight and concentration of PNIPAM-SH on grafting efficiency were investigated. Apparently, the uncoated AuNPs were smaller than all of the PNIPAM-AuNPs. For the AuNPs surrounded by PNIPAM-SH, the particle size was increased with elevating molecular weight of PNIPAM (from 4 kDa to 8 kDa). As illustrated in **Figure 1.4d-e**, the expansion of shell thickness was also evidenced as a function of PNIPAM-SH concentration. It was found that the proper concentration of PNIPAM-SH was 0.2 mM because it was the minimum concentration that still gave AuNPs with thermoresponsive property which can be realized from color transition of the AuNPs solution upon thermal treatment, the detail of which will be described in the following section.

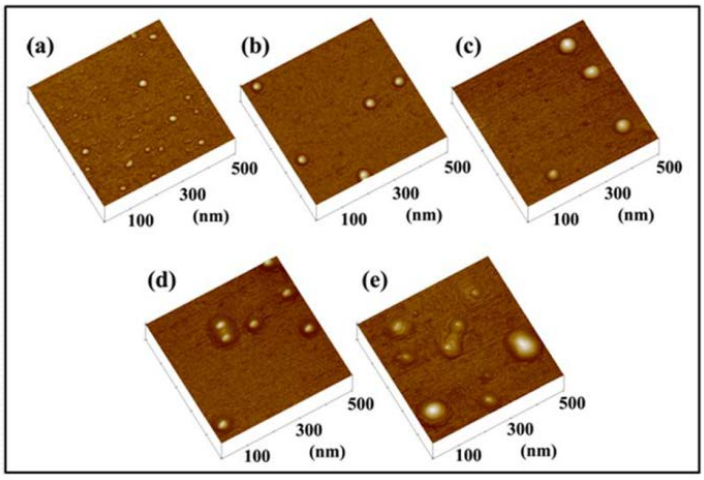


**Figure 1.4** AFM images of (a) uncoated citrated-stabilized AuNPs and AuNPs coated with (b) 0.2 mM of 4k PNIPAM-SH, (c) 0.2 mM of 8k PNIPAM-SH, (d) 0.5 mM of 4k PNIPAM-SH, and (e) 0.5 mM of 8k PNIPAM-SH.

Moreover, the grafting quantity of the two PNIPAM-SH having different molecular weights (4 and 8 kDa) on flat gold surface was determined by using SPR analysis. In brief, the bare cleaned gold-coated SPR disk was first seated in the SPR cell and the SPR angle

was recorded. Then, the formation of PNIPAM brushes on the gold-coated SPR disk was performed by immersing the bare disk in 0.2 mM PNIPAM-SH solution at 4°C for 48 h. After that, excess PNIPAM-SH was removed from SPR disk by shaking in Milli-Q water for 12 h. Finally, the SPR angle of the SPR disk bearing PNIPAM brushes was recorded and the angle shift between before and after polymer grafting was used to calculate the amount of polymer by using a sensitivity factor of 120 mDegree of angle shift = 100 ng/cm$^2$ of molecule bound onto the gold surface. From the data shown in **Table 1.2**, 4k PNIPAM could be grafted with higher density and more consistent than 8k PNIPAM.

**Table 1.2** Amount of PNIPAM chains grafted on the surface of flat gold-coated SPR disk.

| Molecular weight of PNIPAM | 4k PNIPAM | | 8k PNIPAM | |
|---|---|---|---|---|
| Channel | 1 | 2 | 1 | 2 |
| Amount of polymer (ng/cm$^2$) | 824.25 | 824.25 | 229.42 | 373.83 |

Surface plasmon band of AuNPs is known to be sensitive to the size of the particles and their surrounding environment. As demonstrated in **Figure 1.5a**, a solution of highly dispersed citrated-stabilized AuNPs exhibit red color with an absorption band around 520 nm. According to TEM analysis, the particles were spherical in shape and showed uniform size distribution around 13 nm (**Figure 1.5b**). In principle, PNIPAM chains should be collapsed upon increasing temperature above its LCST of 32$^{\circ}$C which is a consequence of hydrogen bonding between water and PNIPAM being destroyed at elevated temperature. **Figure 1.5c** shows UV-vis absorption spectra of 4k PNIPAM-AuNPs at 25°C (NP1) and 40°C (NP2) in PBS solution. The absorption maximum of the plasmon band of 530 nm at 25 °C shifted to 551 nm when the temperature was increased to 40°C. The color of the solution changed from red to blue-purple (from NP1 to NP2) without precipitation. The particles were still spherical in shape and consisted of 13 nm gold core and 1 nm PNIPAM shell, as can be seen in TEM image **(Figure 1.5d)**. **Figure 1.5e** shows UV-vis absorption spectra of 8k PNIPAM-AuNPs at 25°C (NP3) and 40 °C (NP4) in PBS solution. The absorption maximum of the plasmon band of 530 nm at 25 °C only slightly shifted to 541 nm after heating to 40 °C. This slightly red shift might be attributed to a high thickness of PNIPAM shell which prevented an aggregation of the AuNPs. This result was consistent

with the color of the solution in that the solution was altered from red to pink-purple (from NP3 to NP4) without precipitation. It was found that the particles were spherical in shape with well defined core/shell nanostructures having 13 nm gold core and 14-17 nm PNIPAM shell (**Figure 1.5f**). The data depicted in **Table 1.3** also suggested that the relative dimension of the particles measured by AFM was larger than those analyzed by TEM. This may be ascribed to the fact that AFM analysis was performed under semi-dried conditions.

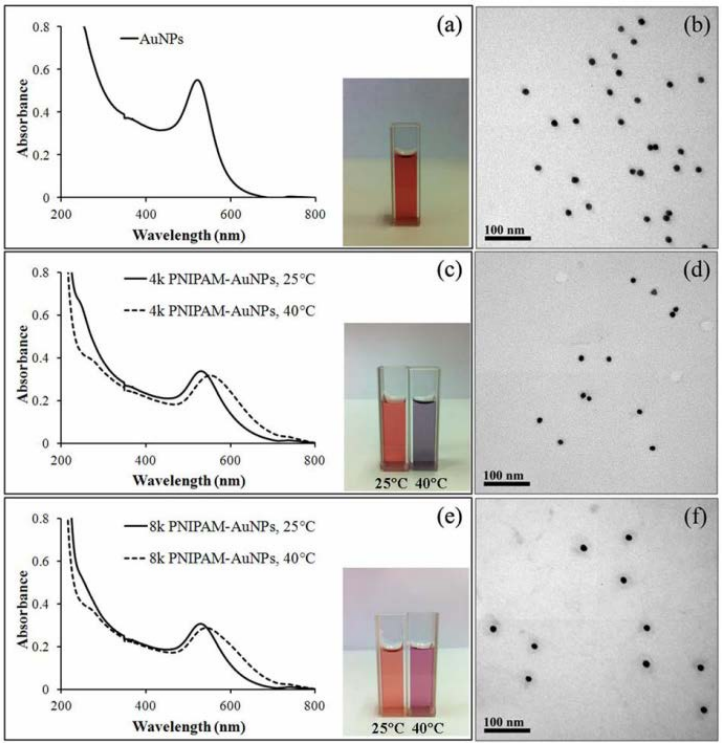


**Figure 1.5** UV-vis spectra (a,c,e) and TEM images (b,d,f) of citrated-stabilized AuNPs (a,b), 4k PNIPAM-AuNPs (c,d), and 8k PNIPAM-AuNPs (e,f). The insets of c and e show color transition of PNIPAM-AuNPs solution upon heating from 25 to 40 $^{\circ}$C.

**Table 1.3** Particle size of AuNPs obtained from AFM and TEM analysis.

| Particles | Size (nm) | |
|---|---|---|
| | AFM[a] | TEM[b] |
| AuNPs | 19.86 ± 5.9 | 13.98 ± 0.91 |
| 4k PNIPAM-AuNPs | 39.39 ± 1.49 | 15.36 ± 0.86 |
| 8k PNIPAM-AuNPs | 59.90 ± 4.51 | 42.08 ± 6.30 |

[a] measured from 10 particles of AuNPs by using Semafore program
[b] measured from 20 particles of AuNPs by using Semafore program

It should also be emphasized that the thermoresponsive property upon this thermal treatment condition is not reversible. The solution color as well as absorption maxima of plasmon bands of both NP2 and NP4 remained unaltered although their solutions were quenched down to ambient temperature (25°C) for such a long period of time (up to 2h) implying that both NP2 and NP4 maintained at their aggregated states and did not turn back to their original NP1 and NP3, respectively, at least within a period of measurements. This contradictory outcome is not completely unknown. In fact, it has been previously reported on the system of magnetic nanoparticles coated with PNIPAM-containing copolymers having relatively low graft density.[43] Our PNIPAM-AuNPs were prepared by grafting-to method so their graft density may not be that high which may be the reason of their irreversible thermal transition.

It has also been reported by Yusa *et al*.[19] that the thermoresponsive property of PNIPAM-AuNPs in terms of color transition (shift in absorption maximum of surface plasmon band) cannot be observed unless salt was added. They have explained that the color transition, in principle, should be driven by both PNIPAM shrinkage upon heating above its LCST and inter-particle aggregation of the PNIPAM-AuNPs. Thermal treatment above LCST should cause PNIPAM shrinkage (which can be realized by change in hydrodynamic radius usually determined by light scattering), however, the thermal energy is apparently not enough to bring together the collapsed PNIPAM-AuNPs that should lead to

aggregation and subsequent change in optical characteristic (color change). They have rationalized this as a consequence of strong hydrogen bonding between water and the PNIPAM particularly at the outer layer of the PNIPAM-AuNPs that prevent aggregation. Introducing salt to the system helped increasing ionic strength so that such strong hydrogen bonding can be destroyed and allows the aggregation to take place. For this reason, we also conducted additional experiments by incorporating 50 mM NaCl to the PNIPAM-AuNPs solution and performed 2 cycles of heating-quenching between 25 and 40°C and found that the color transition from red to blue-purple can be promptly accelerated and the process was also reversible as can be demonstrated in **Figure 1.6**. Such results have suggested that whether or not the visible thermoresponsiveness is reversible truly depends on the solution properties (i.e. ionic strength).

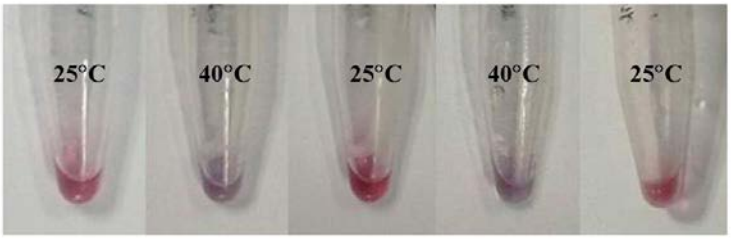


**Figure 1.6** Physical appearance of 4k PNIPAM-AuNPs solution in the presence of 50 mM NaCl upon 2 cycles of heating-quenching between 25°C and 40°C.

In this research, it is our intention not to add any salt to the solution which may complicate the mode of protein classification that relies on the interactions among three counterparts (PNIPAM-AuNPs, fluorophore, and protein). For this reason, the thermoresponsive transition solely relied on thermal energy introduced to the system by heating. Such treatment seems to be working except that the thermoresponsiveness of the PNIPAM-AuNPs is not reversible which may presumably be caused by the relatively low graft density of the PNIPAM as mentioned above. On the other hand, it may also be possible that prolong heating (> 15 min in this research) caused extensive PNIPAM collapse and dehydration making inter-particle aggregation a permanent process. Nevertheless, the irreversibility is truly beneficial for the mode of detection proposed in this

research work in that both NP2 and NP4 maintained their optical characteristic throughout the experiment suggesting that the method is reliable.

**Protein Identification.** To put the synthesized PNIPAM-AuNPs in an array-based sensing platform, a preliminary investigation on quenching efficiency of four tribranched phenylene-ethynylene fluorophores having different charges (structure shown in **Scheme 1.1c**) by 4k PNIPAM-AuNPs at 25°C was performed. It should be emphasized that these specific fluorophores were chosen because their charge characteristic can be tuned by varying the peripheral groups of the branch in the fluorophore structure without affecting their size. This is beneficial from the point that the impact of the charge on the quenching/recovery of the fluorophore can be determined without having to be concerned about the size and dimension variation of the fluorophore. As presented in **Figure 1.7a-d**, when 4k PNIPAM-AuNPs was used as a quencher, the $C^{-}2N^{0}$ and $2C^{-}N^{+}$ fluorophores were slightly quenched (5% and 11%, respectively), while the $3N^{+}$ and $C^{0}2N^{+}$ fluorophores were largely quenched (44% and 46%, respectively). The $C^{-}2N^{0}$ fluorophore has one carboxylic acid and two amino groups providing -1 net electronic charge whereas the $2C^{-}N^{+}$ fluorophore has two carboxylic acid groups and one quaternary ammonium group also netting -1 electronic charge. Therefore, there should be the repulsive force between the fluorophores and PNIPAM-AuNPs which have lone paired electrons of nitrogen and oxygen in the repeating unit resulting in ineffective fluorescence quenching. On the other hand, $3N^{+}$ and $C^{0}2N^{+}$ fluorophores have +3 and +2 net electronic charges. As a result, the electrostatic attraction between these positively charged fluorophores and PNIPAM-AuNPs yielded more effective quenching. For this reason, only $3N^{+}$ and $C^{0}2N^{+}$ fluorophores were selected for further investigation. Furthermore, to assure that the fluorescence response would originate from quenching by the PNIPAM-AuNPs, the interactions between the fluorophore and protein were investigated. In principle, the fluorophore having the least response with proteins is more desirable to be used for the development of protein sensor based on our designed fluorescence quenching.

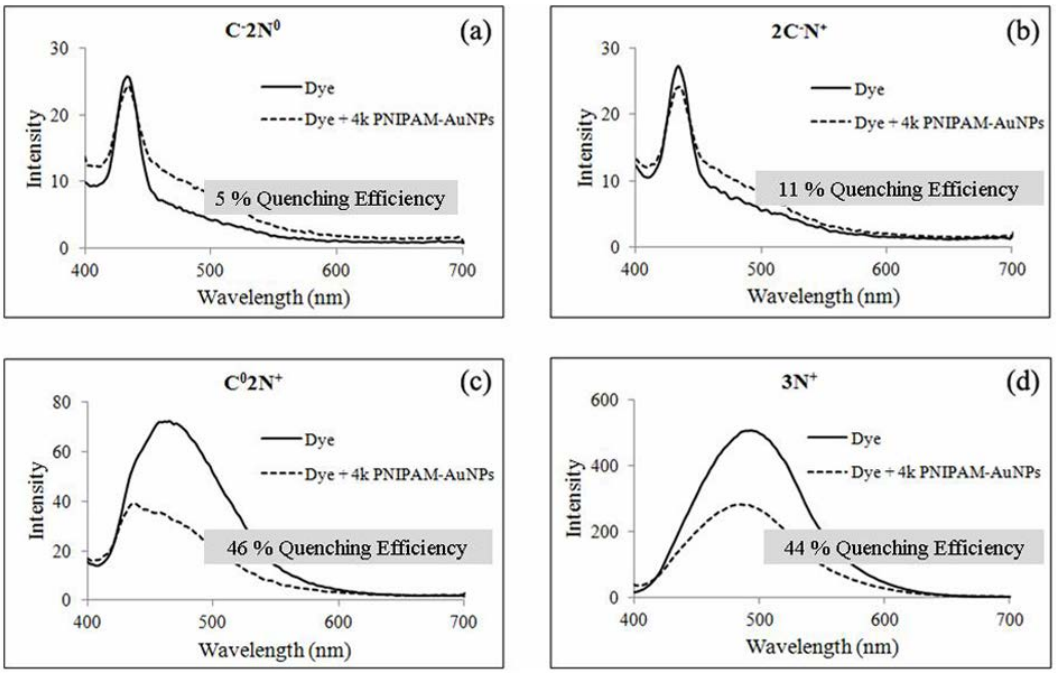


**Figure 1.7** Emission spectra demonstrating quenching behavior of four phenylene-ethynylene fluorophores: (a) $C^{-}2N^{0}$, (b) $2C^{-}N^{+}$ (c) $3N^{+}$, and (d) $C^{0}2N^{+}$ by using 4k PNIPAM-AuNPs (NP1) as a quencher.

As can be seen in **Figure 1.8a-d**, the emission intensity of $3N^{+}$ fluorophore was minimally affected by BSA. Therefore, $3N^{+}$ fluorophore was selected for further investigation. The much lower fluorescence response of $3N^{+}$ towards BSA than that previously reported by Niamnont and coworkers[32] could be described as a result of the protein concentration used in this research (3.3 μg/mL having $A_{280}$ = 0.0028) being lower than that ($A_{280}$ = 0.01) used in the previous work. Such lower protein concentration used in this sensing system was presumably not high enough for the BSA to act as effective surfactant that help deaggregating the fluorophore ($3N^{+}$) which should lead to fluorescence signal enhancement, the principle determined quenching efficiency described in their work. Nevertheless, we find this as a potential benefit given that the fluorescence response of $3N^{+}$ is more sensitive to lower protein concentration when used in combination with PNIPAM-AuNPs. To confirm that the $3N^{+}$ fluorophore was a proper dye, it was also tested with other five different types of protein having different pI and MW (Lys, Fib, Con A, Hgb,

and TF) and was found that all types of proteins did not enhance fluorescence intensity of $3N^{+}$ (**Figure 1.8e**).

To study the effect of polymer conformation grafted on AuNPs surface on the quenching efficiency, NP1 and NP2 were compared and found that the quenching efficiency of NP2 was higher than that of NP1 (**Figure 1.9**). This may be because the conformation of PNIPAM changed from stretched to coil-like structure upon heating to above its LCST resulting in the decreasing of distance between the gold core of NP2 and the fluorophore that in turn enhanced the quenching efficiency. To determine the effect of polymer molecular weight grafted on AuNPs surface on the quenching efficiency, NP1 and NP3 were compared. It was found that the quenching efficiency of NP1 was greater than that of NP3. This may be explained as a result of the PNIPAM layer on the NP1 being thinner than that on the NP3. The closer distance between the gold core and fluorophore in the case of NP1 when compared to that of the NP3 thus promotes the quenching process.

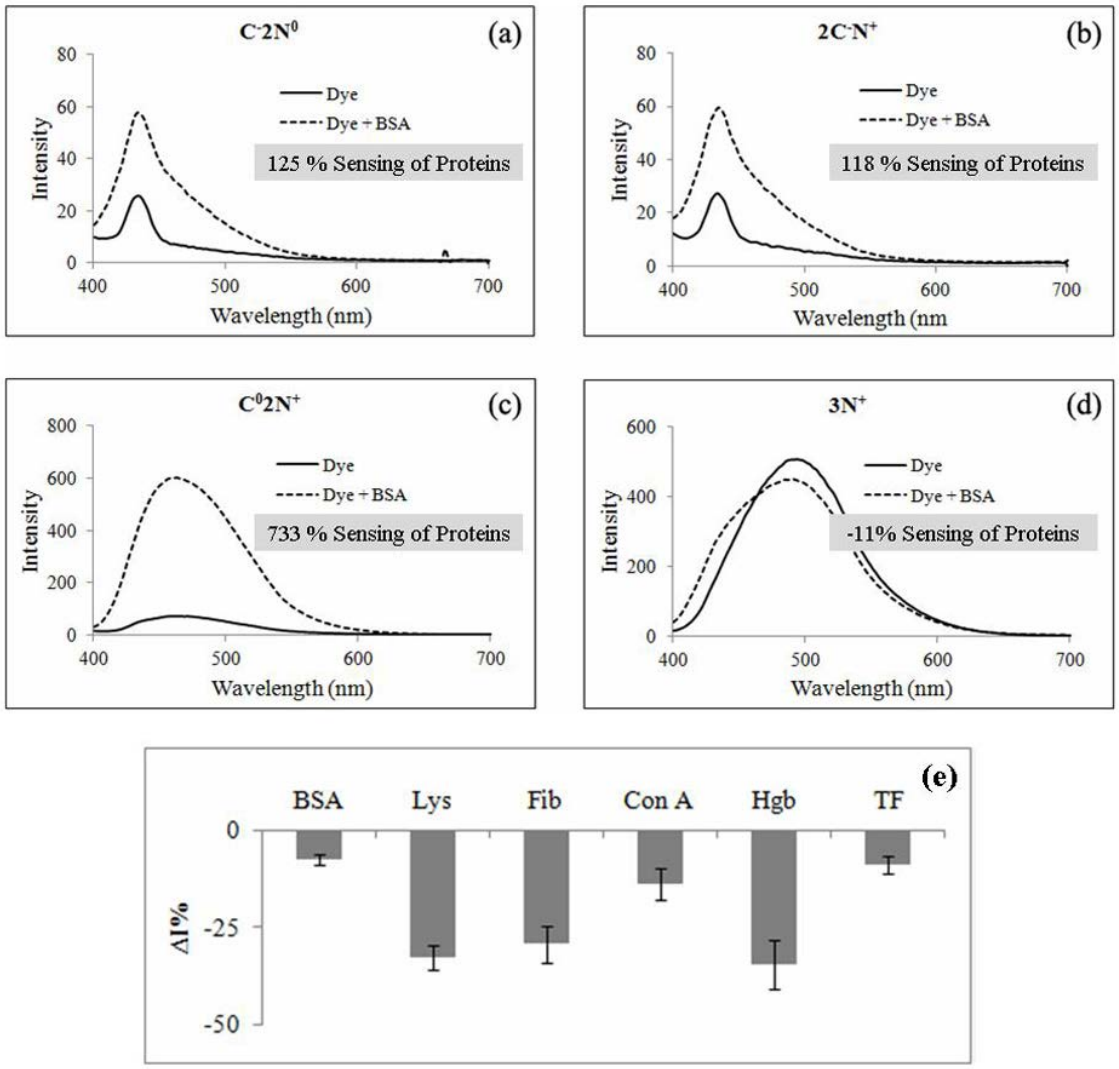


**Figure 1.8** Emission spectra demonstrating the change in fluorescence intensity of four tribranched phenylene-ethynylene fluorophores: (a) $C^{-}2N^{0}$, (b) $2C^{-}N^{+}$, (c) $3N^{+}$, (d) $C^{0}2N^{+}$ upon BSA addition, and (e) percentage of the change in emission intensity of $3N^{+}$ fluorophore when tested with six proteins.

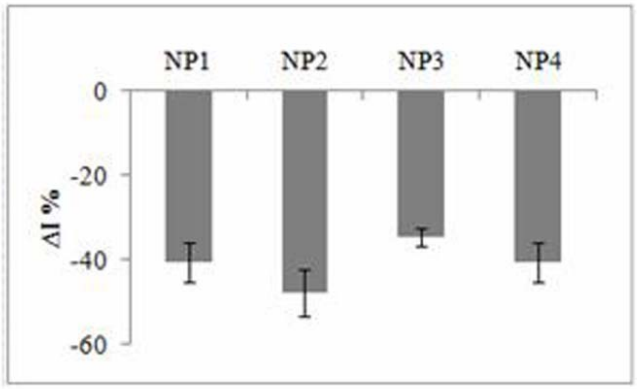


**Figure 1.9** Quenching efficiency of four types of PNIPAM-AuNPs with $3N^+$ fluorophore.

The data shown in **Table 1.4** demonstrated that all PNIPAM-AuNPs initially possessed negative zeta potential values, all of which became less negative upon $3N^+$ addition. These evidently supported the assumption that the quenching was driven by electrostatic attraction between the positive charge of the $3N^+$ fluorophore and the lone paired electrons of nitrogen and oxygen in the repeating unit of PNIPAM on the PNIPAM-AuNPs. Taking NP1 as a representative of PNIPAM-AuNPs, an equilibrium constant of association with the $3N^+$ fluorophore determined using Stern-Volmer analysis (Ksv) was found to be $8.21 \times 10^8\ M^{-1}$ (**Figure 1.10**).

To assure that the structures of PNIPAM-AuNPs maintained their physical characteristic throughout the period of protein classification, UV absorption of NP1 and NP2 both before and after $3N^+$ addition and after protein addition (BSA was chosen as a representative protein for this set of experiment). The results shown in **Figure 1.11** truly demonstrate that the fluorescence quenching/recovery event happened without causing any changes in the PNIPAM-AuNPs characteristic (shift in absorption maximum of surface plasmon band, aggregation). Similar outcome was also observed in the cases of NP3 and NP4 (data not shown).

**Table 1.4** Zeta potential values of all PNIPAM-AuNPs both before and after $3N^+$ fluorophore addition.

| Particles | Zeta-potential ± SD (mV) |
|---|---|
| NP1 | -14.13±1.4 |
| NP1 + $3N^+$ | -10.60±1.2 |
| NP2 | -15.10±0.52 |
| NP2 + $3N^+$ | -11.90±1.7 |
| NP3 | -9.01±0.37 |
| NP3 + $3N^+$ | 0.25±0.78 |
| NP4 | -28.90±0.45 |
| NP4 + $3N^+$ | -7.71±0.58 |

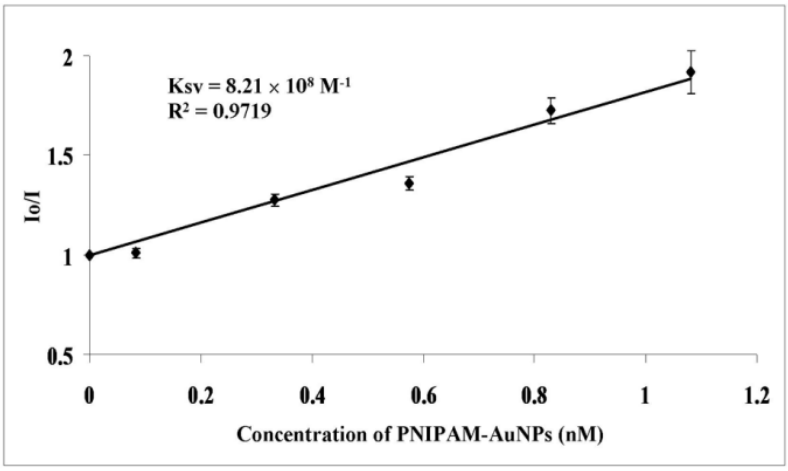


**Figure 1.10**. The Ksv plot between $3N^+$ and NP1.

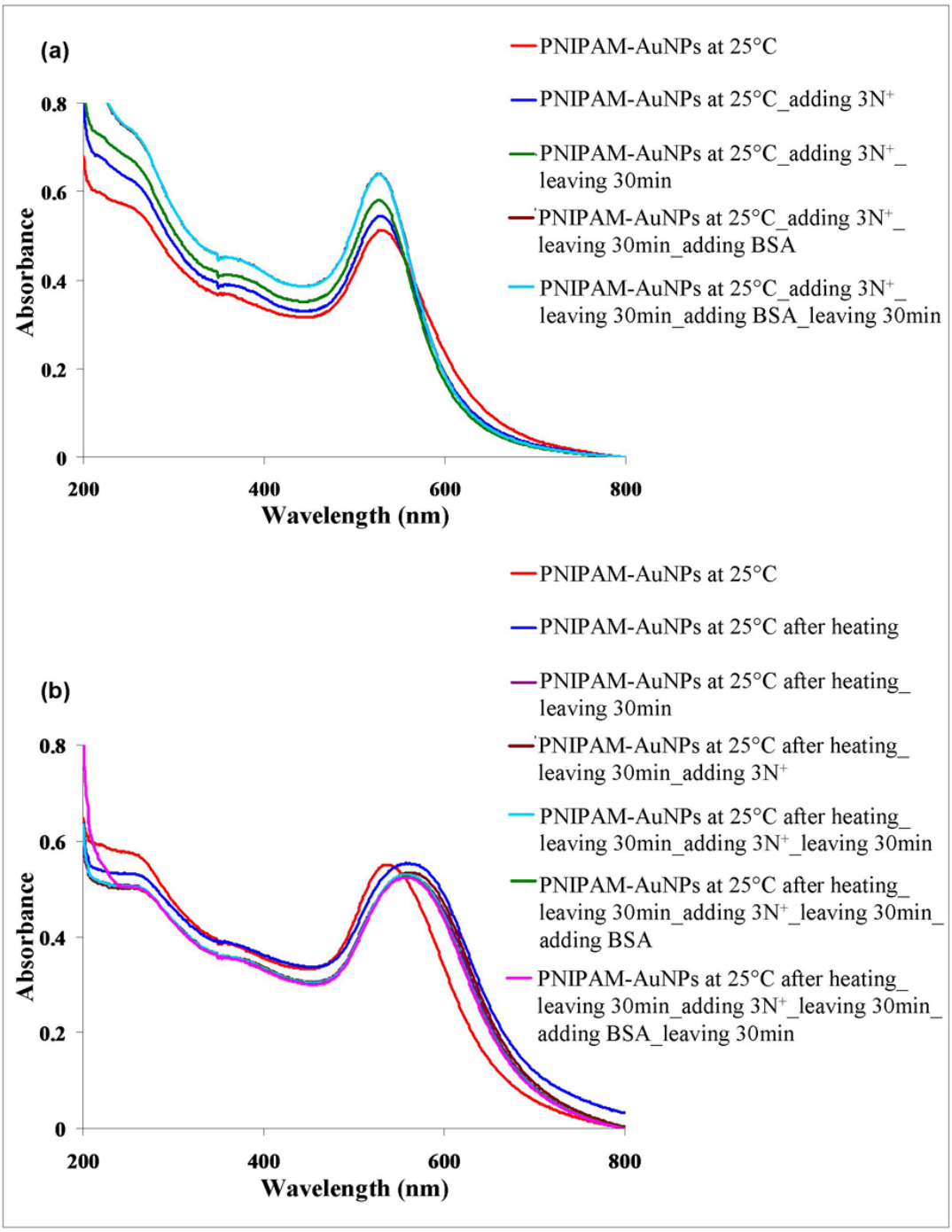


**Figure 1.11** UV-vis absorption spectra of (a) NP1 and (b) NP2 during the process of protein classification starting from fluorophore (3N+) addition followed by protein (BSA) addition.

For the determination of protein based on fluorescence quenching, six types of proteins were analyzed by using NP1-NP4 with the $3N^+$ fluorophore. The obtained results are illustrated in **Figure 1.12a**. Each type of PNIPAM-AuNPs exhibited different responses to different proteins. The fluorescence intensities of six proteins in response to NP1 were larger than those in response to other three types of PNIPAM-AuNPs. Unlike NP1, NP2 with its thinner PNIPAM layer may provide stronger interactions with the fluorophore as evidenced by its greater quenching efficiency when compared with NP1 (See **Figure 1.9**). For this reason, it might be difficult for the fluorophore to be released from NP2 surface upon the protein addition. It is believed that this outcome was influenced by protein resistance property of the PNIPAM brushes which is more prominent at the collapsed state as has been previously described by Xue *et al.*[44] This may be explained as a result of the collapsed PNIPAM layer of NP2 being denser than that of NP1 so that it is more difficult for the protein to access the fluorophore situated within the PNIPAM layer. That is why the signal responses were lower. In the case of NP3, of which PNIPAM layer was thicker than that of NP1, the change in fluorescence response was proportionally smaller. We explained this as a consequence of the quenching being initially low even before the protein addition due to the long distance between the gold core and the fluorophore. After the addition of protein, the fluorescence signal was not much affected and therefore gave the relatively low response.

Despite the facts that the PNIPAM layer of NP4 was thinner than that of the NP3 and its initial quenching efficiency was as high as that of NP1, overall signal responses of NP4 were relatively small and followed the same trend that observed in the case of NP3. We suspect that the same explanation previously used for NP2 based on limited accessability of the protein to the fluorophore in the condensed layer of PNIPAM can be applied here. In addition, to demonstrate the protein detection profile of the developed sensing array based on four types of PNIPAM-AuNPs, the histogram in **Figure 1.12a** was replotted for each protein and shown in **Figure 1.12b**. It is obvious that the responsive patterns of AuNPs were varied with the type of protein because of the difference in charge and molecular weight of protein. At pH 7.4, the $3N^+$ fluorophore bound on the AuNPs surface via charge-dipole interactions. Therefore, when the negatively charged proteins (BSA, Fib, Con A, Hgb, and TF) were added, the release of $3N^+$ fluorophore from the

AuNPs surface driven by the electrostatic interactions between negatively charged proteins in solution and $3N^+$ fluorophore can take place so that the quenched fluorescence signal can be recovered. Although being negatively charged proteins, Fib and TF did not provide responses against some types of AuNPs.

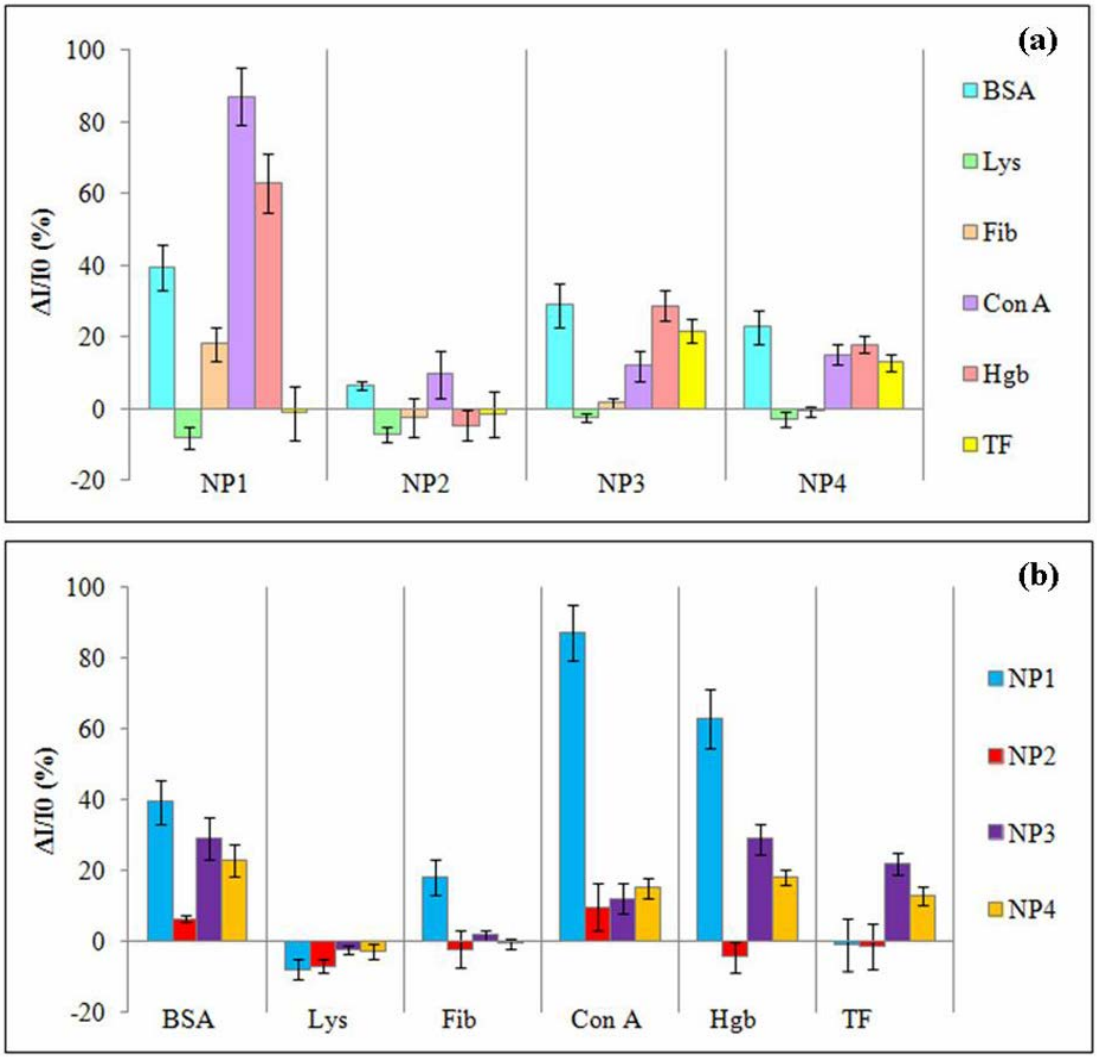


**Figure 1.12** Histogram plot of fluorescence response ($\Delta$I/I0) patterns of $3N^+$ fluorophore: (a) in the presence of six proteins in PBS for each type PNIPAM-AuNPs and (b) in the presence of PNIPAM-AuNPs for each type of proteins in PBS (responses are averages of six measurements and error bars are standard deviations).

These might be caused by their high molecular weight being obstacle for effective binding with $3N^+$ fluorophore and thus hampering the fluorescence signal recovery. In the case of Lys, a relatively small and positively charged protein, it was found that the signal recovery did not happen. This may be attributed to the repulsive forces between Lys and the $3N^+$ fluorophore. In fact, further quenching was also observed as can be realized from the negative response of the signal. We describe the decrease of fluorescence signal as a result of additional quenching of $3N^+$ in the solution that was initially unbound to the PNIPAM-AuNPs. This is likely possible given that it was demonstrated earlier in **Figure 1.8e** that the $3N^+$ fluorophore was slightly quenched by proteins. The explanation for the impact of characteristic charge and molecular weight of protein on fluorescence signal recovery is schematically summarized in **Figure 1.13**.

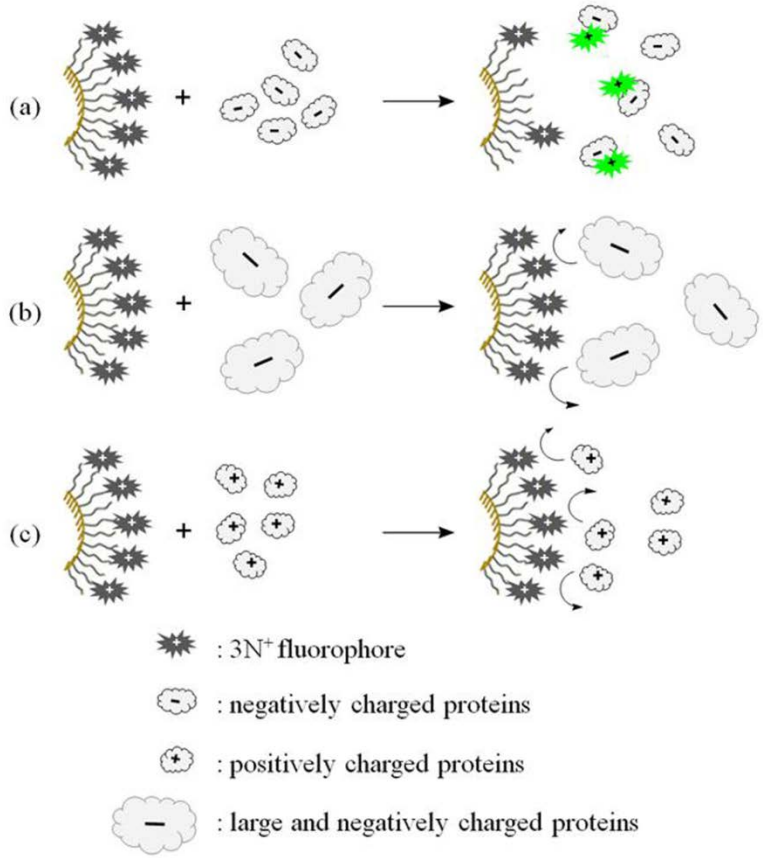


**Figure 1.13** Schematic representation of mechanism explaining the fluorescence signal recovery upon the addition of proteins having different size and charge.

Although the results demonstrated in **Figure 1.12b** suggested that the developed sensing platform using the PNIPAM-AuNPs in combination with $3N^{+}$ fluorophore was applicable for protein identification, the fact that the changes in fluorescence response ($\Delta I/I0$) determined from the maximum emission intensity independent of the wavelength was not intuitively accurate. Such estimation also ruled out the possibility that the wavelength of the emission maxima may be shifted upon protein addition which was found to be the case in some systems. For more accuracy, the whole spectra obtained before and after adding proteins were taken into consideration when performing subtraction. As can be seen in **Figure1.14a-d**, the subtracted spectra of each protein apparently exhibited different characteristic. The intensity values in wavelength range of 400-600 nm of spectra were used to identify each protein as they show the highest variation of $\%\Delta I$ and the highest shifted $\lambda_{max}$ towards the proteins. Although the histogram plot and characteristic spectrum already showed different patterns of the fluorescence responses towards each protein analyte, discrimination of these proteins based on this multi-dimensional data set (4 AuNPs × 6 proteins × 6 replicates) was further simplified using multivariate statistical analyses. In this study, principal component analysis (PCA) was used to transform the data set of fluorescence intensity differences ($\%\Delta I$) into principle component (PC) scores.[45] Based on the data similarity, a two dimension PC score plot (PC1 and PC2) suitably generated six clusters on the PC space corresponding to six types of proteins indicating an encouraging level of protein classification (**Figure 1.14e-h**). To quantify the classification accuracy, PCA-LDA was applied by performing LDA on the PC scores with a total variance > 95% and then validate the discriminating ability using Leave-One-Out (LOO) cross validation technique.[34] After PCA/LDA routines performed on the data by using each type of AuNPs (NP1-NP4), the results showed that the data which used NP3 gave the highest classification accuracy of 97.22%. The data obtained implied that the aggregation of PNIPAM layer induced by thermal treatment (NP2 and NP4) may deteriorate the efficiency of protein classification. However, we found that the 100% of classification accuracy can be obtained by combining NP1 data set with NP4 data set. The PCA score plot of NP1 associated with NP4 is shown in **Figure 1.14i**. These results strongly indicate the high potential of the developed sensing platform given that proteins can be identified with 100% accuracy by using only two types of PNIPAM-AuNPs.

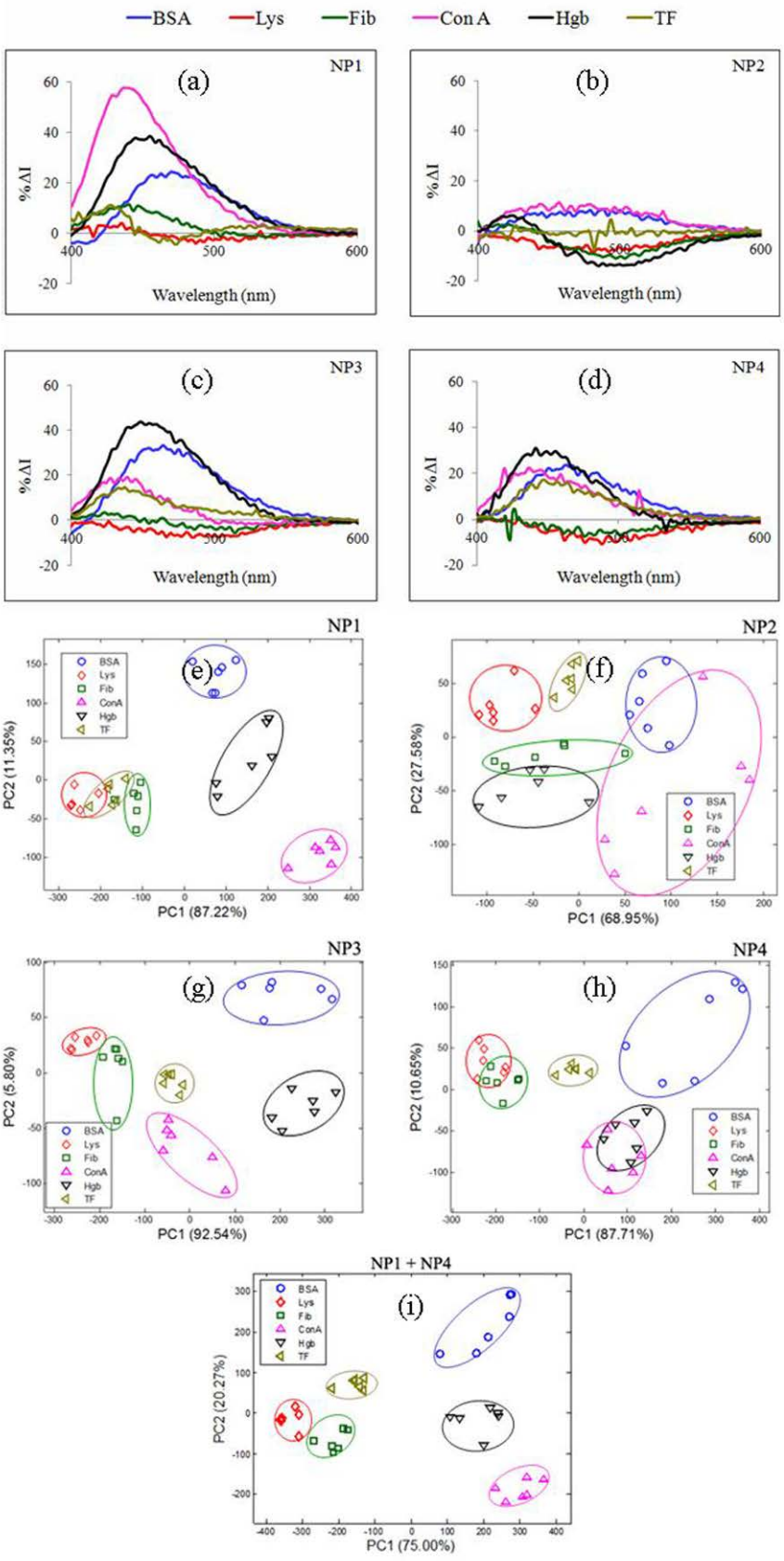
BSA
Lys
Fib
Con A
Hgb
TF
NP1
(a)
NP2
(b)
NP3
(c)
NP4
(d)
%ΔI
Wavelength (nm)
(e)
(f)
(g)
(h)
(i)
PC1 (87.22%)
PC2 (11.35%)
PC1 (68.95%)
PC2 (27.58%)
PC1 (92.54%)
PC2 (5.80%)
PC1 (87.71%)
PC2 (10.65%)
NP1 + NP4
PC1 (75.00%)
PC2 (20.27%)

**Figure 1.14** Characteristic emission spectra of $3N^+$ fluorophore in the presence of (a) NP1, (b) NP2, (c) NP3, (d) NP4 for each type of proteins in PBS (obtained by the subtraction of spectra before and after protein addition) and PCA score plot of $\%\Delta I$ data set obtained from 6 replicates of 6 proteins including fluorescence responses of $3N^+$ fluorophore using (e) NP1, (f) NP2, (g) NP3, (h) NP4, and (i) NP1+NP4.

## CONCLUSIONS

This investigation has demonstrated that the thermoresponsive AuNPs can be prepared by using citrate-stabilized AuNPs grafted with PNIPAM-SH synthesized via RAFT polymerization. The prepared PNIPAM-AuNPs have a spherical morphology and uniform size distribution and their shell thickness depended on the PNIPAM-SH molecular weight. Upon molecular weight variation and heat treatment, 4 types of PNIPAM-AuNPs (NP1-NP4) having different quenching efficiency against $3N^+$ fluorophore were generated. After protein addition, the fluorescence signal of $3N^+$ fluorophore can be recovered. The different pattern of fluorescence signal recovery which is varied with the types of both proteins and PNIPAM-AuNPs can be used to generate an array-based protein classification. Based on LDA analysis using Leave One Out (LOO) approach, a 100% accuracy of protein classification can be achieved using a combination of NP1 data set and NP4 data set. The results have suggested that an array-based sensing platform based on chemical nose approach can be developed from PNIPAM-AuNPs when combined with positively charged phenylene-ethynylene fluorophore.

## REFERENCES

1. Ishii, T.; Otsuka, H.; Kataoka, K.; Nagasaki, Y. Preparation of functionally PEGylated gold nanoparticles with narrow distribution through autoreduction of auric cation by alpha-biotinyl-PEG-block-[poly(2-(N,N-dimethylamino)ethyl methacrylate)]. *Langmuir* **2004,** *20,* (3), 561-564.
2. Mirkin, C. A.; Letsinger, R. L.; Mucic, R. C.; Storhoff, J. J. A DNA-based method for rationally assembling nanoparticles into macroscopic materials. *Nature* **1996,** *382,* (6592), 607-609.
3. Storhoff, J. J.; Lazarides, A. A.; Mucic, R. C.; Mirkin, C. A.; Letsinger, R. L.; Schatz, G. C. What controls the optical properties of DNA-linked gold nanoparticle assemblies? *J. Am. Chem. Soc.* **2000,** *122* (19), 4640-4650.

4. Li, D. X.; He, Q.; Li, J. B. Smart core/shell nanocomposites: Intelligent polymers modified gold nanoparticles. *Adv. Colloid Interface Sci.* **2009,** *149* (1-2), 28-38.
5. Hussain, I.; Graham, S.; Wang, Z. X.; Tan, B.; Sherrington, D. C.; Rannard, S. P.; Cooper, A. I.; Brust, M. Size-controlled synthesis of near-monodisperse gold nanoparticles in the 1-4 nm range using polymeric stabilizers. *J. Am. Chem. Soc.* **2005,** *127* (47), 16398-16399.
6. Cui, Y.; Tao, C.; Zheng, S. P.; He, Q.; Ai, S. F.; Li, J. B. Synthesis of thermosensitive PNIPAM-co-MBAA nanotubes by atom transfer radical polymerization within a porous membrane. *Macromol. Rapid Commun.* **2005,** *26* (19), 1552-1556.
7. Gil, E. S.; Hudson, S. M. Stimuli-reponsive polymers and their bioconjugates. *Prog. Polym. Sci.* **2004,** *29* (12), 1173-1222.
8. Hu, Z. B.; Chen, Y. Y.; Wang, C. J.; Zheng, Y. D.; Li, Y. Polymer gels with engineered environmentally responsive surface patterns. *Nature* **1998,** *393* (6681), 149-152.
9. Schilli, C. M.; Zhang, M. F.; Rizzardo, E.; Thang, S. H.; Chong, Y. K.; Edwards, K.; Karlsson, G.; Muller, A. H. E. A new double-responsive block copolymer synthesized via RAFT polymerization: Poly(*N*-isopropylacrylamide)-*block*-poly(acrylic acid). *Macromolecules* **2004,** *37* (21), 7861-7866.
10. Bohrisch, J.; Wendler, U.; Jaeger, W. Controlled radical polymerization of 4-vinylpyridine. *Macromol. Rapid Commun.* **1997,** *18* (11), 975-982.
11. Mika, A. M.; Childs, R. F. Acid/base properties of poly(4-vinylpyridine) anchored within microporous membranes. *J. Membr. Sci.* **1999,** *152* (1), 129-140.
12. Ista, L. K.; Mendez, S.; Perez-Luna, V. H.; Lopez, G. P. Synthesis of poly(*N*-isopropylacrylamide) on initiator-modified self-assembled monolayers. *Langmuir* **2001,** *17* (9), 2552-2555.
13. Fischer, A.; Brembilla, A.; Lochon, P. Nitroxide-mediated radical polymerization of 4-vinylpyridine: Study of the pseudo-living character of the reaction and influence of temperature and nitroxide concentration. *Macromolecules* **1999,** *32* (19), 6069-6072.
14. Zhang, J.; Pelton, R. The dynamic behavior of poly(*N*-isopropylacrylamide) at the air/water interface. *Colloids Surf. A:Physicochem. Eng. Aspects* **1999,** *156* (1-3), 111-122.
15. Wu, C.; Zhou, S. Q. Thermodynamically stable globule state of a single poly(*N*-isopropylacrylamide) chain in water. *Macromolecules* **1995,** *28* (15), 5388-5390.
16. Wang, X. H.; Wu, C. Light-scattering study of coil-to-globule transition of a poly(*N*-isopropylacrylamide) chain in deuterated water. *Macromolecules* **1999,** *32* (13), 4299-4301.
17. Kratz, K.; Hellweg, T.; Eimer, W. Structural changes in PNIPAM microgel particles as seen by SANS, DLS, and EM techniques. *Polymer* **2001,** *42* (15), 6631-6639.
18. Zhu, M. Q.; Wang, L. Q.; Exarhos, G. J.; Li, A. D. Q. Thermosensitive gold nanoparticles. *J. Am. Chem. Soc.* **2004,** *126* (9), 2656-2657.

19. Yusa, S. I.; Fukuda, K.; Yamamoto, T.; Iwasaki, Y.; Watanabe, A.; Akiyoshi, K.; Morishima, Y. Salt effect on the heat-induced association behavior of gold nanoparticles coated with Poly(*N*-isopropylacrylamide) prepared via reversible addition - Fragmentation chain transfer (RAFT) radical polymerization. *Langmuir* **2007,** *23* (26), 12842-12848.
20. Shan, J.; Nuopponen, M.; Jiang, H.; Kauppinen, E.; Tenhu, H. Preparation of poly(*N*-isopropylacrylamide)-monolayer-protected gold clusters: Synthesis methods, core size, and thickness of monolayer. *Macromolecules* **2003,** *36* (12), 4526-4533.
21. Shan, J.; Chen, J.; Nuopponen, M.; Tenhu, H. Two phase transitions of poly(*N*-isopropylacrylamide) brushes bound to gold nanoparticles. *Langmuir* **2004,** *20* (11), 4671-4676.
22. Chakraborty, S.; Bishnoi, S. W.; Perez-Luna, V. H. Gold nanoparticles with poly(*N*-isopropylacrylamide) formed via surface initiated atom transfer free radical polymerization exhibit unusually slow aggregation kinetics. *J. Phys. Chem. C* **2010,** *114* (13), 5947-5955.
23. Phillips, R. L.; Miranda, O. R.; You, C. C.; Rotello, V. M.; Bunz, U. H. F. Rapid and efficient identification of bacteria using gold-nanoparticle - Poly(para-phenyleneethynylene) constructs. *Angew. Chem. Int. Ed.* **2008,** *47* (14), 2590-2594.
24. Miranda, O. R.; Creran, B.; Rotello, V. M. Array-based sensing with nanoparticles: 'Chemical noses' for sensing biomolecules and cell surfaces. *Curr. Opin. Chem. Biol.* **2010,** *14* (6), 728-736.
25. De, M.; You, C. C.; Srivastava, S.; Rotello, V. M. Biomimetic interactions of proteins with functionalized nanoparticles: A thermodynamic study. *J. Am. Chem. Soc.* **2007,** *129* (35), 10747-10753.
26. De, M.; Rana, S.; Akpinar, H.; Miranda, O. R.; Arvizo, R. R.; Bunz, U. H. F.; Rotello, V. M. Sensing of proteins in human serum using conjugates of nanoparticles and green fluorescent protein. *Nature Chem.* **2009,** *1* (6), 461-465.
27. Schilli, C.; Lanzendorfer, M. G.; Muller, A. H. E. Benzyl and cumyl dithiocarbamates as chain transfer agent in the RAFT polymerization of *N*-isopropylacrylamide. In situ FT-NIR and MALDI-TOF MS investigation. *Macromolecules* **2002,** *35* (18), 6819-6827.
28. Ray, B.; Isobe, Y.; Morioka, K.; Habaue, S.; Okamoto, Y.; Kamigaito, M.; Sawamoto, M. Synthesis of isotactic poly(*N*-isopropylacrylamide) by RAFT polymerization in the presence of Lewis acid. *Macromolecules* **2003,** *36* (3), 543-545.
29. Kujawa, P.; Segui, F.; Shaban, S.; Diab, C.; Okada, Y.; Tanaka, F.; Winnik, F. M. Impact of end-group association and main-chain hydration on the thermosensitive properties of hydrophobically modified telechelic poly(*N*-isopropylacrylamides) in water. *Macromolecules* **2006,** *39* (1), 341-348.
30. Ganachaud, F.; Monteiro, M. J.; Gilbert, R. G.; Dourges, M. A.; Thang, S. H.; Rizzardo, E. Molecular weight characterization of poly(*N*-isopropylacrylamide) prepared by living free-radical polymerization. *Macromolecules* **2000,** *33* (18), 6738-6745.

31. Convertine, A. J.; Ayres, N.; Scales, C. W.; Lowe, A. B.; McCormick, C. L. Facile, controlled, room-temperature RAFT polymerization of *N*-isopropylacrylamide. *Biomacromolecules* **2004,** *5* (4), 1177-1180.
32. Niamnont, N.; Mungkarndee, R.; Techakriengkrai, I.; Rashatasakhon, P.; Sukwattanasinitt, M. Protein discrimination by fluorescent sensor array constituted of variously charged dendritic phenylene-ethynylene fluorophores. *Biosens. Bioelectron.* **2010,** *26* (2), 863-867.
33. Hayat, A. Colloidal gold: principles, methods, and applications. *J. Anat.* **1989,** *176,* 215-216.
34. Brereton, R. G. *Chemometrics for pattern recognition*; Wiley & Sons: Chichester, 2009.
35. Varmuza, K. *Chemometrics in practical applications*; InTech publisher: Rijeka, 2012.
36. Lloyd, G. R.; Orr, L. E.; Christie-Brown, J.; McCarthy, K.; Rose, S.; Thomas, M.; Stone, N. Discrimination between benign, primary and secondary malignancies in lymph nodes from the head and neck utilising Raman spectroscopy and multivariate analysis. *Analyst* **2013,** *138* (14), 3900-8.
37. Smit, S.; van Breemen, M. J.; Hoefsloot, H. C. J.; Smilde, A. K.; Aerts, J. M. F. G.; de Koster, C. G. Assessing the statistical validity of proteomics based biomarkers. *Anal. Chim. Acta* **2007,** *592* (2), 210-217.
38. van der Werf, M. J.; Pieterse, B.; van Luijk, N.; Schuren, F.; van der Werff-van der Vat, B.; Overkamp, K.; Jellema, R. H. Multivariate analysis of microarray data by principal component discriminant analysis: prioritizing relevant transcripts linked to the degradation of different carbohydrates in Pseudomonas putida S12. *Microbiology* **2006,** *152*, 257-272.
39. Nakayama, M.; Okano, T. Polymer terminal group effects on properties of thermoresponsive polymeric micelles with controlled outer-shell chain lengths. *Biomacromolecules* **2005,** *6* (4), 2320-2327.
40. Andersson, M.; Hietala, S.; Tenhu, H.; Maunu, S. L. Polystyrene latex particles coated with crosslinked poly(*N*-isopropylacrylamide). *Colloid. Polym. Sci.* **2006,** *284* (11), 1255-1263.
41. Chen, Q.; Xu, K.; Zhang, W. D.; Song, C. L.; Wang, P. X. Preparation and characterization of poly (*N*-isopropylacrylamide)/polyvinylamine core-shell microgels. *Colloid. Polym. Sci.* **2009,** *287* (11), 1339-1346.
42. Scales, C. W.; Convertine, A. J.; McCormick, C. L. Room-temperature polymerization of *N*-isopropylacrylamide via RAFT and subsequent conjugation of fluorescent labels. *Abstr. Pap. Am. Chem. Soc.* **2005,** *230,* U4233-U4234.
43. Du, B. Y.; Mei, A. X.; Tao, P. J.; Zhao, B.; Cao, Z.; Nie, J. J.; Xu, J. T.; Fan, Z. Q. Poly[*N*-isopropylacrylamide-co-3-(trimethoxysilyl)-propylmethacrylate] coated aqueous dispersed thermosensitive $Fe_3O_4$ nanoparticles. *J. Phys. Chem. C* **2009,** *113* (23), 10090-10096.

44. Xue, C. Y.; Yonet-Tanyeri, N.; Brouette, N.; Sferrazza, M.; Braun, P. V.; Leckband, D. E. Protein adsorption on poly(*N*-isopropylacrylamide) brushes: dependence on grafting density and chain collapse. *Langmuir* **2011,** *27* (14), 8810-8818.

45. Poulli, K. I.; Mousdis, G. A.; Georgiou, C. A. Classification of edible and lampante virgin olive oil based on synchronous fluorescence and total luminescence spectroscopy. *Anal. Chim. Acta* **2005,** *542* (2), 151-156.

# Chapter II

## Patterned Poly(acrylic acid) Brushes containing Gold Nanoparticles for Peptide Detection By Surface-Assisted Laser Desorption/Ionization Mass Spectrometry

### INTRODUCTION

Separation and analysis of biomarkers such as peptides found in trace level play crucial roles in medical diagnosis. A number of peptides have been proposed as potential biomarkers. For example, bradykinin, des-Arg9-bradykinin, and Hyp3-bradykinin are potential biomarkers of breast cancer.[1] Glutathione (GSH), thiol-containing peptides, are also recognized as important biomarkers in human.[2,3] GSH is an antioxidant and a tripeptide composed of L-cysteine, glycine, and γ-glutamic acid, that can prevent damage to important cellular components caused by reactive oxygen species such as free radicals and peroxides.[4] An usual range of GSH concentrations in healthy human is in a range of 684 -2525 and 2.22-11.36 mmol.$L^{-1}$ in blood and plasma, respectively. [5] Abnormal level of GSH is an indication of diseases such as Alzheimer's, Parkinson's, Huntington's disease, cancers, aging, and heart problems.[4] Cysteine (Cys) is the only amino acid with a thiol functional group that serves as a unique unit in protein construction, enzyme active sites and cofactors.[6] Cys is also an amino acid component of GSH. Cys exists in almost all human proteins (89.3 % contain at least one) and 17.2% of tryptic peptides contain one or more cysteine residues.[6,7] Analysis of biomarker generally requires highly sensitive analytical tools such as electrochemistry,[8] fluorescence spectroscopy,[9] UV-Vis spectrophotometry[10] surface plasmon resonance[11] and mass spectrometry.[12,13]

Surface-assisted laser desorption/ionization mass spectrometry (SALDI-MS), in particular, is a widely used technique for biomarker identification especially peptides due to its high sensitivity and accuracy.[9,14] The major benefit of this method lies in its ability to be implemented in specific modification of chip surfaces, recently developed by using nanomaterials as matrices to absorb the laser energy and transfer to analyte in ionization step. This technique is capable of detecting analyte with low mass range (<

500 m/z) without the interference from matrix signal. Metal nanoparticles, for example, ZnS, $TiO_2$, $Fe_3O_4$ and Au are extensively used as matrices in SALDI-MS analysis.[15,16] Unlike conventional organic matrices, metal nanoparticles provide low matrix background, homogeneous sample and insignificant fragmentation. It was also found that each type of nanoparticles have their own suitable range of analyte that can be evaluated. For example, gold nanoparticles (AuNPs) are suitable for sample with a mass range of 300-1300 m/z. $TiO_2$ and $Fe_2O_3$ are appropriate for analyzing samples with a mass range of 1,200-12,000 and 1,200-25,000, respectively.[15] In addition, some metal nanoparticles such as AuNPs and silver nanoparticles (AgNPs) can also function as concentrating and selective probes for pre-concentration and separation of thiol-containing peptide from the peptide mixture.[16-19]

Recently, polymer has been used together with nanoparticles for modifying chip surface not only to improve nanoparticles dispersion that can enhance ionization efficiency, but also help trapping the nanoparticles from coming off during ionization. There are reports about modification of substrate with nanoparticles for SALDI-MS analysis. Aminlashgari *et al.*[20] utilized nanocomposite films based on polylactide embedded with nanoparticles of $TiO_2$, $SiO_2$, MgO, hydroxyapatite, montmorillonite nanoclay, halloysite nanoclay, silicon nitride and graphitized carbon black as matrices for SALDI-MS analysis of small molecules, namely, acebutolol, propranolol and carbamazepine. They found that the advantages of nanocomposite films as compared to the free nanoparticles used in earlier studies are the ease of handling and reduction of instrument contamination because the particles were immobilized within the polymer matrix. Kawasaki *et al.*[21] successfully modified silicon substrate with self-assembled multilayer films of poly(allylamine hydrochloride) and ammonium citrate capped AuNPs $(AuNPs/PAHC)_n$ for analyzing peptides (angiotensin I, cytochrome C) by SALDI-MS. It was found that the sensitivity of the peptide was increased with increasing number of multilayer films. However, a small matrix background of the AuNPs still appeared in the mass spectra. As demonstrated by Tarui *et al.,* the silicon substrate modified with nanocomposite film of cationic diblock copolymer micelles of poly(styrene-b-*N*-methyl-4-vinyl pyridinium iodide) and ammonium citrate stabilized AuNPs, offered superior performance to the AuNPs alone by providing high ionization efficiency of angiotensin I and insulin with low matrix background from Au clusters.[22]

Polymer brushes are one of interesting materials that can be used for chip surface modification. Having chain ends attached covalently on surface, they are more

stable than physically adsorbed polymer film. Polymer brushes with well-controlled molecular weight and polydispersity index can be prepared via surface-initiated polymerization based on a number of controlled radical polymerization such as atom transfer radical polymerization (ATRP) and reversible addition-fragmentation chain transfer (RAFT).[23,24] Having multiple functional groups per surface area, polymer brushes are quite attractive material for bioanalytical analysis. Bruening and co-workers[25-27] have developed an efficient platform for phosphopeptide enrichment prior to MS analysis. The platform is based on polymer brushes of poly(2-hydroxyethyl methacrylate) (PHEMA) or poly(acrylic acid) immobilized with Fe(III)-nitrilotriacetate (NTA). The substrates offered higher recoveries with fewer interfering peaks than those analysed by commercially-available Fe(III)-containing materials. A femtomol-level detection limit can also be reached even in the presence of as high as 10-fold molar excess of non-phosphorylated peptides.[26,27] Kim *et al*.[28] have employed surface-immobilized polymer brushes of poly(oligo(ethylene glycol) methacrylate) (pOEGMA) as non-biofouling polymeric platform for immobilizing peptide-conjugated AuNPs. A label-free assay of matrix metalloproteinase (MMP) activity was evaluated from the peptide segments cleaved from the peptide-conjugated AuNPs using time-of-flight secondary ion mass spectrometry. The use of pOEGMA together with AuNPs synergistically improved the sensitivity of MMP activity assays in human serum, in which a number of interfering proteins are present.

Poly(acrylic acid) (PAA) brushes have been recognized as versatile polymeric entities often used for biosensing and analytical applications. Its greater density of carboxyl groups provides active functionality for specific biomolecule immobilization and detection as reported earlier by a number of research groups.[29-33] In particular, we have previously demonstrated that the surface-grafted PAA brushes can serve as a three-dimensional platform for attachment of biosensing probes. As determined by surface plasmon resonance (SPR), their properties are superior to a SAM of a carboxyl-terminated alkanethiol in terms of both signal enhancement and the ability to prevent non-specific adsorption.[29] The best performance for both the biotin-streptavidin and BSA-anti-BSA systems was found on the sensor platform developed from the surface-grafted PAA brushes with a 50% graft density.[30]

Here in this research, we are interested to develop a substrate for SALDI-MS analysis based on surface-grafted PAA brushes containing AuNPs. Photolithography was first used to generate the hydrophobic/hydrophilic pattern to provide a visible

contrast between the analyte spot and prevent cross-contamination of sample solution from one spot to another. PAA brushes were then grafted on the hydrophilic area of the pattern via surface-initiated RAFT polymerization of acrylic acid (AA). Thereafter, AuNPs were generated *in situ* within the PAA brushes by having carboxylate groups of PAA acting as reducing moieties for gold ions ($Au^{3+}$), without having to use an additional reducing agent.[34,35] The substrate modified with PAA brushes containing AuNPs (AuNPs-PAA) were then used for SALDI-MS analysis of a number of peptides, such as bradykinin which is a biomarker of breast cancer, thiol-containing peptides, namely glutathione and ICNKQDCPILE. It is anticipated that this developed patterned platform can be used for pre-concentration and separation of thiol-containing peptide from the peptide mixture in a high throughput fashion.

## EXPERIMENTAL

### Materials

Hydrogen tetrachloroaurate ($HAuCl_4.3H_2O$), acrylic acid (AA), dimethyl formamide (DMF), 4,4-bis(4-cyanovaleic acid) (ACVA), 4-(dimethylamino)pyridine (DMAP), 4-cyano-4-(phenyl carbonothioylthio)pentanoic acid (chain transfer agent or CTA), dicyclohexyl carbodiimide (DCC), hydrogen peroxide ($H_2O_2$), dialysis bag (cut-off molecular weight of 3,500 g/mol), phosphate buffered saline pH 7.4 (PBS), 3-aminopropyltriethoxysilane (APTES), 1H,1H,2H,2H-perfluorooctyltrichlorosilane (PFOTCS), $\alpha$-cyano-4-hydroxycinnamic acid (CHCA), sucrose and cholesterol were obtained from Sigma-Aldrich. Acetone, toluene, hexane, ethanol, dichloromethane, and sulfuric acid were purchased from Merck (Germany). Positive photoresist S1813 and developer MFTM-321 were purchased from Rohm and Hass (USA). Glass slides were obtained from S.E. Supply (Thailand). AA was purified by vacuum distillation. Glutathione (GSH), bradykinin, ICNKQDCPILE peptide were obtained from American Peptide company. Citrate-stabilized gold nanoparticles were prepared according to a method modified from that of Hayat *et al*.[36] All solutions were made using ultrapure distilled water that was obtained after purification using a Millipore Milli-Q system (USA) that involves reverse osmosis, ion exchange, and a filtration step (18.2 MΩ cm resistance).

### Surface Patterning by Photolithography

A glass slide (i.d.= 1.8 cm) was cleaned in a plasma cleaner (Harrick Plasma PDC-32G, Power 18 W) for 5 min before exposed to vapor of 100 µL APTES in a 50 mL vial sealed with a cap in an oven at 80°C for 72 h and rinsed sequentially with toluene, acetone, and deionized water to yield Si-$NH_2$ (**Scheme 2.1, Step I**). Positive photoresist S1813 was then spin-coated at 4,000 rpm for 3 min on the surface of Si-$NH_2$ and cured at 115 °C for 1 min. A photomask was placed on the photoresist-coated surface before irradiation with UV light (365 nm, 500W) for 15 sec. The irradiated pattern was treated with developer MFTM-321 for 1 min and rinsed with deionized water followed by treatment in the plasma cleaner for 5 min to destroy the APTES layer and recover back the silanol groups on the unmasked area (**Scheme 2.1, Step II**). The obtained patterned Si-$NH_2$/OH was exposed to vapor of 100 µL PFOTCS in a 50 mL vial sealed with a cap in the oven at 80 °C for 72 h and rinsed sequentially with toluene, acetone, and deionized water. The recovered silanol groups of the patterned Si-$NH_2$/OH would react with PFOTCS to form patterned Si-$NH_2$/O$(CH_2)_2(CF_2)_5CF_3$ (**Scheme 2.1, Step III**). At this point, the photoresist on the masked area was also removed so that the amino groups of APTES were readily available for initiator immobilization in the next step.

**Grafting of PAA Brushes on Patterned Surface**

The ACVA (0.21 g, 1 mmol), DCC (0.19 g, 1 mmol), and DMAP (0.01 g, 0.1 mmol) were dissolved in 20 mL DMF. The solution was stirred for 4 h at room temperature before transferred to the glass slide having patterned Si-$NH_2$/O$(CH_2)_2(CF_2)_5CF_3$ in a vial then sealed with a rubber septum. The solution was stirred under nitrogen atmosphere at room temperature for 20 h. Then, the glass slide was taken out from the vial and rinsed with ethanol and deionized water to yield Si-I/O$(CH_2)_2(CF_2)_5CF_3$ (**Scheme 2.1, Step IV**). ACVA (0.014 g, 0.05 mmol) and CTA (0.056 g, 0.2 mmol) were dissolved in 20 mL PBS buffer (pH 7.4). AA (1.37 mL, 20 mmol) was added to the mixture which was later transferred into a vial containing patterned Si-I/O$(CH_2)_2(CF_2)_5CF_3$ then sealed with a rubber septum. The surface-initiated RAFT polymerization of AA was allowed to proceed under nitrogen atmosphere at 70ºC for 20 h. The resulting patterned Si-PAA/O$(CH_2)_2(CF_2)_5CF_3$ was then obtained after rinsing with ethanol and deionized water (**Scheme 2.1, Step V**).

***In situ* Synthesis of AuNPs on PAA brushes**

The glass slide having patterned Si-PAA/O$(CH_2)_2(CF_2)_5CF_3$ was subjected to 5 cycles of alternate dipping in aqueous solution of $HAuCl_4$ (5 mL, 1 mM) and deionized water. Then, the glass slide was immersed in deionized water at 100 °C for 1 h followed by an aqueous solution of $HAuCl_4$ (5 mL, 1 mM) at 100 °C for another 4 h. The glass slide was then rinsed with deionized water and dried with stream of nitrogen to obtain the patterned PAA brushes containing AuNPs (**Scheme 2.1, Step VI**).

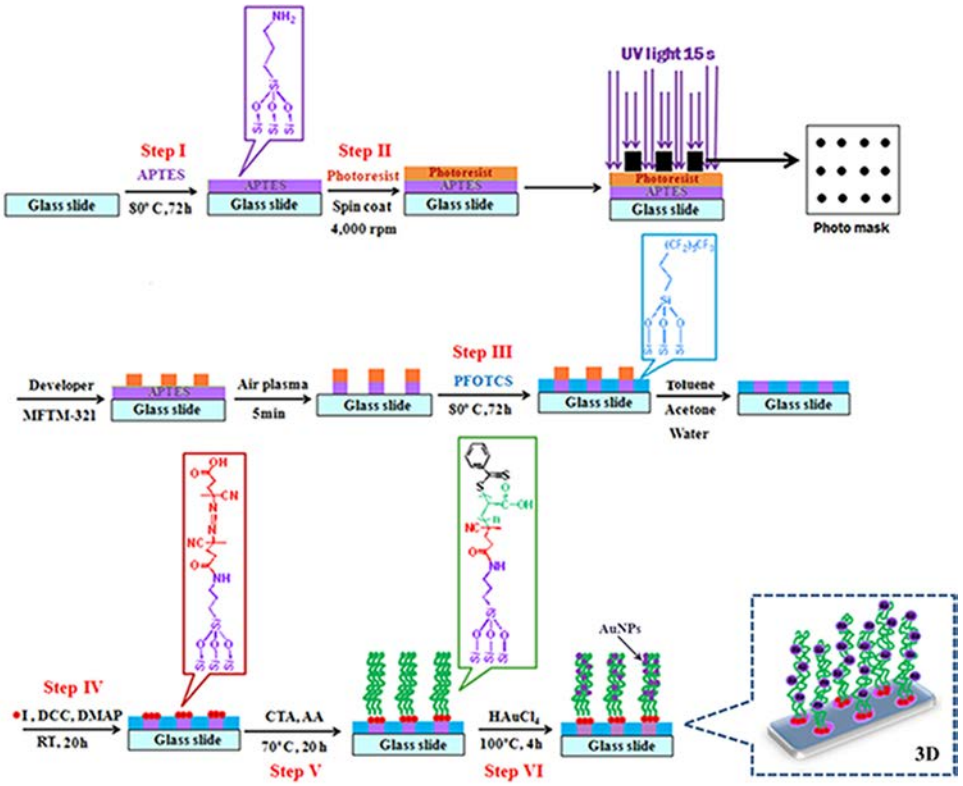


**Scheme 2.1** Schematic representation of stepwise method demonstrating how to prepare patterned PAA brushes containing AuNPs supported on glass slide: (I) reaction with APTES, (II) surface patterning by photolithography, (III) attachment of perfluorooctylsilyl groups, (IV) attachment of initiator, (V) surface-initiated RAFT polymerization of AA, and (VI) *in situ* synthesis of AuNPs on PAA brushes.

**Characterization**

PAA formed in solution during surface-initiated RAFT polymerization was characterized by Varian, model Mercury-400 nuclear magnetic resonance spectrometer (USA) operating at 400 MHz using $D_2O$ as a solvent. The FT-IR spectra of surface-

modified silica particles prepared as KBr discs were recorded in a frequency range of 400-4000 $cm^{-1}$ by a FT-IR spectrometer (Nicolet, USA), model Impact 410, with 32 scans at resolution 4 $cm^{-1}$ using TGS detector. The morphology and size of gold particles were analyzed by a JEOL JEM-2010 transmission electron microscopy (Japan) operating at 200 keV. The TEM samples were prepared by first scrapping the glass slide on the area covered with PAA brushes and AuNPs followed by adding a small quantity of Milli-Q water on the scrapped area. Approximately 10 µL of the generated solution was taken then dropped on the carbon-coated copper grid before being dried in a dessicator before analysis. The average diameters of the observed AuNPs were reported from measurements of 30 random particles for each sample using Semafore software. The dynamic advancing ($\theta_A$) and receding ($\theta_R$) water contact angles of surface-modified glass substrates were measured using a contact angle goniometer (Ramé-Hart, Inc., USA, model 100-00), equipped with a Gilmont syringe and a 24-gauge flat-tipped needle. All of the measurements were carried out in air at ambient temperature. The reported angle is an average of 5 measurements on different area of each sample. Atomic compositions of the surface-modified glass substrates were determined by x-ray photoelectron spectroscopy (XPS) on a Scienta ESCA 200 spectrometer (Uppsala, Sweden) with Al Kα x-rays at a takeoff angle of 90°. AuNPs generated on the PAA brushes were digested by aqueous solution of aqua regia (1$HNO_3$:3HCl) at room temperature for 15 min before quantified by Inductively Coupled Plasma-Mass Spectrometry (ICP-MS; Thermo scientific, model iCAP 6500 ICP-OES), using a calibration curve generated from $Au^{3+}$ solutions having concentration in a range of $10^{-7}$ – $10^{-6}$ M.

**Analysis of Single Peptide**

Each peptide sample was dissolved and diluted in Milli-Q water to a final concentration of 500 nM. For SALDI-MS analysis, the samples (3 µL) were directly deposited onto the glass slide modified with patterned PAA brushes containing AuNPs. The modified glass slide was attached onto MALDI target plate by a two-side conductive tape and then introduced into a Bruker Microflex/Autoflex III MALDI-TOF mass spectrometer for SALDI-MS analyses. The $N_2$ laser (337 nM) with 50% laser intensities and 100 laser shots were used for all analyses.

For MALDI-MS analysis, each peptide sample was mixed with CHCA matrix in a ratio of 1:9 (v/v) of sample: CHCA matrix (CHCA dissolved in 1:1(v/v) of 0.1%

trifluoroacetic acid (TFA) in acetonitrile: 0.1% TFA in Milli-Q) and then deposited onto MALDI target plate. After solvent evaporation and sample crystallization, the target plate was introduced into the mass spectrometer for MALDI-MS analysis.

**Selective Analysis of Thiol-containing Peptide in a Mixture**

A mixture of 500 nM thiol-containing peptide (GSH or ICNKQDCPILE) and 500 nM non thiol-containing peptide (sucrose and cholesterol or bradykinin) was deposited onto the glass slide modified with patterned PAA brushes containing AuNPs. The deposited mixture was incubated on the modified target plates at room temperature for 10 min. Then the unbounded peptides were rinsed out from the target for five times each by PBS buffer (pH 7.4) followed by Milli-Q water. For each rinsing cycle, multiple drops of washing solution were added on and promptly retracted back from the target using a micropipette. After solvent evaporation, the target plate was introduced into the mass spectrometer for both SALDI-MS and MALDI-MS analyses.

## RESULTS AND DISCUSSION

**Preparation and Characterization of Patterned PAA Brushes containing AuNPs**

Water contact angle measurement was used as a tool to monitor the success of stepwise surface modification of the glass substrate. The data are expressed in terms of advancing/receding contact angle ($\theta_A/\theta_R$) as shown in **Table 2.1**. An extremely hydrophilic glass substrate having generated silanol groups after cleaning by plasma treatment $(\theta_A \sim 0)$ became hydrophobic after reacting with APTES and yielded Si-$NH_2$ with $\theta_A/\theta_R$ of 84.7°/52.1°. The substrate turned slightly less hydrophobic when being immobilized with initiator via the reaction with ACVA. Upon surface-initiated RAFT polymerization, the water contact of the glass substrate was further decreased to 16.6° implying that hydrophilic PAA brushes was grafted onto the surface. In contrast, the glass surface was highly hydrophobic with contact angles of 127.6°/74.5° after being modified with perfluorooctylsilyl groups.

**Table 2.1** Water contact angles of the glass substrates after stepwise modification.

| Surface Functionality | $\theta_A$ | $\theta_R$ |
|---|---|---|
| Si-OH | 0 | N/A |
| Si-$NH_2$ | $84.7^{\circ} \pm 5.7^{\circ}$ | $52.1^{\circ} \pm 2.6^{\circ}$ |
| Si-initiator | $75.8^{\circ} \pm 2.9^{\circ}$ | $46.6^{\circ} \pm 6.3^{\circ}$ |
| Si-PAA | $16.6^{\circ}$ | N/A |
| Si-$OSi(CH_2)_2(CF_2)_5CF_3$ | $127.6^{\circ} \pm 2.7^{\circ}$ | $74.5^{\circ} \pm 4.3^{\circ}$ |

N/A: Not measurable

Molecular weight ($\overline{M}_n$) and functional group of PAA simultaneously formed in solution from the "added" initiator, ACVA were determined by $^1$H NMR analysis. As depicted in **Figure 2.1**, the characteristic $^1$H NMR peaks of the methylene proton in the AA unit (–C<u>H</u>(COOH)) and those aromatic protons of the dithiobenzoate group at the chain end of PAA appeared at 2.1-2.3 and 7.2-7.9 ppm, respectively. The average $M_n$ of PAA was calculated from the relative ratio between the peak integration of methylene proton from the PAA backbone and the peak integration of protons from the dithiobenzoate groups using eqn. 2.1. The fact that the calculated $M_n$ of 6,005 g/mol closely resembled the anticipated value (6,158 g/mol) for the target degree of polymerization (DP) of 100 suggested that the RAFT process was well controlled.

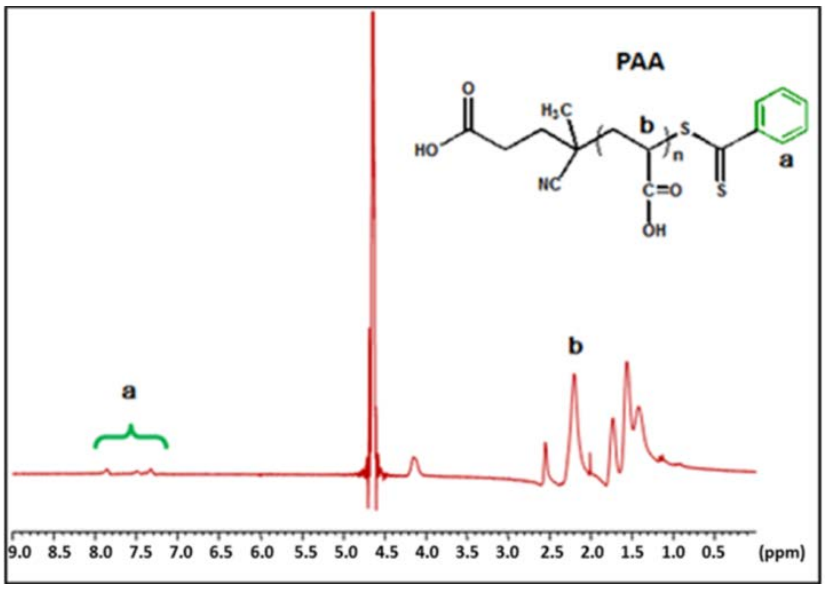


**Figure 2.1** $^1$H NMR spectrum of PAA formed in solution.

$$\text{Average } M_n = \left\{ \frac{\text{intergral of the } H_b \times M_{n\,(\text{acrylic acid})}}{\left( \frac{\text{intergral of the } H_a}{5} \right)} \right\} + M_{n\,(\text{CTA})} \qquad \text{(eq.2.1)}$$

$M_{n(\text{acrylic acid})} = 72.06$ g/mol, $M_{n(\text{CTA})} = 279.38$ g/mol

The success of PAA surface grafting was confirmed by FT-IR analysis of silica particles grafted with PAA brushes. **Figure 2.2c** reveals characteristic absorption bands of C=O stretching at 1635 $cm^{-1}$(Amide I), N-H bending at 1562 $cm^{-1}$(Amide II) suggesting that amide linkage has been formed between the terminal amino groups of APTES and carboxyl groups of the initiator, ACVA. Strong signal of C=O stretching of carboxylic acid apparently emerged at 1718 $cm^{-1}$ after surface-initiated RAFT polymerization took place as an indication of PAA brushes formation as shown in **Figure 2.2d**.

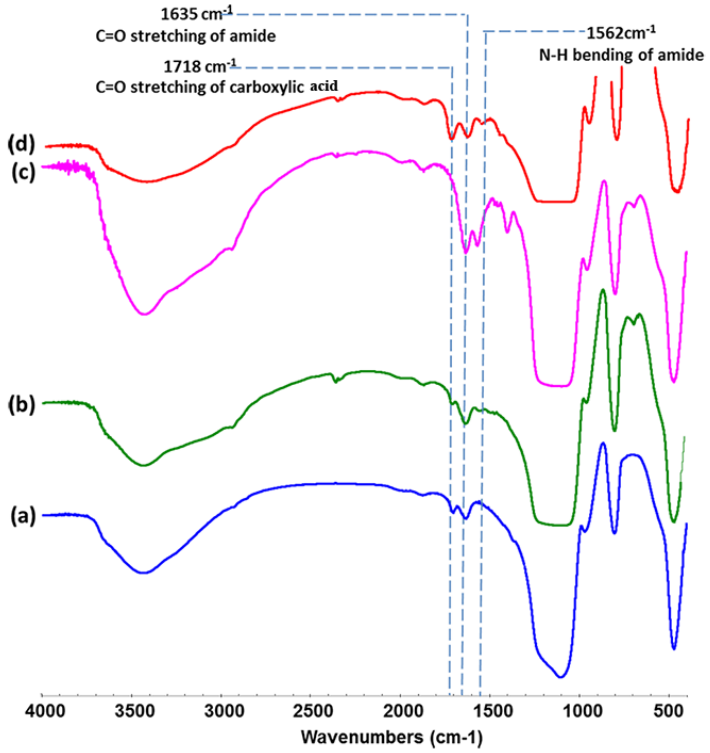


**Figure 2.2** FT-IR spectra of silica particles (a) before and after functionalized with (b) APTES, (c) ACVA initiator, and (d) PAA brushes.

A number of alternate dipping cycle between $HAuCl_4$ solution and deionized water was varied to determine its effect on AuNPs formation on the PAA-modified glass substrate. As shown in **Figure 2.3**, the substrate became slightly darker upon increasing the number of cycle from 1 to 5 implying that there was greater amount of AuNPs as a function of dipping cycle. This may be explained as a consequence of pH-dependent conformational change of the PAA.[30] Because pKa of PAA is 4.2, PAA chains would adopt extended conformation when being soaked in deionized water, having pH of approximately 6.0, due to ionic repulsion of the carboxylate groups along the chains **(Scheme 2.2, Step I,)**. Once the PAA-modified surface was immersed in $HAuCl_4$ solution, having pH of 1.7 **(Scheme 2.2, Step II)**, some carboxylate groups of the PAA chains should electrostatically interact with $Au^{3+}$ and may partially reduce it to $Au^0$. At the same time, the rest of carboxylate groups were protonated and became less extended and more coil-like, therefore can trap $Au^{3+}$ as well as the generated $Au^0$. It is quite unfortunate that exact mechanism on how carboxylate groups can reduce $Au^{3+}$ has not yet been directly proven. To attain such information requires an additional mechanistic study which is beyond a scope of our investigation. However, it can be postulated that the reduction would follow a similar pathway as polyacid compounds commonly used for AuNPs synthesis such as citrate and oxalate anions which involves ligand exchange and simultaneously induction of a concerted decarboxylation and reduction of Au(III).[37] Another most relevant work that was found on the literature suggested that PAA can undergo decarboxylation through radical mechanism in the presence of $Fe^{3+}$ which eventually leads to degradation. The process can be accelerated especially at high temperature.[38]

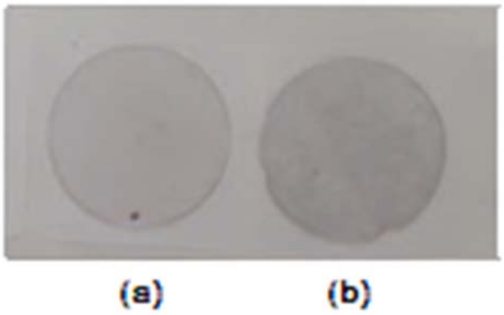


**Figure 2.3** PAA-modified glass slide containing AuNPs generated by (a) 1 cycle of dipping and (b) 5 cycles of dipping in between 1 mM $HAuCl_4$ solution and deionized water.

By repetitive performing this cycle of dipping, the more $Au^{3+}$ can associate with the carboxylate groups and the more $Au^{0}$ can be generated upon subsequent heat treatment **(Scheme 2.2, Step III)**. It should be emphasized at this point that the carboxyl groups can act as effective reducing moieties for $Au^{3+}$ leading to the formation of AuNPs. This would add simplicity to the method because the reduction can be done without having to use additional reducing agent. According to ICP-MS analysis, a surface coverage of the AuNPs was found to be $2.90\times10^{-9}$ and $4.62\times10^{-9}$ mol/cm$^2$ for the 1- and 5-cycled dipping, respectively. The calibration curve used for AuNPs quantification is illustrated in **Figure 2.4**. Effect of number of dipping cycle on the substrate efficiency in analysis of two single peptides (bradykinin and GSH) was evaluated. Although increasing dipping cycle further to 10 yielded approximately 1.3 higher AuNPs coverage than that obtained from the 5-cycled dipping, %RSD values of signal intensity detected on the substrate prepared by 10-cycled dipping was significantly higher than those detected on the substrate prepared by 5-cycled dipping (**See Figure 2.5**). For this reason, the 5-cycled dipping was therefore selected as the optimal condition for substrate preparation to be used for further analysis.

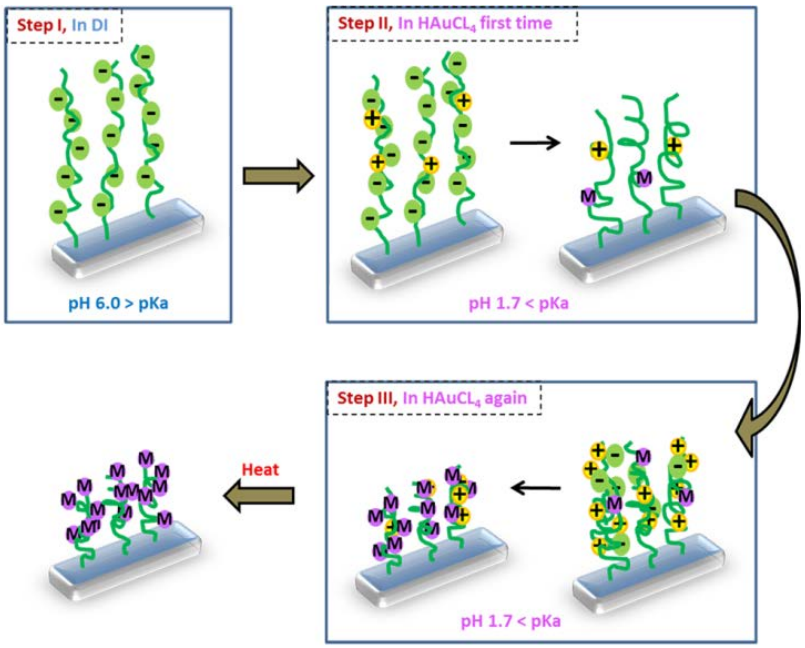


**Scheme 2.2** Schematic representation of stepwise method showing that carboxyl groups of PAA brushes can act as reducing moieties for *in situ* synthesis of AuNPs: (I) PAA-modified surface in deionized water, (II) PAA-modified surface in $HAuCl_4$ (aq) first time, (III) PAA-modified surface in $HAuCl_4$ solution after 5 alternate dipping cycles between deionized water and $HAuCl_4$ (aq) followed by $Au^{3+}$ reduction to $Au^{0}$ by heating.

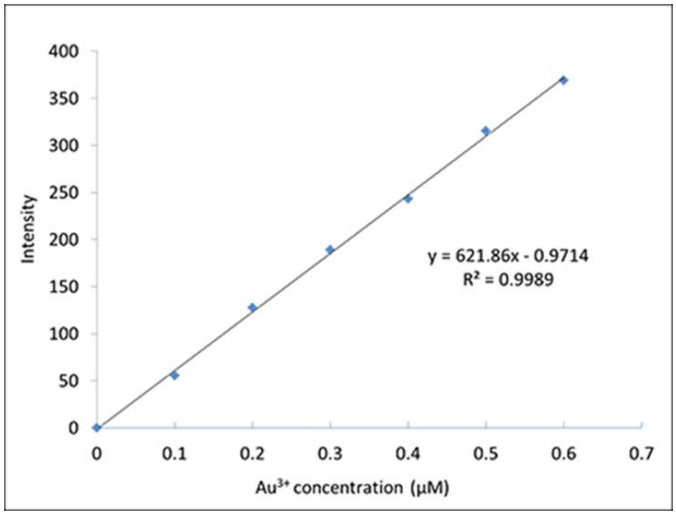


**Figure 2.4** Calibration curve used for AuNPs quantification by ICP-MS generated from $Au^{3+}$ solution.

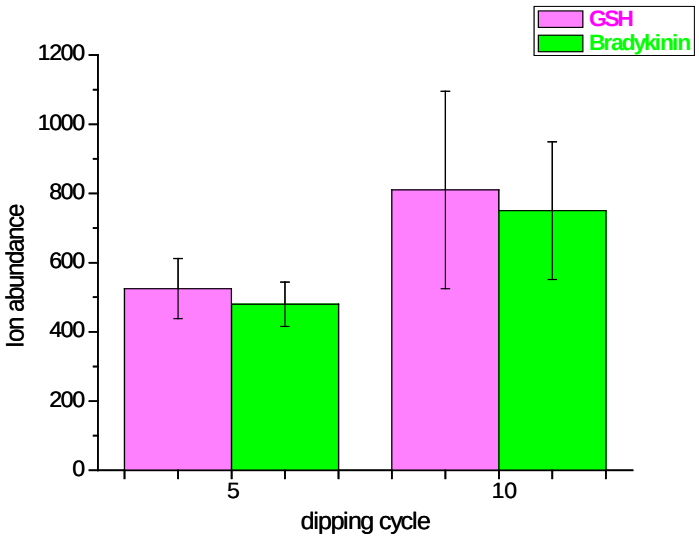


**Figure 2.5** Ion abundance of bradykinin and GSH measured on the AuNPs-PAA substrate prepared by 5 and 10 cycles of dipping.

Formation of AuNPs on the patterned PAA brushes can be demonstrated in **Figure 2.6**. The area covered with UV-sensitive resist after surface patterning by photolithography using the pattern shown in **Figure 2.6a** to generate photomask (**Step II in Scheme 2.1**) can be seen as bright yellow spots. After surface grafting of PAA brushes, the greater hydrophilicity of the PAA brushes than the surrounding area which was covered with perfluorooctylsilyl groups can be demonstrated by the ability to sustain water droplets as shown in **Figure 2.6b**. Subsequent AuNPs formation within

the PAA brushes can be visualized as dark spots on the glass substrate appearing in **Figure 2.6c** at the same positions as those previously covered with UV-sensitive resist in **Figure 2.6a** and water droplets in **Figure 2.6b**. It should also be noted that the diameter of each spot on the glass slide shown in **Figure 2.6a-c** is the same as that of the individual spot on the MALDI target plate underneath the glass substrate appearing in **Figure 2.6d**.

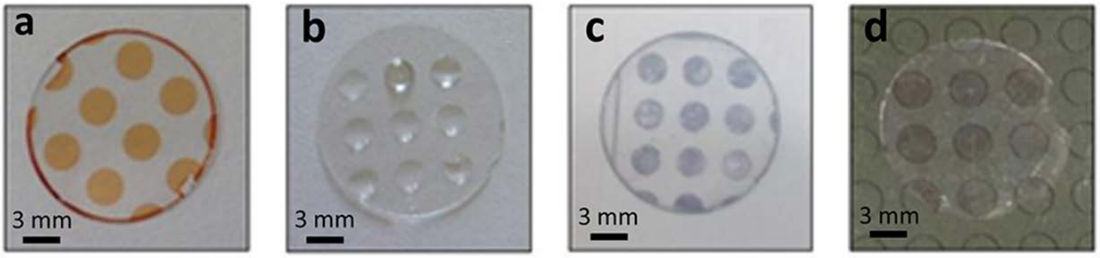


**Figure 2.6** Patterned glass substrates with (a) coated positive UV-sensitive resist after photolithography step, (b) grafted PAA brushes holding water droplets demonstrating their higher hydrophilicity than the surrounding area, grafted PAA brushes having *in situ* generated AuNPs (c) alone, and (d) together with the MALDI target plate.

Morphology of the immobilized AuNPs on the glass substrate was determined from the material scrapped of the glass slide by TEM. As can be seen in **Figure 2.7**, the AuNPs were not quite uniform in shape. This outcome agrees quite well with the work previously reported by Hussain *et al*. [35] The diameter estimated from the AuNPs that are quite spherical was in a range of 25.13±3.20 nm.

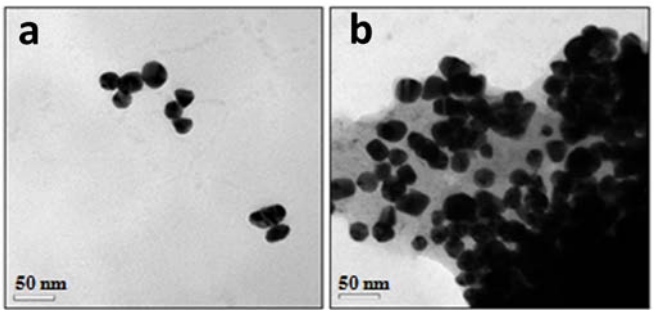


**Figure 2.7** Representative TEM images (a, b) of AuNPs immobilized on PAA-modified glass substrate

The presence of AuNPs on the PAA-modified glass surface was also verified by XPS measurement. **Figure 2.8** shows XPS spectra of the PAA-modified glass surface both before and after AuNPs immobilization. As shown in **Figure 2.8b**, besides the signals of carbon ($C_{1s}$, binding energy of 287 eV) and oxygen ($O_{1s}$, binding energy of 533 eV) of PAA, trace signals of $Au_{4f7/2}$ and $Au_{4f5/2}$ at binding energy of 84 and 88 eV, characteristic binding energies of Au(0) [39] were also observed implying the success of *in situ* synthesis of AuNPs on the PAA brushes modified on glass substrate with 0.67% composition. It should also be emphasized that the ratio of C:O of approximately 3:2 matched very well with the theoretical value estimated from the repeat unit of PAA (-$CH_2CCOOH$-). Percentages of elemental composition of all samples are also shown in **Table 2.2**.

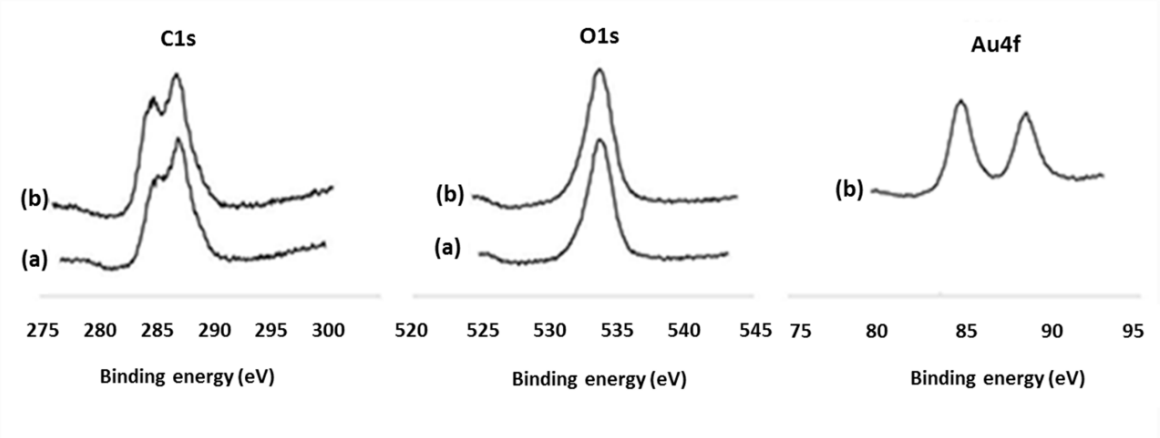


**Figure 2.8** XPS spectra of (a) PAA-modified glass substrate and (b) PAA-modified glass substrate containing AuNPs.

**Table 2.2** Elemental composition of surface-modified glass substrates analyzed by XPS

| Element | PAA-modified glass surface (%) | PAA-modified glass surface containing AuNPs (%) |
|---|---|---|
| $C_{1s}$ | 56.76 | 59.44 |
| $O_{1s}$ | 43.24 | 39.89 |
| $Au_{4f}$ | - | 0.67 |

**SALDI-MS Analysis of Single Peptide on the AuNPs-PAA Substrate**

To determine the applicability of the PAA-modified glass substrate immobilized with AuNPs (AuNPs-PAA) as substrate for SALDI-MS analysis, bradykinin (MW = 1060.21 g/mol), a cancer biomarker, was chosen as a standard peptide for analysis in comparison with the use of citrate-stabilized AuNPs as a MALDI matrix. As illustrated in **Figure 2.9**, the citrate-stabilized AuNPs alone gave such a high background signal which is probably caused by partial ionization of the AuNPs. Therefore, poor signal of bradykinin was detected with relatively strong background when the analysis was done in the presence of citrate-stabilized AuNPs as can be seen in **Figure 2.9b**. On the other hand, a characteristic peak of bradykinin at m/z of 1060 was clearly observed without signal interference from the AuNPs when the analysis was performed on a spot of PAA brushes containing AuNPs (**Figure 2.9c**). This result strongly indicated that the PAA brushes effectively trapped and prevented the AuNPs from coming off the substrate so that their ionization was suppressed. The fact that the ion abundance of bradykinin was relatively high in **Figure 2.9c** suggested that the ionization efficiency was also improved perhaps by a better distribution of the AuNPs within the matrix of PAA and PAA itself being a good proton source. To determine the stability of the mass spectrum, we have also performed analysis of bradykinin on a number of modified targets and found that %RSD of ion abundance is less than 5%. This relatively low %RSD suggests that the mass spectra are quite stable.

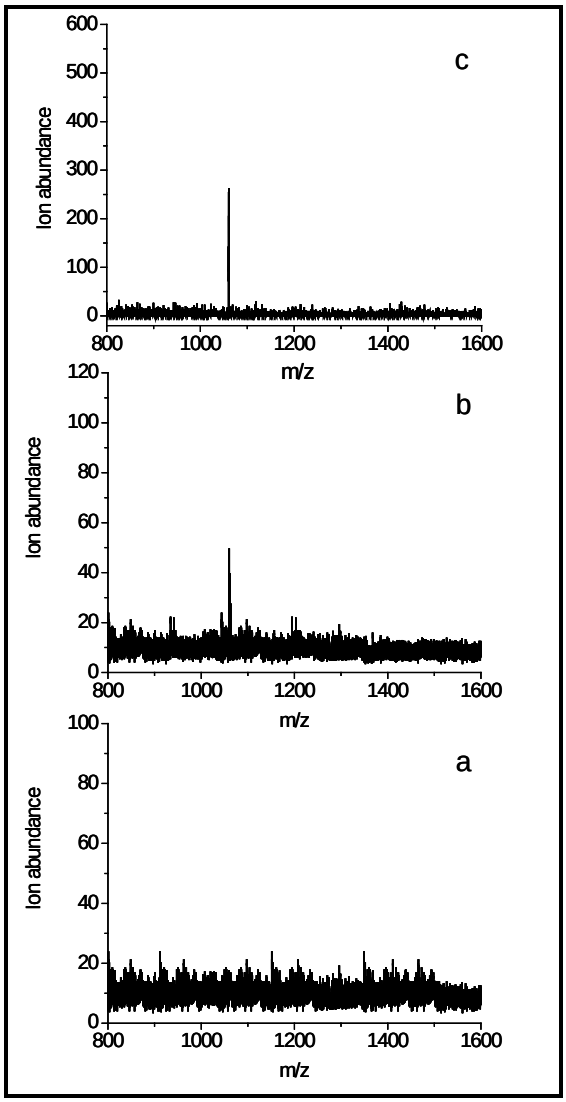


**Figure 2.9** Mass spectra of (a) AuNPs, (b) bradykinin mixed with citrate-stabilized AuNPs matrix, and (c) bradykinin on AuNPs-PAA substrate.

Besides the analysis of bradykinin peptide, the AuNPs-PAA substrate was also subjected to analysis of low molecular weight peptide, GSH (MW 307.08 g/mol). As revealed in **Figure 2.10a**, by using CHCA matrix, GSH was undetectable due to the interference ion peaks from CHCA matrix at low mass region (m/z $\leq$ 600). This common phenomenon limits the application of MALDI-MS technique for small molecule detection. Interestingly, when GSH was analyzed on our developed modified substrate, it was readily detected without interference peak as shown in **Figure 2.10b**. There are two dominant peaks in the mass spectrum, which represent $[GSH+H]^+$ (m/z 308) and $[2GSH+H]^+$ (m/z 615). Dimerization of GSH caused by oxidation of the cysteine side chain thiols, linking two chains together by a disulfide bridge, seems to be favorable at

relatively high concentration, 500 nM in this case. This is the reason why $[2GSH+H]^+$ (m/z 615) was not detected in subsequent investigation where rinsing was involved for selective analysis from mixture (**Figure 2.11a**) and LOD determination (**Figure 2.13a**) of which GSH concentration was as low as 0.1 nM. Similar observation on GSH dimerization was also reported by Cui and co-workers.[40] Moreover, the lower laser energy (50% laser 100 shots) was required in the detection on the AuNPs-PAA substrate when compared to the unmodified substrate (using CHCA matrix), indicating the potential of this substrate for low molecular weight compound detection. This newly developed substrate provides an alternative approach for the analysis of small molecules by SALDI-MS technique.

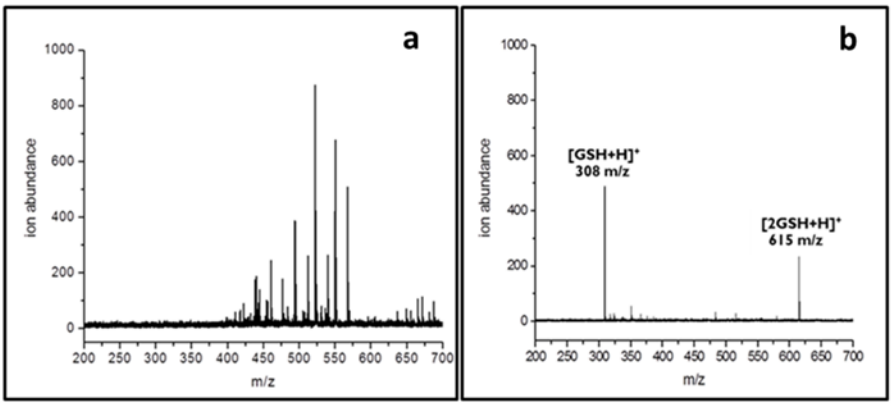


**Figure 2.10** Mass spectra of GSH (500 nM) analyzed (a) by using CHCA matrix and (b) on AuNPs-PAA substrate.

**Selective Detection of Thiol-containing Peptide on the AuNPs-PAA Substrate by SALDI-MS**

Based upon the inherently strong binding interactions between Au and thiol (-SH) group,[41] the selectivity of the AuNPs-PAA substrate towards thiol-containing peptides (*i.e.* GSH, ICNKQDCPILE) was investigated. Firstly, a solution mixture of three small molecules (m/z $\leq$ 500) which are GSH (m/z 307.32), sucrose (m/z 342) and cholesterol (m/z 386.65) was incubated on the AuNPs-PAA substrate and the substrate was simply rinsed with PBS buffer and Milli-Q water before SALDI-MS analysis. The result shown in **Figure 2.11a** indicates that only GSH was detectable on the modified substrate, which may be explained as a consequence of selective binding between Au on the modified substrate and the thiol group of GSH. Apparently, there was no non-

specific adsorption of the non-thiol-containing peptides by either the AuNPs or the PAA brushes. By using our modified substrate, the thiol-containing peptide can be directly detected on the target plate without the requirement for separation by centrifugation as employed by aforementioned research.[16,42] This truly add simplicity by reducing cost and time of sample preparation.

Then, the selectivity of the substrate was further evaluated with peptides having higher mass (MW ≥ 1000 g/mol) from a solution mixture of ICNKQDCPILE (m/z 1274) and bradykinin (m/z 1060.21). As can be seen in **Figure 2.11b**, only ICNKQDCPILE that contains thiol groups on cysteine unit was selectively detected at m/z of 1275 $[M+H]^+$. This high selectivity of the modified substrate towards thiol-containing peptide is very useful for the applications that require high specificity for the detection of thiol-containing peptides in complex biological samples (*e.g.* human serum, cell lysates).

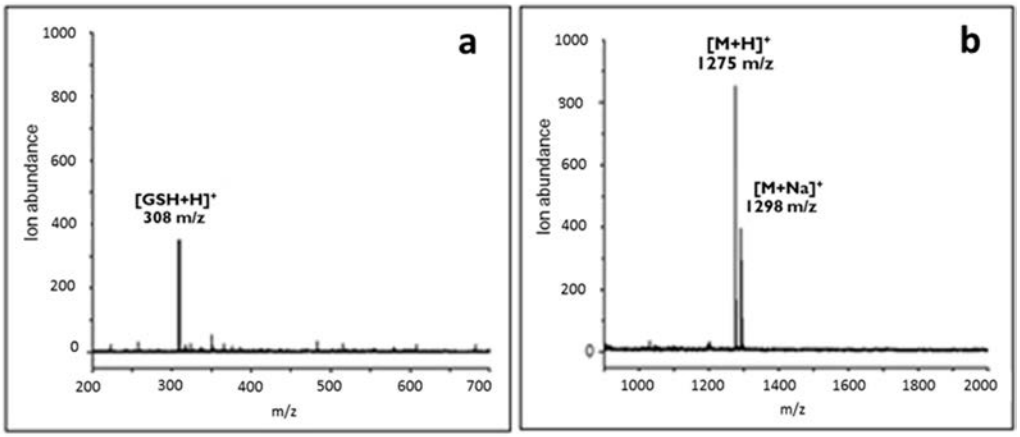


**Figure 2.11** Mass spectra of (a) a mixture of 500 nM GSH, sucrose, cholesterol and (b) a mixture of 500 nM bradykinin and ICNKQDCPILE analyzed on AuNPs-PAA substrate by SALDI-MS.

To demonstrate that the substrate also works in biological matrices, a similar analysis was conducted in human serum by spiking a solution mixture of ICNKQDCPILE (m/z 1274), bradykinin (m/z 1060), and angiotensin I (m/z 1296) at a concentration of 500 nM each into a 10x diluted human serum. After the high abundance serum proteins (*e.g. HSA, IgG*) was removed using an antibody column, the leftover of solution was incubated on the modified substrate for 15 min to selectively bind with thiol-containing peptide. After washing with PBS (pH 7.0) and Milli-Q water, the peptide attached on the modified target was directly analyzed by MS. As shown in a **Figure 2.12**, only ICNKQDCPILE that contains thiol group on cysteine unit is selectively

detected at m/z of 1275 $[M+H]^+$. This result truly verifies the powerfulness of our modified substrate for selective binding and direct MS detection of cysteine-containing peptide in complex biological matrices.

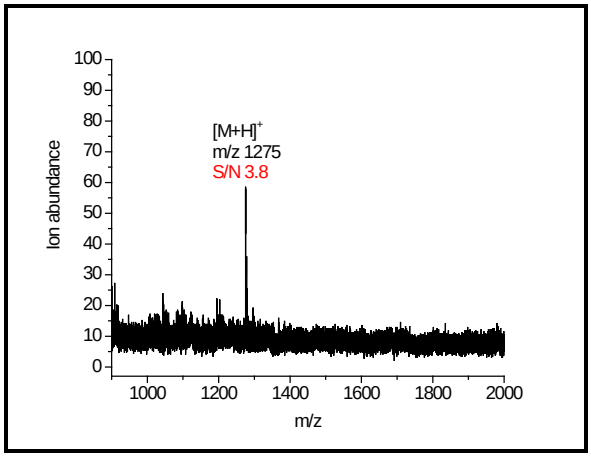


**Figure 2.12** Mass spectra of ICNKQDCPILE spiked in 10x diluted human serum analyzed on AuNPs-PAA substrate by SALDI-MS after depletion of high abundance proteins in human serum.

The detection limit of thiol-containing peptides (GSH, ICNKQDCPILE) on these substrates was also estimated. As shown in **Figure 2.13**, the limit of detection (LOD) of GSH and ICNKQDCPILE were found to be 0.1 nM (S/N = 6.4) and 0.05 nM (S/N = 3.8), respectively on the AuNPs-PAA substrate. Thus, by using our modified substrate, the thiol-containing peptide can be selectively and sensitively detected without the use of organic matrix.

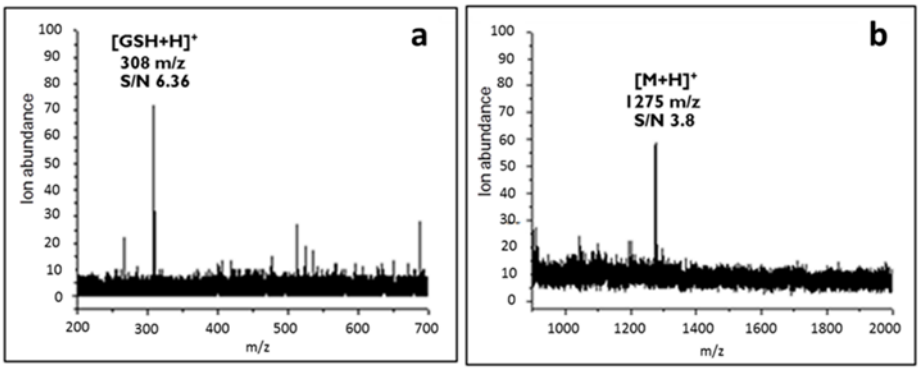


**Figure 2.13** Mass spectra of (a) 0.1 nM GSH and (b) 0.05 nM ICNKQDCPILE analyzed on AuNPs-PAA substrate.

## CONCLUSIONS

The present study has demonstrated that patterned PAA brushes can be formed by photolithography and surface-initiated RAFT polymerization of AA. The AuNPs can be generated *in situ* within the matrix of PAA brushes without the use of additional reducing agent. The presence of AuNPs in the form of $Au^0$ was verified by XPS. TEM analysis suggested that the AuNPs were not quite uniform in shape and had estimated diameter in a range of 25.13±3.20 nm. As determined by ICP-MS, a surface coverage of up to $4.62\times10^{-9}$ mol/cm$^2$ was achieved upon using an optimal dipping cycle of 5 in $HAuCl_4$ and Milli-Q water. The PAA brushes embedded with AuNPs can be used as substrate for SALDI-MS analysis which was capable of detecting both small peptide having m/z $\leq$ 600 (GSH) and large peptides having m/z $\geq$ 1000 (bradykinin, ICNKQDCPILE) without the interference from matrix signal. Moreover, by employing AuNPs as the capture probe, the PAA-AuNPs substrate can selectively identify thiol-containing peptides (GSH, ICNKQDCPILE) from the peptide mixtures with LOD as low as 0.1 nM and 0.05 nM for GSH and ICNKQDCPILE, respectively. An ability to selectively detect ICNKQDCPILE in diluted human serum strongly demonstrates the potential of the developed substrate for peptide analysis in complex biological matrices. In addition, the procedure of separation is simple, time-saving and efficient because sample can be spotted and thiol-containing peptides can be separated directly on the target plate by using micropipette without the requirement for tedious washing/rinsing steps. It should also be emphasized that the analysis can be accomplished without the requirement for extra proton source because carboxyl groups of PAA brushes can serve as internal proton source.

## REFERENCES


(1) Cao, C.; Li, X.; Lee, J.; Sim, S. J. *Biosens. Bioelectron.* **2009**, *24*, 1292-1297.

(2) Afonso, A. S.; Zanetti, B. F.; Santiago, A. C.; Henrique-Silva, F.; Mattoso, L. H. C.; Faria, R. C. *Talanta* **2013**, *104*, 193-197.

(3) Nguyen, H. P.; Chandel, N. S.; DeBerardinis, R. J.; Schug, K. A. *J. Sep. Sci.* **2013**, *36*, 3303-3309.

(4) Smith, Z. M.; Terry, J. M.; Barnett, N. W.; Gray, L. J.; Wright, D. J.; Francis, P. S. *Analyst* **2010**, *139*, 2416-2422.

(5) Hu, B.; Cao, X.; Zhang, P. *New J. Chem.* **2013**, *37*, 3853-3856.

(6) Chen, S.; Hong, Y.; Liu, J.; Tseng, N.-W.; Liu, Y.; Zhao, E.; Lam, J. W. Y.; Tang, B. Z. *J. Mat. Chem. B* **2014**, *2*, 3919-3923.

(7) McKeague, M.; Foster, A.; Miguel, Y.; Giamberardino, A.; Verdin, C.; Chan, J. Y. S.; DeRosa, M. C. *RSC Advances* **2013**, *3*, 24415-24422.

(8) Li, T.; Shu, B.; Jiang, B.; Ding, L.; Qi, H.; Yang, M.; Qu, F. *Sens. Actuator B-Chem.* **2013**, *186*, 768-773.

(9) Wang, Y.; Wu, L.; Zhou, X.; Wong, T. I.; Zhang, J.; Bai, P.; Li, E. P.; Liedberg, B. *Sens. Actuator B-Chem.* **2013**, *186*, 205-211.

(10) Grant, C. S.; Louda, J. W. *Org. Geochem.* **2013**, *65*, 29-36.

(11) Shabani, A.; Tabrizian, M. *Analyst* **2013**, *138*, 6052-6062.

(12) Cerasoli, E.; Rakowska, P. D.; Horgan, A.; Ravi, J.; Bradley, M.; Vincent, B.; Ryadnov, M. G. *Mol. Biosyst.* **2010**, *6*, 2214-2217.

(13) Rodthongkum, N.; Ramireddy, R.; Thayumanavan, S.; Richard, W. V. *Analyst* **2012**, *137*, 1024-1030.

(14) Kailasa, S. K.; Wu, H.-F. *Analyst* **2010**, *135*, 1115-1123.

(15) Chiang, C.-K.; Chiang, N.-C.; Lin, Z.-H.; Lan, G.-Y.; Lin, Y.-W.; Chang, H.-T. *J. Am. Soc. Mass Spectrom.* **2010**, *21*, 1204-1207.

(16) Shrivas, K.; Wu, H.-F. *Rapid Commun. Mass Spectrom.* **2008**, *22*, 2863-2872.

(17) Chen, C.-T.; Chen, W.-J.; Liu, C.-Z.; Chang, L.-Y.; Chen, Y.-C. *Chem. Commun.* **2009**, 7515-7517.

(18) Kailasa, S. K.; Wu, H.-F. *Analyst* **2012**, *137*, 1629-1638.

(19) Li, L.; Li, B. *Analyst* **2009**, *134*, 1361-1365.

(20) Aminlashgari, N.; Shariatgorji, M.; Ilag, L. L.; Hakkarainen, M. *Anal. Methods* **2011**, *3*, 192-197.

(21) Kawasaki, H.; Sugitani, T.; Watanabe, T.; Yonezawa, T.; Moriwaki, H.; Arakawa, R. *Anal. Chem.* **2008**, *80*, 7524-7533.

(22) Tarui, A.; Kawasaki, H.; Taiko, T.; Watanabe, T.; Yonezawa, T.; Arakawa, R. *J. Nanosci. Nanotechnol.* **2009**, *9*, 159-164.

(23) Zhao, B.; Brittain, W. J. *Prog. Polym. Sci.* **2000**, *25*, 677-710.

(24) Barbey, R.; Lavanant, L.; Paripovic, D.; Schuwer, N.; Sugnaux, C.; Tugulu, S.; Klok, H.-A. *Chem. Rev.* **2009**, *109*, 5437-5527.

(25) Dunn, J. D.; Igrisan, E. A.; Palumbo, A. M.; Reid, G. E.; Bruening, M. L. *Anal. Chem.* **2008**, *80*, 5727-5735.

(26) Dunn, J. D.; Watson, J. T.; Bruening, M. L. *Anal. Chem.* **2006**, *78*, 1574-1580.

(27) Wang, W.-H.; Bruening, M. L. *Analyst* **2009**, *134*, 512-518.

(28) Kim, Y.-P.; Lee, B. S.; Kim, E.; Choi, I. S.; Moon, D. W.; Lee, T. G.; Kim, H.-S. *Anal. Chem.* **2008**, *80*, 5094-5102.

(29) Akkahat, P.; Hoven, V. P. *Colloid Surf. B-Biointerfaces* **2011**, *86*, 198-205.

(30) Akkahat, P.; Mekboonsonglarp, W.; Kiatkamjornwong, S.; Hoven, V. P. *Langmuir* **2012**, *28*, 5302-5311.

(31) Dong, R.; Krishnan, S.; Baird, B. A.; Lindau, M.; Ober, C. K. *Biomacromolecules* **2007**, *8*, 3082-3092.

(32) Qu, Z.; Hu, F.; Chen, K.; Duan, Z.; Gu, H.; Xu, H. *J. Colloid Interface Sci.* **2013**, *398*, 82-87.

(33) Wang, Y.-M.; Cui, Y.; Cheng, Z.-Q.; Song, L.-S.; Wang, Z.-Y.; Han, B.-H.; Zhu, J.-S. *Appl. Surf. Sci.* **2013**, *266*, 313-318.

(34) Ballarin, B.; Cassani, M. C.; Tonelli, D.; Boanini, E.; Albonetti, S.; Blosi, M.; Gazzano, M. *J. Phys. Chem. C* **2010**, *114*, 9693-9701.

(35) Hussain, I.; Brust, M.; Papworth, A. J.; Cooper, A. I. *Langmuir* **2003**, *19*, 4831-4835.

(36) Hayat, A. *J. Anat.* **1989**, *176*, 215-216.

(37) Ojea-Jimenez, I.; Romero, F. M.; Bastus, N. G.; Puntes, V. *J. Phys. Chem. C* **2010**, *114*, 1800-1804.

(38) Neira, A.; Tarraga, M.; Catalan, R. *J. Chil. Chem. Soc.* **2007**, *52*, 1314-1317.

(39) Cheng, W. L.; Dong, S. J.; Wang, E. K. *Langmuir* **2003**, *19*, 9434-9439.

(40) Cui, S. Y.; Kim, S. J.; Jo, S. C.; Lee, Y. M.; Lee, Y. I. *Bull. Korean Chem. Soc.* **2005**, *26*, 1235-1240.

(41) Carr, J. A.; Wang, H.; Abraham, A.; Gullion, T.; Lewis, J. P. *J. Phys. Chem. C* **2012**, *116*, 25816-25823.

(42) Chiu, T.-C.; Chang, L.-C.; Chiang, C.-K.; Chang, H.-T. *J. Am. Soc. Mass Spectrom.* **2008**, *19*, 1343-1346.

# Chapter III

## Clickable and Anti-fouling Platform of Poly[(propargyl methacrylate)-*ran*-(2-methacryloyloxyethyl phosphorylcholine)] for Biosensing Applications

### INTRODUCTION

Effective functionalization with biomolecules is important in the development of materials for biotechnology-related applications such as biosensors, protein/cell microarrays, microfluidic devices, and tissue engineering. Polymeric platforms are becoming increasingly attractive for biomolecule immobilization because a variety of functional groups can be conveniently incorporated and proportionally customized using combinations of specific monomers in the polymerization step. The superiority of this approach, which provides a three-dimensional platform and therefore offers a higher functional group density for biomolecular probe binding per surface area than in the case of a conventional two-dimensional platform based on self-assembled monolayers (SAMs)[1-3] of end-functionalized alkanethiols, for biosensing applications has been shown by our group[4,5] and other researchers.[6-9]

Most biomolecules (e.g., proteins, antibodies, enzymes, and DNA) carry carboxyl and/or amino groups. Polymers with versatile functionalities that can accommodate covalent bond formation, particularly via hydrolytically stable amide linkages, including poly[oligo(ethylene glycol) methacrylate],[8,10,11] poly(2-hydroxyethyl methacrylate),[12,13] and poly(acrylic acid) (PAA),[4, 5,14-19] are therefore commonly used as platforms for biomolecule conjugation. However, an additional activation step using an appropriate coupling reagent is required for biomolecule conjugation to such polymers. PAA, in particular, suffers from non-specific adsorption of positively charged components such as lysozyme (LYZ) because its carboxyl groups (–COOH) can be ionized to negatively charged carboxylate ions ($–COO^-$).[5] This is problematic in the analyses of complex samples. Precursor polymers have recently

emerged as alternative and ready-to-use functional materials that can directly bind with designated nucleophilic modifiers such as an amino-containing biomolecules, without having to undergo activation. Well-known precursor polymeric systems include polymers bearing succimidyl ester[20-22] or pentafluorophenyl ester groups,[23,24] poly[propargyl (me)thacrylate] [PPg(M)A],[25,26] and poly(glycidyl methacrylate) (PGMA).[27,28] From the perspective of chemical robustness, PPg(M)A is a good choice because the alkynyl side group in each repeat unit specifically undergoes a Huisgen 1,3-dipolar azide–alkyne cycloaddition with azide-containing molecules, or thiol–yne reactions with thiol-containing molecules; the reaction yields under mild conditions are high and no by-products are generated. Socaci and coworkers[25] prepared core–shell nanoparticles consisting of magnetite cores and poly(*O*-propargyl acrylate) shells. They showed that acryloyl-containing phosphonates or methacryloyl phosphates anchored to the magnetic nanoparticle (MNP) surfaces acted as initiating sites for polymerization of a series of alkyne-terminated acrylate monomers with different spacers between the carboxyl oxygen atom and the alkyne moiety. The ability of the alkyne moieties on MNPs to form triazole linkages via azide–alkyne cycloaddition was tested using azide-terminated biotin fluorescently labeled with dansyl groups. Wang and co-workers[26] successfully developed an alkyne-functionalized microporous polypropylene membrane via a combination of plasma treatment and UV-induced graft polymerization of 3-(trimethylsilyl)propargyl methacrylate. The PPgMA-modified membrane obtained after trimethylsilyl removal can directly bind with a thiol-containing carbohydrate ligand, 2,3,4,6-tetra-*O*-acetyl-β-D-glucopyranoside thiol, and yields a glycosylated membrane via a thiol–yne click reaction. The glycosyl density of the glycosylated membrane can be tuned based on the polymer graft density, and the membrane showed specific adsorption of lectin concanavalin A over peanut agglutinin.

Specific detection of target molecules rather than the non-targeted components or the ability to resist non-specific adsorption, known as anti-fouling, is another key element in biosensor development, especially for the analysis of real biologically relevant samples in which numerous types of interference exist concurrently. A number of copolymeric platforms have therefore been designed to incorporate biocompatible and highly hydrophilic polymers along with precursor polymers. Among the developed hydrophilic polymers, zwitterionic polymers, which contain positively and negatively charged moieties within the same structure, such as poly(2-methacryloyloxyethyl phosphorylcholine) (PMPC),

poly(carboxybetaine methacrylate) (PCBMA), and poly(sulfobetaine methacrylate) (PSBMA) have received growing attention for use in new-generation anti-fouling materials.[29-31] Emmenegger and co-workers[30] reported that plasma protein adsorption completely suppressed on surface-immobilized PCBMA, whereas PMPC and PSBMA prevented adsorption of the main plasma proteins (human serum albumin, IgG, Fbg, and LYZ) from single-protein solutions, but could not prevent plasma deposition. In this study, based on our previous work using MPC-containing copolymer brushes between PMPC and poly(methacrylic acid) (PMA) as precursor layers for biosensor applications,[14] we used PMPC as an anti-fouling zwitterionic polymer to prevent non-specific adsorption. It has been proven that PMPC helps to suppress undesirable non-specific adsorption of proteins and cells,[32-36] and also provides a suitable environment for preserving the stability and activity of immobilized biomolecular probes.[37-39] Ishihara and co-workers[39] used monitoring with a quartz crystal balance to show that poly[2-methacryloyloxyethyl phosphorylcholine (MPC)-*co*-*n*-butyl methacrylate (BMA)-*co*-*p*-nitrophenyloxycarbonyl poly(ethylene glycol) methacrylate (MEONP)] (PMBN), adsorbed on a gold-coated substrate and conjugated with anti-C-reactive protein antibodies via nitrophenyloxycarbonyl active ester binding sites in the MEONP unit can specifically bind with the respective antigens. The developed platform simultaneously prevented adsorption of bovine serum albumin and γ-globulin. PMBN physically adsorbed on poly(methyl methacrylate) microchips and polystyrene well plates has also been used for antigen detection via ELISA-based assays, and for affinity-based protein separation when deposited on poly(L-lactic acid) nanoparticles.[40-43] Iwata et al.[44] generated block copolymer brushes of PGMA, another precursor polymer, and PMPC via surface-initiated atom-transfer radical polymerization. An antibody fragment was conjugated to the surface-grafted copolymer brushes via a thiol–disulfide interchange reaction with pyridyl disulfide linkages, previously introduced by epoxide ring opening of GMA repeat units in the copolymer. The activity of the conjugated antibody fragment in antigen detection was better for the PMPC copolymer platform than those for platforms based on PGMA alone or epoxysilane.

Inspired by the research described above, the aim of this study was to develop a multifunctional copolymer platform based on clickable PPgMA and anti-fouling PMPC, a combination that, to the best of our knowledge, has never been explored. The alkyne moiety of the PgMA unit should serve as an active site for binding of azide-containing

molecules via a Cu-catalyzed azide/alkyne cycloaddition (CuAAC) click reaction, without the need for activation. The hydrophilic monomeric unit, MPC, should enable the copolymer to suppress non-specific adsorption. The copolymer poly[(propargyl methacrylate)-*ran*-(2-methacryloyloxyethyl phosphorylcholine)] (PPgMAMPC) was first synthesized by reversible addition-fragmentation chain-transfer (RAFT) polymerization. Thiol-terminated PPgMAMPC (PPgMAMPC-SH), obtained by aminolysis of PPgMAMPC, was immobilized on a gold-coated substrate using a "grafting to" method via Au–S bond formation between the thiol end groups of the copolymer and the gold surface. Azide-containing biotin and peptide nucleic acid (PNA) were used as model probes to demonstrate the potential of the surface-attached PPgMAMPC for probe immobilization and subsequent detection of target molecules, namely streptavidin (SA) and deoxyribonucleic acid (DNA), using a surface plasmon resonance (SPR) technique. The parameters that may affect the sensitivity and specificity, in terms of the signal-to-noise (*S*/*N*) ratio, in detecting SA in a complex sample using a biotin-based sensor were also investigated. The hybridization efficiency (%HE) and mismatch discrimination (%MD) for DNA detection were evaluated for the PNA-based sensor.

## EXPERIMENTAL SECTION

**Materials.** MPC was purchased from the NOF Corp. (Japan). Methacrylic acid (MA), 4,4′-azobis(4-cyanovaleric acid) (ACVA), 4-cyano-4-(phenylcarbonothioylthio)pentanoic acid (CPADB), azide-$PEG_3$-biotin conjugate (biotin-$N_3$), copper(I) acetate, bovine serum albumin (BSA), and LYZ were purchased from Aldrich. MA was distilled under reduced pressure to remove monomethyl ether hydroquinone, a polymerization inhibitor, prior to use. Phosphate-buffered saline (PBS; pH 7.4) was purchased from Sigma. Hydrazine monohydrate and *N,N*′-diisopropylethylamine (DIEA) were purchased from Sigma-Aldrich. SA was purchased from Thermo Fisher Scientific Inc. PgMA was synthesized using the method reported He et al.[45] DNA was purchased from the Pacific Science Co., Ltd. PNA was synthesized by solid-phase peptide synthesis on Tentagel S RAM resin (Fluka) preloaded with 9-fluorenylmethoxycarbonyl-L-lysine(*tert*-butoxycarbonyl)-pentafluorophenyl (Fmoc-L-Lys(Boc)-oPfp) (CalbiochemNovabiochem Co., Ltd.) using a previously reported procedure.[46] The PNA was modified at the N-terminus by reductive alkylation with $N_3(CH_2)_3CHO$ to prepare azide-terminated PNA (PNA-$N_3$).[47] After

cleavage of PNA-$N_3$ from the solid support using trifluoroacetic acid, the crude PNA-$N_3$ was purified using reverse-phase HPLC and analyzed by matrix assisted laser desorption/ionization-time of flight (MALDI-TOF) mass spectrometry (Bruker Daltonik GmbH, Germany) (see **Figure 3.1** for chromatogram and mass spectra). Ethylenediaminetetraacetic acid (EDTA) was purchased from Fluka. Human platelet-poor plasma was donated by a healthy volunteer. Milli-Q water was purified using an ultrapure water system with a Millipak-40 filter unit (0.22 μm, Millipore) and a Millipore Milli-Q system that involved reverse osmosis followed by ion exchange and filtration steps (18.2 MΩ). All reagents and materials were analytical grade and used without further purification unless specified.

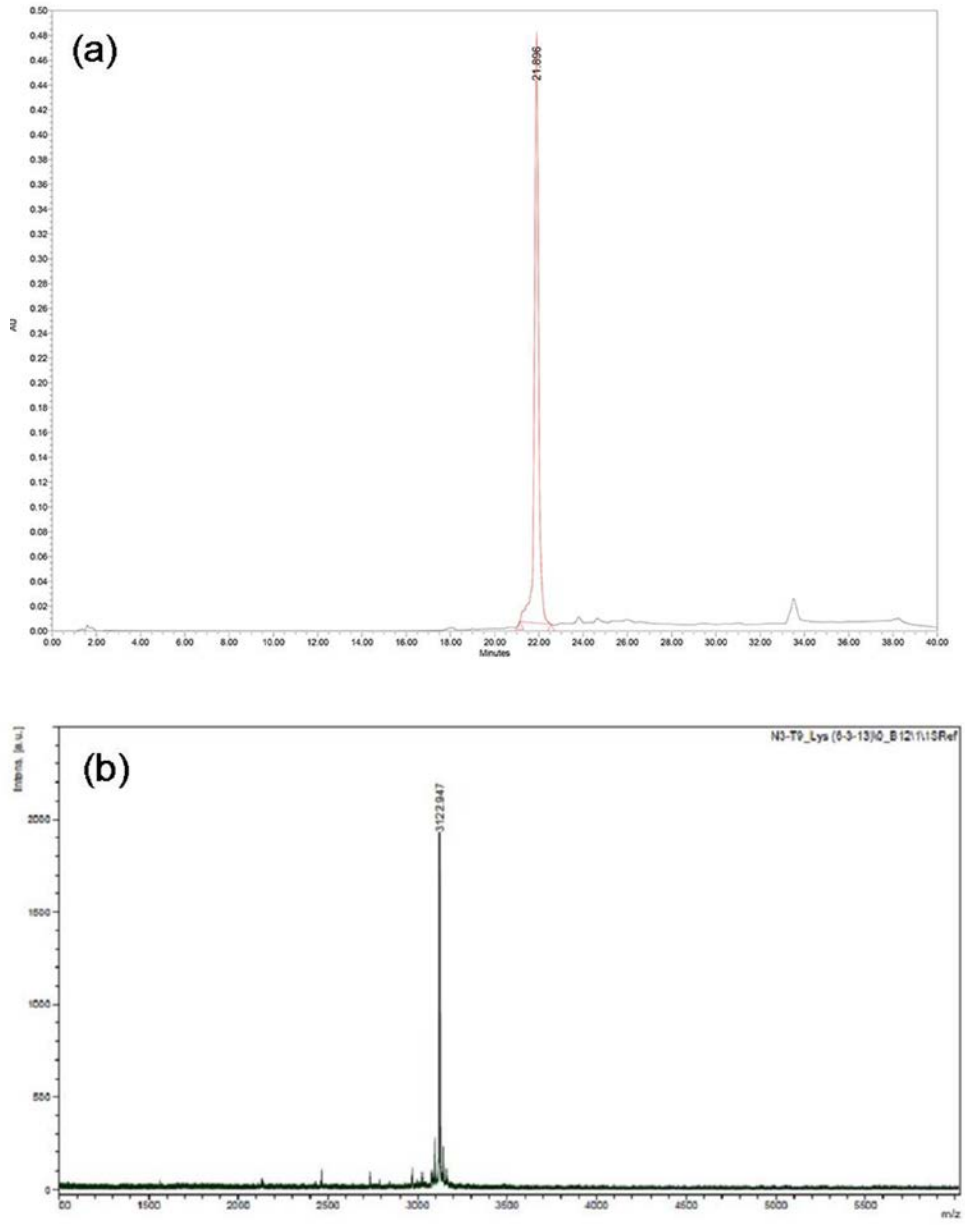


**Figure 3.1** (a) HPLC chromatogram (260 nm) and (b) MALDI-TOF mass spectrum of PNA-$N_3$ ($N_3$-TTT TTT TTT-Lys$NH_2$).

**Synthesis of Thiol-terminated Poly[(propargyl methacrylate)-*ran*-(2-methacryloyloxyethyl phosphorylcholine)] (PPgMAMPC-SH).** MPC monomer (0.59 g, 2.0 mmol), ACVA (0.7 mg, 2.5 μmol), and CPADB (5.6 mg, 20 μmol) were dissolved in 2 mL of an EtOH:THF (1:1 v/v) mixture. PgMA (0.25 mL, 2.0 mmol) was added to the solution under magnetic stirring. The clear pink solution was purged with nitrogen gas for

30 min and then immersed in an oil bath at 70°C and polymerization was performed for a set reaction time. The reaction was terminated in an ice bath. The resulting PPgMAMPC was purified, using a dialysis membrane (molecular weight cut-off = 3500 g/mol), against EtOH for 2 d, and then against deionized water for 2 d. An orange cotton-like material was obtained after lyophilization. The copolymer composition was varied by varying the molar ratio of PgMA to MPC in the feed. PPgMAMPC was characterized using $^1$H NMR and FTIR spectroscopies. The molar percentage contents of PgMA and MPC units in the copolymer ($PPgMA_mMPC_n$) were denoted by *m* and *n*, respectively.

$^1$H NMR (400 MHz, $CD_3OD$) $\delta$ (ppm): characteristic peaks of PgMA unit (–C≡C*H* 3.10, –O–C$H_2$–C≡CH 4.55–4.80), MPC unit [(–N(C$H_3$)$_3$ 3.25, –N–C$H_2$CH$_2$–O– 3.75 ppm, –POC$H_2$CH$_2$N–, –COOC$H_2$, –C$H_2$OP 4.0–4.4], and aromatic protons (–$C_6H_5$ 7.40–7.95).

PPgMAMPC-SH was prepared by aminolysis of the dithioester groups at the chain ends of the copolymer with hydrazine monohydrate (**Scheme 3.1a**).[48] PPgMAMPC (0.2 g) was dissolved in EtOH (3 mL) for $PPgMA_{38}MPC_{62}$-SH and $PPgMA_{45}MPC_{55}$-SH, or a mixture of EtOH and THF (7:3 v/v) for $PPgMA_{65}MPC_{35}$-SH, until the solution was clear. Hydrazine monohydrate (30 mol equiv with respect to dithioester groups) was added to the copolymer solution under magnetic stirring. When addition was complete, the solution was stirred for 2 h at ambient temperature and then added dropwise to aqueous 1.0 M HCl (10 mL) and stirred for 1 h. The obtained PPgMAMPC-SH was purified using a dialysis membrane (molecular weight cut-off = 3500 g/mol) against aqueous HCl, pH 3–4, for 2 d, and then against deionized water for 2 d. A white cotton-like product was obtained after lyophilization. The copolymer was characterized using $^1$H NMR, FTIR, and UV-vis spectroscopies.

**Immobilization of PPgMAMPC-SH on Gold-Coated SPR Chip.** A gold-coated SPR chip was cleaned with air plasma in a plasma cleaner (Harrick Plasma PDC-32G, Power 18 W) for 5 min, washed with Milli-Q water for 5 min, and dried under a nitrogen stream. The cleaned SPR sensor chip was immersed in 3 mL of a 0.1 mM copolymer solution [$PPgMA_{38}MPC_{62}$-SH and $PPgMA_{45}MPC_{55}$-SH in EtOH, $PPgMA_{65}MPC_{35}$-SH in EtOH/THF (7:3 v/v)] at ambient temperature for 48 h. The modified SPR chip was removed from the solution and rinsed five times by constant agitation, for 5 min each time, in EtOH for Au-

$PPgMA_{38}MPC_{62}$ and Au-$PPgMA_{45}MPC_{55}$, and in EtOH/THF (7:3 v/v) for Au-$PPgMA_{65}MPC_{35}$. The SPR sensor chip with the immobilized copolymer was dried under a nitrogen stream and characterized using contact angle and SPR measurements and attenuated total reflection (ATR)-FTIR spectroscopy.

**Characterization.** Dynamic advancing ($\theta_A$) water contact angles were measured using a contact angle goniometer equipped with a Gilmont syringe and a 24-gauge flat-tipped needle (Rame-Hart, model 200-F1). All measurements were performed in air at ambient temperature. Data for each sample were collected from five different areas of the substrate and analyzed using DROPimage standard 2.0 software. The characteristic functional groups of the copolymer brushes on the SPR sensor chip were characterized using ATR-FTIR spectroscopy (Nicolet 6700 FTIR spectrometer). Spectra were recorded in the IR region (4000−650 $cm^{-1}$) based on 32 scans, at a spectral resolution of 4 $cm^{-1}$. $^1H$ NMR spectra were recorded in $CD_3OD$ using a Varian NMR spectrometer (Mercury-400; USA) operated at 400 MHz. The disappearance of the dithioester groups of the copolymer was monitored using UV-vis spectroscopy (CARY 100Bio UV-visible spectrophotometer, Varian Inc., Palo Alto, CA, USA). Gel permeation chromatography (GPC) was performed using a refractive index detector equipped with a Shodex Asahipak GF-1G guard column and a 7.0 μm bead GF-7M HQ column (exclusion limit ~$10^7$) at 40 °C and a flow rate of 0.6 mL/min. A phosphate buffer (pH 9) containing 10 vol% acetonitrile was used as the eluent. The $M_n$ and $M_w/M_n$ values were calibrated with standard sodium poly(styrene sulfonate) samples. The elemental composition on a selected SPR chip with an immobilized copolymer was determined by X-ray photoelectron spectroscopy (XPS; AXIS Ultra DLD, Kratos Analytical Ltd., Manchester, UK) using an Al Kα X-ray source. All XPS data were collected at a take-off angle of 90°. Atomic force microscopy (AFM) images were obtained using a scanning probe microscope (NanoScope®IV, Veeco, Plainview, NY, USA). Measurements were performed in air in tapping mode with a silicon nitride tip at a resonance frequency of 267–295 kHz and a spring constant of 20–80 N/m. The thickness of the polymer brushes was measured using a spectroscopic ellipsometer (J. A. Woollam Co., Lincoln, NE, USA) at an incident angle of 70–80° in steps of 5°. The calculation was performed based on a Cauchy layer model with assumed refractive index of 1.34±0.09 for gold-coated substrate at 632.8 nm.

**SPR Measurements.** SPR measurements were performed using a double-channel AutoLab ESPR instrument (Eco Chemie, Utrecht, The Netherlands) at 25 °C, with the plane face of the prism coupled to the gold-coated glass via an index-matching fluid. The instrument uses a laser diode at a wavelength of 670 nm and a vibrating mirror to modulate the angle of incidence of the p-polarized light beam on the SPR substrate. An autosampler was used to inject the test solution and the SPR angle shift measurements were performed under non-flow liquid conditions. The SPR angle shift at the end-point of each step and after baseline subtraction (angle shift) was used to calculate the density of molecules bound to the surface or the target density, using a sensitivity factor of 120 mDegree, equal to 100 ng/cm$^2$. This sensitivity factor is specifically calibrated for the AutoLab ESPR, which uses an N-BK 7 prism refractive index of 1.518, and incident light wavelength of 670 nm. Each gold-coated SPR chip bearing PPgMAMPC was first seated in an SPR cell before being stabilized with a running solution of 10 mM PBS (pH 7.4). When the equilibrium SPR angle frequency in the buffer solution was obtained, the substrate was ready to be used.

**Probe Conjugation on Copolymer-Modified SPR Chip by CuAAC Reaction.** For conjugation of biotin-$N_3$ (**Scheme 3.1b**), Cu(I) acetate (1.23 mg, 0.01 mmol) and biotin-$N_3$ (0.5 M, 4.0 μL, 2.0 μmol) were dissolved in 10 mM PBS (pH 7.4, 2 mL) for 10 min to obtain a final biotin-$N_3$ concentration of 1.0 mM. The PPgMAMPC-modified SPR chip was immersed in the mixture, with constant agitation for 5 min. DIEA (1.71 μL, 0.01 mmol) was added to the reaction mixture and the SPR chip was immersed in the mixture for 24 h under constant agitation at ambient temperature. The modified SPR chip was removed from the solution and then rinsed by constant agitation in 10 mM EDTA for 1 min and 10 mM PBS (pH 7.4) five times for 5 min each. The azide-containing PNA (PNA-$N_3$) probe was immobilized on the PPgMAMPC-modified SPR chip (**Scheme 3.1c**) by dissolving Cu(I) acetate (0.1 mg, 8.2 μmol) and PNA-$N_3$ (10 nmol) in methanol (2 mL) for 10 min to obtain a final PNA-$N_3$ concentration of 5.0 μM. The modified SPR chip was immersed in the solution with constant agitation for 5 min. A solution of DIEA (50 μM, 1.0 mL) was added to the reaction mixture and then the SPR chip was immersed in this mixture for 24 h under constant agitation at ambient temperature. The modified SPR chip was removed from the solution and rinsed by constant agitation in 10 mM EDTA for 1 min and in methanol five

times for 5 min each. The SPR sensor chip was dried under a nitrogen stream and characterized using contact angle and SPR measurements and ATR-FTIR spectroscopy.

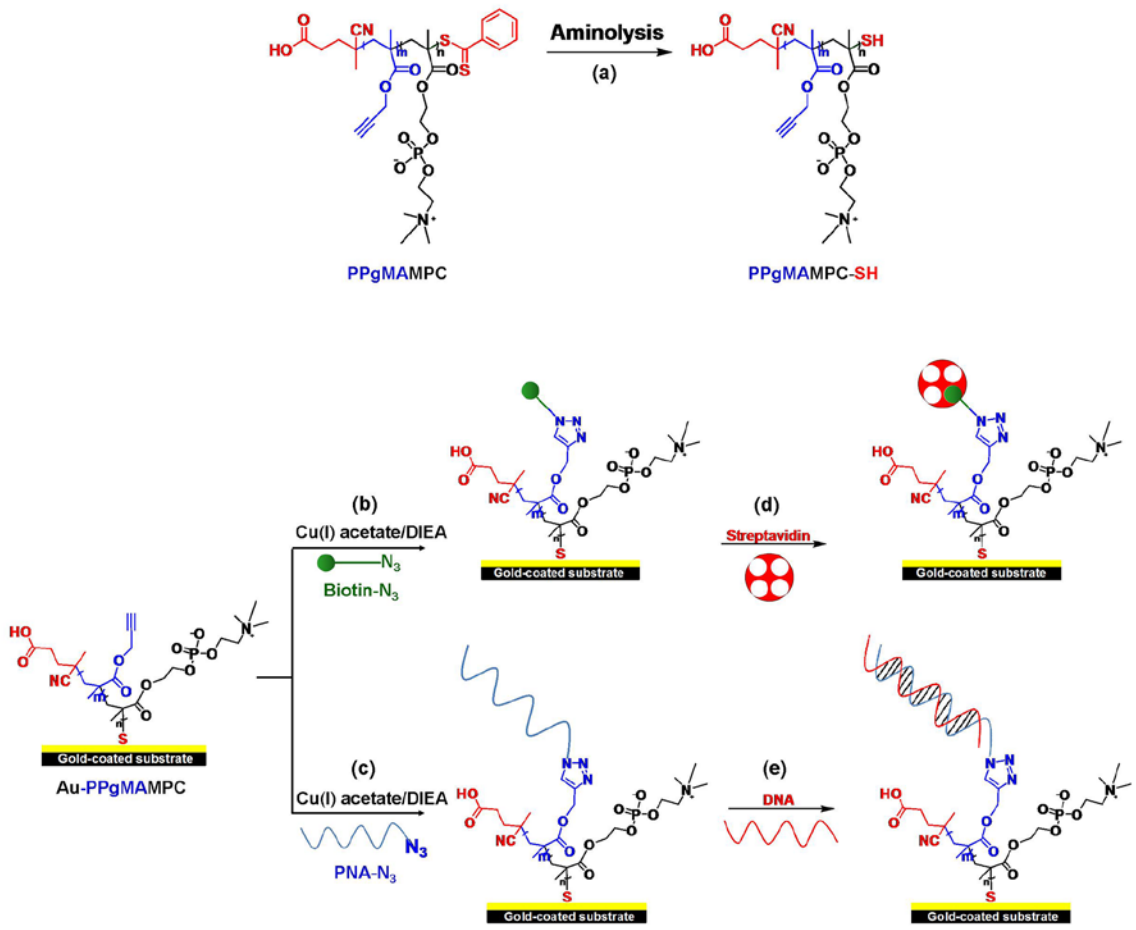


**Scheme 3.1** Schematic Diagram of (a) Preparation of PPgMAMPC-SH, (b, c) Immobilization of Biotin-$N_3$ and PNA-$N_3$ on PPgMAMPC-Modified SPR Chip, and (d, e) Specific Binding between Conjugated Probe and Target Molecule

**Specific Interactions between Conjugated Probes and Target Molecules.** A PPgMAMPC-modified SPR chip conjugated with the desired probe was seated in an SPR cell and then rinsed with a running solution of 10 mM PBS buffer (pH 7.4). Once the baseline SPR response was stable, the target molecule was applied to the chip. In the case of the PPgMAMPC-modified SPR chip conjugated with biotin-$N_3$ (**Scheme 3.1d**), SA (0.1

mg/mL, equivalent to 1.9 μM) in blood plasma solution (0.1 mg/mL, 0.14% in PBS buffer) was applied to the surface and left for 15 min. Unbound SA was removed by washing with 10 mM PBS buffer (pH 7.4) for 5 min. The specific binding of SA was quantified from the shift in the SPR response angle at the end-point of the washing step and after baseline subtraction. Non-specific binding (binding in the absence of SA in blood plasma solution) was also determined to quantify the specific binding of SA in blood plasma in terms of the *S*/*N* ratio; this ratio was calculated using the following equation:

$$S/N = \frac{\text{SPR angle shift after exposure to blood plasma with streptavidin}}{\text{SPR angle shift after exposure to blood plasma without streptavidin}} \quad \text{(eq.3.1)}$$

For the PPgMAMPC-modified SPR chip conjugated with a PNA-$N_3$ probe (**Scheme 3.1e**), DNA (50 μM) in 10 mM PBS (pH 7.4) containing 100 mM NaCl was applied to the surface and left for 15 min. Unbound DNA was removed by washing with PBS for 5 min. The specific binding of DNA was quantified from the shift in the SPR response angle at the end-point of the washing step and after baseline subtraction. The sensor was regenerated by washing with 50 mM NaOH for 5 min. The %HE and %MD were calculated using the following equations:

$$\%HE = \frac{\text{target density}}{\text{probe density}} \times 100 \quad \text{(eq.3.2)}$$

$$\%MD = \frac{\%HE \text{ of complementary DNA} - \%HE \text{ of mismatched DNA}}{\%HE \text{ of complementary DNA}} \times 100 \quad \text{(eq.3.3)}$$

## RESULTS AND DISCUSSION

**Synthesis and Characterization of Thiol-Terminated Poly[(propargyl methacrylate)-*ran*-(2-methacryloyloxyethyl phosphorylcholine)] (PPgMAMPC-SH).** A PPgMAMPC copolymer was synthesized via RAFT polymerization using CPADB and ACVA as the chain transfer agent (CTA) and radical initiator (In), respectively. The molar percentage contents of PgMA and MPC units in the copolymer ($PPgMA_mMPC_n$) are denoted by *m* and *n*, respectively. Our survey suggested that the optimum [CTA]/[In] ratio for obtaining a

copolymer with a well-controlled molecular weight was 8; the data are shown in **Table 3.1**. The control over the copolymerization process was also demonstrated for a targeted degree of polymerization (DP) of 200 based on the linear first-order relationship between $\ln[M]_0/[M]$ and the polymerization time (**Figure 3.2**), suggesting that the polymeric radical concentration remained unaltered throughout the polymerization. $^1$H NMR spectroscopy (**Figure 3.3**) showed that the copolymer composition varied as a function of the monomer ratio in the feed (**Table 3.2**). The molecular weight of the copolymer was close to the target (35,375–46,327 kDa). We also attempted to determine the molecular weight and polydispersity indices (PDIs) of the copolymers using GPC. The data are shown in **Figure 3.4**. It should be emphasized that it is not possible to dissolve the copolymers in a common polar protic solvent (such as methanol) generally used for GPC analysis of MPC-based copolymers. And it was rather difficult to dissolve them in the mobile phase used for GPC analysis, phosphate buffer (pH 9) containing 10 vol% acetonitrile, especially the copolymer having high PgMA composition, $PPgMA_{65}MPC_{35}$, of which molecular weight information cannot be obtained. The fact that the $\overline{M}_n$ determined by GPC analysis are underestimated and proportionally decreased as a function of PgMA content suggested that the molecular weight information obtained via GPC analysis is somewhat not reliable. Besides, PDI values were high which may be ascribed to possible copolymer self-assembly in the phosphate buffer solution. This is why $^1$H NMR spectroscopy was used as the main tool for determining the molecular weight of the copolymer. Despite the relatively high PDI, the unimodal distribution evidenced from GPC chromatograms (also shown in **Figure 3.4**) is reasonable evidence of copolymer formation. The functional groups in the synthesized copolymer were identified using FTIR spectroscopy (**Figure 3.5)**. The characteristic peaks for C=O (ester) stretching, at 1725 $cm^{-1}$, asymmetric O=P-O- stretching, at 1240 $cm^{-1}$, symmetric O=P-O stretching, at 1087 $cm^{-1}$, and $-N^+(CH_3)_3$, at 960 $cm^{-1}$ for the MPC units were observed; a –C≡C– stretching peak was observed at 2127 $cm^{-1}$, and its intensity increased proportionally with the PgMA content. These results confirm copolymer formation.

**Table 3.1** Effect of [CTA]/[In] on molecular weight of PPgMAMPC synthesized by RAFT polymerization for 24 h using PgMA:MPC molar ratio of 20:80 and targeted DP of 100

| Monomer composition in feed (%) | | Monomer composition in copolymer (%)[a] | | [CTA]/[In] | Target $\overline{M}_n$ (kDa) | $\overline{M}_n$ [a] (kDa) |
|---|---|---|---|---|---|---|
| PgMA | MPC | PgMA | MPC | | | |
| 20 | 80 | 15 | 85 | 4 | 26.3 | 66.8 |
| 20 | 80 | 15 | 85 | 8 | 26.3 | 20.1 |

[a]Calculated from $^1$H NMR data

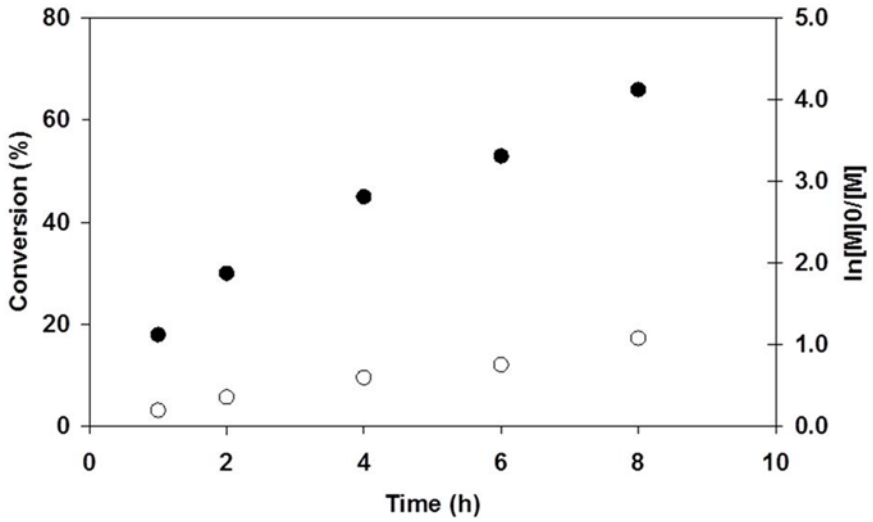


**Figure 3.2** Percentage of MPC conversion (●) and corresponding semi-logarithmic plot (○) as function of time for $PPgMA_{45}MPC_{55}$ with targeted DP of 200.

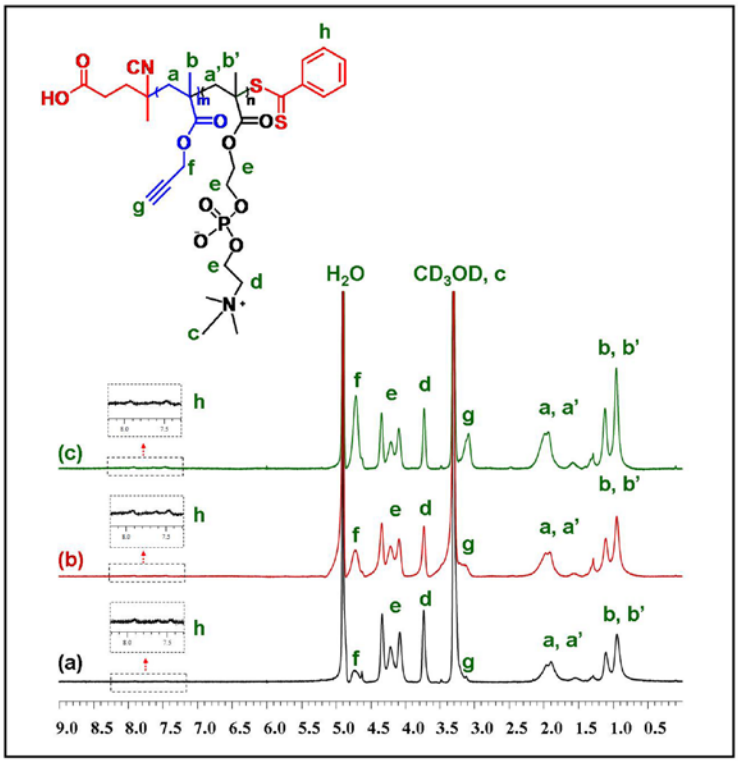


**Figure 3.3** $^{1}$H NMR spectra ($CD_3OD$) of (a) $PPgMA_{38}MPC_{62}$ (40.0 kDa), (b) $PPgMA_{45}MPC_{55}$ (46.7 kDa), and (c) $PPgMA_{65}MPC_{35}$ (38.4 kDa).

**Table 3.2** Copolymer Compositions and Molecular Weights of PPgMAMPC (Target DP 200) Synthesized by RAFT Polymerization

| Monomer composition in feed (mol%) | | Monomer composition in copolymer (mol%)[a] | | $\overline{M}_n$[a] (kDa) | DP[a] | Copolymer abbreviation |
|---|---|---|---|---|---|---|
| PgMA | MPC | PgMA | MPC | | | |
| 70 | 30 | 65 | 35 | 38.4 | 208 | $PPgMA_{65}MPC_{35}$ |
| 50 | 50 | 45 | 55 | 46.7 | 213 | $PPgMA_{45}MPC_{55}$ |
| 30 | 70 | 38 | 62 | 40.0 | 173 | $PPgMA_{38}MPC_{62}$ |

[a] Calculated from $^{1}$H NMR data

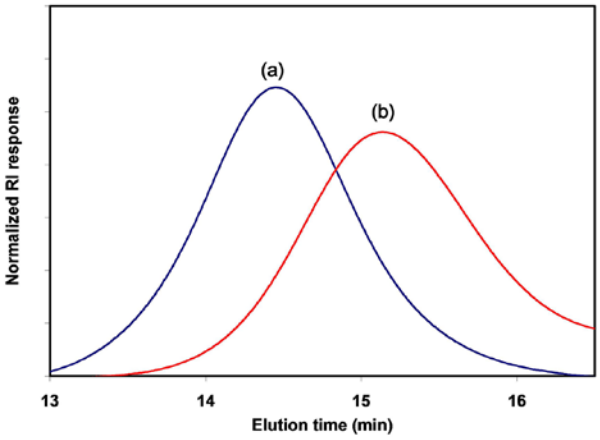


| Copolymer | $\overline{M}_n$ | PDI ($M_w/M_n$) |
|---|---|---|
| (a) $PPgMA_{38}MPC_{62}$ | 13,849 | 1.524 |
| (b) $PPgMA_{45}MPC_{55}$ | 6,048 | 1.520 |

**Figure 3.4** GPC chromatogram (top) and molecular weight and polydispersity index (PDI) (table below) determined by GPC of (a) $PPgMA_{38}MPC_{62}$ (40.0 kDa) and (b) $PPgMA_{45}MPC_{55}$ (46.7 kDa).

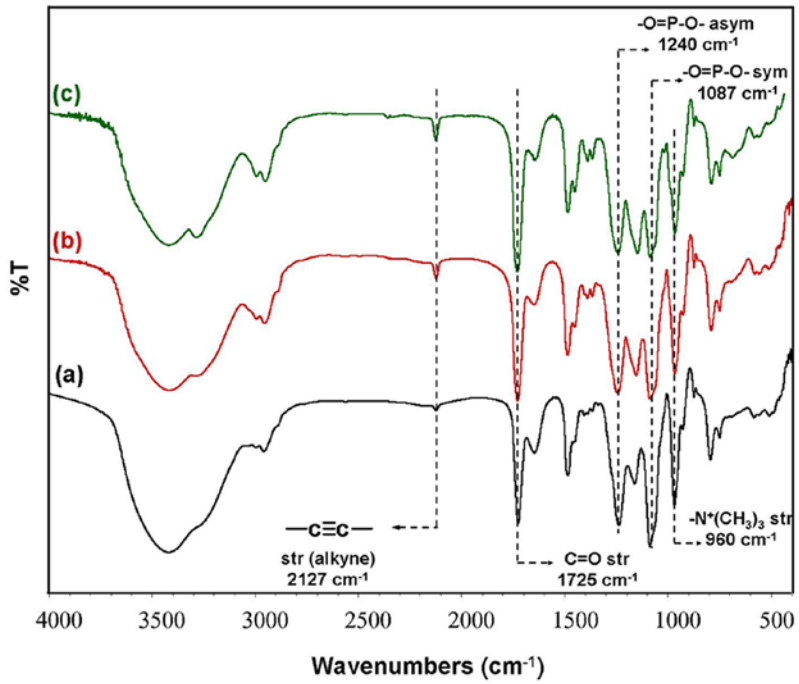


**Figure 3.5** FTIR spectra of (a) $PPgMA_{38}MPC_{62}$ (40.0 kDa), (b) $PPgMA_{45}MPC_{55}$ (46.7 kDa), and (c) $PPgMA_{65}MPC_{35}$ (38.4 kDa).

Aminolysis with hydrazine transformed the dithiobenzoate groups at the chain ends of the PPgMAMPC copolymer into thiol groups, yielding PPgMAMPC-SH,[48] as shown by the disappearance after aminolysis of the aromatic proton signals at 7.40–7.95 ppm in the $^1$H NMR spectrum and the UV-vis absorption peak at 305 nm (**Figure 3.6**).

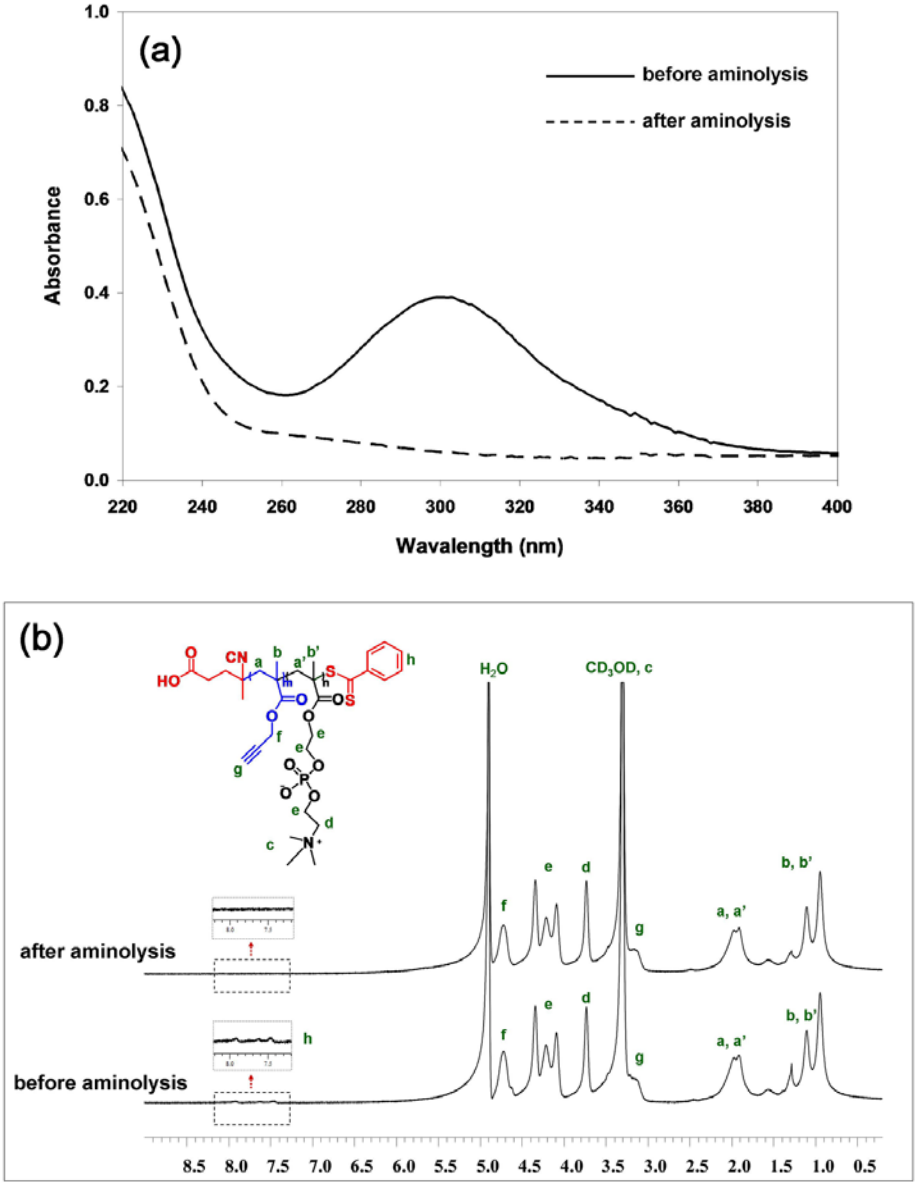


**Figure 3.6** (a) UV-vis absorption spectra and (b) $^1$H NMR spectra of $PgMA_{65}MPC_{35}$ (38.4 kDa) before and after aminolysis.

**Immobilization of PPgMAMPC-SH on Gold-Coated SPR Chip.** Unlike $PPgMA_{38}MPC_{62}$-SH and $PPgMA_{45}MPC_{55}$-SH, $PPgMA_{65}MPC_{35}$-SH, which has a higher content of the more hydrophobic PgMA unit, is not soluble in EtOH but dissolves in a mixture of EtOH and THF (7:3 v/v). Au–S bond formation between the gold layer of the SPR chip and the thiol-terminated copolymer (PPgMAMPC-SH**)** via a "grafting to" approach was performed at ambient temperature for 48 h. The presence of PPgMAMPC brushes on the SPR chip was confirmed using water contact angle measurements, and SPR, ATR-FTIR, and XPS analyses. The data in **Table 3.3** show that the advancing ($\theta_A$) water contact angle of the SPR chip decreased from 71.9 $\pm$ 1.3° to 44.6 $\pm$ 0.9° and 46.6 $\pm$ 3.5° upon immobilization of $PPgMA_{38}MPC_{62}$-SH and $PPgMA_{45}MPC_{55}$-SH, respectively, indicating their highly hydrophilic characters. The copolymer with the highest content of hydrophobic PgMA, i.e., $PPgMA_{65}MPC_{35}$-SH, yielded a gold surface with a contact angle (87.9 $\pm$ 4.2°) higher than that of the pristine gold surface. Chemisorption of the copolymer brushes on the gold-coated SPR chip was monitored using an SPR technique. The SPR angle shift upon PPgMAMPC-SH immobilization was used to calculate the amount of copolymer bound to the surface, using a sensitivity factor of 120 mDegree, which is equivalent to 100 ng/cm$^2$ (**Table 3.3**).[49, 50]

**Table 3.3** Water Contact Angle and SPR Data for Gold-Coated SPR Chips after PPgMAMPC-SH Immobilization and Subsequent Conjugation with Biotin-$N_3$

| Sample | Advancing water contact angle ($^{\circ}$) | SPR data | |
|---|---|---|---|
| | | Angle shift (mDegree) | Amount adsorbed for each modification step (ng/cm$^2$) |
| Au | 71.9 ± 1.3 | - | - |
| Au-PPgMA$_{38}$MPC$_{62}$ | 44.6 ± 0.9 | 1024.8 ± 81.8 | 854.0 ± 68.1 |
| Au-PPgMA$_{45}$MPC$_{55}$ | 46.6 ± 3.5 | 882.1 ± 166.6 | 735.0 ± 138.9 |
| Au-PPgMA$_{65}$MPC$_{35}$ | 87.9 ± 4.2 | 1323.1 ± 56.1 | 1102.0 ± 46.8 |
| Au-PPgMA$_{38}$MPC$_{62}$-biotin | 32.7 ± 2.7 | 15.2 ± 7.4 | 12.7 ± 6.1 |
| Au-PPgMA$_{45}$MPC$_{55}$-biotin | 41.6 ± 1.3 | 229.5 ± 50.4 | 191.2 ± 42.0 |
| Au-PPgMA$_{65}$MPC$_{35}$-biotin | 62.2 ± 1.7 | 209.5 ± 6.7 | 174.5 ± 5.6 |

**Figures 3.7** shows the XPS atomic spectra of the gold-coated substrate with immobilized PPgMA$_{45}$MPC$_{55}$-SH and the substrate before immobilization (bare gold). At a take-off angle of 90°, phosphorus ($P_{2p}$) and nitrogen ($N_{1s}$) signals attributed to the phosphorylcholine group of the MPC units were observed on the substrate, indicating that the copolymer is bound to the gold-coated substrate. The $S_{2p}$ signal of the bound thiol, at a binding energy of 163 eV, was also detected, implying that the copolymer was strongly adsorbed on the substrate by interactions between the thiol groups of the copolymer and the gold surface. The characteristic absorption peaks of the MPC unit, i.e., C=O stretching (ester) at 1725 cm$^{-1}$, O=P-O-$_{asym}$ stretching at 1264 cm$^{-1}$, O=P-O-$_{sym}$ stretching at 1091 cm$^{-1}$, and -N$^{+}$(CH$_3$)$_3$ stretching at 968 cm$^{-1}$, were observed in the ATR-FTIR spectra (**Figure 3.8**), but the characteristic absorption peak of the PgMA unit, i.e., –C≡C– stretching at 2127 cm$^{-1}$, was not clearly observed because of overlap with the characteristic peak of diamond (in the region 1500–2650 cm$^{-1}$), which is the reflectance material used for

ATR-FTIR measurements. This signal from diamond dominates the other signals, particularly when the adsorbed material to be characterized is very thin, 1.89–3.12 nm in our case (estimated by ellipsometry).

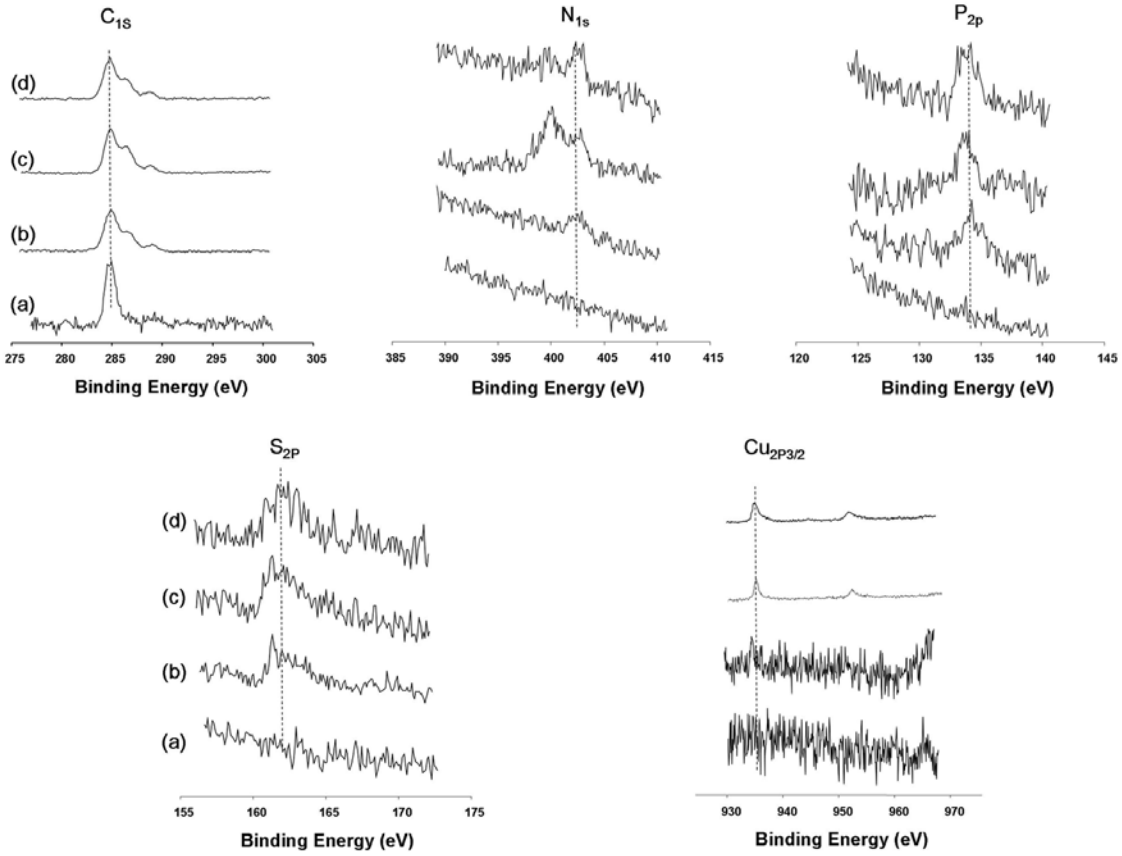


**Figure 3.7** XPS atomic spectra of gold-coated substrate (a) before and (b) after adsorption of $PPgMA_{45}MPC_{55}$-SH and $PPgMA_{45}MPC_{55}$-SH platform after (c) biotin immobilization and (d) PNA immobilization.

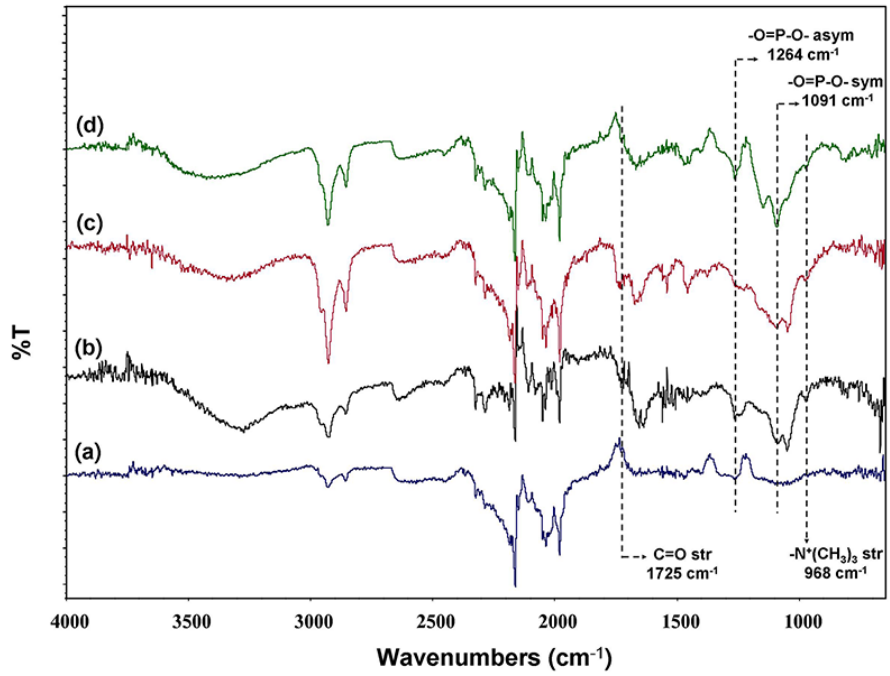


**Figure 3.8** ATR-FTIR spectra of gold-coated SPR chips (a) before immobilization, and after immobilization of (b) $PPgMA_{38}MPC_{62}$-SH (40.0 kDa), (c) $PPgMA_{45}MPC_{55}$-SH (46.7 kDa), and (d) $PPgMA_{65}MPC_{35}$-SH (38.4 kDa).

Surface grafting of PPgMAMPC brushes on the gold-coated substrate was confirmed using AFM. The surface roughness before and after grafting with PPgMAMPC brushes were similar (1.5 vs 1.3 nm), suggesting that the gold surface was smooth and homogeneously covered with the copolymer. The thicknesses ($t$), measured using ellipsometry, of $PPgMA_{38}MPC_{62}$, $PPgMA_{45}MPC_{55}$, and $PPgMA_{65}MPC_{35}$ were 1.89 ± 0.12, 2.66 ± 0.26, and 3.12 ± 0.19 nm, respectively. The thickness can be used to calculate the graft density ($\sigma$) as follows:

$$\sigma = \frac{t\rho N_A}{Mn} \qquad \text{(eq.3.4)}$$

where $\rho$ is the mass density (1.1 g/cm$^3$ for $PPgMA_{65}MPC_{35}$ and 1.2 g/cm$^3$ for $PPgMA_{45}MPC_{55}$ and $PPgMA_{38}MPC_{62}$), $\overline{M}_n$ is the molecular weight of the free polymer, and $N_A$ is Avogadro's number. The copolymer mass densities were estimated proportionally

using $\rho_{PMPC}$ = 1.3 g/cm$^3$ [38] and $\rho_{PPgMA}$ = 1.085 g/cm$^3$, on the assumption that they are equal to that of poly(propyl methacrylate),[51] which has the same number of carbon atoms. For the copolymer synthesized with $\overline{M}_n$ in the range 38.4–46.7 kDa (DP 173–213), the calculated graft densities of surface-grafted $PPgMA_{38}MPC_{62}$, $PPgMA_{45}MPC_{55}$, and $PPgMA_{65}MPC_{35}$ were 0.04, 0.04, and 0.05 chain/nm$^2$, respectively. These values are below 0.08 chains/nm$^2$,[52] which suggests that the PPgMAMPC brushes can be categorized as being in the "mushroom regime."

**Biotin Conjugation on Copolymer-Modified SPR Chip by CuAAC Reaction and Subsequent Binding with Streptavidin.** Biotin was used as the first sensing probe model. It has a high binding affinity with SA (dissociation constant $K_D \approx 10^{-4}$ M).[53] Biotin-$N_3$ was immobilized on the PPgMAMPC-modified SPR chip outside the SPR instrument by CuAAC.[54, 55] The data in **Table 3.3** show that the water contact angles of the PPgMAMPC-modified SPR chip decreased after biotin attachment, indicating that the hydrophobic alkyne moieties from the PgMA repeat units were consumed and bound with biotin with three repeat units of the hydrophilic PEG spacer. The amounts of immobilized biotin increased significantly, from 12.7 $\pm$ 6.1 to 191.2 ± 42.0 ng/cm$^2$, when the PgMA content of the copolymer was increased from 38% to 45%. However, further increasing the PgMA composition to 65% reduced the quantity of bound probe, implying that biotin may have limited access to the alkyne moieties of copolymers with high PgMA contents, in which the swellability would be suppressed because of the inherent hydrophobicity. This is confirmed by the water contact angle (87.9 $\pm$ 4.2°) being much higher than those of the PPgMAMPC-modified SPR chips with PgMA contents of 38% and 45% (44.6 $\pm$ 0.9° and 46.6 $\pm$ 3.5°, respectively). As shown in Figure S6 in supporting information, similar characteristic atomic spectra of the PPgMAMPC-modified SPR chips were observed after biotin and PNA immobilization but with much better signal especially for $N_{1s}$, $S_{2p}$, $P_{2p}$ peaks in comparison with those before probe immobilization. A Cu peak appears in the Au-PPgMAMPC spectra after probe immobilization (both biotin and PNA), suggesting that Cu remained after the click reaction, although the surface was thoroughly rinsed with 10 mM EDTA and 10 mM PBS (pH 7.4). However, we believe that the Cu contamination should not affect the target molecule detection efficiency.

Non-specific adsorption of the biotin-modified PPgMAMPC copolymer platform with different copolymer compositions on gold-coated SPR chips was investigated by comparison of adsorption of non-targeted proteins, bovine serum albumin (BSA; 69 kDa, pI = 4.8), LYZ (14 kDa, pI = 12), and 0.14% blood plasma (equivalent to 0.1 mg/mL of protein in PBS buffer, pH 7.4) with that of a targeted analyte, SA (60 kDa, pI = 5). BSA and LYZ were selected as model proteins with negative and positive charges, respectively, at pH 7.4 in PBS. Blood plasma is a complex biological-mimic medium comprising about 7% (70 mg of proteins per milliliter of plasma) of different proteins, e.g., fibrinogen, albumin, and globulin, and other components such as water, inorganic ions, and organic compounds.[56] As anticipated, the biotin-conjugated PPgMAMPC platform was specifically bound to the targeted SA (**Figure 3.9**). The bound content of SA increased with increasing PgMA content in the copolymer and increasing biotin content (**Table 3.3**). Non-specific adsorption of the non-targeted proteins (BSA, LYZ, 0.14% blood plasma) was greatly suppressed on the biotin-conjugated PPgMAMPC platform compared with that on the bare gold surface. These results indicate that the MPC units in the PPgMAMPC copolymer are of paramount importance in suppressing non-specific protein adsorption. This agrees well with reported studies of other MPC–containing (co)polymers.[14, 34, 37, 57] Although the copolymer platform with the highest PgMA content, i.e., 65%, had the greatest bound SA content, it also gave the highest non-specific adsorption of blood plasma.

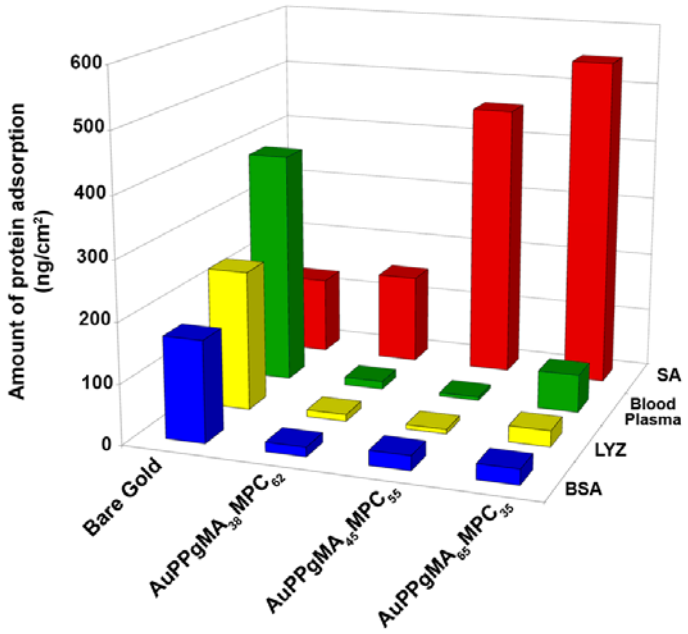


**Figure 3.9** Protein adsorption on biotin-conjugated PPgMAMPC platforms with various copolymer compositions.

In principle, the biotin/SA binding ratio should be four if all biotin molecules can be bound to SA. However, the biotin/SA binding ratios, listed in **Figure 3.10**, were much higher than the theoretical values, indicating that not all of the conjugated biotin molecules were bound to SA. The biotin/SA binding ratios were extremely high for the Au-PPgMAMPC platforms with high contents of hydrophobic PPgMA (45% and 65%). This may be because of the limited accessibility of SA, which is a large protein (MW = 60 kDa), to the immobilized biotin embedded inside the inner layer of the polymer brushes. Au-$PPgMA_{38}MPC_{62}$ had the lowest immobilized biotin content, because it had the lowest content of PgMA, which provides active binding sites for biotin immobilization, and because its assembled layer on the gold-coated SPR chip was very thin (1.89 ± 0.12 nm). Although the amount of biotin bound on the Au-$PPgMA_{65}MPC_{35}$ platform (0.78 ± 0.02 nmol/cm$^2$) was lower than that on the $PPgMA_{45}MPC_{55}$ platform (0.85 ± 0.19 nmol/cm$^2$), it had a higher content of bound SA. To verify this contradictory outcome, we performed additional experiments to determine the non-specific adsorption of SA (0.1 mg/mL SA in 10 mM PBS) on Au-$PPgMA_{45}MPC_{55}$ and Au-$PPgMA_{65}MPC_{35}$ before biotin immobilization, using an SPR

technique. The data shown in **Figure 3.11** in the Supporting Information indicate that non-specific adsorption of SA on the Au-PPgMA$_{65}$MPC$_{35}$ platform was approximately three times higher than that on the PPgMA$_{45}$MPC$_{55}$ brushes. This helps to explain why the Au-PPgMA$_{65}$MPC$_{35}$ platform (with the highest PgMA content) bound the most SA, although it bound slightly less biotin than did the Au-PPgMA$_{45}$MPC$_{55}$ platform. SA can bind to the biotin-conjugated Au-PPgMAMPC platform not only by specific interactions with biotin probes but also by non-specific interactions with the PgMA units of the copolymers.

The amount of SA adsorbed on the biotin-modified PPgMAMPC was low, particularly on the Au-PPgMA$_{38}$MPC$_{62}$-biotin platform. The adsorbed quantity of SA, 149.8 ± 12.3 ng/cm$^2$, was less than that in the SA monolayer adsorbed on a mixed monolayer containing 10% thiol-terminated biotin and 90% thiol-terminated ethylene glycol (379.7 ng/cm$^2$), as reported by Su *et al.*[50] This seems reasonable because the amount of biotin immobilized on the Au-PPgMA$_{38}$MPC$_{62}$ platform was lower than the amounts adsorbed on the platforms based on PPgMA$_{45}$MPC$_{55}$ and PPgMA$_{65}$MPC$_{35}$. Nevertheless, the amounts of SA adsorbed on Au-PPgMA$_{45}$MPC$_{55}$-biotin and Au-PPgMA$_{65}$MPC$_{35}$-biotin, i.e., 457.8 ± 28.6 and 549.5 ± 14.8 ng/cm$^2$, respectively, were well above that in the monolayer, suggesting three-dimensional character of the deposited copolymer in binding with the biotin probes.

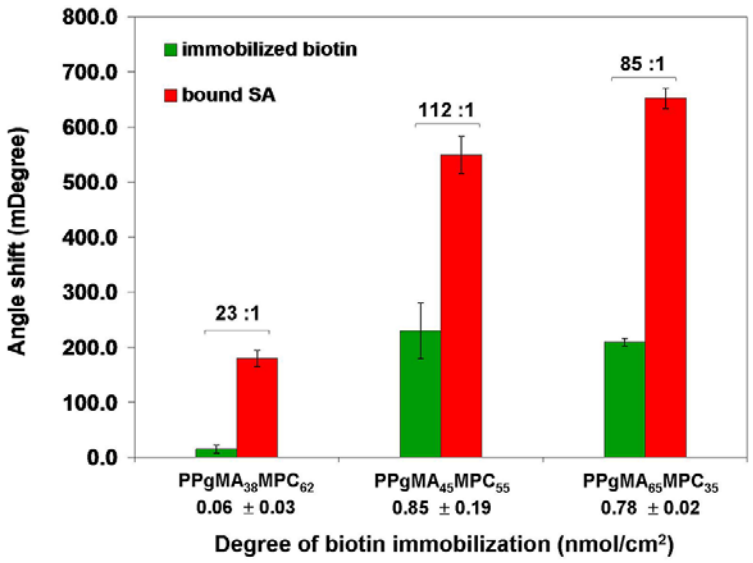


**Figure 3.10** SPR angle shifts corresponding to the amounts of immobilized biotin, and subsequent SA (0.1 mg/mL) binding in PBS solution (10 mM, pH 7.4) on SPR chip modified with PPgMAMPC copolymers of various compositions. Biotin/SA binding ratio is shown on each set of bar charts.

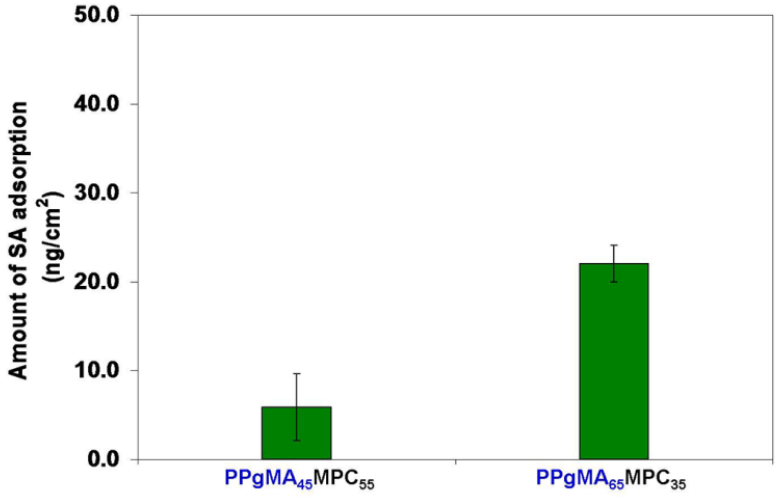


**Figure 3.11** Amounts of SA (0.1 mg/mL in 10 mM PBS) adsorbed on PPgMAMPC platforms with various copolymer compositions.

The biotin-modified PPgMAMPC platforms with different copolymer compositions were further investigated to determine the lowest SA concentration detectable in a complex protein sample (blood plasma). The SA concentration was varied in the range 0.19–190 nM (equivalent to 0.01 to 0.1 mg/mL) in 0.14% blood plasma (0.1 mg/mL). Non-specific binding with 0.14% blood plasma (in the absence of SA) was also measured to evaluate the sensor efficiency in terms of the *S*/*N* ratio, as shown in **Figure 3.12**. The *S*/*N* ratio can be calculated from eq 3.1.[8, 14] The SPR angle shift obtained for the complex sample containing SA is considered to be the signal, whereas that obtained from the sample without SA, i.e., the target molecules, is considered to be background or noise. The results shown in **Figure 3.12** indicate that the SPR chip modified with a copolymer platform containing 65% PgMA ($PPgMA_{65}MPC_{35}$-SH) showed the highest non-specific binding with blood plasma in a control experiment (absence of SA in 0.14% blood plasma). This may be the result of non-specific adsorption between the remaining alkyne moieties on the copolymer platform and non-targeted proteins in the blood plasma. The limits of detection (LODs) of the sensor platforms that can discriminate between target and non-targeted binding signals ($S/N \geq 3$) were 190, 0.95, and 190 nM for $PMA_{38}MPC_{62}$-SH, $PMA_{45}MPC_{55}$-SH, and $PMA_{65}MPC_{35}$-SH, respectively. These results suggest that the platform based on a copolymer containing 45% PgMA was the most efficient for detecting SA in blood plasma solution. The LOD of this $PPgMA_{45}MPC_{55}$ platform (0.95 nM) was even lower than that (1.5 nM) obtained for a platform based on poly[(methacrylic acid)-*ran*-(2-methacryloyloxyethyl phosphorylcholine)] (PMAMPC), previously developed by our group, and approximately 158 times lower than that of a platform based on a SAM of mercaptoundecanoic acid.[14] The fact that the PPgMAMPC sensor platform can directly immobilize an azide-containing biotin probe via a click reaction, without a functional group activation step, as required for the PMAMPC platform, makes it an attractive copolymer platform for probe binding in biosensing applications.

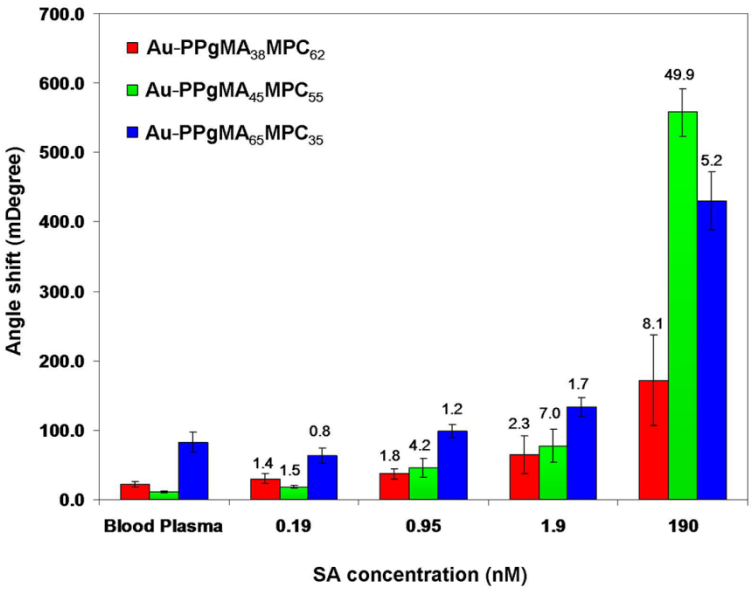


**Figure 3.12** SPR angle shifts corresponding to SA binding on Au-PPgMAMPC-biotin platforms from SA solutions of various concentrations in 0.14% blood plasma. *S*/*N* ratios are shown as number above each bar graph.

The developed PPgMAMPC platforms with clickable PgMA units for probe binding and MPC anti-fouling units were also used to immobilize a PNA-$N_3$ probe to explore its applicability as a DNA sensor. PNA is a DNA mimic with a peptide-like backbone, first introduced by Nielsen and coworkers in 1991.[58] Because it is uncharged, PNA·DNA hybrids are more stable than DNA·DNA hybrids, because electrostatic repulsion between negatively charged phosphate groups in the DNA backbone are absent. This, together with its greater specificity for complementary DNA than mismatched DNA, makes PNA an attractive nucleotide probe with potential applications as a DNA sensor. In this study, a conformationally restricted pyrrolidinyl PNA with D-prolyl-2-aminocyclopentanecarboxylic acid backbones (*acpc*PNA), developed by Vilaivan and coworkers, was selected as a model nucleic acid probe. It has been reported that its binding affinity and sequence specificity toward DNA are higher than those of Nielsen's PNA.[46,59,60] We previously showed that *acpc*PNA can act as an effective probe for DNA detection when immobilized on a gold-coated SPR chip either by Au–S bond formation between thiolated PNA (PNA-SH) and the gold surface[61] or by biotin–SA–biotin linkage between biotinylated PNA (PNA-biotin) and an SA layer assembled on a biotin-functionalized gold substrate.[59] Besides,

blocking which is a necessary step in most SAM-based sensors, the longer and greater hydrophilicity of the spacer between the PNA part and the thiol end of the thiolated PNA has a positive impact on the %HE of the platform developed by direct immobilization of thiolated PNA. Both %HE and %MD were significantly improved for the platform later developed by indirect PNA conjugation via biotin–SA–biotin linkage, which yielded PNA with a reasonably well-controlled density and orientation (see **Table 3.4** for comparison). The results of these two studies suggest that the clickable and anti-fouling PPgMAMPC platforms developed in the current study should meet all the above-mentioned criteria for developing an effective PNA-based sensor for DNA detection. Anchoring the copolymer to the gold surface prior to PNA binding should provide a reasonable distance between the immobilized PNA probes and the gold substrate, and allow the PNA molecules to interact freely with the incoming DNA targets. PMPC provides a hydrophilic environment for the platform so that non-specific adsorption of non-targeted DNA can be suppressed. It is anticipated that good control of the content of clickable PgMA units in the copolymer will enable the density of immobilized PNA to be tailored using efficient CuAAC-based reactions.

**Table 3.4** Values of $\%HE_{com}$ and %MD for DNA Detection by Surface-Modified Gold-Coated SPR Chips Conjugated with PNA

| Sample | $\%HE_{com}$ | %MD |
|---|---|---|
| Au-PPgMA$_{38}$MPC$_{62}$-PNA | 20 | 32 |
| Au-PPgMA$_{45}$MPC$_{55}$-PNA | 61 | 52 |
| Au-PPgMA$_{65}$MPC$_{35}$-PNA | 71 | 58 |
| Au-S-PNA[61] | 20 | >54 |
| Au-biotin-SA-biotin-PNA[59] | 58 | >90 |

In this work, azide-terminated PNA with a $T_9$ sequence (PNA-$N_3$), selected as a PNA probe model, was immobilized by the alkyne moieties of sensing platforms with various copolymer compositions, i.e., PPgMA$_{38}$MPC$_{62}$-SH, PPgMA$_{45}$MPC$_{55}$-SH, and PPgMA$_{65}$MPC$_{35}$-SH, via CuAAC reactions. Specific binding of 50 μM DNA in 10 mM PBS

was monitored using an SPR technique. The %HE and %MD were calculated using eqs 2 and 3, respectively, to evaluate the efficiency of the sensor. As shown in **Figure 3.13**, the sensing platform based on Au-PPgMA$_{65}$MPC$_{35}$-PNA, which had the highest amount of PgMA units, gave the greatest detectable signal, corresponding to binding of the complementary DNA sequence, $A_9$ (85.5 $\pm$ 10.9 mDegree), with a %HE of 71%, which is higher than those for sensing platforms based on Au-S-PNA[61] and Au-biotin-PNA,[59] as shown in Table 3. However, this copolymer platform still showed high non-specific interactions toward a single mismatched DNA sequence (AAAA<u>T</u>AAAA), therefore its %MD was not satisfactorily high compared with that for a platform based on Au-biotin-SA-biotin-PNA. Despite this limitation, a %HE as high as 71% may be suitable for other DNA-based applications, such as affinity-based DNA separation, in which the mismatch discrimination efficiency is not a critical issue. There is also room for improvement in terms of %MD. For example, possible non-specific interactions between the remaining unreacted alkyne moieties of PgMA and mismatched DNA may be decreased by blocking the unreacted PgMA with hydrophilic molecules, enabling %HE of mismatched DNA to be minimized. Stable triazole linkages between the PNA probe and the sensing platform should have the additional advantage of being more robust to the regeneration conditions than Au-S or Au-biotin-SA-biotin linkages. This should enable probe recycling, making the process economically viable.

| PNA probe | $N_3$-TTT TTT TTT-Lys$NH_2$ |
|---|---|
| Complementary DNA | 5'-AAA AAA AAA-3' |
| Single mismatch DNA | 5'-AAA ATA AAA-3' |

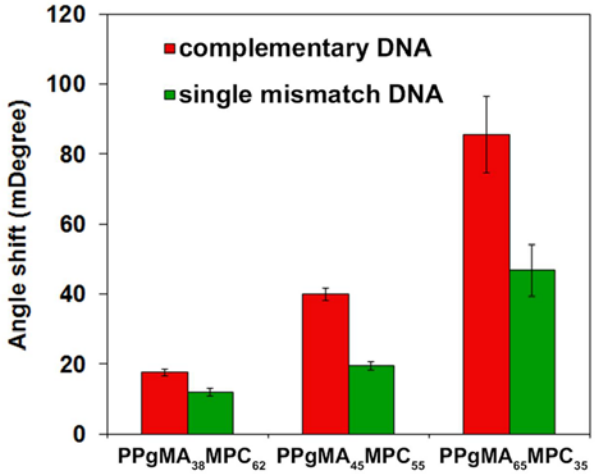


**Figure 3.13** SPR angle shifts corresponding to DNA binding to Au-PPgMAMPC-PNA platforms in 10 mM PBS.

**Conclusions**

Clickable and anti-fouling PPgMAMPC copolymer platforms were successfully synthesized by RAFT polymerization. The dithioester end groups of the copolymer were converted to thiol groups before surface immobilization on a gold-coated SPR chip via a "grafting to" approach. The alkyne moieties of PgMA bound azide-containing molecules (biotin-$N_3$ and PNA-$N_3$) via a CuAAC reaction, and the hydrophilic monomeric MPC unit suppressed non-specific adsorption of non-targeted analytes, namely BSA, LYZ, and blood plasma. Specific detection of SA by biotin probes conjugated with the PPgMAMPC platforms in 0.14% blood plasma was investigated using an SPR technique. Among all the platforms investigated, copolymer brushes of $PPgMA_{45}MPC_{55}$ performed best, giving the lowest detection limit, i.e., 0.95 nM. The potential of the surface-attached PPgMAMPC as a sensing layer for DNA detection was investigated by conjugating a PNA-$N_3$ probe with PPgMAMPC platforms with various copolymer compositions. The sensor platform based on Au-$PPgMA_{65}MPC_{35}$-PNA detected the highest amount of complementary DNA sequence, with 71%HE, and a reasonable degree of mismatch discrimination (58%MD) between the fully complementary DNA and single-mismatched DNA. These results suggest that substrate-modified PPgMAMPC brushes are potential copolymer platforms for azide-

containing probe immobilization for detecting target molecules in diagnostic and related applications. Both types of probe functioned effectively, which shows the versatility of the developed platform, and suggests that it can be used for both antibody-based and DNA-based biosensors.

## REFERENCES


1. Nakamura, F.; Ito, E.; Hayashi, T.; Hara, M., Fabrication of COOH-Terminated Self-Assembled Monolayers for DNA Sensors. *Colloid Surf. A-Physicochem. Eng. Asp.* **2006,** *284-285*, 495-498.
2. Senaratne, W.; Andruzzi, L.; Ober, C. K., Self-Assembled Monolayers and Polymer Brushes in Biotechnology: Current Applications and Future Perspectives. *Biomacromolecules* **2005,** *6* (5), 2427-48.
3. Su, X. L.; Li, Y., A Self-Assembled Monolayer-Based Piezoelectric Immunosensor for Rapid Detection of *Escherichia coli* O157:H7. *Biosens. Bioelectron.* **2004,** *19* (6), 563-574.
4. Akkahat, P.; Hoven, V. P., Introducing Surface-Tethered Poly(acrylic acid) Brushes as 3D Functional Thin Film for Biosensing Applications. *Colloid Surf. B-Biointerfaces* **2011,** *86* (1), 198-205.
5. Akkahat, P.; Mekboonsonglarp, W.; Kiatkamjornwong, S.; Hoven, V. P., Surface-Grafted Poly(acrylic acid) Brushes as a Precursor Layer for Biosensing Applications: Effect of Graft Density and Swellability on the Detection Efficiency. *Langmuir* **2012,** *28* (11), 5302-5311.
6. Henry, O. Y.; Mehdi, A. D.; Kirwan, S.; Sanchez, J. L.; O'Sullivan, C. K., Three-Dimensional Arrangement of Short DNA Oligonucleotides at Surfaces via the Synthesis of DNA-Branched Polyacrylamide Brushes by SI-ATRP. *Macromol. Rapid Commun.* **2011,** *32* (18), 1405-1410.
7. Kurosawa, S.; Aizawa, H.; Talib, Z. A.; Atthoff, B.; Hilborn, J., Synthesis of Tethered-Polymer Brush by Atom Transfer Radical Polymerization from a Plasma-Polymerized-Film-Coated Quartz Crystal Microbalance and Its Application for Immunosensors. *Biosens. Bioelectron.* **2004,** *20* (6), 1165-1176.
8. Lee, B. S.; Chi, Y. S.; Lee, K.-B.; Kim, Y.-G.; Choi, I. S., Functionalization of Poly(oligo(ethylene glycol) methacrylate) Films on Gold and Si/$SiO_2$ for Immobilization of Proteins and Cells: SPR and QCM studies. *Biomacromolecules* **2007,** *8* (12), 3922-3929.
9. Yang, N.; Su, X.; Tjong, V.; Knoll, W., Evaluation of Two- and Three-Dimensional Streptavidin Binding Platforms for Surface Plasmon Resonance Spectroscopy Studies of DNA Hybridization and Protein-DNA Binding. *Biosens. Bioelectron.* **2007,** *22* (11), 2700-2706.
10. Jeong, S. P.; Lee, B. S.; Kang, S. M.; Ko, S.; Choi, I. S.; Lee, J. K., Binding Behaviors of Protein on Spatially Controlled Poly[oligo(ethylene glycol) methacrylate] Brushes Grafted from Mixed Self-Assembled Monolayers on Gold. *Chem. Commun.* **2014,** *50* (40), 5291-5293.

11. Trmcic-Cvitas, J.; Hasan, E.; Ramstedt, M.; Li, X.; Cooper, M. A.; Abell, C.; Huck, W. T. S.; Gautrot, J. E., Biofunctionalized Protein Resistant Oligo(ethylene glycol)-Derived Polymer Brushes as Selective Immobilization and Sensing Platforms. *Biomacromolecules* **2009,** *10* (10), 2885-2894.
12. Gam-Derouich, S.; Lamouri, A.; Redeuilh, C.; Decorse, P.; Maurel, F.; Carbonnier, B.; Beyazit, S.; Yilmaz, G.; Yagci, Y.; Chehimi, M. M., Diazonium Salt-Derived 4-(Dimethylamino)phenyl Groups as Hydrogen Donors in Surface-Confined Radical Photopolymerization for Bioactive Poly(2-hydroxyethyl methacrylate) Grafts. *Langmuir* **2012,** *28* (21), 8035-8045.
13. Vaisocherova, H.; Sevcu, V.; Adam, P.; Spac□kova, B.; Hegnerova, K.; de los Santos Pereira, A.; Rodriguez-Emmenegger, C.; Riedel, T.; Houska, M.; Brynda, E.; Homola, J., Functionalized Ultra-Low Fouling Carboxy- and Hydroxy-Functional Surface Platforms: Functionalization Capacity, Biorecognition Capability and Resistance to Fouling from Undiluted Biological Media. *Biosens. Bioelectron.* **2014,** *51*, 150-157.
14. Akkahat, P.; Kiatkamjornwong, S.; Yusa, S.-i.; Hoven, V. P.; Iwasaki, Y., Development of a Novel Antifouling Platform for Biosensing Probe Immobilization from Methacryloyloxyethyl Phosphorylcholine-Containing Copolymer Brushes. *Langmuir* **2012,** *28* (13), 5872-5881.
15. Audouin, F.; Larragy, R.; Fox, M.; O'Connor, B.; Heise, A., Protein Immobilization onto Poly(acrylic acid) Functional Macroporous PolyHIPE Obtained by Surface-Initiated ARGET ATRP. *Biomacromolecules* **2012,** *13* (11), 3787-3794.
16. Cullen, S. P.; Liu, X.; Mandel, I. C.; Himpsel, F. J.; Gopalan, P., Polymeric Brushes as Functional Templates for Immobilizing Ribonuclease A: Study of Binding Kinetics and Activity. *Langmuir* **2007,** *24* (3), 913-920.
17. Dai, J. H.; Bao, Z. Y.; Sun, L.; Hong, S. U.; Baker, G. L.; Bruening, M. L., High-Capacity Binding of Proteins by Poly(acrylic acid) Brushes and Their Derivatives. *Langmuir* **2006,** *22* (9), 4274-4281.
18. Qu, Z.; Chen, K.; Gu, H.; Xu, H., Covalent Immobilization of Proteins on 3D Poly(acrylic acid) Brushes: Mechanism Study and a More Effective and Controllable Process. *Bioconjugate Chem.* **2014,** *25* (2), 370-378.
19. Thilakarathne, V.; Briand, V. A.; Zhou, Y.; Kasi, R. M.; Kumar, C. V., Protein Polymer Conjugates: Improving the Stability of Hemoglobin with Poly(acrylic acid). *Langmuir* **2011,** *27* (12), 7663-7671.
20. Baek, M.-G.; Roy, R., Relative Lectin Binding Properties of T-Antigen-Containing Glycopolymers: Copolymerization of *N*-Acryloylated T-Antigen Monomer vs. Graft Conjugation of Aminated T-Antigen Ligands onto Poly(*N*-acryloxysuccinimide). *Macromol. Biosci.* **2001,** *1* (7), 305-311.
21. Chen, J.-P.; Chiu, S.-H., A Poly(*N*-isopropylacrylamide-*co*-*N*-acryloxysuccinimide-*co*-2-hydroxyethyl methacrylate) Composite Hydrogel Membrane for Urease Immobilization to Enhance Urea Hydrolysis Rate by Temperature Swing. *Enzyme Microb. Technol.* **2000,** *26* (56), 359-367.

22. Minard-Basquin, C.; Chaix, C.; D'Agosto, F.; Charreyre, M.-T.; Pichot, C., Oligonucleotide Synthesis onto Poly(*N*-acryloylmorpholine-*co*-*N*-acryloxysuccinimide): Assessment of The Resulting Conjugates in a DNA Sandwich Hybridization Test. *J. Appl. Polym. Sci.* **2004,** *92* (6), 3784-3795.
23. Duque, L.; Menges, B.; Borros, S.; Forch, R., Immobilization of Biomolecules to Plasma Polymerized Pentafluorophenyl Methacrylate. *Biomacromolecules* **2010,** *11* (10), 2818-2823.
24. McRae, S.; Chen, X.; Kratz, K.; Samanta, D.; Henchey, E.; Schneider, S.; Emrick, T., Pentafluorophenyl Ester-Functionalized Phosphorylcholine Polymers: Preparation of Linear, Two-Arm, and Grafted Polymer-Protein Conjugates. *Biomacromolecules* **2012,** *13* (7), 2099-2109.
25. Socaci, C.; Rybka, M.; Magerusan, L.; Nan, A.; Turcu, R.; Liebscher, J., Magnetite Nanoparticles Coated with Alkyne-Containing Polyacrylates for Click Chemistry. *J. Nanopart. Res. C7 - 1747* **2013,** *15* (6), 1-14.
26. Wang, C.; Fan, Y.; Hu, M. X.; Xu, W.; Wu, J.; Ren, P. F.; Xu, Z. K., Glycosylation of the Polypropylene Membrane Surface via Thiol-Yne Click Chemistry for Lectin Adsorption. *Colloid Surf. B-Biointerfaces* **2013,** *110*, 105-112.
27. Liu, Y.; Li, C. M.; Hu, W.; Lu, Z., High Performance Protein Microarrays Based on Glycidyl Methacrylate-Modified Polyethylene Terephthalate Plastic Substrate. *Talanta* **2009,** *77* (3), 1165-1171.
28. Xiu, K. M.; Cai, Q.; Li, J. S.; Yang, X. P.; Yang, W. T.; Xu, F. J., Anti-Fouling Surfaces by Combined Molecular Self-Assembly and Surface-Initiated ATRP for Micropatterning Active Proteins. *Colloid Surf. B-Biointerfaces* **2012,** *90*, 177-183.
29. Chang, Y.; Shu, S.-H.; Shih, Y.-J.; Chu, C.-W.; Ruaan, R.-C.; Chen, W.-Y., Hemocompatible Mixed-Charge Copolymer Brushes of Pseudozwitterionic Surfaces Resistant to Nonspecific Plasma Protein Fouling. *Langmuir* **2010,** *26* (5), 3522-3530.
30. Rodriguez Emmenegger, C.; Brynda, E.; Riedel, T.; Sedlakova, Z.; Houska, M.; Alles, A. B., Interaction of Blood Plasma with Antifouling Surfaces. *Langmuir* **2009,** *25* (11), 6328-6333.
31. Zhang, Z.; Zhang, M.; Chen, S.; Horbett, T. A.; Ratner, B. D.; Jiang, S., Blood Compatibility of Surfaces with Superlow Protein Adsorption. *Biomaterials* **2008,** *29* (32), 4285-4291.
32. Fuchs, A. V.; Ritz, S.; Putz, S.; Mailander, V.; Landfester, K.; Ziener, U., Bioinspired Phosphorylcholine Containing Polymer Films with Silver Nanoparticles Combining Antifouling and Antibacterial Properties. *Biomater. Sci.* **2013,** *1* (5), 470-477.
33. Fuchs, A. V.; Walter, C.; Landfester, K.; Ziener, U., Biomimetic Silver-Containing Colloids of Poly(2-methacryloyloxyethyl phosphorylcholine) and Their Film-Formation Properties. *Langmuir* **2012,** *28* (11), 4974-4983.
34. Ishihara, K.; Nomura, H.; Mihara, T.; Kurita, K.; Iwasaki, Y.; Nakabayashi, N., Why do Phospholipid Polymers Reduce Protein Adsorption? *J. Biomed. Mater. Res.* **1998,** *39* (2), 323-330.

35. Ishihara, K.; Ueda, T.; Nakabayashi, N., Preparation of Phospholipid Polymers and Their Properties as Polymer Hydrogel Membranes. *Polym. J.* **1990,** *22* (5), 355-360.
36. Iwasaki, Y.; Fujiike, A.; Kurita, K.; Ishihara, K.; Nakabayashi, N., Protein Adsorption and Platelet Adhesion on Polymer Surfaces Having Phospholipid Polar Group Connected with Oxyethylene Chain. *J. Biomater. Sci.-Polym. Ed.* **1996,** *8* (2), 91-102.
37. Ishihara, K.; Oshida, H.; Endo, Y.; Ueda, T.; Watanabe, A.; Nakabayashi, N., Hemocompatibility of Human Whole Blood on Polymers with a Phospholipid Polar Group and Its Mechanism. *J. Biomed. Mater. Res.* **1992,** *26* (12), 1543-1552.
38. Iwata, R.; Suk-In, P.; Hoven, V. P.; Takahara, A.; Akiyoshi, K.; Iwasaki, Y., Control of Nanobiointerfaces Generated from Well-Defined Biomimetic Polymer Brushes for Protein and Cell Manipulations. *Biomacromolecules* **2004,** *5* (6), 2308-2314.
39. Park, J.; Kurosawa, S.; Takai, M.; Ishihara, K., Antibody Immobilization to Phospholipid Polymer Layer on Gold Substrate of Quartz Crystal Microbalance Immunosensor. *Colloid Surf. B-Biointerfaces* **2007,** *55* (2), 164-172.
40. Goto, Y.; Matsuno, R.; Konno, T.; Takai, M.; Ishihara, K., Polymer Nanoparticles Covered with Phosphorylcholine Groups and Immobilized with Antibody for High-Affinity Separation of Proteins. *Biomacromolecules* **2008,** *9* (3), 828-833.
41. Mark, S. S.; Nishizawa, K.; Takai, M.; Ishihara, K., A Bioconjugated Phospholipid Polymer Biointerface with Nanometer-Scaled Structure for Highly Sensitive Immunoassays. In *Bioconjugation Protocols*, Mark, S. S., Ed. Humana Press: New York, USA, 2011; Vol. 751, pp 491-502.
42. Nishizawa, K.; Konno, T.; Takai, M.; Ishihara, K., Bioconjugated Phospholipid Polymer Biointerface for Enzyme-Linked Immunosorbent Assay. *Biomacromolecules* **2008,** *9* (1), 403-407.
43. Sakai-Kato, K.; Kato, M.; Ishihara, K.; Toyo'oka, T., An Enzyme-Immobilization Method for Integration of Biofunctions on a Microchip Using a Water-Soluble Amphiphilic Phospholipid Polymer Having a Reacting Group. *Lab Chip* **2004,** *4* (1), 4-6.
44. Iwata, R.; Satoh, R.; Iwasaki, Y.; Akiyoshi, K., Covalent Immobilization of Antibody Fragments on Well-Defined Polymer Brushes via Site-Directed Method. *Colloid Surf. B-Biointerfaces* **2008,** *62* (2), 288-298.
45. He, H.; Zhang, Y.; Gao, C.; Wu, J., 'Clicked' Magnetic Nanohybrids with a Soft Polymer Interlayer. *Chem. Commun.* **2009,** (13), 1655-1657.
46. Vilaivan, T.; Srisuwannaket, C., Hybridization of Pyrrolidinyl Peptide Nucleic Acids and DNA: Selectivity, Base-Pairing Specificity, and Direction of Binding. *Org. Lett.* **2006,** *8* (9), 1897-1900.
47. Ditmangklo, B.; Boonlua, C.; Suparpprom, C.; Vilaivan, T., Reductive Alkylation and Sequential Reductive Alkylation-Click Chemistry for On-Solid-Support Modification of Pyrrolidinyl Peptide Nucleic Acid. *Bioconjugate Chem. 24* (4), 614-625.

48. Shen, W.; Qiu, Q.; Wang, Y.; Miao, M.; Li, B.; Zhang, T.; Cao, A.; An, Z., Hydrazine as a Nucleophile and Antioxidant for Fast Aminolysis of RAFT Polymers in Air. *Macromol. Rapid Commun.* **2010,** *31* (16), 1444-1448.
49. Metallo, S. J.; Kane, R. S.; Holmlin, R. E.; Whitesides, G. M., Using Bifunctional Polymers Presenting Vancomycin and Fluorescein Groups to Direct Anti-Fluorescein Antibodies to Self-Assembled Monolayers Presenting d-Alanine-d-Alanine Groups. *J. Am. Chem. Soc.* **2003,** *125* (15), 4534-4540.
50. Su, X.; Wu, Y.-J.; Knoll, W., Comparison of Surface Plasmon Resonance Spectroscopy and Quartz Crystal Microbalance Techniques for Studying DNA Assembly and Hybridization. *Biosens. Bioelectron.* **2005,** *21* (5), 719-726.
51. Ellis, B.; Smith, R., *Polymers: A property database*. 2nd edition ed.; Taylor and Francis Group: Boca Raton, Florida, USA, 2008.
52. Wu, T.; Gong, P.; Szleifer, I.; Vlcek, P.; Subr, V.; Genzer, J., Behavior of Surface-Anchored Poly(acrylic acid) Brushes with Grafting Density Gradients on Solid Substrates:1. Experiment. *Macromolecules* **2007,** *40* (24), 8756-8764.
53. Green, N. M., Avidin. *Adv. Protein Chem.* **1975,** *29*, 85-133.
54. Huisgen, R., 1,3-Dipolar cycloadditions. Past and future. *Angew. Chem-Int. Edit.* **1963,** *2* (10), 565-598.
55. Tornoe, C. W.; Christensen, C.; Meldal, M., Peptidotriazoles on Solid phase: [1,2,3]-Triazoles by Regiospecific Copper(I)-Catalyzed 1,3-Dipolar Cycloadditions of Terminal Alkynes to Azides. *J. Org. Chem.* **2002,** *67* (9), 3057-3064.
56. Hansen, J. T., *Netter's Clinical Anatomy*. 3rd Edition ed.; Elsevier Inc: Philadelphia, PA, 2014.
57. Kim, G.; Park, S.; Jung, J.; Heo, K.; Yoon, J.; Kim, H.; Kim, I. J.; Kim, J. R.; Lee, J. I.; Ree, M., Novel Brush Polymers with Phosphorylcholine Bristle Ends: Synthesis, Structure, Properties, and Biocompatibility. *Adv. Funct. Mater.* **2009,** *19* (10), 1631-1644.
58. Nielsen, P.; Egholm, M.; Berg, R.; Buchardt, O., Sequence-Selective Recognition of DNA by Strand Displacement with a Thymine-Substituted Polyamide. *Science* **1991,** *254* (5037), 1497-1500.
59. Ananthanawat, C.; Vilaivan, T.; Hoven, V. P.; Su, X., Comparison of DNA, Aminoethylglycyl PNA and Pyrrolidinyl PNA as Probes for Detection of DNA Hybridization Using Surface Plasmon Resonance Technique. *Biosens. Bioelectron.* **2010,** *25* (5), 1064-1069.
60. Suparpprom, C.; Srisuwannaket, C.; Sangvanich, P.; Vilaivan, T., Synthesis and Oligodeoxynucleotide Binding Properties of Pyrrolidinyl Peptide Nucleic Acids Bearing Prolyl-2-Aminocyclopentanecarboxylic Acid (ACPC) Backbones. *Tetrahedron Lett.* **2005,** *46* (16), 2833-2837.
61. Ananthanawat, C.; Vilaivan, T.; Mekboonsonglarp, W.; Hoven, V. P., Thiolated Pyrrolidinyl Peptide Nucleic Acids for the Detection of DNA Hybridization Using Surface Plasmon Resonance. *Biosens. Bioelectron.* **2009,** *24* (12), 3544-3549.

# Chapter IV

## Filter Paper Grafted With PNA-Conjugated Copolymer Brushes for Colorimetric DNA Sequence Determination

### INTRODUCTION

DNA sequence determination is crucially important for clinical diagnosis, forensic identification as well as pathogen detection in food and agricultural products.[1] Basic principle for DNA detection is generally based on the concept that DNA target is detected via specific binding to complementary nucleic acid probe, following Watson-Crick base-pairing rule.[2] Peptide nucleic acid (PNA), firstly introduced by Nielsen and co-workers in 1991[3] is a synthetic DNA analogue having an uncharged peptide-like backbone. The suppressed electrostatic repulsion between the neutral PNA and the negatively charged DNA bring about a number of favorable DNA binding characteristics including high thermal stability, greater sequence specificity and mismatch discrimination sensitivity, and less salt-dependent affinity. Among PNA variants being investigated so far, a conformationally rigid pyrrolidinyl PNA derived from D-prolyl-2-aminocyclopentane carboxylic acid (acpc) backbones (acpcPNA) developed by Vilaivan and co-workers[4] truly stands out as potential and effective nucleic acid probe for DNA biosensor in that it can form a PNA·DNA duplex with even higher affinity and specificity than the original Nielsen's aminoethylglycyl PNA. The success of using acpcPNA as probe for DNA sequence determination have been continuously demonstrated by many techniques including MALDI-TOF mass spectrometry,[5,6] quartz crystal microbalance (QCM),[7] surface plasmon resonance (SPR),[8,9] electrochemistry[10-12] most of which require advanced instruments and have to be done in well-equipped laboratories. The development of highly sensitive and specific, yet simple and economical test kit/assays without the demand for sophisticated instruments, suitable for point-of-care usages still remains a challenge.

Inspired by research work firstly reported by Whitesides and coworkers on paper-based microfluidic devices[13] and a number of relevant publications following thereafter,[14] paper-based DNA sensing platforms employing acpcPNA as probes have

been recently developed. The first assay is based on the concept of “Dot blot hybridization” in which filter paper grafted with quaternized poly(2-(dimethylamino)ethyl methacrylate) (QPDMAEMA) brushes was used as positively charged platform that can selectively capture PNA·DNA hybrids and prevent non-specific adsorption of non-target analytes. The hybridization event can then be visualized by an enzyme-based calorimetric assay employing horseradish peroxidase streptavidin (SA–HRP) conjugate and a chromogenic substrate.[15] Although quite an impressive detection limit (10 fmol, equivalent to 1 mL of 10 nM of DNA) can be reached by naked eye detection, the technique has a limitation for detection of DNA mixtures because the DNA was deposited on the membrane via non-specific electrostatic interactions. There will most likely be binding competition among different DNA sequences so it may not be possible to detect the desired target. To overcome the above-mentioned problem, the second platform most recently reported relies on direct immobilization of the acpc PNA probes on cellulose paper. Upon contacting with DNA analyte via capillary method, cationic dyes were introduced to electrostatically intereact with negatively charged hybridized DNA to monitor the PNA-DNA binding event. A lowest detectable DNA concentration of 200 nM or 3.3 pmol per spot has been achieved.[16]

The information gained from this latest development is very fruitful in that acpcPNA covalently immobilized directly onto the paper still functions efficiently in binding with the DNA targets. Together with our well-established strategy to enhance active binding sites per surface area of material by using surface-grafted polymer brushes,[17-19] this research aims to develop another paper-based DNA sensor that can bind directly to the PNA probes. The filter paper was first grafted with poly[glycidyl methacrylate-*co*-poly(ethylene glycol)methacrylate] (P(GMA-*co*-PEGMA) via surface-initiated reversible addition fragmentation chain transfer polymerization (SI-RAFT). This copolymeric system was chosen to generate active layer for PNA binding due to the following reasons: (1) the epoxide group of the GMA unit can act as versatile active site for binding with PNA capture probe via epoxide ring opening without having to use additional coupling agent so that no by-product would be released.[17,18,20-22] Hydroxyl group generated as an outcome of epoxide ring opening is well known as non-charged hydrophilic entity under neutral pH, a general DNA hybridization condition, that should not interfere, but synergistically facilitate the detection. (2) the PEGMA unit incorporated as hydrophilic entity should prevent non-specific adsorption of non-target DNA as well as non-DNA components that may deteriorate the detection sensitivity. This latter issue

is extremely important because it determines the fate of the developed platform when subjected to analysis of real biological samples. Signal amplification used in this research relies on sandwich-hybridization assay employing biotinylated acpcPNA probe (b-PNA) as reporter probe together with horseradish peroxidase streptavidin (SA-HRP) and *o*-phenylenediamine (OPD) substrate can be visualized by an enzyme-based colorimetric assay.[23] The concept for this developed filter paper-based DNA sequence determination is demonstrated in **Scheme 4.1**.

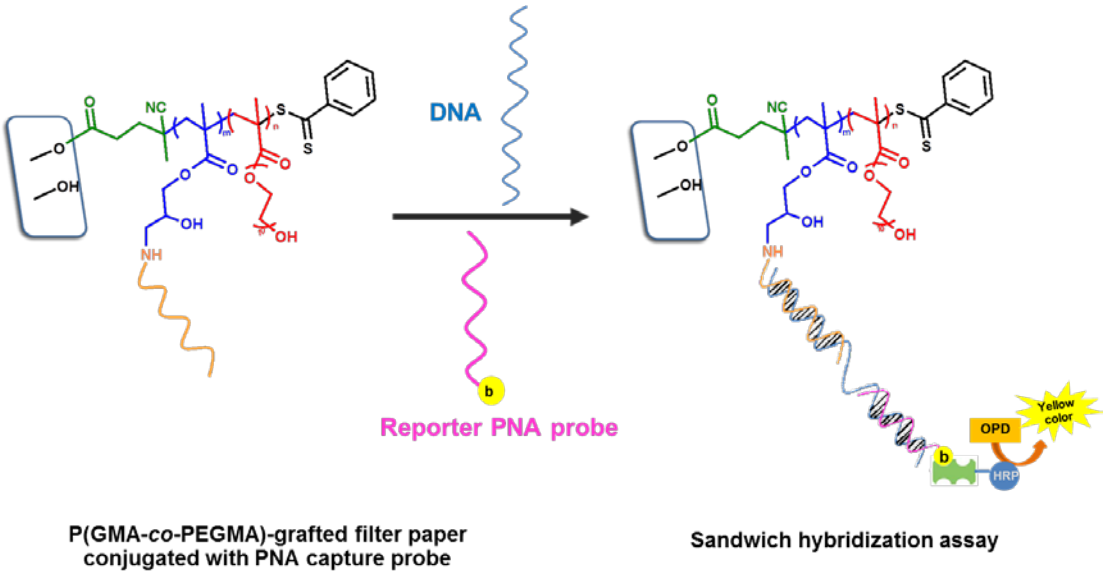


**Scheme 4.1.** Schematic representation of enzymatic amplified colorimetric detection of DNA following sandwich-hybridization assay employing biotinylated acpcPNA probe (b-PNA) as reporter probe and filter paper-grafted (P(GMA-*co*-PEGMA) brushes conjugated with acpcPNA capture probe as substrate.

## MATERIALS AND METHODS

### Materials

Whatman No. 1 filter paper was used as the membrane. PEGMA (98%), GMA (99%), dimethylformamide (DMF), 4,4-azobis(4-cyanovaleic acid) (ACVA), 4-cyano-4-(phenylcarbonothio) pentanoic acid (CPD), 4-(dimethylamino)pyridine (DMAP), *N,N'*-Dicyclohexylcarbodiimide (DCC), *O*-phenylene- diamine (OPD), bovine serum albumin (BSA), urea–hydrogen peroxide (urea–$H_2O_2$) and streptavidin–horseradish peroxidase conjugate (SA–HRP) were bought from Aldrich (USA). PEGMA and GMA were purified through a column filled with basic alumina to remove the inhibitor prior to use. All reagents and materials are analytical grade and used without further purification.

Oligonucleotides were purchased from Bioservice Unit, National Science and Technology Development Agency (Thailand). Ultrapure distilled water was obtained after purification using a Millipore Milli-Q system (USA) that involves reverse osmosis, ion exchange, and a filtration step.

**Instrumentation**

$^1$H NMR spectra of the copolymer formed in solution were recorded in solution of $CDCl_3$ or DMSO-$d_6$ on a Varian Mercury-400 nuclear magnetic resonance spectrometer operating at 400 MHz. Chemical shifts were reported in part per million (ppm) relative to tetramethylsilane (TMS). Infrared spectra of materials scraped from the surface-modified filter paper and prepared as KBr disks were obtained from a FT-IR spectrometer (Nicolet, USA), model Impact 410, with 32 scans at resolution 4 $cm^{-1}$, in a frequency range of 400-4000 $cm^{-1}$ using TGS detector. The surface morphology of the filter paper before and after modification was examined by scanning electron microscopy (SEM) on a JEOL (JSM-6610LV) instrument. The elemental compositions of the surface-modified filter paper were characterized by x-ray photoelectron spectroscopy (XPS) on a Physical Electronics Quantum 2000, using monochromatic Al K-$\alpha$ x-rays, and standard dual ion-electron neutralization.

The crude acpcPNA was purified by reversed-phase HPLC with UV detection at 260 nm. A Varian Polaris C18 analytical HPLC column (3 mm particle size 4.6 × 50 mm) was used and eluted with a gradient of 0.1% TFA in MeOH and 0.1% TFA in water. MALDI-TOF mass spectra of acpcPNAs were obtained on Microflex MALDI-TOF mass spectrometer (Bruker Daltonics, Germany). The samples (1 μL) were mixed with 10 μL of the matrix solution consisting of $\alpha$-cyano-4-hydroxycinnamic acid (CCA) in 0.1% trifluoroacetic acid (TFA) in acetonitrile:water (1:1) solution. This mixture (1 μL) was spotted onto the target, allowed to dry, and analyzed in positive ion linear time-of-fight mode with an accelerating voltage +20 kV. All spectra were processed by averaging between 20 and 30 individual laser shots. Melting temperature ($T_m$) measurements of PNA·DNA complex was performed on a CARY 100 Bio UV-Visible spectrophotometer (Varian, Inc., USA) equipped with a thermal melt system.

The scanned images of the tested results on filter papers were recorded on an Epson Perfection V33 scanner in 24 bits Professional mode. The brightness/contrast/resolution was set to 128/128/300. The images were saved as TIFF-files. The intensity of each spot was determined using Scion Image software by first

converting to gray scale at 300 dpi. Intensity measurements were carried out using the Line tool to select an area for analysis to obtain profile images.

**Preparation of P(GMA-*co*-PEGMA)-grafted filter paper**

The filter paper was first immobilized with initiator (**Step I, Scheme 4.2**). The initiator, ACVA (0.21 g, 1 mmol), DMAP (9.14 mg, 0.1 mmol) and DCC (0.19 g, 1 mmol) were dissolved in 20 mL DMF. The solution was stirred for 4 h at room temperature under nitrogen atmosphere before transferred to a vial containing filter paper ($4\times8$ $cm^2$) . After the reaction proceeded for 20 h, the filter paper was removed from the solution and thoroughly rinsed with DMF and ethanol for three times each and dried under nitrogen gas flow. The obtained initiator-immobilized filter paper was then placed in a vial containing ACVA (3.5 mg, 0.05 mmol) and CPD (14 mg, 0.0125 mmol) in 5 mL of DMF. GMA (0.928 mL, 7 mmol or 0.4 mL, 3 mmol) and PEGMA (2.28 mL, 3 mmol or 0.98 mL, 7 mmol) were then added into the mixture. The vial was then sealed with a rubber septum. The solution was deoxygenated by purging with nitrogen gas for 30 min. The SI-RAFT was then performed at 70 $^{\circ}C$ for 4 h (**Step II, Scheme 4.2**). The filter paper was removed from the vial and rinsed thoroughly with DMF and ethanol.

**Synthesis of acpcPNA probes**

acpcPNA Probes were synthesized using solid phase peptide synthesis according to procedures previously reported in literatures.[24] For the reporter probe, biotin was attached at the N-termini of acpcPNA while still on the solid support via two successive aminoethoxyethoxyacetyl (egl) linkers employing biotin pentafluorophenyl ester in the presence of hydroxyl-7-azabenzotriazole/N-ethyldiisopropylamine. For pentafluorobenzenesulfonyl-labeled PNA (penta-TTTTTTTTT-Lys$NH_2$), acpcPNA (T9) oligomer was capped with pentafluorobenzenesulfonyl chloride at room temperature for 5 days. For the fluorescence-labeled PNA (flu-o-TTTTTTTTT-Lys$NH_2$) was synthesized. After nucleobase side-chain deprotection and cleavage from the solid support, the crude acpcPNA was purified by reversed-phase HPLC. After purification, the solution of PNA was lyophilized and the identity of the acpcPNA oligomers was verified by MALDI-TOF mass spectrometry and thermal denaturation experiments (after hybridization with complementary DNA sequences) (**Table 4.1**).

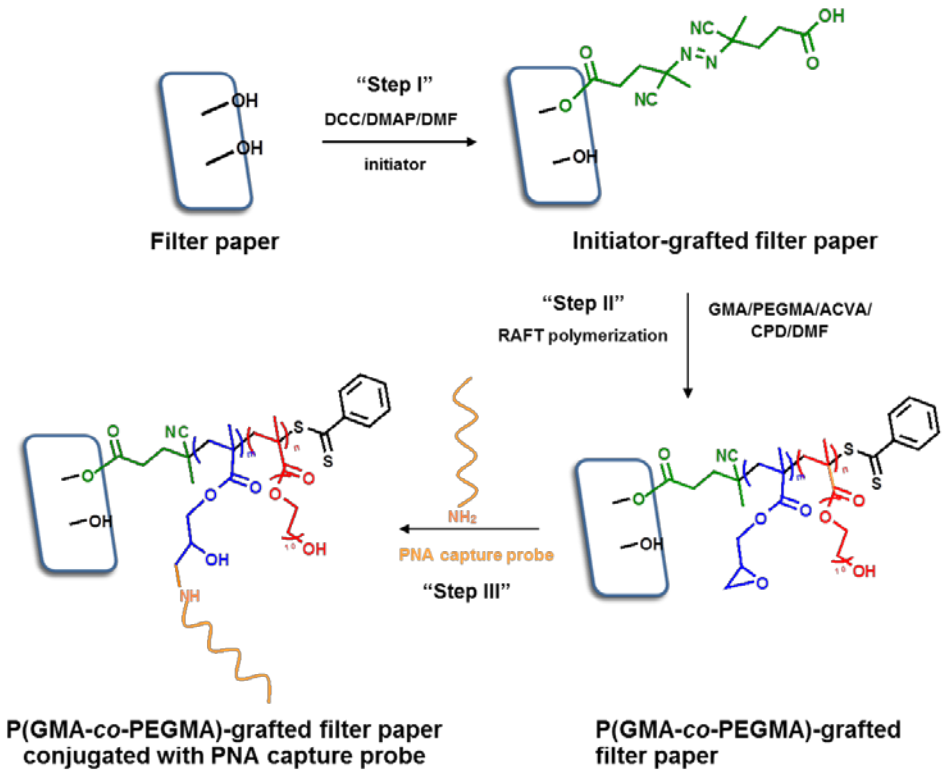


**Scheme 4.2** Preparation of P(GMA-*co*-PEGMA)–grafted filter paper via SI-RAFT followed by PNA capture probe immobilization.

**Table 4.1** Characteristics of *acpc*PNA oligomers synthesized by solid phase method.

| Name | Sequence | m/z (calculated) | m/z (observed) | $T_m$ (°C) |
|---|---|---|---|---|
| PNA (Cap) | *N*-Ac-GGAACCTGCGCG-LysNH$_2$-*C* | 4259.55 | 4259.38 | 77.6 |
| b-PNA(Ser) | *N*-biotin-(egl)$_2$-AACACACAGACT- SerOH -*C* | 4630.02 | 4630.99 | 62.2 |
| b-PNA(Lys) | *N*-biotin-(egl)$_2$-AACACACAGACT- LysNH$_2$ -*C* | 4670.12 | 4669.21 | not measured |
| penta-PNA(T9) | *N*-penta-TTTTTTTTT-LysNH$_2$-*C* | 3368.47 | 3368.63 | not measured |
| PNA(T9) | *N*-flu-(egl)-TTTTTTTTT-LysNH$_2$-*C* | - | - | - |

**Immobilization of PNA capture probe on the P(GMA-*co*-PEGMA)-grafted filter paper**

P(GMA-*co*-PEGMA)-grafted filter paper was incubated in an aqueous solution containing PNA capture probe (Ac-GGAACCTGCGCG-Lys$NH_2$, 2 nmol) in 2 mL 0.1 M phosphate buffered saline (PBS, pH 7.4) and a designated quantity of triethylamine (TEA) was added into the mixture. The solution was shaken for 24 h at room temperature and washed with 0.1 M PBS buffer, pH 7.4 and Milli-Q water, dried with nitrogen gas flow to obtain the P(GMA-*co*-PEGMA)-filter paper conjugated with PNA capture probe (**Step III, Scheme 4.2**). A biotinylated PNA (b-o-o-AACACACAGACT-Lys$NH_2$, b-PNA, 2 nmol) as a positive control was also immobilized on P(GMA-*co*-PEGMA)-filer paper using the same procedure.

**Determination of immobilization efficiency of PNA capture probe**

This investigation was performed to determine the effect of triethylamine (TEA) concentration or buffer having different pH on immobilization efficiency of PNA capture probe. Firstly, the fluorescence-labeled PNA (flu-o-TTTTTTTTT-Lys$NH_2$) was used as a model for PNA capture probe. The aqueous PNA solution having designated quantity of TEA (0.1, 0.2 and 0.3 μM) was added into 0.1 M PBS pH 7.4. 0.5 μL (200 μM) of the PNA was spotted on the marked P(GMA-*co*-PEGMA)-grafted filter paper and dried for 24 h at room temperature. The P(GMA-*co*-PEGMA)-grafted filter paper was then rinsed by acetonitrile: Milli-Q water (1:1) , 0.1 M phosphate buffer pH 7.4 and Milli-Q water three times each, then blow-dried with nitrogen gas. A similar procedure was applied for the investigation on the effect of pH of buffer (8.0, 9.0 and 10.0) by using the designated buffer to dissolve PNA without TEA addition (0.1 M phosphate buffer pH 8.0, 0.1 M carbonate-bicarbonate buffer pH 9.0, 0.1 M carbonate-bicarbonate buffer pH 10.0). The extent of fluorescence-labeled PNA immobilization was monitored under fluorescence microscope.

To determine immobilization efficiency of PNA capture probe on P(GMA-*co*-PEGMA)-grafted filter paper by XPS analysis, the pentafluorobenzenesulfonyl-labeled PNA (penta-TTTTTTTTT-Lys$NH_2$) was employed as a probe. P(GMA-*co*-PEGMA)-grafted filer paper was incubated in an aqueous solution containing PNA (3.58 μL, 2 nmol) dissolved in 2 mL of 0.1 M PBS pH 7.4 with designated quantity of TEA (0.1 and 0.3 μM TEA) or 0.1 M carbonate-bicarbonate buffer pH 10.0.

**Colorimetric detection for DNA sequence by sandwich-hybridization assay**

All PNA and DNA sequences used in this study are displayed in **Table 4.2**. The P(GMA-*co*-PEGMA) grafted filter paper immobilized with PNA capture probe was cut into 1×4.9 $cm^2$ piece and spot positions were marked with a pencil. Description of DNA and PNA sequences used for each spot positions of the test are listed in **Table 4.3**. 2 µL of the DNA sample (1 µM in 0.5 mM phosphate buffer, pH 7.0) was spotted on the marked filter paper on position 2, 3, and 4. The filter paper was rinsed with 0.1% Tween 20 in 0.1 M phosphate buffer pH 7.4, 0.1 M phosphate buffer pH 7.4 and Milli-Q water three times each followed by incubation in a blocking solution (1% w/v BSA in 0.1 M PBS pH 7.4) for 30 min. A 2 µL of the biotinylated acpcPNA probe, as reporter probe (b-o-o-AACACACAGACT-SerOH), (1 µM in 0.1 M phosphate buffer, pH 7.4) was spotted on filter paper at position 3, 4 and 5. After that the filter paper was rinsed with 0.1% Tween 20 in 0.1 M phosphate buffer pH 7.4, 0.1 M phosphate buffer pH 7.4 and Milli-Q water three times each and incubated in the blocking solution for 30 min again. A 2 µL of SA-HRP was spotted on the filter paper at all positions followed by rinsing with 0.1 M phosphate buffer (pH 7.4), Milli-Q water and 0.1 M citrate buffer (CTB, pH 5.0) three times each. 5 µL of a solution consisting of 250 µL of OPD substrate (1.6 mg/mL) and 250 µL of urea-$H_2O_2$ (1.6 mg/mL) was spotted on the filter paper at all positions for 1 min and was finally washed with Milli-Q water.

**Table 4.2** PNA and DNA sequences used in this study.

| Code | Sequence | Description |
|---|---|---|
| PNA (Cap) | Ac-GGAACCTGCGCG-Lys$NH_2$ | Capture probe |
| b-PNA (Lys) | b-o-o-AACACACAGACT-Lys$NH_2$ | Positive control |
| b-PNA (Ser) | b-o-o-AACACACAGACT-SerOH | Reporter probe |
| b-DNA | d(5'-CGCGCAGGTTCC-b-3') | Positive control |
| DNA 1 | d(5'-**CGCGCAGGTTCC**GCTAAGT CTGTGTGTT-3') | Complementary to PNA(Cap) |
| DNA 2 | d(5'-CGCGC**T**GGTTCCGCTAAGTC TGTGTGTT-3') | Single mismatch to PNA(Cap) |
| DNA 3 | d(5'-TATATCAAGGTTGCTACAGT GAGAGAGG-3') | Non-complementary PNA(Cap) |

**Table 4.3** Description of DNA and PNA sequences used for each spot on the P(GMA-*co*-PEGMA)-grafted filter paper conjugated with PNA capture probe of the test results shown in Figure 4.6-4.8.

| Spot position | DNA | PNA | Remark[a] |
|---|---|---|---|
| **1** | - | b-PNA(Lys) | (+) |
| **2** | b-DNA HLA-B*1502 | - | (+) |
| **3** | DNA 1 HLA-B*1502 | b-PNA (Ser) | (+) |
| **4** | DNA 3 | b-PNA (Ser) | (-) |
| **5** | | b-PNA (Ser) | (-) |
| **6** | - | - | (-) |

[a](+) = positive result, (-) = negative result

**Results and Discussion**

**Preparation and characterization of P(GMA-*co*-PEGMA)-grafted filter paper**

The initiator was immobilized on filter paper via esterification of hydroxyl groups on the filter paper with ACVA using DCC as coupling agent and DMAP as catalyst. The P(GMA-*co*-PEGMA) was then grafted on filter paper via SI-RAFT polymerization to insure that the molecular weight and copolymer composition can be well manipulated. In this research, a target degree of polymerization was set at 200 and the copolymer composition was varied from GMA:PEGMA of 30:70 to 70:30. $^{1}$H NMR spectra of the copolymers formed in solution from ACVA also added in solution are displayed (**Figure 4.1**). As determined by $^{1}$H NMR analysis (**Table 4.4),** the molecular weight ($\overline{M}_n$) of P(GMA-*co*-PEGMA) formed in solution closely resembled the theoretical value for the feed composition GMA:PEGMA 70:30, but was much lower than expected for the feed composition GMA:PEGMA 30:70. The copolymer composition also coincides well with the monomer feed ratio suggesting that the copolymerization was reasonably under control.

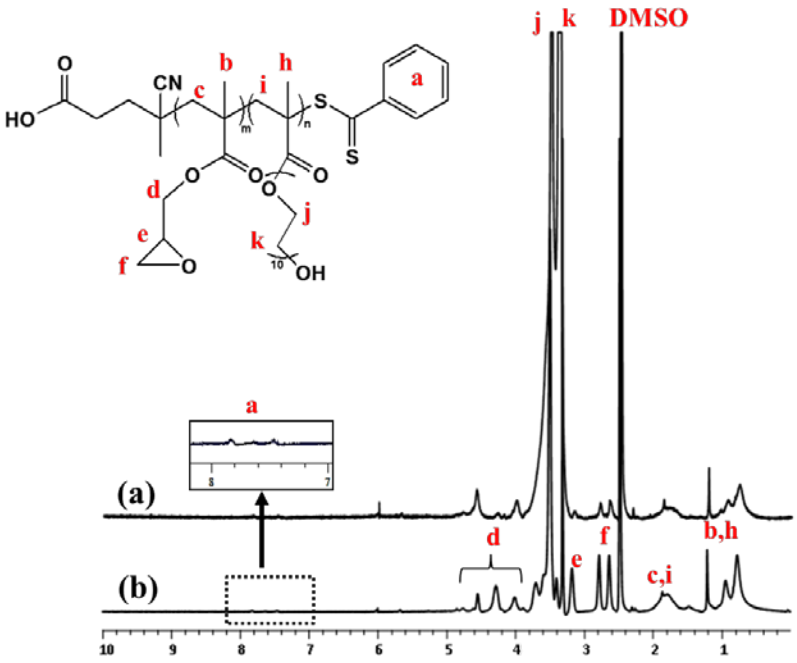


**Figure 4.1** $^{1}$H NMR spectra of P(GMA-*co*-PEGMA) in solution prepared by RAFT polymerization having GMA:PEGMA of (a) 30:70 and (b) 70:30.

**Table 4.4** Characteristics of P(GMA-*co*-PEGMA) synthesized by RAFT polymerization.

| Entry | GMA:PEGMA mole ratio (target) | GMA:PEGMA mole ratio (observed) | Mn (calculated) | Mn (observed) |
|---|---|---|---|---|
| 1 | 30:70 | 21:79 | 59199 | 51921 |
| 2 | 70:30 | 74:26 | 41759 | 43883 |

The success of stepwise surface modification of filter paper was confirmed by FT-IR as displayed in **Figure 4.2**. The FT-IR spectrum of the initiator-immobilized filter paper **(Figure 4.2b)** shows a band at 1738 $cm^{-1}$ (C=O stretching) which does not appear in the unmodified filter paper (**Figure 4.2a**) suggesting that ester linkage was formed between the filter paper and carboxyl-containing initiator. The spectrum of P(GMA-*co*-PEGMA)-grafted filter paper (**Figure 4.2c**) exhibits a band at the same position which is also a characteristic C=O stretching of ester groups in the copolymer and a band at 910 $cm^{-1}$ corresponding to C-O-C stretching of epoxide group of GMA. The relative peak intensity ratio between C-O-C stretching (910 $cm^{-1}$) and C=O

stretching (1738 $cm^{-1}$) was found to be correspondingly increased as a function of GMA content in the copolymer (**Figure 4.2c and 4.2d**). The intensity decrease of C-O-C stretching at 910 $cm^{-1}$ found in the spectrum of P(GMA-*co*-PEGMA)-grafted filter paper after being conjugated with PNA capture probe (**Figure e**) suggested that the epoxide groups were consumed by reacting with the PNA capture probe via epoxide ring opening.

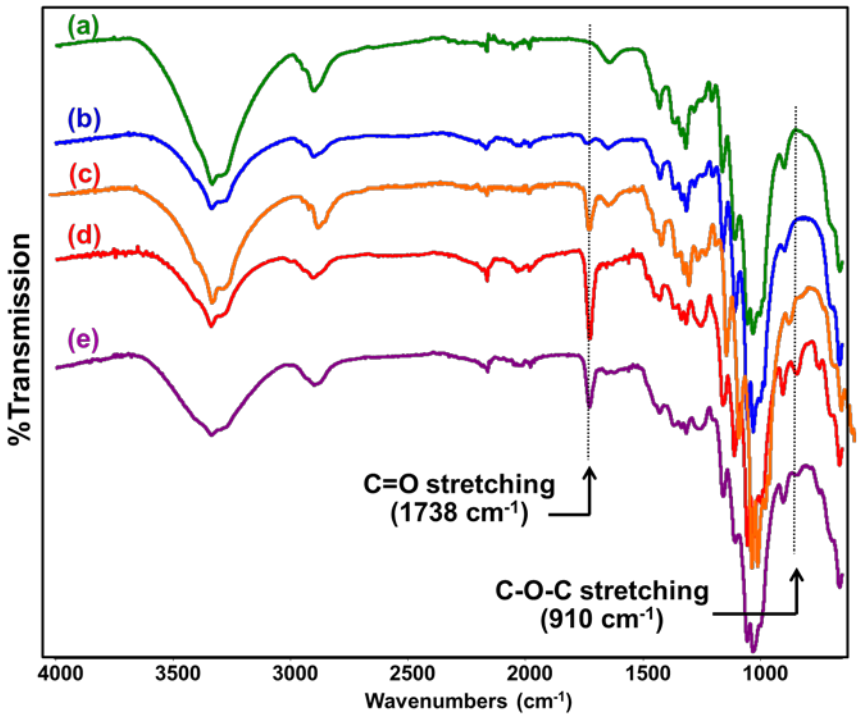


**Figure 4.2** FT-IR spectra of the filter paper: (a) unmodified, (b) immobilized with initiator, grafted with P(GMA-*co*-PEGMA) having GMA:PEGMA of (c) 30:70 and (d) 70:30, and (e) grafted with P(GMA-*co*-PEGMA) having GMA:PEGMA = 70:30 and conjugated with PNA capture probe.

As illustrated in **Figure 4.3**, there were no noticeable microscopic changes in morphology of the filter paper undergoing initiator immobilization and copolymer grafting suggesting that the coated polymer layer is relatively thin. Nevertheless, the filter paper grafted with P(GMA-*co*-PEGMA) exhibits better tearing resistance as opposed to the unmodified filter paper, especially after repetitive exposure to variety of solutions during PNA probe conjugation and DNA hybridization studies.

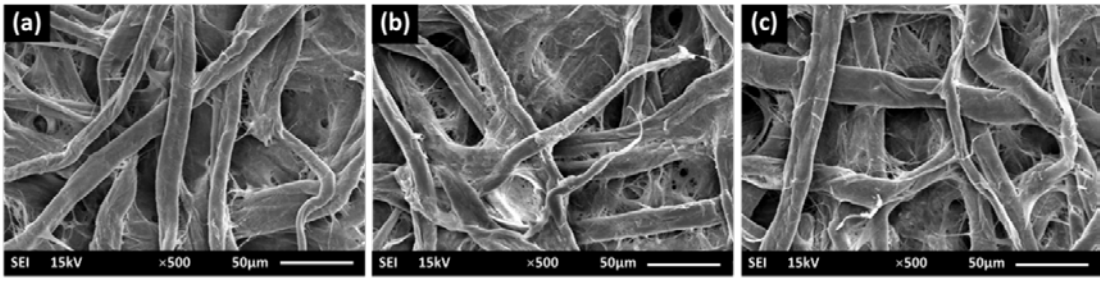


**Figure 4.3** SEM images of the filter paper: (a) unmodified, (b) immobilized with initiator, and (c) grafted with P(GMA-*co*-PEGMA) having GMA:PEGMA = 70:30.

**Immobilization of PNA capture probe on the P(GMA-co-PEGMA)-grafted filter paper**

In principle, the epoxide ring opening can be promoted under basic condition. To be able to monitor the effect of a base (TEA in this particular case) addition or pH of buffer on immobilization efficiency by fluorescence microscopy, the fluorescence-labeled PNA (flu-o-PNA(T9)-Lys$NH_2$) was used as a model for PNA capture probe. Firstly, different TEA concentration (0.1, 0.2 and 0.3 μM) was introduced to PNA solution dissolved in 0.1 M phosphate buffer. According to the fluorescence images shown in **Figure 4.4**, an intensity of green illumination of the spots became stronger as a function of TEA concentration indicating that the PNA conjugation was quantitatively improved upon base addition. It should be noted that pH of the PNA solution was not altered after TEA addition. Alternatively, the enhancement of PNA conjugation was much more pronounced once buffer solution was used instead of the 0.1 M phosphate buffer (**Figure 4.5**). The strongest fluorescence intensity which indicated the maximum immobilization quantity, was achieved for the conjugation in buffer solution having pH 10.0 (0.1 M $NaCO_3$-$NaHCO_3$ buffer). Notably, low background illumination was also found on most of the controlled unmodified filter paper implying a certain level of nonspecific adsorption of the flu-o-PNA(T9)-Lys$NH_2$.

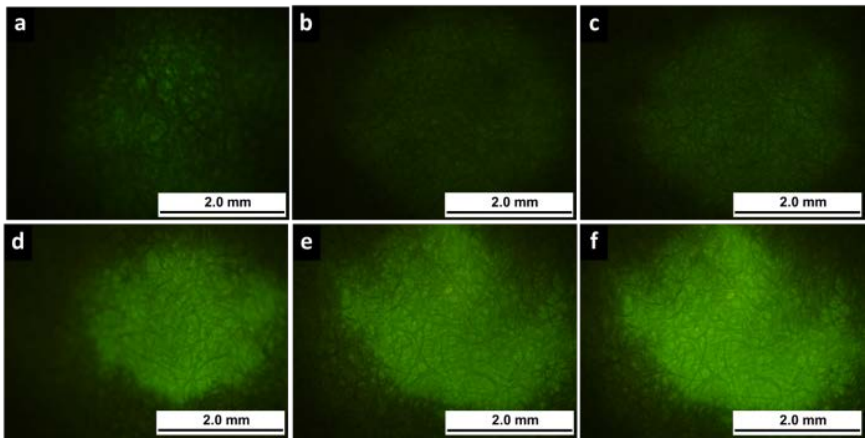


**Figure 4.4** Fluorescence images of filter paper after flu-o-PNA(T9)-Lys$NH_2$ conjugation in 0.1 M phosphate buffer with added TEA of (a,d) 0.1, (b,e) 0.2, and (c,f) 0.3 μM : (a-c) unmodified filter paper; (d-f) P(GMA-*co*-PEGMA)-grafted filter paper (GMA:PEGMA = 70:30)

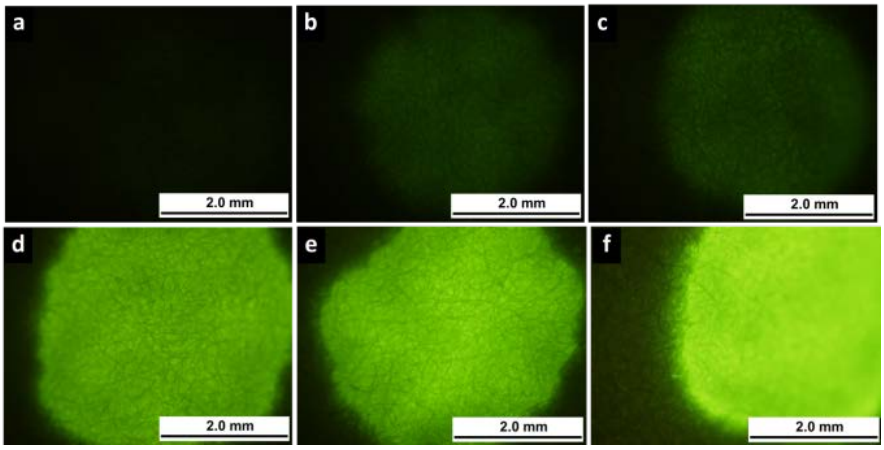


**Figure 4.5** Fluorescence images of filter paper after flu-o-PNA(T9)-Lys$NH_2$ conjugation in buffer solution having pH of (a,d) 8.0, (b,e) 9.0, and (c,f) 10.0: (a-c) unmodified filter paper; (d-f) P(GMA-*co*-PEGMA)-grafted filter paper (GMA:PEGMA = 70:30).

To further chemically identify whether the PNA capture probe can be bound onto the P(GMA-*co*-PEGMA)-grafted filter paper, XPS analysis of the P(GMA-*co*-PEGMA)-grafted filter paper after conjugation with another model of PNA capture probe, the pentafluorobenzenesulfonyl-labeled PNA (penta-PNA(T9)-Lys$NH_2$) using the selected solutions previously employed for fluorescence studies: 0.1 M phosphate buffer with added 0.1, 0.2, and 0.3 mm TEA and buffer solution of pH 10 was performed. This

fluorine-tagged PNA provides additional fluorine atoms in its structure enabling a convenient identification of its existence from fluorine composition. From the XPS atomic composition data presented in **Table 4.5**, the fluorine content of ~0.6 %. was detected on all substrates after conjugation verifying that the top most surface (< 5 nm, the sampling depth of XPS technique) of the P(GMA-*co*-PEGMA)-grafted filter paper were saturatedly covered with relatively same amount of penta-PNA(T9)-Lys$NH_2$, independent of conjugation condition. From application viewpoint, fluorescence technique is therefore more appropriate to probe the extent of PNA conjugation than the highly surface sensitive technique like XPS, given that the detection relies not only on solution adsorption on top of the surface but also absorption to a certain depth within the paper-based platform.

This investigation suggested that the attachment of PNA probe is apparently more efficient under basic condition so that the conditions with added 0.1 μM TEA in 0.1 phosphate buffer and in buffer solution of pH 10 were selected for the step of PNA capture probe immobilization on P(GMA-*co*-PEGMA)-grafted filter paper to be further analyzed for DNA detection.

**Table 4.5** Atomic composition of surface-modified filter paper as determined by XPS analysis.

| Sample | Atomic composition (%) | | | | |
|---|---|---|---|---|---|
| | C | O | N | F | S |
| Immobilized with initiator | 53.41 | 43.45 | 3.15 | - | - |
| Grafted with P(GMA-*co*-PEGMA) | 57.00 | 41.15 | 1.58 | - | 0.27 |
| Immobilized with penta-PNA(T9)-$LysNH_2$ in 0.1 M PBS pH 7.4 | 57.20 | 39.98 | 1.95 | 0.60 | 0.28 |
| Immobilized with penta-PNA(T9)-$LysNH_2$ in 0.1 M PBS pH 7.4 with 0.1 μM TEA | 61.14 | 36.41 | 1.53 | 0.59 | 0.34 |
| Immobilized with penta-PNA(T9)-$LysNH_2$ in 0.1 M PBS pH 7.4 with 0.3 μM TEA | 64.09 | 33.73 | 1.23 | 0.65 | 0.29 |
| Immobilized with penta-PNA(T9)-$LysNH_2$ in 0.1 M $NaCO_3$-$NaHCO_3$ pH 10.0 | 61.84 | 35.72 | 1.51 | 0.62 | 0.31 |

**Colorimetric detection for DNA sequence by sandwich-hybridization assay**

The P(GMA-*co*-PEGMA)-grafted filter paper was tested for its efficiency as a sensing platform for DNA sequence analysis by sandwich-hybridization assay employing two PNA probes of which sequences are designed in response to DNA sequences in human leukocyte antigen (HLA) alleles. In particular, this research focuses on HLA-B*1502 alleles having strong correlation with a severe skin disorder called Stevens-Johnson syndrome in response to carbamazepine (a drug used to treat seizures).[25] PNA(Cap) of a 12-base sequence of Ac-GGAACCTGCGCG-$LysNH_2$ was used as the capture probe to be immobilized on the surface of P(GMA-*co*-PEGMA)-grafted filter paper for capturing the DNA target. b-PNA (Ser), a biotinylated PNA probe having a sequence of b-o-o-AACACACAGACT-SerOH was used as a reporter probe to generate a signal upon enzymatic amplification using the optimal condition (in terms of substrate/enzyme concentration and activation time) previously identified by Laopa *et al*.[15] Two formats of the test results are displayed: scanned images (column A) and

profile images as analyzed by Scion Image (column B). The profile image provides the semi-quantitative intensity of the colorimetric readout. Details of DNA and PNA sequences and the description of samples/probes applied in each spot (1–6) are shown in **Table 4.2 and 4.3,** respectively. A biotinylated PNA (b-PNA(Lys)) having the same sequence as the reporter probe (b-PNA(Ser)) was immobilized on the position 1 as a positive control to illustrate the maximum signal generated by the enzymatic reaction. A biotinylated DNA (b-DNA) was spotted on the position 2 as another positive control to demonstrate that enzymatic signal amplification via hybridization can be achieved once the PNA is complementary with the DNA.

From the results shown in **Figure 4.6**, the position 3 with DNA 1 which is complementary to the PNA capture probe (PNA(Cap)) shows yellow spots visible by the naked eyes with similar intensity to that of the positive control on the position 2 but with much stronger intensity than that of the position 4 with the non-complementary DNA 2. Apparently, the filter paper grafted with the copolymer with greater composition of PEGMA (GMA:PEGMA = 30:70) shows a much better signal readout implying that the ability to suppress non-specific adsorption by hydrophilic PEGMA entities are very important for the detection efficiency.

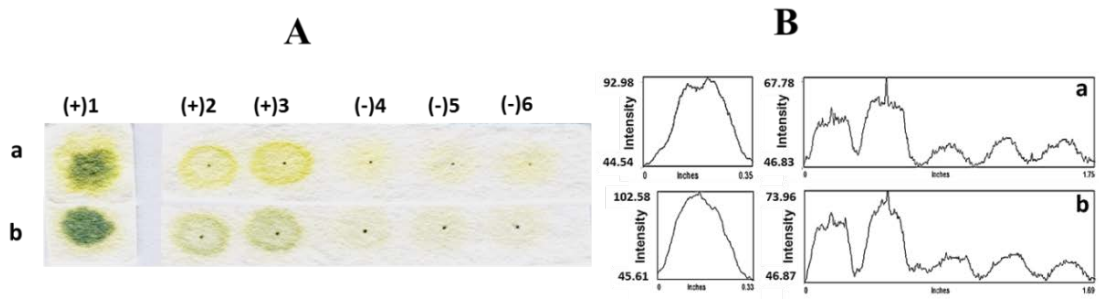


**Figure 4.6** Representative images (column A: scanned image and column B: profile image) of the test results demonstrating the copolymer composition of GMA:PEGMA (a) 30:70, (b) 70:30.

Another test was conducted on the P(GMA-*co*-PEGMA)-grafted filter paper conjugated with PNA(Cap) in 0.1 phosphate buffer containing 0.1 M TEA to determine an impact of ionic strength of DNA binding solution on DNA hybridization efficiency. As revealed in **Figure 4.7**, very strong signal readout on position 1 and 2 which was spotted with b-PNA(Lys) as a control for reporter probe indicated that the signal amplification through biotin-SA-HRP conjugation function efficiently. A relatively

strong signal appearing at position 3 spotted with the complementary DNA sequence preliminarily signify the specificity of the test. Upon increasing ionic strength of DNA hybridization step by NaCl addition from 10 mM to 100 mM NaCl not only can increase the signal intensity, but also suppressed non-specific adsorption from non-complementary DNA sequence [(-4)], reporter probe [(-5)], and SA-HRP [(-6)], allowing more effective discrimination. It was found that 0.5 mM phosphate buffer pH 7.4 with added 100 mM NaCl (**row C, Figure 4.7**) gave highest signal. For this reason, it was chosen as the hybridization buffer for all subsequent experiments.

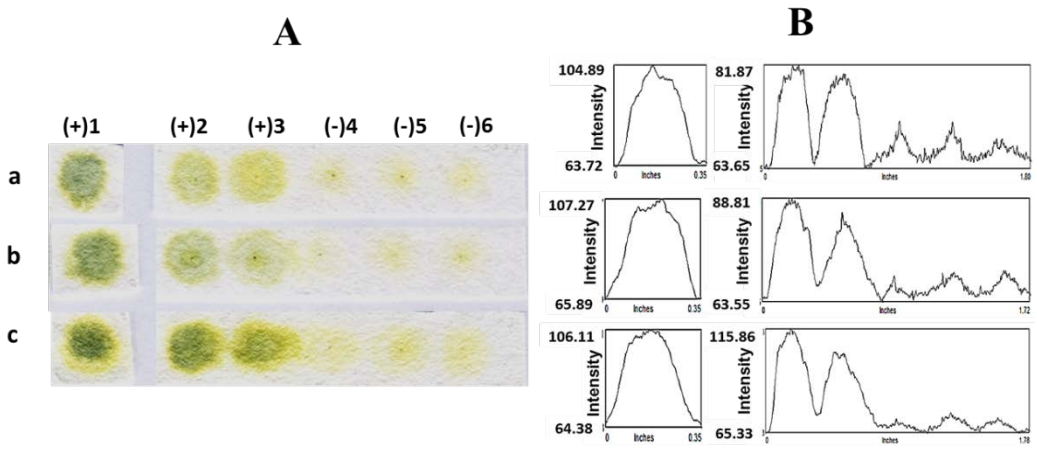


**Figure 4.**7 Representative images (column A: scanned image and column B: profile image) of the test results demonstrating the effect of salt addition to the hybridization buffer (0.5 mM phosphate buffer) : (a) 10 mM NaCl, (b) 50 mM NaCl, and (c) 100 mM NaCl.

To compare the effect of PNA capture probe bound quantity and binding efficiency, three conditions for PNA(Cap) conjugation on the P(GMA-*co*-PEGMA)-grafted filter paper were employed: in 0.1 PBS pH7.4 with added 0.1 or 0.3 μM TEA and in buffer solution of pH 10, which supposedly yielded varied quantity of bound PNA(Cap) from low to high as previously identified by fluorescence microscopic analysis. The results shown in **Figure 4.8** demonstrate that the detection efficiency which can be judged from the ability to provide high intensity signal to the complementary DNA 1[(+3)] as opposed to the non-complementary DNA3[(-4)] and simultaneously suppress non-specific adsorption of b-PNA(Ser) [(-5)] and SA–HRP [(-6)] seems to be inversely proportional to the immobilized PNA(Cap) quantity. This unexpected outcome may be

described as a result of the high probe density that restricts the accessibility of the target DNA. Therefore, the quantity of PNA(Cap) immobilized on the P(GMA-*co*-PEGMA)-grafted filter paper which was obtained from the immobilization in 0.1 M PBS pH 7.4 containing 0.1 μM TEA was optimal for DNA hybridization.

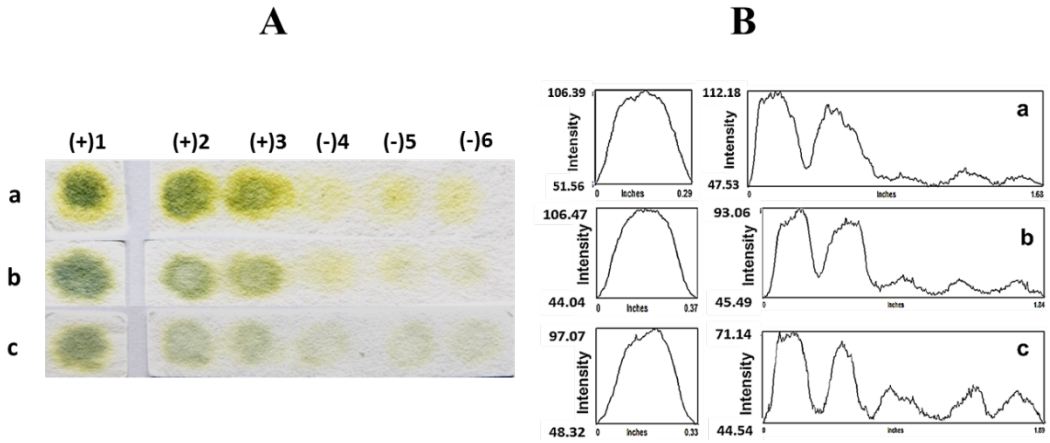


**Figure 4.8** Representative images (column A: scanned image and column B: profile image) of the test results demonstrating the effect of PNA(Cap) immobilization condition: in 0.1 M PBS pH 7.4 with added TEA of (a) 0.1 and (b) 0.3μM , and (c) in buffer solution pH 10.

DNA 2, another DNA sequence having one base mismatch from the complementary DNA, DNA1 was subjected to the test. Detail of DNA and PNA sequences and description of samples/probes applied in each spot (1-7) of this particular test are illustrated in **Table 4.6**. From the results shown in **Figure 4.9**, the DNA 1[(+3)] which is complementary to the PNA(cap) show green spots visible by the naked eyes with similar intensity to that of the positive control b-PNA(Lys) [(+1)] and b-DNA [(+2)]. This illustrated an excellent specificity to distinguish single base mismatches [(-4)] and non-complementary [(-5)] in the DNA targets.

**Table 4.6** Description of DNA and PNA sequences used for each spot of the test results shown in Figure 4.9

| Sequence | Spot position | | | | | | |
|---|---|---|---|---|---|---|---|
| | **1** | **2** | **3** | **4** | **5** | **6** | **7** |
| DNA | - | b-DNA | DNA 1 | DNA 2 | DNA 3 | - | - |
| PNA | b-PNA(Lys) | - | b-PNA(Ser) | b-PNA(Ser) | b-PNA (Ser) | b-PNA (Ser) | - |
| [a]Remark | (+) | (+) | (+) | (-) | (-) | (-) | (-) |

[a](+) = positive result, (-) = negative result

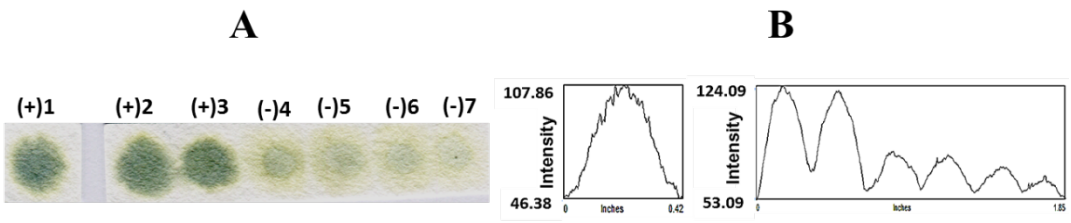


**Figure 4.9** Representative images (column A: scanned image and column B: profile image) of the test results demonstrating the specificity and efficiency of PNA(Cap) and b-PNA(Ser) to distinguish complementary, single mismatched and non-complementary DNA targets. The positive results are shown at b-PNA(Lys) [(+1)], b-DNA [(+2)] and DNA 1 [(+)3].

To determine the minimal quantity of DNA targets that can still allow a clear differentiation between fully complementary and single-mismatched DNA, the immobilized PNA(Cap) probe was hybridized with DNA1 and DNA2 at different concentrations ranging from 2 pmol to 10 fmol and detected using 2 pmol of b-PNA(Ser) probe. As presented in **Figure 4.10**, the detection limit of this colorimetric method is at least down to 100 fmol (equivalent to 1 µL of 100 nM DNA). Although this platform is 10 times less sensitive than the previously developed platform based on filter paper grafted with QPDMAEMA brushes (10 fmol detection limit), the inferior performance can be forgiven considering that the limitation of detection of DNA mixtures

can be overcome. Besides, the fact that the discrimination power was not sacrified via sandwich-hybridization assay of which the use of two PNA probes was required truly highlights the specificity of this acpcPNA system. It should be emphasized that the assay developed in this research does not at all require stringent washing condition (i.e. 20% acetonitrile in PBS buffer) to remove non-specific binding. This outcome suggested that the grafting of copolymer having ability to resist non-specific adsorption is also another key to the success of this developed assay.

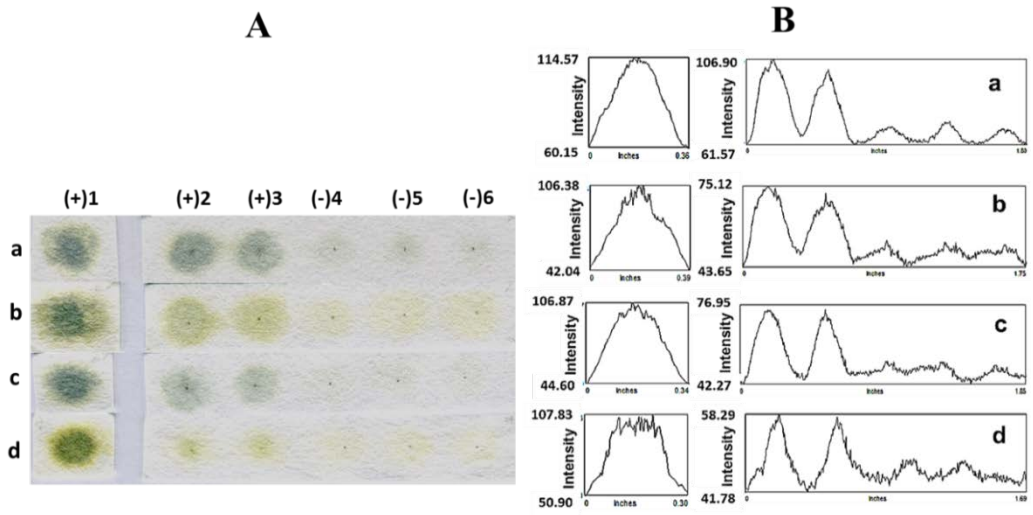


**Figure 4.10** Representative images (column A: scanned image and column B: profile image) of the test results demonstrating detection limit of complementary DNA 1 and single mismatched DNA 2 using 2 µL of 1 µM b-PNA(Ser) as probe: (a) 2 pmol (2 µL of 1 µM), (b) 1 pmol (1 µL of 1 µM), (c) 100 fmol (1 µL of 100 nM), and (d) 50 fmol (0.5 µL of 100 nM).

## CONCLUSIONS

In this work, it has been demonstrated that the P(GMA-*co*-PEGMA)-grafted filter paper can be prepared by SI-RAFT as characterized by FT-IR. Upon PNA capture probe immobilization, the developed paper-based platform can be used for DNA sequence determination using sandwich-hybridization assay. Immobilization of PNA capture probe in 0.1 M PBS pH 7.4 with added 0.1 µM TEA was the optimal condition. The best hybridization efficiency could be achieved at pH 7.0 in 0.5 mM phosphate buffer having added 100 mM NaCl. The enzymatic signal amplification by SA–HRP and OPD can discriminate complementary from single-mismatched and non-complementary

DNA targets at a detection limit of at least 100 fmol that can be observed by naked eye. It is anticipated that this P(GMA-*co*-PEGMA)-grafted filter paper can potentially be developed into an alternative paper-based platform for DNA sequence determination in a high throughput format.

## REFERENCES


1. Noor, M.O.; Hrovat, D.; Moaxami-Goudarzi, M.; Espi, G.S.; Krull, U.J., Ratiometric fluorescence transduction by hybridization after isothermal amplification for determination of zeptomole quantities of oligonucleotide biomarkers with a paper-based platform and camera-based detection. *Analytica Chimica Acta***2015**, *885*, 156-65.
2. Hyrup, B.; Nielsen, P. E., Peptide nucleic acids (PNA): Synthesis, properties and potential applications. *Bioorganic & Medicinal Chemistry* **1996,** *4* (1), 5-23.
3. Nielsen, P. E.; Egholm, M.; Berg, R. H.; Buchardt, O., Sequence-selective recognition of DNA by strand displacement with a thymine-substituted polyamide. *Science* **1991,** *254*, 1497-1500.
4. Vilaivan, T.; Srisuwannaket, C., Hybridization of pyrrolidinyl peptide nucleic acids and DNA: Selectivity, base-pairing specificity, and direction of binding. *Organic Letters* **2006,** *8* (9), 1897-1900.
5. Theppaleak, T., et al., Magnetite Nanoparticle with Positively Charged Surface for Immobilization of Peptide Nucleic Acid and Deoxyribonucleic Acid. *Journal of Biomedical Nanotechnology* **2013**, ***9(9)***, 1509-1520.
6. Boontha, B.; Nakkuntod, J.; Hirankarn, N.; Chaumpluk, P.; Vilaivan, T., Multiplex mass spectrometric genotyping of single nucleotide polymorphisms employing pyrrolidinyl peptide nucleic acid in combination with ion-exchange capture. *Analytical Chemistry* **2008,** *80* (21), 8178-8186.
7. Ananthanawat, C.; Vilaivan, T.; Hoven, V. P., Synthesis and immobilization of thiolated pyrrolidinyl peptide nucleic acids on gold-coated piezoelectric quartz crystals for the detection of DNA hybridization. *Sensors and Actuators B-Chemical* **2009,** *137* (1), 215-221.
8. Ananthanawat, C.; Vilaivan, T.; Mekboonsonglarp, W.; Hoven, V. P., Thiolated pyrrolidinyl peptide nucleic acids for the detection of DNA hybridization using surface plasmon resonance. *Biosensors and Bioelectronics* **2009,** *24* (12), 3544-3549.
9. Ananthanawat, C.; Vilaivan, T.; Hoven, V. P.; Su, X., Comparison of DNA, aminoethylglycyl PNA and pyrrolidinyl PNA as probes for detection of DNA hybridization using surface plasmon resonance technique. *Biosensors and Bioelectronics* **2010,** *25* (5), 1064-1069.
10. Thipmanee, O.; Samanman, S.; Sankoh, S.; Numnuam, A.; Limbut, W.; Kanatharana, P.; Vilaivan, T.; Thavarungkul, P., Label-free capacitive DNA sensor using immobilized pyrrolidinyl PNA probe: effect of the length and terminating head group of the blocking thiols. *Biosensor and Bioelectronics* **2012,** *38* (1), 430-435.

11. Sankoh, S.; Samanman, S.; Thipmanee, O.; Numnuam, A.; Limbut, W.; Kanatharana, P.; Vilaivan, T.; Thavarungkul, P., A comparative study of a label-free DNA capacitive sensor using a pyrrolidinyl peptide nucleic acid probe immobilized through polyphenylenediamine and polytyramine non-conducting polymers. *Sensors and Actuators B: Sensors and Actuators B: Chemical* **2013,** *177*, 543-554.
12. Jampasa, S.; Wonsawat, W.; Rodthongkum, N.; Siangproh, W.; Yanatatsaneejit, P.; Vilaivan, T.; Chailapakul, O., Electrochemical detection of human papillomavirus DNA type 16 using a pyrrolidinyl peptide nucleic acid probe immobilized on screen-printed carbon electrodes. *Biosensors and Bioelectronics* **2014,** *54*, 428-434.
13. Liang, L.; Su, M.; Li, L.; Lan F.; Yang, G.; Ge, S.; Yu, J.; Song, X., Aptamer-based fluorescent and visual biosensor for multiplexed monitoring of cancer cells in microfluidic paper-based analytical devices. *Sensors and Actuators B: Chemical* **2016**, *229*, 347-354.
14. Zhou, F., M.; Noor, O.; Krull, U., J., A Paper-Based Sandwich Format Hybridization Assay for Unlabeled Nucleic Acid Detection Using Upconversion Nanoparticles as Energy Donors in Luminescence Resonance Energy Transfer. *Nanomaterials* **2015**, *5(4*), 1556-1570.
15. Laopa, P.S.; Vilaivan, T.; Hoven, V. P., Positively charged polymer brush-functionalized filter paper for DNA sequence determination following Dot blot hybridization employing a pyrrolidinyl peptide nucleic acid probe. *Analyst* **2013,** *138* (1), 269-277.
16. Jirakittiwut, N.; Panyain, N.; Nuanyai, T.; Vilaivan, T.; Praneenararat, T., Pyrrolidinyl peptide nucleic acids immobilised on cellulose paper as a DNA sensor. *RSC Advances* **2015,** *5* (31), 24110-24114.
17. Liu, Y.; Wang, W.; Hu, W.; Lu, Z.; Zhou, X.; Li, C. M., Highly sensitive poly[glycidyl methacrylate-co-poly(ethylene glycol) methacrylate] brush-based flow-through microarray immunoassay device. *Biomedical Microdevices* **2011,** *13* (4), 769-777.
18. Akkahat, P.; Hoven, V. P., Introducing surface-tethered poly(acrylic acid) brushes as 3D functional thin film for biosensing applications. *Colloids and Surfaces. B, Biointerfaces* **2011,** *86* (1), 198-205.
19. Li, X.; Wang, M.; Wang, L.; Shi, X.; Xu, Y.; Song, B.; Chen, H., Block copolymer modified surfaces for conjugation of biomacromolecules with control of quantity and activity. *Langmuir* **2013,** *29* (4), 1122-1128.
20. Li, C. Y.; Xu, F. J.; Yang W. T., Simple strategy to functionalize polymeric substrates via surface-initiated ATRP for biomedical applications. *Langmuir* **2013,** *29* (5), 1541-1550.
21. Hansson, S.; Östmark, E.; Carlmark, A.; Malmström, E., ARGET ATRP for versatile grafting of cellulose using various monomers. *ACS Applied Materials & Interfaces* **2009,** *1* (11), 2651-2659.
22. Bernand-Mantel, D.; Chehimi, M. M.; Millot, M. C.; Carbonnier, B., Protein-functionalized ultrathin glycidyl methacrylate polymer grafts on gold for the development of optical biosensors : An SPR investigation. *Surface and Interface Analysis* **2010,** *42* (6-7), 1035-1040.

23. Zhang, N.; Appella, D. H., Colorimetric detection of Anthrax DNA with a peptide nucleic acid sandwich-hybridization assay. *Journal of the American Chemical Society* **2007,** *129* (27), 8424-8425.
24. Ananthawat, C., Development of DNA sensor based on peptide nucleic acid and surface plasmon resonance. Doctoral disertation, Program in Macromolecular Science, Faculty of Science, Chulalongkorn University, 2009.
25. Ferrell, P. B. Jr.; McLeod, H. L., Carbamazepine, HLA-B*1502 and risk of Stevens- Johnson syndrome and toxic epidermal necrolysis: US FDA recommendations. *Pharmacogenomics* **2008,** *9* (10), 1543-1546.

# Chapter V

## Formation of Thermo-Sensitive and Cross-Linkable Micelles by Self-Assembly of Poly(pentafluorophenyl acrylate)-containing Block Copolymer

### INTRODUCTION

Amphiphilic block copolymer micelles assembled from thermo-responsive polymers have been extensively investigated for various applications in the field of controlled drug/gene delivery and biotechnology.[1-5] Poly(*N*-isopropylacrylamide) (PNIPAM) is one of the most investigated temperature-sensitive component to be incorporated into block copolymers due to its lower critical solution temperature (LCST) of approximately 32$^{o}$C in aqueous solution, being close to human body temperature.[6] When combined with a hydrophobic block, PNIPAM yields copolymer that would self-assemble into micelles having thermo-responsive shell, which is capable of encapsulating hydrophobic molecules within the core. Upon heating above the LCST, the micellar structure should be deformed and released the hydrophobic molecules. Okano's research team has performed pioneering work on polymeric micelles with temperature-triggered drug release mechanisms using block copolymers comprising PNIPAM and various hydrophobic polymers.[7,8] Temperature-responsive micelles with biodegradable cores have been also developed.[9,10] Similar works have been studied by Liu *et al.*[11] and Zhu *et al.*[12] for the release of doxorubicin and paclitaxel, respectively.

However, a major drawback of these self-assembled micelles is their instabilities under certain changes in biological systems. Stabilization has often been achieved by chemical cross-linking of the shell or the core of the micelles.[3,13,14] One of the most effective methods is to incorporate reactive functional groups onto the backbone of the copolymers. The constructed micelles undergo cross-linking upon an addition of a bifunctional reagent. In 2007, Zhang and co-workers fabricated double hydrophilic block copolymer micelles from poly(ethylene oxide)-*b*-poly(*N*-isopropylacrylamide-*co*-*N*-

acryloxysuccinimide) (PEO-*b*-P(NIPAM-*co*-NAS), which formed micelles by heating a copolymer solution above its LCST. Stabilization of the P(NIPAM-*co*-NAS) cores was accomplished via the reaction of NAS residues with cystamine.[15] Similarly, Li and co-workers prepared thermally responsive micelles by self-assembly of triblock copolymer of poly(ethylene oxide)-*block*-(*N,N′*-dimethylacrylamide-*stat*-*N*-acryloxysuccinimide)-*block*-poly(*N*-isopropylacrylamide) (PEO-*b*-(DMA-*s*-NAS)-*b*-NIPAM). Incorporation of the NAS units into the triblock copolymer allows for shell cross-linked (SCL) micelles by reaction with difunctional primary amines. These SCL micelles swell when the solution temperature is lower than the LCST. of the NIPAM block.[16] Despite its high reactivity, *N*-acryloxysuccinimide (NAS) suffers from its hydrolytic instability and limited solubility in organic media (only soluble in dimethylformamide or dimethyl sulfoxide) that restrict their applications. Monomer having active pentafluorophenyl ester, pentafluorophenyl (meth)acrylate (PFP(M)A), has been recently introduced as alternative to NAS due to its better solubility in many common organic solvents and higher hydrolytic stability in water and air than NAS.[17,18] Additional advantage lies on the fact that the reaction of the pentafluorophenyl ester groups can be conveniently monitored by $^{19}$F NMR spectroscopy.[19] Duong and co-workers prepared well-defined functional nanoparticles from poly(oligo(ethylene glycol) methyl ether acrylate)-*block*-poly(vinylbenzyl chloride-*co*-pentafluorophenyl acrylate) (P(OEG-A)-*b*-P(VBC-*co*-PFPA)). The nanoparticles were subsequently stabilized by a reaction of active pentafluorophenyl moieties with diamine. The polymer nanoparticles were found to be suitable for hydrophobic drug encapsulation.[20] Recently, Zhuang and co-workers have developed water-dispersible nanogels based on random copolymer of pentafluorophenyl acrylate and poly(ethylene glycol methacrylate) having diamine as a cross-linker. Isopropylamine and *N,N′*-dimethylethylene diamine were incorporated onto the core-cross-linked nanogel to demonstrate the possibility of surface engineering. These nanogels can encapsulate lipophilic guest molecules during the cross-linking step of the nanogel synthesis.[21]

Another interesting approach to obtain stable micelles is using photo/UV-labile linker. In general, a light-responsive behavior of polymer can either be reversible or irreversible, depending on the chromophore that is attached to the polymeric backbone or to the chain end. Recently, an irreversible light-responsive moiety of *ortho*-nitrobenzyl (ONB) derivatives has attracted increasing interest in biochemistry and synthetic chemistry

as photo-labile protecting groups and has been introduced to polymer structure as photo-cleavable units.[22,23] Jiang and co-workers nicely demonstrated the use of ONB as a side chain functionality to prepare light-responsive block copolymeric micelles of poly(ethylene oxide) (PEO) and poly(2-nitrobenzyl methacrylate) (PNBM). The micelles were capable of entrapping dyes with the intention of releasing them at a defined time and location.[24] However, controlling the polymerization of ONB-containing monomers is still difficult because nitroaromatic compounds can act as inhibitors/retardants during the radical polymerization process.[25] Post-polymerization modification is a versatile method for the introduction of such chemical functionality that would otherwise interfere with the polymerization process.[25]

Reversible addition-fragmentation chain transfer (RAFT), a commonly used controlled radical polymerization process, provides a versatile route to the generation of amphiphilic block copolymer with controllable features, such as block length, structure, and molecular weight.[26-28] It is compatible with a wide range of functional monomers and does not require the use of (transition metal) catalyst. One can achieve precisely defined reactive polymer structures. This procedure enables the synthesis of polymeric architectures, which cannot be realized by the classical way of radical copolymerization.[29]

This research aims to develop thermo-responsive micelles of which cores are cross-linkable via light-trigger process from block copolymers consisting of pentafluorophenyl acrylate (PFPA) and *N*-isopropylacrylmide (NIPAM), to the best of our knowledge, has never been reported before. It is anticipated that RAFT polymerization under optimized conditions can yield well-defined block copolymers with controlled molecular weights and narrow polydispersities. Subsequent post-polymerization modification of the copolymers is performed to incorporate light-responsive moieties of *ortho*-nitrobenzyl (ONB) into the PFPA block of the copolymers. Finally, the ONB-containing copolymers are self-assembled into micelles. The stabilization of core is subsequently induced by UV irradiation. It is anticipated that the residual PFPA moieties in the copolymers should be available for further chemical modification with bioactive species and allow for physical encapsulation of desired hydrophobic molecules. These should make the developed core-cross-linked (CCL) micelles of PNIPAM-containing copolymers more useful in many advanced applications.

## EXPERIMENTAL

### Materials

All solvents used for reactions are reagent grade and used as received, unless otherwise specified. Anhydrous 1,4-dioxane (99.9%) were obtained from Merck. Anhydrous tetrahydrofuran (THF, 99.9%) was obtained from Sigma-Aldrich. Dichloromethane was dried over $CaH_2$ under reflux and nitrogen atmosphere. Solutions were made with Milli-Q water purified by Millipore Milli-Q system that involves reverse osmosis, ion exchange, and filtration steps (18.2 MΩ). The NMR solvents such as $CDCl_3$ (99.8% D), DMSO-d6 (99.9%), and $D_2O$ (99.9% D) were obtained from Cambridge Isotope Laboratories, Inc. (USA). 4-Cyanopentanoic acid dithiobenzoate (CPADB, 97%), triethylamine (TEA, 99.5%), 4-Nitro-7-piperazino-2,1,3-benzoxadiazole (NBD) (99.0%), pyrene (98%), 2-nitrobenzyl bromide (98%), and *N,N′*-dimethylethylenediamine (85%) were purchased from Sigma-Aldrich and used as received. *N*-isopropylacrylamide (NIPAM, 97%) was obtained from Sigma-Aldrich and recrystallized twice in hexane before use. Pentafluorophenol (99%) was commercially available from Merck and used as received. Azobisisobutyronitrile (AIBN, 98%) was obtained from Fluka and used as received. Acryloyl chloride was purchased from Acros and used as received.

### Instrumentation

$^{1}$H NMR spectra were recorded on a Varian, model Mercury-400 nuclear magnetic resonance spectrometer (USA) operating at 400 MHz, and $^{19}$F NMR spectra were recorded on a Bruker DRX 400 FT-NMR spectrometer. Chemical shifts ($\delta$) were reported in part per million (ppm) relative to tetramethylsilane (TMS) signal as a reference. FT-IR spectra were recorded with a Nicolet Impact 6700 FT-IR spectrometer with 32 scans at a resolution of 4 $cm^{-1}$ in a frequency range of 400-4000 $cm^{-1}$. Samples were pressed into potassium bromide (KBr) pellets. UV-vis spectra were recorded on an Agilent 8453 UV-vis spectroscopy. Molecular weight and molecular weight distribution of synthesized (co)polymers were analyzed by gel permeation chromatography (GPC) using Waters 600 controller chromatograph equipped with HR1 and HR4 columns (Waters, MW resolving range =100-500,000 g/mol) at 35$^{o}$C and refractive index (RI) detector (Waters 2414). THF was used as an eluent with the flow rate of 1.0 mL/min. Sample injection volume was 80 µL. Five polystyrene standards (996-188,000 g/mol) were used for generating a calibration curve.

The hydrodynamic diameters of micelles were measured using a dynamic light scattering (DLS) instrument (Zetasizer Nano ZS, Malvern Instrument Ltd., U.K. equipped with a He-Ne laser beam at 658 nm) at a fixed scattering angle of 173°. The sample refractive index (RI) was set at 1.59 for polystyrene. The dispersant viscosity and RI were set to 0.89 $Ns \cdot m^2$ and 1.33, respectively. All samples (1.0 mg/mL) were filtered through a 0.45 μm syringe filter prior to analysis, and each measurement was repeated at least ten times to obtain the average value with an equilibrium time of 5 min before each measurement. Transmission electron microscopy (TEM) studies were performed on a JEOL Model JEM-2100 electron microscope operating at an acceleration voltage of 100 kV. Samples were prepared by drop-casting of a given micelle solution onto carbon-coated copper grid and excess solution was carefully blotted off using filter paper. The samples were then air-dried at room temperature before measurement.

**Synthesis of *ortho*-nitrobenzyl (ONB) protected diamine**

ONB-protected diamine was synthesized according to a method modified from that of Zhao *et al.*[25] 2-Nitrobenzyl bromide (1.0 g, 4.6 mmol), *N,N′*-diethylethylenediamine (4 mL, 37.2 mmol), and dry dichloromethane (20 mL) were added into a round bottom flask. The reaction mixture was stirred in the dark place at room temperature overnight. After that, the solution was extracted with distilled water for 3 times. The filtrate was dried over anhydrous sodium sulfate ($Na_2SO_4$) and dichloromethane was then removed using rotary evaporator. The pure yellow liquid was obtained (0.69 g (3.2 mmol, 70% yield). $^1$H NMR (400 MHz, $CDCl_3$): $\delta$/ppm: 7.89-7.27 (m, 4H), 3.79 (d, 2H), 2.63-2.52 (m, 4H), 2.46 (s, 3H), 2.04 (s, 3H).

**Synthesis of pentafluorophenyl acrylate (PFPA)**

Pentafluorophenyl acrylate (PFPA) was synthesized according to the method of Jochum *et al.*[30] Pentafluorophenol (40.0 g, 0.22 mol) was dissolved in 250 mL of dry dichloromethane in round bottom flask. Triethylamine (TEA) (36.2 mL, 0.26 mol) was slowly added to the reaction mixture on ice bath, and acryloyl chloride (21.1 mL, 0.26 mol) was then slowly added. After being removed from the ice bath, the reaction mixture was stirred at room temperature overnight. The precipitate of triethylamine hydrochloride salt was filtered, washed thoroughly with dichloromethane. The filtrate was extracted twice with

acidic water (pH=2.0), and twice with basic solution ($Na_2CO_3$), and finally twice with DI water. The organic phase was dried over anhydrous sodium sulfate ($Na_2SO_4$), and dichloromethane was removed using rotary evaporator. The crude product was further purified by column chromatography (column material: silica gel; solvent: petroleum ether). The pure colorless liquid was obtained (26.3 g, 0.16 mol, 75% yield) and stored in refrigerator at -20°C. $^1$H NMR (400 MHz, $CDCl_3$): $\delta$/ppm: 6.70 (d, 1H), 6.35 (dd, 1H), 6.16 (d, 1H); $^{19}$F NMR ($CDCl_3$): $\delta$/ppm: -162 (d, 2F), -157 (t, 1F), -153 (d, 2F); FT-IR (ATR-mode): 1772 cm$^{-1}$ (C=O reactive ester band), 1516 cm$^{-1}$ (C=C aromatic band).

**Synthesis of poly(pentafluorophenyl acrylate) (PPFPA)**

PPFPA was synthesized according to the method published recently.[30] Briefly, PFPA monomer (4.80 g, 20 mmol), CPADB (11 mg, 0.04 mmol), and AIBN (0.65 mg, 0.004 mmol) were added to a vial followed by 10 mL of dry 1,4-dioxane. The vial was sealed with a rubber septum and the solution was purged with argon gas for 30 min. The vial was then immersed into a thermo-stated oil bath at 70°C for 2 h. After immersing for 2 h, the polymer solution was precipitated in methanol, centrifuged, and dried under vacuum at room temperature. The dried polymer was then dissolved in THF and precipitated again in methanol. This procedure was repeated two times. The product was obtained as pink powder in 65% yield (3.10 g, 13 mmol). $^1$H NMR (400 MHz, $CDCl_3$): $\delta$/ppm: 3.10 (br, $CH_2C\underline{H}$), 2.51 (br, $C\underline{H_2}CH$), 2.13 (br, $C\underline{H_2}CH$); $^{19}$F NMR ($CDCl_3$): $\delta$/ppm: -163, -159, -153. FT-IR (ATR-mode): 1782 cm$^{-1}$ (C=O reactive ester band), 1515 cm$^{-1}$ (C=C aromatic band), 1090 cm$^{-1}$ (C-O ester band). The resulting PPFPA homopolymer was subsequently used as a macro chain transfer agent (macro CTA) for the polymerization of NIPAM.

**Synthesis of poly(PFPA)-*block*-poly(NIPAM) (PPFPA-*b*-PNIPAM)**

For the synthesis of diblock PPFPA-*b*-PNIPAM copolymer using RAFT polymerization, it is advisable to start with the monomer that shows higher transfer ability for the selected CTA.[31,32] In this case, PPFPA was first synthesized and used as a macro CTA for PNIPAM synthesis (**Scheme 5.1**). The purified PPFPA (0.32 g, 0.05 mmol), NIPAM (0.57 g, 5.04 mmol), and AIBN (0.5 mg, 0.003 mmol) were added to a vial followed by 6 mL of dry 1,4-dioxane. The vial was sealed with a rubber septum and the solution was purged with nitrogen gas for 30 min. Polymerization was conducted under nitrogen

atmosphere at 70°C for 12 h. The polymer solution was precipitated in hexane, centrifuged, and finally dried under vacuum at room temperature. The dried copolymer was then dissolved in THF and precipitated again in hexane. This procedure was repeated two times. The product was obtained as pink powder in 72% yield (1.29 g, 3.66 mmol). $^{1}$H NMR (400 MHz, $CDCl_3$): δ/ppm: 4.10 (br,–NHC<u>H</u>$(CH_3)_2$), 3.10 (br, $CH_2C\underline{H}$), 2.51-1.50 (m, protons in backbone), 1.13 (br, –NHCH($C\underline{H}_3)_2$); $^{19}$F NMR (DMSO-d6): δ/ppm: -172, -166, -162. FT-IR (ATR-mode): 1782 cm$^{-1}$ (C=O reactive ester band), 1645 cm$^{-1}$ (C=O of amide), 1515 cm$^{-1}$ (C=C aromatic band), 1090 cm$^{-1}$ (C-O ester band).

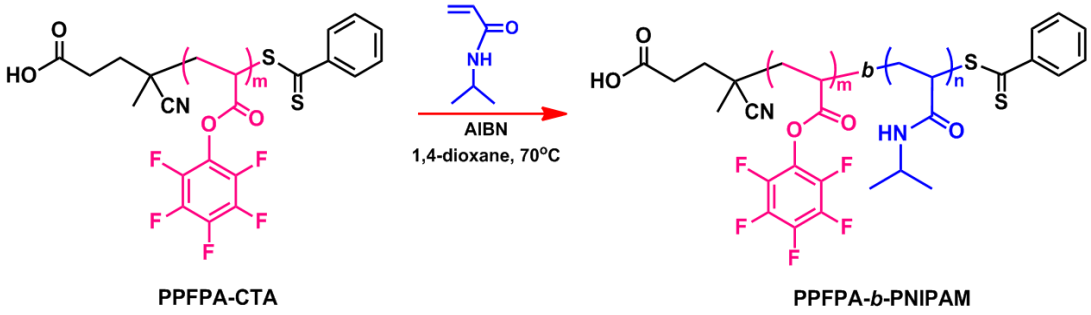


**PPFPA-CTA** **PPFPA-*b*-PNIPAM**

**Scheme 5.1** Synthetic pathway of PPFPA-*b*-PNIPAM by RAFT polymerization.

**Post-polymerization modification of PPFPA-*b*-PNIPAM with ONB-protected diamine**

Light-responsive moieties in the form of an ONB-protected diamine were introduced to PPFPA-*b*-PNIPAM via post-polymerization modification of the PFPA part in the block copolymer (**Scheme 5.2**). The copolymer (0.5 g, 1 equiv. of PFPA unit) was dissolved in 5 mL of dry THF under nitrogen atmosphere for 30 min. Separately, ONB-protected diamine (0.5 equiv.) and TEA (0.1 equiv) was dissolved in 1 mL of dry THF. The ONB-protected diamine solution was quickly added to the polymer solution and continued purging with nitrogen gas for 20 min. The solution was stirred in the dark at room temperature for 24 h. The resulting copolymer was purified by precipitation in diethyl ether, centrifuged, and vacuum dried at room temperature overnight. The product was obtained as pale yellow powder in 67% yield (0.55 g, 0.95 mmol). $^{1}$H NMR (400 MHz, $CDCl_3$) δ/ppm: 7.52-8.09 (br, protons in *o*-nitrobenzene), 4.10 (br, –NHC<u>H</u>$(CH_3)_2$), 3.2-1.5 (m, protons in backbone and linker of ONB), 1.13 (br, –NHCH($C\underline{H}_3)_2$). $^{19}$F NMR (DMSO-d6): δ/ppm: -170, -165, -162. FT-IR (ATR-mode): 1782 cm$^{-1}$ (C=O reactive ester band), 1645 cm$^{-1}$ (C=O of amide band), 1515 cm$^{-1}$ (C=C aromatic band), 1090 cm$^{-1}$ (C-O ester band).

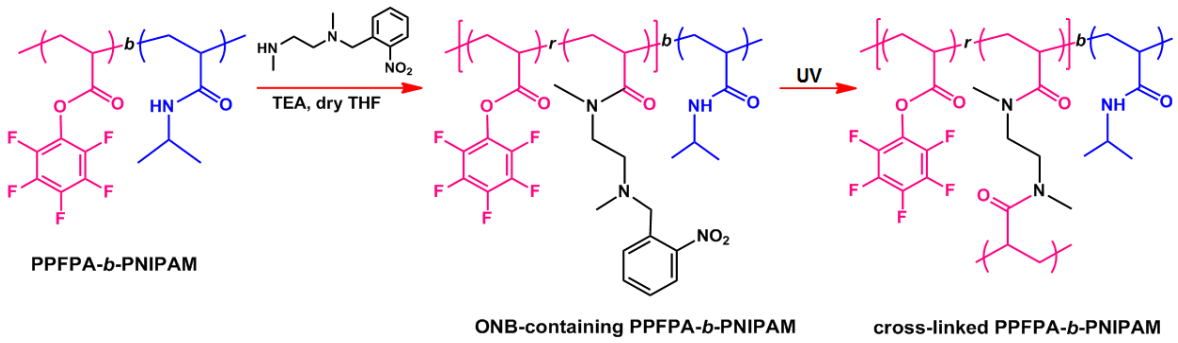


**Scheme 5.2** Synthetic pathway for the preparation of ONB-containing PPFPA-*b*-PNIPAM via post-polymerization modification and cross-linked PPFPA-*b*-PNIPAM induced by UV irradiation.

**Preparation of non-cross-linked (NCL) and core-cross-linked (CCL) micelles**

Non-cross-linked (NCL) micelles were formed by gradually adding DI water into a solution of PPFPA-*b*-PNIPAM in THF (50 mg/mL). THF was evaporated by stirring the solution in air to yield a micellar solution of NCL. For core-cross-linked (CCL) micelles, a micellar solution was first prepared from ONB-containing PPFPA-*b*-PNIPAM using a similar procedure as mentioned above for the NCL micelles followed by exposure to UV light (365 nm) for 2 h. After irradiation, the solution was dialyzed consecutively against THF for 2 days and DI water for 1 day to remove by-products (non-cross-linked polymer and nitrosobenzaldehyde) and THF, respectively. The aqueous solution in the dialysis tube was collected and filtered with a 0.45 μm pore-sized syringe filter and then lyophilized yielding a pale yellow powder of dry CCL micelles.

**Chemical incorporation of amino-containing dye into micelles**

NBD as an amino-functionalized fluorescent dye was selected as a model compound that can chemically bind with unreacted PFPA in the core of micelles via post-functionalization. The dry CCL micelles (5 mg, 1 equiv. of residual PFPA unit) were dispersed in 5 mL of dry THF. The micellar solution was purged with nitrogen gas for 30 min. Separately, TEA (0.1 equiv) and NBD (2 equiv.) were dissolved in 1 mL of dry THF. The mixed solution of TEA and NBD was quickly added to the micellar solution and continued purging with nitrogen gas for 20 min. The solution was stirred in the dark at room

temperature for 24 h. The solution was then purified by dialysis consecutively against THF for 2 days and DI water for 1 day to remove free NBD and THF, respectively. The aqueous solution in the dialysis tube was collected and filtered with a 0.45 μm pore-sized syringe filter and lyophilized yielding an orange powder of dry micelles.

For comparison, NBD incorporation was also performed prior to micelles formation and UV-induced cross-linking to compare loading contents of NBD from the two methods. Briefly, the mixed solution of TEA and NBD having the same concentration as above was added directly to 5 mL of ONB-containing PPFPA-*b*-PNIPAM solution in THF (1 mg/mL). The solution was purged with nitrogen gas for 20 min and stirred in the dark at room temperature for 24 h. The solution was then purified by dialysis against THF for 2 days to remove free NBD. Core-cross-linked (CCL) micelles incorporated with NBD were then formed using the same procedure as that for the preparation of CCL micelles as mentioned above.

**Physical encapsulation of hydrophobic dye into micelles**

To determine the ability to encapsulate hydrophobic molecule into the core of the micelles, pyrene was selected as a model. The dry CCL micelles (5 mg) were dispersed in 2 mL of THF. Pyrene solution in THF (2 mg/mL) was added dropwise into the micellar solution and stirred vigorously for 1 h. DI water was gradually added dropwise to the solution and then THF was evaporated by stirring the solution in air. The solution was then dialyzed against DI water at room temperature for 2 days to remove THF. The aqueous solution in the dialysis tube was collected and filtered with a 0.45 μm pore-sized syringe filter and lyophilized to yield a white powder of dry micelles.

For comparison, pyrene encapsulation into the ONB-containing PPFPA-*b*-PNIPAM was also performed prior to micelles formation and UV-induced cross-linking to compare loading contents of pyrene from the two methods. Briefly, the ONB-containing PPFPA-*b*-PNIPAM (5 mg) was dissolved in 2 mL of THF. Pyrene solution in THF (2 mg/mL) was added directly to the polymer solution and stirred vigorously for 1 h. CCL micelles encapsulated with pyrene were then formed using the same procedure as that for the preparation of CCL micelles as mentioned above except that the dialysis was only performed against DI water after UV-irradiation.

**Determination of dye loading content**

The contents of NBD chemically incorporated and pyrene physically encapsulated into the micelles were determined by dissolving the micelles in THF before analyzed by UV spectroscopy at 478 and 336 nm, respectively using standard calibration curves experimentally obtained with NBD/THF or pyrene/THF solutions (**Figure 5.1**). The dye content was calculated according to the following equation:

$$\text{Dye loading content (mg/g)} = \frac{\text{weight of dye loaded in micelles (mg)}}{\text{weight of dye – loaded micelles (g)}} \quad \text{(eq.5.1)}$$

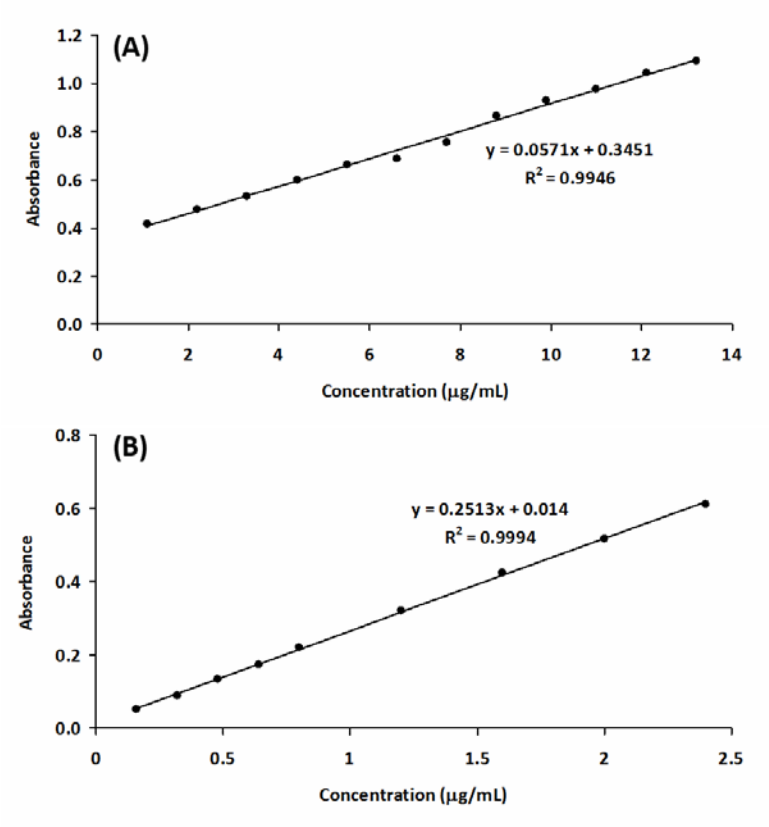


**Figure 5.1** Calibration curves of (A) NBD and (B) pyrene absorbance as a function of dye concentration in THF.

## RESULTS AND DISCUSSION

**Preparation of PPFPA-*b*-PNIPAM by RAFT polymerization**

For the synthesis of diblock copolymers of PPFPA-*b*-PNIPAM using RAFT polymerization, it is advisable to start with the monomer that shows higher transfer ability for the selected CTA.[31,32] Comparative polymerization kinetics of PFPA and NIPAM are shown in **Figure 5.2**. In this case, PPFPA was first synthesized and used as a macro CTA for the PNIPAM synthesis (**Scheme 5.1**). The PPFPA macro-CTAs with two molecular weights of 6.5 and 22.1 kDa were prepared (see **Table 5.1**). GPC chromatograms of the PPFPA and diblock copolymers are shown in **Figure 5.3**. A single peak was observed for each of the copolymers. A decrease in retention time as well as progressive peak broadening is seen with each block addition. The PPFPA with the two molecular weights of 6.5 and 22.1 kDa yielded block copolymer of the PPFPA-*b*-PNIPAM with molecular weights of 11.5 kDa and 30.4 kDa, respectively. The slight shoulder appearing in the GPC traces of the resulting block copolymers especially in the case of higher molecular weight one (30.4 kDa) implied that there was a significant amount of the inactive PPFPA macro CTA which did not participate in chain extension of the PNIPAM block. This may be described as a result of the PFPA polymerization being allowed to proceed to a rather high conversion (74%). This would raise a chance of chain termination. It is also likely that the PPFPA macro-CTA with higher molecular weight (22.1 kDa) would possess lower mobility so as the rate of chain transfer than that of the 6.5 kDa, resulting in the potential loss of polymerization controllability.

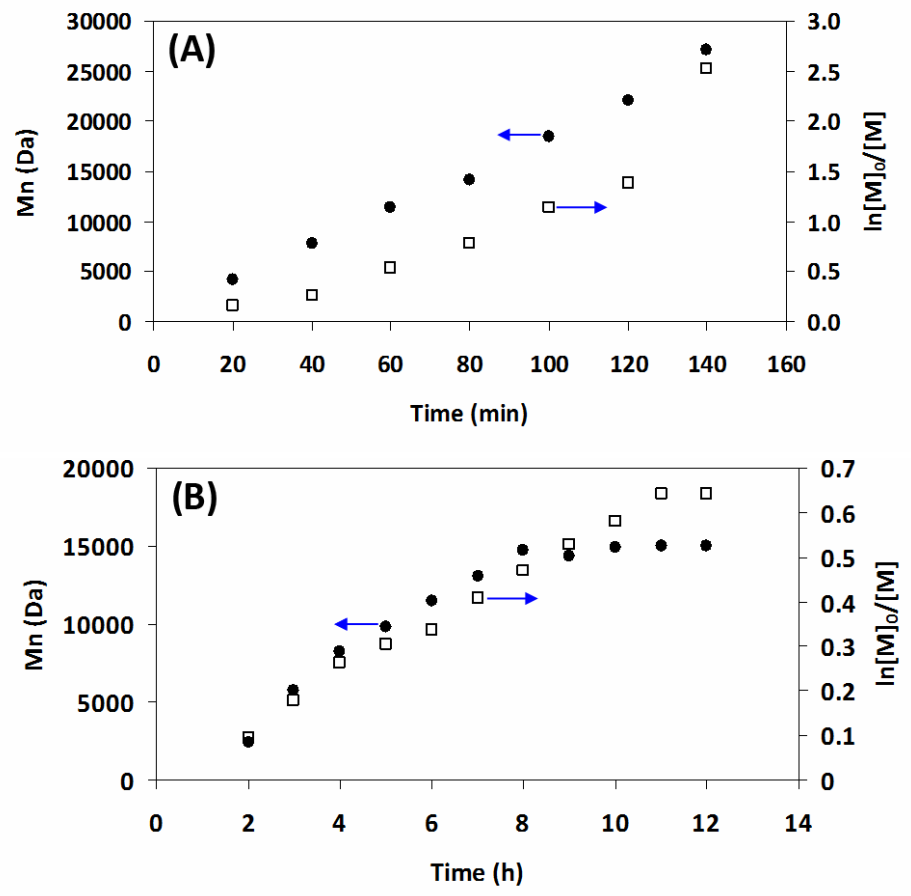


**Figure 5.2** Kinetics of RAFT polymerization of (A) PFPA and (B) NIPAM using 4-cyanopentanoic acid dithiobenzoate (CPADB) and azobisisobutyronitrile (AIBN) as CTA and initiator, respectively in 1,4-dioxane at 70°C.

**Table 5.1** Molecular weight information of PPFPA-*b*-PNIPAAm copolymers synthesized by RAFT polymerization.

| First block (PPFPA-CTA) | | | | PPFPA-*b*-PNIPAM | | | | |
|---|---|---|---|---|---|---|---|---|
| $M_n$[a] (kDa) | $M_w$[a] (kDa) | PDI | % conversion[b] | $M_n$[a] (kDa) | $M_w$[a] (kDa) | PDI | NIPAM[b] (mol-%) | PFPA[b] (mol-%) |
| 6.5 | 7.1 | 1.10 | 61 | 11.5 | 14.9 | 1.30 | 74 | 26 |
| 22.1 | 28.7 | 1.30 | 74 | 30.4 | 41.3 | 1.36 | 77 | 23 |

[a]The molecular weights were determined by GPC in THF, PS standard.

[b] %conversion and copolymer compositions were determined by $^1$H NMR

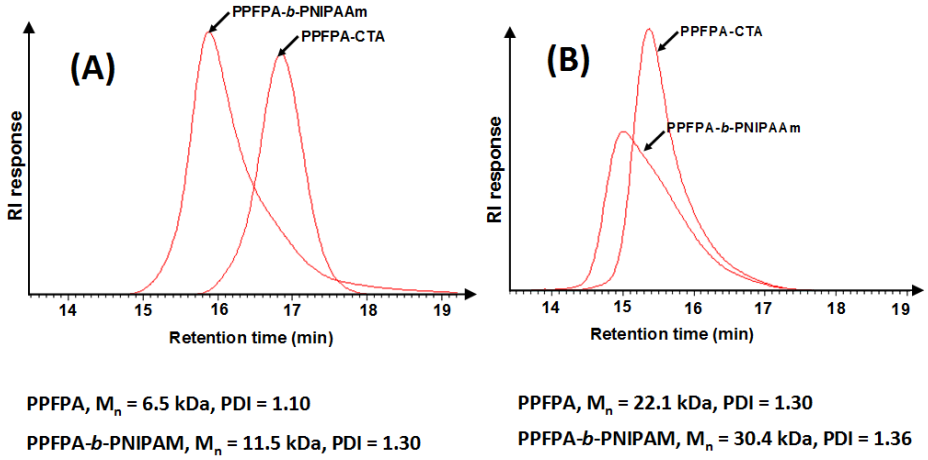


**Figure 5.3** GPC traces of PPFPA molecular weights of 6.5 kDa (A) and 22.1 kDa (B) and their corresponding block copolymers.

Additionally, **Table 5.1** gives an overview of the molecular weight information of the block copolymers prepared by RAFT polymerizations. The molecular weight ($M_n$) of the block increased with increasing [monomer]/[PPFPA macro-CTA] ratio. The content of the NIPAM in the block copolymer was determined from $^1$H NMR data by selecting the area of the signal at 4.10 ppm (for methine proton of NIPAM) in relation to the area of the signal at 3.10 ppm of the PPFPA polymer backbone. The contents of NIPAM in the block copolymers were 74 and 77 mol% for the PPFPA-CTA with $M_n$ of 6.5 and 22.1 kDa, respectively. $^1$H NMR measurement showed the appearance of a new signal at 4.10 ppm attributed to -C<u>H</u>$(CH_3)_2$, the methine proton of NIPAM (**Figure 5.4**). The characteristic proton signals of PPFPA at 3.10, 2.50, and 2.12 ppm attributed to CH and $CH_2$ groups of polymer backbone. The combination of a single GPC peak (**Figure 5.3**) and the presence of characteristic protons of both PPFPA and PNIPAM led to the assumption that diblock copolymers were successfully synthesized. Apparently, the RAFT process enables the synthesis of well-defined block copolymer of PPFPA-*b*-PNIPAM with predetermined molecular weight and narrow molecular weight distribution.

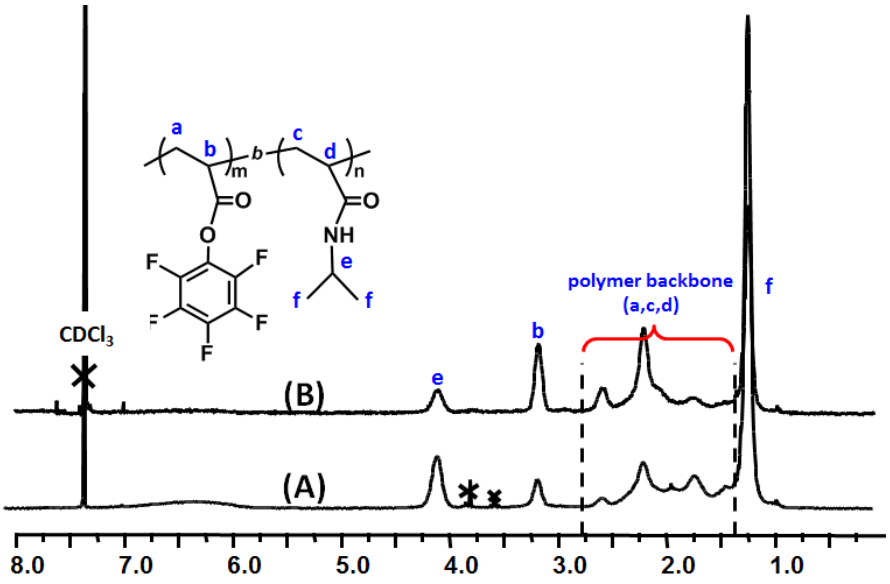


**Figure 5.4** $^{1}$H NMR spectra of PPFPA-*b*-PNIPAM in $CDCl_3$ having PPFPA:PNIPAM compositions of (A) 23:77 and (B) 71: 29.

**Post-polymerization modification of PPFPA-*b*-PNIPAM with ONB-protected diamine**

Herein, light-responsive moieties of ONB were prepared via post polymerization modification of PFPA moieties with a mono ONB-protected diamine.[25] Upon UV irradiation at 365 nm for 2 h, a new peak of nitrosobenzaldehyde appeared at around 350 nm (**Figure 5.5**) confirming the formation of the cleaved by-product.[23,25,33] In addition, FT-IR spectrum showed the appearance of C=O peak of nitrosobenzaldehyde at 1725 $cm^{-1}$. (**Figure 5.6**). The ONB-protected diamine group should be released, which can subsequently induce cross-linking via activated ester-amine chemistry resulting in network formation as shown in **Scheme 5.2**.

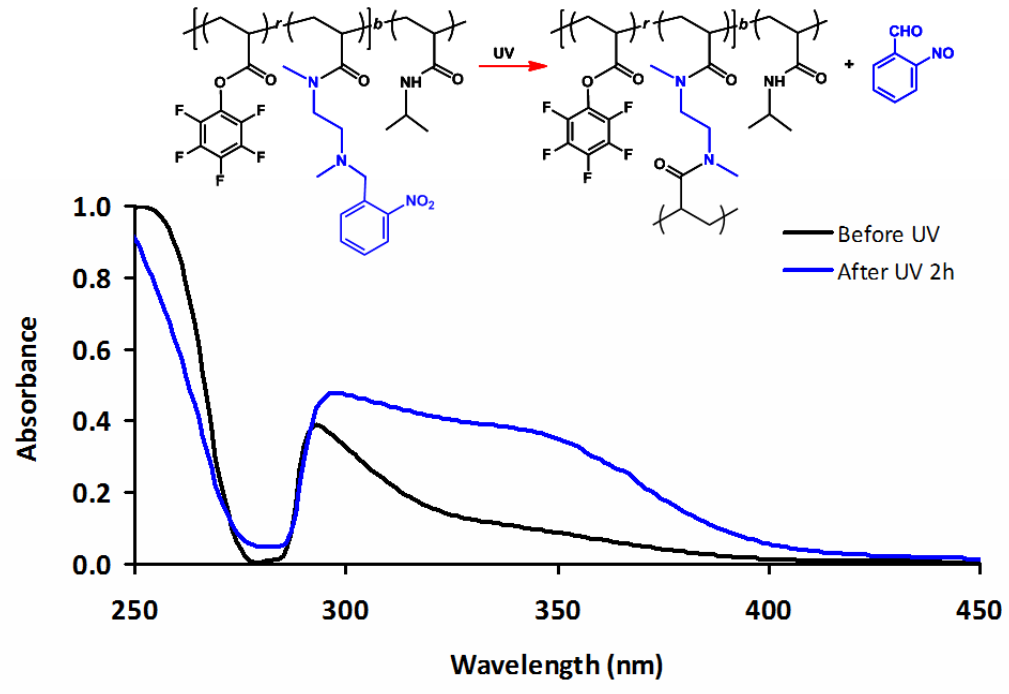


**Figure 5.5** UV spectra of ONB-containing PPFPA-*b*-PNIPAM before and after UV irradiation at 365 nm.

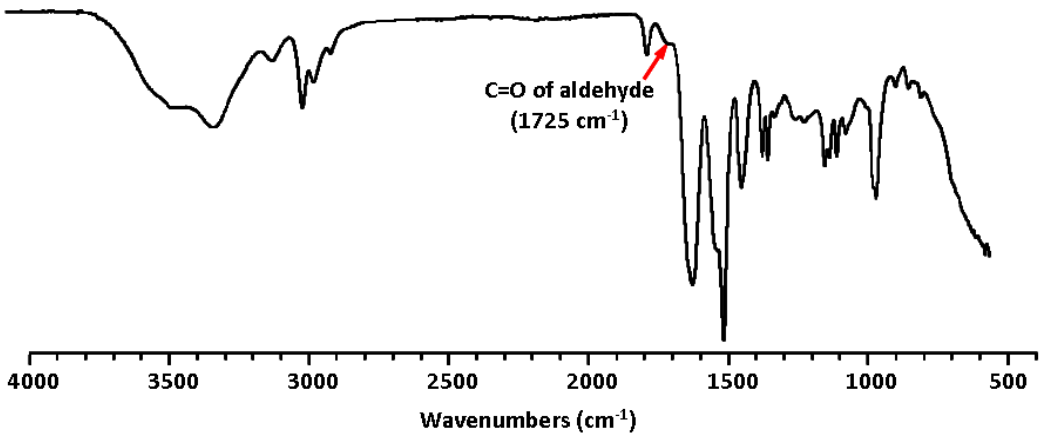


**Figure 5.6** FT-IR spectrum of cross-linked PPFPA-*b*-PNIPAM after UV irradiation at 365 nm.

A successful reaction can be demonstrated by the results from $^{1}$H NMR and FT-IR analysis. **Figure 5.7(A)** represents $^{1}$H NMR spectrum of the ONB-containing PPFPA-*b*-

PNIPAM. The signals of the four aromatic protons of the ONB moieties in a range of $\delta$=7.52-8.09 ppm clearly confirmed the attachment of the ONB groups to the block copolymer. The amount of incorporated ONB-protected diamine in the copolymer can be calculated by $^{1}$H NMR from the relative ratio between the peak integration of the four aromatic protons around $\delta$ = 7.52-8.09 ppm and the peak integration of one proton around $\delta$ = 3.10 ppm of the PPFPA polymer backbone. As reported earlier by Zhao *et al*.[25], the percentage of ONB incorporation (%ONB) can be varied as a function of the amount of ONB-protected diamine. Here in this research, the %ONB in the block copolymer of approximately 20% were chosen to assure that a certain portion of PFPA were cross-linked via incorporated ONB-protected diamine and allowed for the majority of the unreacted PFPA to be available for subsequent post functionalization with other active species of which we chose NBD in this case. Additionally, the successful conversion of the parent PPFPA in the copolymer to the corresponding ONB-protected group was also confirmed by FT-IR analysis from the decrement of C=O peak at 1782 cm$^{-1}$ of PPFPA and the increment of the amide carbonyl group at 1645 cm$^{-1}$ (**Figure 5.7(B)**). After the post- polymerization modification, the molecular weight of the ONB-containing block copolymer was slightly shifted to higher value in comparison to the GPC trace of the precursor block copolymer due to the increment of molecular weight per repeating unit (**Figure 5.8**).

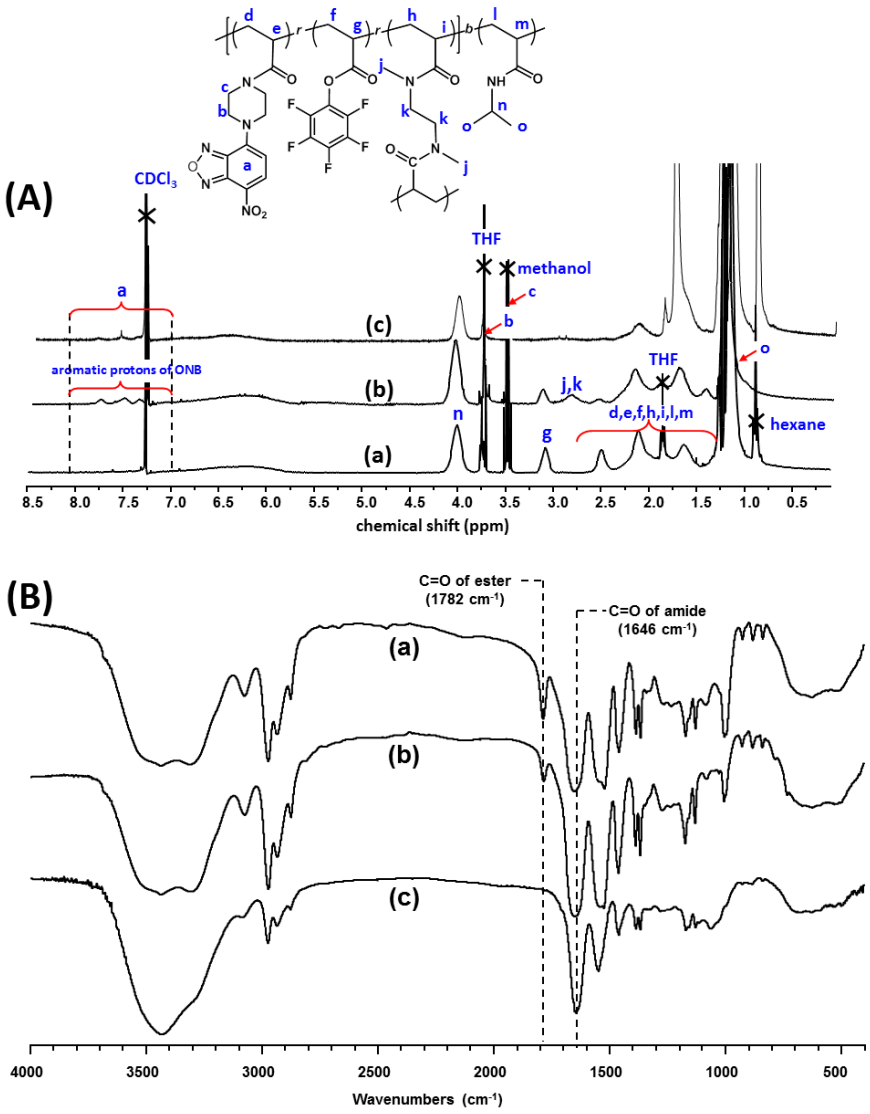


**Figure 5.7** $^{1}$H NMR spectra in $CDCl_3$ (A) and FT-IR spectra (B) of (a) PPFPA-*b*-PNIPAM, (b) ONB-containing PPFPA-*b*-PNIPAM, and (c) NBD-incorporated CCL micelles.

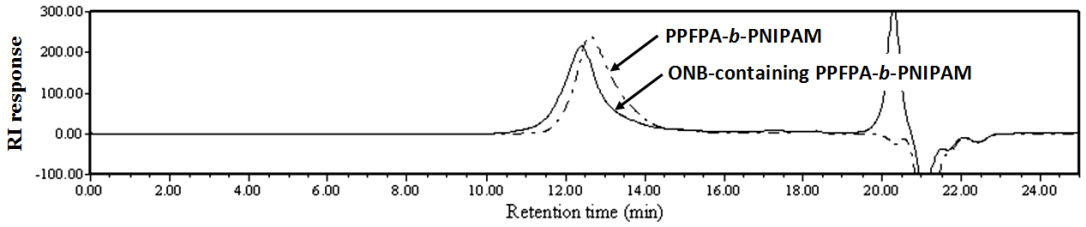


**Figure 5.8** GPC traces of PPFPA-*b*-PNIPAM and ONB-containing PPFPA-*b*-PNIPAM.

**Preparation of core-cross-linked (CCL) micelles of PPFPA-*b*-PNIPAM**

In this part, we introduce a new methodology for polymeric micelles preparation from diblock copolymer having PPFPA as hydrophobic part, PNIPAM as hydrophilic part, and ONB-protected diamine as a photo-induced cross-linker molecule of which the strategy is shown in **Scheme 5.3**. The molecular weight of PPFPA-*b*-PNIPAM and the %ONB were fixed at around 30 kDa and 20%, respectively, while the copolymer composition of PPFPA:PNIPAM was varied from 23:77 to 71:29. Micellization of the diblock copolymers in aqueous solution was confirmed by DLS and TEM. DLS studies (**Table 5.2**) revealed that the sizes of both NCL and CCL micelles above LCST became smaller than those below the LCST due to the outer shell of PNIPAM dehydrated and collapsed. After UV irradiation at 365 nm for 2 h, the average sizes of the CCL micelles were found to be smaller than those of the NCL micelles implying that covalently cross-linked network of ONB-protected diamine with the PFPA part in the core were formed. It should be emphasized at this point that complete cross-linking via the reaction between PFPA moieties and ONB can be achieved upon the UV-irradiation at 365 nm for 2 h as monitored by UV-vis spectroscopy. This agrees well with the report by Zhao *et al*.[25] Moreover, the average size of the micelles having a copolymer composition of 71:29 PPFPA:PNIPAM is smaller than that with the ratio of 23:77 PPFPA:PNIPAM implying that the size of the micelles corresponds with the block length of the PNIPAM outer shell. In addition, size distribution profiles measured by DLS showed that all of the micelles have a unimodal size distribution. The micelles did not precipitate above the LCST because the DLS measurement was carried out at a very low concentration (1 mg/mL) allowing us to determine their size by DLS. TEM images revealed well-defined spherical shapes with slightly smaller diameters than those observed in DLS, which is attributed to the shrinkage of the micelles after solvent evaporation during TEM sample preparation as shown in **Figure 5.9**.

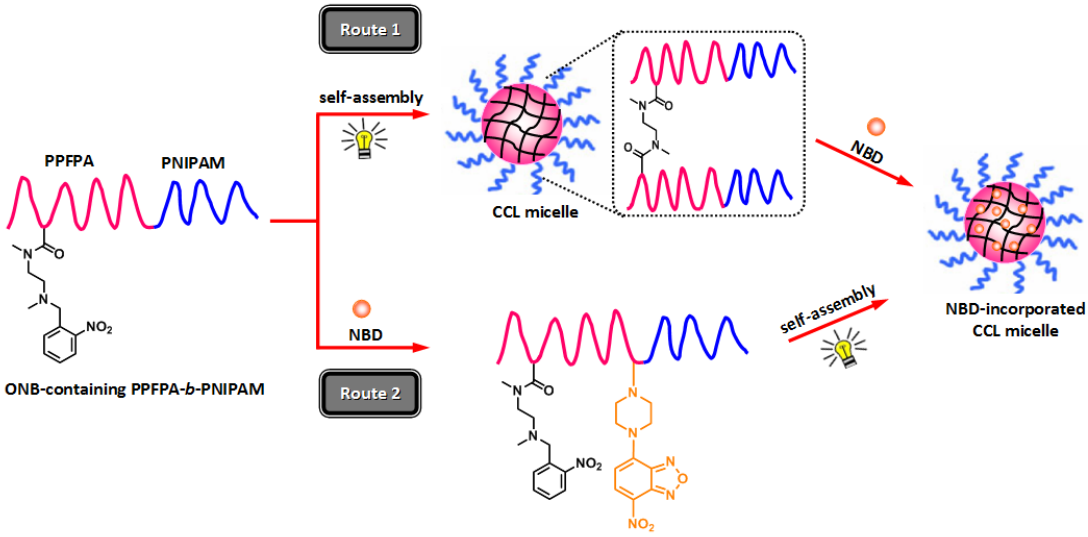


**Scheme 5.3** Schematic representation of NBD-incorporated CCL micelles preparation by performing cross-linking/self-assembly before (**Route 1**) or after (**Route 2**) chemical incorporation of NBD.

**Table 5.2** Summary of average sizes of the NCL and CCL micelles of PPFPA-*b*-PNIPAM and NBD-incorporated CCL micelles determined by DLS measurement in aqueous media.

| PPFPA:PNIPAM (% mol ratio) | Average size (nm) | | | | | |
|---|---|---|---|---|---|---|
| | PPFPA-*b*-PNIPAM NCL micelles | | PPFPA-*b*-PNIPAM CCL micelles | | NBD-incorporated CCL micelles | |
| | 10°C | 40°C | 10°C | 40°C | 10°C | 40°C |
| 23:77 ($M_n$ = 30.4 kDa) | 257 ± 5 | 178 ± 2 | 146 ± 3 | 97 ± 1 | 182 ± 2 | 135.9 ± 0.3 |
| 71:29 ($M_n$ = 32.5 kDa) | 122 ± 3 | 81.2 ± 0.2 | 58 ± 2 | 42.1 ± 0.2 | 67 ± 1 | 41.4 ± 0.7 |

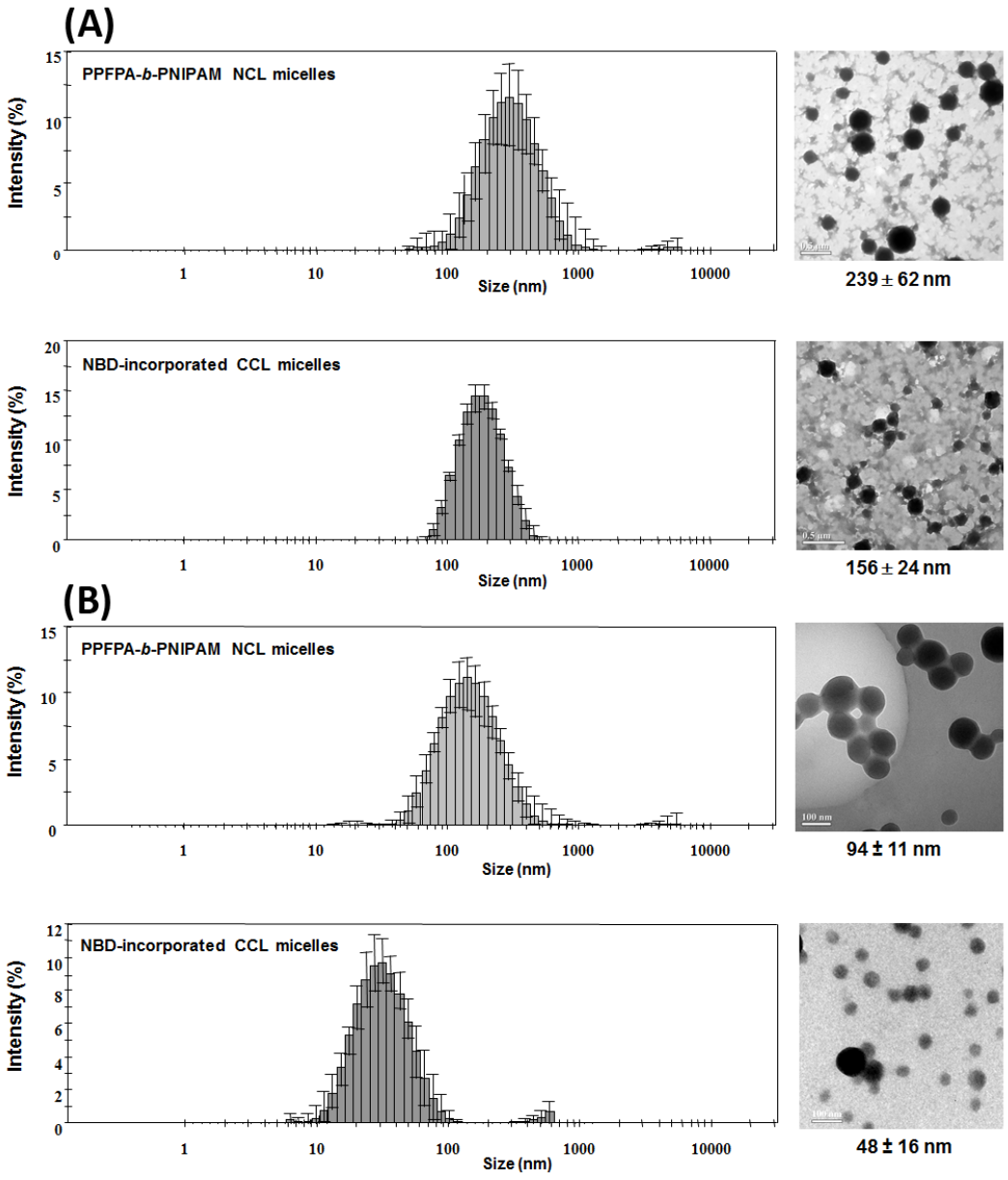


**Figure 5.9** Size distribution profiles evaluated by DLS (left column) and TEM images (right column) of the PPFPA-*b*-PNIPAM NCL micelles and the NBD-incorporated CCL micelles formulated from the copolymer with PPFPA:PNIPAM composition of (A) 23:77 (scale bar 0.5 μm) and (B) 71:29 (scale bar 100 nm). DLS measurements were carried out at 10°C with a micelle concentration of 1 mg/mL.

Furthermore, we have performed DLS and TEM measurements of the CCL micelles after placing them in THF, a good solvent for both PPFPA and PNIPAM blocks, to demonstrate that the synthesized CCL micelles were stable. From the DLS data, the average sizes of the CCL micelles having PPFPA:PNIPAM composition of 23:77 and 71:29 were 189 and 80 nm, respectively. These average sizes of the CCL micelles in THF are larger than those determined in aqueous media (See **Table 5.2** for comparison) as a result of THF being a good solvent and thus causing the CCL micelles to swell. According to TEM images shown in **Figure 5.10**, the CCL micelles maintained their spherical shape with their diameters around 82 and 38 nm for the copolymer having PPFPA:PNIPAM composition of 23:77 and 71:29, respectively. The size measured by the DLS is larger than that observed by TEM because the size measured by DLS is based on the swollen micelles in solution whereas that observed by TEM is for the dried micelles.

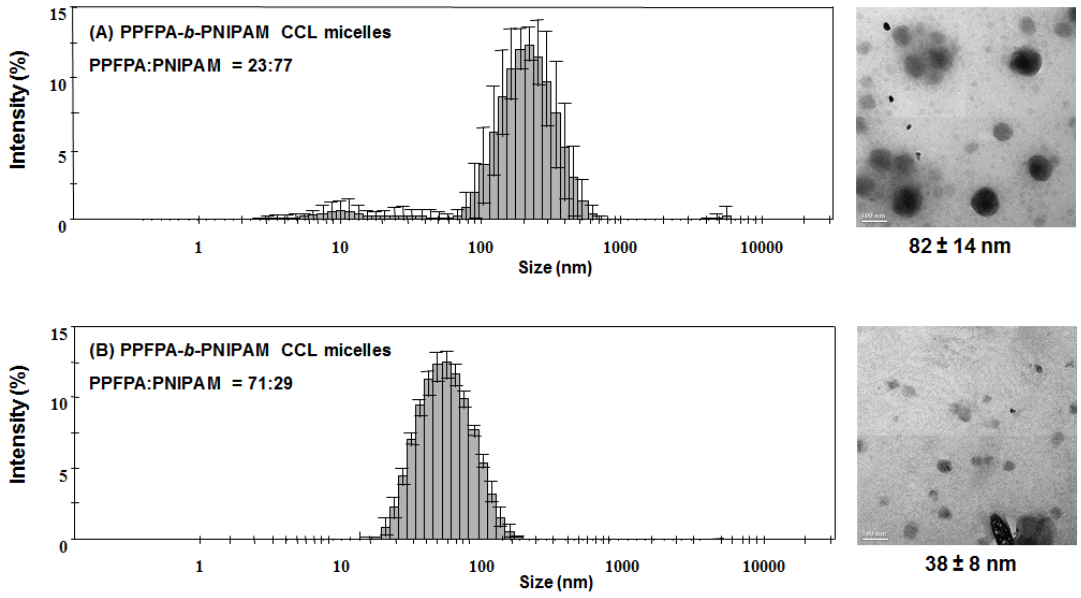


**Figure 5.10** Size distribution profiles evaluated by DLS and TEM images (scale bar 100 nm) of the CCL micelles after UV irradiation for 2 h, formulated from the ONB-containing PPFPA-*b*-PNIPAM with PPFPA:PNIPAM compositions of (A) 23:77 and (B) 71:29 after placing them in THF.

**Chemical incorporation and physical encapsulation of dyes into micelles**

NBD was covalently incorporated onto the residual PFPA moieties in the core of the CCL micelles to demonstrate the possibility for additional post-functionalization, as shown in **Scheme 5.3**. A successful incorporation of NBD was confirmed by FT-IR, $^{1}$H NMR, $^{19}$F NMR, and UV-vis spectroscopy. The disappearance of ester carbonyl group of activated PFPA at 1782 $cm^{-1}$ and appearance of amide carbonyl group at 1646 $cm^{-1}$ suggest that the PFPA units were fully converted to amide upon reacting with NBD (**Figure 5.7(B)**). Similar explanation can also be applied for the $^{1}$H NMR spectrum that showed the disappearance of the proton at $\delta$ = 3.10 ppm of the PPFPA backbone (**Figure 5.7(A)**). Complementary $^{19}$F NMR analysis confirmed that the three signals at -170, -165, and -162 ppm attributed to the pentafluorophenyl ester groups in the block copolymer completely disappeared when 2 equiv. of NBD dye was reacted, suggesting that all residual PFPA groups in the core of the micelles were totally consumed upon chemical incorporation of NBD (**Figure 5.11**).

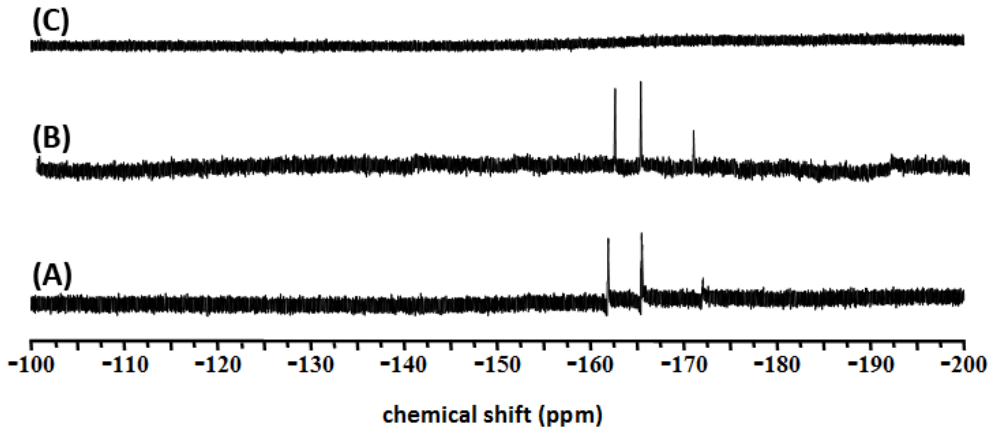


**Figure 5.11** $^{19}$F NMR spectra in DMSO-d6 of (A) PPFPA-*b*-PNIPAM, ONB-containing PPFPA-*b*-PNIPAM having PPFPA:PNIPAM compositions of 71:29 (B) before and (C) after reacting with NBD.

UV-vis spectroscopy was also used to confirm the incorporation of NBD into the core of micelles via post-functionalization modification of the residual PFPA units. As seen in **Figure 5.12 (A)**, an absorbance of NBD-incorporated CCL micelles, which corresponds to an absorbance of free NBD appears at $\lambda_{max}$= 478 nm indicating the presence of NBD in

the micelles. The loading content of NBD into the CCL micelles after UV-induced cross-linking (**Scheme 5.3, Route 1**) of the copolymer having PPFPA:PNIPAM composition of 23:77 and 71:29 was found to be 3.8 and 7.7 mg/g (NBD/copolymer), respectively. Furthermore, the physical encapsulation of pyrene into the CCL micelles was also determined (**Scheme 5.4, Route 1**). The typical UV-vis spectrum of pyrene-encapsulated CCL micelles is similar to that of free pyrene **Figure 5.12 (B)**, suggesting no significant change of pyrene structure when being encapsulated within the CCL micelles. The loading content of pyrene into the CCL micelles after UV-induced cross-linking of the copolymer having PPFPA:PNIPAM composition of 23:77 and 71:29 was 1.2 and 2.9 mg/g (pyrene/copolymer), respectively. We have also performed additional experiments by conducting UV-induced cross-linking after dye loading (**Route 2 of both Scheme 5.3 and 5.4**). It was found that the loading content of NBD into the CCL micelles formulated from the copolymer having PPFPA:PNIPAM composition of 23:77, and 71:29 was 3.9 and 8.0 mg/g (NBD/copolymer), respectively. Whereas, the loading content of pyrene into the CCL micelles formulated from the block copolymer having PPFPA:PNIPAM composition of 23:77, and 71:29 was 3.7 and 4.8 mg/g (pyrene/copolymer), respectively. Apparently, the loading contents of both NBD and pyrene into the core of micelles can be elevated as a function of the PPFPA composition in the block copolymer. The fact that the loading content of NBD prior to UV-induced cross-linking was essentially the same as that after UV-induced cross-linking indicated that enthalpic gain via chemical reactions between the residual PFPA groups and NBD was so powerful that it can overcome the restriction of dye permeability through the cross-linked polymeric network. The procedure based on the sequence of cross-linking/self-assembly followed by encapsulation should provide a better stability to micelles. This also gives additional benefit from practical perspective because any designated molecules can be chemically incorporated into ready-to-use cross-linked micelles which are quite stable. However, this seems not to be the case for pyrene of which physical encapsulation is mainly driven by weaker hydrophobic interactions. Cross-linking exhibited a significant impact on pyrene encapsulation so that its loading was more effective if being performed prior to cross-linking.

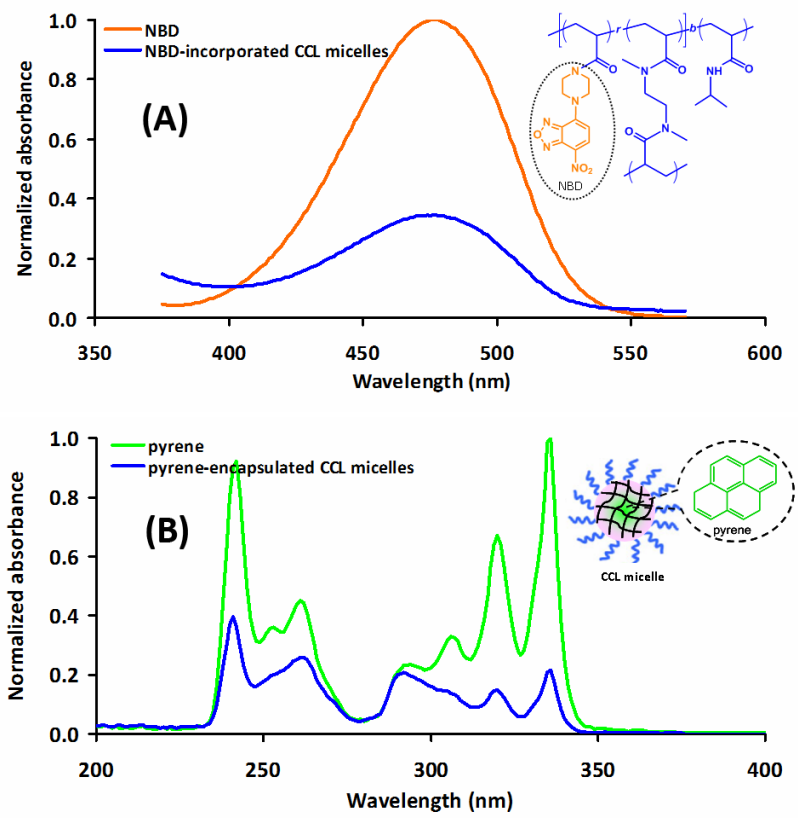


**Figure 5.12** Normalized absorbance of (A) NBD and the NBD-incorporated CCL micelles and (B) pyrene and the pyrene-encapsulated CCL micelles.

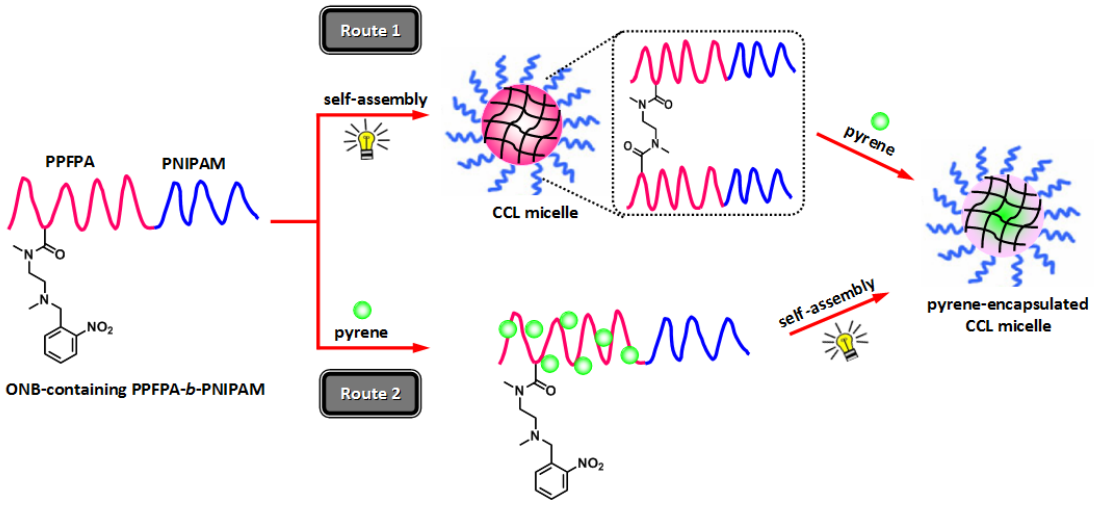


**Scheme 5.4** Schematic representation of pyrene-encapsulated CCL micelles preparation by performing cross-linking/self-assembly before (**Route 1**) or after (**Route 2**) physical encapsulation of pyrene.

## CONCLUSIONS

In this research, well-defined block copolymer consisting of PFPA and NIPAM were first synthesized by RAFT polymerization. The kinetic analysis and gel permeation chromatography (GPC) measurements confirmed that polymerization was well controlled. The cross-linked amphiphilic polymeric micelles of PPFPA-*b*-PNIPAM were prepared via post- polymerization modification of PFPA moieties with the ONB protected diamine. The ONB groups can be released upon UV irradiation which subsequently induced an *in situ* cross-linking by a spontaneous reaction with the remaining PFPA and yielded cross-linked micelles. Micellization of the copolymers was confirmed by DLS and TEM. The sizes of the NCL and CCL micelles can be controlled by changing the external temperature above or below their LCSTs. Our results have demonstrated that the copolymer micelles having residual PFPA moieties in their cores are capable of not only chemically incorporating amino-containing molecule, NBD via post-functionalization but also physically encapsulating hydrophobic molecule, pyrene, suggesting their potential to be used as alternative cargos for biomedical applications.

## REFERENCES


(1) Ganta, S.; Devalapally, H.; Shahiwala, A.; Amiji, M. *Journal of Controlled Release* **2008**, *126*, 187.

(2) Rapoport, N. *Progress in Polymer Science* **2007**, *32*, 962.

(3) Read, E. S.; Armes, S. P. *Chemical Communications* **2007**, 3021.

(4) Wei, H.; Cheng, S.-X.; Zhang, X.-Z.; Zhuo, R.-X. *Progress in Polymer Science* **2009**, *34*, 893.

(5) Zhuang, J.; Gordon, M. R.; Ventura, J.; Li, L.; Thayumanavan, S. *Chemical Society Reviews* **2013**, *42*, 7421.

(6) Schild, H. G. *Progress in Polymer Science* **1992**, *17*, 163.

(7) Chung, J. E.; Yokoyama, M.; Okano, T. *Journal of Controlled Release* **2000**, *65*, 93.

(8) Chung, J. E.; Yokoyama, M.; Yamato, M.; Aoyagi, T.; Sakurai, Y.; Okano, T. *Journal of Controlled Release* **1999**, *62*, 115.

(9) Kohori, F.; Sakai, K.; Aoyagi, T.; Yokoyama, M.; Yamato, M.; Sakurai, Y.; Okano, T. *Colloids and Surfaces B: Biointerfaces* **1999**, *16*, 195.

(10) Nakayama, M.; Okano, T.; Miyazaki, T.; Kohori, F.; Sakai, K.; Yokoyama, M. *Journal of Controlled Release* **2006**, *115*, 46.

(11) Liu, S. Q.; Tong, Y. W.; Yang, Y.-Y. *Biomaterials* **2005**, *26*, 5064.

(12) Zhu, J.-L.; Zhang, X.-Z.; Cheng, H.; Li, Y.-Y.; Cheng, S.-X.; Zhuo, R.-X. *Journal of Polymer Science Part A: Polymer Chemistry* **2007**, *45*, 5354.

(13) O'Reilly, R. K.; Hawker, C. J.; Wooley, K. L. *Chemical Society Reviews* **2006**, *35*, 1068.

(14) van Nostrum, C. F. *Soft Matter* **2011**, *7*, 3246.

(15) Zhang, J.; Jiang, X.; Zhang, Y.; Li, Y.; Liu, S. *Macromolecules* **2007**, *40*, 9125.

(16) Li, Y.; Lokitz, B. S.; McCormick, C. L. *Macromolecules* **2005**, *39*, 81.

(17) Eberhardt, M.; Théato, P. *Macromolecular Rapid Communications* **2005**, *26*, 1488.

(18) Theato, P. *Journal of Polymer Science Part A: Polymer Chemistry* **2008**, *46*, 6677.

(19) Eberhardt, M.; Mruk, R.; Zentel, R.; Théato, P. *European Polymer Journal* **2005**, *41*, 1569.

(20) Duong, H. T. T.; Marquis, C. P.; Whittaker, M.; Davis, T. P.; Boyer, C. *Macromolecules* **2011**, *44*, 8008.

(21) Zhuang, J.; Jiwpanich, S.; Deepak, V. D.; Thayumanavan, S. *ACS Macro Letters* **2012**, *1*, 175.

(22) Schumers, J.-M.; Fustin, C.-A.; Gohy, J.-F. *Macromolecular Rapid Communications* **2010**, *31*, 1588.

(23) Zhao, H.; Sterner, E. S.; Coughlin, E. B.; Theato, P. *Macromolecules* **2012**, *45*, 1723.

(24) Jiang, J.; Tong, X.; Morris, D.; Zhao, Y. *Macromolecules* **2006**, *39*, 4633.

(25) Zhao, H.; Theato, P. *Polymer Chemistry* **2013**, *4*, 891.

(26) Ahmed, M.; Narain, R. *Progress in Polymer Science* **2013**, *38*, 767.

(27) Smith, A. E.; Xu, X.; McCormick, C. L. *Progress in Polymer Science* **2010**, *35*, 45.

(28) York, A. W.; Kirkland, S. E.; McCormick, C. L. *Advanced Drug Delivery Reviews* **2008**, *60*, 1018.

(29) Boyer, C.; Bulmus, V.; Davis, T. P.; Ladmiral, V.; Liu, J.; Perrier, S. *Chemical Reviews* **2009**, *109*, 5402.

(30) Jochum, F. D.; Theato, P. *Macromolecules* **2009**, *42*, 5941.

(31) Gibson, M. I.; Fröhlich, E.; Klok, H.-A. *Journal of Polymer Science Part A: Polymer Chemistry* **2009**, *47*, 4332.

(32) Vega-Rios, A.; Licea-Claveríe, A. *Journal of the Mexican Chemical Society* **2011**, *55*, 21.

(33) Chen, L.; Goh, Y. K.; Cheng, H. H.; Smith, B. W.; Xie, P.; Montgomery, W.; Whittaker, A. K.; Blakey, I. *Journal of Polymer Science Part A: Polymer Chemistry* **2012**, *50*, 4255.

# Chapter VI

## Thermo-Responsive and Active Functional Fibers for Cultured Cell Recovery

### INTRODUCTION

Tissue engineering has gained much popularity because of its use in repair and replacement of damaged tissues or part by providing 3D scaffolds for cell growth and subsequent tissue organization. The cells inside body attach to extracellular matrix (ECM) in order to proliferate, migrate and differentiate into specific tissue. It is generally known that the process of cell culture requires a method to recover cells from the culture surface. Trypsin is an enzyme commonly used to digest cells. This agent would cleave off the cells adhered to the cultured material and unavoidably destroy cell-to-cell junctions as well as ECM which may affect cell viability.[1,2]

The use of thermo-responsive polymers has attracted considerable attention in the field of tissue engineering. Poly(*N*-isopropylacrylamide) (PNIPAM), in particular, is a well-known and best studied thermo-responsive polymer featuring a phase separation in aqueous media below its lower critical solution temperature (LCST) at 32$^{o}$C. It exhibits a reversible phase transition between hydrophilicity (below LCST) and hydrophobicity (above LCST) because of intermolecular and intramolecular hydrogen bonding.[3] Accordingly, cells can attach and grow on the PNIPAM surface above the LCST and can be spontaneously released by simply cooling the cell culture medium below the LCST and without requiring enzymes.[4,5] Okano's research team has performed pioneering work on grafting PNIPAM chains onto tissue culture polystyrene dish (TCPS).[2,6-11] However, cell detachment from PNIPAM-grafted TCPS is a relatively slow process which might have negative impact on cell functions.[2] The use of porous membranes grafted with PNIPAM as culture substrates have recently been reported to facilitate the rapid cell sheet detachment.[12-16] Recently in 2014, Oh *et al.* prepared thermo-responsive polystyrene (PS) nanofibrous mats by grafting thermo-sensitive PNIPAM chains onto PS nanofibrous mats via electron beam irradiation. Cells were well attached and proliferated more on the PNIPAM-grafted PS nanofibrous mats than on

the flat PS dish surfaces. Moreover, cells cultured on the PNIPAM-grafted PS mats were detached more rapidly than those on the PNIPAM-grafted PS dishes. These results demonstrated that thermo-responsive nanofibrous mats are attractive substrates for recovery of cultured cells.[17]

Functional polymer nanofibers produced via electrospinning are very attractive materials for diversified applications. It is recognized as one of the most promising and versatile method for preparing 3D porous nanofibers with high porosity and high surface area.[18] The ECM-mimic structure render electrospun fibrous material an excellent candidate for using in tissue engineering.[19-22] However, electrospun nanofibers of PNIPAM homopolymer are not stable in water and disperse easily which limits its application in some bio-related areas, especially in tissue engineering and regenerative medicine.[23,24]

Copolymerizing NIPAM with comonomers having active functionalities that can undergo crosslinking is a promising strategy to obtain stable nanofibers in an aqueous medium. Monomers having active pentafluorophenyl ester, pentafluorophenyl (meth)acrylate (PFP(M)A), are quite desirable choices for copolymerization with NIPAM due to their resulting copolymers are hydrolytically stable is water.[25,26] Moreover, these active PFP functional groups are readily available for further chemical modification with bioactive molecules via activated ester-amine chemistry. Designing and producing three-dimensional (3D) of PFP-containing functional nanofibrous structure via electrospinning have been recently reported. Gentsch and coworkers[27] successfully prepared reactive fiber meshes based on pentafluorophenyl methacrylate (PFPMA) for the first time. The fiber mesh is a versatile platform for simple immobilization of sugar molecules via post-polymerization modification. The sugar-functionalized fiber meshes enhance the cytokine production of macrophages which triggered specific interaction with biological systems.

Here is this research, random copolymer of P(PFPA-*r*-NIPAM) is introduced as electrospinnable and crosslinkable polymeric material that could combine thermoresponsiveness and active functionality for further biofunctionalization. Partial post-polymerization modification of the copolymer was firstly performed to incorporate light responsive moieties of *ortho*-nitrobenzyl (ONB) group into the PFPA part. The ONB group is known to undergo irreversible transformation upon irradiation with UV. Finally, the ONB-containing copolymers were then electrospun into fibers. Cross-linked and stable fibers were then formed after UV irradiation. The cross-linked copolymer fibers

were utilized as functional fibers to immobilize GRGDS peptide, a well-known cell adhesive peptide sequence, which could promote cell growth. It is strongly believed that the nanofibrous structure of the copolymer should accelerate the recovery process of intact cultured cells which is highly beneficial for tissue engineering applications.

## EXPERIMENTAL SECTION

**Materials.** Triethylamine (TEA, 99.5%), 2-nitrobenzyl bromide (98%), *N,N′*-dimethylethylenediamine (85%), 4-cyanopentanoic acid dithiobenzoate (CPADB, 97%), and bovine serum albumin-fluorescein isothiocyanate conjugate (BSA-FITC) were purchased from Sigma-Aldrich and used as received. *N*-isopropylacrylamide (NIPAM, 97%) was obtained from Sigma-Aldrich and recrystallized twice in hexane before use. Acrylic acid (AA, 99%) was obtained from Sigma-Aldrich and purified by distillation under reduced pressure prior to use. Pentafluorophenol (99.0%) was commercially available from Merck and used as received. Azobisisobutyronitrile (AIBN, 98%) was obtained from Fluka and used as received. Acryloyl chloride (98%) was purchased Acros and used as received. H-Gly-Arg-Gly-Asp-Ser-OH (GRGDS) was purchased from Genscript (USA). Fetal bovine serum (FBS) and RPMI 1640 medium were purchased from InVitromex. Fibroblast (L929) cell line was obtained from ATCC. All solvents used for reactions are reagent grade and used as received, unless otherwise specified. Anhydrous 1,4-dioxane (99.9%) were obtained from Merck. Anhydrous tetrahydrofuran (THF, 99.9%) was obtained from Sigma-Aldrich. Dichloromethane was dried over $CaH_2$ under reflux and nitrogen atmosphere. Phosphate buffered saline (PBS) pH 7.4 was purchased from Sigma-Aldrich. The NMR solvents such as $CDCl_3$ (99.8% D) and DMSO-d6 (99.9%) were obtained from Cambridge Isotope Laboratories, Inc. (USA). ONB-protected diamine was synthesized according to a method of Graisuwan *et al.*[28] and PFPA was synthesized according to the method of Jochum *et al.*[29]

**Methods.** $^1$H NMR spectra were recorded on a Varian, model Mercury-400 nuclear magnetic resonance spectrometer (USA) operating at 400 MHz. Chemical shifts ($\delta$) were reported in part per million (ppm) relative to tetramethylsilane (TMS) signal as a reference. FT-IR spectra were recorded with a Nicolet Impact 6700 FT-IR spectrometer with 32 scans at a resolution of 4 $cm^{-1}$ in a frequency range of 400-4000 $cm^{-1}$. Molecular weight and molecular weight distribution of synthesized polymers were analyzed by gel permeation chromatography (GPC) using Waters 600 controller

chromatograph equipped with HR1 and HR4 columns (Waters, MW resolving range =100-500,000 g/mol) at 35°C and refractive index (RI) detector (Waters 2414). THF was used as an eluent with the flow rate of 1.0 mL/min. Sample injection volume was 80 µL. Five polystyrene standards (996-188,000 g/mol) were used for generating a calibration curve. The surface morphology of electrospun fibers was observed using a JEOL Model JSM-6610/LV scanning electron microscope (SEM) and analyzed with an accelerating voltage of 15 kV. A small piece of electrospun fibers on aluminum foil was cut and placed on SEM stub using a double-sided adhesive carbon tape. Sample was sputter-coated with gold prior to imaging. The fiber diameters were measured by using a SemAfore 5.21 for 50 fibers per sample. A contact angle goniometer model 100-00 equipped with a Gilmont syringe and a 24-gauge flat-tipped needle (Ramé-Hart, Inc., USA) was used for the determination of water contact angles. A droplet of Milli-Q water was placed on the tested surface by bringing the surface into contact with a droplet suspended from a needle on the syringe. The measurements were carried out in air at room temperature. The reported angle is an average of 10 measurements on different areas of each sample.

**Synthesis of poly(PFPA-*ran*-NIPAM) (P(PFPA-*r*-NIPAM)).** PFPA (2.38 g, 10 mmol), NIPAM (1.13 g, 10 mmol), CPADB (2.79 mg, 0.01 mmol), and AIBN (0.21 mg, $1.28 \times 10^{-3}$ mmol), were added to a vial followed by 10 mL of dry 1,4-dioxane. The vial was sealed with a rubber septum and the solution was purged with nitrogen gas for 30 min under stirring. Polymerization was conducted under nitrogen atmosphere at 70°C for 24 h. The polymer solution was precipitated in diethyl ether, centrifuged, and finally dried under vacuum at room temperature. The dried copolymer was then dissolved in THF and precipitated again in diethyl ether. This procedure was repeated two times. The product was obtained as pink powder in 80% yield (2.81 g, 8 mmol). $^1$H NMR (400 MHz, $CDCl_3$): $\delta$/ppm: 4.10 (br,–NHC<u>H</u>$(CH_3)_2$), 3.10 (br, $CH_2C$<u>H</u>), 2.51-1.50 (m, protons in backbone), 1.13 (br, –NHCH(C<u>H</u>$_3)_2$). FT-IR (ATR-mode): 1782 cm$^{-1}$ (C=O reactive ester band), 1645 cm$^{-1}$ (C=O of amide), 1515 cm$^{-1}$ (C=C aromatic band), 1090 cm$^{-1}$ (C-O ester band). GPC (THF) : $M_n$ = 47 kDa; PDI = 1.62 and $M_n$ = 60 kDa; PDI = 1.98.

**Post-polymerization modification of P(PFPA-*r*-NIPAM) with ONB-protected diamine.** Light-responsive moieties in the form of an ONB-protected diamine were introduced to the PFPA part of P(PFPA-*r*-NIPAM) via post-polymerization modification.[28]

The P(PFPA-*r*-NIPAM) (1.0 g, 1 equiv. of PFPA unit) was dissolved in 10 mL of dry THF under nitrogen atmosphere for 30 min. Separately, ONB-protected diamine (0.5 equiv.) and TEA (0.1 equiv) were dissolved in 1 mL of dry THF. The ONB-protected diamine solution was quickly added to the polymer solution and continued purging with nitrogen gas for 20 min. The solution was stirred in the dark at room temperature for 24 h. The resulting copolymer was purified by precipitation in diethyl ether, centrifuged, and vacuum dried at room temperature overnight. The product was obtained as pale yellow powder in 71% yield (1.16 g, 2.02 mmol). $^{1}$H NMR (400 MHz, $CDCl_3$): $\delta$/ppm: 7.52-8.09 (br, protons in *o*-nitrobenzene), 4.10 (br, –NHC<u>H</u>$(CH_3)_2$), 3.2-1.5 (m, protons in backbone and linker of ONB), 1.13 (br, –NHCH(C<u>H</u>$_3)_2$). FT-IR (ATR-mode): 1782 cm$^{-1}$ (C=O reactive ester band), 1645 cm$^{-1}$ (C=O of amide I band), 1515 cm$^{-1}$ (C=C aromatic band), 1090 cm$^{-1}$ (C-O ester band).

**Electrospinning of P(PFPA-*r*-NIPAM), ONB-containing P(PFPA-*r*-NIPAM) and Polystyrene (PS) fibers.** Electrospinning technique was employed to fabricate the P(PFPA-*r*-NIPAM), ONB-containing P(PFPA-*r*-NIPAM) and PS as fibers. The electrospinning apparatus consisted of a variable syringe pump (ProSense B.V. Laboratory & process equipment model NE1000, Netherlands) and a high voltage power supply (Gamma High Voltage Research, model ES30P, USA).

The copolymers of P(PFPA-*r*-NIPAM) and ONB-containing P(PFPA-*r*-NIPAM) with different concentrations (10-30% w/v) were dissolved in a mixture of THF/DMF (3:1, v/v). The polymer solutions were then stirred at room temperature for 24 h. The polymer solution was loaded in a 5 mL plastic syringe equipped with a metallic needle of 0.7 mm inner diameter. The syringe was fixed horizontally on the syringe pump and an electrode of high power supply was clamped to the metal needle tip. A grounded stationary rectangular metal collector covered with a piece of clean aluminum foil was used for the fiber collection. The distance between the needle tip and the collector was set to 20 cm. The flow rate of polymer solution was fixed at 3 mL/h, and the applied voltage was set at 20 kV. The electrospun fibers were collected on a flat aluminum foil and then vacuum dried at room temperature overnight prior to further studies.

For preparation of cross-linked P(PFPA-*r*-NIPAM) fibers, the electrospun fibers of ONB-containing P(PFPA-*r*-NIPAM) fibers were exposed to UV light for 2 h to generate cross-linked networks.

For preparation of PS fibers, 0.2 g of PS was dissolved in a mixture of THF/DMF (3:2, v/v) 2 mL to generate a 10% wt of PS solution. The electrospinning process was then performed using the same procedure as that for the preparation of the P(PFPA-*r*-NIPAM) as mentioned above. The PS fibers were then plasma treated in air for 5 min prior to use for cell study.

**Immobilization of GRGDS peptide on the electrospun fibers.** GRGDS peptide was dissolved in PBS buffer pH 7.4. The electrospun fibers of P(PFPA-*r*-NIPAM), and cross-linked P(PFPA-*r*-NIPAM) were cut into small circle pieces with diameter of 15 mm and placed into the bottom of 24-well tissue culture polystyrene (TCPS) plates. The GRGDS peptide solution was then pipetted into each well of the electrospun fibers. After immobilization for 24 h, the samples were rinsed twice with PBS and DI water, respectively. The electrospun fibers were then air dried overnight.

**Cell viability using MTT Assay.** Fibroblast (L929) cell line was used to study cell adhesion and proliferation of the electrospun fibers. The L929 cells were cultured in RPMI 1640 medium supplemented with 5% fetal bovine serum (FBS), penicillin (100,000 U/L) and streptomycin (100 mg/mL). They were incubated at $37^{\circ}C$ in atmosphere containing 5% $CO_2$ where the culture medium was changed every 3 days. For cell culture, the electrospun fibers in 24-well TCPS plates were sterilized with UV light overnight prior to use. Eight replicated samples were used for each condition. Approximately $2x10^4$ of the L929 cells in 200 μL culture medium were pipetted into each well containing the substrates as well as into the bottom of TCPS plates as a control and then incubated under 5% $CO_2$ at $37^{\circ}C$. MTT assay was used to investigate cell adhesion and proliferation. After cell culture for a set of incubation time, the culture medium was removed to discard the unattached cell and the 200 μL of fresh culture medium was pipetted into each well followed by 10 μL of 0.5 mg/mL of MTT in normal saline solution. After incubation for 1 h, the supernatant solution was removed and 150 μL of DMSO was pipetted into each well to dissolve the purple crystals of formazan. Next, 25 μL of 0.1 M glycine (pH 10.5) was added. The optical density of sample was measured using a microplate reader at the wavelength at 540 nm. For the cell adhesion studies, the cells were allowed to attach on the surfaces for 6 h. For the cell proliferation studies, the cells after having been allowed to attach on the surfaces for 6

h, were cultured for either 1, 3, and 5 days. The viability of the attached and proliferated cells was quantified by MTT assay.

**Recovery of cultured cells.** Detachment of single cells was achieved by lowering temperature after incubation for 5 days. For lowering temperature, spread cells on each surface were transferred to a controlled temperature incubator fixed at 20$^{o}$C. The morphology and detachment rate were observed with SEM and MTT assay as a function of lowering temperature treatment time.

**Statistical Analysis.** For the cell adhesion and proliferation tests, the data are expressed as the mean ±standard deviation (S.D.) Statistical analysis to test for significant differences between means was performed using the Statistical Package for the Social Science (SPSS) version 17.0 software, using One-Way Analysis of Variance (ANOVA) with the Least Square Difference (LSD) tests were used for post hoc evaluations of differences between groups. The threshold level for accepting statistical significance was set at $p < 0.05$.

## RESULTS AND DISCUSSION

**Preparation of P(PFPA-*r*-NIPAM) by RAFT polymerization.** The success of P(PFPA-*r*-NIPAM) synthesis was confirmed by $^{1}$H NMR and FT-IR analyses as shown in **Figure 6.1 and 6.2**, respectively. The characteristic proton signal of NIPAM appeared at 4.10 ppm which can be assigned to the methine proton of NIPAM part. The characteristic proton signal at 3.10 ppm assignable to the CH group from PFPA part. The signals around $\delta$ = 2.51-1.13 ppm can be attributed to the protons of polymer backbone from both of PFPA and NIPAM units. In addition, FT-IR spectra also showed the characteristic peaks of both of PFPA (C=O of ester at 1782 cm$^{-1}$) and NIPAM (C=O of amide I at a 1645 cm$^{-1}$) as shown in **Figure 6.2 (a)**. The comonomer composition (mol%) of PFPA to NIPAM in the copolymer was determined from $^{1}$H NMR data based on relative integration of the peak at 4.10 ppm (for methine proton of NIPAM) to that of the peak at 3.10 ppm of the PFPA. The comonomer ratio of PFPA to NIPAM was found to be 28:72.

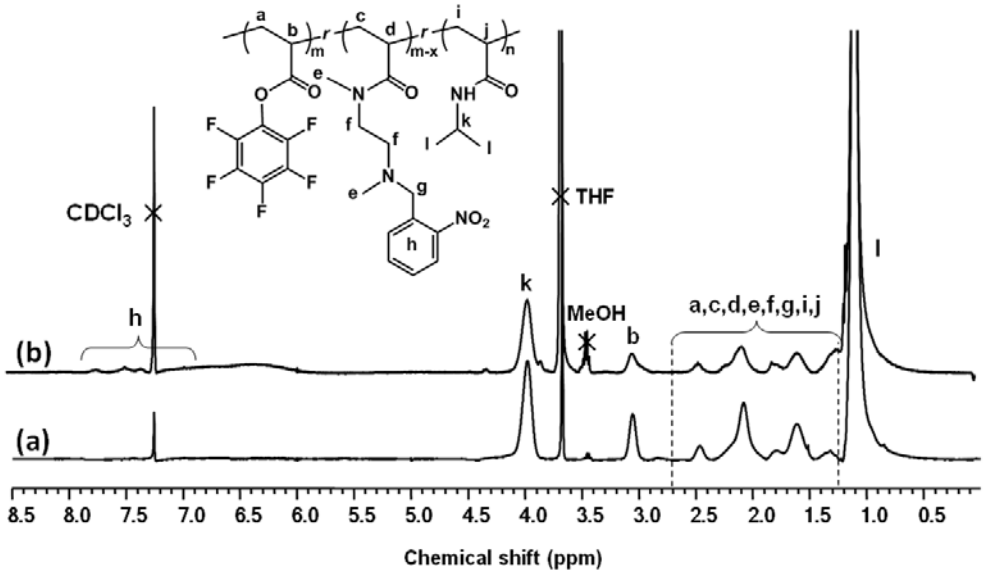


**Figure 6.1** $^{1}$H NMR spectra in $CDCl_3$ of (a) P(PFPA-*r*-NIPAM), (b) ONB-containing P(PFPA-*r*-NIPAM).

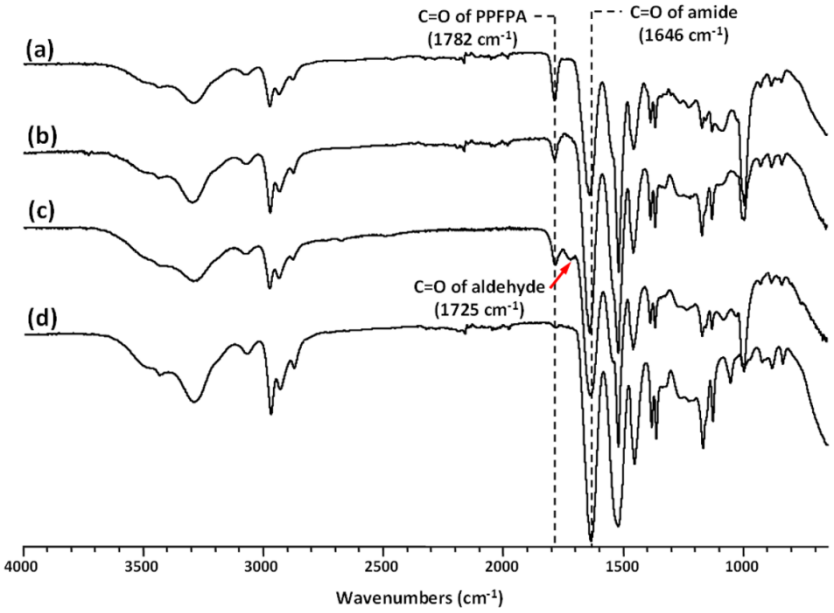


**Figure 6.2** FT-IR spectra of (a) P(PFPA-*r*-NIPAM), ONB-containing P(PFPA-*r*-NIPAM) (b) before and (c) after crosslinking by UV irradiation, and (d) cross-linked P(PFPA-*r*-NIPAM) fibers after GRGDS immobilization.

**Post-polymerization modification of P(PFPA-*r*-NIPAM).** Light responsive ONB-containing P(PFPA-*r*-NIPAM) were prepared via post-polymerization modification of PFPA units in the copolymer with a mono ONB-protected diamine. Upon UV irradiation at 365 nm, the ONB-protected diamine group should be released, which can subsequently induce cross-linking via activated ester-amine chemistry resulting in a network formation as shown in **Scheme 6.1**. A successful reaction can be demonstrated

by the results from $^{1}$H NMR and FTIR analyses. **Figure 6.1 (b)** represents $^{1}$H NMR spectrum of ONB-containing P(PFPA-*r*-NIPAM). The signals of the four aromatic protons of the ONB moieties in a range of δ=7.52-8.09 ppm clearly confirmed the attachment of the ONB groups to the P(PFPA-*r*-NIPAM). The amount of incorporated ONB-protected amine in the copolymer can be calculated by $^{1}$H NMR from the relative ratio between the peak integration of the four aromatic protons (δ=7.52-8.09 ppm) and the peak integration of one proton at 3.10 ppm of the PPFPA polymer backbone. The percentage of ONB incorporation (%ONB) was found to be 20%. Here in this research, the %ONB in the copolymer of 20% were chosen to assure that a certain portion of PFPA were cross-linked via incorporated ONB-protected diamine and allowed for the majority of the unreacted PFPA to be available for subsequent post-functionalization with biomolecules of which we chose GRGDS peptide in this case. Additionally, the successful conversion of the parent PPFPA in the copolymer to the corresponding ONB-protected group was also confirmed by FT-IR analysis from the decrement of C=O peak at 1782 cm$^{-1}$ of active ester group in the PPFPA and the increment of the amide carbonyl group at 1645 cm$^{-1}$ (**Figure 6.2 (b)**). After UV irradiation, a new peak of C=O of nitrosobenzaldehyde appeared at 1725 cm$^{-1}$ confirming the formation of the cleaved by-product as shown in **Figure 6.2 (c)**.

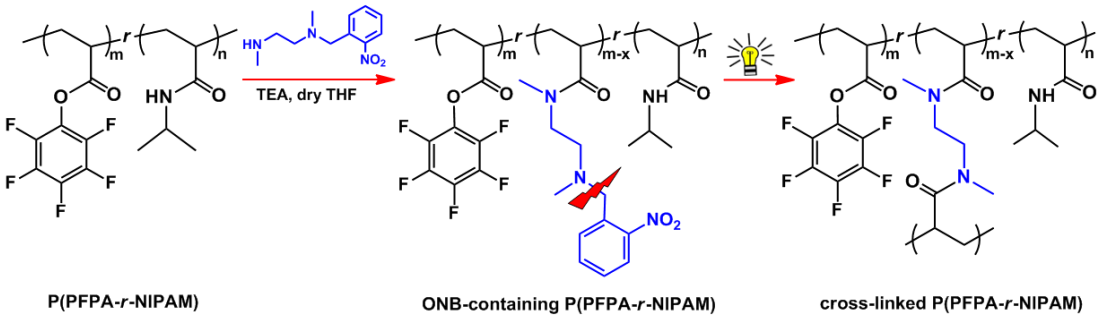


**Scheme 6.1** Synthetic pathway for the preparation of ONB-containing P(PFPA-*r*-NIPAM) via post-polymerization modification and cross-linked reaction induced by UV irradiation.

**Fiber fabrication by electrospinning process**. The P(PFPA-*r*-NIPAM) was fabricated into fibers by electrospinning technique. The effects of solvent, molecular weight and polymer solution concentration were investigated in order to get optimal conditions that yield fibers with uniform size distribution.

***Effect of solvent.*** The P(PFPA-*r*-NIPAM) having $M_n$ of 47 kDa was electrospun from THF and a binary mixtures of THF/DMF (3:1 v/v) to study the effect of solvent on fibers formation (**Figure 6.3**). For each solvent system, the polymer solution concentration was varied from 10 to 30% (w/v). The fibers electrospun from THF showed only beads and beads with some fibers on the collector at polymer concentration of 10 and 20% w/v, respectively. The average diameter of the fibers electrospun from THF at 30% (w/v) was 2.02 ± 0.84 μm. The fibers electrospun from the binary mixtures of THF/DMF (3:1 v/v) formed beads with fibers at a polymer concentration of 30% (w/v). Moreover, the average diameter of fibers electrospun from the THF/DMF had smaller diameter than that of the fibers electrospun from THF. DMF with relatively high dielectric constant (36.4) as compared with that of THF (7.6), DMF can increase elongational force within the solution jet so that fibers electrospun from THF/DMF became smaller in diameter.[30] Therefore, the binary mixtures of THF/DMF (3:1 v/v) was selected and used for further investigation.

| $M_n$ (kDa) | Solvent | 10% w/v | 20% w/v | 30% w/v |
|---|---|---|---|---|
| 47 | THF | 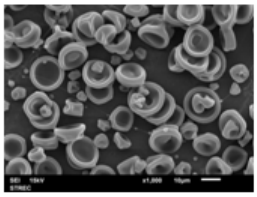 beads | 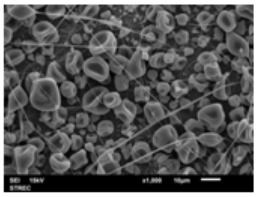 beads | 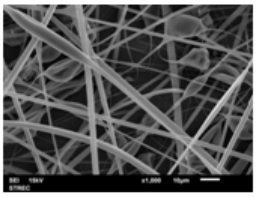 2.02 ± 0.84 μm |
| | THF/DMF (3:1 v/v) | 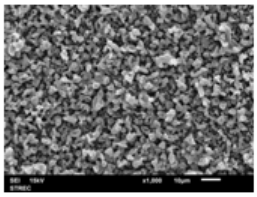 beads | 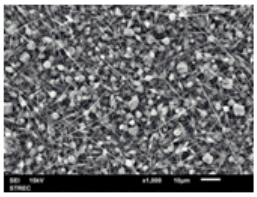 0.18 ± 0.07 μm | 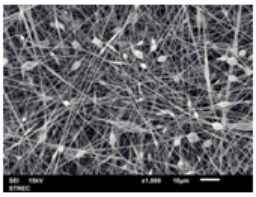 0.29 ± 0.10 μm |
| 60 | THF/DMF (3:1 v/v) | 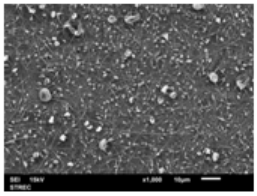 0.16 ± 0.05 μm | 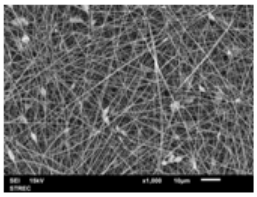 0.33 ± 0.13 μm | 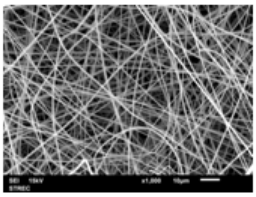 0.62 ± 0.16 μm |

**Figure 6.3** SEM micrographs of P(PFPA-*r*-NIPAM) fibers electrospun from two molecular weights (47 and 60 kDa) in THF and binary mixture of THF/DMF (3:1(v/v)) with different polymer concentrations from 10 to 30% w/v at a constant voltage of 20 kV, a flow rate of 3 mL/h. Number appearing below each micrograph is an average diameter of the electrospun fibers (scale bar 10 μm).

***Effect of molecular weight and polymer solution concentration.*** The molecular weight and polymer solution concentration are the important parameters that pose strong impact on fiber formation. **Figure 6.3** shows SEM micrographs of the P(PFPA-*r*-NIPAM) electrospun fibers fabricated from two molecular weights (47 kDa and 60 kDa) with different polymer concentrations (10-30% (w/v)) at a constant voltage of 20 kV and a flow rate of 3 mL/h. For the copolymer with $M_n$ of 47 kDa, a concentration of 10% (w/v) was too low to provide reasonable chain entanglement and viscosity so that only beads were formed  Under the same concentration, beads with some fibers were observed for the copolymer with $M_n$ of 60 kDa. At 20% (w/v), beaded fibers with diameter of 0.18 ± 0.07 μm were formed for the copolymer with $M_n$ of 47 kDa. In contrast, the copolymer with $M_n$ of 60 kDa yielded fibers with fewer beads. As the concentration of polymer in solution was increased to 30%(w/v), chain entanglement and viscosity were high enough to give a well-defined fibers without beads especially in the case of copolymer with high molecular weight. Moreover, the fiber diameter of the P(PFPA-*r*-NIPAM) was correspondingly increased as a function of polymer concentration. Therefore, the optimal molecular weight and polymer concentration of the P(PFPA-*r*-NIPAM) were 60 kDa and 30 %(w/v), respectively.

Following the optimal condition formerly identified for the electrospinning of P(PFPA-*r*-NIPAM) fibers, ONB-containing P(PFPA-*r*-NIPAM) fibers were fabricated using a polymer solution concentration of 30% w/v, a constant voltage of 20 kV, and a flow rate was 3 mL/h. The average fiber diameter of ONB-containing P(PFPA-*r*-NIPAM) was 0.78 ± 0.21 μm. After UV irradiation, the average fiber diameter of cross-linked (CL) fibers was found to be slightly smaller than those of uncross-linked (UCL) fibers implying that the covalently cross-linked network of the ONB-protected diamine with PFPA part were formed as shown in **Figure 6.4**.

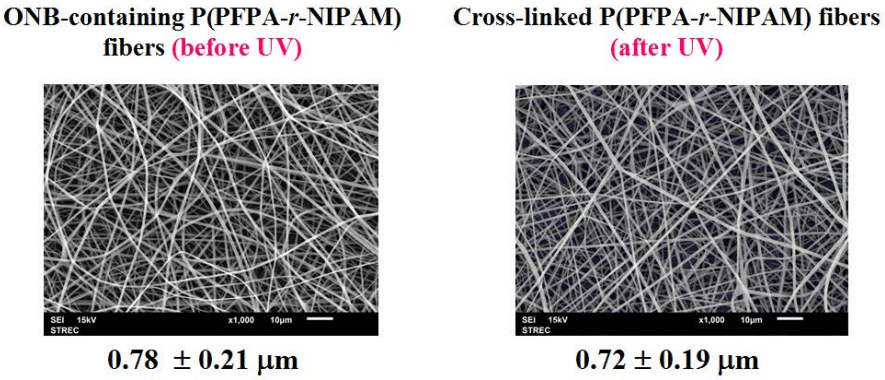


**Figure 6.4** SEM micrographs of ONB-containing P(PFPA-*r*-NIPAM) fibers electrospun from a binary mixture of THF/DMF (3:1) at a constant voltage of 20 kV, a flow rate of 3 mL/h. Number appearing below each micrograph is an average diameter of the electrospun fibers (scale bar 10 μm).

**Stability of of P(NIPAM-*r*-PFPA) fibers.** The stability of UCL and CL fibers of P(PFPA-*r*-NIPAM) were evaluated in BSA-FITC solution and phosphate-buffered saline (10 mM PBS, pH 7.4). Samples were immersed in the solutions for 24 h at room temperature and then washed with distilled water twice, followed by drying overnight under ambient condition and then vacuum dried for another 24 h. The morphological changes of the samples were observed by SEM. The fiber diameters were measured on at least 50 samples to evaluate swelling of the fibers. The morphological changes and the diameters of the electrospun fibers before and after treatment with the solutions are shown in **Figure 6.5**. Before immersion, all the samples were of similar diameters (around 600-700 nm). After immersion in the solutions for 24 h, both of the UCL and CL electrospun fibers could maintain their fibrous structure, although the diameters of both fibers slightly increased as a result from swelling of PNIPAM.

| | Before immersion in PBS | After immersion in PBS | After immersion in BSA-FITC |
|---|---|---|---|
| Uncross-linked P(PFPA-*r*-NIPAM) | 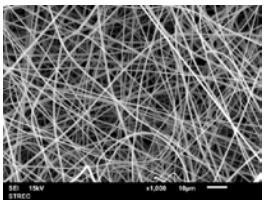 | 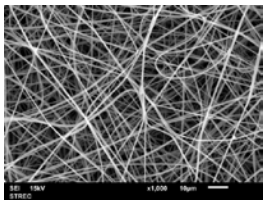 | 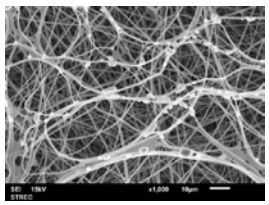 |
| | 0.62 ± 0.16 μm | 0.80 ± 0.19 μm | 0.81 ± 0.24 μm |
| Cross-linked P(PFPA-*r*-NIPAM) | 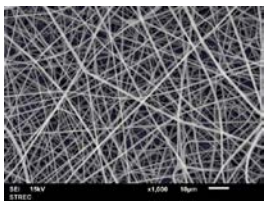 | 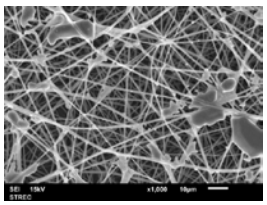 | 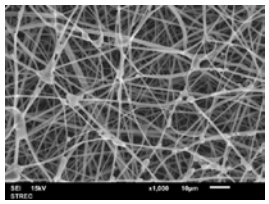 |
| | 0.72 ± 0.19 μm | 0.88 ± 0.16 μm | 0.91 ± 0.22 μm |

**Figure 6.5** SEM micrographs of uncross-linked and cross-linked P(PFPA-*r*-NIPAM) fibers before and after immersion in PBS and BSA-FITC for 24 h (scale bar 10 μm).

**Immobilization of GRGDS peptide on the P(PFPA-*r*-NIPAM) fibers.** Prior to immobilization of GRGDS peptide on both UCL and CL fibrous mats, Bovine serum albumin-fluorescein isothiocyanate conjugate (BSA-FITC) was used as a fluorescent-labeled biomolecule model to prove whether or not amino-containing molecules can react with the active ester groups of PFPA units in the copolymer. **Figure 6.6** shows fluorescence images of uncross-linked and cross-linked P(PFPA-*r*-NIPAM) fibers both before and after conjugation. The green illumination of both UCL and CL fibers on the right column indicated the successful immobilization of the BSA-FITC onto the fibers. Even dye distribution along the fibers also implies a homogeneous distribution of PPFPA moieties on the fiber surface. Change in wettability of the fibrous surfaces was monitored by water contact angle measurements (shown in **Table 6.1**). The UCL fibers exhibited much higher water contact angle than the CL fibers which is a strong indication of hydrophobic PFP groups being greater in composition at the fiber surface before crosslinking. The water contact angle became significantly decreased after reacting with GRGDS peptide, indicating that some of hydrophobic moieties of PFPA units have been replaced by the more hydrophilic GRGDS peptide.

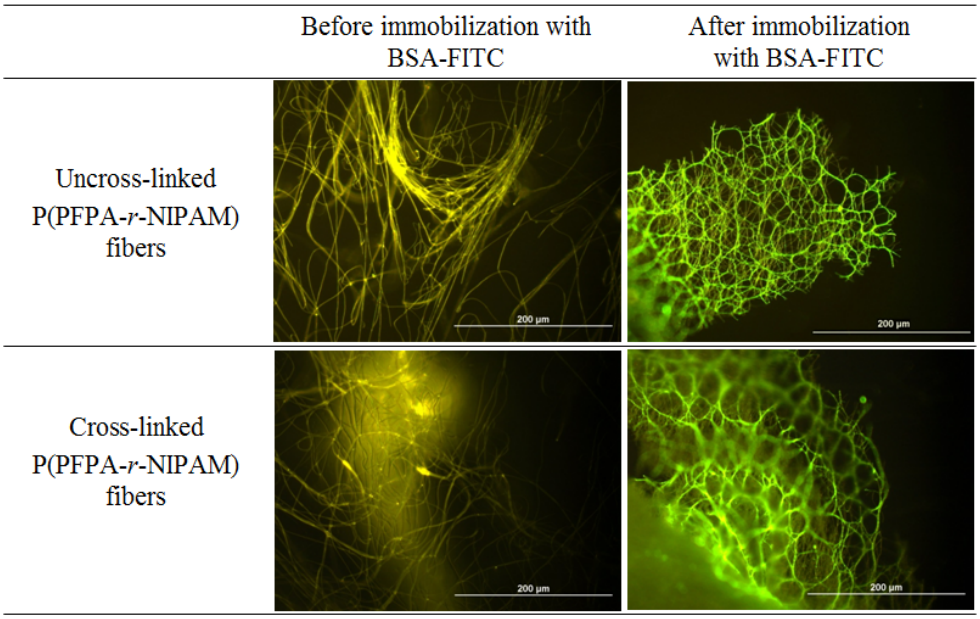


**Figure 6.6** Fluorescence micrographs of UCL and CL P(PFPA-*r*-NIPAM) fibers before and after immobilization with BSA-FITC (scale bar 200 µm).

**Table 6.1** Water contact angles of UCL and CL fibers of P(PFPA-*r*-NIPAM) before and after immobilization of GRGDS peptide.

| Sample | Water contact angle (degree) | |
|---|---|---|
| | before GRGDS immobilization | after GRGDS immobilization |
| UCL fibers | 157.6 ± 8.33 | 105.6 ± 4.16 |
| CL fibers | 129.2 ± 6.29 | 80.3 ± 2.93 |

**Cytocompatibility test.** In this research, *in vitro* cytocompatibility of both uncross-linked and cross-linked P(PFPA-*r*-NIPAM) fibers after GRGDS immobilization which is designated as GRGDS-UC and GRGDS-C fibers, respectively was carried out against mice L929 fibroblast cell line. To investigate the mitochondrial functions of the cultured L929, reduction of MTT reagent was used as an assay of mitochondrial redox activity. MTT reagent is a pale yellow substance that is reduced to a dark blue formazan product when incubating with viable cells by mitochondrial succinate dehydrogenase in complex II, which plays a critical role in both oxidative phosphorylation and tricarboxylic acid cycle. Therefore, the production of formazan can

reflect the level of cell viability. The cell adhesion was determined at 6 h and cell proliferation was evaluated at 1 day, 3 days and 5 days of cell culture. The results are reported in terms of the cell adhesion and proliferation ratio (% relative to TCPS) which is directly correlated to the number of viable cells.

After 6 h of cell culture, the cell adhesion ratios (% relative to TCPS) on UC and C fibers were 35 and 49%, respectively whereas much higher cell adhesion ratios of 60 and 109% were found on GRGDS-UC, and GRGDS-C fibers respectively. Such an outcome strongly suggested that the immobilized GRGDS peptide can efficiently support cell adhesion at 6 h (**Figure 6.7 (a)**). We explain the inferior cellular adhesion in both the UC and C fibers before peptide immobilization as a consequence of the hydrophobic nature of the fibers as opposed to the TCPS and the fibers after peptide immobilization. Apparently, the degree of cell adhesion corresponded quite well with the hydrophobicity of the fibers (See water contact angle data in **Table 6.1**). Besides, initial cell attachment on the plasma treated-polystyrene (abbreviated as t-PS) fibers was higher than TCPS surface. This truly emphasizes the positive influence of material porosity on cell adhesion.

Cell proliferation was observed on 1 day, 3 days, and 5 days of cell culture. The data of cell proliferation ratio (% relative to TCPS) are displayed in **Figure 6.7(b)**. The percentage of live cells increases with an increase in cell culture time. The percentage of live cells for GRGDS-C fibers was higher than those of GRGDS-UC fibers. This outcome suggested that not only the immobilized peptide but also the hydrophilicity of the surfaces are important parameters that dictate cell growth. Once again, the percentage of live cells on t-PS fibers was the highest and higher than that of TCPS, emphasizing the fact that three dimensional fibrous structure of t-PS fibers are superior substrate for supporting cell growth than the flat TCPS.

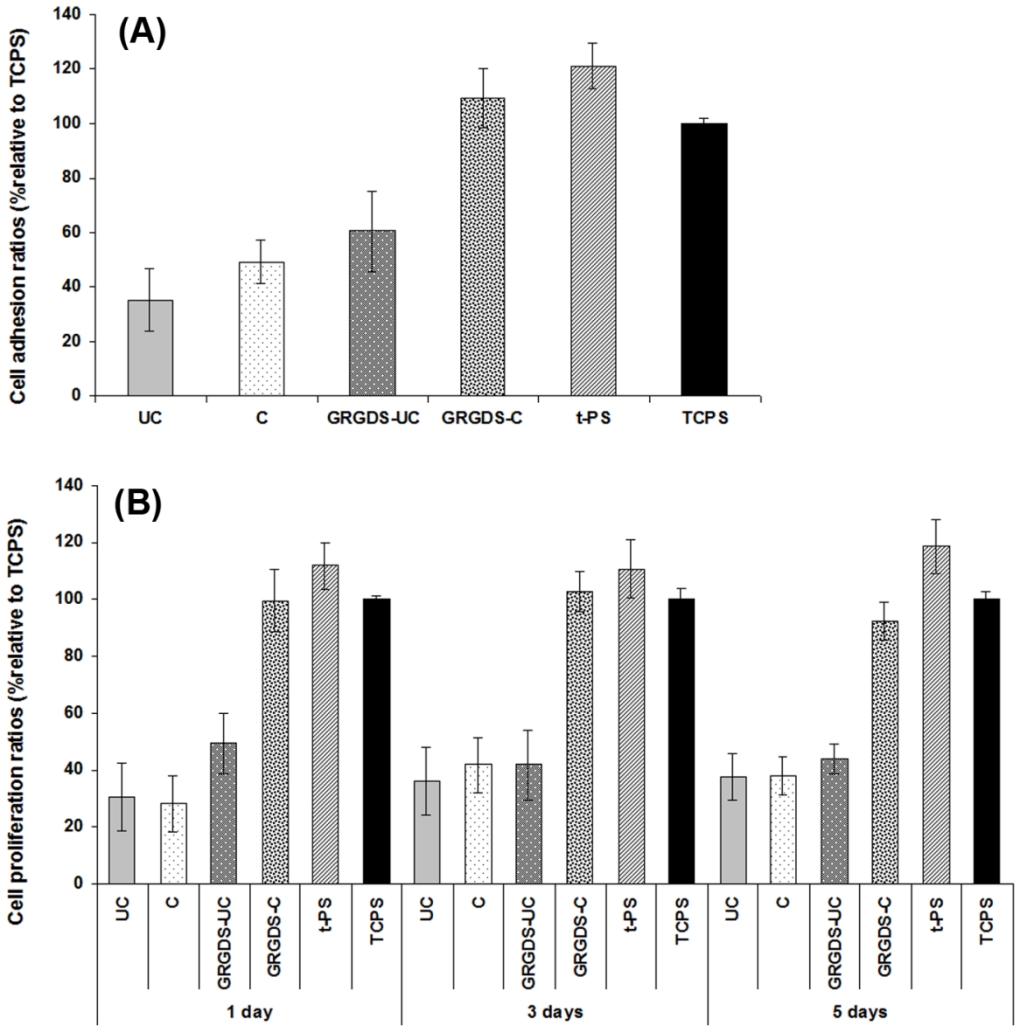


**Figure 6.7** Responses of L929 cells (% relative to TCPS) with a seeding density of $2.0x10^4$ cells/well on uncross-linked (UC), cross-linked (C), GRGDS-immobilized uncross-linked (GRGDS-UC) and cross-linked (GRGDS-C) fibers, t-PS fibers and TCPS in terms of (A) the cell adhesion ratios at 6 h and (B) the cell proliferation ratios at 1, 3 and 5 days. Statistical significance with $p < 0.05$ is compared with the control (TCPS).

For cell detachment treatment, spread cells were transferred to an incubator equipped with a cooling unit fixed at 20°C. The morphology of both attached and detached cells were observed by SEM. When the culture temperature was reduced to 20°C after incubation at 37°C for 5 days, the spread cells became rounded and detached from both GRGDS-UC and GRGDS-C fibers. Spread cells were more slightly detached from the GRGDS-C fibers than the GRGDS-UC fibers. This may be ascribed to the GRGDS-C fibers being more hydrophilic than the GRGDS-UC fibers. In addition, Ebara *et al.*,[31] reported that at temperatures below the grafted polymer's LCST, integrin-RGDS association decreases due to loss of cell tension and surface anchoring,

prompting cells to round and then detach. This surface property changes obviously weakened cellular adhesion, resulting in spontaneous cell detachment as shown in **Figure 6.8**.

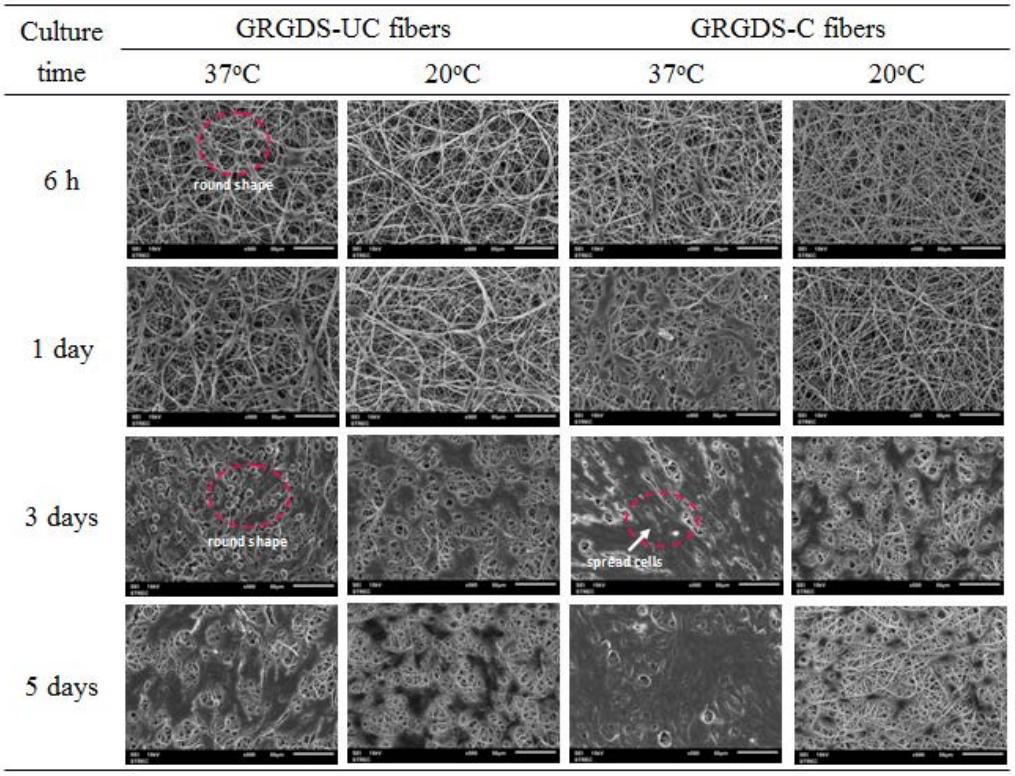


**Figure 6.8** SEM micrographs of fibroblasts on the GRGDS-UC fibers (left column) and GRGDS-C fibers (right column): cell attachment at 37°C for a set culture time and cell detachment at 20°C for 30 min (scale bar 50 μm).

As demonstrated in **Figure 6.9**, the percentage of attached cells on the surfaces after temperature reduction from 37 to 20 °C decreased rapidly on both GRGDS-UC and GRGDS-C fibrous mats (decrease around 45% within 30 min), while there were no cells detached from t-PS fiber and TCPS of which surfaces are lack of thermo-responsive property. The cell detachment was almost complete within 90 min of incubation. The prompt cell detachment from both GRGDS-UC and GRGDS-C fibrous mats may be explained as a result of water molecules being capable of efficiently reaching PNIPAM chains within the fiber through pores from both underneath and side. Therefore, hydration of PNIPAM molecules happened so quickly and thus accelerated detachment of the attached cells.

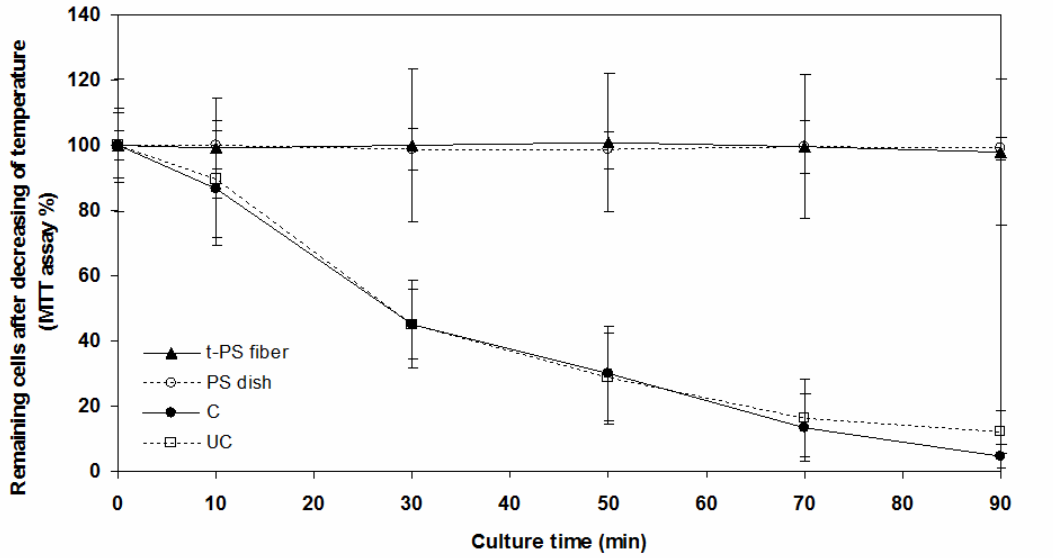


**Figure 6.9** The percentage of remaining cells on GRGDS-immobilized uncross-linked (GRGDS-UC) and cross-linked fibers (GRGDS-C), t-PS fibers and TCPS as a function of incubation time at 20°C.

Biocompatibility is the main requirement for any polymeric synthetic materials to be useful in tissue engineering. It should not leach any toxic substances that may cause harm to cells or otherwise interfere with the physiological responses of the cells that come in contact with these substances. Moreover, initial cell attachment, rapid proliferation, and rapid intact cell recovery are important to maintain biological functions and viability of cell source for the fields of regenerative medicine. From this view point, the GRGDS-C fibers could be a promising biomaterial to recover intact cultured cells for cell culture and tissue engineering applications.

## CONCLUSIONS

In this research, random copolymer of P(PFPA-*r*-NIPAM) was successfully synthesized by RAFT polymerization having relatively high molecular weights ($M_n$ of 47 and 60 kDa). The ONB groups introduced via post-polymerization modification of PFPA moieties in P(PFPA-*r*-NIPAM) with the ONB-protected diamine can be released upon UV irradiation which subsequently induced an *in situ* cross-linking by spontaneous reaction with the remaining PFPA and yielded cross-linked fibers. GRGDS peptide was then grafted onto the surface of cross-linked fibers via post-functionalization. From the cell study results, cells were well attached and proliferated on GRGDS-grafted cross-linked fibers more than that on GRGDS-grafted uncross-linked fibers. Moreover, cells

were spontaneously detached on both GRGDS-grafted uncross-linked and cross-linked fibers. From this point of view, GRGDS-grafted cross-linked fibers could be a promising material to recover intact cultured cells.

## REFERENCES


(1) Guillame-Gentil, O.; Semenov, O.; Roca, A. S.; Groth, T.; Zahn, R.; Vörös, J.; Zenobi-Wong, M. *Advanced Materials* **2010**, *22*, 5443.

(2) Tang, Z.; Akiyama, Y.; Okano, T. *Polymers* **2012**, *4*, 1478.

(3) Schild, H. G. *Progress in Polymer Science* **1992**, *17*, 163.

(4) Yamato, M.; Okano, T. *Materials Today* **2004**, *7*, 42.

(5) Yamato, M.; Akiyama, Y.; Kobayashi, J.; Yang, J.; Kikuchi, A.; Okano, T. *Progress in Polymer Science* **2007**, *32*, 1123.

(6) Yamada, N.; Okano, T.; Sakai, H.; Karikusa, F.; Sawasaki, Y.; Sakurai, Y. *Die Makromolekulare Chemie, Rapid Communications* **1990**, *11*, 571.

(7) Okano, T.; Yamada, N.; Okuhara, M.; Sakai, H.; Sakurai, Y. *Biomaterials* **1995**, *16*, 297.

(8) Uchida, K.; Sakai, K.; Ito, E.; Hyeong Kwon, O.; Kikuchi, A.; Yamato, M.; Okano, T. *Biomaterials* **2000**, *21*, 923.

(9) Nandkumar, M. A.; Yamato, M.; Kushida, A.; Konno, C.; Hirose, M.; Kikuchi, A.; Okano, T. *Biomaterials* **2002**, *23*, 1121.

(10) Mizutani, A.; Kikuchi, A. *Biomaterials* **2008**, *29*, 2073.

(11) Arisaka, Y.; Kobayashi, J.; Yamato, M.; Akiyama, Y.; Okano, T. *Biomaterials* **2013**, *34*, 4214.

(12) Yoshida, R.; Uchida, K.; Kaneko, Y.; Sakai, K.; Kikuchi, A.; Sakurai, Y.; Okano, T. *Nature* **1995**, *374*, 240.

(13) Kaneko, Y.; Nakamura, S.; Sakai, K.; Aoyagi, T.; Kikuchi, A.; Sakurai, Y.; Okano, T. *Macromolecules* **1998**, *31*, 6099.

(14) Kaneko, Y.; Nakamura, S.; Sakai, K.; Kikuchi, A.; Aoyagi, T.; Sakurai, Y.; Okano, T. *Polymer Gels and Networks* **1998**, *6*, 333.

(15) Kwon, O. H.; Kikuchi, A.; Yamato, M.; Sakurai, Y.; Okano, T. *Journal of Biomedical Materials Research* **2000**, *50*, 82.

(16) Hyeong Kwon, O.; Kikuchi, A.; Yamato, M.; Okano, T. *Biomaterials* **2003**, *24*, 1223.

(17) Oh, H. H.; Ko, Y.-G.; Uyama, H.; Park, W. H.; Cho, D.; Kwon, O. H. *BioMed Research International* **2014**, *2014*, 9.

(18) Bhardwaj, N.; Kundu, S. C. *Biotechnology Advances* **2010**, *28*, 325.

(19) Quynh P. Pham, U. S., Antonios G. Mikos *Tissue Engineering* **2006**, *12*, 1197.

(20) Sill, T. J.; von Recum, H. A. *Biomaterials* **2008**, *29*, 1989.

(21) Agarwal, S.; Wendorff, J. H.; Greiner, A. *Polymer* **2008**, *49*, 5603.

(22) Beachley, V.; Wen, X. *Progress in Polymer Science* **2010**, *35*, 868.

(23) Rockwood, D. N.; Chase, D. B.; Akins Jr, R. E.; Rabolt, J. F. *Polymer* **2008**, *49*, 4025.

(24) Okuzaki, H.; Kobayashi, K.; Yan, H. *Synthetic Metals* **2009**, *159*, 2273.

(25) Eberhardt, M.; Théato, P. *Macromolecular Rapid Communications* **2005**, *26*, 1488.

(26) Theato, P. *Journal of Polymer Science Part A: Polymer Chemistry* **2008**, *46*, 6677.

(27) Gentsch, R.; Pippig, F.; Nilles, K.; Theato, P.; Kikkeri, R.; Maglinao, M.; Lepenies, B.; Seeberger, P. H.; Börner, H. G. *Macromolecules* **2010**, *43*, 9239.

(28) Graisuwan, W.; Zhao, H.; Kiatkamjornwong, S.; Theato, P.; Hoven, V. P. *Journal of Polymer Science Part A: Polymer Chemistry* **2015**, *53*, 1103.

(29) Jochum, F. D.; Theato, P. *Macromolecules* **2009**, *42*, 5941.

(30) Eda, G.; Shivkumar, S. *Journal of Applied Polymer Science* **2007**, *106*, 475.

(31) Ebara, M.; Yamato, M.; Aoyagi, T.; Kikuchi, A.; Sakai, K.; Okano, T. *Biomacromolecules* **2004**, *5*, 505.

# Chapter VII

## Thermoresponsive Polymer Brushes Prepared by Post-Polymerization Modification of Poly(pentafluorophenyl acrylate) for Tissue Engineering Applications

### INTRODUCTION

Thermoresponsive polymers belong to a class of smart materials that have the ability to alter their physical properties in response to temperature change. Poly(*N*-isopropylacrylamide) (PNIPAM) is the most well-known in its class, exhibiting a lower critical solution temperature (LCST) of about 32°C in water. Below the LCST, PNIPAM forms an expanded structure and soluble in solution. In contrast, PNIPAM forms denser globular structure and becomes insoluble in the solution once the temperature is raised above the LCST.[1,2] Since its LCST is close to body temperature, PNIPAM is currently recognized as valuable materials for a variety of biomedical applications e.g. drug delivery, biomolecules separation, and tissue engineering.[3-5]

A tissue-like cellular monolayer or cell sheet has become one of the most effective platforms for tissue engineering because they can be directly transplanted to host tissues without the demand for biodegradable scaffolds which are often the cause of inflammatory response. The direct transplantation has been recently applied to several diseased organs e.g. eye, heart and kidney.[6] To prepare this platform, the thermoresponsive PNIPAM has been developed as cell-culture substrates for cell sheet preparation. At above the LCST, cultured cells can adhere and proliferate on PNIPAM surface. When reducing temperature below the LCST, cell sheet can be harvested intact with associated extracellular matrix (ECM) without EDTA or enzymatic treatment.[7-9]

To improve properties of the thermoresponsive brushes, terminal functionalization and synthesis of PNIPAM containing more active functional group such as carboxyl group have been reported by Okano and coworkers.[5,10,11] They have found that modification of PNIPAM chain end with hydrophilic maleimide derivatives demonstrated can improve cell adhesion property of thermoresponsive surfaces. In

particular, the maleimide derivative containing carboxyl group enhanced the ability to promote cell sheet detachment within 30 min after low temperature treatment. In addition, the immobilization of biomolecules for enhance cell adhesion property through carbodiimide chemistry of carboxyl groups in PNIPAM brushes has been reported. 3-Mercaptopropionic acid was used as chain transfer agent for polymerization of NIPAM providing carboxyl group at chain end. It was reported that the terminal carboxyl groups of PNIPAM brushes showed the ability to immobilize protein and promote cell adhesion and detachment of surfaces.

Immobilizing cell-specific biomolecules is one of effective ways to improve cell adhesion property of materials. Such strategy cannot be directly applied to PNIPAM, of which its amide side chains are hydrolytically stable, unless complicated synthetic techniques are employed.[5,11,12] Poly(pentafluorophenyl acrylate) (PPFPA) is an attractive precursor polymer containing active pentafluorophenyl (PFPA) moieties in its side chains. The active PPFPA also provide a good hydrolytic stability and good solubility in a wide range of organic solvents.[13,14] The active PFPA groups can react with hydrophilic amine compounds including isopropylamine (IPA) under mild conditions via post-polymerization modification yielding the thermoresponsive PNIPAM.[15] In principle, these highly reactive ester groups should readily available for interacting with N-terminus of protein/peptide rendering effective biomolecule immobilization.[16,17]

Here in this research, active PPFPA grafted substrates were prepared by either “grafting from” or “grafting to” methods via RAFT polymerization and converted to thermoresponsive PNIPAM brushes by post-polymerization modification with IPA The composition of P(PFPA-*co*-NIPAM) can be controlled by IPA concentration and reaction time. The resulting surface-grafted copolymer brushes of P(PFPA-co-NIPAM) were then immobilized with collagen type I, a cell adhesion promoter (CAPs). PAA brushes have been shown to have the capacity to resist cell adhesion and promote cell detachment property.[5,18] Because the pentafluorophenyl esters can be transformed to acrylic acid under suitable hydrolytic condition, another series of surface-grafted polymer brushes based on poly(acrylic acid-co- *N*-isopropylacrylamide) or P(AA-*co*-NIPAM) were also prepared by hydrolysis of P(PFPA-*co*-NIPAM). Both collagen type I immobilized P(PFPA-co-NIPAM) and P(AA-*co*-NIPAM) brushes were investigated as thermoresponsive substrates for cell sheet fabrication. This research aims to demonstrate the versatility of active-ester containing PPFPA as precursor polymer capable of undergoing tandam post-polymerization with the right choice of active

molecules and yield multifunctional polymeric platform for tissue engineering applications.

## EXPERIMENTAL SECTION

**Materials.** Acrylic acid (AA), 4-dimethylaminopyridine (DMF), 4,4′-azobis(4-cyanovaleric acid) (ACVA), and 4-cyanopentanoic acid dithiobenzoate (CPD) (chain transfer agent or CTA) were obtained from Aldrich (USA). AA was purified by vacuum distillation. Pentafluorophenol, acetone, toluene, hexane, ethanol, dichloromethane, 1,4-dioxane and tetrahydrofuran (THF) were purchased from Merck (Germany). Dicyclohexyl carbodiimide (DCC), phosphate buffered saline pH 7.4 (PBS), 3-aminopropyltriethoxysilane (APTES), triethylamine (TEA), isopropylamine (IPA) were obtained from Sigma-Aldrich (USA). Glass slides were supplied by S.E. SUPPLY LTD PART. Pentafluorophenyl acrylate (PFPA) was synthesized according a published procedure.[1] Keratinocyte cells and collagen type I were purchased from STEMCELL Technologies. Ultrapure distilled water that was obtained after purification using a Millipore Milli-Q system (USA) that involves reverse osmosis, ion exchange, and a filtration step (18.2 MΩ cm resistance).

### Preparation of P(PFPA-co-NIPAM) by post-polymerization modification

PPFPA was first synthesized via RAFT polymerization. PFPA (1.48mL, 1 M), CPD (2.5, 5, 20 mM) and ACVA (0.31, 0.62, 2.5 mM) were dissolved in 1,4-dioxane (9 mL). The solution was heated up to 70ºC for 20 h and then cooled down to room temperature before precipitated in methanol. Purified PPFPA was obtained as pink powder after re-precipitation twice from polymer solution in 1,4-dioxane into methanol.

P(PFPA-*co*-NIPAM) was then prepared by post-polymerization modification of PPFPA with IPA at 45ºC. The mole equivalent of IPA to PFPA unit in the PPFPA was varied in a range of 0.25-1. The reaction time was also varied to determine the kinetics of post-polymerization modification. At the end of modification period, the obtained (co)polymer product was precipitated in hexane or diethyl ether.

### Preparation of surface-grafted (co)polymer Brushes

Glass coverslips were cleaned by air plasma cleaner (Harrick, USA, model PDC-32G) with power of 18 W for 5 min prior to use. APTES was immobilized on the cleaned glass substrates via vapor-phase deposition method. APTES (100 µL) was

added to a reaction vial containing the cleaned glass substrates and then heated to 80 °C. After 72 h, the APTES-modified substrates were rinsed with toluene, acetone and DI water, respectively.

The active PPFPA were grafted on glass surfaces via “grafting from” or “grafting onto” methods (**Scheme 7.1**). For the “grafting from” method, the APTES-modified substrates were immersed in DMF containing ACVC (37.5 mM), DCC (47.0 mM) and DMAP (3.74 mM) at room temperature for 20 h under nitrogen atmosphere to yield initiator-immobilized substrates. The substrates were rinsed thoroughly with DMF and ethanol. The initiator-immobilized substrates were immersed in 1,4-dioxane containing PFPA (1 M) and CTA (2.5, 5, 20 mM) and then heated to 70 °C for 20 h under nitrogen atmosphere. The resulting surface-grafted PPFPA were rinsed thoroughly with 1,4-dioxane. Free PPFPA formed simultaneously in solution was also recovered by precipitation with methanol. The surface-grafted PNIPAM and P(PFPA-*co*-NIPAM) were then obtained by post polymerization modification of the surface-grafted PPFPA. Briefly, the surface-grafted PPFPA were immersed in THF containing IPA (10 mM) and TEA (10 mM) at room temperature for 5, 10, 30 and 60 min then rinsed with THF and acetone, respectively.

For the “grafting onto” method, APTES-modified substrates were immersed in 1,4-dioxane containing 0.5 M of P(PFPA-*co*-NIPAM) synthesized by post-polymerization modification of PPFPA at room temperature. After 16 h, the substrates were rinsed with 1,4-dioxane. For the surface-grafted P(AA-*co*-NIPAM) brushes, P(PFPA-*co*-NIPAM) brushes obtained from both “grafting from” and “grafting onto” method were immersed in Milli-Q water containing 0.5 M of TEA at room temperature. After 20 h, the substrates were rinsed thoroughly with Milli-Q water.

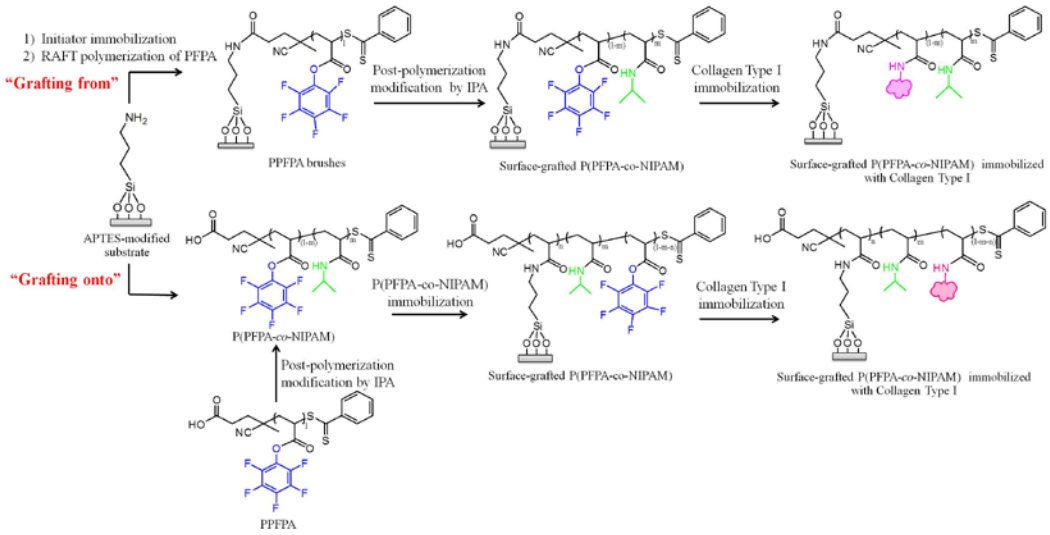


**Scheme 7.1** Preparation of surface-grafted polymer brushes by "grafting from" and "grafting onto" methods followed by collagen type I immobilization.

**Characterization of surface-grafted (co)polymer brushes**

Molecular weight and PDI of PPFPA grafted on glass substrates were analyzed from free PPFPA in solution using a NMR spectrophotometer (Varian, USA, model Mercury-400) operating at 400 MHz and gel permeation chromatography (GPC) using Waters 600 controller chromatograph equipped with HR1 and HR4 columns (Waters, USA) at 35°C and refractive index (RI) detector (Waters, USA, model 2414). THF was used as mobile phase with a flow rate of 1.0 mL/min. A calibration curve was obtained using polystyrene standards. Wettability of the modified surfaces were determined by water contact angle measurement using a contact angle goniometer (Ramé-Hart, Inc., USA, model 100-00), equipped with a Gilmont syringe and a 24-gauge flat-tipped needle. All of measurements were carried out in air at ambient temperature. Advancing ($\theta_A$) and receding ($\theta_R$) were recorded and averaged from a measurements of different area of each sample. The composition of the copolymer grafted on substrates was determined by attenuated total reflectance-Fourier transform infrared (ATR-FTIR) spectrometer (Thermo Scientific Nicolet, USA, model 6700). Surface elemental composition was characterized by an x-ray photoelectron spectroscopy (XPS) (Scienta, Sweden, model ESCA 200) with Al $K_\alpha$ x-rays. All the XPS data were collected at takeoff angles of 90°. Thickness of samples was analyzed by atomic force microscopy (AFM) recorded with Scanning Probe Microscope (Veeco, USA, model NanoScope®IV). Measurements were performed in air using tapping mode. Silicon nitride tips with a resonance frequency of 267-295 KHz and a spring constant 20-80 N/m were used.

**Protein immobilization**

The P(PFPA-*co*-NIPAM) brushes with various %PNIPAM composition were immersed in PBS buffer (pH 7.4) containing collagen type I (10 µg/mL) and stirred for 12 h at 4ºC. The substrates were rinsed with PBS buffer and Milli-Q water, respectively.

**Cell sheet preparation**

Keratinocyte cells were cultured in keratinocyte Growth Medium on tissue culture dishes at 37$^{o}$C, 5% $CO_{2.}$ After 10 days, keratinocyte cells were trypsinized and seeded at 1x10$^{4}$ cells/cm$^{2}$ onto the desired substrates, followed by incubation at 37 ºC. After reaching confluency, the adherent cells were observed by optical microscope (ZEISS, Germany, model Axio Oserver Z1 Motorized) and harvested by decreasing temperature from 37ºC to 25ºC.

**RESULTS AND DISCUSSION**

**Preparation of P(PFPA-*co*-NIPAM) by post-polymerization modification**

PPFPA with different MW was synthesized via RAFT polymerization. The MW and polydispersity index (PDI) were characterized by $^{1}$H NMR and GPC, respectively. The data shown in **Table 7.1** indicated that the polymerization was well-controlled for the targeted degree of polymerization (DP) of 50 and 200 with narrow MWD and the MW being close to the expected MW. Less control over the polymerization of higher targeted DP (400) was observed as indicated by the PDI being deviated from 1.0.

**Table 7.1** Molecular weight information of PPFPA synthesized by RAFT polymerization

| Targeted DP | Theoretical $M_n$ | $M_n$ determined by $^{1}$H NMR | PDI determined by GPC |
|---|---|---|---|
| 50 | 11,905 | 10,238 | 1.37 |
| 200 | 47,622 | 50,003 | 1.24 |
| 400 | 95,244 | 112,507 | 1.72 |

Effects of IPA concentration and reaction time on the extent of post-polymerization modification of PPFPA in solution were determined in order to obtain appropriate conditions that gave P(PFPA-*co*-NIPAM) with varied PNIPAM composition. PPFPA having MW of 112,507 was used for this investigation. As evaluated by FT-IR (**Figure 7.1**), %conversion from PPFPA to PNIPAM or %PNIPAM composition in the

resulting P(PFPA-*co*-NIPAM) can be calculated from a relative intensity ratio of amide C=O stretching of PNIPAM at 1650 $cm^{-1}$ to that of ester C=O stretching of PPFPA. For example, treating PPFPA with 0.25 eq. IPA for 16 h gave 30% conversion meaning that 30% of PPFPA was converted to PNIPAM whereas 70% PPFPA remained unreacted. In other words, such condition yielded P(PFPA-*co*-NIPAM) with 30%PNIPAM composition. As demonstrated in **Figure 7.2**, %PNIPAM composition can be varied as a function of both IPA concentration and reaction time.

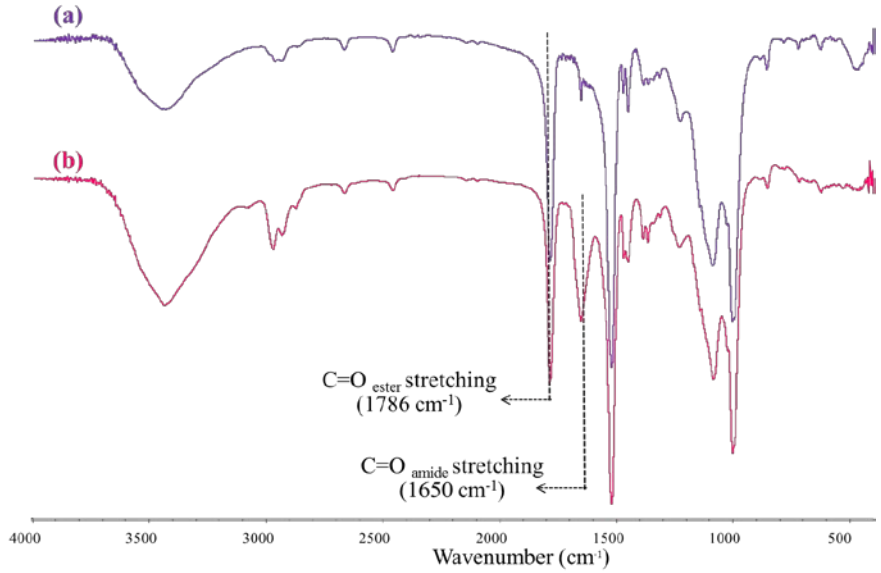


**Figure 7.1** FTIR spectra of PPFPA (a) before and (b) after a reaction with 0.25 eq. IPA for 16 h.

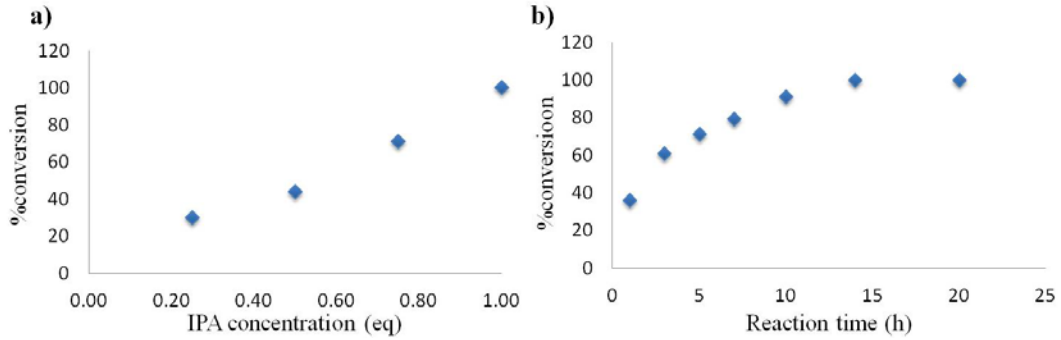


**Figure 7.2** %Conversion from PPFPA to PNIPAM in solution upon post-polymerization modification with IPA as determined by FT-IR as a function of: (a) IPA concentration for 16 h, (b) reaction time using 1 eq. IPA.

**Preparation and Characterization of Surface-grafted (Co)polymer brushes**

Surface-grafted P(PFPA-*co*-NIPAM) brushes were fabricated by two methods (See **Scheme 7.1** for detail). The first method was based on "grafting from" approach which began with surface-initiated RAFT polymerization of PFPA from initiator-immobilized substrates (having $\theta_A/\theta_R$ of 80.1°/43.7°) that resulted in surface-grafted PPFPA followed by post-polymerization modification with IPA. Formation of the surface-grafted P(PFPA-*co*-NIPAM) brushes was monitored by water contact angle measurements. As shown in **Figure 7.3**, the water contact angle rapidly decreased from 98°/67° of the surface-grafted PPFPA to 90/56° after 5 min of exposure to 10 mM of IPA. Decreasing of water contact angle still continued and reached a minimum of 84/52° after 20 min. The water contact angle remained unchanged despite the longer reaction time suggesting that the PPFPA was completely transformed into PNIPAM. This set of data have demonstrated that the surface-grafted P(PFPA-*co*-NIPAM) brushes with varied PNIPAM composition can be prepared by post-polymerization modification of the surface-grafted PPFPA brushes initially prepared by "grafting from" approach.

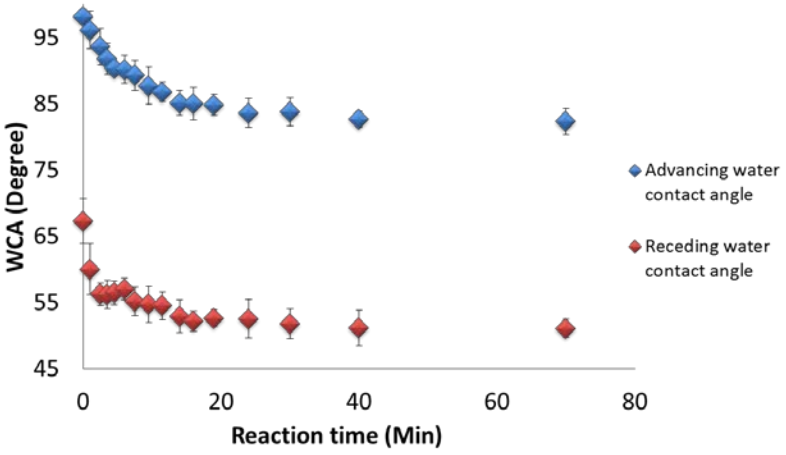


**Figure 7.3** Kinetics of post-polymerization modification of the surface-grafted PPFPA brushes prepared by "grafting from" approach after exposure to 10 mM of IPA.

The ability to control the extent of post-polymerization modification of PPFPA by IPA in solution by varying IPA concentration (as shown in **Figure 7.2(a)**) allows for the preparation of P(PFPA-*co*-NIPAM) with varied %PNIPAM via the second method based on "grafting onto" approach. This can be accomplished by a reaction between remaining PFP groups in the copolymers after the first post-polymerization modification with IPA and amino groups on the surface of the APTES-modified substrates. A series of

P(PFPA-*co*-NIPAM) having of 40, 60, 75 %PNIPAM obtained from post-polymerization modification described earlier were selected for this investigation.

As shown in **Table 7.2**, the surface-grafted P(PFPA-*co*-NIPAM) brushes became more hydrophilic with lower water contact angles as a function of %PNIPAM. Notably, similar water contact angle values were observed for both the surface-grafted PPFPA and PNIPAM prepared by the "grafting onto" method suggesting their comparable surface properties to those prepared by "grafting from" method despite their different preparation methods.

**Table 7.2** Water contact angle data of the surface-grafted (co)polymer brushes prepared by "grafting onto" approach.

| Surfaces | Water contact angle (Degree) |
|---|---|
| APTES-modified | 84.7/50.4 |
| PPFPA brushes | 99.5/64.0 |
| P(PFPA-*co*-NIPAM) brushes | |
| - 40% PNIPAM | 92.4/50.1 |
| - 60% PNIPAM | 89.7/46.1 |
| - 75% PNIPAM | 82.4/52.3 |
| PNIPAM brushes | 77.1/33.9 |

The surface grafted P(PFPA-*co*-NIPAM) brushes prepared by this "grafting onto" approach were also characterized by FT-IR analysis (**Figure 7.4**). The characteristic peaks assigned to ester C=O stretching of PPFPA and amide C=O stretching of PNIPAM appeared at 1786 and 1650 $cm^{-1}$, respectively. The relative intensity between the former and latter peak became correspondingly decreased as the %PNIPAM in the copolymer increased from 40 to 75%.

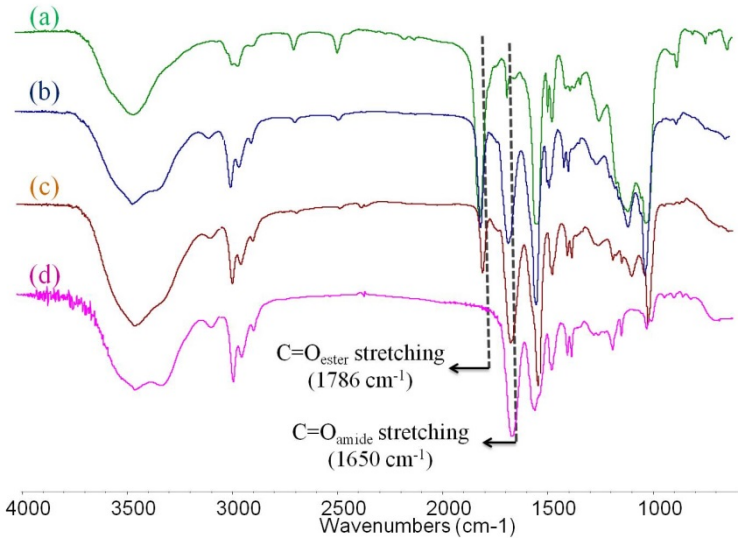


**Figure 7.4** FTIR spectra of the surface-grafted (co)polymer brushes prepared by "grafting onto" approach: (a) PPFPA, P(PFPA-*co*-NIPAM) with %PNIPAM of (b) 40 and (c) 75, and (d) PNIPAM.

To identify the varied copolymer composition (PPFPA vs PNIPAM) on the surface-grafted P(PFPA-*co*-NIPAM) brushes, XPS analysis has been performed on two series of substrates: one prepared by the "grafting from" approach and the other prepared by "grafting onto" approach. In the case of "grafting from" approach of which XPS data are shown in **Table 7.3**, fluorine composition correspondingly decreased as a function of reaction time with IPA suggesting the PFP groups were eliminated as a result of post polymerization modification. The decreasing F/N ratio indicated the greater %PNIPAM as the reaction time increased. As anticipated, the %F as well as F/N ratio also decreased as the %PNIPAM in the copolymer used for "grafting onto" the APTES-modified substrates increased as demonstrated in **Table 7.4**.

**Table 7.3** Atomic composition of the surface-grafted P(PFPA-*co*-NIPAM) brushes prepared by "grafting from" approach by post-polymerization modification of the surface-grafted PPFPA in 10 mM of IPA for different period of time.

| Reaction time with IPA (min) | Atomic composition (%) | | | | | | Atomic ratio |
|---|---|---|---|---|---|---|---|
| | C | N | O | F | Si | S | F/N |
| 0 | 61.10 | 2.59 | 23.79 | 5.67 | 6.39 | 0.46 | 2.189 |
| 5 | 60.06 | 3.66 | 25.87 | 2.55 | 7.41 | 0.46 | 0.697 |
| 10 | 61.42 | 4.77 | 25.30 | 1.43 | 6.78 | 0.30 | 0.300 |
| 30 | 61.35 | 3.95 | 26.15 | 0.55 | 7.6 | 0.33 | 0.140 |
| 60 | 58.59 | 4.93 | 27.02 | 0.46 | 8.43 | 0.57 | 0.093 |

**Table 7.4** Atomic composition of the surface-grafted P(PFPA-*co*-NIPAM) brushes prepared by "grafting onto" approach from P(PFPA-co-NIPAM) obtained from post-polymerization modification of PPFPA with varied equivalence of IPA for 16 h

| %PNIPAM | Atomic composition (%) | | | | | | Atomic ratio |
|---|---|---|---|---|---|---|---|
| | C | N | O | F | Si | S | F/N |
| 30 | 62.22 | 2.31 | 25.87 | 1.44 | 7.69 | 0.48 | 0.623 |
| 45 | 56.71 | 3.15 | 28.69 | 1.63 | 9.00 | 0.82 | 0.517 |
| 59 | 61.53 | 2.64 | 25.39 | 1.21 | 8.84 | 0.38 | 0.458 |
| 78 | 54.92 | 4.03 | 30.21 | 1.05 | 9.08 | 0.72 | 0.261 |

**Determination of Graft Density and Thickness of the Surface-grafted (Co)polymer Brushes**

It has been reported by Okano and co-workers[19] that the thickness of surface-grafted PNIPAM exhibits a strong influence on its thermo-responsiveness and therefore determines its success in subsequent application for cell sheet fabrication. Grafting quantity of PPFPA on glass substrates can be first determined by FT-IR. As the base substrate was glass, a strong adsorption of Si–O was observed at 1000 $cm^{-1}$ and the characteristic C=O stretching peak of PPFPA appeared at 1786 $cm^{-1}$. The peak intensity

ratio of Si-O and C=O can be used to determine the amount of PPFPA grafted onto surfaces using a calibration curve prepared by a known amount of PPFPA cast on APTES-modified glass surfaces (**Figure 7.5**).

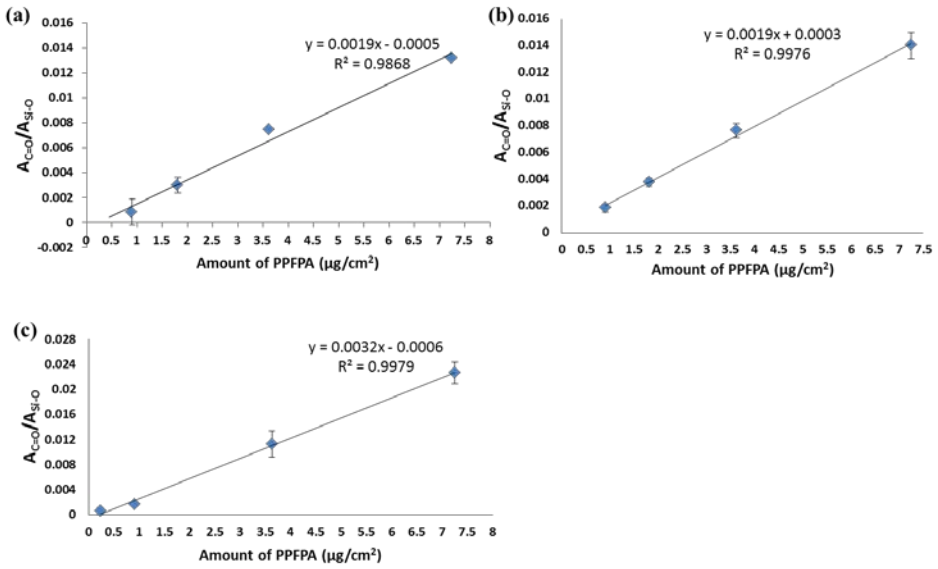


**Figure 7.5** Calibration curves of PPFPA casted on glass substrates for grafted amount determination; DP of (a) 50, (b) 200, and (c) 400.

As outlined in **Table 7.5**, the grafted quantity of PPFPA on the glass surface proportionally increased as a function of molecular weight of PPFPA. Apparently, grafting amount of the surface-grafted PPFPA prepared by “grafting onto” approach was smaller and less dependent on the PPFPA molecular weight than that obtained via “grafting from” approach. The “grafting onto” method is known to yield low graft density. This is mainly because the incoming polymer chains usually suffer entropic barrier due to the crowding of the initially grafted polymer chains that inhibits further insertion of the polymer chains. The limitation becomes more problematic for polymer with high molecular weight. As determined by AFM, the thickness values of the surface-grafted PNIPAM obtained after post-polymerization modification agree well with the PPFPA grafted amount previously quantified by FT-IR. The greater the grafted quantity of PPFPA yielded thicker PNIPAM layer. The thickness of the PNIPAM can be more broadly and efficiently tuned by the “grafting from” method than the “grafting onto” method.

**Table 7.5** Grafting amount of the surface-grafted PPFPA and thickness of the surface-grafted PNIPAM prepared by both “grafting from” and “grafting onto” approach

| Targeted DP | Grafted amount of PPFPA[a] (μg/cm$^2$) | | Thickness of PNIPAM[b] (nm) | |
|---|---|---|---|---|
| | Grafting from | Grafting onto | Grafting from | Grafting onto |
| 50 | 1.18±0.23 | 1.28±0.07 | 3.76±0.09 | 5.05±0.48 |
| 200 | 3.54±0.20 | 1.66±0.05 | 20.89±3.54 | 8.18±1.45 |
| 400 | 4.48±0.20 | 1.95±0.14 | 34.64±7.14 | 12.50±3.10 |

[a]estimated by FT-IR analysis

[b]determined by AFM measurements

**Hydrolysis and Collagen immobilization of the Surface-grafted P(PFPA-*co*-NIPAM)**

To highlight the benefit of having active PFP groups available in the grafted copolymer structure that are capable of undergoing tandem post-polymerization modification, two reactions were performed. Firstly, the surface-grafted P(PFPA-*co*-NIPAM) brushes obtained from both “grafting from” and “grafting onto” methods were subjected to hydrolysis to convert the PFP to carboxyl groups. The extent of this subsequent modification was monitored by water contact angle measurements. Data shown in **Table 7.6** indicated that the hydrolyzed surface-grafted P(PFPA-*co*-NIPAM) was more hydrophilic with lower water contact angle than its counterpart, P(PFPA-*co*-NIPAM) implying the presence of more hydrophilic carboxyl groups in the copolymer structure after hydrolysis. It was also found that the grafted P(PFPA-*co*-NIPAM) with greater PPFPA composition would give the copolymer with higher carboxyl group content upon hydrolysis. The second modification which is quite relevant to the application of this developed thermoresponsive platform for cell sheet fabrication is based on collagen type I immobilization. Collagen type I is known to promote cell adhesion and growth. Upon collagen immobilization, all substrates became highly hydrophilic with advancing water contact angles in a range of 42-67$^{o}$ depending on the initial PPFPA composition. The larger content of active PPFPA apparently allows for more of collagen type I to be immobilized.

**Table 7.6** Water contact angle data of the surface-grafted P(PFPA-*co*-NIPAM) brushes after hydrolysis and collagen immobilization.

| Grafting Methods | Conditions | Advancing Water contact Angle (Degree) | | |
|---|---|---|---|---|
| | | P(PFPA-*co*-NIPAM) | Hydrolyzed P(PFPA-*co*-NIPAM) | Collagen Type I immobilized P(PFPA-*co*-NIPAM) |
| Grafting From | Reaction time with IPA(min) | | | |
| | 0 | 96.49 ± 1.75 | 84.32 ± 3.72 | 59.14 ± 6.28 |
| | 5 | 88.05 ± 1.97 | 73.87 ± 1.99 | 46.82 ± 6.06 |
| | 10 | 84.20 ± 2.33 | 74.33 ± 4.46 | 53.63 ± 2.50 |
| | 30 | 87.40 ± 2.09 | 68.01 ± 0.69 | 61.24 ± 4.50 |
| | 60 | 78.33 ± 3.04 | 71.91 ± 0.33 | 63.27 ± 7.62 |
| Grafting Onto | IPA Concentration (eq) | | | |
| | 0.2 | 94.07 ± 1.25 | 54.00 ± 5.31 | 41.74 ± 3.33 |
| | 0.4 | 92.36 ± 4.07 | 63.89 ± 4.40 | 48.85 ± 1.31 |
| | 0.6 | 89.43 ± 1.92 | 57.19 ± 5.59 | 56.91 ± 1.45 |
| | 0.8 | 84.80 ± 1.55 | 77.88 ± 1.92 | 66.73 ± 0.72 |

The success of hydrolysis was also confirmed by FT-IR analysis. As shown in **Figure 7.6**, the characteristic peak assigned to ester C=O stretching of PPFPA completely disappeared and replaced by C=O stretching of COOH of PAA at 1710 $cm^{-1}$. The relative intensity between the peak at 1710 $cm^{-1}$ and amide C=O stretching of PNIPAM became correspondingly decreased as the %PNIPAM in the copolymer increased.

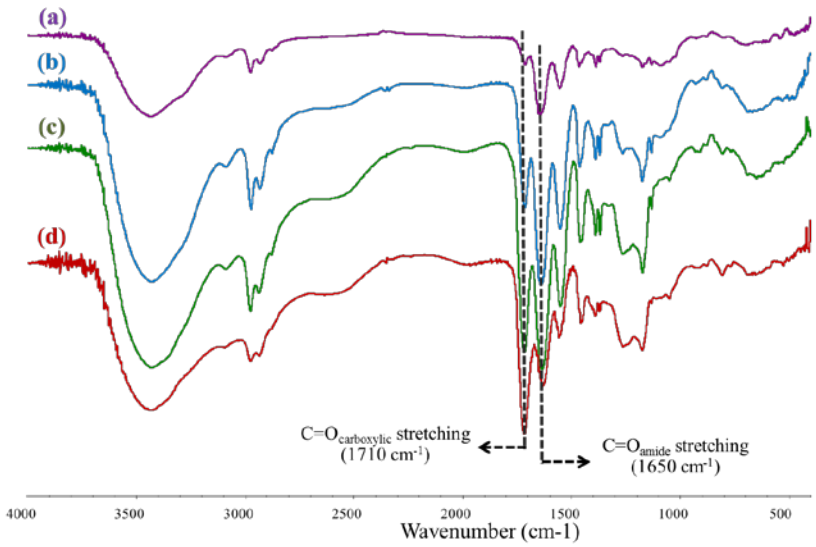


**Figure 7.6** FTIR spectra of hydrolyzed P(PFPA-*co*-NIPAM) with %PNIPAM of (a) 78, (b) 59, (c) 45, and (d) 30.

**Cell sheet fabrication**

Because the thickness of thermoresponsive brushes is an important factor for cell adhesion and cell detachment properties, different MW of PNIPAM brushes prepared by post-polymerization modification of PPFPA brushes both “grafting from” and grafting onto” methods were investigated. In cell culture process, the thermoresponsive substrate which is generally based on PNIPAM has to be coated with CAPs such as collagen, laminin or fibronectin before cell seeding to promote cell adhesion and growth. After incubated at 37°C, the adherent cells were observed to study cell adhesion property of polymer brushes. PNIPAM brushes prepared via “grafting onto” method showed the impressive result for cell adhesion property. Because of the smaller thickness, keratinocyte cells easier adhere and reach confluency on PNIPAM brushes prepared via “grafting onto” method (having thickness of 5.1-12.5 nm) than the surface-grafted PNIPAM brushes prepared via “grafting from” method (having thickness of 3.8-34.6 nm). Although all of PNIPAM brushes prepared via “grafting onto” method exhibited the good property for cell adhesion, cell sheet could be harvested with DP of 400 only (entry 3, last column, **Table 7.7**). Since swelling and mobility of the PNIPAM chains of the surface-grafted PNIPAM brushes with DP 50 and 200, having low thickness were limited (5.1 and 8.2 nm, respectively), the adherent cells could not detach from these surfaces as a cell sheet. A similar behaviour was also observed for the surface-grafted PNIPAM brushes prepared by “grafting from” approach having DP of

50 with the thickness of 3.8 nm. These results strongly suggest that there is a minimum thickness of PNIPAM layer required for this cell sheet harvesting application.

**Table 7.7** Microscopic photographs of keratinocyte cells sheet preparation on PNIPAM brushes with various MW obtained from post-polymerization modification of “grafting from” and “grafting onto” PPFPA brushes.

| DP | Grafting From | | Grafting Onto | |
|---|---|---|---|---|
| | Adhesion | Detachment | Adhesion | Detachment |
| 50 | 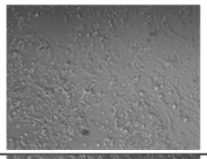 | 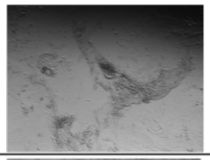 | 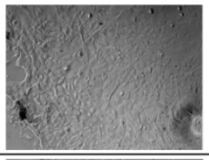 | 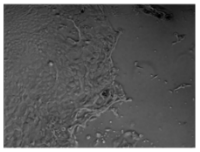 |
| 200 | 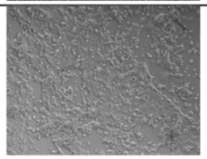 |  | 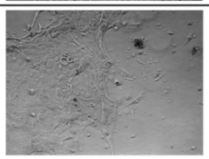 | 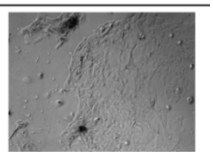 |
| 400 | 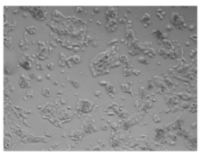 | 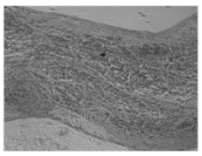 | 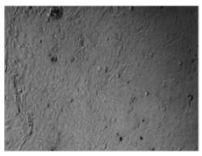 | 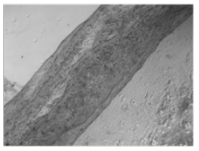 |

In contrast, the surface-grafted PNIPAM brushes prepared by “grafting from” method showed the good property for cell sheet detachment. Although keratinocyte cells were difficultly adhere and reach confluency when the thickness of PNIPAM increased, the cell sheet can easily detach after low temperature treatment because of the mobility of long PNIPAM chains on the surface-grafted PNIPAM of higher DP with thicker PNIPAM layer. As shown in **Table 7.7**, the surface-grafted PNIPAM brushes with DP of 400 fabricated by “grafting from” and “grafting onto” approach could be used to provide the keratinocyte cell sheets. Therefore PPFPA with DP of 400 was selected for next investigation.

To further investigate the potential use of the developed thermoresponsive platform for cell sheet preparation, the surface-grafted P(PFPA-*co*-NIPAM) brushes with various PNIPAM composition prepared by “grafting from” and “grafting onto” approach were used for collagen type I immobilization. The active PFP ester groups in the copolymer are readily available for covalent immobilization with collagen type I. Because collagen type I was covalently immobilized on P(PFPA-*co*-NIPAM) brushes, keratinocyte cells could easily adhere without CAPs coating step. As shown in **Table 7.8**, the collagen type I immobilized P(PFPA-*co*-NIPAM) brushes with various PNIPAM composition prepared by “grafting from” method demonstrated that PPFPA brushes immersed in IPA solution with less reaction time showed more amount of adherent cell because there were more collagen type I on the surfaces. Therefore the PPFPA brushes reacted with IPA for 5 minutes that yielded P(PFPA-co-NIPAM) brushes with highest remaining PFP moieties and thus highest immobilized collagen type I quantity showed the best property for cell adhesion while the smallest amount of adherent cells were observed on PPFPA surfaces reacted with IPA for 60 minutes that gave P(PFPA-co-NIPAM) brushes with lowest remaining PFP moieties and thus lowest immobilized collagen type I quantity (**Table 7.8**). For cell sheet harvesting step, the keratinocyte cell sheet could be obtained from all of collagen type I immobilized P(PFPA-*co*-NIPAM) substrates but cell sheet on the PPFPA brushes reacted with IPA for 5 minutes difficultly detach as a cell sheet from the surface. Moreover, the residual cells were observed on cell culture substrates because thermoresponsive property of substrates was limited by a little PNIPAM composition in copolymer. PPFPA brushes reacted with IPA for the longer reaction time provided more composition of PNIPAM in copolymer. Thus cell sheet could be easily harvested without the residual cells from PPFPA brushes reacted with IPA for 60, 30 and 10 minutes, respectively.

**Table 7.8** Microscopic photographs of keratinocyte cells adhesion and detachment on collagen type I immobilized P(PFPA-*co*-NIPAM) brushes fabricated via “grafting from method”.

| | Reaction time in 10mM IPA | | | |
|---|---|---|---|---|
| | 5 min in IPA | 10 min in IPA | 30 min in IPA | 60 min in IPA |
| Day1 | 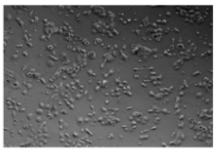 | 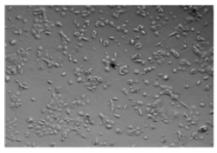 | 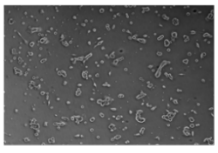 | 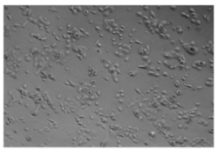 |
| Day2 | 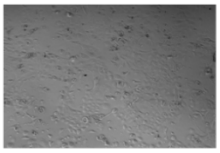 | 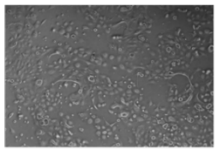 | 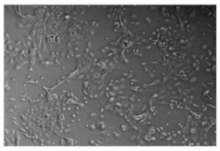 | 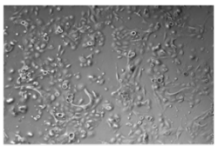 |
| Day3 | 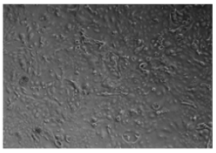 | 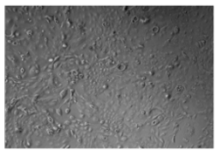 | 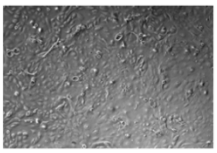 | 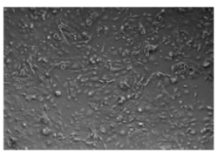 |
| cell sheet | 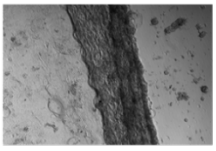 | 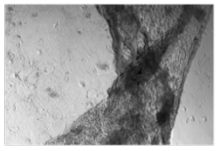 | 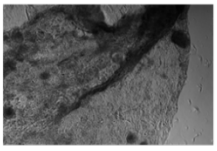 | 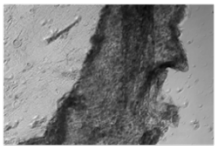 |

The similar results were observed from the collagen type I immobilized P(PFPA-*co*-NIPAM) brushes prepared by “grafting onto” method (**Table 7.9**). Thermoresponsive substrates containing less %PNIPAM composition exhibited the ability to promote cell adhesion property while cell sheet detachment process was slow. On the other hand, the substrates containing more % PNIPAM composition showed the detachment of cell sheet in a short time after low temperature treatment. As shown in **Table 7.9**, there are more adherent cells on collagen type I immobilized P(PFPA-NIPAM) with 20% PNIPAM surfaces than copolymer surface with 40, 60 and 80% PNIPAM, respectively. Although, the adhesion of cells on the surface-grafted P(PFPA-*co*-NIPAM) with 78% PNIPAM surfaces was slow, the detachment of cell sheet rapidly occurred without residual cells on substrates.

**Table 7.9** Microscopic photographs of keratinocyte cells adhesion and detachment on collagen type I immobilized P(PFPA-*co*-NIPAM) brushes fabricated via “grafting onto method”.

| | P(PFPA-NIPAM with 20% PNIPAM | P(PFPA-NIPAM with 40% PNIPAM | P(PFPA-NIPAM with 60% PNIPAM | P(PFPA-NIPAM with 80% PNIPAM |
|---|---|---|---|---|
| Day1 | 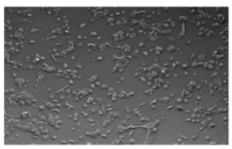 | 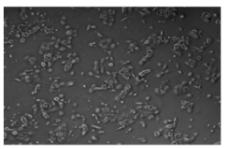 | 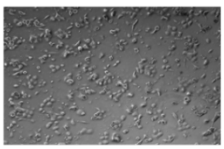 | 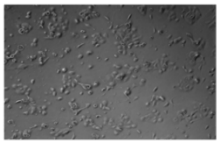 |
| Day2 | 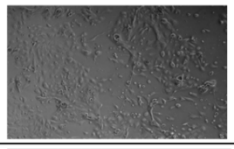 | 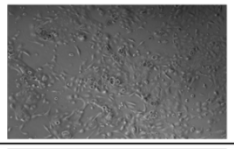 | 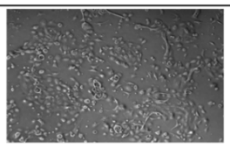 | 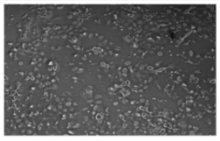 |
| Day3 | 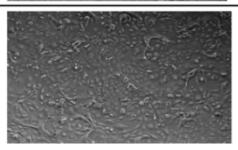 | 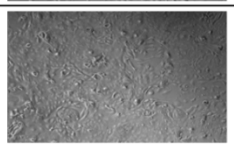 | 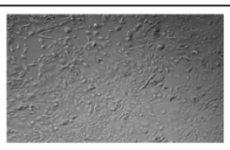 | 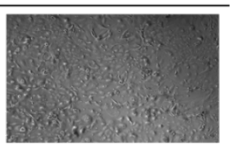 |
| cell sheet | 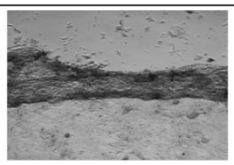 | 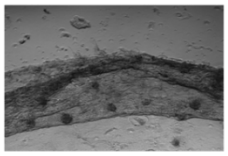 | 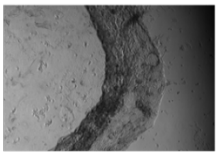 | 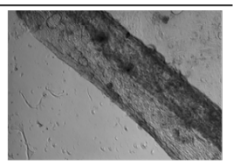 |

This study indicated that the amount of collagen type I immobilized on copolymer surface through active PFP groups, improved cell adhesion property of the thermoresponsive surfaces. However, the % PNIPAM composition in copolymer was importance for cell sheet detachment after temperature reducing.

In addition, the resulting P(AA-*co*-PNIPAM) brushes with various %PAA in copolymer obtained from hydrolysis of P(PFPA-*co*-NIPAM) were investigated to study the effect of hydrophilic groups for cell sheet preparation. The hydrolyzed P(PFPA-*co*-NIPAM) brushes prepared by “grafting from” and “grafting onto” method showed the poor property of cell adhesion (**Table 7.10 - 7.11**). The process of cell growth and confluency reaching apparently consumed much longer time when compared with collagen type I immobilized P(PFPA-*co*-NIPAM) surfaces. For P(AA-*co*-PNIPAM) brushes prepared via “grafting from” method, the composition of PAA in copolymer was controlled by reaction time of PPFPA brushes with IPA solution. Thus PPFPA brushes reacted with IPA for a short time provided high density of PAA in the copolymer surfaces. The difficulty of cell adhesion and spreading is shown in **Table 7.10** and the

hydrolyzed P(PFPA-*co*-NIPAM) brushes obtained from reaction of PPFPA with IPA for 5 minutes also showed the worst cell adhesion property.

**Table 7.10** Microscopic photographs of keratinocyte cells adhesion and detachment on hydrolyzed P(PFPA-*co*-NIPAM) brushes fabricated via “grafting from method”.

| | Reaction time in 10mM IPA | | | |
|---|---|---|---|---|
| | 5 min | 10 min | 30 min | 60 min |
| Day1 | 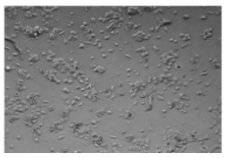 | 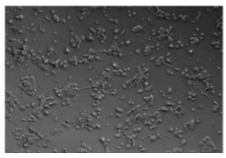 | 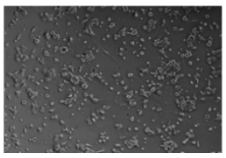 | 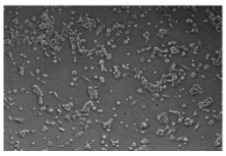 |
| Day4 | 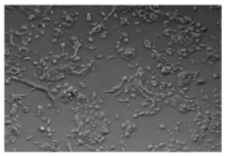 | 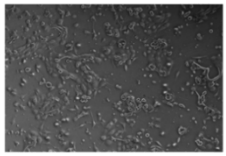 | 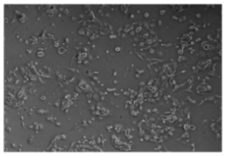 | 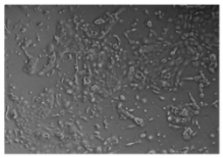 |
| Day6 | 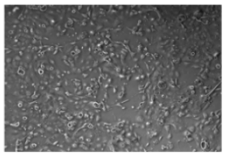 | 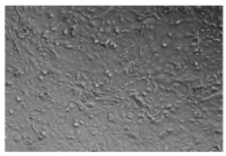 | 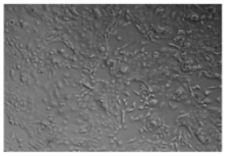 | 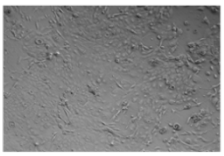 |
| cell sheet | 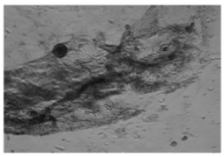 | 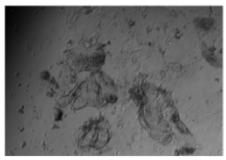 | 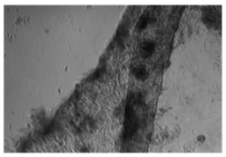 | 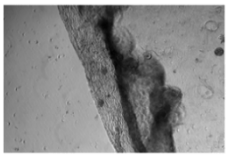 |

For the hydrolyzed copolymer brushes obtained from reaction of the surface-grafted PPFPA with IPA for 60 min, cells could easier adhered and spread on the surfaces because the PPFPA brushes were almost completely converted to PNIPAM brushes. In this experiment the keratinocyte cell sheet was obtained from the copolymer brushes prepared by reaction of PPFPA in IPA solution with reaction time 30 and 60 min only because there was much PNIPAM composition enough to perform thermoresponsive property. Adherent cells on other surfaces could be detached but not as a cell sheet. Hydrolyzed P(AA-*co*-PNIPAM) brushes prepared via “grafting onto” method were investigated for cell sheet preparation and the result demonstrated in **Table 7.11** that cell sheet couldn’t detach from all % PAA composition of copolymer brushes. Although keratinocyte cells could adhere onto the substrates, it couldn’t detach after low temperature treatment because the “grafting onto” method provided low polymer film thickness.

**Table 7.11** Microscopic photographs of keratinocyte cells adhesion and detachment on hydrolyzed P(PFPA-*co*-NIPAM) brushes fabricated via “grafting onto method”.

| | P(PFPA-NIPAM with 20% PNIPAM | P(PFPA-NIPAM with 40% PNIPAM | P(PFPA-NIPAM with 60% PNIPAM | P(PFPA-NIPAM with 80% PNIPAM |
|---|---|---|---|---|
| Day1 | 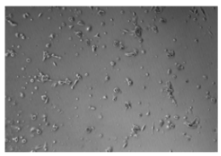 | 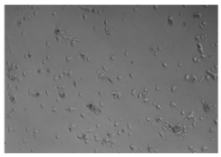 | 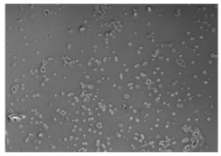 | 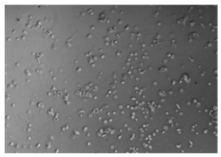 |
| Day4 | 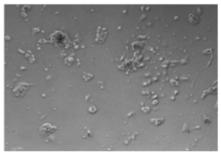 | 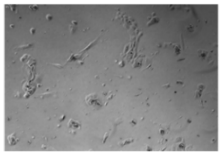 | 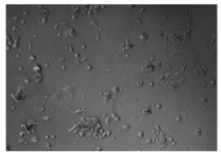 | 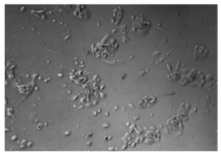 |
| Day6 | 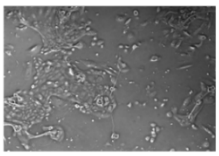 | 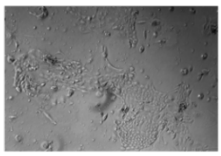 | 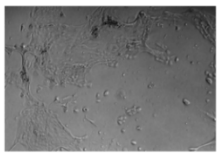 | 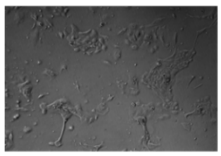 |
| cell sheet | 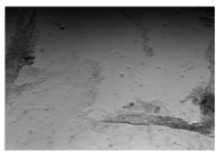 | 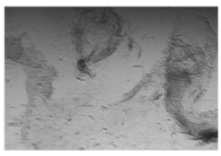 | 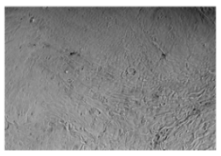 | 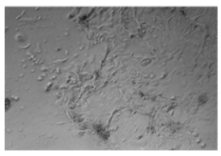 |

## CONCLUSIONS

PPFPA with well-controlled molecular weight was synthesized by RAFT polymerization. As monitored by FT-IR, post-polymerization modification of PPFPA yielded P(PFPA-*co*-NIPAM) of which PNIPAM composition can be varied as a function of both IPA concentration and reaction time. Surface-grafted P(PFPA-*co*-NIPAM) brushes were fabricated by two methods. The first method relied on “grafting from” approach, involving surface-initiated RAFT polymerization of PFPA from initiator-immobilized substrates followed by post-polymerization modification with IPA. The second method was based on “grafting onto” approach which was accomplished by a reaction between PFP groups in P(PFPA-*co*-NIPAM) previously obtained from post-polymerization modification of PPFPA and amino groups on the surface of the APTES-modified substrates. The success of grafting by both methods was verified by contact angle measurements, FT-IR and XPS analyses. Results from FT-IR and AFM analyses indicated that the “grafting onto” approach gave the surface-grafted polymer brushes with lower grafted amount and thickness than those prepared by “grafting from” approach.

The remaining PFP units on the surface-grafted P(PFPA-*co*-NIPAM) brushes prepared by both methods were readily available for tandem post-polymerization modification. Hydrolysis of the surface-grafted P(PFPA-*co*-NIPAM) brushes yielded surface-grafted P(AA-*co*-NIPAM) brushes. Whereas the attachment of collagen type I to the surface-grafted P(PFPA-*co*-NIPAM) brushes can be effectively done without having to use coupling agent. An optimum targeted DP that gave surface-grafted PNIPAM having the ability to prepare keratinocyte cell sheet was 400. Both hydrolyzed- and collagen type I-immobilized surface-grafted P(PFPA-*co*-NIPAM) brushes with the same targeted DP prepared by both “grafting from” and “grafting onto” were also tested for their applicability for cell sheet preparation. It was found that cell adhesion property was proportionally improved on collagen type I immobilized P(PFPA-*co*-NIPAM) as a function of %PPFPA composition. On the other hand, the substrates containing lower %PPFPA composition showed better characteristic for cell detachment. While the hydrolyzed surface-grafted P(PFPA-*co*-NIPAM) brushes with high %PPFPA were not suitable for cell sheet preparation because their highly hydrophilic surfaces resisted the adhesion and proliferation of cells. This study has demonstrated that multifunctional thermoresponsive platform for cell sheet fabrication can be developed from the surface-grafted PPFPA brushes via the “grafting from” and “grafting onto” approach.

**References**


1. Ward, M. A.; Georgiou, T. K. *Polymers* **2011**, 3, 1215-1242.
2. Fukumori, K.; Akiyama, Y.; Yamato, M.; Kobayashi, J.; Sakai, K.; Okano, T. *Acta Biomaterialia* **2009**, 5, 470-476.
3. Tan, L.; Liu, J.; Zhou, W.; Wei, J.; Peng, Z. *Materials Science and Engineering: C* **2014**, 45, 524-529.
4. Nagase, K.; Hatakeyama, Y.; Shimizu, T.; Matsuura, K.; Yamato, M.; Takeda, N.; Okano, T. *Biomacromolecules* **2013**, 14, 3423-33.
5. Takahashi, H.; Matsuzaka, N.; Nakayama, M.; Kikuchi, A.; Yamato, M.; Okano, T. *Biomacromolecules* **2012**, 13, 253-260.
6. Masuda, S.; Shimizu, T.; Yamato, M.; Okano, T. *Advanced Drug Delivery Reviews* **2008**, 60, 277-285.
7. Kumashiro, Y.; Yamato, M.; Okano, T. *Annuals of Biomedical Engineering* **2010**, 38, 1977-1988.
8. Patel, N.G.; Zhang, G. *Organogenesis* **2013**, *9(2)*, 93-100.

9. Takahashi, H.; Nakayama, M.; Yamato, M.; Okano, T. *Biomacromolecules* **2010**, 11, 1991-1999.
10. Takei, Y. G.; Aoki, T.; Sanui, K.; Ogata, N.; Okano, T.; Sakurai, Y. Bioconjugate Chemistry 1993, 4(1), 42-46.
11. Matsuzaka, N.; Nakayama, M.; Takahashi, H.; Yamato, M.; Kikuchi, A.; Okano, T. *Biomacromolecules* **2013**, 14, 3164-3171.
12. Oezyuerek, Z.; Franke, K.; Nitschke, M.; Schulze, R.; Simon, F.; Eichhorn, K.-J.; Pompe, T.; Werner, C.; Voit, B. *Biomaterials* **2009**, 30, 1026-1035.
13. Arnold, R. M.; Sheppard, G. R.; Locklin, J. *Macromolecules* **2012**, 45, 5444-5450.
14. Zhuang, J.; Jiwpanich, S.; Deepak, V. D.; Thayumanavan, S. *ACS Macro Letters* **2012**, 1, 175-179.
15. Gunay, K. A.; Schuwer, N.; Klok, H.-A. *Polymer Chemistry* **2012**, 3, 2186-2192.
16. Kessler, D.; Roth, P. J.; Theato, P. *Langmuir* **2009**, 25, 10068-10076.
17. Deng, X.; Eyster, T. W.; Elkasabi, Y.; Lahann, J. *Macromolecular Rapid Communications* **2012**, 33 (8), 640-645.
18. Chiang, E. N.; Dong, R.; Ober, C. K.; Baird, B. A. *Langmuir* **2011**, *27(11)*, 7016-7023.
19. Mizutani, A.; Kikichi, A.; Yamato, M.; Kanazawa, H.; Okano, T. Biomaterials, 2008, 29(13), 2073-2081.

# OUTPUT

**International Publication**

1. Kusolkamabot, K.; Sae-ung, P.; Niamnont, N.; Wongravee, K.; Sukwattanasinitt, M.; **Hoven, V. P. "**Poly(n-isopropylacrylamide)-stabilized Gold Nanoparticles in Combination with Tricationic Branched Phenylene-ethynylene Fluorophore for Protein Identification " *Langmuir* **2013**, *29,* 12317-12327.
2. Graisuwan, W.; Zhao, H.; Kiatkamjornwong, S.; Theato, P.; **Hoven, V. P.** "Formation of Thermo-sensitive and Cross-Linkable Micelles by Self-Assembly of Poly(pentafluorophenyl acrylate)-containing Block Copolymer" *J. Polym. Sci. Polym. Chem.,* **2015**, *53*, 1103-1113.
3. Sangsuwan, A.; Narupai, B.; Rodthongkum, N.; **Hoven, V. P.** "Patterned Poly(acrylic acid) Brushes Containing Gold Nanoparticles for Peptide Detection by Surface-assisted Laser Desorption/Ionization Mass Spectrometry" *Anal.Chem.,* **2015***, 87(21),* 10738-10746.
4. Wiarachai, O.; Vilavan, T.; Iwasaki, Y.; **Hoven, V. P.** "Clickable and Anti-fouling Copolymer Platform of Poly[(propargyl methacrylate)-*ran*-(2-methacryloyloxyethyl phosphorylcholine)] for Biosensing Applications**"***, Langmuir***, 2016**, *32* (4), 1184–1194.
5. Graisuwan, W.; Zhao, H.; Puthong, S.; Kiatkamjornwong, S.; Theato, P.; **Hoven, V. P.** "Thermo-responsive and Active Functional Fibers for Cultured Cell Recovery", *Manuscript in Preparation*
6. Leekrajang, M.; Vilaivan, T.; **Hoven, V. P.** "Filter Paper Grafted with PNA-conjugated Copolymer Brushes for Colorimetric DNA Sequence Determination**"** , *Manuscript in Preparation*
7. Bunwanna, M.; Khramchantuk, S.; Isarasena, N.; **Hoven, V. P.** "Thermoresponsive Polymer Brushes Prepared by Post-Polymerization Modification of Poly(pentafluorophenyl acrylate) for Tissue Engineering Applications", *Manuscript in Preparation*

**Patent**

1. วรวีร์ โฮเว่น, นาฏนัดดา รอดทองคำ, อะรุณี แสงสุวรรณ เรื่อง "แผ่นกระจกตรึงด้วยพอลิแอคริลิกแอซิดบรัชที่มีอนุภาคนาโนทองเป็นองค์ประกอบในลักษณะแพทเทิร์น สำหรับใช้ในการแยกและวิเคราะห์เพปไทด์ กรรมวิธีการผลิตและวิธีการวิเคราะห์" **สิทธิบัตรเลขที่คำขอ 1501000575 วันยื่นคำขอ 4 กุมภาพันธ์ 2558**

2. พนิดา ธัญญศรีสังข์, เอมวิกา วิทยาประสิทธิ์, วรวีร์ โฮเว่น เรื่อง “กรรมวิธีการเตรียมสารประกอบอนุภาคที่สามารถจับกับเชื้อก่อโรคฟันพุได้อย่างจำเพาะสำหรับใช้ในการแยกและตรวจวัดเชื้อก่อโรคฟันผุเชิงกึ่งปริมาณได้ด้วยตาเปล่า” **สิทธิบัตรเลขที่คำขอ 1601003554 วันยื่นคำขอ 16 มิ.ย. 2559**
3. พนิดา ธัญญศรีสังข์, เอมวิกา วิทยาประสิทธิ์, วรวีร์ โฮเว่น เรื่อง “สารประกอบอนุภาคที่สามารถจับกับเชื้อก่อโรคฟันพุได้อย่างจำเพาะสำหรับใช้ในการแยกและตรวจวัดเชื้อก่อโรคฟันผุเชิงกึ่งปริมาณได้ด้วยตาเปล่า” **อนุสิทธิบัตรเลขที่คำขอ 1603001055 วันยื่นคำขอ 16 มิ.ย.2559**

**International Presentation**

1. Hoven, V. P. “Tunable Platform for Biomolecule Immobilization Based on Surface-grafted Polymer Brushes for Biosensing and Biomedical Applications”, *The 3rd Polymer Conference of Thailand*, March 28-29, **2013**, Pathumwan Princess Hotel, Bangkok, Thailand, Invited presentation
2. **Hoven, V. P.** “Tunable Platform for Biomolecule Immobilization Based on Surface-grafted Polymer Brushes for Biosensing and Biomedical Applications”, *The 3rd Polymer Conference of Thailand*, March 28-29, **2013**, Pathumwan Princess Hotel, Bangkok, Thailand, Invited presentation
3. **Hoven, V. P.** “Surface-grafted Polymer Brushes: Tunable Platform for Biosensing Applications” *The 45th International Symposium on Macromolecules-IUPAC World Polymer Congress (MACRO 2014)*, July 6 - 11, **2014**, Chiangmai, Thailand, Invited Presentation
4. Sangsuwan, A.; Rodthongkum, N.; **Hoven, V. P.** “Patterned Poly(acrylic acid) Brushes Containing Gold Nanoparticles for Peptide Detection by Surface-assisted Laser Desorption/Ionization Mass Spectrometry” *International Symposium in Science and Technology at Kansai University 2013,* August 21-23, **2013**, Osaka, Japan, Poster.
5. Wiarachai, O.; Vilaivan, T.; Iwasaki, Y.; **Hoven, V. P. “**Clickable and Anti-fouling Copolymer of Poly[(propargyl methacrylate)-*ran*-(2-methacryloyloxyethyl phosphorylcholine)] for Biosensing Applications” *The 8th International Symposium in Science and Technology at Kansai University 2013,* August 21-23, **2013**, Osaka, Japan, Poster.
6. Graisuwan, W.; Theato, P.; Kiatkamjornwong, S.; **Hoven, V. P.** “Synthesis and Characterization of Stimuli-responsive Reactive Copolymers via Post-functionalization of

Poly(pentafluorophenyl acrylate)" *International Symposium in Science and Technology at Kansai University 2013,* August 21-23, **2013**, Osaka, Japan*,* Poster.

7. Graisuwan, W. Theato, P.; Kiatkamjornwong, S.; **Hoven, V. P.** "Self-assembly of Thermo-sensitive Block Copolymer Micelles based on Poly(*N*-isopropylacrylamide)" *The 45th International Symposium on Macromolecules-IUPAC World Polymer Congress (MACRO 2014)*, July 6 - 11, **2014**, Chiangmai, Thailand, Oral.
8. Wiarachai, O.; Vilavan, T.; Iwasaki, Y.; **Hoven, V. P.** "Clickable and Anti-fouling Copolymer Platform of Poly[(propargyl methacrylate)-*ran*-(2-methacryloyloxyethyl phosphorylcholine)] for Biosensing Applications**"** *The 45th International Symposium on Macromolecules-IUPAC World Polymer Congress (MACRO 2014)*, July 6 - 11, **2014**, Chiangmai, Thailand, Poster.
9. Bunwanna, M.; **Hoven, V. P.** "Thermoresponsive Polymer Brushes Prepared by Post-Polymerization Modification of Poly(pentafluorophenyl acrylate) for Tissue Engineering Applications" *The 45th International Symposium on Macromolecules-IUPAC World Polymer Congress (MACRO 2014)*, July 6 - 11, **2014**, Chiangmai, Thailand, Poster.
10. Leekrajang, M.; Vilaivan, T.; **Hoven, V. P.** "Filter Paper Grafted with PNA-containing Copolymer Brushes for Colorimetric DNA Sequence Determination**"** *The 45th International Symposium on Macromolecules-IUPAC World Polymer Congress (MACRO 2014)*, July 6 - 11, **2014**, Chiangmai, Thailand, Poster.
11. **Hoven, V. P.** "Thermoresponsive Materials Developed from Pentafluorophenyl Ester-based Polymer for Biomedical Applications" *The 110th TRF Seminar Series in Basic Science: Materials Advancement via Organic Synthesis,* August 11, **2015***,* Department of Chemistry, Faculty of Science, Chulalongkorn University, Thailand*,* Invited Presentation.

# Appendix

Langmuir

Article

pubs.acs.org/Langmuir

# Poly(*N*-isopropylacrylamide)-Stabilized Gold Nanoparticles in Combination with Tricationic Branched Phenylene-Ethynylene Fluorophore for Protein Identification

Keerati Kusolkamabot,[†,‡] Pornpen Sae-ung,[§] Nakorn Niamnont,[∥] Kanet Wongravee,[⊥] Mongkol Sukwattanasinitt,[#] and Voravee P. Hoven*[,#]

[†]Program in Petrochemistry and Polymer Science, Faculty of Science, Chulalongkorn University, Phayathai Road, Pathumwan, Bangkok 10330, Thailand

[‡]Center of Excellence on Petrochemical and Materials Technology, Chulalongkorn University, Phayathai Road, Pathumwan, Bangkok 10330, Thailand

[§]Program in Macromolecular Science, Faculty of Science, Chulalongkorn University, Phayathai Road, Pathumwan, Bangkok 10330, Thailand

[∥]Department of Chemistry, Faculty of Science, King Mongkut's University of Technology Thonburi, Pracha-Uthit Road, Thung Khru, Bangkok 10140, Thailand

[⊥]Sensor Research Unit, Department of Chemistry, Faculty of Science, Chulalongkorn University, Phayathai Road, Pathumwan, Bangkok 10330, Thailand

[#]Organic Synthesis Research Unit, Department of Chemistry, Faculty of Science, Chulalongkorn University, Phayathai Road, Pathumwan, Bangkok 10330, Thailand

Supporting Information

**ABSTRACT:** Gold nanoparticles stabilized by thermoresponsive polymer, poly(*N*-isopropylacrylamide) (PNIPAM-AuNPs) were prepared by surface grafting of thiol-terminated PNIPAM onto citrate-stabilized AuNPs. The color change of the PNIPAM-AuNPs solution from red to blue-purple without precipitation when the solution was heated to 40 °C, above the lower critical solution temperature (LCST) of PNIPAM, indicated the thermoresponsive property of the synthesized AuNPs. PNIPAM-AuNPs were used to detect proteins by chemical nose approach based on fluorescence quenching of fluorophore by AuNPs. An array-based sensing platform for detection of six proteins, namely bovine serum albumin, lysozyme, fibrinogen, concanavalin A, hemoglobin, holo-transferrin human can be successfully developed from the PNIPAM-AuNPs having different molecular weights (4 and 8 kDa) and conformation (varied heat treatment from 25 to 40 °C) in combination with a tricationic branched phenylene-ethynylene fluorophore. From principal component analysis (PCA) followed by linear discriminant analysis (LDA), 100% accuracy of protein classification using a leave-one-out (LOO) approach can be achieved by using only two types of PNIPAM-AuNPs.

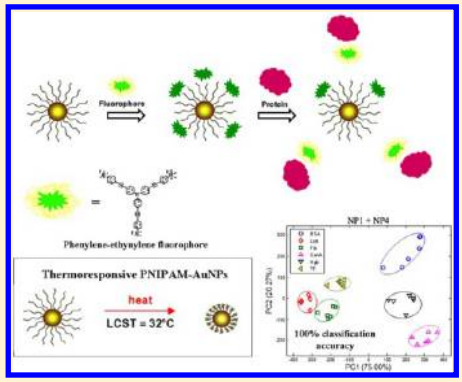


## INTRODUCTION

Gold nanoparticles (AuNPs) have been the focus of considerable interest due to their potential applications for catalysis, diagnosis, and photoelectronic devices. Highly dispersed AuNP solutions exhibit a red color with an absorption band around 520 nm due to the excitation of surface plasmon by incident light. The association of the AuNPs dispersed in the solution induces a color change from red to blue-purple, which can be applied for the development of colloidal sensors.[1−3] Considerable effort has been devoted to synthesis of AuNPs, focusing on control over their size, shape, solubility, stability, and functionality. In general, AuNPs in solution are susceptible to aggregation themselves. To improve their dispersibility and introduce functionality to particle surfaces, the AuNPs may be coated with a water-soluble polymer having a functionality that can interact with gold. It has been reported that some polymers are effective stabilizing agents because they are capable of providing both electrostatic and steric stabilizations to the gold particles.[4,5]

Intelligent polymers, also known as "stimuli-responsive" or "environmentally sensitive" polymers,[6−9] can undergo relatively large and abrupt, physical, or chemical changes in response to small external stimuli in the environmental conditions.[10−13] One of the most recognizable polymers in the class is poly(*N*-

Received: June 5, 2013
Revised: August 22, 2013
Published: August 23, 2013

  

Scheme 1[a]

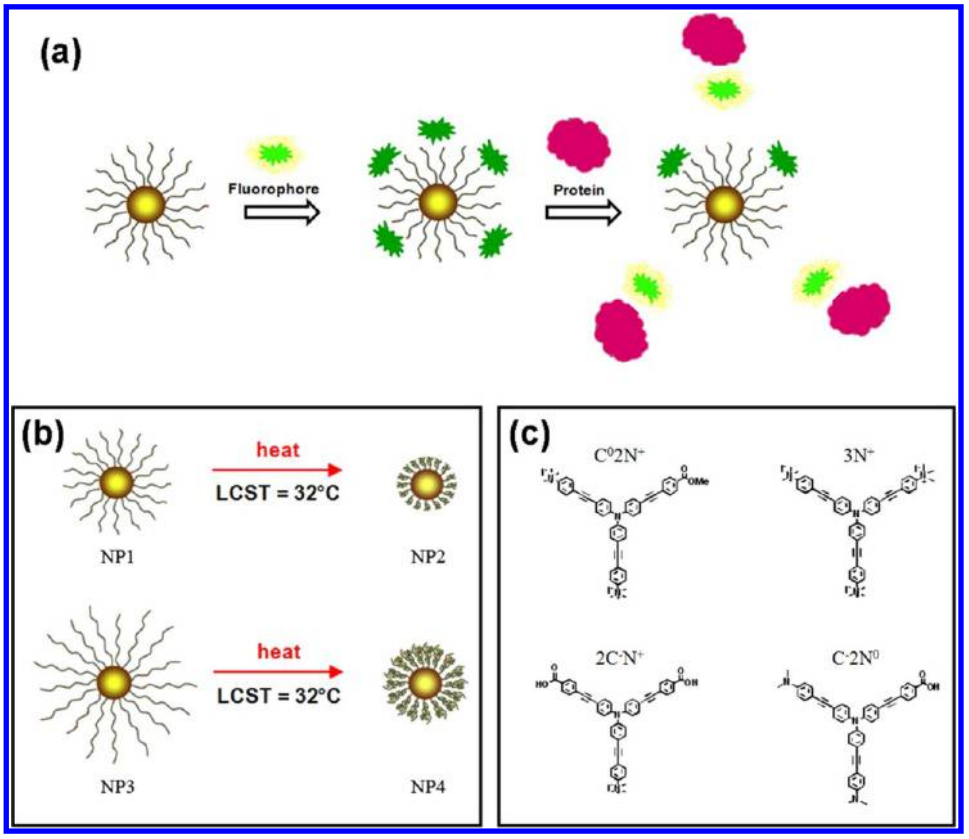


[a](a) Concept of sensor based on competitive binding of PNIPAM-AuNPs and protein with fluorophore that has an impact on fluorescence quenching, (b) four different types of PNIPAM-AuNPs (NP1-NP4), and (c) chemical structures of four tribranched phenylene-ethynylene fluorophores.

isopropylacrylamide) (PNIPAM). PNIPAM dissolves in water assuming a random coil conformation at room temperature, but it separates from the aqueous phase when heated above 31−32 °C, its lower critical solution temperature (LCST).[14−17] Such thermoresponsive behavior is also maintained for PNIPAM grafted on AuNPs (PNIPAM-AuNPs) which can be evidenced from color transition of a AuNPs aqueous solution above and below the LCST. The solution would turn from red to blue upon the collapse of extended brushlike PNIPAM chains above LCST and caused AuNPs aggregation.[18−22]

Recently, it has been reported that protein as a biomarker can be detected by chemical nose approach based on fluorescence quenching of fluorophore by functionalized AuNPs.[23−26] The binding equilibrium between fluorophore and AuNPs would be altered because of competitive binding of protein analyte. Upon an addition of protein analyte, quenched fluorophore adsorbed on the AuNPs surface can be replaced by protein resulting in the recovery of fluorescence signal from the fluorophore. The fluorescence response may be positive or negative depending on the binding affinity of protein toward AuNPs and fluorophore. Although the chemical nose approach relies very much on nonspecific interactions between protein and AuNPs, it is selective enough to be used for identifying the type of individual protein based on the variation of quenching ability of AuNPs having different functionality and the binding strength between the functionalized AuNPs and different kind of protein.[26]

Taking advantage of the PNIPAM-AuNPs being capable of undergoing thermoresponsive conformational transition of the surface-grafted PNIPAM between extended brushes to collapsed chains upon heat treatment above or below the LCST, it is anticipated that the distance between the core of AuNPs and fluorophore as well as protein in solution and so the degree of fluorescence quenching/recovery and the binding strength with the protein should be altered upon heat treatment. This would be highly beneficial if these PNIPAM-AuNPs are to be put in an array-based protein detection following chemical nose approach strategy because the other kind of AuNPs can be obtained by simply heating the existing AuNPs. Considering that PNIPAM is a polymer, such distance may also be varied as a function of PNIPAM molecular weight. In particular, reversible addition−fragmentation chain transfer (RAFT) polymerization has been well recognized as an effective controlled radical polymerization process for PNIPAM synthesis. Not only can a precise control over molecular weight and polydispersity of PNIPAM be achieved, but the terminal dithioester group at the PNIPAM chain end can also be converted to thiol group which is readily available for grafting onto the surface of gold.[27−31]

This research aims to combine the thermoresponsive behavior of PNIPAM and the fluorescence quenching properties of AuNPs to create hybrid materials to be used for protein detection, a mode of biosensing application, to the best of our knowledge, that has never been described before. Together with phenylene-ethynylene tribranched fluorophores having tunable charge characteristic, synthetic dyes successfully used for protein discrimination based on a chemical nose approach,[32] an array-based chemical nose sensor for protein


dx.doi.org/10.1021/la402139g | Langmuir 2013, 29, 12317−12327

detection was developed based on the concept of fluorescence quenching schematically described in Scheme 1a.

## EXPERIMENTAL SECTION

**Materials.** Hydrogen tetrachloroaurate ($HAuCl_4 \cdot 3H_2O$), 4,4′-azobis(4-cyanopentanoic acid) (ACPA), 4-cyano-4-(thiobenzoylthio)-pentanoic acid (CPD), tris(2-carboxyethyl)phosphine hydrochloride (TCEP), and *N*-isopropylacrylamide (NIPAM) were obtained from Aldrich. Bovine serum albumin (BSA), lysozyme (Lys), fibrinogen (Fib), concanavalin A (Con A), hemoglobin (Hgb), holo-transferrin human (TF), dialysis bag (cut-off molecular weight of 3500 g/mol), and phosphate buffered saline pH 7.4 (PBS) were bought from Sigma. 2-Ethanolamine and trisodium citrate dihydrate ($Na_3C_6H_5O_7 \cdot 2H_2O$) were obtained from Fluka (Switzerland). The above chemicals as well as all solvents used (1,4-dioxane, tetrahydrofuran (THF), methanol (MeOH)) were analytical grade and used as received without further purification except NIPAM which was recrystallized in a mixture of benzene and *n*-hexane (3:7, v/v) prior to use. Four fluorophores ($C^0 2N^+$, $3N^+$, $2C^- N^+$, and $C^- 2N^0$) having different charges were synthesized according to a published procedure reported by Niamnont et al.[32] All solutions were prepared using ultrapure distilled water that was obtained after purification using a Millipore Milli-Q system that involves reverse osmosis, ion exchange, and a filtration step (18.2 MΩ cm resistance).

**Characterization.** Molecular weight of the synthesized PNIPAM was analyzed by GPC using a Waters 600 controller chromatograph equipped with HR1 and HR4 columns (Waters, MW resolving range = 100−500 000) at 35 °C and refractive index detector (Waters 2414). THF was used as eluent with a flow rate of 1.0 mL/min. Five polystyrene standards (996−188 000 Da) were used for generating a calibration curve. Fluorescence signals of the fluorophores were recorded by using a Perkin-Elmer precisely (LS 45) luminescence spectrometer (PerkinElmer Inc., UK) in a scanning wavelength range of 400−700 nm. The presence of the polymer around the AuNPs was confirmed by using a Seiko SPA 400 atomic force microscope (SII Nanotechnology Inc., Japan). Measurements were performed in air at ambient temperature using tapping mode and silicon tips with a resonance frequency of 115−190 kHz. Surface plasmon resonance (SPR) measurements used for the determination of PNIPAM coverage on gold surface were conducted using a double channel, AutoLab ESPR (Eco Chemie, Netherlands). The morphology and actual size of AuNPs were analyzed by using a JEOL JEM-2010 transmission electron microscope (Japan) operating at 80 keV. The average diameters of AuNPs were reported from measurements of 30 random particles for each sample using Semafore software. The zeta ($\zeta$) potential of AuNPs were determined using Nanosizer Nano-ZS (Malvern Instruments, UK). The analysis was performed at 25 °C using a scattering angle of 173°. The data were calculated using the Helmholtz-Smoluchowski equation.

**Synthesis of Thiol-Terminated PNIPAM (PNIPAM-SH).** PNIPAM having two different target degrees of polymerization (DP = 40 and 70) were prepared by RAFT polymerization. According to a method modified from that of Yusa et al.,[19] CPD (17.5 mg, 62.5 μmol) and ACPA (8.8 mg, 31.3 μmol) were added to a NIPAM (565.8 mg, 5.0 mmol) solution in 1,4-dioxane (5 mL). The solution was degassed by purging with nitrogen gas for 30 min, and then heated at 70 °C for 24 h. After being cooled down in an ice bath, the reaction mixture was dialyzed against DI water at 4 °C for 3 days, before the PNIPAM was recovered by lyophilization. To remove the terminal dithiobenzoate group, an aqueous solution of PNIPAM was treated with 2-ethanolamine (30 mol equiv of PNIPAM) and a trace amount (3−5 mg) of TCEP at 25 °C for 24 h. The solution was dialyzed against DI water at 4 °C for 3 days. The PNIPAM-SH was then obtained after lyophilization. The condition mentioned above was used to prepare PNIPAM with targeted DP = 40 (targeted molecular weight = 4805.78 g/mol). To prepare PNIPAM with targeted DP = 70 (targeted molecular weight = 8200.58 g/mol), CPD (11.1 mg, 39.7 μmol) and ACPA (4.5 mg, 15.9 μmol) were used instead.

**Preparation of AuNPs Stabilized by PNIPAM (PNIPAM-AuNPs).** PNIPAM-AuNPs were prepared by surface grafting of PNIPAM-SH onto citrate-stabilized AuNPs. In the first step, citrate-AuNPs were synthesized according to a method modified from that of Hayat.[33] An aqueous solution of trisodium citrate (1% w/v, 1.75 mL) was added to a boiling aqueous solution of $HAuCl_4$ (0.01% w/v, 50 mL). Then, the mixture was heated for 30 min and cooled down to ambient temperature. At this point, the color of the solution was changed from gray to red. Finally, the synthesized AuNPs were stored at 4 °C prior to use. It should be noted that all glassware used for the synthesis of AuNPs was washed with freshly prepared aqua regia solution ($HCl/HNO_3$ = 3:1, v/v) and rinsed thoroughly with distilled water prior to use. PNIPAM-AuNPs were obtained by grafting to method modified from that of Zhu et al.[18] PNIPAM-SH (2.0 μmol) was dissolved in 10 mL of citrate-stabilized AuNPs solution obtained from the first step and kept at 4 °C for 48 h. After that, excess PNIPAM-SH was removed from the PNIPAM-AuNPs by centrifugation twice (MIKRO 120, Hettich, Germany) at 14 000 rpm for 15 min intervals. After redispersion in Milli-Q water, a red solution of PNIPAM-AuNPs was obtained and kept at 4 °C.

**Determination of Fluorescence Quenching of Fluorophores by PNIPAM-AuNPs.** Quenching efficiency of four tribranched phenylene-ethynylene fluorophores having different charges of which structures are shown in Scheme 1c was evaluated with PNIPAM-AuNPs to find the fluorophores that can be highly quenched by AuNPs. The abbreviated names of the fluorophores are assigned according to the number and types of the functional groups on their peripheries in which $C^0$, $C^-$, $N^0$, and $N^+$ stand for carboxylate ester, carboxylic acid (or carboxylate anion in basic condition), amino, and quaternary ammonium groups, respectively. For example, $C^0 2N^+$ possesses one carboxylate ester and two quaternary ammonium groups on its periphery. To determine quenching efficiency, the initial fluorescence signal of fluorophore was determined by diluting the fluorophore stock solution (10.0 μM, 100 μL) in 2.9 mL of PBS solution and measured by using a luminescence spectrometer. The quenching efficiency of PNIPAM-AuNPs was determined by mixing the fluorophore stock solution (10.0 μM, 100 μL) and 500 μL of PNIPAM-AuNPs solution in 2.4 μL of PBS solution in a cuvette. To ensure that the equilibrium was attained, the mixture was allowed to stand at ambient temperature for 30 min before the measurement of the emission spectrum.

**Determination of Fluorescence Response of Fluorophore by Proteins.** All of the fluorophores were tested with BSA. The selected fluorophore (10.0 μM, 100 μL) was first dissolved in 2.9 mL of PBS solution in a cuvette. After the solution was left for 30 min, the initial fluorescence emission of fluorophore was analyzed by using a luminescence spectrometer. BSA (10 μL, 1 mg/mL) was then added to the mixture obtained from the first step. To ensure that the equilibrium was attained, the mixture was analyzed by using a luminescence spectrometer after leaving for 30 min. To maximize the fluorescence quenching effect of the PNIPAM-AuNPs on the fluorophores, the fluorophores showing the least response to proteins were selected for developing a sensor platform based on the chemical nose approach.

**Protein Detection Based on Fluorescence Quenching.** The synthesized PNIPAM-AuNPs were put in an array-based sensing platform. Six types of proteins (BSA, Lys, Fib, Con A, Hgb, and TF) were analyzed by using four different types of PNIPAM-AuNPs having varied PNIPAM molecular weight and conformation (induced by thermal treatment) together with the selected phenylene-ethynylene fluorophore. There are four different types of PNIPAM-AuNPs used for this investigation. Two types were obtained from the AuNPs stabilized by 4 kDa of PNIPAM-SH (4k PNIPAM-AuNPs). The first type is 4k PNIPAM-AuNPs at 25 °C (NP1) which was obtained directly from the subsection "Preparation of AuNPs Stabilized by PNIPAM (PNIPAM-AuNPs)" above. The second type is 4k PNIPAM-AuNPs at 40 °C (NP2) which was obtained by heating NP1 for 15 min and cool it down to 25 °C and leave it for 30 min before conducting further experiment. Another two types were obtained from AuNPs stabilized by 8 kDa of PNIPAM-SH (8k


dx.doi.org/10.1021/la402139g | Langmuir 2013, 29, 12317−12327

PNIPAM-AuNPs). The third type is 8k PNIPAM-AuNPs at 25 °C (NP3) and the forth type is 8k PNIPAM-AuNPs at 40 °C (NP4) obtained by a similar heat treatment as mentioned above of NP3. The detection of protein was done as follows. In the first step, 0.5 mL of NP1 was dissolved in 2.4 mL of PBS. After that, $3N^+$ fluorophore ($1 \times 10^{-5}$ M, 100 $\mu$L) was then added and analyzed via luminescence spectrometer after 30 min allowed for the equilibrium time. The second step, BSA (10 $\mu$L, 1 mg/mL), was added to the previous mixture and analyzed via luminescence spectrometer again after the equilibrium time. BSA was subjected to the same analysis with NP2, NP3, and NP4. To generate an array-based sensing platform, other types of proteins were also tested with NP1, NP2, NP3, and NP4.

**Data Analysis.** All data analysis program were written in-house using MATLAB version R2011b. The software for principal component analysis (PCA) and linear discriminant analysis (LDA) was programmed using the algorithm described elsewhere.[34] In our case, LDA was not directly performed to the original data set where the number of variables (wavelengths) exceeds the number of samples as the inverse of the pooled variance-covariance matrix is impossible to be calculated.[34,35] To avoid the problem, the procedure called "PCA-LDA" was used to demonstrate the classification power.[36−38] The approach is to compress the dimension of the data into a low number of principal component (PC) using PCA and LDA is then performed on the resulting PC scores to quantify the discriminant ability.

## RESULTS AND DISCUSSION

**Preparation and Characterization of PNIPAM-SH.** Here in this research, PNIPAM was synthesized by RAFT polymerization of which molecular weight and polydispersity can be well controlled by using a chain transfer agent. Besides, the dithioester group at the polymer chain end can be converted to a thiol group that is readily available for grafting onto the gold surface.[39] The chemical structure of the synthesized PNIPAM was verified by $^1$H NMR (Figure S1, Supporting Information). Its characteristic signals were consistent with those reported in the literature.[40,41] As determined by $^1$H NMR data, it was found that the percent conversion and the average $M_n$ of PNIPAM were 41% and 4053 g/mol, and 42% and 7015 g/mol for targeted DP of 40 and 70, respectively.

Cleavage of the terminal dithiobenzoate group at the PNIPAM chain end was confirmed by UV−vis analysis. Upon aminolysis by using 2-ethanolamine, the UV absorption band around 300 nm corresponding to the dithiobenzoate group disappeared resulting in the formation of thiol group and yielded PNIPAM-SH (Figure S2 in the Supporting Information). The success of aminolysis was also confirmed by the appearance of PNIPAM which changed from pink-orange to white as a result of dithiobenzoate group removal. Since the thiol-terminated polymers can easily be oxidized by oxygen, internal disulfide linkage may be formed and possibly yielded an overestimated molecular weight. To ensure that such incidence did not occur, the molecular weights of PNIPAM-SH were also determined by GPC. The data shown in Table 1 indicated that the $M_n$ and PDI ($M_w/M_n$) values of PNIPAM before aminolysis and after aminolysis (PNIPAM-SH) were closely resembled, implying that the disulfide bond formation was absent.[42] The fact that all PDI values are very close to one another verifies that the molecular weight distribution is narrow and that the RAFT polymerization is well-controlled.

**Preparation and Characterization of PNIPAM-AuNPs.** PNIPAM-SH obtained from the previous section was directly grafted onto the surface of AuNPs through sulfur−gold interaction. As compared with the Fourier transform infrared (FTIR) spectrum of PNIPAM (Figure S3a, Supporting Information), the FTIR spectrum of the PNIPAM-AuNPs

**Table 1. Molecular Weight and Polydispersity Values of PNIPAM and PNIPAM-SH**

| | target | | | | | |
|---|---|---|---|---|---|---|
| polymer | DP | $M_n$ | [M]/[I]/[CTA] (mmol) | $M_n$[a] | PDI[a] | $M_n$[b] |
| PNIPAM | 40 | 4526 | 1.600/0.01/0.020 | 3816 | 1.09 | 4053 |
| | 70 | 7921 | 3.145/0.01/0.025 | 8552 | 1.13 | 7015 |
| PNIPAM-SH | 40 | 4526 | 1.600/0.01/0.020 | 4180 | 1.11 | n/a |
| | 70 | 7921 | 3.145/0.01/0.025 | 8788 | 1.14 | n/a |

[a]Determined by GPC analysis using THF as eluent. [b]Calculated from $^1$H NMR data.

(Figure S3b, Supporting Information) has characteristic peaks of N−H stretching from secondary amide at 3276 cm$^{-1}$ and C−H deformation of isopropyl groups with a 1:1 intensity ratio at 1386 and 1367 cm$^{-1}$ which indicated the success of PNIPAM-SH coating on the surface of AuNPs.

The layer of PNIPAM shell surrounding the AuNPs can be visualized from atomic force microscopy (AFM) images shown in comparison with that of the uncoated AuNPs stabilized by citrate ions in Figure 1. In addition, the effects of molecular

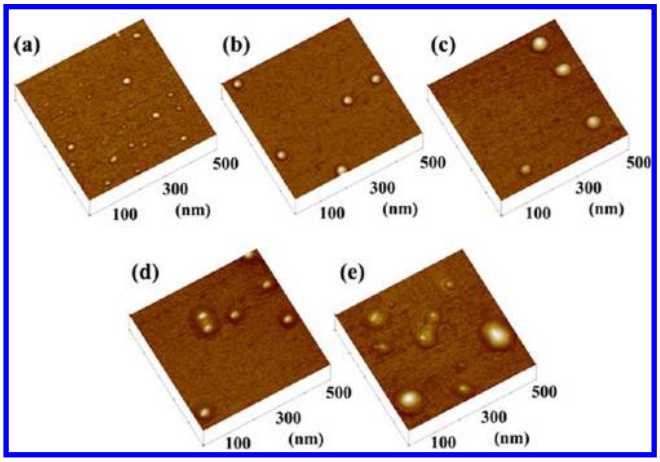


**Figure 1.** AFM images of (a) uncoated citrated-stabilized AuNPs and AuNPs coated with (b) 0.2 mM 4k PNIPAM-SH, (c) 0.2 mM 8k PNIPAM-SH, (d) 0.5 mM 4k PNIPAM-SH, and (e) 0.5 mM 8k PNIPAM-SH.

weight and concentration of PNIPAM-SH on grafting efficiency were investigated. Apparently, the uncoated AuNPs were smaller than all of the PNIPAM-AuNPs. For the AuNPs surrounded by PNIPAM-SH, the particle size was increased with elevating molecular weight of PNIPAM (from 4 to 8 kDa). As illustrated in Figure 1d and e, the expansion of shell thickness was also evidenced as a function of PNIPAM-SH concentration. It was found that the proper concentration of PNIPAM-SH was 0.2 mM because it was the minimum concentration that still gave AuNPs with thermoresponsive property which can be realized from color transition of the AuNPs solution upon thermal treatment, the detail of which will be described in the following section. Moreover, the grafting quantity of the two PNIPAM-SH having different molecular weights (4 and 8 kDa) on a flat gold surface was determined by using SPR analysis (detailed experimental procedure is included along with the data shown in Table S1 in the Supporting Information). Apparently, 4k PNIPAM could


dx.doi.org/10.1021/la402139g | Langmuir 2013, 29, 12317−12327

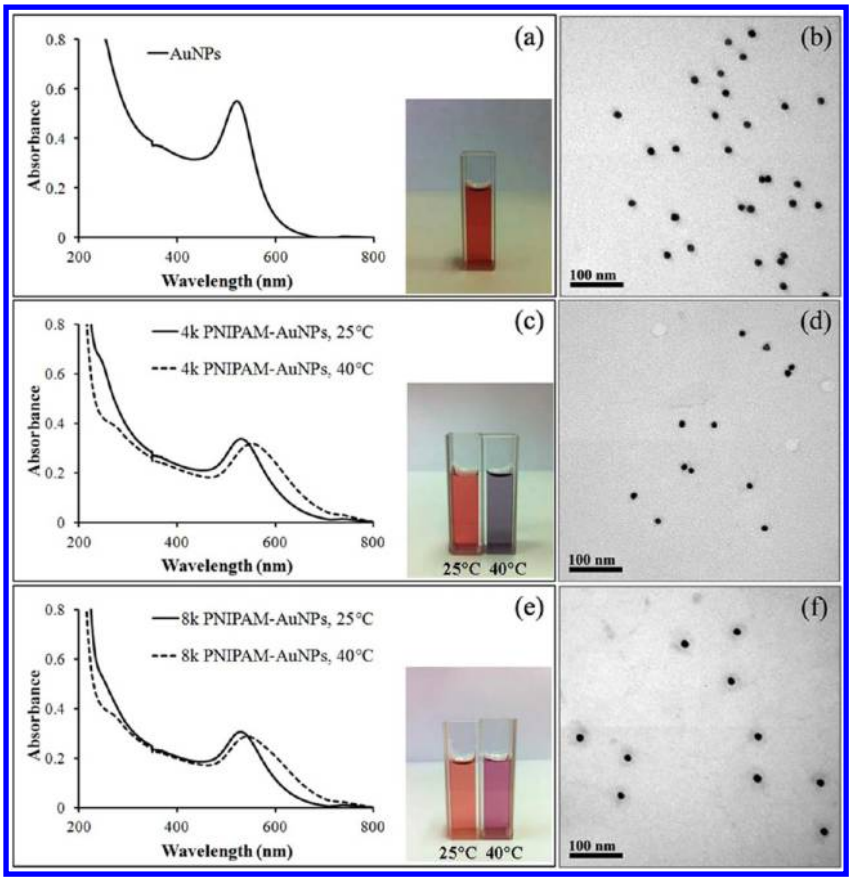


**Figure 2.** UV−vis spectra (a,c,e) and TEM images (b,d,f) of citrated-stabilized AuNPs (a,b), 4k PNIPAM-AuNPs (c,d), and 8k PNIPAM-AuNPs (e,f). The insets of (c) and (e) show the color transition of PNIPAM-AuNPs solution upon heating from 25 to 40 °C.

be grafted with higher density and more consistently than 8k PNIPAM.

The surface plasmon band of AuNPs is known to be sensitive to the size of the particles and their surrounding environment. As demonstrated in Figure 2a, a solution of highly dispersed citrated-stabilized AuNPs exhibits red color with an absorption band around 520 nm. According to transmission electron microscopy (TEM) analysis, the particles were spherical in shape and showed uniform size distribution around 13 nm (Figure 2b). In principle, PNIPAM chains should be collapsed upon increasing temperature above its LCST of 32 °C which is a consequence of hydrogen bonding between water and PNIPAM being destroyed at elevated temperature. Figure 2c shows UV−vis absorption spectra of 4k PNIPAM-AuNPs at 25 °C (NP1) and 40 °C (NP2) in PBS solution. The absorption maximum of the plasmon band of 530 nm at 25 °C shifted to 551 nm when the temperature was increased to 40 °C. The color of the solution changed from red to blue-purple (from NP1 to NP2) without precipitation. The particles were still spherical in shape and consisted of 13 nm gold core and 1 nm PNIPAM shell, as can be seen in the TEM image (Figure 2d). Figure 2e shows UV−vis absorption spectra of 8k PNIPAM-AuNPs at 25 °C (NP3) and 40 °C (NP4) in PBS solution. The absorption maximum of the plasmon band of 530 nm at 25 °C only slightly shifted to 541 nm after heating to 40 °C. This slight red shift might be attributed to a high thickness of PNIPAM shell which prevented an aggregation of the AuNPs. This result was consistent with the color of the solution in that the solution was altered from red to pink-purple (from NP3 to NP4) without precipitation. It was found that the particles were spherical in shape with well-defined core/shell nanostructures having 13 nm gold core and 14−17 nm PNIPAM shell (Figure 2f). The data depicted in Table S2 in the Supporting Information also suggested that the relative dimension of the particles measured by AFM was larger than those analyzed by TEM. This may be ascribed to the fact that AFM analysis was performed under semidried conditions.

It should also be emphasized that the thermoresponsive property upon this thermal treatment condition is not reversible. The solution color as well as absorption maxima of plasmon bands of both NP2 and NP4 remained unaltered although their solutions were quenched down to ambient temperature (25 °C) for a long period of time (up to 2 h), implying that both NP2 and NP4 maintained at their aggregated states and did not turn back to their original NP1 and NP3, respectively, at least within the period of measurements. This irreversibility is not completely unknown. In fact, it has been previously reported on the system of magnetic nanoparticles coated with PNIPAM-containing copolymers having relatively low graft density.[43] Our PNIPAM-AuNPs were prepared by grafting-to method so their graft density may not be that high which could be the reason of their irreversible thermal transition.

It has also been reported by Yusa et al.[19] that the thermoresponsive property of PNIPAM-AuNPs in terms of color transition (shift in absorption maximum of surface plasmon band) cannot be observed unless salt was added. They have explained that the color transition, in principle, should be driven by both PNIPAM shrinkage upon heating above its LCST and interparticle aggregation of the PNIPAM-AuNPs.


dx.doi.org/10.1021/la402139g | Langmuir 2013, 29, 12317−12327

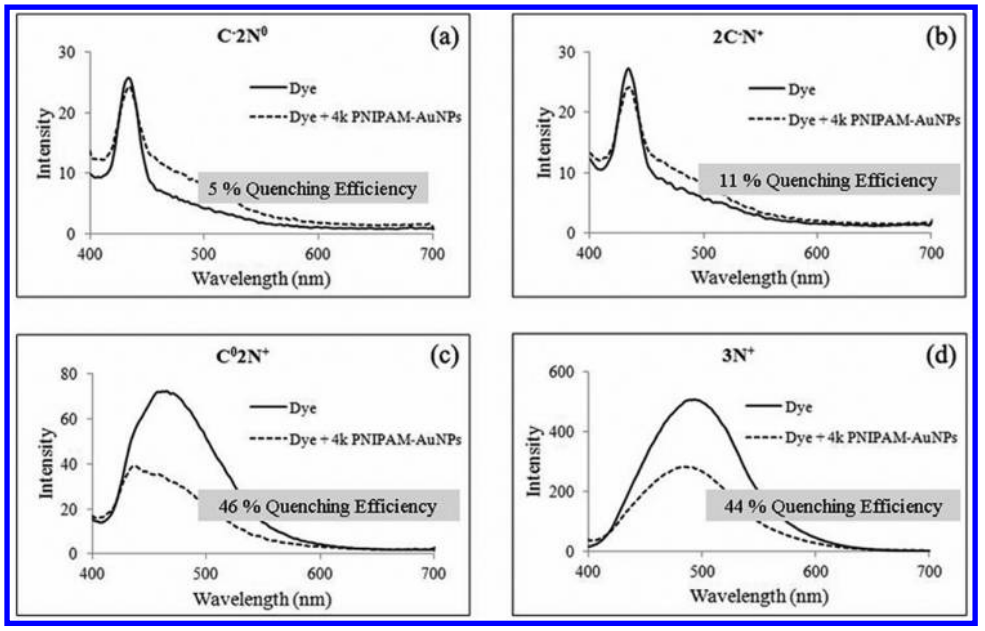


**Figure 3.** Emission spectra demonstrating quenching behavior of four phenylene-ethynylene fluorophores: (a) $C^{-}2N^{0}$, (b) $2C^{-}N^{+}$ (c) $C^{0}2N^{+}$, and (d) $3N^{+}$ by using 4k PNIPAM-AuNPs (NP1) as a quencher.

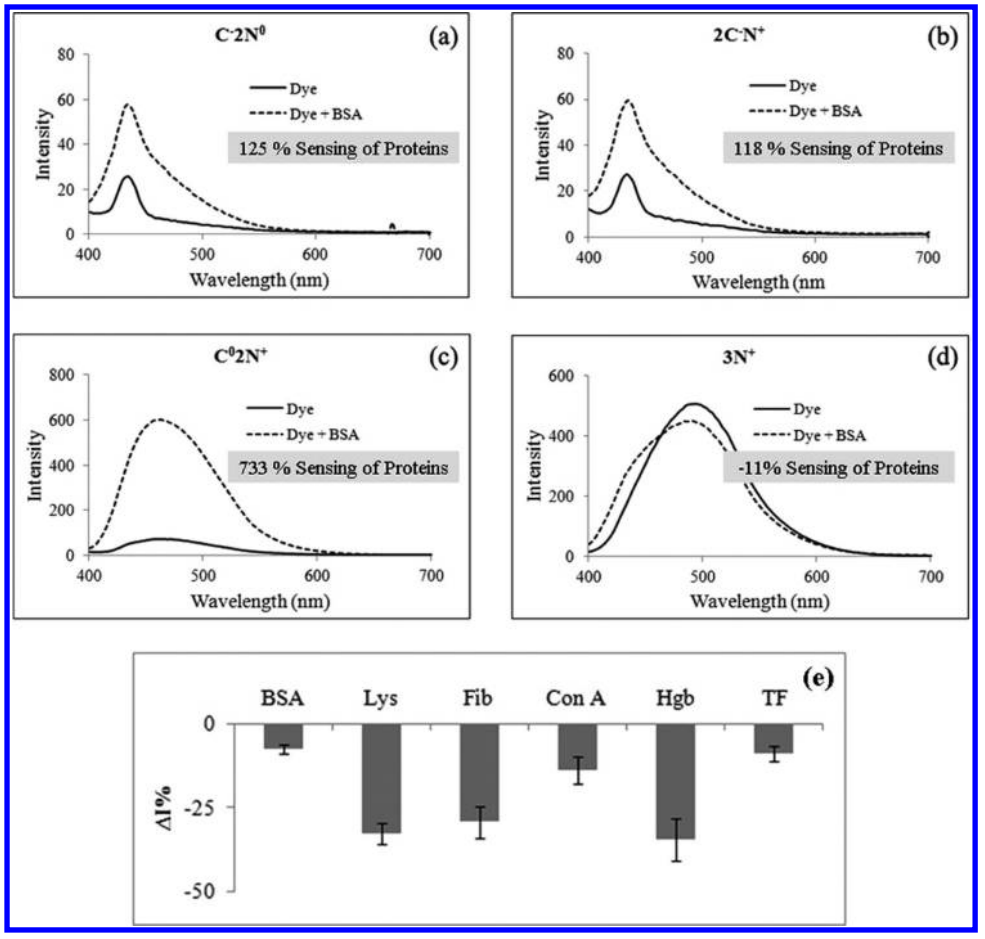


**Figure 4.** Emission spectra demonstrating the change in fluorescence intensity of four tribranched phenylene-ethynylene fluorophores: (a) $C^{-}2N^{0}$, (b) $2C^{-}N^{+}$, (c) $C^{0}2N^{+}$, and (d) $3N^{+}$ upon BSA addition, and (e) percentage of the change in emission intensity of $3N^{+}$ fluorophore when tested with six proteins.

Thermal treatment above LCST should cause PNIPAM shrinkage (which can be realized by change in hydrodynamic radius usually determined by light scattering), however, the thermal energy is apparently not enough to bring together the collapsed PNIPAM-AuNPs that should lead to aggregation and subsequent change in optical characteristic (color change). This


dx.doi.org/10.1021/la402139g | *Langmuir* 2013, 29, 12317−12327

may be rationalized as a consequence of strong hydrogen bonding between water and the PNIPAM particularly at the outer layer of the PNIPAM-AuNPs that prevent aggregation. Introducing salt to the system helped increasing ionic strength so that such strong hydrogen bonding can be destroyed and allows the aggregation to take place. For this reason, we also conducted additional experiments by incorporating 50 mM NaCl to the PNIPAM-AuNPs solution and performed two cycles of heating-quenching between 25 and 40 °C and found that the color transition from red to blue-purple can be promptly accelerated and the process was also reversible as can be demonstrated in Figure S4 (Supporting Information). Such results have suggested that whether the visible thermoresponsiveness is reversible truly depends on the solution properties (i.e., ionic strength).

In this research, it is our intention not to add any salt to the solution which may complicate the protein classification that relies on the interactions among three counterparts (PNIPAM-AuNPs, fluorophore, and protein). For this reason, the thermoresponsive transition solely relied on thermal energy introduced to the system by heating. The thermoresponsiveness of the PNIPAM-AuNPs was not reversible which was presumably caused by the relatively low graft density of the PNIPAM as mentioned above. On the other hand, it was also possible that prolonged heating (>15 min in this research) caused extensive PNIPAM collapse and dehydration, making interparticle aggregation a permanent process. Nevertheless, the irreversibility is truly beneficial for the mode of detection proposed in this research work in that both NP2 and NP4 maintained their optical characteristic throughout the experiment, suggesting that the method is reliable.

**Protein Identification.** To put the synthesized PNIPAM-AuNPs in an array-based sensing platform, a preliminary investigation on quenching efficiency of four tribranched phenylene-ethynylene fluorophores having different charges (structure shown in Scheme 1c) by 4k PNIPAM-AuNPs at 25 °C was performed. It should be emphasized that these specific fluorophores were chosen because their charge characteristic can be tuned by varying the peripheral groups of the branch in the fluorophore structure without affecting their size. This is beneficial from the point that the impact of the charge on the quenching/recovery of the fluorophore can be determined without having to be concerned about the size and dimension variation of the fluorophore. As presented in Figure 3, when 4k PNIPAM-AuNPs were used as a quencher, the $C^{-}2N^{0}$ and $2C^{-}N^{+}$ fluorophores were slightly quenched (5% and 11%, respectively), while the $3N^{+}$ and $C^{0}2N^{+}$ fluorophores were largely quenched (44% and 46%, respectively). The $C^{-}2N^{0}$ fluorophore has one carboxylic acid and two amino groups providing −1 net electronic charge, whereas the $2C^{-}N^{+}$ fluorophore has two carboxylic acid groups and one quaternary ammonium group also netting −1 electronic charge. Therefore, there should be the repulsive force between the fluorophores and PNIPAM-AuNPs which have lone paired electrons of nitrogen and oxygen in the repeating unit resulting in ineffective fluorescence quenching. On the other hand, $3N^{+}$and $C^{0}2N^{+}$ fluorophores have +3 and +2 net electronic charges. As a result, the electrostatic attraction between these positively charged fluorophores and PNIPAM-AuNPs yielded more effective quenching. For this reason, only $3N^{+}$ and $C^{0}2N^{+}$ fluorophores were selected for further investigation. Furthermore, to ensure that the fluorescence response would originate from quenching by the PNIPAM-AuNPs, the interactions between the fluorophore and protein were investigated. In principle, the fluorophore having the least response with proteins is more desirable to be used for the development of protein sensor based on our designed fluorescence quenching.

As can be seen in Figure 4, the emission intensity of $3N^{+}$ fluorophore was minimally affected by BSA. Therefore, $3N^{+}$ fluorophore was selected for further investigation. The much lower fluorescence response of $3N^{+}$ toward BSA than that previously reported by Niamnont and co-workers[32] could be described as a result of the protein concentration used in this research (3.3 $\mu$g/mL having $A_{280}$ = 0.0028) being lower than that ($A_{280}$ = 0.01) used in the previous work. Such lower protein concentration used in this sensing system was presumably not high enough for the BSA to act as effective surfactant that help deaggregating the fluorophore ($3N^{+}$) which should lead to fluorescence signal enhancement, the principle determined quenching efficiency described in their work. Nevertheless, we find this as a potential benefit given that the fluorescence response of $3N^{+}$ is more sensitive to lower protein concentration when used in combination with PNIPAM-AuNPs. To confirm that the $3N^{+}$fluorophore was a proper dye, it was also tested with other five different types of protein having different pI and MW (Lys, Fib, Con A, Hgb, and TF) and was found that all types of proteins did not enhance fluorescence intensity of $3N^{+}$ (Figure 4e).

To study the effect of polymer conformation grafted on AuNPs surface on the quenching efficiency, NP1 and NP2 were compared and found that the quenching efficiency of NP2 was higher than that of NP1 (Figure S5 in the Supporting Information). This may be because the conformation of PNIPAM changed from stretched to coil-like structure upon heating to above its LCST, resulting in the decreasing of distance between the gold core of NP2 and the fluorophore that in turn enhanced the quenching efficiency. To determine the effect of polymer molecular weight grafted on AuNPs surface on the quenching efficiency, NP1 and NP3 were compared. It was found that the quenching efficiency of NP1 was greater than that of NP3. This may be explained as a result of the PNIPAM layer on the NP1 being thinner than that on the NP3. The closer distance between the gold core and fluorophore in the case of NP1 when compared to that of the NP3 thus promotes the quenching process. The data shown in Table S3 in the Supporting Information demonstrated that all PNIPAM-AuNPs initially possessed negative zeta potential values, all of which became less negative upon $3N^{+}$ addition. These evidently supported the assumption that the quenching was driven by electrostatic attraction between the positive charge of the $3N^{+}$ fluorophore and the lone paired electrons of nitrogen and oxygen in the repeating unit of PNIPAM on the PNIPAM-AuNPs. Taking NP1 as a representative of PNIPAM-AuNPs, an equilibrium constant of association with the $3N^{+}$ fluorophore determined using Stern−Volmer analysis ($K_{SV}$) was found to be $8.21 \times 10^{8}$ $M^{-1}$ (Figure S6, Supporting Information).

To ensure that the structures of PNIPAM-AuNPs maintained their physical characteristic throughout the period of protein classification, UV absorption of NP1 and NP2 both before and after $3N^{+}$ addition and after protein addition (BSA was chosen as a representative protein for this set of experiment) was measured. The results shown in Figure S7 (Supporting Information) truly demonstrate that the fluorescence quenching/recovery event happened without causing any changes in the PNIPAM-AuNPs characteristic (shift in absorption

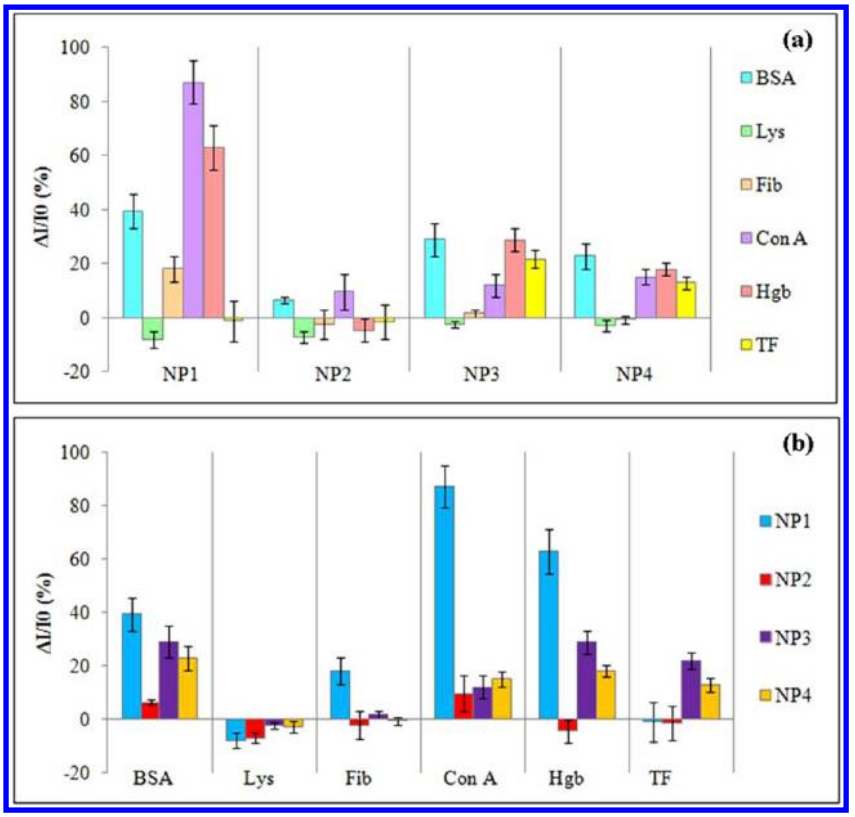


**Figure 5.** Histogram plot of fluorescence response ($\Delta I/I_0$) patterns of $3N^+$ fluorophore: (a) in the presence of six proteins in PBS for each type PNIPAM-AuNPs and (b) in the presence of PNIPAM-AuNPs for each type of proteins in PBS (responses are averages of six measurements, and error bars are standard deviations).

maximum of surface plasmon band, aggregation). Similar outcome was also observed in the cases of NP3 and NP4 (data not shown).

For the determination of protein based on fluorescence quenching, six types of proteins were analyzed by using NP1-NP4 with the $3N^+$ fluorophore. The obtained results are illustrated in Figure 5a. Each type of PNIPAM-AuNPs exhibited different responses to different proteins. The fluorescence intensities of six proteins in response to NP1 were larger than those in response to other three types of PNIPAM-AuNPs. Unlike NP1, NP2 with its thinner PNIPAM layer may provide stronger interactions with the fluorophore as evidenced by its greater quenching efficiency when compared with NP1 (See Figure S5 in Supporting Information). For this reason, it might be difficult for the fluorophore to be released from NP2 surface upon the protein addition. It is believed that this outcome was influenced by protein resistance property of the PNIPAM brushes which is more prominent at the collapsed state as has been previously described by Xue et al.[44] This may be explained as a result of the collapsed PNIPAM layer of NP2 being denser than that of NP1 so that it is more difficult for the protein to access the fluorophore situated within the PNIPAM layer. That is why the signal responses were lower. In the case of NP3, of which PNIPAM layer was thicker than that of NP1, the change in fluorescence response was proportionally smaller. We explained this as a consequence of the quenching being initially low even before the protein addition due to the long distance between the gold core and the fluorophore. After the addition of protein, the fluorescence signal was not much affected and therefore gave the relatively low response.

Despite the facts that the PNIPAM layer of NP4 was thinner than that of the NP3 and its initial quenching efficiency was as high as that of NP1, overall signal responses of NP4 were relatively small and followed the same trend that observed in the case of NP3. We suspect that the same explanation previously used for NP2 based on limited accessability of the protein to the fluorophore in the condensed layer of PNIPAM can be applied here. In addition, to demonstrate the protein detection profile of the developed sensing array based on four types of PNIPAM-AuNPs, the histogram in Figure 5a was replotted for each protein and shown in Figure 5b. It is obvious that the responsive patterns of AuNPs were varied with the type of protein because of the difference in charge and molecular weight of protein. At pH 7.4, the $3N^+$ fluorophore bound on the AuNPs surface via charge−dipole interactions. Therefore, when the negatively charged proteins (BSA, Fib, Con A, Hgb, and TF) were added, the release of $3N^+$ fluorophore from the AuNPs surface driven by the electrostatic interactions between negatively charged proteins in solution and $3N^+$ fluorophore can take place so that the quenched fluorescence signal can be recovered. Although being negatively charged proteins, Fib and TF did not provide responses against some types of AuNPs. These might be caused by their high molecular weight being obstacle for effective binding with $3N^+$ fluorophore and thus hampering the fluorescence signal recovery. In the case of Lys, a relatively small and positively charged protein, it was found that the signal recovery did not happen. This may be attributed to the repulsive forces between Lys and the $3N^+$ fluorophore. In fact, further quenching was also observed as can be realized from the negative response of the signal. We describe the decrease of fluorescence signal as a


dx.doi.org/10.1021/la402139g | *Langmuir* 2013, 29, 12317−12327

result of additional quenching of $3N^+$ in the solution that was initially unbound to the PNIPAM-AuNPs. This is likely possible given that it was demonstrated earlier in Figure 4e that the $3N^+$fluorophore was slightly quenched by proteins. The explanation for the impact of characteristic charge and molecular weight of protein on fluorescence signal recovery is schematically summarized in Figure 6.

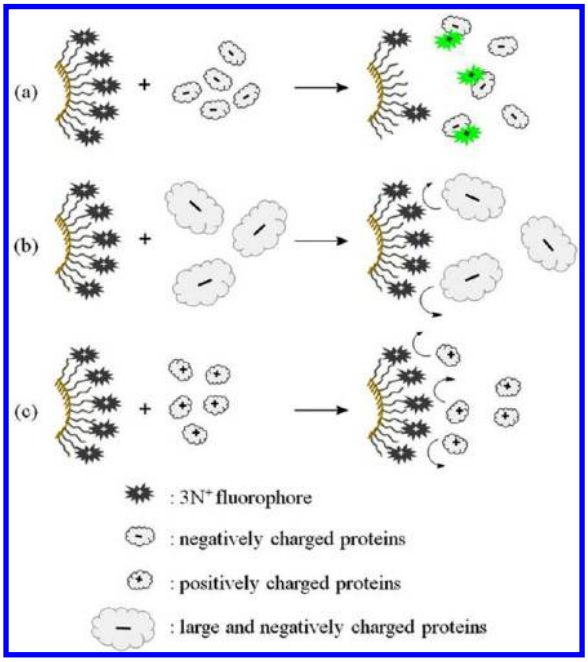


**Figure 6.** Schematic representation of mechanism explaining the fluorescence signal recovery upon the addition of proteins having different size and charge.

Although the results demonstrated in Figure 5b suggested that the developed sensing platform using the PNIPAM-AuNPs in combination with $3N^+$ fluorophore was applicable for protein identification, the fact that the changes in fluorescence response ($\Delta I/I_0$) determined from the maximum emission intensity independent of the wavelength was not intuitively accurate. Such estimation also ruled out the possibility that the wavelength of the emission maxima may be shifted upon protein addition which was found to be the case in some systems. For more accuracy, the whole spectra obtained before and after adding proteins were taken into consideration when performing subtraction. As can be seen in Figure 7a–d, the subtracted spectra of each protein apparently exhibited different characteristic. The intensity values in wavelength range of 400–600 nm of spectra were used to identify each protein as they show the highest variation of $\%\Delta I$ and the highest shifted $\lambda_{max}$ toward the proteins. Although the histogram plot and characteristic spectrum already showed different patterns of the fluorescence responses toward each protein analyte, discrimination of these proteins based on this multidimensional data set (4 AuNPs × 6 proteins × 6 replicates) was further simplified using multivariate statistical analyses. In this study, principal component analysis (PCA) was used to transform the data set of fluorescence intensity differences ($\%\Delta I$) into principle component (PC) scores.[45] Based on the data similarity, a two-dimensional PC score plot (PC1 and PC2) suitably generated six clusters on the PC space corresponding to six types of proteins indicating an encouraging level of

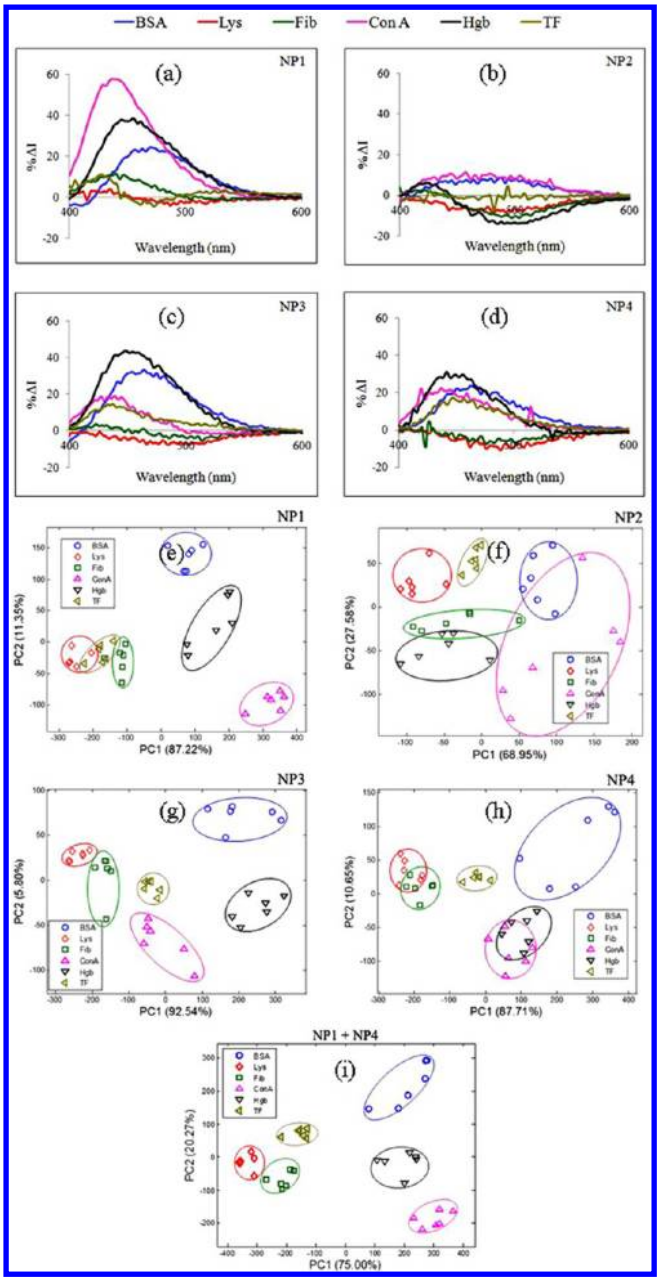


**Figure 7.** Characteristic emission spectra of $3N^+$ fluorophore in the presence of (a) NP1, (b) NP2, (c) NP3, and (d) NP4 for each type of proteins in PBS (obtained by the subtraction of spectra before and after protein addition) and PCA score plot of $\%\Delta I$ data set obtained from 6 replicates of 6 proteins including fluorescence responses of $3N^+$ fluorophore using (e) NP1, (f) NP2, (g) NP3, (h) NP4, and (i) NP1+NP4.

protein classification (Figure 7e–h). To quantify the classification accuracy, PCA-LDA was applied by performing LDA on the PC scores with a total variance of >95% and then validate the discriminating ability using leave-one-out (LOO) cross validation technique.[34] After PCA-LDA routines were performed on the data by using each type of AuNPs (NP1-NP4), the results showed that the data which used NP3 gave the highest classification accuracy of 97.22%. The obtained data implied that the aggregation of PNIPAM layer induced by thermal treatment (NP2 and NP4) may deteriorate the efficiency of protein classification. However, we found that the 100% of classification accuracy can be obtained by


dx.doi.org/10.1021/la402139g | Langmuir 2013, 29, 12317–12327

combining NP1 data set with NP4 data set. The PCA score plot of NP1 associated with NP4 is shown in Figure 7i. These results strongly indicate the high potential of the developed sensing platform given that proteins can be identified with 100% accuracy by using only two types of PNIPAM-AuNPs.

## CONCLUSIONS

This investigation has demonstrated that the thermoresponsive AuNPs can be prepared by using citrate-stabilized AuNPs grafted with PNIPAM-SH synthesized via RAFT polymerization. The prepared PNIPAM-AuNPs have a spherical morphology and uniform size distribution and their shell thickness depended on the PNIPAM-SH molecular weight. Upon molecular weight variation and heat treatment, four types of PNIPAM-AuNPs (NP1-NP4) having different quenching efficiency against $3N^+$ fluorophore were generated. After protein addition, the fluorescence signal of $3N^+$ fluorophore can be recovered. The different pattern of fluorescence signal recovery which is varied with the types of both proteins and PNIPAM-AuNPs can be used to generate an array-based protein classification. Based on LDA analysis using the LOO approach, a 100% accuracy of protein classification can be achieved using a combination of NP1 data set and NP4 data set. The results have suggested that an array-based sensing platform based on chemical nose approach can be developed from PNIPAM-AuNPs when combined with a positively charged phenylene-ethynylene fluorophore.

## ASSOCIATED CONTENT

### Supporting Information

$^1$H NMR spectra of PNIPAM, UV−vis absorption spectra of PNIPAM and PNIPAM-SH, FTIR spectra of PNIPAM and PNIPAM-AuNPs, amount of grafted PNIPAM chains, particle size of AuNPs obtained from AFM and TEM analysis, physical appearance of PNIPAM-AuNPs solution after two heating cycles upon salt addition, and quenching efficiency of four types of PNIPAM-AuNPs with $3N^+$ fluorophore, zeta potential values of all PNIPAM-AuNPs both before and after $3N^+$ fluorophore addition, $K_{SV}$ plot between $3N^+$ and NP1, and UV−vis absorption spectra of NP1 and NP2 during the process of protein classification. This material is available free of charge via the Internet at http://pubs.acs.org.

## AUTHOR INFORMATION

### Corresponding Author

*E-mail: vipavee.p@chula.ac.th. Tel: +66-2218-7627. Fax: +66-2218-7598.

### Notes

The authors declare no competing financial interest.

## ACKNOWLEDGMENTS

This research was financially supported by Chulalongkorn University Centenary Academic Development Project (Under the Center of Innovative Nanotechnology, Chulalongkorn University), the National Research University Project of Thailand, Office of the Higher Education Commission (AM1006A), the Thailand Research Fund (DBG5580003), the Ratchadaphiseksomphot Endowment Fund of Chulalongkorn University (RES560530126-AM), and the Thai Government Stimulus Package 2 (TKK2555), under the Project for Establishment of Comprehensive Center for Innovative Food, Health Products and Agriculture.

## REFERENCES

(1) Ishii, T.; Otsuka, H.; Kataoka, K.; Nagasaki, Y. Preparation of functionally PEGylated gold nanoparticles with narrow distribution through autoreduction of auric cation by alpha-biotinyl-PEG-block-[poly(2-(*N*,*N*-dimethylamino)ethyl methacrylate)]. *Langmuir* **2004**, *20* (3), 561−564.

(2) Mirkin, C. A.; Letsinger, R. L.; Mucic, R. C.; Storhoff, J. J. A DNA-based method for rationally assembling nanoparticles into macroscopic materials. *Nature* **1996**, *382* (6592), 607−609.

(3) Storhoff, J. J.; Lazarides, A. A.; Mucic, R. C.; Mirkin, C. A.; Letsinger, R. L.; Schatz, G. C. What controls the optical properties of DNA-linked gold nanoparticle assemblies? *J. Am. Chem. Soc.* **2000**, *122* (19), 4640−4650.

(4) Li, D. X.; He, Q.; Li, J. B. Smart core/shell nanocomposites: Intelligent polymers modified gold nanoparticles. *Adv. Colloid Interface Sci.* **2009**, *149* (1−2), 28−38.

(5) Hussain, I.; Graham, S.; Wang, Z. X.; Tan, B.; Sherrington, D. C.; Rannard, S. P.; Cooper, A. I.; Brust, M. Size-controlled synthesis of near-monodisperse gold nanoparticles in the 1−4 nm range using polymeric stabilizers. *J. Am. Chem. Soc.* **2005**, *127* (47), 16398−16399.

(6) Cui, Y.; Tao, C.; Zheng, S. P.; He, Q.; Ai, S. F.; Li, J. B. Synthesis of thermosensitive PNIPAM-co-MBAA nanotubes by atom transfer radical polymerization within a porous membrane. *Macromol. Rapid Commun.* **2005**, *26* (19), 1552−1556.

(7) Gil, E. S.; Hudson, S. M. Stimuli-reponsive polymers and their bioconjugates. *Prog. Polym. Sci.* **2004**, *29* (12), 1173−1222.

(8) Hu, Z. B.; Chen, Y. Y.; Wang, C. J.; Zheng, Y. D.; Li, Y. Polymer gels with engineered environmentally responsive surface patterns. *Nature* **1998**, *393* (6681), 149−152.

(9) Schilli, C. M.; Zhang, M. F.; Rizzardo, E.; Thang, S. H.; Chong, Y. K.; Edwards, K.; Karlsson, G.; Muller, A. H. E. A new double-responsive block copolymer synthesized via RAFT polymerization: Poly(*N*-isopropylacrylamide)-*block*-poly(acrylic acid). *Macromolecules* **2004**, *37* (21), 7861−7866.

(10) Bohrisch, J.; Wendler, U.; Jaeger, W. Controlled radical polymerization of 4-vinylpyridine. *Macromol. Rapid Commun.* **1997**, *18* (11), 975−982.

(11) Mika, A. M.; Childs, R. F. Acid/base properties of poly(4-vinylpyridine) anchored within microporous membranes. *J. Membr. Sci.* **1999**, *152* (1), 129−140.

(12) Ista, L. K.; Mendez, S.; Perez-Luna, V. H.; Lopez, G. P. Synthesis of poly(*N*-isopropylacrylamide) on initiator-modified self-assembled monolayers. *Langmuir* **2001**, *17* (9), 2552−2555.

(13) Fischer, A.; Brembilla, A.; Lochon, P. Nitroxide-mediated radical polymerization of 4-vinylpyridine: Study of the pseudo-living character of the reaction and influence of temperature and nitroxide concentration. *Macromolecules* **1999**, *32* (19), 6069−6072.

(14) Zhang, J.; Pelton, R. The dynamic behavior of poly(*N*-isopropylacrylamide) at the air/water interface. *Colloids Surf., A* **1999**, *156* (1−3), 111−122.

(15) Wu, C.; Zhou, S. Q. Thermodynamically stable globule state of a single poly(*N*-isopropylacrylamide) chain in water. *Macromolecules* **1995**, *28* (15), 5388−5390.

(16) Wang, X. H.; Wu, C. Light-scattering study of coil-to-globule transition of a poly(*N*-isopropylacrylamide) chain in deuterated water. *Macromolecules* **1999**, *32* (13), 4299−4301.

(17) Kratz, K.; Hellweg, T.; Eimer, W. Structural changes in PNIPAM microgel particles as seen by SANS, DLS, and EM techniques. *Polymer* **2001**, *42* (15), 6631−6639.

(18) Zhu, M. Q.; Wang, L. Q.; Exarhos, G. J.; Li, A. D. Q. Thermosensitive gold nanoparticles. *J. Am. Chem. Soc.* **2004**, *126* (9), 2656−2657.

(19) Yusa, S. I.; Fukuda, K.; Yamamoto, T.; Iwasaki, Y.; Watanabe, A.; Akiyoshi, K.; Morishima, Y. Salt effect on the heat-induced association behavior of gold nanoparticles coated with Poly(*N*-isopropylacrylamide) prepared via reversible addition - Fragmentation chain transfer (RAFT) radical polymerization. *Langmuir* **2007**, *23* (26), 12842−12848.

(20) Shan, J.; Nuopponen, M.; Jiang, H.; Kauppinen, E.; Tenhu, H. Preparation of poly(*N*-isopropylacrylamide)-monolayer-protected gold clusters: Synthesis methods, core size, and thickness of monolayer. *Macromolecules* **2003**, *36* (12), 4526−4533.
(21) Shan, J.; Chen, J.; Nuopponen, M.; Tenhu, H. Two phase transitions of poly(*N*-isopropylacrylamide) brushes bound to gold nanoparticles. *Langmuir* **2004**, *20* (11), 4671−4676.
(22) Chakraborty, S.; Bishnoi, S. W.; Perez-Luna, V. H. Gold nanoparticles with poly(*N*-isopropylacrylamide) formed via surface initiated atom transfer free radical polymerization exhibit unusually slow aggregation kinetics. *J. Phys. Chem. C* **2010**, *114* (13), 5947−5955.
(23) Phillips, R. L.; Miranda, O. R.; You, C. C.; Rotello, V. M.; Bunz, U. H. F. Rapid and efficient identification of bacteria using gold-nanoparticle- Poly(para-phenyleneethynylene) constructs. *Angew. Chem., Int. Ed.* **2008**, *47* (14), 2590−2594.
(24) Miranda, O. R.; Creran, B.; Rotello, V. M. Array-based sensing with nanoparticles: 'Chemical noses' for sensing biomolecules and cell surfaces. *Curr. Opin. Chem. Biol.* **2010**, *14* (6), 728−736.
(25) De, M.; You, C. C.; Srivastava, S.; Rotello, V. M. Biomimetic interactions of proteins with functionalized nanoparticles: A thermodynamic study. *J. Am. Chem. Soc.* **2007**, *129* (35), 10747−10753.
(26) De, M.; Rana, S.; Akpinar, H.; Miranda, O. R.; Arvizo, R. R.; Bunz, U. H. F.; Rotello, V. M. Sensing of proteins in human serum using conjugates of nanoparticles and green fluorescent protein. *Nat. Chem.* **2009**, *1* (6), 461−465.
(27) Schilli, C.; Lanzendorfer, M. G.; Muller, A. H. E. Benzyl and cumyl dithiocarbamates as chain transfer agent in the RAFT polymerization of *N*-isopropylacrylamide. In situ FT-NIR and MALDI-TOF MS investigation. *Macromolecules* **2002**, *35* (18), 6819−6827.
(28) Ray, B.; Isobe, Y.; Morioka, K.; Habaue, S.; Okamoto, Y.; Kamigaito, M.; Sawamoto, M. Synthesis of isotactic poly(*N*-isopropylacrylamide) by RAFT polymerization in the presence of Lewis acid. *Macromolecules* **2003**, *36* (3), 543−545.
(29) Kujawa, P.; Segui, F.; Shaban, S.; Diab, C.; Okada, Y.; Tanaka, F.; Winnik, F. M. Impact of end-group association and main-chain hydration on the thermosensitive properties of hydrophobically modified telechelic poly(*N*-isopropylacrylamides) in water. *Macromolecules* **2006**, *39* (1), 341−348.
(30) Ganachaud, F.; Monteiro, M. J.; Gilbert, R. G.; Dourges, M. A.; Thang, S. H.; Rizzardo, E. Molecular weight characterization of poly(*N*-isopropylacrylamide) prepared by living free-radical polymerization. *Macromolecules* **2000**, *33* (18), 6738−6745.
(31) Convertine, A. J.; Ayres, N.; Scales, C. W.; Lowe, A. B.; McCormick, C. L. Facile, controlled, room-temperature RAFT polymerization of *N*-isopropylacrylamide. *Biomacromolecules* **2004**, *5* (4), 1177−1180.
(32) Niamnont, N.; Mungkarndee, R.; Techakriengkrai, I.; Rashatasakhon, P.; Sukwattanasinitt, M. Protein discrimination by fluorescent sensor array constituted of variously charged dendritic phenylene-ethynylene fluorophores. *Biosens. Bioelectron.* **2010**, *26* (2), 863−867.
(33) Hayat, A. Colloidal gold: principles, methods, and applications. *J. Anat.* **1989**, *176*, 215−216.
(34) Brereton, R. G. *Chemometrics for pattern recognition*; Wiley & Sons: Chichester, 2009.
(35) Varmuza, K. *Chemometrics in practical applications*; InTech publisher: Rijeka, 2012.
(36) Lloyd, G. R.; Orr, L. E.; Christie-Brown, J.; McCarthy, K.; Rose, S.; Thomas, M.; Stone, N. Discrimination between benign, primary and secondary malignancies in lymph nodes from the head and neck utilising Raman spectroscopy and multivariate analysis. *Analyst* **2013**, *138* (14), 3900−3908.
(37) Smit, S.; van Breemen, M. J.; Hoefsloot, H. C. J.; Smilde, A. K.; Aerts, J. M. F. G. de Koster, C. G. Assessing the statistical validity of proteomics based biomarkers. *Anal. Chim. Acta* **2007**, *592* (2), 210−217.
(38) van der Werf, M. J.; Pieterse, B.; van Luijk, N.; Schuren, F.; van der Werff-van der Vat, B.; Overkamp, K.; Jellema, R. H. Multivariate analysis of microarray data by principal component discriminant analysis: prioritizing relevant transcripts linked to the degradation of different carbohydrates in *Pseudomonas putida* S12. *Microbiology* **2006**, *152*, 257−272.
(39) Nakayama, M.; Okano, T. Polymer terminal group effects on properties of thermoresponsive polymeric micelles with controlled outer-shell chain lengths. *Biomacromolecules* **2005**, *6* (4), 2320−2327.
(40) Andersson, M.; Hietala, S.; Tenhu, H.; Maunu, S. L. Polystyrene latex particles coated with crosslinked poly(*N*-isopropylacrylamide). *Colloid Polym. Sci.* **2006**, *284* (11), 1255−1263.
(41) Chen, Q.; Xu, K.; Zhang, W. D.; Song, C. L.; Wang, P. X. Preparation and characterization of poly (*N*-isopropylacrylamide)/polyvinylamine core-shell microgels. *Colloid Polym. Sci.* **2009**, *287* (11), 1339−1346.
(42) Scales, C. W.; Convertine, A. J.; McCormick, C. L. Room-temperature polymerization of *N*-isopropylacrylamide via RAFT and subsequent conjugation of fluorescent labels. *Abstr. Pap. Am. Chem. Soc.* **2005**, *230*, U4233−U4234.
(43) Du, B. Y.; Mei, A. X.; Tao, P. J.; Zhao, B.; Cao, Z.; Nie, J. J.; Xu, J. T.; Fan, Z. Q. Poly[*N*-isopropylacrylamide-*co*-3-(trimethoxysilyl)-propylmethacrylate] coated aqueous dispersed thermosensitive $Fe_3O_4$ nanoparticles. *J. Phys. Chem. C* **2009**, *113* (23), 10090−10096.
(44) Xue, C. Y.; Yonet-Tanyeri, N.; Brouette, N.; Sferrazza, M.; Braun, P. V.; Leckband, D. E. Protein adsorption on poly(*N*-isopropylacrylamide) brushes: dependence on grafting density and chain collapse. *Langmuir* **2011**, *27* (14), 8810−8818.
(45) Poulli, K. I.; Mousdis, G. A.; Georgiou, C. A. Classification of edible and lampante virgin olive oil based on synchronous fluorescence and total luminescence spectroscopy. *Anal. Chim. Acta* **2005**, *542* (2), 151−156.

# Formation of Thermo-Sensitive and Cross-Linkable Micelles by Self-Assembly of Poly(pentafluorophenyl acrylate)-Containing Block Copolymer

**Wilaiporn Graisuwan,[1] Hui Zhao,[2] Suda Kiatkamjornwong,[3] Patrick Theato,[2] Voravee P. Hoven[4]**

[1]Program in Petrochemistry, Faculty of Science, Chulalongkorn University, Phayathai Road, Pathumwan, Bangkok 10330, Thailand
[2]Institute for Technical and Macromolecular Chemistry, University of Hamburg, Bundesstrasse 45, D-20146, Hamburg, Germany
[3]Department of Imaging and Printing Technology, Faculty of Science, Chulalongkorn University, Phayathai Road, Pathumwan, Bangkok 10330, Thailand
[4]Department of Chemistry, Organic Synthesis Research Unit, Faculty of Science, Chulalongkorn University, Phayathai Road, Pathumwan, Bangkok 10330, Thailand
Correspondence to: V. P. Hoven (E-mail: vipavee.p@chula.ac.th) and P. Theato (E-mail: theato@chemie.uni-hamburg.de)

Received 14 July 2014; accepted 29 December 2014; published online 7 February 2015
**DOI: 10.1002/pola.27541**

**ABSTRACT**: Poly(pentafluorophenyl acrylate)-*block*-poly(*N*-isopropylacrylamide) (PPFPA-*b*-PNIPAM) is synthesized by reversible addition-fragmentation chain transfer (RAFT) polymerization. Light-responsive moieties of *ortho*-nitrobenzyl (ONB)-protected diamine are partially introduced to the PFPA moieties via post-polymerization modification. The amphiphilic block copolymers are assembled into micelles in water. The ONB-protected diamine group in the micelle core is released upon UV irradiation, which subsequently induces an *in situ* cross-linking by a spontaneous reaction with the remaining PFPA groups in the core and yields stable cross-linked micelles. Micellization of the copolymers is confirmed by dynamic light scattering (DLS) and transmission electron microscopy (TEM). 4-Nitro-7-piperazino-2,1,3-benzoxadiazole (NBD) and pyrene are loaded in the core of cross-linked micelles to demonstrate the possibility for additional post-functionalization of residual PFPA moieties and hydrophobic molecule encapsulation, respectively. It is anticipated that these micelles can be alternative cargos for incorporating active compounds that may be useful for advanced applications. © 2015 Wiley Periodicals, Inc. J. Polym. Sci., Part A: Polym. Chem. **2015**, *53*, 1103–1113

**KEYWORDS**: block copolymers; crosslinking; micelles; post-functionalization; PPFPA; RAFT polymerization

**INTRODUCTION** Amphiphilic block copolymer micelles assembled from thermo-responsive polymers have been extensively investigated for various applications in the field of controlled drug/gene delivery and biotechnology.[1–5] Poly(*N*-isopropylacrylamide) (PNIPAM) is one of the most investigated temperature-sensitive component to be incorporated into block copolymers due to its lower critical solution temperature (LCST) of approximately 32 °C in aqueous solution, being close to human body temperature.[6] When combined with a hydrophobic block, PNIPAM yields copolymer that would self-assemble into micelles having thermo-responsive shell, which is capable of encapsulating hydrophobic molecules within the core. Upon heating above the LCST, the micellar structure should be deformed and released the hydrophobic molecules. Okano's research team has performed pioneering work on polymeric micelles with temperature-triggered drug release mechanisms using block copolymers comprising PNIPAM and various hydrophobic polymers.[7,8] Temperature-responsive micelles with biodegradable cores have been also developed.[9,10] Similar works have been studied by Liu et al.[11] and Zhu et al.[12] for the release of doxorubicin and paclitaxel, respectively.

However, a major drawback of these self-assembled micelles is their instabilities under certain changes in biological systems. Stabilization has often been achieved by chemical cross-linking of the shell or the core of the micelles.[3,13,14] One of the most effective methods is to incorporate reactive functional groups onto the backbone of the copolymers. The constructed micelles undergo cross-linking upon an addition of a bifunctional reagent. In 2007, Zhang et al. fabricated double hydrophilic block copolymer micelles from

Additional Supporting Information may be found in the online version of this article.

poly(ethylene oxide)-*b*-poly(*N*-isopropylacrylamide-*co*-*N*-acryloxysuccinimide) (PEO-*b*-P(NIPAM-*co*-NAS), which formed micelles by heating a copolymer solution above its LCST. Stabilization of the P(NIPAM-*co*-NAS) cores was accomplished via the reaction of NAS residues with cystamine.[15] Similarly, Li et al. prepared thermally responsive micelles by self-assembly of triblock copolymer of poly(ethylene oxide)-*block*-(*N,N′*-dimethylacrylamide-*stat*-*N*-acryloxysuccinimide)-*block*-poly(*N*-isopropylacrylamide) (PEO-*b*-(DMA-*s*-NAS)-*b*-NIPAM). Incorporation of the NAS units into the triblock copolymer allows for shell-cross-linked (SCL) micelles by reaction with difunctional primary amines. These SCL micelles swell when the solution temperature is lower than the LCST of the NIPAM block.[16] Despite its high reactivity, *N*-acryloxysuccinimide (NAS) suffers from its hydrolytic instability and limited solubility in organic media (only soluble in dimethylformamide or dimethyl sulfoxide) that restrict their applications. Monomer having active pentafluorophenyl ester, pentafluorophenyl (meth)acrylate (PFP(M)A), has been recently introduced as alternative to NAS due to its better solubility in many common organic solvents and higher hydrolytic stability in water and air than NAS.[17,18] Additional advantage lies on the fact that the reaction of the pentafluorophenyl ester groups can be conveniently monitored by $^{19}$F NMR spectroscopy.[19] Duong et al. prepared well-defined functional nanoparticles from poly(oligo(ethylene glycol) methyl ether acrylate)-*block*-poly(vinylbenzyl chloride-*co*-pentafluorophenyl acrylate) (P(OEG-A)-*b*-P(VBC-*co*-PFPA)). The nanoparticles were subsequently stabilized by a reaction of active pentafluorophenyl moieties with diamine. The polymer nanoparticles were found to be suitable for hydrophobic drug encapsulation.[20] Recently, Zhuang et al. have developed water-dispersible nanogels based on random copolymer of pentafluorophenyl acrylate and poly(ethylene glycol methacrylate) having diamine as a cross-linker. Isopropylamine and *N,N′*-dimethylethylene diamine were incorporated onto the core-cross-linked nanogel to demonstrate the possibility of surface engineering. These nanogels can encapsulate lipophilic guest molecules during the cross-linking step of the nanogel synthesis.[21]

Another interesting approach to obtain stable micelles is using photo/UV-labile linker. In general, a light-responsive behavior of polymer can either be reversible or irreversible, depending on the chromophore that is attached to the polymeric backbone or to the chain end. Recently, an irreversible light-responsive moiety of *ortho*-nitrobenzyl (ONB) derivatives has attracted increasing interest in biochemistry and synthetic chemistry as photo-labile protecting groups and has been introduced to polymer structure as photo-cleavable units.[22,23] Jiang et al. nicely demonstrated the use of ONB as a side chain functionality to prepare light-responsive block copolymeric micelles of poly(ethylene oxide) (PEO) and poly(2-nitrobenzyl methacrylate) (PNBM). The micelles were capable of entrapping dyes with the intention of releasing them at a defined time and location.[24] However, controlling the polymerization of ONB-containing monomers is still difficult because nitroaromatic compounds can act as inhibitors/retardants during the radical polymerization process.[25] Post-polymerization modification is a versatile method for the introduction of such chemical functionality that would otherwise interfere with the polymerization process.[25]

Reversible addition-fragmentation chain transfer (RAFT), a commonly used controlled radical polymerization process, provides a versatile route to the generation of amphiphilic block copolymer with controllable features, such as block length, structure, and molecular weight.[26–28] It is compatible with a wide range of functional monomers and does not require the use of (transition metal) catalyst. One can achieve precisely defined reactive polymer structures. This procedure enables the synthesis of polymeric architectures, which cannot be realized by the classical way of radical copolymerization.[29]

This research aims to develop thermo-responsive micelles of which cores are cross-linkable via light-trigger process from block copolymers consisting of pentafluorophenyl acrylate (PFPA) and *N*-isopropylacrylmide (NIPAM), to the best of our knowledge, has never been reported before. It is anticipated that RAFT polymerization under optimized conditions can yield well-defined block copolymers with controlled molecular weights and narrow polydispersities. Subsequent post-polymerization modification of the copolymers is performed to incorporate light-responsive moieties of *ortho*-nitrobenzyl (ONB) into the PFPA block of the copolymers. Finally, the ONB-containing copolymers are self-assembled into micelles. The stabilization of core is subsequently induced by UV irradiation. It is anticipated that the residual PFPA moieties in the copolymers should be available for further chemical modification with bioactive species and allow for physical encapsulation of desired hydrophobic molecules. These should make the developed core-cross-linked (CCL) micelles of PNIPAM-containing copolymers more useful in many advanced applications.

## EXPERIMENTAL

### Materials

All solvents used for reactions are reagent grade and used as received, unless otherwise specified. Anhydrous 1,4-dioxane (99.9%) were obtained from Merck. Anhydrous tetrahydrofuran (THF, 99.9%) was obtained from Sigma-Aldrich. Dichloromethane was dried over $CaH_2$ under reflux and nitrogen atmosphere. Solutions were made with Milli-Q water purified by Millipore Milli-Q system that involves reverse osmosis, ion exchange, and filtration steps (18.2 MΩ). The NMR solvents such as $CDCl_3$ (99.8% D), DMSO-d6 (99.9%), and $D_2O$ (99.9% D) were obtained from Cambridge Isotope Laboratories, Inc. (USA); 4-cyanopentanoic acid dithiobenzoate (CPADB, 97%), triethylamine (TEA, 99.5%), 4-nitro-7-piperazino-2,1,3-benzoxadiazole (NBD) (99.0%), pyrene (98%), 2-nitrobenzyl bromide (98%), and *N,N′*-dimethylethylenediamine (85%) were purchased from Sigma-Aldrich and used as received. *N*-isopropylacrylamide (NIPAM, 97%) was obtained from Sigma-Aldrich and recrystallized twice in hexane before use. Pentafluorophenol (99%) was commercially available from Merck and used as received.

Azobisisobutyronitrile (AIBN, 98%) was obtained from Fluka and used as received. Acryloyl chloride (98%) was purchased from Acros and used as received.

### Instrumentation

$^1$H NMR spectra were recorded on a Varian, model Mercury-400 nuclear magnetic resonance spectrometer (USA) operating at 400 MHz, and $^{19}$F NMR spectra were recorded on a Bruker DRX 400 FT-NMR spectrometer. Chemical shifts ($\delta$) were reported in part per million (ppm) relative to tetramethylsilane (TMS) signal as a reference. FT-IR spectra were recorded with a Nicolet Impact 6700 FT-IR spectrometer with 32 scans at a resolution of 4 cm$^{-1}$ in a frequency range of 400 to 4000 cm$^{-1}$. Samples were pressed into potassium bromide (KBr) pellets. UV-Vis spectra were recorded on an Agilent 8453 UV-Vis spectroscopy. Molecular weight and molecular weight distribution of synthesized (co)polymers were analyzed by gel permeation chromatography (GPC) using Waters 600 controller chromatograph equipped with HR1 and HR4 columns (Waters, MW resolving range = 100–500,000 g/mol) at 35 °C and refractive index (RI) detector (Waters 2414). THF was used as an eluent with the flow rate of 1.0 mL/min. Sample injection volume was 80 μL. Five polystyrene standards (996–188,000 g/mol) were used for generating a calibration curve. The hydrodynamic diameters of micelles were measured using a dynamic light scattering (DLS) instrument (Zetasizer Nano ZS, Malvern Instrument Ltd., U.K. equipped with a He-Ne laser beam at 658 nm) at a fixed scattering angle of 173°. The sample refractive index (RI) was set at 1.59 for polystyrene. The dispersant viscosity and RI were set to 0.89 Ns m$^2$ and 1.33, respectively. All samples (1.0 mg/mL) were filtered through a 0.45 μm syringe filter before analysis, and each measurement was repeated at least 10 times to obtain the average value with an equilibrium time of 5 min before each measurement. Transmission electron microscopy (TEM) studies were performed on a JEOL Model JEM-2100 electron microscope operating at an acceleration voltage of 100 kV. Samples were prepared by drop-casting of a given micelle solution onto carbon-coated copper grid and excess solution was carefully blotted off using filter paper. The samples were then air-dried at room temperature before measurement.

### Synthesis of *Ortho*-Nitrobenzyl (ONB) Protected Diamine

ONB-protected diamine was synthesized according to a method modified from that of Zhao and Theato.[25] 2-Nitrobenzyl bromide (1.0 g, 4.6 mmol), *N,N′*-diethylethylenediamine (4 mL, 37.2 mmol), and dry dichloromethane (20 mL) were added into a round bottom flask. The reaction mixture was stirred in the dark place at room temperature overnight. After that, the solution was extracted with distilled water for three times. The filtrate was dried over anhydrous sodium sulfate ($Na_2SO_4$) and dichloromethane was then removed using rotary evaporator. The pure yellow liquid was obtained (0.69 g (3.2 mmol, 70% yield). $^1$H NMR (400 MHz, $CDCl_3$): $\delta$/ppm: 7.89–7.27 (m, 4H), 3.79 (d, 2H), 2.63-2.52 (m, 4H), 2.46 (s, 3H), 2.04 (s, 3H).

### Synthesis of Pentafluorophenyl Acrylate (PFPA)

PFPA was synthesized according to the method of Jochum and Theato[30] Pentafluorophenol (40.0 g, 0.22 mol) was dissolved in 250 mL of dry dichloromethane in round bottom flask. Triethylamine (TEA) (36.2 mL, 0.26 mol) was slowly added to the reaction mixture on ice bath, and acryloyl chloride (21.1 mL, 0.26 mol) was then slowly added. After being removed from the ice bath, the reaction mixture was stirred at room temperature overnight. The precipitate of triethylamine hydrochloride salt was filtered, washed thoroughly with dichloromethane. The filtrate was extracted twice with acidic water (pH = 2.0), and twice with basic solution ($Na_2CO_3$), and finally twice with DI water. The organic phase was dried over anhydrous sodium sulfate ($Na_2SO_4$), and dichloromethane was removed using rotary evaporator. The crude product was further purified by column chromatography (column material: silica gel; solvent: petroleum ether). The pure colorless liquid was obtained (26.3 g, 0.16 mol, 75% yield) and stored in refrigerator at −20 °C.

$^1$H NMR (400 MHz, $CDCl_3$): $\delta$/ppm: 6.70 (d, 1H), 6.35 (dd, 1H), 6.16 (d, 1H); $^{19}$F NMR ($CDCl_3$): $\delta$/ppm: −162 (d, 2F), −157 (t, 1F), −153 (d, 2F); FT-IR (ATR-mode): 1772 cm$^{-1}$ (C═O reactive ester band), 1516 cm$^{-1}$ (C═C aromatic band)

### Synthesis of Poly(pentafluorophenyl acrylate) (PPFPA)

PPFPA was synthesized according to the method published recently.[30] Briefly, PFPA monomer (4.80 g, 20 mmol), CPADB (11 mg, 0.04 mmol), and AIBN (0.65 mg, 0.004 mmol) were added to a vial followed by 10 mL of dry 1,4-dioxane. The vial was sealed with a rubber septum and the solution was purged with argon gas for 30 min. The vial was then immersed into a thermo-stated oil bath at 70 °C for 2 h. After immersing for 2 h, the polymer solution was precipitated in methanol, centrifuged, and dried under vacuum at room temperature. The dried polymer was then dissolved in THF and precipitated again in methanol. This procedure was repeated two times. The product was obtained as pink powder in 65% yield (3.10 g, 13 mmol).

$^1$H NMR (400 MHz, $CDCl_3$): $\delta$/ppm: 3.10 (br, $CH_2C\underline{H}$), 2.51 (br, $C\underline{H}_2CH$), 2.13 (br, $C\underline{H}_2CH$); $^{19}$F NMR ($CDCl_3$): $\delta$/ppm: −163, −159, −153. FT-IR (ATR-mode): 1782 cm$^{-1}$ (C═O reactive ester band), 1515 cm$^{-1}$ (C═C aromatic band), 1090 cm$^{-1}$ (C—O ester band). The resulting PPFPA homopolymer was subsequently used as a macro chain transfer agent (macro-CTA) for the polymerization of NIPAM.

### Synthesis of Poly(PFPA)-*block*-poly(NIPAM) (PPFPA-*b*-PNIPAM)

For the synthesis of diblock PPFPA-*b*-PNIPAM copolymer using RAFT polymerization, it is advisable to start with the monomer that shows higher transfer ability for the selected CTA.[31,32] In this case, PPFPA was first synthesized and used as a macro-CTA for PNIPAM synthesis (Scheme 1). The purified PPFPA (0.32 g, 0.05 mmol), NIPAM (0.57 g, 5.04 mmol), and AIBN (0.5 mg, 0.003 mmol) were added to a vial followed by 6 mL of dry 1,4-dioxane. The vial was sealed with a rubber septum and the solution was purged with nitrogen gas for

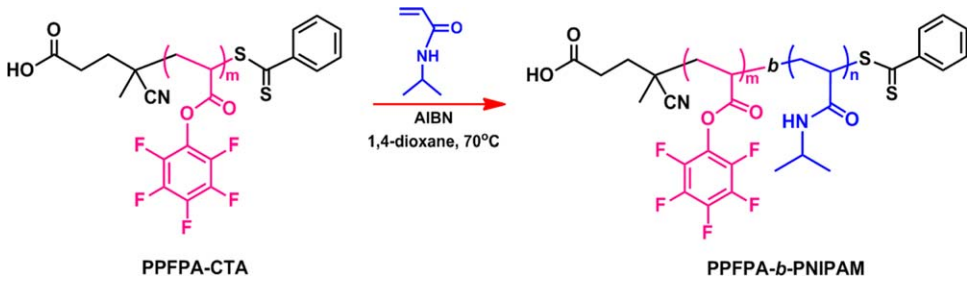


**SCHEME 1** Synthetic pathway of PPFPA-*b*-PNIPAM by RAFT polymerization. [Color figure can be viewed in the online issue, which is available at wileyonlinelibrary.com.]

30 min. Polymerization was conducted under nitrogen atmosphere at 70 °C for 12 h. The polymer solution was precipitated in hexane, centrifuged, and finally dried under vacuum at room temperature. The dried copolymer was then dissolved in THF and precipitated again in hexane. This procedure was repeated two times. The product was obtained as pink powder in 72% yield (1.29 g, 3.66 mmol).

$^1$H NMR (400 MHz, $CDCl_3$): $\delta$/ppm: 4.10 (br, —NHC$\underline{H}$($CH_3$)$_2$), 3.10 (br, $CH_2C\underline{H}$), 2.51–1.50 (m, protons in backbone), 1.13 (br, —NHCH($C\underline{H}_3$)$_2$); $^{19}$F NMR (DMSO-d6): $\delta$/ppm: −172, −166, −162. FT-IR (ATR-mode): 1782 cm$^{-1}$ (C═O reactive ester band), 1645 cm$^{-1}$ (C═O of amide), 1515 cm$^{-1}$ (C═C aromatic band), 1090 cm$^{-1}$ (C—O ester band).

### Post-Polymerization Modification of PPFPA-*b*-PNIPAM with ONB-Protected Diamine

Light-responsive moieties in the form of an ONB-protected diamine were introduced to PPFPA-*b*-PNIPAM via post-polymerization modification of the PFPA part in the block copolymer. The copolymer (0.5 g, 1 equiv. of PFPA unit) was dissolved in 5 mL of dry THF under nitrogen atmosphere for 30 min. Separately, ONB-protected diamine (0.5 equiv.) and TEA (0.1 equiv) was dissolved in 1 mL of dry THF. The ONB-protected diamine solution was quickly added to the polymer solution and continued purging with nitrogen gas for 20 min. The solution was stirred in the dark at room temperature for 24 h. The resulting copolymer was purified by precipitation in diethyl ether, centrifuged, and vacuum dried at room temperature overnight. The product was obtained as pale yellow powder in 67% yield (0.55 g, 0.95 mmol).

$^1$H NMR (400 MHz, $CDCl_3$) $\delta$/ppm: 7.52–8.09 (br, protons in *o*-nitrobenzene), 4.10 (br, —NHC$\underline{H}$($CH_3$)$_2$), 3.2–1.5 (m, protons in backbone and linker of ONB), 1.13 (br, —NHCH($C\underline{H}_3$)$_2$). $^{19}$F NMR (DMSO-d6): $\delta$/ppm: −170, −165, −162. FT-IR (ATR-mode): 1782 cm$^{-1}$ (C═O reactive ester band), 1645 cm$^{-1}$ (C═O of amide band), 1515 cm$^{-1}$ (C═C aromatic band), 1090 cm$^{-1}$ (C—O ester band).

### Preparation of Noncross-Linked (NCL) and Core-Cross-Linked (CCL) Micelles

Noncross-linked (NCL) micelles were formed by gradually adding DI water into a solution of PPFPA-*b*-PNIPAM in THF (50 mg/mL). THF was evaporated by stirring the solution in air to yield a micellar solution of NCL. For core-cross-linked (CCL) micelles, a micellar solution was first prepared from ONB-containing PPFPA-*b*-PNIPAM using a similar procedure as mentioned above for the NCL micelles followed by exposure to UV light (365 nm) for 2 h. After irradiation, the solution was dialyzed consecutively against THF for 2 days and DI water for 1 day to remove by-products (noncross-linked polymer and nitrosobenzaldehyde) and THF, respectively. The aqueous solution in the dialysis tube was collected and filtered with a 0.45 μm pore-sized syringe filter and then lyophilized yielding a pale yellow powder of dry CCL micelles.

### Chemical Incorporation of Amino-Containing Dye into Micelles

NBD as an amino-functionalized fluorescent dye was selected as a model compound that can chemically bind with unreacted PFPA in the core of micelles via post-functionalization. The dry CCL micelles (5 mg, 1 equiv. of residual PFPA unit) were dispersed in 5 mL of dry THF. The micellar solution was purged with nitrogen gas for 30 min. Separately, TEA (0.1 equiv) and NBD (2 equiv.) were dissolved in 1 mL of dry THF. The mixed solution of TEA and NBD was quickly added to the micellar solution and continued purging with nitrogen gas for 20 min. The solution was stirred in the dark at room temperature for 24 h. The solution was then purified by dialysis consecutively against THF for 2 days and DI water for 1 day to remove free NBD and THF, respectively. The aqueous solution in the dialysis tube was collected and filtered with a 0.45 μm pore-sized syringe filter and lyophilized yielding an orange powder of dry micelles.

For comparison, NBD incorporation was also performed before micelles formation and UV-induced cross-linking to compare loading contents of NBD from the two methods. Briefly, the mixed solution of TEA and NBD having the same concentration as above was added directly to 5 mL of ONB-containing PPFPA-*b*-PNIPAM solution in THF (1 mg/mL). The solution was purged with nitrogen gas for 20 min and stirred in the dark at room temperature for 24 h. The solution was then purified by dialysis against THF for 2 days to remove free NBD. Core-cross-linked (CCL) micelles incorporated with NBD were then formed using the same procedure as that for the preparation of CCL micelles as mentioned above.

### Physical Encapsulation of Hydrophobic Dye into Micelles

To determine the ability to encapsulate hydrophobic molecule into the core of the micelles, pyrene was selected as a

**TABLE 1** Molecular Weight Information of PPFPA-*b*-PNIPAM Copolymers Synthesized by RAFT Polymerization

| First block (PPFPA-CTA) | | | | PPFPA-*b*-PNIPAM | | | | |
|---|---|---|---|---|---|---|---|---|
| $M_n$[a] (kDa) | $M_w$[a] (kDa) | PDI | % Conversion[b] | $M_n$[a] (kDa) | $M_w$[a] (kDa) | PDI | NIPAM[b] (mol %) | PFPA[b] (mol %) |
| 6.5 | 7.1 | 1.10 | 61 | 11.5 | 14.9 | 1.30 | 74 | 26 |
| 22.1 | 28.7 | 1.30 | 74 | 30.4 | 41.3 | 1.36 | 77 | 23 |

[a] The molecular weights were determined by GPC in THF, PS standard.

[b] %Conversion and copolymer compositions were determined by $^1$H NMR.

model. The dry CCL micelles (5 mg) were dispersed in 2 mL of THF. Pyrene solution in THF (2 mg/mL) was added dropwise into the micellar solution and stirred vigorously for 1 h. DI water was gradually added dropwise to the solution and then THF was evaporated by stirring the solution in air. The solution was then dialyzed against DI water at room temperature for 2 days to remove THF. The aqueous solution in the dialysis tube was collected and filtered with a 0.45 μm pore-sized syringe filter and lyophilized to yield a white powder of dry micelles.

For comparison, pyrene encapsulation into the ONB-containing PPFPA-*b*-PNIPAM was also performed before micelles formation and UV-induced cross-linking to compare loading contents of pyrene from the two methods. Briefly, the ONB-containing PPFPA-*b*-PNIPAM (5 mg) was dissolved in 2 mL of THF. Pyrene solution in THF (2 mg/mL) was added directly to the polymer solution and stirred vigorously for 1 h. CCL micelles encapsulated with pyrene were then formed using the same procedure as that for the preparation of CCL micelles as mentioned above except that the dialysis was only performed against DI water after UV irradiation.

### Determination of Dye Loading Content

The contents of NBD chemically incorporated and pyrene physically encapsulated into the micelles were determined by dissolving the micelles in THF before analyzed by UV-Vis spectroscopy at 478 and 336 nm, respectively using standard calibration curves experimentally obtained with NBD/THF or pyrene/THF solutions (Fig. S1 in Supporting Information). The dye content was calculated according to the following equation:

$$\text{Dye loading content (mg/g)} = \frac{\text{weight of dye loaded in micelles (mg)}}{\text{weight of dye-loaded in micelles (g)}}$$

## RESULTS AND DISCUSSION

### Preparation of PPFPA-*b*-PNIPAM by RAFT Polymerization

For the synthesis of diblock copolymers of PPFPA-*b*-PNIPAM using RAFT polymerization, it is advisable to start with the monomer that shows higher transfer ability for the selected CTA.[31,32] Comparative polymerization kinetics of PFPA and NIPAM are shown in Figure S2 (Supporting Information). In this case, PPFPA was first synthesized and used as a macro-CTA for the PNIPAM synthesis (Scheme 1). The PPFPA macro-CTAs with two molecular weights of 6.5 and 22.1 kDa were prepared (see Table 1). GPC chromatograms of the PPFPA and diblock copolymers are shown in Figure 1. A single peak was observed for each of the copolymers. A decrease in retention time as well as progressive peak

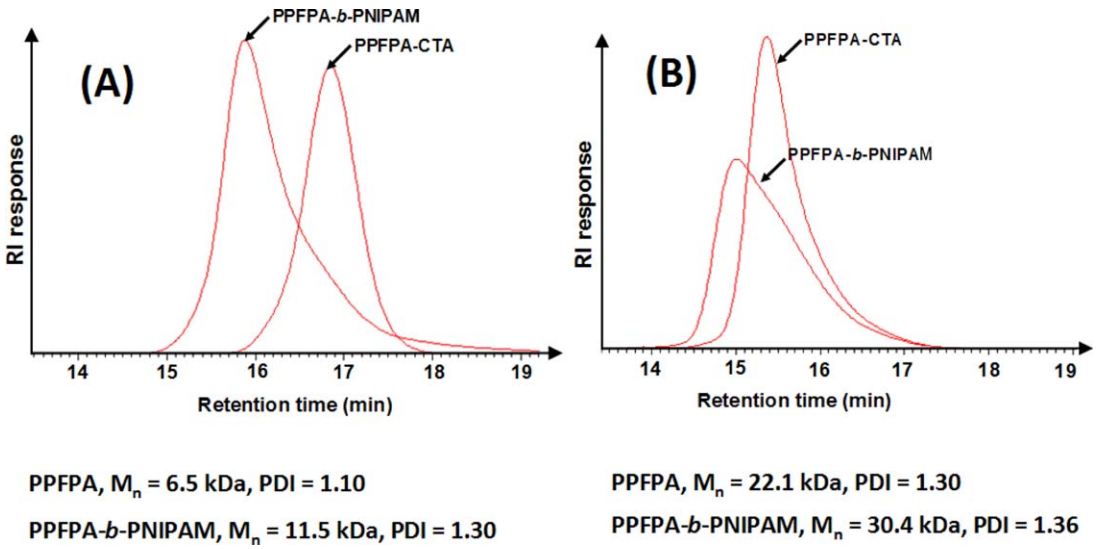


**FIGURE 1** GPC traces of PPFPA molecular weights of 6.5 kDa (A) and 22.1 kDa (B) and their corresponding block copolymers. [Color figure can be viewed in the online issue, which is available at wileyonlinelibrary.com.]

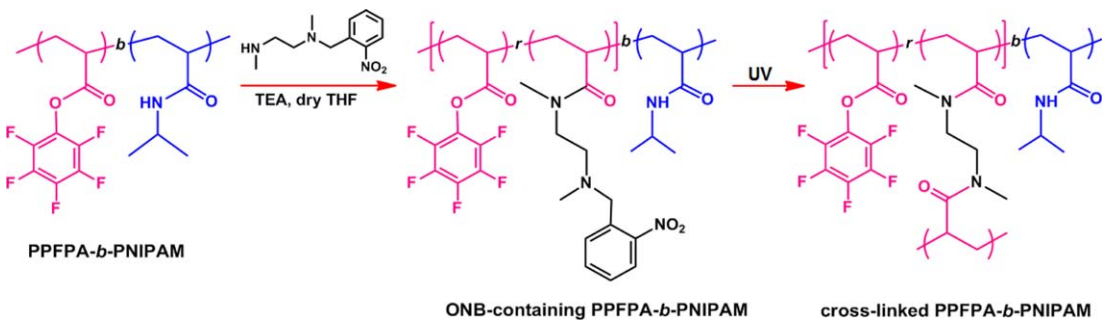


**SCHEME 2** Synthetic pathway for the preparation of ONB-containing PPFPA-*b*-PNIPAM via post-polymerization modification and cross-linked PPFPA-*b*-PNIPAM induced by UV irradiation. [Color figure can be viewed in the online issue, which is available at wileyonlinelibrary.com.]

broadening is seen with each block addition. The PPFPA with the two molecular weights of 6.5 and 22.1 kDa yielded block copolymers of the PPFPA-*b*-PNIPAM with molecular weights of 11.5 kDa and 30.4 kDa, respectively. The slight shoulder appearing in the GPC traces of the resulting block copolymers especially in the case of higher molecular weight one (30.4 kDa) implied that there was a significant amount of the inactive PPFPA macro-CTA which did not participate in chain extension of the PNIPAM block. This may be described as a result of the PFPA polymerization being allowed to proceed to a rather high conversion (74%). This would raise a chance of chain termination. It is also likely that the PPFPA macro-CTA with higher molecular weight (22.1 kDa) would possess lower mobility so as the rate of chain transfer than that of the 6.5 kDa, resulting in the potential loss of polymerization controllability. Additionally, Table 1 gives an overview of the molecular weight information of the block copolymers prepared by RAFT polymerizations. The molecular weight ($M_n$) of the block increased with increasing [NIPAM]/[PPFPA macro-CTA] ratio. The content of the NIPAM in the block copolymer was determined from $^1$H NMR data by selecting the area of the signal at 4.10 ppm (for methine proton of NIPAM) in relation to the area of the signal at 3.10 ppm of the PPFPA polymer backbone. The contents of NIPAM in the block copolymers were 74 and 77 mol % for the PPFPA-CTA with $M_n$ of 6.5 and 22.1 kDa, respectively. $^1$H NMR measurement showed the appearance of a new signal at 4.10 ppm attributed to —C<u>H</u>$(CH_3)_2$, the methine proton of NIPAM (Fig. S3 in Supporting Information). The characteristic proton signals of PPFPA at 3.10, 2.50, and 2.12 ppm attributed to CH and $CH_2$ groups of polymer backbone. The combination of a single GPC peak and the presence of characteristic protons of both PPFPA and PNIPAM led to the assumption that diblock PPFPA-*b*-PNIPAM copolymers were successfully synthesized. Apparently, the RAFT process enables the synthesis of well-defined block copolymer of PPFPA-*b*-PNIPAM with predetermined molecular weight and narrow molecular weight distribution.

### Post-Polymerization Modification of PPFPA-*b*-PNIPAM with ONB-Protected Diamine

Herein, light-responsive moieties of ONB were prepared via post-polymerization modification of PFPA moieties with a mono ONB-protected diamine.[25] Upon UV irradiation at 365 nm for 2 h, a new peak of nitrosobenzaldehyde appeared at around 350 nm (Fig. S4 in Supporting Information) confirming the formation of the cleaved by-product.[23,25,33] In addition, FT-IR spectrum showed the appearance of C═O peak of nitrosobenzaldehyde at 1725 cm$^{-1}$ (Fig. S5 in Supporting Information). The ONB-protected diamine group should be released, which can subsequently induce cross-linking via activated ester-amine chemistry resulting in network formation as shown in

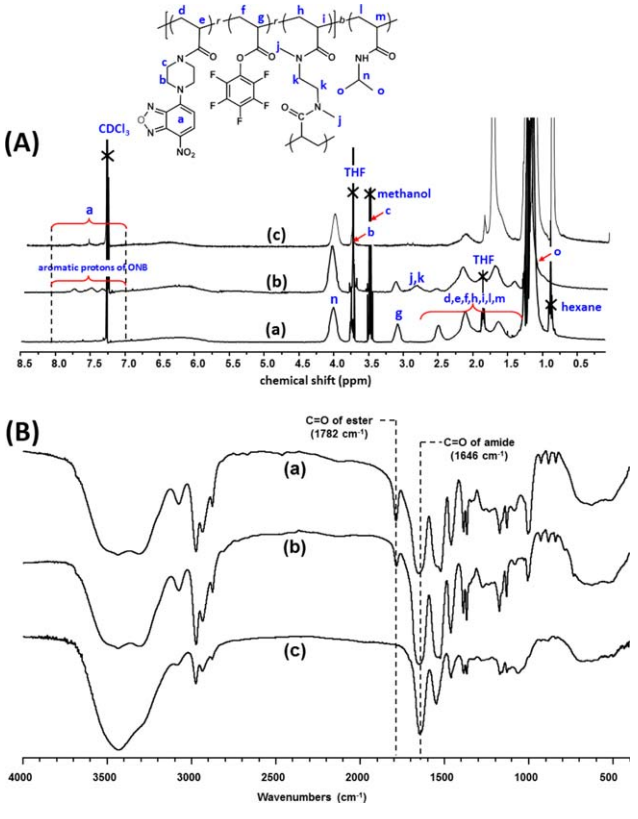


**FIGURE 2** $^1$H NMR spectra in $CDCl_3$ (A) and FT-IR spectra (B) of (a) PPFPA-*b*-PNIPAM, (b) ONB-containing PPFPA-*b*-PNIPAM, and (c) NBD-incorporated CCL micelles. [Color figure can be viewed in the online issue, which is available at wileyonlinelibrary.com.]

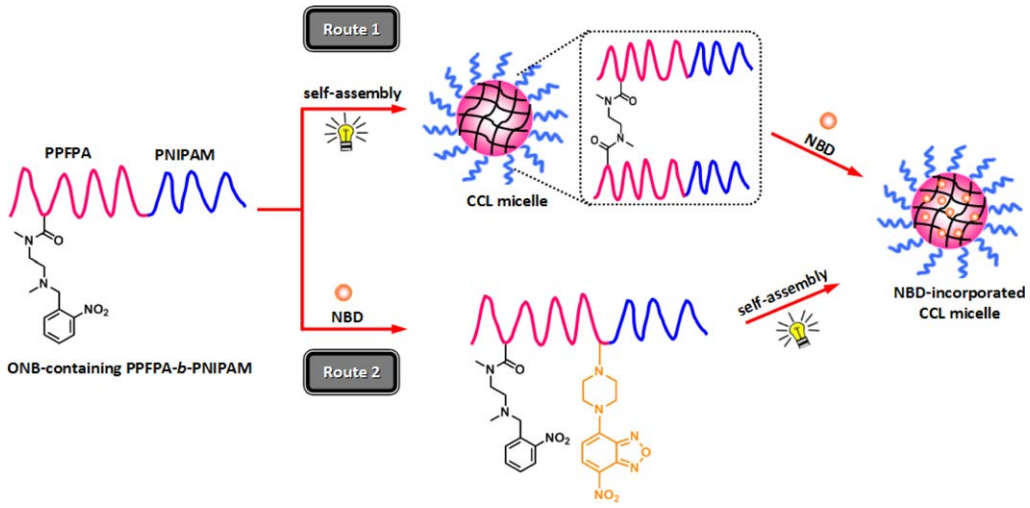


**SCHEME 3** Schematic representation of NBD-incorporated CCL micelles preparation by performing cross-linking/self-assembly before (Route 1) or after (Route 2) chemical incorporation of NBD. [Color figure can be viewed in the online issue, which is available at wileyonlinelibrary.com.]

Scheme 2. A successful reaction can be demonstrated by the results from $^1$H NMR and FT-IR analysis. Figure 2(A) represents $^1$H NMR spectrum of the ONB-containing PPFPA-*b*-PNIPAM. The signals of the four aromatic protons of the ONB moieties in a range of $\delta = 7.52–8.09$ ppm clearly confirmed the attachment of the ONB groups to the block copolymer. The amount of incorporated ONB-protected diamine in the copolymer can be calculated by $^1$H NMR from the relative ratio between the peak integration of the four aromatic protons around $\delta = 7.52–8.09$ ppm and the peak integration of one proton around $\delta = 3.10$ ppm of the PPFPA polymer backbone. As reported earlier by Zhao and Theato.[25] the percentage of ONB incorporation (%ONB) can be varied as a function of the amount of ONB-protected diamine. Here in this research, the %ONB in the block copolymer of approximately 20% were chosen to assure that a certain portion of PFPA were cross-linked via incorporated ONB-protected diamine and allowed for the majority of the unreacted PFPA to be available for subsequent post-functionalization with other active species of which we chose NBD in this case. Additionally, the successful conversion of the parent PPFPA in the copolymer to the corresponding ONB-protected group was also confirmed by FT-IR analysis from the decrement of C═O peak at 1782 cm$^{-1}$ of PPFPA and the increment of the amide carbonyl group at 1645 cm$^{-1}$ [Fig. 2(B)]. After the post-polymerization modification, the molecular weight of the ONB-containing block copolymer was slightly shifted to higher value in comparison to the GPC trace of the precursor block copolymer due to the increment of molecular weight per repeating unit (Fig. S6 in Supporting Information).

### Preparation of Core-Cross-Linked (CCL) Micelles of PPFPA-*b*-PNIPAM

In this part, we introduce a new methodology for polymeric micelles preparation from diblock copolymer having PPFPA as hydrophobic part, PNIPAM as hydrophilic part, and ONB-protected diamine as a photo-induced cross-linker molecule of which the strategy is shown in Scheme 3. The molecular weight of PPFPA-*b*-PNIPAM and the %ONB were fixed at around 30 kDa and 20%, respectively, while the copolymer composition of PPFPA:PNIPAM was varied from 23:77 to 71:29. Micellization of the diblock copolymers in aqueous solution was confirmed by DLS and TEM. DLS studies (Table 2) revealed that the sizes of both NCL and CCL micelles above LCST became smaller than those below the LCST due to the outer shell of PNIPAM dehydrated and collapsed. After UV irradiation at 365 nm for 2 h, the average sizes of the CCL micelles were found to be smaller than those of the NCL micelles implying that covalently cross-linked network of ONB-protected diamine with the PFPA part in the core were formed. It should be emphasized at this point that complete cross-linking via the reaction between PFPA moieties and ONB can be achieved upon the UV irradiation at 365 nm for 2 h as monitored by UV-Vis spectroscopy. This agrees well with the report by Zhao and Theato.[25] Moreover, the average size of the micelles having a copolymer composition of 71:29 PPFPA:PNIPAM is smaller than that with the ratio of 23:77 PPFPA:PNIPAM implying that the size of the micelles corresponds with the block length of the PNIPAM outer shell. In addition, size distribution profiles measured by DLS showed that all of the micelles have a unimodal size distribution. The micelles did not precipitate above the LCST because the DLS measurement was carried out at a very low concentration (1 mg/mL) allowing us to determine their size by DLS. TEM images revealed well-defined spherical shapes with slightly smaller diameters than those observed in DLS, which is attributed to the shrinkage of the micelles after solvent evaporation during TEM sample preparation as shown in Figure 3.

Furthermore, we have performed DLS and TEM measurements of the CCL micelles after placing them in THF, a good

**TABLE 2** Summary of Average Sizes of the NCL and CCL Micelles of PPFPA-*b*-PNIPAM and NBD-Incorporated CCL Micelles Determined by DLS Measurement in Aqueous Media

| | Average Size (nm) | | | | | |
|---|---|---|---|---|---|---|
| | PPFPA-*b*-PNIPAM NCL Micelles | | PPFPA-*b*-PNIPAM CCL Micelles | | NBD-Incorporated CCL Micelles | |
| PPFPA:PNIPAM (% Mol Ratio) | 10 °C | 40 °C | 10 °C | 40 °C | 10 °C | 40 °C |
| 23:77 ($M_n$ = 30.4 kDa) | 257 ± 5 | 178 ± 2 | 146 ± 3 | 97 ± 1 | 182 ± 2 | 135.9 ± 0.3 |
| 71:29 ($M_n$ = 32.5 kDa) | 122 ± 3 | 81.2 ± 0.2 | 58 ± 2 | 42.1 ± 0.2 | 67 ± 1 | 41.4 ± 0.7 |

solvent for both PPFPA and PNIPAM blocks, to demonstrate that the synthesized CCL micelles were stable. From the DLS data, the average sizes of the CCL micelles having PPFPA:PNIPAM composition of 23:77 and 71:29 were 189 and 80 nm, respectively. These average sizes of the CCL micelles in THF are larger than those determined in aqueous

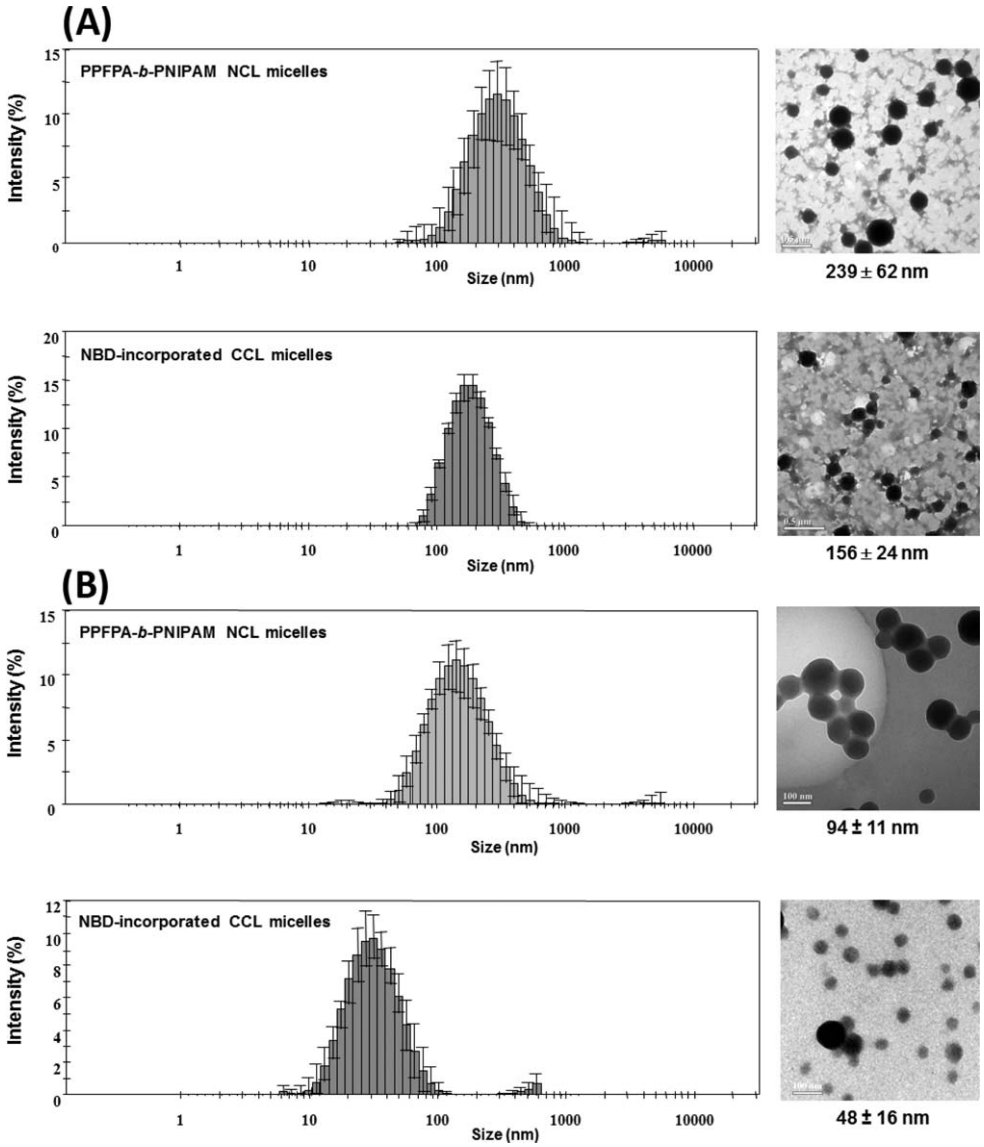


**FIGURE 3** Size distribution profiles evaluated by DLS (left column) and TEM images (right column) of the PPFPA-*b*-PNIPAM NCL micelles and the NBD-incorporated CCL micelles formulated from the copolymer with PPFPA:PNIPAM composition of (A) 23:77 (scale bar 0.5 μm) and (B) 71:29 (scale bar 100 nm). DLS measurements were carried out at 10 °C with a micelle concentration of 1 mg/mL.

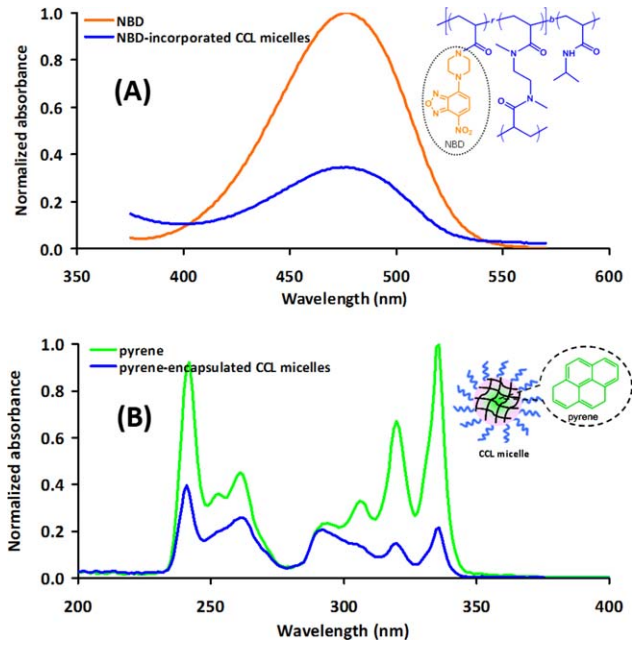


**FIGURE 4** Normalized absorbance of (A) NBD and the NBD-incorporated CCL micelles and (B) pyrene and the pyrene-encapsulated CCL micelles. [Color figure can be viewed in the online issue, which is available at wileyonlinelibrary.com.]

media (see Table 2 for comparison) as a result of THF being a good solvent and thus causing the CCL micelles to swell. According to TEM images shown in Figure S7 of Supporting Information, the CCL micelles maintained their spherical shape with their diameters around 82 and 38 nm for the copolymer having PPFPA:PNIPAM composition of 23:77 and 71:29, respectively. The size measured by the DLS is larger than that observed by TEM because the size measured by DLS is based on the swollen micelles in solution whereas that observed by TEM is for the dried micelles.

### Chemical Incorporation and Physical Encapsulation of Dyes into Micelles

NBD was covalently incorporated onto the residual PFPA moieties in the core of the CCL micelles to demonstrate the possibility for additional post-polymerization, as shown in Scheme 3. A successful incorporation of NBD was confirmed by FT-IR, $^{1}$H NMR, $^{19}$F NMR, and UV-Vis spectroscopy. The disappearance of ester carbonyl group of activated PFPA at 1782 $cm^{-1}$ and appearance of amide carbonyl group at 1646 $cm^{-1}$ suggest that the PFPA units were fully converted to amide upon reacting with NBD [Fig. 2(B)]. Similar explanation can also be applied for the $^{1}$H NMR spectrum that showed the disappearance of the proton at $\delta = 3.10$ ppm of the PPFPA backbone [Fig. 2(A)]. Complementary $^{19}$F NMR analysis confirmed that the three signals at $-170$, $-165$, and $-162$ ppm attributed to the pentafluorophenyl ester groups in the block copolymer completely disappeared when 2 equiv. of NBD dye was reacted, suggesting that all residual PFPA groups in the core of the micelles were totally consumed upon chemical incorporation of NBD (Fig. S8 in Supporting Information).

UV-Vis spectroscopy was also used to confirm the incorporation of NBD into the core of micelles via post-functionalization modification of the residual PFPA units. As seen in Figure 4(A), an absorbance of NBD-incorporated CCL micelles, which corresponds to an absorbance of free NBD appears at $\lambda_{max} = 478$ nm indicating the presence of NBD in the micelles. The loading contents of NBD into the CCL micelles after UV-induced cross-linking (Scheme 3, Route 1) of the copolymers having PPFPA:PNIPAM composition of 23:77 and 71:29 were found to be 3.8 and 7.7 mg/g (NBD/copolymer), respectively. Furthermore, the physical encapsulation of pyrene into the CCL micelles was also determined (Scheme 4, Route 1). The typical UV-Vis spectrum of pyrene-encapsulated CCL micelles is similar to that of free pyrene Figure 4(B), suggesting no significant change of pyrene structure when being encapsulated within the

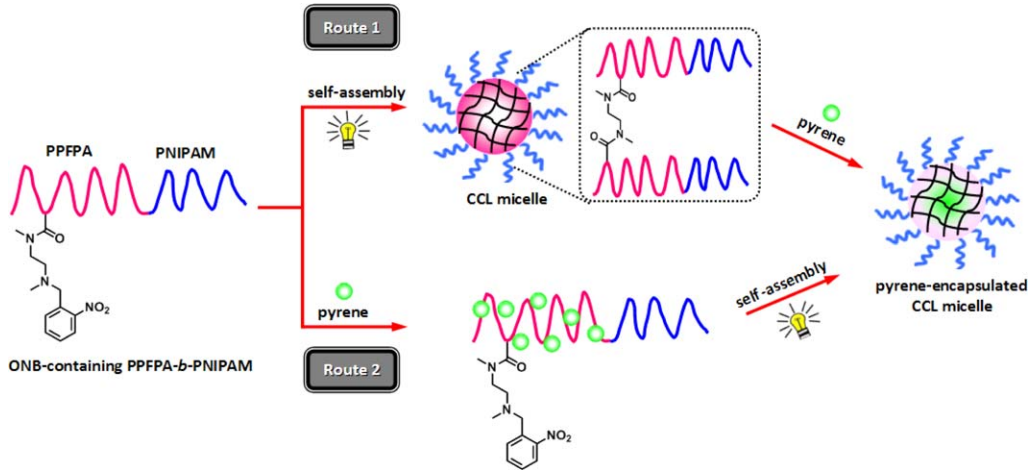


**SCHEME 4** Schematic representation of pyrene-encapsulated CCL micelles preparation by performing cross-linking/self-assembly before (Route 1) or after (Route 2) physical encapsulation of pyrene. [Color figure can be viewed in the online issue, which is available at wileyonlinelibrary.com.]

CCL micelles. The loading contents of pyrene into the CCL micelles after UV-induced cross-linking of the copolymers having PPFPA:PNIPAM composition of 23:77 and 71:29 were 1.2 and 2.9 mg/g (pyrene/copolymer), respectively. We have also performed additional experiments by conducting UV-induced cross-linking after dye loading (Route 2 of both Schemes 3 and 4). It was found that the loading contents of NBD into the CCL micelles formulated from the copolymers having PPFPA:PNIPAM composition of 23:77, and 71:29 were 3.9 and 8.0 mg/g (NBD/copolymer), respectively. Whereas, the loading contents of pyrene into the CCL micelles formulated from the copolymers having PPFPA:PNIPAM composition of 23:77, and 71:29 were 3.7 and 4.8 mg/g (pyrene/copolymer), respectively. Apparently, the loading contents of both NBD and pyrene into the core of micelles can be elevated as a function of the PPFPA composition in the block copolymer. The fact that the loading content of NBD before UV-induced cross-linking was essentially the same as that after UV-induced cross-linking indicated that enthalpic gain via chemical reactions between the residual PFPA groups and NBD was so powerful that it can overcome the restriction of dye permeability through the cross-linked polymeric network. The procedure based on the sequence of cross-linking/self-assembly followed by encapsulation should provide a better stability to micelles. This also gives additional benefit from practical perspective because any designated molecules can be chemically incorporated into ready-to-use cross-linked micelles which are quite stable. However, this seems not to be the case for pyrene of which physical encapsulation is mainly driven by weaker hydrophobic interactions. Cross-linking exhibited a significant impact on pyrene encapsulation so that its loading was more effective if being performed before cross-linking.

## CONCLUSIONS

In this research, well-defined block copolymer consisting of PFPA and NIPAM were first synthesized by RAFT polymerization. The kinetic analysis and gel permeation chromatography (GPC) measurements confirmed that polymerization was well controlled. The cross-linked amphiphilic polymeric micelles of PPFPA-*b*-PNIPAM were prepared via post-polymerization modification of PFPA moieties with the ONB protected diamine. The ONB groups can be released upon UV irradiation which subsequently induced an *in situ* cross-linking by a spontaneous reaction with the remaining PFPA and yielded cross-linked micelles. Micellization of the copolymers was confirmed by DLS and TEM. The sizes of the NCL and CCL micelles can be controlled by changing the external temperature above or below their LCSTs. Our results have demonstrated that the copolymer micelles having residual PFPA moieties in their cores are capable of not only chemically incorporating amino-containing molecule, NBD via post-functionalization but also physically encapsulating hydrophobic molecule, pyrene, suggesting their potential to be used as alternative cargos for biomedical applications.

## ACKNOWLEDGMENTS

This research was financially supported by Thailand Research Fund (DBG5580003), the Ratchadaphiseksomphot Endowment Fund of Chulalongkorn University (RES560530126-AM), and the Thai Government Stimulus Package 2 (TKK2555), under the Project for Establishment of Comprehensive Center for Innovative Food, Health Products and Agriculture. W. Graisuwan gratefully acknowledges the Commission on Higher Education, Thailand for the program Strategic Scholarships for Frontier Research Network for the Joint Ph.D. Program Thai Doctoral degree.

## REFERENCES AND NOTES

**1** S. Ganta, H. Devalapally, A. Shahiwala, M. Amiji, *J. Controlled Release* **2008**, *126*, 187.

**2** N. Rapoport, *Prog. Polym. Sci.* **2007**, *32*, 962.

**3** E. S. Read, S. P. Armes, *Chem. Commun.* **2007**, *29*, 3021.

**4** H. Wei, S. -X. Cheng, X. -Z. Zhang, R. -X. Zhuo, *Prog. Polym. Sci.* **2009**, *34*, 893.

**5** J. Zhuang, M. R. Gordon, J. Ventura, L. Li, S. Thayumanavan, *Chem. Soc. Rev.* **2013**, *42*, 7421.

**6** H. G. Schild, *Prog. Polym. Sci.* **1992**, *17*, 163.

**7** J. E. Chung, M. Yokoyama, T. Okano, *J. Controlled Release* **2000**, *65*, 93.

**8** J. E. Chung, M. Yokoyama, M. Yamato, T. Aoyagi, Y. Sakurai, T. Okano, *J. Controlled Release* **1999**, *62*, 115.

**9** F. Kohori, K. Sakai, T. Aoyagi, M. Yokoyama, M. Yamato, Y. Sakurai, T. Okano, *Colloids Surf. B* **1999**, *16*, 195.

**10** M. Nakayama, T. Okano, T. Miyazaki, F. Kohori, K. Sakai, M. Yokoyama, *J. Controlled Release* **2006**, *115*, 46.

**11** S. Q. Liu, Y. W. Tong, Y. -Y. Yang, *Biomaterials* **2005**, *26*, 5064.

**12** J. -L. Zhu, X. -Z. Zhang, H. Cheng, Y. -Y. Li, S. -X. Cheng, R. -X. Zhuo, *J. Polym. Sci. Part A: Polym. Chem.* **2007**, *45*, 5354.

**13** R. K. O'Reilly, C. J. Hawker, K. L. Wooley, *Chem. Soc. Rev.* **2006**, *35*, 1068.

**14** C. F. van Nostrum, *Soft Matter* **2011**, *7*, 3246.

**15** J. Zhang, X. Jiang, Y. Zhang, Y. Li, S. Liu, *Macromolecules* **2007**, *40*, 9125.

**16** Y. Li, B. S. Lokitz, C. L. McCormick, *Macromolecules* **2005**, *39*, 81.

**17** M. Eberhardt, P. Théato, *Macromol. Rapid Commun.* **2005**, *26*, 1488.

**18** P. Theato, *J. Polym. Sci. Part A: Polym. Chem.* **2008**, *46*, 6677.

**19** M. Eberhardt, R. Mruk, R. Zentel, P. Théato, *Eur. Polym. J.* **2005**, *41*, 1569.

**20** H. T. T. Duong, C. P. Marquis, M. Whittaker, T. P. Davis, C. Boyer, *Macromolecules* **2011**, *44*, 8008.

**21** J. Zhuang, S. Jiwpanich, V. D. Deepak, S. Thayumanavan, *ACS Macro Lett.* **2012**, *1*, 175.

**22** J. -M. Schumers, C. -A. Fustin, J. -F. Gohy, *Macromol. Rapid Commun.* **2010**, *31*, 1588.

**23** H. Zhao, E. S. Sterner, E. B. Coughlin, P. Theato, *Macromolecules* **2012**, *45*, 1723.

**24** J. Jiang, X. Tong, D. Morris, Y. Zhao, *Macromolecules* **2006**, *39*, 4633.

**25** H. Zhao, P. Theato, *Polym. Chem.* **2013**, *4*, 891.

**26** M. Ahmed, R. Narain, *Prog. Polym. Sci.* **2013**, *38*, 767.

**27** A. E. Smith, X. Xu, C. L. McCormick, *Prog. Polym. Sci.* **2010**, *35*, 45.

**28** A. W. York, S. E. Kirkland, C. L. McCormick, *Adv. Drug Deliv. Rev.* **2008**, *60*, 1018.

**29** C. Boyer, V. Bulmus, T.P. Davis, V. Ladmiral, J. Liu, S. Perrier, *Chem. Rev.* **2009**, *109*, 5402.

**30** F. D. Jochum, P. Theato, *Macromolecules* **2009**, *42*, 5941.

**31** M. I. Gibson, E. Fröhlich, H. -A. Klok, *J. Polym. Sci. Part A: Polym. Chem.* **2009**, *47*, 4332.

**32** A. Vega-Rios, A. Licea-Claveríe, *J. Mexican Chem. Soc.* **2011**, *55*, 21.

**33** L. Chen, Y. K. Goh, H. H. Cheng, B. W. Smith, P. Xie, W. Montgomery, A. K. Whittaker, I. Blakey, *J. Polym. Sci. Part A: Polym. Chem.* **2012**, *50*, 4255.

analytical chemistry

Article

pubs.acs.org/ac

# Patterned Poly(acrylic acid) Brushes Containing Gold Nanoparticles for Peptide Detection by Surface-Assisted Laser Desorption/Ionization Mass Spectrometry

Arunee Sangsuwan,[†] Benjaporn Narupai,[‡] Pornpen Sae-ung,[§] Sasithon Rodtamai,[‡] Nadnudda Rodthongkum,[∥] and Voravee P. Hoven*[,‡]

[†]Program in Petrochemistry and Polymer Science, Faculty of Science, [‡]Organic Synthesis Research Unit, Department of Chemistry, Faculty of Science, [§]Program in Macromolecular Science, Faculty of Science, and [∥]Metallurgy and Materials Science Research Institute, Chulalongkorn University, Phayathai Road, Pathumwan, Bangkok 10330, Thailand

Supporting Information

**ABSTRACT:** Patterned poly(acrylic acid) (PAA) brushes was successfully generated via photolithography and surface-initiated reversible addition−fragmentation chain transfer (RAFT) polymerization of acrylic acid as verified by water contact angle measurements and FT-IR analysis. The carboxyl groups of PAA brushes can act as reducing moieties for in situ synthesis of gold nanoparticles (AuNPs), without the use of additional reducing agent. The formation of AuNPs was confirmed by transmission electron microscopy and X-ray photoelectron spectroscopy. The glass surface-modified by PAA brushes and immobilized with AuNPs (AuNPs-PAA) can be used as a substrate for SALDI-MS analysis, which is capable of detecting both small peptides having $m/z \leq 600$ (glutathione) and large peptides having $m/z \geq 1000$ (bradykinin, ICNKQDCPILE) without the interference from matrix signal suggesting that AuNPs were stably trapped within the PAA brushes and the carboxyl groups of PAA can serve as internal proton source. By employing AuNPs as the capture probe, the AuNPs-PAA substrate can selectively identify thiol-containing peptides from the peptide mixtures with LOD as low as 0.1 and 0.05 nM for glutathione and ICNKQDCPILE, respectively. An ability to selectively detect ICNKQDCPILE in a diluted human serum is also demonstrated. The patterned format together with its high sensitivity and selectivity render this newly developed substrate a potential platform for high-throughput analysis of other biomarkers, especially those with low molecular weight in complex biological samples.

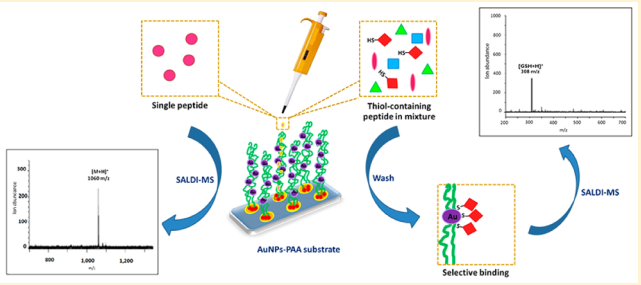


Separation and analysis of biomarkers such as peptides found in trace levels play crucial roles in medical diagnosis. A number of peptides have been proposed as potential biomarkers. For example, bradykinin, des-Arg9-bradykinin, and Hyp3-bradykinin are potential biomarkers of breast cancer.[1] Glutathione (GSH), thiol-containing peptides, are also recognized as important biomarkers in human.[2,3] GSH is an antioxidant and a tripeptide composed of L-cysteine, glycine, and γ-glutamic acid, that can prevent damage to important cellular components caused by reactive oxygen species such as free radicals and peroxides.[4] The usual range of GSH concentrations in a healthy human is in a range of 684−2525 and 2.22−11.36 mmol $L^{-1}$ in blood and plasma, respectively.[5] An abnormal level of GSH is an indication of diseases such as Alzheimer's, Parkinson's, Huntington's disease, cancers, aging, and heart problems.[4] Cysteine (Cys) is the only amino acid with a thiol functional group that serves as a unique unit in protein construction, enzyme active sites, and cofactors.[6] Cys is also an amino acid component of GSH. Cys exists in almost all human proteins (89.3% contain at least one), and 17.2% of tryptic peptides contain one or more cysteine residues.[6,7] Analysis of biomarker generally requires highly sensitive analytical tools such as electrochemistry,[8] fluorescence spectroscopy,[9] UV−vis spectrophotometry,[10] surface plasmon resonance,[11] and mass spectrometry.[12,13]

Surface-assisted laser desorption/ionization mass spectrometry (SALDI-MS), in particular, is a widely used technique for biomarker identification, especially peptides due to their high sensitivity and accuracy.[9,14] The major benefit of this method lies in its ability to be implemented in specific modification of chip surfaces, recently developed by using nanomaterials as matrices to absorb the laser energy and transfer to analyte in the ionization step. This technique is capable of detecting analyte with a low mass range (<500 $m/z$) without the interference from matrix signal. Metal nanoparticles, for example, ZnS, $TiO_2$, $Fe_3O_4$, and Au, are extensively used as matrices in SALDI-MS analysis.[15,16] Unlike conventional organic matrices, metal nanoparticles provide low matrix background, homogeneous sample, and insignificant fragmen-

**Received:** February 23, 2015
**Accepted:** October 3, 2015
**Published:** October 4, 2015





DOI: 10.1021/acs.analchem.5b00734
*Anal. Chem.* 2015, 87, 10738−10746

tation. It was also found that each type of nanoparticle has their own suitable range of analyte that can be evaluated. For example, gold nanoparticles (AuNPs) are suitable for samples with a mass range of 300−1300 $m/z$. $TiO_2$ and $Fe_2O_3$ are appropriate for analyzing samples with a mass range of 1200−12000 and 1200−25000, respectively.[15] In addition, some metal nanoparticles, such as AuNPs and silver nanoparticles (AgNPs), can also function as concentrating and selective probes for preconcentration and separation of thiol-containing peptide from the peptide mixture.[16−19]

Recently, polymer has been used together with nanoparticles for modifying the chip surface not only to improve nanoparticles dispersion that can enhance ionization efficiency, but also help trapping the nanoparticles from coming off during ionization. There are reports about modification of substrate with nanoparticles for SALDI-MS analysis. Aminlashgari et al.[20] utilized nanocomposite films based on polylactide embedded with nanoparticles of $TiO_2$, $SiO_2$, MgO, hydroxyapatite, montmorillonite nanoclay, halloysite nanoclay, silicon nitride, and graphitized carbon black as matrices for SALDI-MS analysis of small molecules, namely, acebutolol, propranolol, and carbamazepine. They found that the advantages of nanocomposite films as compared to the free nanoparticles used in earlier studies are the ease of handling and reduction of instrument contamination because the particles were immobilized within the polymer matrix. Kawasaki et al.[21] successfully modified silicon substrate with self-assembled multilayer films of poly(allylamine hydrochloride) and ammonium citrate capped AuNPs $(AuNPs/PAHC)_n$ for analyzing peptides (angiotensin I, cytochrome C) by SALDI-MS. It was found that the sensitivity of the peptide was increased with increasing number of multilayer films. However, a small matrix background of the AuNPs still appeared in the mass spectra. As demonstrated by Tarui et al., the silicon substrate modified with nanocomposite film of cationic diblock copolymer micelles of poly(styrene-*b*-*N*-methyl-4-vinylpyridinium iodide) and ammonium citrate stabilized AuNPs offered superior performance to the AuNPs alone by providing high ionization efficiency of angiotensin I and insulin, with a low matrix background from Au clusters.[22]

Polymer brushes are one of the interesting materials that can be used for chip surface modification. Having chain ends attached covalently on the surface, they are more stable than physically adsorbed polymer film. Polymer brushes with well-controlled molecular weight and polydispersity index can be prepared via surface-initiated polymerization based on a number of controlled radical polymerization such as atom transfer radical polymerization (ATRP) and reversible addition−fragmentation chain transfer (RAFT).[23,24] Having multiple functional groups per surface area, polymer brushes are quite an attractive material for bioanalytical analysis. Bruening and co-workers[25−27] have developed an efficient platform for phosphopeptide enrichment prior to MS analysis. The platform is based on polymer brushes of poly(2-hydroxyethyl methacrylate) (PHEMA) or poly(acrylic acid) immobilized with Fe(III)-nitrilotriacetate (NTA). The substrates offered higher recoveries with fewer interfering peaks than those analyzed by commercially available Fe(III)-containing materials. A femtomol-level detection limit can also be reached, even in the presence of as high as 10-fold molar excess of nonphosphorylated peptides.[26,27] Kim et al.[28] have employed surface-immobilized polymer brushes of poly(oligo(ethylene glycol) methacrylate) (pOEGMA) as nonbiofouling polymeric platform for immobilizing peptide-conjugated AuNPs. A label-free assay of matrix metalloproteinase (MMP) activity was evaluated from the peptide segments cleaved from the peptide-conjugated AuNPs using time-of-flight secondary ion mass spectrometry. The use of pOEGMA, together with AuNPs, synergistically improved the sensitivity of MMP activity assays in human serum, in which a number of interfering proteins are present.

Poly(acrylic acid) (PAA) brushes have been recognized as versatile polymeric entities often used for biosensing and analytical applications. Its greater density of carboxyl groups provides active functionality for specific biomolecule immobilization and detection, as reported earlier by a number of research groups.[29−33] In particular, we have previously demonstrated that the surface-grafted PAA brushes can serve as a three-dimensional platform for attachment of biosensing probes. As determined by surface plasmon resonance (SPR), their properties are superior to a SAM of a carboxyl-terminated alkanethiol in terms of both signal enhancement and the ability to prevent nonspecific adsorption.[29] The best performance for both the biotin−streptavidin and BSA−anti-BSA systems was found on the sensor platform developed from the surface-grafted PAA brushes with a 50% graft density.[30]

Here, in this research, we are interested in developing a substrate for SALDI-MS analysis based on surface-grafted PAA brushes containing AuNPs. Photolithography was first used to generate the hydrophobic/hydrophilic pattern to provide a visible contrast between the analyte spot and prevent cross-contamination of sample solution from one spot to another. PAA brushes were then grafted on the hydrophilic area of the pattern via surface-initiated RAFT polymerization of acrylic acid (AA). Thereafter, AuNPs were generated in situ within the PAA brushes by having carboxylate groups of PAA acting as reducing moieties for gold ions ($Au^{3+}$), without having to use an additional reducing agent.[34,35] The substrate modified with PAA brushes containing AuNPs (AuNPs-PAA) were then used for SALDI-MS analysis of a number of peptides, such as bradykinin, which is a biomarker of breast cancer, thiol-containing peptides, namely, glutathione and ICNKQDCPILE. It is anticipated that this developed patterned platform can be used for preconcentration and separation of thiol-containing peptide from the peptide mixture in a high-throughput fashion.

## EXPERIMENTAL SECTION

**Materials.** Hydrogen tetrachloroaurate ($HAuCl_4 \cdot 3H_2O$), acrylic acid (AA), dimethylformamide (DMF), 4,4-bis(4-cyanovaleic acid) (ACVA), 4-(dimethylamino)pyridine (DMAP), 4-cyano-4-(phenyl carbonothioylthio)pentanoic acid (chain transfer agent or CTA), dicyclohexyl carbodiimide (DCC), dialysis bag (cutoff molecular weight of 3500 g/mol), phosphate buffered saline pH 7.4 (PBS), 3-aminopropyltriethoxysilane (APTES), 1*H*,1*H*,2*H*,2*H*-perfluorooctyltrichlorosilane (PFOTCS), α-cyano-4-hydroxycinnamic acid (CHCA), sucrose, and cholesterol were obtained from Sigma-Aldrich. Acetone, toluene, hexane, ethanol, and dichloromethane were purchased from Merck (Germany). Positive photoresist S1813 and developer MFTM-321 were purchased from Rohm and Hass (U.S.A.). Glass slides were obtained from SE. Supply (Thailand). AA was purified by vacuum distillation. Glutathione (GSH), bradykinin, ICNKQDCPILE peptide were obtained from American Peptide company. Citrate-stabilized gold nanoparticles were prepared according to a method modified from that of Hayat et al.[36] All solutions were made using


DOI: 10.1021/acs.analchem.5b00734
*Anal. Chem.* 2015, 87, 10738−10746

**Scheme 1. Schematic Representation of Stepwise Method Demonstrating How To Prepare Patterned PAA Brushes Containing AuNPs Supported on a Glass Slide**[a]

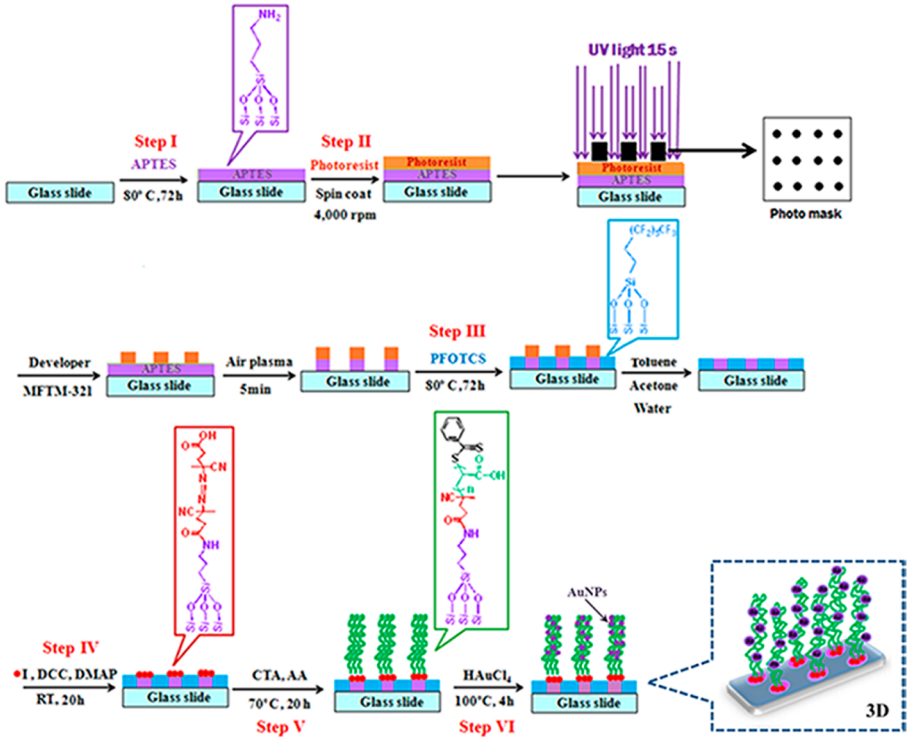


[a](I) reaction with APTES, (II) surface patterning by photolithography, (III) attachment of perfluorooctylsilyl groups, (IV) attachment of initiator, (V) surface-initiated RAFT polymerization of AA, and (VI) in situ synthesis of AuNPs on PAA brushes.

ultrapure distilled water that was obtained after purification using a Millipore Milli-Q system (U.S.A.) that involves reverse osmosis, ion exchange, and a filtration step (18.2 MΩ cm resistance).

**Surface Patterning by Photolithography.** A glass slide (i.d. = 1.8 cm) was cleaned in a plasma cleaner (Harrick Plasma PDC-32G, Power 18 W) for 5 min before exposure to vapor of 100 μL of APTES in a 50 mL vial sealed with a cap in an oven at 80 °C for 72 h and rinsed sequentially with toluene, acetone, and deionized water to yield Si-$NH_2$ (Scheme 1, step I). Positive photoresist S1813 was then spin-coated at 4000 rpm for 3 min on the surface of Si-$NH_2$ and cured at 115 °C for 1 min. A photomask was placed on the photoresist-coated surface before irradiation with UV light (365 nm, 500 W) for 15 s. The irradiated pattern was treated with developer MFTM-321 for 1 min and rinsed with deionized water followed by treatment in the plasma cleaner for 5 min to destroy the APTES layer and recover back the silanol groups on the unmasked area (Scheme 1, step II). The obtained patterned Si-$NH_2$/OH was exposed to vapor of 100 μL of PFOTCS in a 50 mL vial sealed with a cap in the oven at 80 °C for 72 h and rinsed sequentially with toluene, acetone, and deionized water. The recovered silanol groups of the patterned Si-$NH_2$/OH would react with PFOTCS to form patterned Si-$NH_2$/$O(CH_2)_2(CF_2)_5CF_3$ (Scheme 1, step III). At this point, the photoresist on the masked area was also removed so that the amino groups of APTES were readily available for initiator immobilization in the next step.

**Grafting of PAA Brushes on Patterned Surface.** The ACVA (0.21 g, 1 mmol), DCC (0.19 g, 1 mmol), and DMAP (0.01 g, 0.1 mmol) were dissolved in 20 mL of DMF. The solution was stirred for 4 h at room temperature before being transferred to the glass slide having patterned Si-$NH_2$/$O(CH_2)_2(CF_2)_5CF_3$ in a vial then sealed with a rubber septum. The solution was stirred under nitrogen atmosphere at room temperature for 20 h. Then, the glass slide was taken out from the vial and rinsed with ethanol and deionized water to yield Si−I/$O(CH_2)_2(CF_2)_5CF_3$ (Scheme 1, step IV). ACVA (0.014 g, 0.05 mmol) and CTA (0.056 g, 0.2 mmol) were dissolved in 20 mL of PBS buffer (pH 7.4). AA (1.37 mL, 20 mmol) was added to the mixture, which was later transferred into a vial containing patterned Si−I/$O(CH_2)_2(CF_2)_5CF_3$ then sealed with a rubber septum. The surface-initiated RAFT polymerization of AA was allowed to proceed under a nitrogen atmosphere at 70 °C for 20 h. The resulting patterned Si-PAA/$O(CH_2)_2(CF_2)_5CF_3$ was then obtained after rinsing with ethanol and deionized water (Scheme 1, step V).

**In Situ Synthesis of AuNPs on PAA Brushes.** The glass slide having patterned Si-PAA/$O(CH_2)_2(CF_2)_5CF_3$ was subjected to five cycles of alternate dipping in aqueous solution of $HAuCl_4$ (5 mL, 1 mM) and deionized water. Then, the glass slide was immersed in deionized water at 100 °C for 1 h, followed by an aqueous solution of $HAuCl_4$ (5 mL, 1 mM) at 100 °C for another 4 h. The glass slide was then rinsed with deionized water and dried with a stream of nitrogen to obtain the patterned PAA brushes containing AuNPs (Scheme 1, step VI).

**Characterization.** PAA formed in solution during surface-initiated RAFT polymerization was characterized by Varian, model Mercury-400 NMR spectrometer (U.S.A.) operating at 400 MHz using $D_2O$ as a solvent. The FT-IR spectra of surface-modified silica particles prepared as KBr discs were recorded in a frequency range of 400−4000 $cm^{-1}$ by a FT-IR spectrometer (Nicolet, U.S.A.), model Impact 410, with 32 scans at


DOI: 10.1021/acs.analchem.5b00734
Anal. Chem. 2015, 87, 10738−10746

resolution 4 $cm^{-1}$ using TGS detector. The morphology and size of gold particles were analyzed by a JEOL JEM-2010 transmission electron microscopy (Japan) operating at 200 keV. The TEM samples were prepared by first scrapping the glass slide on the area covered with PAA brushes and AuNPs followed by adding a small quantity of Milli-Q water on the scrapped area. Approximately 10 $\mu$L of the generated solution was taken then dropped on the carbon-coated copper grid before being dried in a desiccator before analysis. The average diameters of the observed AuNPs were reported from measurements of 30 random particles for each sample using Semafore software. The dynamic advancing ($\theta_A$) and receding ($\theta_R$) water contact angles of surface-modified glass substrates were measured using a contact angle goniometer (Ramé-Hart, Inc., U.S.A., model 100−00), equipped with a Gilmont syringe and a 24-gauge flat-tipped needle. All of the measurements were carried out in air at ambient temperature. The reported angle is an average of five measurements on different areas of each sample. Atomic compositions of the surface-modified glass substrates were determined by X-ray photoelectron spectroscopy (XPS) on a Scienta ESCA 200 spectrometer (Uppsala, Sweden) with Al K$\alpha$ X-rays at a takeoff angle of 90°. AuNPs generated on the PAA brushes were digested by aqueous solution of aqua regia (1$HNO_3$/3HCl) at room temperature for 15 min before quantified by Inductively Coupled Plasma-Mass Spectrometry (ICP-MS; Thermo scientific, model iCAP 6500 ICP-OES), using a calibration curve generated from $Au^{3+}$ solutions having concentration in a range of $10^{-7}$−$10^{-6}$ M.

**Analysis of Single Peptide.** Each peptide sample was dissolved and diluted in Milli-Q water to a final concentration of 500 nM. For SALDI-MS analysis, the samples (3 $\mu$L) were directly deposited onto the glass slide modified with patterned PAA brushes containing AuNPs. The modified glass slide was attached onto MALDI target plate by a two-side conductive tape and then introduced into a Bruker Microflex/Autoflex III MALDI-TOF mass spectrometer for SALDI-MS analyses. The $N_2$ laser (337 nM) with 50% laser intensities and 100 laser shots were used for all analyses.

For MALDI-MS analysis, each peptide sample was mixed with CHCA matrix in a ratio of 1:9 (v/v) of sample/CHCA matrix (CHCA dissolved in 1:1 (v/v) of 0.1% trifluoroacetic acid (TFA) in acetonitrile/0.1% TFA in Milli-Q) and then deposited onto MALDI target plate. After solvent evaporation and sample crystallization, the target plate was introduced into the mass spectrometer for MALDI-MS analysis.

**Selective Analysis of Thiol-Containing Peptide in a Mixture.** A mixture of 500 nM thiol-containing peptide (GSH or ICNKQDCPILE) and 500 nM nonthiol-containing peptide (sucrose and cholesterol or bradykinin) was deposited onto the glass slide modified with patterned PAA brushes containing AuNPs. The deposited mixture was incubated on the modified target plates at room temperature for 10 min. Then the unbounded peptides were rinsed out from the target for five times each by PBS buffer (pH 7.4), followed by Milli-Q water. For each rinsing cycle, multiple drops of washing solution were added on and promptly retracted back from the target using a micropipette. After solvent evaporation, the target plate was introduced into the mass spectrometer for both SALDI-MS and MALDI-MS analyses.

## RESULTS AND DISCUSSION

**Preparation and Characterization of Patterned PAA Brushes Containing AuNPs.** Water contact angle measurement was used as a tool to monitor the success of stepwise surface modification of the glass substrate. The data are expressed in terms of advancing/receding contact angle ($\theta_A$/$\theta_R$) as shown in Table S-1 (Supporting Information). An extremely hydrophilic glass substrate having generated silanol groups after cleaning by plasma treatment ($\theta_A \sim 0$) became hydrophobic after reacting with APTES and yielded Si-$NH_2$ with $\theta_A/\theta_R$ of 84.7°/52.1°. The substrate turned slightly less hydrophobic when being immobilized with initiator via the reaction with ACVA. Upon surface-initiated RAFT polymerization, the water contact of the glass substrate was further decreased to 16.6°, implying that hydrophilic PAA brushes were grafted onto the surface. In contrast, the glass surface was highly hydrophobic with contact angles of 127.6°/74.5° after being modified with perfluorooctylsilyl groups.

Molecular weight ($\bar{M}_n$) and functional group of PAA simultaneously formed in solution from the "added" initiator, ACVA were determined by $^1$H NMR analysis. As depicted in Figure S-1 (Supporting Information), the characteristic $^1$H NMR peaks of the methylene proton in the AA unit (−C<u>H</u>(COOH)) and those aromatic protons of the dithiobenzoate group at the chain end of PAA appeared at 2.1−2.3 and 7.2−7.9 ppm, respectively. The average $M_n$ of PAA was calculated from the relative ratio between the peak integration of methylene proton from the PAA backbone and the peak integration of protons from the dithiobenzoate groups using eq S1 (Supporting Information). The fact that the calculated $M_n$ of 6005 g/mol closely resembled the anticipated value (6158 g/mol) for the target degree of polymerization (DP) of 100 suggested that the RAFT process was well controlled.

The success of PAA surface grafting was confirmed by FT-IR analysis of silica particles grafted with PAA brushes. Figure 1c reveals characteristic absorption bands of C═O stretching at 1635 $cm^{-1}$ (amide I) and N−H bending at 1562 $cm^{-1}$ (amide II), suggesting that amide linkage has been formed between the terminal amino groups of APTES and carboxyl groups of the

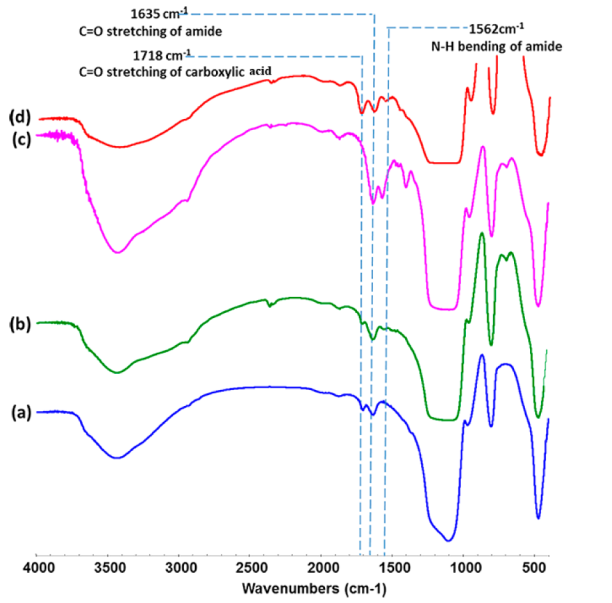


**Figure 1.** FT-IR spectra of silica particles (a) before and after functionalization with (b) APTES, (c) ACVA initiator, and (d) PAA brushes.



DOI: 10.1021/acs.analchem.5b00734
Anal. Chem. 2015, 87, 10738−10746

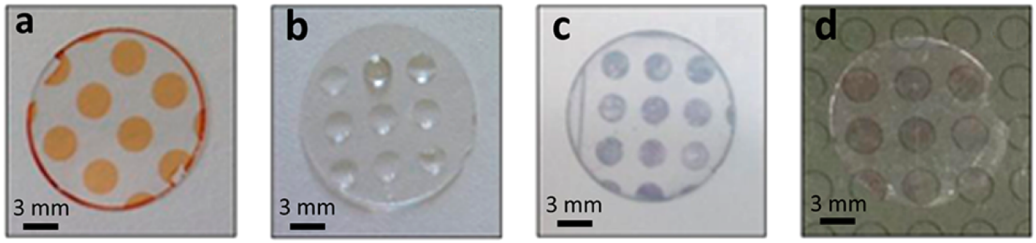


**Figure 2.** Patterned glass substrates with (a) coated positive UV-sensitive resist after photolithography step, (b) grafted PAA brushes holding water droplets demonstrating their higher hydrophilicity than the surrounding area, grafted PAA brushes having in situ generated AuNPs (c) alone, and (d) together with the MALDI target plate.

initiator, ACVA. A strong signal of C═O stretching of carboxylic acid apparently emerged at 1718 $cm^{-1}$ after surface-initiated RAFT polymerization took place as an indication of PAA brushes formation, as shown in Figure 1d.

A number of alternate dipping cycles between $HAuCl_4$ solution and deionized water was varied to determine its effect on AuNPs formation on the PAA-modified glass substrate. As shown in Figure S-2 (Supporting Information), the substrate became slightly darker upon increasing the number of cycles from 1 to 5, implying that there was a greater amount of AuNPs as a function of dipping cycle. This may be explained as a consequence of pH-dependent conformational change of the PAA.[30] Because $pK_a$ of PAA is 4.2, PAA chains would adopt extended conformation when being soaked in deionized water, having a pH of approximately 6.0 due to ionic repulsion of the carboxylate groups along the chains (Scheme S-1, step I, Supporting Information). Once the PAA-modified surface was immersed in $HAuCl_4$ solution, having pH of 1.7 (Scheme S-1, step II, Supporting Information), some carboxylate groups of the PAA chains should electrostatically interact with $Au^{3+}$ and may partially reduce it to $Au^0$. At the same time, the rest of the carboxylate groups were protonated and became less extended and more coil-like, therefore, trapping $Au^{3+}$ as well as the generated $Au^0$. It is quite unfortunate that the exact mechanism on how carboxylate groups can reduce $Au^{3+}$ has not yet been directly proven. To attain such information requires an additional mechanistic study which is beyond a scope of our investigation. However, it can be postulated that the reduction would follow a similar pathway as polyacid compounds commonly used for AuNPs synthesis such as citrate and oxalate anions, which involves ligand exchange and simultaneous induction of a concerted decarboxylation and reduction of Au(III).[37] Another relevant work that was found on the literature suggested that PAA can undergo decarboxylation through radical mechanism in the presence of $Fe^{3+}$, which eventually leads to degradation. The process can be accelerated especially at high temperature.[38]

By repetitive performing this cycle of dipping, the more $Au^{3+}$ can associate with the carboxylate groups and the more $Au^0$ can be generated upon subsequent heat treatment (Scheme S-1, step III, Supporting Information). It should be emphasized at this point that the carboxyl groups can act as effective reducing moieties for $Au^{3+}$ leading to the formation of AuNPs. This would add simplicity to the method because the reduction can be done without having to use additional reducing agent. According to ICP-MS analysis, a surface coverage of the AuNPs was found to be $2.90 \times 10^{-9}$ and $4.62 \times 10^{-9}$ mol/$cm^2$ for the 1- and 5-cycled dipping, respectively. The calibration curve used for AuNPs quantification is illustrated in Figure S-3, Supporting Information. Effect of the number of dipping cycles on the substrate efficiency in analysis of two single peptides (bradykinin and GSH) was evaluated. Although increasing dipping cycle further to 10 yielded approximately 1.3 higher AuNPs coverage than that obtained from the 5-cycled dipping, %RSD values of signal intensity detected on the substrate prepared by 10-cycled dipping was significantly higher than those detected on the substrate prepared by 5-cycled dipping (see Figure S-4, Supporting Information). For this reason, the 5-cycled dipping was therefore selected as the optimal condition for substrate preparation to be used for further analysis.

Formation of AuNPs on the patterned PAA brushes can be demonstrated in Figure 2. The area covered with UV-sensitive resist after surface patterning by photolithography using the pattern shown in Figure 2a to generate photomask (step II in Scheme 1) can be seen as bright yellow spots. After surface grafting of PAA brushes, the greater hydrophilicity of the PAA brushes than the surrounding area, which was covered with perfluorooctylsilyl groups, can be demonstrated by the ability to sustain water droplets, as shown in Figure 2b. Subsequent AuNPs formation within the PAA brushes can be visualized as dark spots on the glass substrate appearing in Figure 2c at the same positions as those previously covered with UV-sensitive resist in Figure 2a and water droplets in Figure 2b. It should also be noted that the diameter of each spot on the glass slide shown in Figure 2a–c is the same as that of the individual spot on the MALDI target plate underneath the glass substrate appearing in Figure 2d.

Morphology of the immobilized AuNPs on the glass substrate was determined from the material scrapped of the glass slide by TEM. As can be seen in Figure 3, the AuNPs were not quite uniform in shape. This outcome agrees quite well with the work previously reported by Hussain et al.[35] The diameter estimated from the AuNPs that are quite spherical was in a range of 25.13 ± 3.20 nm.

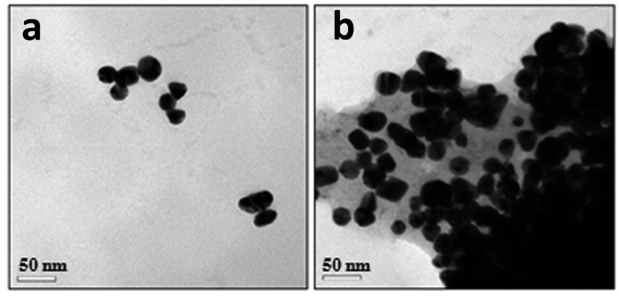


**Figure 3.** Representative TEM images (a, b) of AuNPs immobilized on PAA-modified glass substrate:.



DOI: 10.1021/acs.analchem.5b00734
*Anal. Chem.* 2015, 87, 10738–10746

The presence of AuNPs on the PAA-modified glass surface was also verified by XPS measurement. Figure S-5 in Supporting Information shows XPS spectra of the PAA-modified glass surface both before and after AuNPs immobilization. As shown in Figure S-5b, besides the signals of carbon ($C_{1s}$, binding energy of 287 eV) and oxygen ($O_{1s}$, binding energy of 533 eV) of PAA, trace signals of $Au_{4f7/2}$ and $Au_{4f5/2}$ at binding energies of 84 and 88 eV, characteristic binding energies of Au(0)[39] were also observed, implying the success of in situ synthesis of AuNPs on the PAA brushes modified on glass substrate with 0.67% composition. It should also be emphasized that the ratio of C/O of approximately 3:2 matched very well with the theoretical value estimated from the repeat unit of PAA ($CH_2CHCOOH$). Percentages of elemental composition of all samples are also shown in the table below Figure S-5 (Supporting Information).

**SALDI-MS Analysis of Single Peptide on the AuNPs-PAA Substrate.** To determine the applicability of the PAA-modified glass substrate immobilized with AuNPs (AuNPs-PAA) as substrate for SALDI-MS analysis, bradykinin (MW = 1060.21 g/mol), a cancer biomarker, was chosen as a standard peptide for analysis in comparison with the use of citrate-stabilized AuNPs as a MALDI matrix. As illustrated in Figure 4a, the citrate-stabilized AuNPs alone gave such a high background signal which is probably caused by partial ionization of the AuNPs. Therefore, a poor signal of bradykinin was detected with relatively strong background when the analysis was done in the presence of citrate-stabilized AuNPs, as can be seen in Figure 4b. On the other hand, a characteristic peak of bradykinin at $m/z$ of 1060 was clearly observed without signal interference from the AuNPs when the analysis was performed on a spot of PAA brushes containing AuNPs (Figure 4c). This result strongly indicated that the PAA brushes effectively trapped and prevented the AuNPs from coming off the substrate so that their ionization was suppressed. The fact that the ion abundance of bradykinin was relatively high in Figure 4c suggested that the ionization efficiency was also improved perhaps by a better distribution of the AuNPs within the matrix of PAA and PAA itself being a good proton source. To determine the stability of the mass spectrum, we have also performed analysis of bradykinin on a number of modified targets and found that %RSD of ion abundance is less than 5%. This relatively low %RSD suggests that the mass spectra are quite stable.

Besides the analysis of bradykinin peptide, the AuNPs-PAA substrate was also subjected to analysis of low molecular weight peptide, GSH (MW 307.08 g/mol). As revealed in Figure 5a, by using CHCA matrix, GSH was undetectable due to the interference ion peaks from CHCA matrix at low mass region ($m/z \leq 600$). This common phenomenon limits the application of MALDI-MS technique for small molecule detection. Interestingly, when GSH was analyzed on our developed modified substrate, it was readily detected without interference peak as shown in Figure 5b. There are two dominant peaks in the mass spectrum, which represent $[GSH + H]^+$ ($m/z$ 308) and $[2GSH + H]^+$ ($m/z$ 615). Dimerization of GSH caused by oxidation of the cysteine side chain thiols, linking two chains together by a disulfide bridge, seems to be favorable at relatively high concentration, 500 nM in this case. This is the reason why $[2GSH + H]^+$ ($m/z$ 615) was not detected in subsequent investigation where rinsing was involved for selective analysis from mixture (Figure 6a) and LOD determination (Figure 8a) of which GSH concentration was as low as 0.1 nM. Similar observation on GSH dimerization was also reported by Cui and co-workers.[40] Moreover, the lower laser energy (50% laser 100 shots) was required in the detection on the AuNPs-PAA substrate when compared to the unmodified substrate (using CHCA matrix), indicating the potential of this substrate for low molecular weight compound detection. This newly developed substrate provides an alternative approach for the analysis of small molecules by SALDI-MS technique.

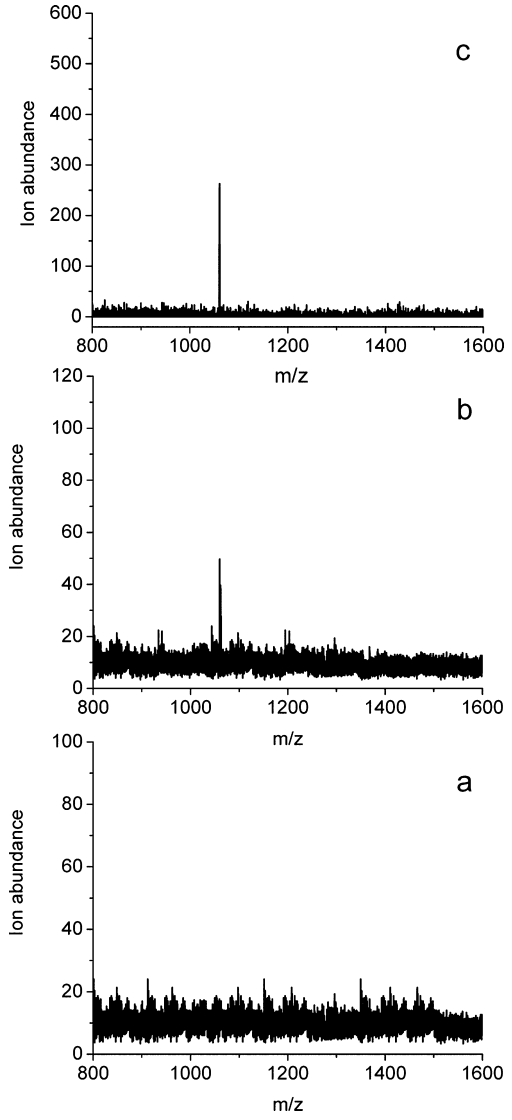


**Figure 4.** Mass spectra of (a) AuNPs, (b) bradykinin mixed with citrate-stabilized AuNPs matrix, and (c) bradykinin on AuNPs-PAA substrate.

**Selective Detection of Thiol-Containing Peptide on the AuNPs-PAA Substrate by SALDI-MS.** Based on the inherently strong binding interactions between Au and the thiol (−SH) group,[41] the selectivity of the AuNPs-PAA substrate toward thiol-containing peptides (i.e., GSH, ICNKQDCPILE) was investigated. First, a solution mixture of three small molecules ($m/z \leq 500$), which are GSH ($m/z$ 307.32), sucrose ($m/z$ 342), and cholesterol ($m/z$ 386.65) was incubated on the AuNPs-PAA substrate and the substrate was simply rinsed with PBS buffer and Milli-Q water before SALDI-MS analysis. The result shown in Figure 6a indicates that only GSH was


DOI: 10.1021/acs.analchem.5b00734
Anal. Chem. 2015, 87, 10738−10746

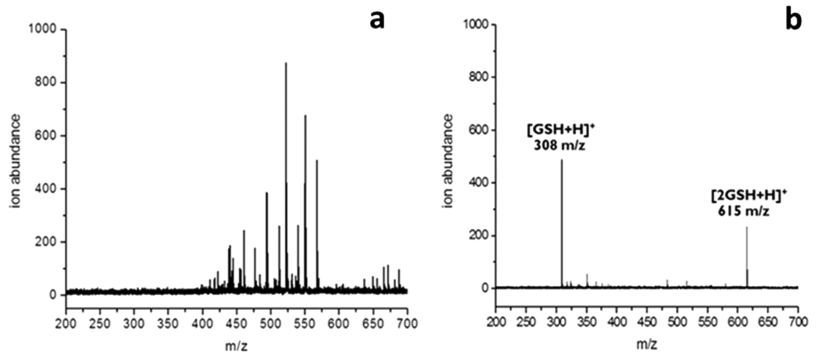


**Figure 5.** Mass spectra of GSH (500 nM) analyzed (a) by using CHCA matrix and (b) on AuNPs-PAA substrate.

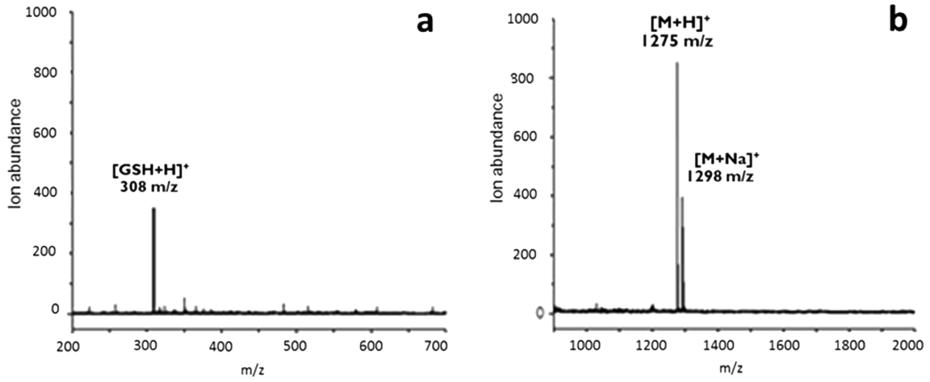


**Figure 6.** Mass spectra of (a) a mixture of 500 nM GSH, sucrose, cholesterol and (b) a mixture of 500 nM bradykinin and ICNKQDCPILE analyzed on AuNPs-PAA substrate by SALDI-MS.

detectable on the modified substrate, which may be explained as a consequence of selective binding between Au on the modified substrate and the thiol group of GSH. Apparently, there was no nonspecific adsorption of the nonthiol-containing peptides by either the AuNPs or the PAA brushes. By using our modified substrate, the thiol-containing peptide can be directly detected on the target plate without the requirement for separation by centrifugation as employed by aforementioned research.[16,42] This truly adds simplicity by reducing cost and time of sample preparation.

Then, the selectivity of the substrate was further evaluated with peptides having higher mass (MW ≥ 1000 g/mol) from a solution mixture of ICNKQDCPILE ($m/z$ 1274) and bradykinin ($m/z$ 1060.21). As can be seen in Figure 6b, only ICNKQDCPILE that contains thiol groups on the cysteine unit was selectively detected at $m/z$ of 1275 $[M + H]^+$. This high selectivity of the modified substrate toward thiol-containing peptide is very useful for the applications that require high specificity for the detection of thiol-containing peptides in complex biological samples (e.g., human serum, cell lysates).

To demonstrate that the substrate also works in biological matrices, a similar analysis was conducted in human serum by spiking a solution mixture of ICNKQDCPILE ($m/z$ 1274), bradykinin ($m/z$ 1060), and angiotensin I ($m/z$ 1296) at a concentration of 500 nM each into a 10x diluted human serum. After the high abundance serum proteins (e.g., HSA, IgG) were removed using an antibody column, the leftover of solution was incubated on the modified substrate for 15 min to selectively bind with thiol-containing peptide. After washing with PBS (pH 7.0) and Milli-Q water, the peptide attached on the modified target was directly analyzed by MS. As shown in Figure 7, only ICNKQDCPILE that contains a thiol group on the cysteine unit is selectively detected at $m/z$ of 1275 $[M + H]^+$. This result truly verifies the powerfulness of our modified substrate for selective binding and direct MS detection of cysteine-containing peptide in complex biological matrices.

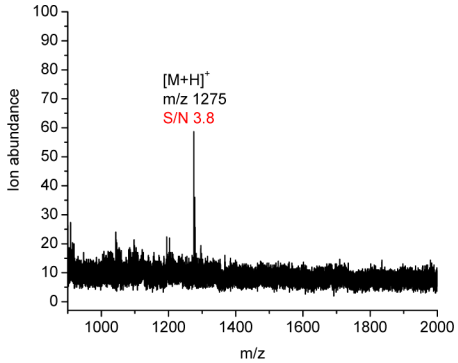


**Figure 7.** Mass spectra of ICNKQDCPILE spiked in 10× diluted human serum analyzed on AuNPs-PAA substrate by SALDI-MS after depletion of high abundance proteins in human serum.

The detection limit of thiol-containing peptides (GSH, ICNKQDCPILE) on these substrates was also estimated. As shown in Figure 8, the limit of detection (LOD) of GSH and ICNKQDCPILE were found to be 0.1 nM (S/N = 6.4) and 0.05 nM (S/N = 3.8), respectively, on the AuNPs-PAA substrate. Thus, by using our modified substrate, the thiol-containing peptide can be selectively and sensitively detected without the use of an organic matrix.



DOI: 10.1021/acs.analchem.5b00734
*Anal. Chem.* 2015, 87, 10738−10746

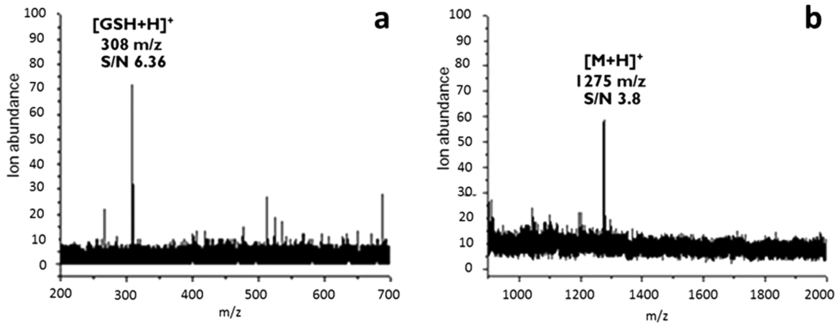


**Figure 8.** Mass spectra of (a) 0.1 nM GSH and (b) 0.05 nM ICNKQDCPILE analyzed on AuNPs-PAA substrate.

## CONCLUSIONS

The present study has demonstrated that patterned PAA brushes can be formed by photolithography and surface-initiated RAFT polymerization of AA. The AuNPs can be generated in situ within the matrix of PAA brushes without the use of additional reducing agent. The presence of AuNPs in the form of $Au^0$ was verified by XPS. TEM analysis suggested that the AuNPs were not quite uniform in shape and had estimated diameter in a range of 25.13 ± 3.20 nm. As determined by ICP-MS, a surface coverage of up to $4.62 \times 10^{-9}$ mol/cm$^2$ was achieved upon using an optimal dipping cycle of 5 in $HAuCl_4$ and Milli-Q water. The PAA brushes embedded with AuNPs can be used as substrate for SALDI-MS analysis which was capable of detecting both small peptide having $m/z \leq 600$ (GSH) and large peptides having $m/z \geq 1000$ (bradykinin, ICNKQDCPILE) without the interference from matrix signal. Moreover, by employing AuNPs as the capture probe, the PAA-AuNPs substrate can selectively identify thiol-containing peptides (GSH, ICNKQDCPILE) from the peptide mixtures with LOD as low as 0.1 and 0.05 nM for GSH and ICNKQDCPILE, respectively. An ability to selectively detect ICNKQDCPILE in diluted human serum strongly demonstrates the potential of the developed substrate for peptide analysis in complex biological matrices. In addition, the procedure of separation is simple, time-saving and efficient because sample can be spotted and thiol-containing peptides can be separated directly on the target plate by using micropipette without the requirement for tedious washing/rinsing steps. It should also be emphasized that the analysis can be accomplished without the requirement for an extra proton source because carboxyl groups of PAA brushes can serve as an internal proton source.

## ASSOCIATED CONTENT

### Supporting Information

The Supporting Information is available free of charge on the ACS Publications website at DOI: 10.1021/acs.analchem.5b00734.

Water contact angle of surface-modified glass substrates, $^1$H NMR spectrum of PAA formed in solution, photograph of PAA-modified glass slide containing AuNPs, schematic representation of stepwise method showing in situ synthesis of AuNPs, calibration curve used for AuNPs quantification by ICP-MS, ion abundance of peptide measured on the AuNPs-PAA substrates prepared by different number of dipping cycle, and XPS spectra and atomic composition of PAA-modified glass substrate with and without AuNPs (PDF).

## AUTHOR INFORMATION

### Corresponding Author

*E-mail: vipavee.p@chula.ac.th. Tel.: +66-2218-7627. Fax: +66-2218-7598.

### Notes

The authors declare no competing financial interest.

## ACKNOWLEDGMENTS

Financial support for this work was provided by the Thailand Research Fund (DBG5580003), the Ratchadaphiseksomphot Endowment Fund of Chulalongkorn University (RES560530126-AM), and the Thai Government Stimulus Package 2 (TKK2555), under the Project for Establishment of Comprehensive Center for Innovative Food, Health Products and Agriculture. The authors appreciate MALDI-TOF mass spectrometer, X-ray photoelectron spectroscopy, and ICP-MS facilities provided by Mass Spectrometric Center, University of Massachusetts, Amherst, Faculty of Chemistry, Materials and Bioengineering, Kansai University, and SciSpec Co., Ltd., respectively.

## REFERENCES

(1) Cao, C.; Li, X.; Lee, J.; Sim, S. J. *Biosens. Bioelectron.* **2009**, *24*, 1292−1297.
(2) Afonso, A. S.; Zanetti, B. F.; Santiago, A. C.; Henrique-Silva, F.; Mattoso, L. H. C.; Faria, R. C. *Talanta* **2013**, *104*, 193−197.
(3) Nguyen, H. P.; Chandel, N. S.; DeBerardinis, R. J.; Schug, K. A. *J. Sep. Sci.* **2013**, *36*, 3303−3309.
(4) Smith, Z. M.; Terry, J. M.; Barnett, N. W.; Gray, L. J.; Wright, D. J.; Francis, P. S. *Analyst* **2014**, *139*, 2416−2422.
(5) Hu, B.; Cao, X.; Zhang, P. *New J. Chem.* **2013**, *37*, 3853−3856.
(6) Chen, S.; Hong, Y.; Liu, J.; Tseng, N.-W.; Liu, Y.; Zhao, E.; Lam, J. W. Y.; Tang, B. Z. *J. Mater. Chem. B* **2014**, *2*, 3919−3923.
(7) McKeague, M.; Foster, A.; Miguel, Y.; Giamberardino, A.; Verdin, C.; Chan, J. Y. S.; DeRosa, M. C. *RSC Adv.* **2013**, *3*, 24415−24422.
(8) Li, T.; Shu, B.; Jiang, B.; Ding, L.; Qi, H.; Yang, M.; Qu, F. *Sens. Actuators, B* **2013**, *186*, 768−773.
(9) Wang, Y.; Wu, L.; Zhou, X.; Wong, T. I.; Zhang, J.; Bai, P.; Li, E. P.; Liedberg, B. *Sens. Actuators, B* **2013**, *186*, 205−211.
(10) Grant, C. S.; Louda, J. W. *Org. Geochem.* **2013**, *65*, 29−36.
(11) Shabani, A.; Tabrizian, M. *Analyst* **2013**, *138*, 6052−6062.
(12) Cerasoli, E.; Rakowska, P. D.; Horgan, A.; Ravi, J.; Bradley, M.; Vincent, B.; Ryadnov, M. G. *Mol. BioSyst.* **2010**, *6*, 2214−2217.
(13) Rodthongkum, N.; Ramireddy, R.; Thayumanavan, S.; Richard, W. V. *Analyst* **2012**, *137*, 1024−1030.
(14) Kailasa, S. K.; Wu, H.-F. *Analyst* **2010**, *135*, 1115−1123.
(15) Chiang, C.-K.; Chiang, N.-C.; Lin, Z.-H.; Lan, G.-Y.; Lin, Y.-W.; Chang, H.-T. *J. Am. Soc. Mass Spectrom.* **2010**, *21*, 1204−1207.
(16) Shrivas, K.; Wu, H.-F. *Rapid Commun. Mass Spectrom.* **2008**, *22*, 2863−2872.



DOI: 10.1021/acs.analchem.5b00734
*Anal. Chem.* 2015, 87, 10738−10746

(17) Chen, C.-T.; Chen, W.-J.; Liu, C.-Z.; Chang, L.-Y.; Chen, Y.-C. *Chem. Commun.* **2009**, 7515−7517.
(18) Kailasa, S. K.; Wu, H.-F. *Analyst* **2012**, *137*, 1629−1638.
(19) Li, L.; Li, B. *Analyst* **2009**, *134*, 1361−1365.
(20) Aminlashgari, N.; Shariatgorji, M.; Ilag, L. L.; Hakkarainen, M. *Anal. Methods* **2011**, *3*, 192−197.
(21) Kawasaki, H.; Sugitani, T.; Watanabe, T.; Yonezawa, T.; Moriwaki, H.; Arakawa, R. *Anal. Chem.* **2008**, *80*, 7524−7533.
(22) Tarui, A.; Kawasaki, H.; Taiko, T.; Watanabe, T.; Yonezawa, T.; Arakawa, R. *J. Nanosci. Nanotechnol.* **2009**, *9*, 159−164.
(23) Zhao, B.; Brittain, W. J. *Prog. Polym. Sci.* **2000**, *25*, 677−710.
(24) Barbey, R.; Lavanant, L.; Paripovic, D.; Schuwer, N.; Sugnaux, C.; Tugulu, S.; Klok, H.-A. *Chem. Rev.* **2009**, *109*, 5437−5527.
(25) Dunn, J. D.; Igrisan, E. A.; Palumbo, A. M.; Reid, G. E.; Bruening, M. L. *Anal. Chem.* **2008**, *80*, 5727−5735.
(26) Dunn, J. D.; Watson, J. T.; Bruening, M. L. *Anal. Chem.* **2006**, *78*, 1574−1580.
(27) Wang, W.-H.; Bruening, M. L. *Analyst* **2009**, *134*, 512−518.
(28) Kim, Y.-P.; Lee, B. S.; Kim, E.; Choi, I. S.; Moon, D. W.; Lee, T. G.; Kim, H.-S. *Anal. Chem.* **2008**, *80*, 5094−5102.
(29) Akkahat, P.; Hoven, V. P. *Colloids Surf., B* **2011**, *86*, 198−205.
(30) Akkahat, P.; Mekboonsonglarp, W.; Kiatkamjornwong, S.; Hoven, V. P. *Langmuir* **2012**, *28*, 5302−5311.
(31) Dong, R.; Krishnan, S.; Baird, B. A.; Lindau, M.; Ober, C. K. *Biomacromolecules* **2007**, *8*, 3082−3092.
(32) Qu, Z.; Hu, F.; Chen, K.; Duan, Z.; Gu, H.; Xu, H. *J. Colloid Interface Sci.* **2013**, *398*, 82−87.
(33) Wang, Y.-M.; Cui, Y.; Cheng, Z.-Q.; Song, L.-S.; Wang, Z.-Y.; Han, B.-H.; Zhu, J.-S. *Appl. Surf. Sci.* **2013**, *266*, 313−318.
(34) Ballarin, B.; Cassani, M. C.; Tonelli, D.; Boanini, E.; Albonetti, S.; Blosi, M.; Gazzano, M. *J. Phys. Chem. C* **2010**, *114*, 9693−9701.
(35) Hussain, I.; Brust, M.; Papworth, A. J.; Cooper, A. I. *Langmuir* **2003**, *19*, 4831−4835.
(36) Hayat, A. *J. Anat.* **1989**, *176*, 215−216.
(37) Ojea-Jimenez, I.; Romero, F. M.; Bastus, N. G.; Puntes, V. *J. Phys. Chem. C* **2010**, *114*, 1800−1804.
(38) Neira, A.; Tarraga, M.; Catalan, R. *J. Chil. Chem. Soc.* **2007**, *52*, 1314−1317.
(39) Cheng, W. L.; Dong, S. J.; Wang, E. K. *Langmuir* **2003**, *19*, 9434−9439.
(40) Cui, S. Y.; Kim, S. J.; Jo, S. C.; Lee, Y. M.; Lee, Y. I. *Bull. Korean Chem. Soc.* **2005**, *26*, 1235−1240.
(41) Carr, J. A.; Wang, H.; Abraham, A.; Gullion, T.; Lewis, J. P. *J. Phys. Chem. C* **2012**, *116*, 25816−25823.
(42) Chiu, T.-C.; Chang, L.-C.; Chiang, C.-K.; Chang, H.-T. *J. Am. Soc. Mass Spectrom.* **2008**, *19*, 1343−1346.



DOI: 10.1021/acs.analchem.5b00734
*Anal. Chem.* 2015, 87, 10738−10746

LANGMUIR

Article

pubs.acs.org/Langmuir

# Clickable and Antifouling Platform of Poly[(propargyl methacrylate)-*ran*-(2-methacryloyloxyethyl phosphorylcholine)] for Biosensing Applications

Oraphan Wiarachai,[†] Tirayut Vilaivan,[‡] Yasuhiko Iwasaki,[§] and Voravee P. Hoven*[,‡]

[†]Program in Petrochemistry, Faculty of Science, and [‡]Organic Synthesis Research Unit, Department of Chemistry, Faculty of Science, Chulalongkorn University, Phayathai Road, Pathumwan, Bangkok 10330, Thailand

[§]Faculty of Chemistry, Materials and Bioengineering, Kansai University, 3-3-35 Yamate-cho, Suita-shi, Osaka 564-8680, Japan

Supporting Information

**ABSTRACT:** A functional copolymer platform, namely, poly[(propargyl methacrylate)-*ran*-(2-methacryloyloxyethyl phosphorylcholine)] (PPgMAMPC), was synthesized by reversible addition−fragmentation chain-transfer polymerization. In principle, the alkyne moiety of propargyl methacrylate (PgMA) should serve as an active site for binding azide-containing molecules via a click reaction, i.e., Cu-catalyzed azide/alkyne cycloaddition (CuAAC), and 2-methacryloyloxyethyl phosphorylcholine (MPC), the hydrophilic monomeric unit, should enable the copolymer to suppress nonspecific adsorption. The copolymers were characterized using Fourier transform infrared (FTIR) and $^1$H NMR spectroscopies. Thiol-terminated, PPgMAMPC-SH, obtained by aminolysis of PPgMAMPC, was immobilized on a gold-coated substrate using a "grafting to" approach via self-assembly. Azide-containing species, namely, biotin and peptide nucleic acid (PNA), were then immobilized on the alkyne-containing copolymeric platform via CuAAC. The potential use of surface-attached PPgMAMPC in biosensing applications was shown by detection of specific target molecules, i.e., streptavidin (SA) and DNA, by the developed sensing platform using a surface plasmon resonance technique. The copolymer composition strongly influenced the performance of the developed sensing platform in terms of signal-to-noise ratio in the case of the biotin−SA system and hybridization efficiency and mismatch discrimination for the PNA−DNA system.

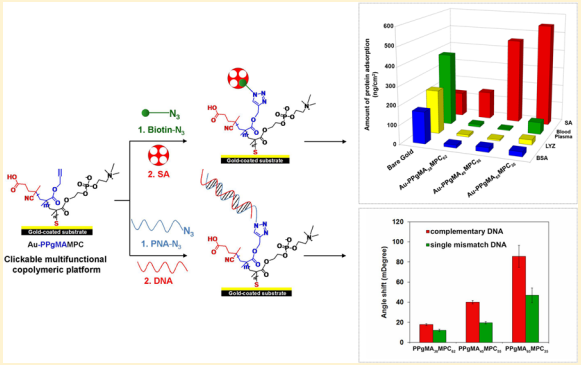


## INTRODUCTION

Effective functionalization with biomolecules is important in the development of materials for biotechnology-related applications such as biosensors, protein/cell microarrays, microfluidic devices, and tissue engineering. Polymeric platforms are becoming increasingly attractive for biomolecule immobilization because a variety of functional groups can be conveniently incorporated and proportionally customized using combinations of specific monomers in the polymerization step. The superiority of this approach, which provides a three-dimensional platform and therefore offers a higher functional group density for biomolecular probe binding per surface area than in the case of a conventional two-dimensional platform based on self-assembled monolayers (SAMs)[1−3] of end-functionalized alkanethiols, for biosensing applications has been shown by our group[4,5] and other researchers.[6−9]

Most biomolecules (e.g., proteins, antibodies, enzymes, and DNA) carry carboxyl and/or amino groups. Polymers with versatile functionalities that can accommodate covalent bond formation, particularly via hydrolytically stable amide linkages, including poly[oligo(ethylene glycol) methacrylate],[8,10,11] poly(2-hydroxyethyl methacrylate),[12,13] and poly(acrylic acid) (PAA),[4,5,14−19] are therefore commonly used as platforms for biomolecule conjugation. However, an additional activation step using an appropriate coupling reagent is required for biomolecule conjugation to such polymers. PAA, in particular, suffers from nonspecific adsorption of positively charged components such as lysozyme (LYZ) because its carboxyl groups (−COOH) can be ionized to negatively charged carboxylate ions (−COO$^-$).[5] This is problematic in the analyses of complex samples. Precursor polymers have recently emerged as alternative and ready-to-use functional materials that can directly bind with designated nucleophilic modifiers such as amino-containing biomolecules, without having to undergo activation. Well-known precursor polymeric systems include polymers bearing succimidyl ester[20−22] or pentafluorophenyl ester groups,[23,24] poly[propargyl (me)thacrylate] [PPg(M)A],[25,26] and poly(glycidyl methacrylate) (PGMA).[27,28] From the perspective of chemical robustness, PPg(M)A is a good choice because the alkynyl side group in

**Received:** July 23, 2015
**Revised:** December 8, 2015
**Published:** December 22, 2015





DOI: 10.1021/acs.langmuir.5b02727
*Langmuir* 2016, 32, 1184−1194

each repeat unit specifically undergoes a Huisgen 1,3-dipolar azide−alkyne cycloaddition with azide-containing molecules, or thiol−yne reactions with thiol-containing molecules; the reaction yields under mild conditions are high, and no byproducts are generated. Socaci and co-workers[25] prepared core−shell nanoparticles consisting of magnetite cores and poly(*O*-propargyl acrylate) shells. They showed that acryloyl-containing phosphonates or methacryloyl phosphates anchored to the magnetic nanoparticle (MNP) surfaces acted as initiating sites for polymerization of a series of alkyne-terminated acrylate monomers with different spacers between the carboxyl oxygen atom and the alkyne moiety. The ability of the alkyne moieties on MNPs to form triazole linkages via azide−alkyne cycloaddition was tested using azide-terminated biotin fluorescently labeled with dansyl groups. Wang and co-workers[26] successfully developed an alkyne-functionalized microporous polypropylene membrane via a combination of plasma treatment and UV-induced graft polymerization of 3-(trimethylsilyl)propargyl methacrylate. The PPgMA-modified membrane obtained after trimethylsilyl removal can directly bind with a thiol-containing carbohydrate ligand, 2,3,4,6-tetra-*O*-acetyl-*β*-D-glucopyranoside thiol, and yields a glycosylated membrane via a thiol−yne click reaction. The glycosyl density of the glycosylated membrane can be tuned based on the polymer graft density, and the membrane showed specific adsorption of lectin concanavalin A over peanut agglutinin.

Specific detection of target molecules rather than the nontargeted components or the ability to resist nonspecific adsorption, known as antifouling, is another key element in biosensor development, especially for the analysis of real biologically relevant samples in which numerous types of interference exist concurrently. A number of copolymeric platforms have therefore been designed to incorporate biocompatible and highly hydrophilic polymers along with precursor polymers. Among the developed hydrophilic polymers, zwitterionic polymers, which contain positively and negatively charged moieties within the same structure, such as poly(2-methacryloyloxyethyl phosphorylcholine) (PMPC), poly(carboxybetaine methacrylate) (PCBMA), and poly(sulfobetaine methacrylate) (PSBMA) have received growing attention for use in new-generation antifouling materials.[29−31] Emmenegger and co-workers[30] reported that plasma protein adsorption completely suppressed on surface-immobilized PCBMA, whereas PMPC and PSBMA prevented adsorption of the main plasma proteins (human serum albumin, IgG, Fbg, and LYZ) from single-protein solutions, but could not prevent plasma deposition. In this study, based on our previous work using MPC-containing copolymer brushes between PMPC and poly(methacrylic acid) (PMA) as precursor layers for biosensor applications,[14] we used PMPC as an antifouling zwitterionic polymer to prevent nonspecific adsorption. It has been proven that PMPC helps to suppress undesirable nonspecific adsorption of proteins and cells,[32−36] and also provides a suitable environment for preserving the stability and activity of immobilized biomolecular probes.[37−39] Ishihara and co-workers[39] used monitoring with a quartz crystal balance to show that poly[2-methacryloyloxyethyl phosphorylcholine (MPC)-*co*-*n*-butyl methacrylate (BMA)-*co*-*p*-nitrophenyloxycarbonyl poly(ethylene glycol) methacrylate (MEONP)] (PMBN), adsorbed on a gold-coated substrate and conjugated with anti-C-reactive protein antibodies via nitrophenyloxycarbonyl active ester binding sites in the MEONP unit can specifically bind with the respective antigens. The developed platform simultaneously prevented adsorption of bovine serum albumin and *γ*-globulin. PMBN physically adsorbed on poly(methyl methacrylate) microchips and polystyrene well plates has also been used for antigen detection via ELISA-based assays, and for affinity-based protein separation when deposited on poly(L-lactic acid) nanoparticles.[40−43] Iwata et al.[44] generated block copolymer brushes of PGMA, another precursor polymer, and PMPC via surface-initiated atom-transfer radical polymerization. An antibody fragment was conjugated to the surface-grafted copolymer brushes via a thiol−disulfide interchange reaction with pyridyl disulfide linkages, previously introduced by epoxide ring opening of GMA repeat units in the copolymer. The activity of the conjugated antibody fragment in antigen detection was better for the PMPC copolymer platform than those for platforms based on PGMA alone or epoxysilane.

Inspired by the research described above, the aim of this study was to develop a multifunctional copolymer platform based on clickable PPgMA and antifouling PMPC, a combination that, to the best of our knowledge, has never been explored. The alkyne moiety of the PgMA unit should serve as an active site for binding of azide-containing molecules via a Cu-catalyzed azide/alkyne cycloaddition (CuAAC) click reaction, without the need for activation. The hydrophilic monomeric unit, MPC, should enable the copolymer to suppress nonspecific adsorption. The copolymer poly[(propargyl methacrylate)-*ran*-(2-methacryloyloxyethyl phosphorylcholine)] (PPgMAMPC) was first synthesized by reversible addition−fragmentation chain-transfer (RAFT) polymerization. Thiol-terminated PPgMAMPC (PPgMAMPC-SH), obtained by aminolysis of PPgMAMPC, was immobilized on a gold-coated substrate using a "grafting to" method via Au−S bond formation between the thiol end groups of the copolymer and the gold surface. Azide-containing biotin and peptide nucleic acid (PNA) were used as model probes to demonstrate the potential of the surface-attached PPgMAMPC for probe immobilization and subsequent detection of target molecules, namely, streptavidin (SA) and deoxyribonucleic acid (DNA), using a surface plasmon resonance (SPR) technique. The parameters that may affect the sensitivity and specificity, in terms of the signal-to-noise (*S*/*N*) ratio, in detecting SA in a complex sample using a biotin-based sensor were also investigated. The hybridization efficiency (%HE) and mismatch discrimination (%MD) for DNA detection were evaluated for the PNA-based sensor.

## EXPERIMENTAL SECTION

**Materials.** MPC was purchased from the NOF Corp. (Japan). Methacrylic acid (MA), 4,4′-azobis(4-cyanovaleric acid) (ACVA), 4-cyano-4-(phenylcarbonothioylthio)pentanoic acid (CPADB), azide-$PEG_3$-biotin conjugate (biotin-$N_3$), copper(I) acetate, bovine serum albumin (BSA), and LYZ were purchased from Aldrich. MA was distilled under reduced pressure to remove hydroquinone monomethyl ether, a polymerization inhibitor, prior to use. Phosphate-buffered saline (PBS; pH 7.4) was purchased from Sigma. Hydrazine monohydrate and *N*,*N*′-diisopropylethylamine (DIEA) were purchased from Sigma-Aldrich. SA was purchased from Thermo Fisher Scientific Inc. PgMA was synthesized using the method reported by He et al.[45] DNA was purchased from the Pacific Science Co., Ltd. PNA was synthesized by solid-phase peptide synthesis on Tentagel S RAM resin (Fluka) preloaded with 9-fluorenylmethoxycarbonyl-L-lysine(*tert*-butoxycarbonyl)-pentafluorophenyl ester (Fmoc-L-Lys(Boc)-oPfp) (CalbiochemNovabiochem Co., Ltd.) using a previously reported procedure.[46] The PNA was modified at the N-terminus by reductive alkylation with $N_3(CH_2)_3CHO$ to prepare azide-terminated PNA (PNA-$N_3$).[47] After cleavage of PNA-$N_3$ from the solid support


DOI: 10.1021/acs.langmuir.5b02727
*Langmuir* 2016, 32, 1184−1194

**Scheme 1. Schematic Diagram of (a) Preparation of PPgMAMPC-SH, (b,c) Immobilization of Biotin-$N_3$ and PNA-$N_3$ on PPgMAMPC-Modified SPR Chip, and (d,e) Specific Binding between Conjugated Probe and Target Molecule**

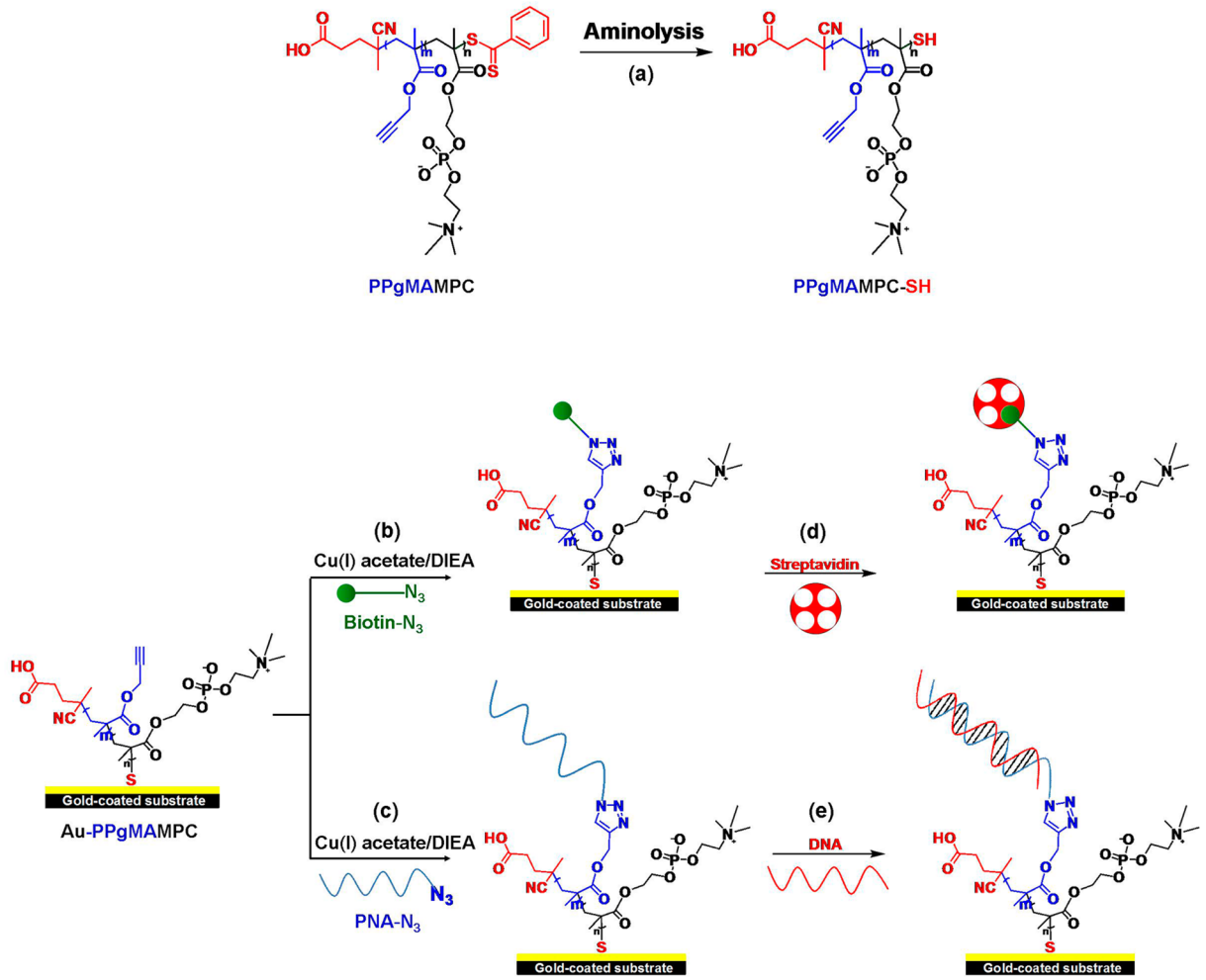


using trifluoroacetic acid, the crude PNA-$N_3$ was purified using reverse-phase high performance liquid chromatography (HPLC) and analyzed by matrix-assisted laser desorption/ionization-time-of-flight (MALDI-TOF) mass spectrometry (Bruker Daltonik GmbH, Germany) (see Figure S1 in the Supporting Information for chromatogram and mass spectra). Ethylenediaminetetraacetic acid (EDTA) was purchased from Fluka. Human platelet-poor plasma was donated by a healthy volunteer. Milli-Q water was purified using an ultrapure water system with a Millipak-40 filter unit (0.22 $\mu$m, Millipore) and a Millipore Milli-Q system that involved reverse osmosis followed by ion exchange and filtration steps (18.2 MΩ). All reagents and materials were analytical grade and used without further purification unless specified.

**Synthesis of Thiol-Terminated Poly[(propargyl methacrylate)-*ran*-(2-methacryloyloxyethyl phosphorylcholine)] (PPgMAMPC-SH).** MPC monomer (0.59 g, 2.0 mmol), ACVA (0.7 mg, 2.5 $\mu$mol), and CPADB (5.6 mg, 20 $\mu$mol) were dissolved in 2 mL of an ethanol/tetrahydrofuran (EtOH:THF) (1:1 v/v) mixture. PgMA (0.25 mL, 2.0 mmol) was added to the solution under magnetic stirring. The clear pink solution was purged with nitrogen gas for 30 min and then immersed in an oil bath at 70 °C, and polymerization was performed for a set reaction time. The reaction was terminated in an ice bath. The resulting PPgMAMPC was purified, using a dialysis membrane (molecular weight cutoff = 3500 g/mol), against EtOH for 2 d, and then against deionized water for 2 d. An orange cotton-like material was obtained after lyophilization. The copolymer composition was varied by varying the molar ratio of PgMA to MPC in the feed. PPgMAMPC was characterized using $^1$H NMR and Fourier transform infrared (FTIR) spectroscopies. The molar percentage contents of PgMA and MPC units in the copolymer ($PPgMA_mMPC_n$) were denoted by $m$ and $n$, respectively.

$^1$H NMR (400 MHz, $CD_3OD$) $\delta$ (ppm): characteristic peaks of PgMA unit (−C≡C*H* 3.10, −O−$CH_2$−C≡CH 4.55−4.80), MPC unit [(−N($CH_3$)$_3$ 3.25, −N−$CH_2CH_2$−O− 3.75, −POC$H_2$C$H_2$N−, −COOC$H_2$, −$CH_2$OP 4.0−4.4], and aromatic protons (−$C_6H_5$ 7.40−7.95).

PPgMAMPC-SH was prepared by aminolysis of the dithioester groups at the chain ends of the copolymer with hydrazine monohydrate (Scheme 1a).[48] PPgMAMPC (0.2 g) was dissolved in EtOH (3 mL) for $PPgMA_{38}MPC_{62}$−SH and $PPgMA_{45}MPC_{55}$−SH, or a mixture of EtOH and THF (7:3 v/v) for $PPgMA_{65}MPC_{35}$−SH, until the solution was clear. Hydrazine monohydrate (30 mol equiv with respect to dithioester groups) was added to the copolymer solution under magnetic stirring. When addition was complete, the solution was stirred for 2 h at ambient temperature and then added dropwise to aqueous 1.0 M HCl (10 mL) and stirred for 1 h. The obtained PPgMAMPC-SH was purified using a dialysis membrane (molecular weight cutoff = 3500 g/mol) against aqueous HCl, pH 3−4, for 2 d, and then against deionized water for 2 d. A white cotton-like product was obtained after lyophilization. The copolymer was characterized using $^1$H NMR, FTIR, and UV−vis spectroscopies.

**Immobilization of PPgMAMPC-SH on Gold-Coated SPR Chip.** A gold-coated SPR chip was cleaned with air plasma in a plasma cleaner (Harrick Plasma PDC-32G, Power 18 W) for 5 min, washed with Milli-Q water for 5 min, and dried under a nitrogen stream. The cleaned SPR sensor chip was immersed in 3 mL of a 0.1


DOI: 10.1021/acs.langmuir.5b02727
*Langmuir* 2016, 32, 1184−1194

mM copolymer solution [$PPgMA_{38}MPC_{62}$–SH and $PPgMA_{45}MPC_{55}$–SH in EtOH, $PPgMA_{65}MPC_{35}$–SH in EtOH/THF (7:3 v/v)] at ambient temperature for 48 h. The modified SPR chip was removed from the solution and rinsed five times by constant agitation, for 5 min each time, in EtOH for Au–$PPgMA_{38}MPC_{62}$ and Au–$PPgMA_{45}MPC_{55}$, and in EtOH/THF (7:3 v/v) for Au–$PPgMA_{65}MPC_{35}$. The SPR sensor chip with the immobilized copolymer was dried under a nitrogen stream and characterized using contact angle and SPR measurements and attenuated total reflection (ATR)-FTIR spectroscopy.

**Characterization.** Dynamic advancing ($\theta_A$) water contact angles were measured using a contact angle goniometer equipped with a Gilmont syringe and a 24-gauge flat-tipped needle (Ramé-Hart, model 200-F1). All measurements were performed in air at ambient temperature. Data for each sample were collected from five different areas of the substrate and analyzed using DROPimage standard 2.0 software. The characteristic functional groups of the copolymer brushes on the SPR sensor chip were characterized using ATR-FTIR spectroscopy (Nicolet 6700 FTIR spectrometer). Spectra were recorded in the IR region (4000–650 $cm^{-1}$) based on 32 scans, at a spectral resolution of 4 $cm^{-1}$. $^1H$ NMR spectra were recorded in $CD_3OD$ using a Varian NMR spectrometer (Mercury-400; USA) operated at 400 MHz. The disappearance of the dithioester groups of the copolymer was monitored using UV–vis spectroscopy (CARY 100Bio UV–visible spectrophotometer, Varian Inc., Palo Alto, CA, USA). Gel permeation chromatography (GPC) was performed using a refractive index detector equipped with a Shodex Asahipak GF-1G guard column and a 7.0 $\mu$m bead GF-7 M HQ column (exclusion limit ~$10^7$) at 40 °C and a flow rate of 0.6 mL/min. A phosphate buffer (pH 9) containing 10 vol % acetonitrile was used as the eluent. The $M_n$ and $M_w/M_n$ values were calibrated with standard sodium poly(styrenesulfonate) samples. The elemental composition on a selected SPR chip with an immobilized copolymer was determined by X-ray photoelectron spectroscopy (XPS; AXIS Ultra DLD, Kratos Analytical Ltd., Manchester, UK) using an Al K$\alpha$ X-ray source. All XPS data were collected at a takeoff angle of 90°. Atomic force microscopy (AFM) images were obtained using a scanning probe microscope (NanoScopeIV, Veeco, Plainview, NY, USA). Measurements were performed in air in tapping mode with a silicon nitride tip at a resonance frequency of 267–295 kHz and a spring constant of 20–80 N/m. The thickness of the polymer brushes was measured using a spectroscopic ellipsometer (J. A. Woollam Co., Lincoln, NE, USA) at an incident angle of 70–80° in steps of 5°. The calculation was performed based on a Cauchy layer model with assumed refractive index of 1.34 ± 0.09 for gold-coated substrate at 632.8 nm.

**SPR Measurements.** SPR measurements were performed using a double-channel AutoLab ESPR instrument (Eco Chemie, Utrecht, The Netherlands) at 25 °C, with the plane face of the prism coupled to the gold-coated glass via an index-matching fluid. The instrument uses a laser diode at a wavelength of 670 nm and a vibrating mirror to modulate the angle of incidence of the p-polarized light beam on the SPR substrate. An autosampler was used to inject the test solution, and the SPR angle shift measurements were performed under nonflow liquid conditions. The SPR angle shift at the end-point of each step and after baseline subtraction (angle shift) was used to calculate the density of molecules bound to the surface or the target density, using a sensitivity factor of 120 mdeg, equal to 100 ng/$cm^2$. This sensitivity factor is specifically calibrated for the AutoLab ESPR, which uses an N-BK 7 prism refractive index of 1.518, and incident light wavelength of 670 nm. Each gold-coated SPR chip bearing PPgMAMPC was first seated in an SPR cell before being stabilized with a running solution of 10 mM PBS (pH 7.4). When the equilibrium SPR angle frequency in the buffer solution was obtained, the substrate was ready to be used.

**Probe Conjugation on Copolymer-Modified SPR Chip by CuAAC Reaction.** For conjugation of biotin-$N_3$ (Scheme 1b), Cu(I) acetate (1.23 mg, 0.01 mmol) and biotin-$N_3$ (0.5 M, 4.0 $\mu$L, 2.0 $\mu$mol) were dissolved in 10 mM PBS (pH 7.4, 2 mL) for 10 min to obtain a final biotin-$N_3$ concentration of 1.0 mM. The PPgMAMPC-modified SPR chip was immersed in the mixture, with constant agitation for 5 min. DIEA (1.71 $\mu$L, 0.01 mmol) was added to the reaction mixture, and the SPR chip was immersed in the mixture for 24 h under constant agitation at ambient temperature. The modified SPR chip was removed from the solution and then rinsed by constant agitation in 10 mM EDTA for 1 min and 10 mM PBS (pH 7.4) five times for 5 min each. The azide-containing PNA (PNA-$N_3$) probe was immobilized on the PPgMAMPC-modified SPR chip (Scheme 1c) by dissolving Cu(I) acetate (0.1 mg, 8.2 $\mu$mol) and PNA-$N_3$ (10 nmol) in methanol (2 mL) for 10 min to obtain a final PNA-$N_3$ concentration of 5.0 $\mu$M. The modified SPR chip was immersed in the solution with constant agitation for 5 min. A solution of DIEA (50 $\mu$M, 1.0 mL) was added to the reaction mixture, and then the SPR chip was immersed in this mixture for 24 h under constant agitation at ambient temperature. The modified SPR chip was removed from the solution and rinsed by constant agitation in 10 mM EDTA for 1 min and in methanol five times for 5 min each. The SPR sensor chip was dried under a nitrogen stream and characterized using contact angle and SPR measurements and ATR-FTIR spectroscopy.

**Specific Interactions between Conjugated Probes and Target Molecules.** A PPgMAMPC-modified SPR chip conjugated with the desired probe was seated in an SPR cell and then rinsed with a running solution of 10 mM PBS buffer (pH 7.4). Once the baseline SPR response was stable, the target molecule was applied to the chip. In the case of the PPgMAMPC-modified SPR chip conjugated with biotin-$N_3$ (Scheme 1d), SA (0.1 mg/mL, equivalent to 1.9 $\mu$M) in blood plasma solution (0.1 mg/mL, 0.14% in PBS buffer) was applied to the surface and left for 15 min. Unbound SA was removed by washing with 10 mM PBS buffer (pH 7.4) for 5 min. The specific binding of SA was quantified from the shift in the SPR response angle at the end-point of the washing step and after baseline subtraction. Nonspecific binding (binding in the absence of SA in blood plasma solution) was also determined to quantify the specific binding of SA in blood plasma in terms of the $S/N$ ratio; this ratio was calculated using the following equation:

$$S/N = \frac{\text{SPR angle shift after exposure to blood plasma with streptavidin}}{\text{SPR angle shift after exposure to blood plasma without streptavidin}} \quad (1)$$

For the PPgMAMPC-modified SPR chip conjugated with a PNA-$N_3$ probe (Scheme 1e), DNA (50 $\mu$M) in 10 mM PBS (pH 7.4) containing 100 mM NaCl was applied to the surface and left for 15 min. Unbound DNA was removed by washing with PBS for 5 min. The specific binding of DNA was quantified from the shift in the SPR response angle at the end-point of the washing step and after baseline subtraction. The sensor was regenerated by washing with 50 mM NaOH for 5 min. The %HE and %MD were calculated using the following equations:

$$\%\text{HE} = \frac{\text{target density}}{\text{probe density}} \times 100 \quad (2)$$

$$\%\text{MD} = \frac{\%\text{HE of complementary DNA} - \%\text{HE of mismatched DNA}}{\%\text{HE of complementary DNA}} \times 100 \quad (3)$$

## RESULTS AND DISCUSSION

**Synthesis and Characterization of Thiol-Terminated Poly[(propargyl methacrylate)-*ran*-(2-methacryloyloxyethyl phosphorylcholine)] (PPgMAMPC-SH).** A PPgMAMPC copolymer was synthesized via RAFT polymerization using CPADB and ACVA as the chain transfer agent (CTA) and radical initiator (In), respectively. The molar percentage contents of PgMA and MPC units in the copolymer ($PPgMA_mMPC_n$) are denoted by $m$ and $n$, respectively. Our survey suggested that the optimum [CTA]/[In] ratio for obtaining a copolymer with a well-controlled molecular weight was 8; the data are shown in Table S1 in the Supporting Information. The control over the copolymerization process



DOI: 10.1021/acs.langmuir.5b02727
*Langmuir* 2016, 32, 1184–1194

was also demonstrated for a targeted degree of polymerization (DP) of 200 based on the linear first-order relationship between $\ln[M]_0/[M]$ and the polymerization time (Figure S2, Supporting Information), suggesting that the polymeric radical concentration remained unaltered throughout the polymerization. $^1$H NMR spectroscopy (Figure S3 and explanation in the Supporting Information) showed that the copolymer composition varied as a function of the monomer ratio in the feed (Table 1). The molecular weight of the copolymer was close to the target (35 375−46 327 kDa). We also attempted to determine the molecular weight and polydispersity indices (PDIs) of the copolymers using GPC. The data are shown in Figure S4 (Supporting Information). It should be emphasized that it is not possible to dissolve the copolymers in a common polar protic solvent (such as methanol) generally used for GPC analysis of MPC-based copolymers. And it was rather difficult to dissolve them in the mobile phase used for GPC analysis, phosphate buffer (pH 9) containing 10 vol % acetonitrile, especially the copolymer having high PgMA composition, $PPgMA_{65}MPC_{35}$, of which molecular weight information cannot be obtained. The fact that the $\bar{M}_n$ determined by GPC analysis are underestimated and proportionally decreased as a function of PgMA content suggested that the molecular weight information obtained via GPC analysis is somewhat not reliable. Additionally, PDI values were high, which may be ascribed to possible copolymer self-assembly in the phosphate buffer solution. This is why $^1$H NMR spectroscopy was used as the main tool for determining the molecular weight of the copolymer. Despite the relatively high PDI, the unimodal distribution evidenced from GPC chromatograms (also shown in Figure S4) is reasonable evidence of copolymer formation. The functional groups in the synthesized copolymer were identified using FTIR spectroscopy (Figure 1). The characteristic peaks for C═O (ester) stretching, at 1725 $cm^{-1}$, asymmetric O═P−O− stretching, at 1240 $cm^{-1}$, symmetric O═P−O− stretching, at 1087 $cm^{-1}$, and $-N^+(CH_3)_3$, at 960 $cm^{-1}$ for the MPC units were observed; a −C≡C− stretching peak was observed at 2127 $cm^{-1}$, and its intensity increased proportionally with the PgMA content. These results confirm copolymer formation.

**Table 1. Copolymer Compositions and Molecular Weights of PPgMAMPC (Target DP 200) Synthesized by RAFT Polymerization**

| monomer composition in feed (mol %) | | monomer composition in copolymer (mol %)[a] | | | | |
|---|---|---|---|---|---|---|
| PgMA | MPC | PgMA | MPC | $\bar{M}_n$[a] (kDa) | DP[a] | copolymer abbreviation |
| 70 | 30 | 65 | 35 | 38.4 | 208 | $PPgMA_{65}MPC_{35}$ |
| 50 | 50 | 45 | 55 | 46.7 | 213 | $PPgMA_{45}MPC_{55}$ |
| 30 | 70 | 38 | 62 | 40.0 | 173 | $PPgMA_{38}MPC_{62}$ |

[a]Calculated from $^1$H NMR data.

Aminolysis with hydrazine transformed the dithiobenzoate groups at the chain ends of the PPgMAMPC copolymer into thiol groups, yielding PPgMAMPC-SH,[48] as shown by the disappearance after aminolysis of the aromatic proton signals at 7.40−7.95 ppm in the $^1$H NMR spectrum and the UV−vis absorption peak at 305 nm (Figure S5, Supporting Information).

**Immobilization of PPgMAMPC-SH on Gold-Coated SPR Chip.** Unlike $PPgMA_{38}MPC_{62}$−SH and $PPgMA_{45}MPC_{55}$−SH, $PPgMA_{65}MPC_{35}$−SH, which has a higher content of the more hydrophobic PgMA unit, is not soluble in EtOH but dissolves in a mixture of EtOH and THF (7:3 v/v). Au−S bond formation between the gold layer of the SPR chip and the thiol-terminated copolymer (PPgMAMPC-SH) via a "grafting to" approach was performed at ambient temperature for 48 h. The presence of PPgMAMPC brushes on the SPR chip was confirmed using water contact angle

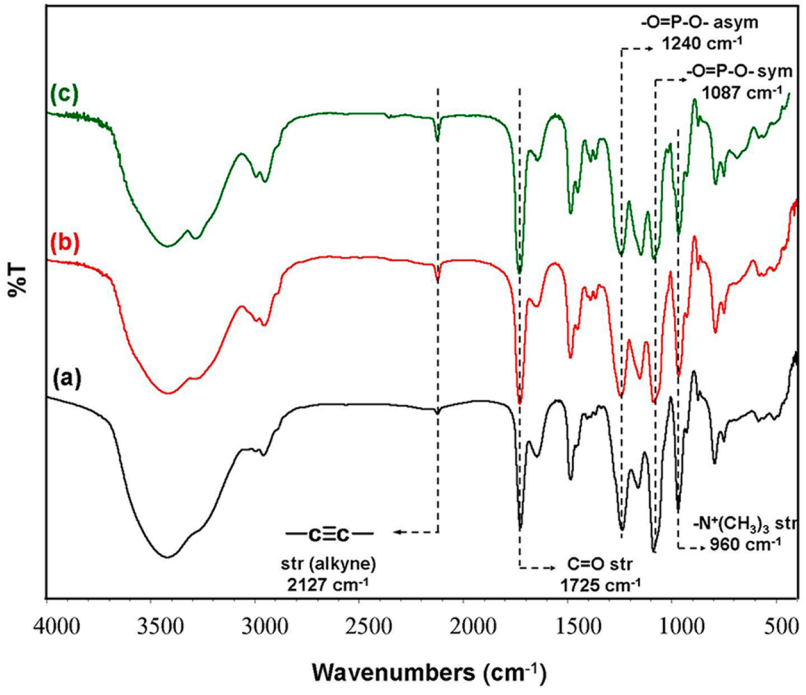


**Figure 1.** FTIR spectra of (a) $PPgMA_{38}MPC_{62}$ (40.0 kDa), (b) $PPgMA_{45}MPC_{55}$ (46.7 kDa), and (c) $PPgMA_{65}MPC_{35}$ (38.4 kDa).



DOI: 10.1021/acs.langmuir.5b02727
Langmuir 2016, 32, 1184−1194

measurements, and SPR, ATR-FTIR, and XPS analyses. The data in Table 2 show that the advancing ($\theta_A$) water contact angle of the SPR chip decreased from 71.9 ± 1.3° to 44.6 ± 0.9° and 46.6 ± 3.5° upon immobilization of $PPgMA_{38}MPC_{62}$–SH and $PPgMA_{45}MPC_{55}$–SH, respectively, indicating their highly hydrophilic characters. The copolymer with the highest content of hydrophobic PgMA, i.e., $PPgMA_{65}MPC_{35}$–SH, yielded a gold surface with a contact angle (87.9 ± 4.2°) higher than that of the pristine gold surface. Chemisorption of the copolymer brushes on the gold-coated SPR chip was monitored using an SPR technique. The SPR angle shift upon PPgMAMPC-SH immobilization was used to calculate the amount of copolymer bound to the surface, using a sensitivity factor of 120 mDegree, which is equivalent to 100 ng/cm$^2$ (Table 2).[49,50]

**Table 2. Water Contact Angle and SPR Data for Gold-Coated SPR Chips after PPgMAMPC-SH Immobilization and Subsequent Conjugation with Biotin-$N_3$**

| | | SPR data | |
|---|---|---|---|
| sample | advancing water contact angle (deg) | angle shift (mDegree) | amount adsorbed for each modification step (ng/cm$^2$) |
| Au | 71.9 ± 1.3 | - | - |
| Au–$PPgMA_{38}MPC_{62}$ | 44.6 ± 0.9 | 1024.8 ± 81.8 | 854.0 ± 68.1 |
| Au–$PPgMA_{45}MPC_{55}$ | 46.6 ± 3.5 | 882.1 ± 166.6 | 735.0 ± 138.9 |
| Au–$PPgMA_{65}MPC_{35}$ | 87.9 ± 4.2 | 1323.1 ± 56.1 | 1102.0 ± 46.8 |
| Au–$PPgMA_{38}MPC_{62}$–biotin | 32.7 ± 2.7 | 15.2 ± 7.4 | 12.7 ± 6.1 |
| Au–$PPgMA_{45}MPC_{55}$–biotin | 41.6 ± 1.3 | 229.5 ± 50.4 | 191.2 ± 42.0 |
| Au–$PPgMA_{65}MPC_{35}$–biotin | 62.2 ± 1.7 | 209.5 ± 6.7 | 174.5 ± 5.6 |

Figure S6 (Supporting Information) shows the XPS atomic spectra of the gold-coated substrate with immobilized $PPgMA_{45}MPC_{55}$–SH and the substrate before immobilization (bare gold). At a takeoff angle of 90°, phosphorus ($P_{2p}$) and nitrogen ($N_{1s}$) signals attributed to the phosphorylcholine group of the MPC units were observed on the substrate, indicating that the copolymer is bound to the gold-coated substrate. The $S_{2p}$ signal of the bound thiol, at a binding energy of 163 eV, was also detected, implying that the copolymer was strongly adsorbed on the substrate by interactions between the thiol groups of the copolymer and the gold surface. The characteristic absorption peaks of the MPC unit, i.e., C═O stretching (ester) at 1725 cm$^{-1}$, O═P–O–$_{asym}$ stretching at 1264 cm$^{-1}$, O═P–O–$_{sym}$ stretching at 1091 cm$^{-1}$, and $-N^+(CH_3)_3$ stretching at 968 cm$^{-1}$, were observed in the ATR-FTIR spectra (Figure S7, Supporting Information), but the characteristic absorption peak of the PgMA unit, i.e., –C≡C– stretching at 2127 cm$^{-1}$, was not clearly observed because of overlap with the characteristic peak of diamond (in the region 1500–2650 cm$^{-1}$), which is the reflectance material used for ATR-FTIR measurements. This signal from diamond dominates the other signals, particularly when the adsorbed material to be characterized is very thin, 1.89–3.12 nm in our case (estimated by ellipsometry).

Surface grafting of PPgMAMPC brushes on the gold-coated substrate was confirmed using AFM. The surface roughness before and after grafting with PPgMAMPC brushes were similar (1.5 vs 1.3 nm), suggesting that the gold surface was smooth and homogeneously covered with the copolymer. The thicknesses ($t$), measured using ellipsometry, of $PPgMA_{38}MPC_{62}$, $PPgMA_{45}MPC_{55}$, and $PPgMA_{65}MPC_{35}$ were 1.89 ± 0.12, 2.66 ± 0.26, and 3.12 ± 0.19 nm, respectively. The thickness can be used to calculate the graft density ($\sigma$) as follows:

$$\sigma = \frac{t\rho N_A}{M_n} \tag{4}$$

where $\rho$ is the mass density (1.1 g/cm$^3$ for $PPgMA_{65}MPC_{35}$ and 1.2 g/cm$^3$ for $PPgMA_{45}MPC_{55}$ and $PPgMA_{38}MPC_{62}$), $\bar{M}_n$ is the molecular weight of the free polymer, and $N_A$ is Avogadro's number. The copolymer mass densities were estimated proportionally using $\rho_{PMPC}$ = 1.3 g/cm$^3$[38] and $\rho_{PPgMA}$ = 1.085 g/cm$^3$, on the assumption that they are equal to that of poly(propyl methacrylate),[51] which has the same number of carbon atoms. For the copolymer synthesized with $\bar{M}_n$ in the range 38.4–46.7 kDa (DP 173-213), the calculated graft densities of surface-grafted $PPgMA_{38}MPC_{62}$, $PPgMA_{45}MPC_{55}$, and $PPgMA_{65}MPC_{35}$ were 0.04, 0.04, and 0.05 chain/nm$^2$, respectively. These values are below 0.08 chains/nm$^2$,[52] which suggests that the PPgMAMPC brushes can be categorized as being in the "mushroom regime."

**Biotin Conjugation on Copolymer-Modified SPR Chip by CuAAC Reaction and Subsequent Binding with Streptavidin.** Biotin was used as the first sensing probe model. It has a high binding affinity with SA (dissociation constant $K_D \approx 10^{-14}$ M).[53] Biotin-$N_3$ was immobilized on the PPgMAMPC-modified SPR chip outside the SPR instrument by CuAAC.[54,55] The data in Table 2 show that the water contact angles of the PPgMAMPC-modified SPR chip decreased after biotin attachment, indicating that the hydrophobic alkyne moieties from the PgMA repeat units were consumed and bound with biotin with three repeat units of the hydrophilic PEG spacer. The amounts of immobilized biotin increased significantly, from 12.7 ± 6.1 to 191.2 ± 42.0 ng/cm$^2$, when the PgMA content of the copolymer was increased from 38% to 45%. However, further increasing the PgMA composition to 65% reduced the quantity of bound probe, implying that biotin may have limited access to the alkyne moieties of copolymers with high PgMA contents, in which the swellability would be suppressed because of the inherent hydrophobicity. This is confirmed by the water contact angle (87.9 ± 4.2°) being much higher than those of the PPgMAMPC-modified SPR chips with PgMA contents of 38% and 45% (44.6 ± 0.9° and 46.6 ± 3.5°, respectively). As shown in Figure S6 in the Supporting Information, similar characteristic atomic spectra of the PPgMAMPC-modified SPR chips were observed after biotin and PNA immobilization but with much better signal, especially for $N_{1s}$, $S_{2p}$, $P_{2p}$ peaks in comparison with those before probe immobilization. A Cu peak appears in the Au–PPgMAMPC spectra after probe immobilization (both biotin and PNA), suggesting that Cu remained after the click reaction, although the surface was thoroughly rinsed with 10 mM EDTA and 10 mM PBS (pH 7.4). However, we believe that the Cu contamination should not affect the target molecule detection efficiency.



DOI: 10.1021/acs.langmuir.5b02727
Langmuir 2016, 32, 1184–1194

Nonspecific adsorption of the biotin-modified PPgMAMPC copolymer platform with different copolymer compositions on gold-coated SPR chips was investigated by comparison of adsorption of nontargeted proteins, bovine serum albumin (BSA; 69 kDa, pI = 4.8), LYZ (14 kDa, pI = 12), and 0.14% blood plasma (equivalent to 0.1 mg/mL of protein in PBS buffer, pH 7.4) with that of a targeted analyte, SA (60 kDa, pI = 5). BSA and LYZ were selected as model proteins with negative and positive charges, respectively, at pH 7.4 in PBS. Blood plasma is a complex biological-mimic medium comprising about 7% (70 mg of proteins per milliliter of plasma) of different proteins, e.g., fibrinogen, albumin, and globulin, and other components such as water, inorganic ions, and organic compounds.[56] As anticipated, the biotin-conjugated PPgMAMPC platform was specifically bound to the targeted SA (Figure 2). The bound content of SA increased with

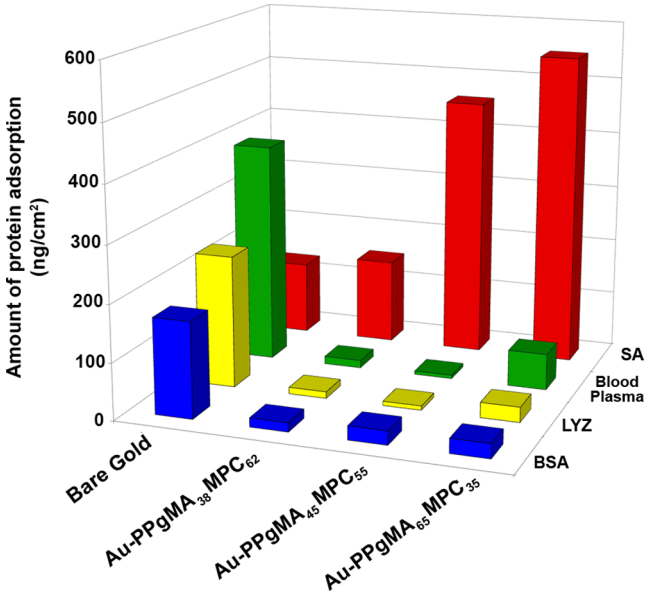


**Figure 2.** Protein adsorption on biotin-conjugated PPgMAMPC platforms with various copolymer compositions.

increasing PgMA content in the copolymer and increasing biotin content (Table 2). Nonspecific adsorption of the nontargeted proteins (BSA, LYZ, 0.14% blood plasma) was greatly suppressed on the biotin-conjugated PPgMAMPC platform compared with that on the bare gold surface. These results indicate that the MPC units in the PPgMAMPC copolymer are of paramount importance in suppressing nonspecific protein adsorption. This agrees well with reported studies of other MPC-containing (co)polymers.[14,34,37,57] Although the copolymer platform with the highest PgMA content, i.e., 65%, had the greatest bound SA content, it also gave the highest nonspecific adsorption of blood plasma.

In principle, the biotin/SA binding ratio should be 4 if all biotin molecules can be bound to SA. However, the biotin/SA binding ratios, listed in Figure 3, were much higher than the theoretical value, indicating that not all of the conjugated biotin molecules were bound to SA. The biotin/SA binding ratios were extremely high for the Au−PPgMAMPC platforms with high contents of hydrophobic PPgMA (45% and 65%). This may be because of the limited accessibility of SA, which is a large protein (MW = 60 kDa), to the immobilized biotin embedded inside the inner layer of the polymer brushes. Au−

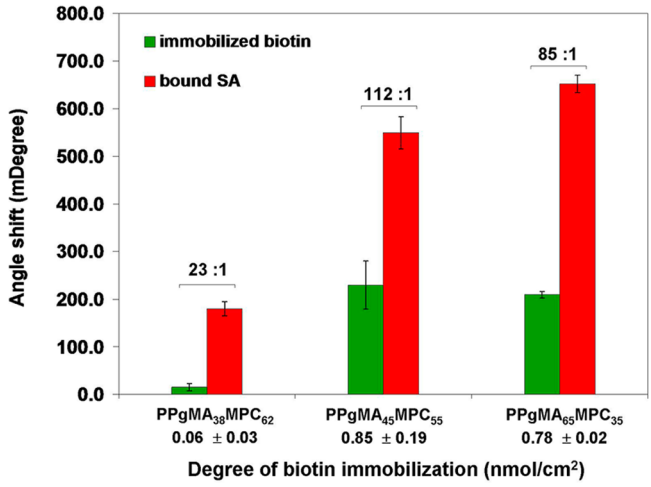


**Figure 3.** SPR angle shifts corresponding to the amounts of immobilized biotin, and subsequent SA (0.1 mg/mL) binding in PBS solution (10 mM, pH 7.4) on SPR chip modified with PPgMAMPC copolymers of various compositions. Biotin/SA binding ratio is shown on each set of bar charts.

$PPgMA_{38}MPC_{62}$ had the lowest immobilized biotin content, because it had the lowest content of PgMA, which provides active binding sites for biotin immobilization, and because its assembled layer on the gold-coated SPR chip was very thin (1.89 ± 0.12 nm). Although the amount of biotin bound on the Au−$PPgMA_{65}MPC_{35}$ platform (0.78 ± 0.02 nmol/cm$^2$) was lower than that on the $PPgMA_{45}MPC_{55}$ platform (0.85 ± 0.19 nmol/cm$^2$), it had a higher content of bound SA. To verify this contradictory outcome, we performed additional experiments to determine the nonspecific adsorption of SA (0.1 mg/mL SA in 10 mM PBS) on Au−$PPgMA_{45}MPC_{55}$ and Au−$PPgMA_{65}MPC_{35}$ before biotin immobilization, using an SPR technique. The data shown in Figure S8 in the Supporting Information indicate that nonspecific adsorption of SA on the Au−$PPgMA_{65}MPC_{35}$ platform was approximately 3 times higher than that on the $PPgMA_{45}MPC_{55}$ brushes. This helps to explain why the Au−$PPgMA_{65}MPC_{35}$ platform (with the highest PgMA content) bound the most SA, although it bound slightly less biotin than did the Au−$PPgMA_{45}MPC_{55}$ platform. SA can bind to the biotin-conjugated Au−PPgMAMPC platform not only by specific interactions with biotin probes but also by nonspecific interactions with the PgMA units of the copolymers.

The amount of SA adsorbed on the biotin-modified PPgMAMPC was low, particularly on the Au−$PPgMA_{38}MPC_{62}$−biotin platform. The adsorbed quantity of SA, 149.8 ± 12.3 ng/cm$^2$, was less than that in the SA monolayer adsorbed on a mixed monolayer containing 10% thiol-terminated biotin and 90% thiol-terminated ethylene glycol (379.7 ng/cm$^2$), as reported by Su et al.[50] This seems reasonable because the amount of biotin immobilized on the Au−$PPgMA_{38}MPC_{62}$ platform was lower than the amounts adsorbed on the platforms based on $PPgMA_{45}MPC_{55}$ and $PPgMA_{65}MPC_{35}$. Nevertheless, the amounts of SA adsorbed on Au−$PPgMA_{45}MPC_{55}$−biotin and Au−$PPgMA_{65}MPC_{35}$−biotin, i.e., 457.8 ± 28.6 and 549.5 ± 14.8 ng/cm$^2$, respectively, were well above that in the monolayer, suggesting three-dimensional character of the deposited copolymer in binding with the biotin probes.



DOI: 10.1021/acs.langmuir.5b02727
Langmuir 2016, 32, 1184−1194

The biotin-modified PPgMAMPC platforms with different copolymer compositions were further investigated to determine the lowest SA concentration detectable in a complex protein sample (blood plasma). The SA concentration was varied in the range 0.19−190 nM (equivalent to 0.01 to 0.1 mg/mL) in 0.14% blood plasma (0.1 mg/mL). Nonspecific binding with 0.14% blood plasma (in the absence of SA) was also measured to evaluate the sensor efficiency in terms of the $S/N$ ratio, as shown in Figure 4. The $S/N$ ratio can be calculated from eq 1.[8,14] The SPR angle shift obtained for the complex sample containing SA is considered to be the signal, whereas that obtained from the sample without SA, i.e., the target molecules, is considered to be background or noise. The results shown in Figure 4 indicate that the SPR chip modified with a copolymer platform containing 65% PgMA ($PPgMA_{65}MPC_{35}$−SH) showed the highest nonspecific binding with blood plasma in a control experiment (absence of SA in 0.14% blood plasma). This may be the result of nonspecific adsorption between the remaining alkyne moieties on the copolymer platform and nontargeted proteins in the blood plasma. The limits of detection (LODs) of the sensor platforms that can discriminate between target and nontargeted binding signals ($S/N \geq 3$) were 190, 0.95, and 190 nM for $PMA_{38}MPC_{62}$−SH, $PMA_{45}MPC_{55}$−SH, and $PMA_{65}MPC_{35}$−SH, respectively. These results suggest that the platform based on a copolymer containing 45% PgMA was the most efficient for detecting SA in blood plasma solution. The LOD of this $PPgMA_{45}MPC_{55}$ platform (0.95 nM) was even lower than that (1.5 nM) obtained for a platform based on poly[(methacrylic acid)-*ran*-(2-methacryloyloxyethyl phosphorylcholine)] (PMAMPC), previously developed by our group, and approximately 158 times lower than that of a platform based on a SAM of mercaptoundecanoic acid.[14] The fact that the PPgMAMPC sensor platform can directly immobilize an azide-containing biotin probe via a click reaction, without a functional group activation step, as required for the PMAMPC platform, makes it an attractive copolymer platform for probe binding in biosensing applications.

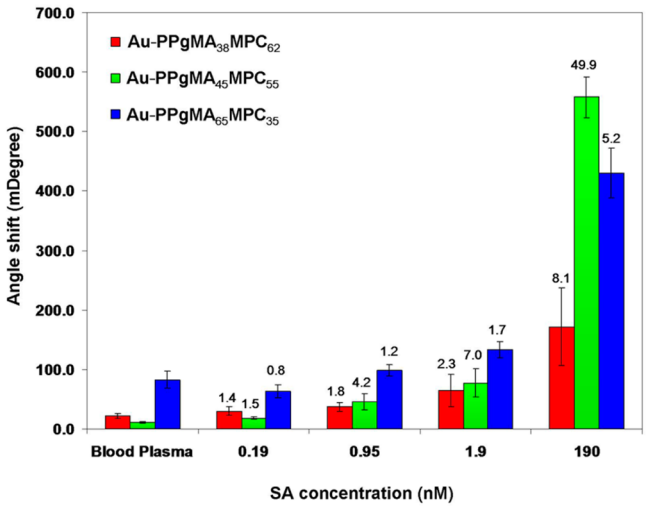


**Figure 4.** SPR angle shifts corresponding to SA binding on Au−PPgMAMPC−biotin platforms from SA solutions of various concentrations in 0.14% blood plasma. $S/N$ ratios are shown as the number above each bar graph.

The developed PPgMAMPC platforms with clickable PgMA units for probe binding and MPC antifouling units were also used to immobilize a PNA-$N_3$ probe to explore its applicability as a DNA sensor. PNA is a DNA mimic with a peptide-like backbone, first introduced by Nielsen and co-workers in 1991.[58] Because it is uncharged, PNA·DNA hybrids are more stable than DNA·DNA hybrids, because electrostatic repulsion between negatively charged phosphate groups in the DNA backbone are absent. This, together with its greater specificity for complementary DNA than mismatched DNA, makes PNA an attractive nucleotide probe with potential applications as a DNA sensor. In this study, a conformationally restricted pyrrolidinyl PNA with D-prolyl-2-aminocyclopentanecarboxylic acid backbones (*acpc*PNA), developed by Vilaivan and co-workers, was selected as a model nucleic acid probe. It has been reported that its binding affinity and sequence specificity toward DNA are higher than those of Nielsen's PNA.[46,59,60] We previously showed that *acpc*PNA can act as an effective probe for DNA detection when immobilized on a gold-coated SPR chip either by Au−S bond formation between thiolated PNA (PNA-SH) and the gold surface[61] or by biotin−SA−biotin linkage between biotinylated PNA (PNA−biotin) and an SA layer assembled on a biotin-functionalized gold substrate.[59] Besides blocking, which is a necessary step in most SAM-based sensors, the longer and greater hydrophilicity of the spacer between the PNA part and the thiol end of the thiolated PNA has a positive impact on the %HE of the platform developed by direct immobilization of thiolated PNA. Both %HE and %MD were significantly improved for the platform later developed by indirect PNA conjugation via biotin−SA−biotin linkage, which yielded PNA with a reasonably well-controlled density and orientation (see Table 3 for comparison). The results of these two studies suggest that the clickable and antifouling PPgMAMPC platforms developed in the current study should meet all the above-mentioned criteria for developing an effective PNA-based sensor for DNA detection. Anchoring the copolymer to the gold surface prior to PNA binding should provide a reasonable distance between the immobilized PNA probes and the gold substrate, and allow the PNA molecules to interact freely with the incoming DNA targets. PMPC provides a hydrophilic environment for the platform so that nonspecific adsorption of nontargeted DNA can be suppressed. It is anticipated that good control of the content of clickable PgMA units in the copolymer will enable the density of immobilized PNA to be tailored using efficient CuAAC-based reactions.

**Table 3. Values of $\%HE_{com}$ and %MD for DNA Detection by Surface-Modified Gold-Coated SPR Chips Conjugated with PNA**

| sample | $\%HE_{com}$ | %MD |
|---|---|---|
| Au−$PPgMA_{38}MPC_{62}$−PNA | 20 | 32 |
| Au−$PPgMA_{45}MPC_{55}$−PNA | 61 | 52 |
| Au−$PPgMA_{65}MPC_{35}$−PNA | 71 | 58 |
| Au−S−PNA[61] | 20 | > 54 |
| Au−biotin−SA−biotin−PNA[59] | 58 | > 90 |

In this work, azide-terminated PNA with a $T_9$ sequence (PNA-$N_3$), selected as a PNA probe model, was immobilized by the alkyne moieties of sensing platforms with various copolymer compositions, i.e., $PPgMA_{38}MPC_{62}$−SH, $PPgMA_{45}MPC_{55}$−SH, and $PPgMA_{65}MPC_{35}$−SH, via CuAAC reactions. Specific binding of 50 $\mu$M DNA in 10 mM PBS was


DOI: 10.1021/acs.langmuir.5b02727
*Langmuir* 2016, 32, 1184−1194

monitored using an SPR technique. The %HE and %MD were calculated using eqs 2 and 3, respectively, to evaluate the efficiency of the sensor. As shown in Figure 5, the sensing

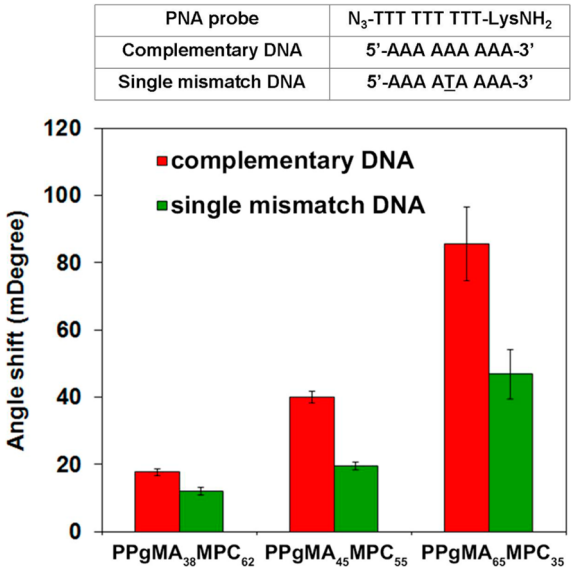


**Figure 5.** SPR angle shifts corresponding to DNA binding to Au–PPgMAMPC–PNA platforms in 10 mM PBS.

platform based on Au–$PPgMA_{65}MPC_{35}$–PNA, which had the highest amount of PgMA units, gave the greatest detectable signal, corresponding to binding of the complementary DNA sequence, $A_9$ (85.5 ± 10.9 mdeg), with a %HE of 71%, which is higher than those for sensing platforms based on Au–S–PNA[61] and Au–biotin–PNA,[59] as shown in Table 3. However, this copolymer platform still showed high nonspecific interactions toward a single mismatched DNA sequence (AAAATAAAA), therefore its %MD was not satisfactorily high compared with that for a platform based on Au–biotin–SA–biotin–PNA. Despite this limitation, a %HE as high as 71% may be suitable for other DNA-based applications, such as affinity-based DNA separation, in which the mismatch discrimination efficiency is not a critical issue. There is also room for improvement in terms of %MD. For example, possible nonspecific interactions between the remaining unreacted alkyne moieties of PgMA and mismatched DNA may be decreased by blocking the unreacted PgMA with hydrophilic molecules, enabling %HE of mismatched DNA to be minimized. Stable triazole linkages between the PNA probe and the sensing platform should have the additional advantage of being more robust to the regeneration conditions than Au–S or Au–biotin–SA–biotin linkages. This should enable probe recycling, making the process economically viable.

## CONCLUSIONS

Clickable and antifouling PPgMAMPC copolymer platforms were successfully synthesized by RAFT polymerization. The dithioester end groups of the copolymer were converted to thiol groups before surface immobilization on a gold-coated SPR chip via a "grafting to" approach. The alkyne moieties of PgMA bound azide-containing molecules (biotin-$N_3$ and PNA-$N_3$) via a CuAAC reaction, and the hydrophilic monomeric MPC unit suppressed nonspecific adsorption of nontargeted analytes, namely BSA, LYZ, and blood plasma. Specific detection of SA by biotin probes conjugated with the PPgMAMPC platforms in 0.14% blood plasma was investigated using an SPR technique. Among all the platforms investigated, copolymer brushes of $PPgMA_{45}MPC_{55}$ performed best, giving the lowest detection limit, i.e., 0.95 nM. The potential of the surface-attached PPgMAMPC as a sensing layer for DNA detection was investigated by conjugating a PNA-$N_3$ probe with PPgMAMPC platforms with various copolymer compositions. The sensor platform based on Au–$PPgMA_{65}MPC_{35}$–PNA detected the highest amount of complementary DNA sequence, with 71%HE, and a reasonable degree of mismatch discrimination (58%MD) between the fully complementary DNA and single-mismatched DNA. These results suggest that substrate-modified PPgMAMPC brushes are potential copolymer platforms for azide-containing probe immobilization for detecting target molecules in diagnostic and related applications. Both types of probe functioned effectively, which shows the versatility of the developed platform, and suggests that it can be used for both antibody-based and DNA-based biosensors.

## ASSOCIATED CONTENT

### Supporting Information

The Supporting Information is available free of charge on the ACS Publications website at DOI: 10.1021/acs.langmuir.5b02727.

HPLC chromatogram and MALDI-TOF MS spectrum of PNA, data and calculations related to RAFT polymerization (% conversion, MW, PDIs, GPC chromatograms, and copolymer composition), $^1$H NMR and UV–vis spectra of copolymer, XPS and ATR-FTIR for copolymer brushes grafted on gold-coated SPR chips, and amounts of SA adsorbed on PPgMAMPC platforms (PDF)

## AUTHOR INFORMATION

### Corresponding Author

* Tel.: +66-2218-7627; fax: +66-2218-7598; E-mail address: vipavee.p@chula.ac.th.

### Notes

The authors declare no competing financial interest.

## ACKNOWLEDGMENTS

This work was financially supported by a Directed Basic Research Grant by the Thailand Research Fund (DBG5580003), a Distinguished Research Professor Grant by the Thailand Research Fund and Chulalongkorn University (DPG5780002), the Ratchadaphiseksomphot Endowment Fund of Chulalongkorn University (RES560530126-AM), and the Thai Government Stimulus Package 2 (TKK2555), under the Project for Establishment of a Comprehensive Center for Innovative Food, Health Products, and Agriculture. O.W. acknowledges receipt of an academic scholarship from Chulalongkorn University Dutsadiphiphat Scholarship for her Ph.D. study. The authors are grateful to Professor Shin-ichi Yusa and Mr. Keita Nakai from the Graduate School of Engineering, University of Hyogo, Japan, for their assistance in GPC analysis.

## REFERENCES

(1) Nakamura, F.; Ito, E.; Hayashi, T.; Hara, M. Fabrication of COOH-Terminated Self-Assembled Monolayers for DNA Sensors. *Colloids Surf., A* **2006**, *284–285*, 495–498.



DOI: 10.1021/acs.langmuir.5b02727
*Langmuir* 2016, 32, 1184–1194

(2) Senaratne, W.; Andruzzi, L.; Ober, C. K. Self-Assembled Monolayers and Polymer Brushes in Biotechnology: Current Applications and Future Perspectives. *Biomacromolecules* **2005**, *6* (5), 2427−48.
(3) Su, X. L.; Li, Y. A Self-Assembled Monolayer-Based Piezoelectric Immunosensor for Rapid Detection of *Escherichia coli* O157:H7. *Biosens. Bioelectron.* **2004**, *19* (6), 563−574.
(4) Akkahat, P.; Hoven, V. P. Introducing Surface-Tethered Poly(acrylic acid) Brushes as 3D Functional Thin Film for Biosensing Applications. *Colloids Surf., B* **2011**, *86* (1), 198−205.
(5) Akkahat, P.; Mekboonsonglarp, W.; Kiatkamjornwong, S.; Hoven, V. P. Surface-Grafted Poly(acrylic acid) Brushes as a Precursor Layer for Biosensing Applications: Effect of Graft Density and Swellability on the Detection Efficiency. *Langmuir* **2012**, *28* (11), 5302−5311.
(6) Henry, O. Y.; Mehdi, A. D.; Kirwan, S.; Sanchez, J. L.; O'Sullivan, C. K. Three-Dimensional Arrangement of Short DNA Oligonucleotides at Surfaces via the Synthesis of DNA-Branched Polyacrylamide Brushes by SI-ATRP. *Macromol. Rapid Commun.* **2011**, *32* (18), 1405−1410.
(7) Kurosawa, S.; Aizawa, H.; Talib, Z. A.; Atthoff, B.; Hilborn, J. Synthesis of Tethered-Polymer Brush by Atom Transfer Radical Polymerization from a Plasma-Polymerized-Film-Coated Quartz Crystal Microbalance and Its Application for Immunosensors. *Biosens. Bioelectron.* **2004**, *20* (6), 1165−1176.
(8) Lee, B. S.; Chi, Y. S.; Lee, K.-B.; Kim, Y.-G.; Choi, I. S. Functionalization of Poly(oligo(ethylene glycol) methacrylate) Films on Gold and Si/$SiO_2$ for Immobilization of Proteins and Cells: SPR and QCM Studies. *Biomacromolecules* **2007**, *8* (12), 3922−3929.
(9) Yang, N.; Su, X.; Tjong, V.; Knoll, W. Evaluation of Two- and Three-Dimensional Streptavidin Binding Platforms for Surface Plasmon Resonance Spectroscopy Studies of DNA Hybridization and Protein-DNA Binding. *Biosens. Bioelectron.* **2007**, *22* (11), 2700−2706.
(10) Jeong, S. P.; Lee, B. S.; Kang, S. M.; Ko, S.; Choi, I. S.; Lee, J. K. Binding Behaviors of Protein on Spatially Controlled Poly[oligo-(ethylene glycol) methacrylate] Brushes Grafted from Mixed Self-Assembled Monolayers on Gold. *Chem. Commun.* **2014**, *50* (40), 5291−5293.
(11) Trmcic-Cvitas, J.; Hasan, E.; Ramstedt, M.; Li, X.; Cooper, M. A.; Abell, C.; Huck, W. T. S.; Gautrot, J. E. Biofunctionalized Protein Resistant Oligo(ethylene glycol)-Derived Polymer Brushes as Selective Immobilization and Sensing Platforms. *Biomacromolecules* **2009**, *10* (10), 2885−2894.
(12) Gam-Derouich, S.; Lamouri, A.; Redeuilh, C.; Decorse, P.; Maurel, F.; Carbonnier, B.; Beyazit, S.; Yilmaz, G.; Yagci, Y.; Chehimi, M. M. Diazonium Salt-Derived 4-(Dimethylamino)phenyl Groups as Hydrogen Donors in Surface-Confined Radical Photopolymerization for Bioactive Poly(2-hydroxyethyl methacrylate) Grafts. *Langmuir* **2012**, *28* (21), 8035−8045.
(13) Vaisocherova, H.; Sevcu, V.; Adam, P.; Spac kova, B.; Hegnerova, K.; de los Santos Pereira, A.; Rodriguez-Emmenegger, C.; Riedel, T.; Houska, M.; Brynda, E.; Homola, J. Functionalized Ultra-Low Fouling Carboxy- and Hydroxy-Functional Surface Platforms: Functionalization Capacity, Biorecognition Capability and Resistance to Fouling from Undiluted Biological Media. *Biosens. Bioelectron.* **2014**, *51*, 150−157.
(14) Akkahat, P.; Kiatkamjornwong, S.; Yusa, S.-i.; Hoven, V. P.; Iwasaki, Y. Development of a Novel Antifouling Platform for Biosensing Probe Immobilization from Methacryloyloxyethyl Phosphorylcholine-Containing Copolymer Brushes. *Langmuir* **2012**, *28* (13), 5872−5881.
(15) Audouin, F.; Larragy, R.; Fox, M.; O'Connor, B.; Heise, A. Protein Immobilization onto Poly(acrylic acid) Functional Macroporous PolyHIPE Obtained by Surface-Initiated ARGET ATRP. *Biomacromolecules* **2012**, *13* (11), 3787−3794.
(16) Cullen, S. P.; Liu, X.; Mandel, I. C.; Himpsel, F. J.; Gopalan, P. Polymeric Brushes as Functional Templates for Immobilizing Ribonuclease A: Study of Binding Kinetics and Activity. *Langmuir* **2008**, *24* (3), 913−920.
(17) Dai, J. H.; Bao, Z. Y.; Sun, L.; Hong, S. U.; Baker, G. L.; Bruening, M. L. High-Capacity Binding of Proteins by Poly(acrylic acid) Brushes and Their Derivatives. *Langmuir* **2006**, *22* (9), 4274−4281.
(18) Qu, Z.; Chen, K.; Gu, H.; Xu, H. Covalent Immobilization of Proteins on 3D Poly(acrylic acid) Brushes: Mechanism Study and a More Effective and Controllable Process. *Bioconjugate Chem.* **2014**, *25* (2), 370−378.
(19) Thilakarathne, V.; Briand, V. A.; Zhou, Y.; Kasi, R. M.; Kumar, C. V. Protein Polymer Conjugates: Improving the Stability of Hemoglobin with Poly(acrylic acid). *Langmuir* **2011**, *27* (12), 7663−7671.
(20) Baek, M.-G.; Roy, R. Relative Lectin Binding Properties of T-Antigen-Containing Glycopolymers: Copolymerization of *N*-Acryloylated T-Antigen Monomer vs. Graft Conjugation of Aminated T-Antigen Ligands onto Poly(*N*-acryloxysuccinimide). *Macromol. Biosci.* **2001**, *1* (7), 305−311.
(21) Chen, J.-P.; Chiu, S.-H. A Poly(*N*-isopropylacrylamide-*co*-*N*-acryloxysuccinimide-*co*-2-hydroxyethyl methacrylate) Composite Hydrogel Membrane for Urease Immobilization to Enhance Urea Hydrolysis Rate by Temperature Swing. *Enzyme Microb. Technol.* **2000**, *26* (56), 359−367.
(22) Minard-Basquin, C.; Chaix, C.; D'Agosto, F.; Charreyre, M.-T.; Pichot, C. Oligonucleotide Synthesis onto Poly(*N*-acryloylmorpholine-*co*-*N*-acryloxysuccinimide): Assessment of The Resulting Conjugates in a DNA Sandwich Hybridization Test. *J. Appl. Polym. Sci.* **2004**, *92* (6), 3784−3795.
(23) Duque, L.; Menges, B.; Borros, S.; Forch, R. Immobilization of Biomolecules to Plasma Polymerized Pentafluorophenyl Methacrylate. *Biomacromolecules* **2010**, *11* (10), 2818−2823.
(24) McRae, S.; Chen, X.; Kratz, K.; Samanta, D.; Henchey, E.; Schneider, S.; Emrick, T. Pentafluorophenyl Ester-Functionalized Phosphorylcholine Polymers: Preparation of Linear, Two-Arm, and Grafted Polymer-Protein Conjugates. *Biomacromolecules* **2012**, *13* (7), 2099−2109.
(25) Socaci, C.; Rybka, M.; Magerusan, L.; Nan, A.; Turcu, R.; Liebscher, J. Magnetite Nanoparticles Coated with Alkyne-Containing Polyacrylates for Click Chemistry. *J. Nanopart. Res.* **2013**, *15* (6), 1747.
(26) Wang, C.; Fan, Y.; Hu, M. X.; Xu, W.; Wu, J.; Ren, P. F.; Xu, Z. K. Glycosylation of the Polypropylene Membrane Surface via Thiol-Yne Click Chemistry for Lectin Adsorption. *Colloids Surf., B* **2013**, *110*, 105−112.
(27) Liu, Y.; Li, C. M.; Hu, W.; Lu, Z. High Performance Protein Microarrays Based on Glycidyl Methacrylate-Modified Polyethylene Terephthalate Plastic Substrate. *Talanta* **2009**, *77* (3), 1165−1171.
(28) Xiu, K. M.; Cai, Q.; Li, J. S.; Yang, X. P.; Yang, W. T.; Xu, F. J. Anti-Fouling Surfaces by Combined Molecular Self-Assembly and Surface-Initiated ATRP for Micropatterning Active Proteins. *Colloids Surf., B* **2012**, *90*, 177−183.
(29) Chang, Y.; Shu, S.-H.; Shih, Y.-J.; Chu, C.-W.; Ruaan, R.-C.; Chen, W.-Y. Hemocompatible Mixed-Charge Copolymer Brushes of Pseudozwitterionic Surfaces Resistant to Nonspecific Plasma Protein Fouling. *Langmuir* **2010**, *26* (5), 3522−3530.
(30) Rodriguez Emmenegger, C.; Brynda, E.; Riedel, T.; Sedlakova, Z.; Houska, M.; Alles, A. B. Interaction of Blood Plasma with Antifouling Surfaces. *Langmuir* **2009**, *25* (11), 6328−6333.
(31) Zhang, Z.; Zhang, M.; Chen, S.; Horbett, T. A.; Ratner, B. D.; Jiang, S. Blood Compatibility of Surfaces with Superlow Protein Adsorption. *Biomaterials* **2008**, *29* (32), 4285−4291.
(32) Fuchs, A. V.; Ritz, S.; Putz, S.; Mailander, V.; Landfester, K.; Ziener, U. Bioinspired Phosphorylcholine Containing Polymer Films with Silver Nanoparticles Combining Antifouling and Antibacterial Properties. *Biomater. Sci.* **2013**, *1* (5), 470−477.
(33) Fuchs, A. V.; Walter, C.; Landfester, K.; Ziener, U. Biomimetic Silver-Containing Colloids of Poly(2-methacryloyloxyethyl phosphorylcholine) and Their Film-Formation Properties. *Langmuir* **2012**, *28* (11), 4974−4983.


DOI: 10.1021/acs.langmuir.5b02727
*Langmuir* 2016, 32, 1184−1194

(34) Ishihara, K.; Nomura, H.; Mihara, T.; Kurita, K.; Iwasaki, Y.; Nakabayashi, N. Why do Phospholipid Polymers Reduce Protein Adsorption? *J. Biomed. Mater. Res.* **1998**, *39* (2), 323−330.
(35) Ishihara, K.; Ueda, T.; Nakabayashi, N. Preparation of Phospholipid Polymers and Their Properties as Polymer Hydrogel Membranes. *Polym. J.* **1990**, *22* (5), 355−360.
(36) Iwasaki, Y.; Fujke, A.; Kurita, K.; Ishihara, K.; Nakabayashi, N. Protein Adsorption and Platelet Adhesion on Polymer Surfaces Having Phospholipid Polar Group Connected with Oxyethylene Chain. *J. Biomater. Sci., Polym. Ed.* **1997**, *8* (2), 91−102.
(37) Ishihara, K.; Oshida, H.; Endo, Y.; Ueda, T.; Watanabe, A.; Nakabayashi, N. Hemocompatibility of Human Whole Blood on Polymers with a Phospholipid Polar Group and Its Mechanism. *J. Biomed. Mater. Res.* **1992**, *26* (12), 1543−1552.
(38) Iwata, R.; Suk-In, P.; Hoven, V. P.; Takahara, A.; Akiyoshi, K.; Iwasaki, Y. Control of Nanobiointerfaces Generated from Well-Defined Biomimetic Polymer Brushes for Protein and Cell Manipulations. *Biomacromolecules* **2004**, *5* (6), 2308−2314.
(39) Park, J.; Kurosawa, S.; Takai, M.; Ishihara, K. Antibody Immobilization to Phospholipid Polymer Layer on Gold Substrate of Quartz Crystal Microbalance Immunosensor. *Colloids Surf., B* **2007**, *55* (2), 164−172.
(40) Goto, Y.; Matsuno, R.; Konno, T.; Takai, M.; Ishihara, K. Polymer Nanoparticles Covered with Phosphorylcholine Groups and Immobilized with Antibody for High-Affinity Separation of Proteins. *Biomacromolecules* **2008**, *9* (3), 828−833.
(41) Mark, S. S.; Nishizawa, K.; Takai, M.; Ishihara, K. A Bioconjugated Phospholipid Polymer Biointerface with Nanometer-Scaled Structure for Highly Sensitive Immunoassays. In *Bioconjugation Protocols*; Mark, S. S., Ed. Humana Press: New York, 2011; Vol. *751*, pp 491−502.
(42) Nishizawa, K.; Konno, T.; Takai, M.; Ishihara, K. Bioconjugated Phospholipid Polymer Biointerface for Enzyme-Linked Immunosorbent Assay. *Biomacromolecules* **2008**, *9* (1), 403−407.
(43) Sakai-Kato, K.; Kato, M.; Ishihara, K.; Toyo'oka, T. An Enzyme-Immobilization Method for Integration of Biofunctions on a Microchip Using a Water-Soluble Amphiphilic Phospholipid Polymer Having a Reacting Group. *Lab Chip* **2004**, *4* (1), 4−6.
(44) Iwata, R.; Satoh, R.; Iwasaki, Y.; Akiyoshi, K. Covalent Immobilization of Antibody Fragments on Well-Defined Polymer Brushes via Site-Directed Method. *Colloids Surf., B* **2008**, *62* (2), 288−298.
(45) He, H.; Zhang, Y.; Gao, C.; Wu, J. 'Clicked' Magnetic Nanohybrids with a Soft Polymer Interlayer. *Chem. Commun.* **2009**, *13*, 1655−1657.
(46) Vilaivan, T.; Srisuwannaket, C. Hybridization of Pyrrolidinyl Peptide Nucleic Acids and DNA: Selectivity, Base-Pairing Specificity, and Direction of Binding. *Org. Lett.* **2006**, *8* (9), 1897−1900.
(47) Ditmangklo, B.; Boonlua, C.; Suparpprom, C.; Vilaivan, T. Reductive Alkylation and Sequential Reductive Alkylation-Click Chemistry for On-Solid-Support Modification of Pyrrolidinyl Peptide Nucleic Acid. *Bioconjugate Chem.* **2013**, *24* (4), 614−625.
(48) Shen, W.; Qiu, Q.; Wang, Y.; Miao, M.; Li, B.; Zhang, T.; Cao, A.; An, Z. Hydrazine as a Nucleophile and Antioxidant for Fast Aminolysis of RAFT Polymers in Air. *Macromol. Rapid Commun.* **2010**, *31* (16), 1444−1448.
(49) Metallo, S. J.; Kane, R. S.; Holmlin, R. E.; Whitesides, G. M. Using Bifunctional Polymers Presenting Vancomycin and Fluorescein Groups to Direct Anti-Fluorescein Antibodies to Self-Assembled Monolayers Presenting d-Alanine-d-Alanine Groups. *J. Am. Chem. Soc.* **2003**, *125* (15), 4534−4540.
(50) Su, X.; Wu, Y.-J.; Knoll, W. Comparison of Surface Plasmon Resonance Spectroscopy and Quartz Crystal Microbalance Techniques for Studying DNA Assembly and Hybridization. *Biosens. Bioelectron.* **2005**, *21* (5), 719−726.
(51) Ellis, B.; Smith, R. *Polymers: A Property Database*, 2nd ed.; Taylor & Francis Group: Boca Raton, FL, 2008.
(52) Wu, T.; Gong, P.; Szleifer, I.; Vlcek, P.; Subr, V.; Genzer, J. Behavior of Surface-Anchored Poly(acrylic acid) Brushes with Grafting Density Gradients on Solid Substrates:1. Experiment. *Macromolecules* **2007**, *40* (24), 8756−8764.
(53) Green, N. M. Avidin. *Adv. Protein Chem.* **1975**, *29*, 85−133.
(54) Huisgen, R. 1,3-Dipolar cycloadditions. Past and future. *Angew. Chem., Int. Ed. Engl.* **1963**, *2* (10), 565−598.
(55) Tornoe, C. W.; Christensen, C.; Meldal, M. Peptidotriazoles on Solid phase: [1,2,3]-Triazoles by Regiospecific Copper(I)-Catalyzed 1,3-Dipolar Cycloadditions of Terminal Alkynes to Azides. *J. Org. Chem.* **2002**, *67* (9), 3057−3064.
(56) Hansen, J. T. *Netter's Clinical Anatomy*, 3rd ed.; Elsevier, Inc: Philadelphia, PA, 2014.
(57) Kim, G.; Park, S.; Jung, J.; Heo, K.; Yoon, J.; Kim, H.; Kim, I. J.; Kim, J. R.; Lee, J. I.; Ree, M. Novel Brush Polymers with Phosphorylcholine Bristle Ends: Synthesis, Structure, Properties, and Biocompatibility. *Adv. Funct. Mater.* **2009**, *19* (10), 1631−1644.
(58) Nielsen, P.; Egholm, M.; Berg, R.; Buchardt, O. Sequence-Selective Recognition of DNA by Strand Displacement with a Thymine-Substituted Polyamide. *Science* **1991**, *254* (5037), 1497−1500.
(59) Ananthanawat, C.; Vilaivan, T.; Hoven, V. P.; Su, X. Comparison of DNA, Aminoethylglycyl PNA and Pyrrolidinyl PNA as Probes for Detection of DNA Hybridization Using Surface Plasmon Resonance Technique. *Biosens. Bioelectron.* **2010**, *25* (5), 1064−1069.
(60) Suparpprom, C.; Srisuwannaket, C.; Sangvanich, P.; Vilaivan, T. Synthesis and Oligodeoxynucleotide Binding Properties of Pyrrolidinyl Peptide Nucleic Acids Bearing Prolyl-2-Aminocyclopentanecarboxylic Acid (ACPC) Backbones. *Tetrahedron Lett.* **2005**, *46* (16), 2833−2837.
(61) Ananthanawat, C.; Vilaivan, T.; Mekboonsonglarp, W.; Hoven, V. P. Thiolated Pyrrolidinyl Peptide Nucleic Acids for the Detection of DNA Hybridization Using Surface Plasmon Resonance. *Biosens. Bioelectron.* **2009**, *24* (12), 3544−3549.


DOI: 10.1021/acs.langmuir.5b02727
*Langmuir* 2016, 32, 1184−1194

**คำขอรับสิทธิบัตร/อนุสิทธิบัตร**

☑ การประดิษฐ์
☐ การออกแบบผลิตภัณฑ์
☐ อนุสิทธิบัตร

ข้าพเจ้าผู้ลงลายมือชื่อในคำขอรับสิทธิบัตร/อนุสิทธิบัตรนี้ ขอรับสิทธิบัตร/อนุสิทธิบัตร ตามพระราชบัญญัติสิทธิบัตร พ.ศ. 2522 แก้ไขเพิ่มเติมโดยพระราชบัญญัติสิทธิบัตร (ฉบับที่ 2) พ.ศ 2535 และพระราชบัญญัติสิทธิบัตร (ฉบับที่ 3) พ.ศ 2542

| สำหรับเจ้าหน้าที่ | |
|---|---|
| วันรับคำขอ -4 ก.พ. 2558 | เลขที่คำขอ 1501000575 |
| วันยื่นคำขอ -4 ก.พ. 2558 | |
| สัญลักษณ์จำแนกการประดิษฐ์ระหว่างประเทศ | |
| ใช้กับแบบผลิตภัณฑ์ ประเภทผลิตภัณฑ์ | |
| วันประกาศโฆษณา | เลขที่ประกาศโฆษณา |
| วันออกสิทธิบัตร/อนุสิทธิบัตร | เลขที่สิทธิบัตร/อนุสิทธิบัตร |
| ลายมือชื่อเจ้าหน้าที่ | |

1.ชื่อที่แสดงถึงการประดิษฐ์/~~การออกแบบผลิตภัณฑ์~~

แผ่นกระจกตรึงด้วยพอลิแอคริลิกแอซิดบรัชที่มีอนุภาคนาโนทองเป็นองค์ประกอบในลักษณะเฟทเทิร์น สำหรับใช้ในการแยกและวิเคราะห์เพปไทด์ กรรมวิธีการผลิตและวิธีการวิเคราะห์

2.คำขอรับสิทธิบัตรการออกแบบผลิตภัณฑ์นี้เป็นคำขอสำหรับแบบผลิตภัณฑ์อย่างเดียวกันและเป็นคำขอลำดับที่
ในจำนวน คำขอ ที่ยื่นในครั้งเดียวกัน



| | |
|---|---|
| 3.ผู้ขอรับสิทธิบัตร/อนุสิทธิบัตร และที่อยู่ (เลขที่ ถนน ประเทศ) ดูที่หน้า 3 | 3.1 สัญชาติ |
| | 3.2 โทรศัพท์ |
| | 3.3 โทรสาร |
| | 3.4 อีเมล์ |
| 4.สิทธิในการขอรับสิทธิบัตร/~~อนุสิทธิบัตร~~ ☐ ผู้ประดิษฐ์/ผู้ออกแบบ ☑ ผู้รับโอน ☐ ผู้ขอรับสิทธิโดยเหตุอื่น | |
| 5.ตัวแทน(ถ้ามี)/ที่อยู่ (เลขที่ ถนน จังหวัด รหัสไปรษณีย์) นายบัญชา วงศ์ณัฐภัทร สถาบันทรัพย์สินทางปัญญาแห่งจุฬาลงกรณ์มหาวิทยาลัย อาคารจัตุรัสจามจุรี ชั้น 12 ยูนิต 13 ถนนพญาไท แขวงปทุมวัน เขตปทุมวัน กรุงเทพฯ 10330 | 5.1 ตัวแทนเลขที่ 2392 |
| | 5.2 โทรศัพท์ 0-2160-5340-2 |
| | 5.3 โทรสาร 0-2160-5343 |
| | 5.4 อีเมล์ |
| 6.ผู้ประดิษฐ์/ผู้~~ออกแบบผลิตภัณฑ์~~ และที่อยู่ ( เลขที่ ถนน ประเทศ ) ดูที่หน้า 3 | |

7. คำขอรับสิทธิบัตร/อนุสิทธิบัตรนี้แยกจากหรือเกี่ยวข้องกับคำขอเดิม

ผู้ขอรับสิทธิบัตร/อนุสิทธิบัตร ขอให้ถือว่าได้ยื่นคำขอรับสิทธิบัตร/อนุสิทธิบัตรนี้ ในวันเดียวกับคำขอรับสิทธิบัตร เลขที่ วันยื่น เพราะคำขอรับสิทธิบัตร/อนุสิทธิบัตรนี้แยกจากหรือเกี่ยวข้องกับคำขอเดิมเพราะ

☐ คำขอเดิมมีการประดิษฐ์หลายอย่าง ☐ ถูกคัดค้านเนื่องจากผู้ขอไม่มีสิทธิ ☐ ขอเปลี่ยนแปลงประเภทของสิทธิ

**หมายเหตุ** ในกรณีที่ไม่อาจระบุรายละเอียดได้ครบถ้วน ให้จัดทำเป็นเอกสารแนบท้ายแบบพิมพ์นี้โดยระบุหมายเลขกำกับข้อและหัวข้อที่แสดงรายละเอียดเพิ่มเติมดังกล่าวด้วย

8.การยื่นคำขอนอกราชอาณาจักร

| วันยื่นคำขอ | เลขที่คำขอ | ประเทศ | สัญลักษณ์จำแนกการประดิษฐ์ระหว่างประเทศ | สถานะคำขอ |
|---|---|---|---|---|
| 8.1 | | | | |
| 8.2 | | | | |
| 8.3 | | | | |

8.4 ☐ ผู้ขอรับสิทธิบัตร/อนุสิทธิบัตรขอสิทธิให้ถือว่าได้ยื่นคำขอนี้ในวันที่ได้ยื่นคำขอรับสิทธิบัตร/อนุสิทธิบัตรในต่างประเทศเป็นครั้งแรกโดย
☐ ได้ยื่นเอกสารหลักฐานพร้อมคำขอนี้ ☐ ขอยื่นเอกสารหลักฐานหลังจากวันยื่นคำขอนี้

9.การแสดงการประดิษฐ์ หรือการออกแบบผลิตภัณฑ์ ผู้ขอรับสิทธิบัตร/อนุสิทธิบัตรได้แสดงการประดิษฐ์ที่หน่วยงานของรัฐเป็นผู้จัด
วันแสดง วันเปิดงานแสดง ผู้จัด

10.การประดิษฐ์เกี่ยวกับจุลชีพ

| 10.1 เลขทะเบียนฝากเก็บ | 10.2 วันที่ฝากเก็บ | 10.3 สถาบันฝากเก็บ/ประเทศ |
|---|---|---|
| | | |

11.ผู้ขอรับสิทธิบัตร/อนุสิทธิบัตร ขอยื่นเอกสารภาษาต่างประเทศก่อนในวันยื่นคำขอนี้ และจะจัดยื่นคำขอรับสิทธิบัตร/อนุสิทธิบัตรนี้ที่จัดทำเป็นภาษาไทยภายใน 90 วัน นับจากวันยื่นคำขอนี้ โดยขอยื่นเป็นภาษา
☐ อังกฤษ ☐ ฝรั่งเศส ☐ เยอรมัน ☐ ญี่ปุ่น ☐ อื่นๆ

12.ผู้ขอรับสิทธิบัตร/อนุสิทธิบัตร ขอให้อธิบดีประกาศโฆษณาคำขอรับสิทธิบัตร หรือรับจดทะเบียน และประกาศโฆษณาอนุสิทธิบัตรนี้ หลังจากวันที่ เดือน พ.ศ
☐ ผู้ขอรับสิทธิบัตร/อนุสิทธิบัตรขอให้ใช้รูปเขียนหมายเลข ในการประกาศโฆษณา

13.คำขอรับสิทธิบัตร/~~อนุสิทธิบัตร~~นี้ประกอบด้วย
ก. แบบพิมพ์คำขอ 3 หน้า
ข. รายละเอียดการประดิษฐ์
~~หรือคำพรรณนาแบบผลิตภัณฑ์~~ 9 หน้า
ค. ข้อถือสิทธิ 2 หน้า
ง. รูปเขียน 2 รูป 2 หน้า
จ. ภาพแสดงแบบผลิตภัณฑ์
☐ รูปเขียน รูป หน้า
☐ ภาพถ่าย รูป หน้า
ฉ. บทสรุปการประดิษฐ์ 1 หน้า

14.เอกสารประกอบคำขอ
☐ เอกสารแสดงสิทธิในการขอรับสิทธิบัตร/อนุสิทธิบัตร
☐ หนังสือรับรองการแสดงการประดิษฐ์/การออกแบบผลิตภัณฑ์
☐ หนังสือมอบอำนาจ
☐ เอกสารรายละเอียดเกี่ยวกับจุลชีพ
☐ เอกสารการขอนับวันยื่นคำขอในต่างประเทศเป็นวันยื่นคำขอในประเทศไทย
☐ เอกสารขอเปลี่ยนแปลงประเภทของสิทธิ
☐ เอกสารอื่น ๆ

15. ข้าพเจ้าขอรับรองว่า
☑ การประดิษฐ์นี้ไม่เคยยื่นขอรับสิทธิบัตร/ อนุสิทธิบัตรมาก่อน
☐ การประดิษฐ์นี้ได้พัฒนาปรับปรุงมาจาก.....

16.ลายมือชื่อ ( ☐ ผู้ขอรับสิทธิบัตร / อนุสิทธิบัตร; ☑ ตัวแทน )
นายบัญชา วงศ์ณัฐภัทร

**หมายเหตุ** บุคคลใดยื่นขอรับสิทธิบัตรการประดิษฐ์หรือการออกแบบผลิตภัณฑ์ หรืออนุสิทธิบัตร โดยการแสดงข้อความอันเป็นเท็จแก่พนักงานเจ้าหน้าที่ เพื่อให้ได้ไปซึ่งสิทธิบัตรหรืออนุสิทธิบัตร ต้องระวางโทษจำคุกไม่เกินหกเดือน หรือปรับไม่เกินห้าพันบาท หรือทั้งจำทั้งปรับ

3.ผู้ขอรับสิทธิบัตร/~~อนุสิทธิบัตร~~ และที่อยู่ (เลขที่ ถนน ประเทศ)

จุฬาลงกรณ์มหาวิทยาลัย

อยู่ที่ จุฬาลงกรณ์มหาวิทยาลัย ถนนพญาไท แขวงวังใหม่ เขตปทุมวัน

กรุงเทพฯ 10330

3.1 สัญชาติ ไทย 3.2 โทรศัพท์ 0-2160-5340-42 3.3 โทรสาร 0-2160-5343

สำนักงานกองทุนสนับสนุนการวิจัย

อยู่ที่ ชั้น 14 อาคารเอส เอ็ม ทาวเวอร์ เลขที่ 979/17-21 ถนนพหลโยธิน แขวงสามเสนใน เขตพญาไท กรุงเทพฯ 10400

3.1 สัญชาติ ไทย 3.2 โทรศัพท์ 0-2278-8200 3.3 โทรสาร 0-2278-8248

6.ผู้ประดิษฐ์/~~ผู้ออกแบบผลิตภัณฑ์~~ และที่อยู่ (เลขที่ ถนน ประเทศ)

นางวรวีร์ โฮเว่น

อยู่ที่ คณะวิทยาศาสตร์ จุฬาลงกรณ์มหาวิทยาลัย เขตปทุมวัน กรุงเทพฯ 10330

นางสาวนาฏนัดดา รอดทองคำ

อยู่ที่ สถาบันวิจัยโลหะและวัสดุ จุฬาลงกรณ์มหาวิทยาลัย เขตปทุมวัน กรุงเทพฯ 10330

นางสาวอะรุณี แสงสุวรรณ

อยู่ที่ คณะวิทยาศาสตร์ จุฬาลงกรณ์มหาวิทยาลัย เขตปทุมวัน กรุงเทพฯ 10330

## รายละเอียดการประดิษฐ์

### ชื่อที่แสดงถึงการประดิษฐ์

แผ่นกระจกตรึงด้วยพอลิแอคริลิกแอซิดบรัชที่มีอนุภาคนาโนทองเป็นองค์ประกอบในลักษณะแพทเทิร์น สำหรับใช้ในการแยกและวิเคราะห์เพปไทด์ กรรมวิธีการผลิตและวิธีการวิเคราะห์

### สาขาวิทยาการที่เกี่ยวข้องกับการประดิษฐ์

สาขาเคมีในส่วนที่เกี่ยวข้องกับแผ่นกระจกตรึงด้วยพอลิแอคริลิกแอซิดบรัชที่มีอนุภาคนาโนทองเป็นองค์ประกอบในลักษณะแพทเทิร์น สำหรับใช้ในการแยกและวิเคราะห์เพปไทด์ กรรมวิธีการผลิตและวิธีการวิเคราะห์

### ภูมิหลังของศิลปะหรือวิทยาการที่เกี่ยวข้อง

เทคนิคเซอร์เฟสแอสซิสเตดเลเซอร์ดีซอร์ปชันไอออไนเซชัน-แมสสเปกโทรเมตรี (Surface assisted laser desorption ionization-mass spectrometry; SALDI-MS) เป็นเทคนิคหนึ่งที่ได้รับความนิยมในการนำมาใช้วิเคราะห์สารชีวโมเลกุล เนื่องจากมีความไวและแม่นยำสูง โดยเทคนิคนี้จะมีการพัฒนาวัสดุบนพื้นผิวสับสเตรทในการทำหน้าที่ดูดซับและถ่ายโอนพลังงานจากแสงเลเซอร์ไปยังสารตัวอย่างเพื่อทำให้สารตัวอย่างเกิดการแตกตัวเป็นไอออน โดยวัสดุดังกล่าวจะไม่แตกตัวเป็นไอออน เช่น อนุภาคนาโนของโลหะ ซิลิกอน คาร์บอน (Adv. Mater., Vol 24, p 4211–4216, 2012), (Anal. Chem., Vol 66, p 1227-1242, 2011) และ (Anal. Sci., Vol 26, p 1229-1240, 2010) จึงไม่ส่งสัญญาณรบกวนการวิเคราะห์สารตัวอย่างโดยเฉพาะอย่างยิ่งสารตัวอย่างที่มีน้ำหนักโมเลกุลต่ำ (< 500 มวลต่อประจุ) ซึ่งแตกต่างจากเทคนิคดั้งเดิม คือ เมทริกซ์แอสซิสเตดเลเซอร์ดีซอร์ปชันไอออไนเซชัน-แมสสเปกโทรเมตรี ที่จำเป็นต้องใช้สารอินทรีย์ทำหน้าที่เป็นเมทริกซ์ เช่น แอลฟาไซยาโน-4-ไฮดรอกซีซินนามิกแอซิด (α-cyano-4-hydroxycinnamic acid, CCA) และ 2,5-ไดไฮดรอกซีเบนโซอิกแอซิด (2,5-dihydroxybenzoic acid, DHB) โดยเมทริกซ์เหล่านี้สามารถแตกตัวเป็นไอออนได้ เกิดเป็นสัญญาณรบกวนซึ่งเป็นข้อจำกัดในการวิเคราะห์สารที่มีโมเลกุลขนาดเล็ก

ในปัจจุบันการแยกและตรวจวิเคราะห์ชนิดหรือปริมาณของสารชีวโมเลกุล เช่น เอนไซม์ กรดแอมิโน เพปไทด์ โปรตีน หรือดีเอ็นเอ โดยเฉพาะอย่างยิ่งที่เป็นสารบ่งชี้ทางชีวภาพ (biomarker) ซึ่งสามารถบ่งบอกความผิดปกติหรือการเกิดโรคต่างๆ เช่น โรคมะเร็ง โรคอัลไซเมอร์ โรคเบาหวาน และโรคไตเป็นต้น มีความสำคัญอย่างยิ่งต่อการตรวจวินิจฉัยและการบำบัดรักษาทางการแพทย์ จำเป็นต้องใช้เทคนิคที่มีความถูกต้องและว่องไวสูง เนื่องจากหากมีการเปลี่ยนแปลงปริมาณสารบ่งชี้ทางชีวภาพเหล่านี้ภายในร่างกายเพียงเล็กน้อยก็อาจส่งผลอันตรายแก่ชีวิตได้

อนุภาคนาโนโลหะเป็นวัสดุหนึ่งที่ได้รับความนิยมในการนำมาปรับปรุงพื้นผิวสับสเตรทที่ใช้ในเทคนิคเซอร์เฟสแอสซิสเตดเลเซอร์ดีซอร์ปชันไอออไนเซชัน-แมสสเปกโทรเมตรี เพื่อทำหน้าที่เป็นเมทริกซ์สำหรับการตรวจวิเคราะห์สารบ่งชี้ทางชีวภาพ (Anal. Bioanal. Chem., Vol 402, p 601-623, 2012) เนื่องจากอนุภาคนาโนโลหะมีพื้นที่ผิวสูง มีสมบัติการดูดซับและถ่ายโอนพลังงานไปยังโมเลกุลสารที่ต้องการวิเคราะห์ได้ดี ช่วยเพิ่มพลังงานในการแตกตัวของสารให้อยู่ในรูปของไอออนได้มากขึ้น มีความเสถียรสูงจึงไม่แตกตัวเป็นไอออนเกิดเป็นสัญญาณรบกวนการวิเคราะห์สารตัวอย่าง สามารถช่วยเพิ่มสัญญาณในการตรวจวิเคราะห์ได้ โดยมีรายงานว่าอนุภาคนาโนโลหะแต่ละชนิดมีความเหมาะสมกับช่วงน้ำหนักโมเลกุลของสารตัวอย่างที่นำมาวิเคราะห์แตกต่างกัน เช่น อนุภาคนาโนทองเหมาะกับสารตัวอย่างที่มีช่วงน้ำหนักโมเลกุล 300-1300 อนุภาคนาโนไททาเนียมออกไซด์เหมาะกับช่วง 1,200 – 12,000 อนุภาคนาโนเหล็กออกไซด์ เหมาะกับช่วง 1,200 – 25,000 (J. Am. Soc. Mass Spectrom., Vol 21, p 1204–1207, 2010)

มีสิทธิบัตรรายงานการนำโลหะชนิดต่างๆ ทั้งในรูปของอนุภาคนาโนและฟิล์มมาทำหน้าที่เป็นเมทริกซ์ในการวิเคราะห์เพปไทด์ โดยเทคนิคแมสสเปกโทรเมตรีแทนการใช้เมทริกซ์ที่เป็นสารอินทรีย์ เช่น ซิลเวอร์ (Ag) ไททาเนียมออกไซด์ ($TiO_2$) ซิงค์ออกไซด์ (ZnO) ทินไดออกไซด์ ($SnO_2$) และเซอร์โคเนียมออกไซด์ (ZrO) โดยจากการรายงานพบว่า สามารถลดปัญหาอันเนื่องมาจากสัญญาณรบกวนของสารอินทรีย์ที่เป็นเมทริกซ์และปัญหาจากการที่เมทริกซ์กับสารตัวอย่างไม่ผสมเป็นเนื้อเดียวกันได้ตามสิทธิบัตรประเทศสหรัฐอเมริกาเลขที่ 8,610,058 และสิทธิบัตรประเทศสหรัฐอเมริกาเลขที่ 7,122,792

มีรายงานการปรับปรุงผื้นผิวสับสเตรทด้วยฟิล์มอะลูมินัมที่มีรูพรุนขนาดนาโนร่วมกับทองโดยการฉาบด้วยเครื่อง sputter coater ลงบนแผ่นกระจก ในการวิเคราะห์เพปไทด์ด้วยเครื่องแมสสเปกโทรเมตรี และศึกษาผลจากขนาดรูพรุนของฟิล์มอะลูมินัมและความหนาของชั้นทองพบว่า เมื่อเพิ่มขนาดรูพรุนของฟิล์มอะลูมินัมจนมีความกว้างของรูพรุนตั้งแต่ 100 นาโนเมตรขึ้นไปจะทำให้สัญญาณในการวิเคราะห์ลดลง และจากการศึกษาความหนาของชั้นทอง 30 ถึง 220 นาโนเมตร พบว่าที่ความหนา 90 นาโนเมตรให้สัญญาณการวิเคราะห์สารตัวอย่างดีที่สุด (Anal. Chem., Vol 79, p 4950-4956, 2007)

นอกจากนี้มีรายงานการนำอนุภาคนาโนทองในรูปของอนุภาคทองซิเตรต (AuNPs- citrate) มาใช้ในการปรับปรุงพื้นผิวสับสเตรทร่วมกับพอลิแอลลิลเอมีนไฮโดรคลอไรด์(poly(allylamine hydrochloride) (PAHC)) ในลักษณะของแผ่นฟิล์มทำการเปรียบเทียบความแตกต่างของผลการวิเคราะห์เพปไทด์จากการเคลือบพอลิเมอร์ฟิล์มสลับกับชั้นของอนุภาคทองซิเตรต 1, 3 และ 5 ชั้น พบว่าการเพิ่มจำนวนชั้นของพอลิเมอร์ฟิล์มและอนุภาคทองนั้น ทำให้สัญญาณการวิเคราะห์สารตัวอย่างดีขึ้นแต่ยังพบสัญญาณรบกวนจากอนุภาคทองทำให้ไม่สามารถวิเคราะห์สารในช่วงน้ำหนักโมเลกุลต่ำได้ (Anal. Chem., Vol 80, p 7524–7533, 2008) และมีรายงานการใช้อนุภาคทองร่วมกับพอลิเมอร์ชนิดอื่นๆ ใน

รูปแบบของฟิล์มในการปรับปรุงสับสเตรท แต่ยังปรากฏสัญญาณของอนุภาคทองรบกวนการวิเคราะห์เช่นกัน (Anal. Chem., Vol 80, p 5094–5102, 2008)

มีงานวิจัยที่รายงานการใช้อนุภาคนาโนโลหะร่วมกับพอลิเมอร์เพื่อปรับปรุงพื้นผิวสับสเตรท โดยใช้ไททาเนียมไดออกไซด์ ($TiO_2$), แมกนีเซียมออกไซด์ (MgO) และซิลิกอนไดออกไซด์ ($SiO_2$) เป็นเมทริกซ์ในการวิเคราะห์สารตัวอย่างที่มีน้ำหนักโมเลกุลต่ำได้แก่ อะซิบูโทลอล (acebutolol), โพรพราโนลอล (propranolol) และคาร์บามาซิพิน (carbamazepine) โดยทำการตรึงอนุภาคนาโนโลหะลงบนพอลิแลกไทด์ (polylactide; PLA) ที่ทำหน้าที่จับยึดอนุภาคไม่ให้หลุดออกและปนเปื้อนภายในเครื่องมือ ซึ่งพบว่าอนุภาคนาโนโลหะทำหน้าที่เป็นเมทริกซ์ได้และกระจายตัวได้ดีในพอลิเมอร์ อย่างไรก็ตามงานวิจัยดังกล่าวยังประสบปัญหาการรบกวนสัญญาณจากเมทริกซ์อยู่ (Anal. Methods, Vol 3, p 192-197, 2011)

นอกจากนี้มีรายงานการนำพอลิเมอร์มาใช้ร่วมกับอนุภาคนาโนทองเพื่อทำหน้าที่ในการตรึงอนุภาค ช่วยลดการหลุดออกของอนุภาคในภาวะความดันต่ำซึ่งจะทำให้เกิดการปนเปื้อนภายในแหล่งกำเนิดไอออนของเครื่องมือได้ โดยมีงานวิจัยที่นำพอลิเมอร์นาโนคอมพอสิตที่เตรียมจากพอลิ (สไตรีน-บล็อก-เอ็น-เมทิล-4-ไวนิลไพริดิเนียมไอโอไดด์) (poly(styrene-b-*N*-methyl-4-vinylpyridinium iodide)) และอนุภาคนาโนทองในการปรับปรุงพื้นผิวของแผ่นซิลิกอนสำหรับใช้ในการตรวจวิเคราะห์ด้วยเทคนิคเซอร์เฟสแอสซิส เตดเลเซอร์ดีซอร์ปชันไอออไนเซชัน-แมสสเปกโทรเมตรี จากผลการทดลองพบว่า พื้นผิวดังกล่าวสามารถนำมาใช้เป็นวัสดุในการวิเคราะห์เพปไทด์ได้ โดยพบว่า พอลิเมอร์ช่วยเพิ่มประสิทธิภาพในการแตกตัวเป็นไอออนของสารตัวอย่างเมื่อเทียบกับการใช้อนุภาคเพียงอย่างเดียว เนื่องจากพอลิเมอร์ช่วยให้อนุภาคเกิด การกระจายตัวได้ดีขึ้น ซึ่งถึงแม้จะไม่ปรากฏสัญญาณรบกวนจากอนุภาคนาโนทอง แต่ยังจำเป็นต้องมีการเติมสารละลายซิเตรตบัฟเฟอร์สำหรับเป็นแหล่งให้โปรตอนจากภายนอกอยู่ (J. Nanosci. Nanotechnol., Vol 9, p 159–164, 2009)

แนวทางหนึ่งที่น่าสนใจในการปรับปรุงพื้นผิวของวัสดุด้วยพอลิเมอร์คือ การเตรียมเป็นพอลิ เมอร์บรัช (polymer brushes) ซึ่งเป็นพอลิเมอร์ที่มีปลายของโซ่ด้านหนึ่งยึดติดบนพื้นผิวด้วยพันธะโควาเลนต์ ทำให้มีเสถียรภาพในการยึดติดบนพื้นผิวสูงกว่าการดูดซับทางกายภาพ การเตรียมพอลิเมอร์บรัชนิยมเตรียมด้วยปฏิกิริยาพอลิเมอไรเซชันริเริ่มจากพื้นผิว (surface-initiated polymerization) ทั้งนี้สามารถควบคุมความยาวของโซ่พอลิเมอร์ได้หากใช้ปฏิกิริยาพอลิเมอไรเซชันแบบควบคุม (controlled polymerization) เช่น atom transfer radical polymerization (ATRP) และ reversible addition-fragmentation chain transfer (RAFT) (Prog. Polym. Sci., Vol 25, p 677-710, 2000) และ (Chem. Rev., Vol 109, p 5437-5527, 2009) โดยสมบัติทางเคมีและกายภาพของพอลิเมอร์บรัชขึ้นกับชนิดของ มอนอเมอร์ที่เลือกใช้ในการสังเคราะห์ การประดิษฐ์นี้เป็นการสังเคราะห์พอลิเมอร์บรัชของพอลิแอคริลิกแอซิด (poly(acrylic acid; PAA) เนื่องจากในโครงสร้างประกอบด้วยหมู่คาร์บอกซิลซึ่งสามารถแตกตัวเป็นหมู่คาร์บอกซิเลตที่มีประจุลบได้ สามารถจับและรีดิวซ์ออเรทไอออน (aurate ion: $Au^{3+}$) ทำให้เกิดเป็น

อนุภาคนาโนทองอยู่ภายในพอลิแอคริลิกแอซิดด้วยวิธีสังเคราะห์ภายใน (*in situ*) ได้โดยไม่ต้องเติมตัวรีดิวซ์จากภายนอก ทั้งนี้มีรายงานความสำเร็จในการใช้ PAA ในรูปของสารละลาย poly(acrylic acid) sodium salt ในการรีดิวซ์ $Au^{3+}$ เป็นอนุภาคนาโนทองมาแล้ว (Langmuir, Vol 19, p 4831-4835, 2003) และ (J. Phys. Chem. C., Vol 114, p 9693-9701, 2010) จากการที่หมู่คาร์บอกซิลในโครงสร้างของพอลิแอคริลิกแอซิดสามารถแตกตัวให้โปรตอนได้ จึงสามารถทำหน้าที่เป็นแหล่งให้โปรตอนกับสารตัวอย่างเกิดการแตกตัวเป็นไอออนได้ง่ายขึ้นอีกด้วยโดยไม่ต้องเติมแหล่งให้โปรตอนจากภายนอก (Anal. Lett., Vol 41, p 260-267, 2008)

แผ่นกระจกตรึงด้วยพอลิแอคริลิกแอซิดบรัชที่มีอนุภาคนาโนทองเป็นองค์ประกอบในลักษณะแพทเทิร์นตามการประดิษฐ์นี้พบว่า พอลิเมอร์บรัชของพอลิแอคริลิกแอซิดสามารถยึดจับอนุภาคนาโนทองไว้ได้อย่างมีประสิทธิภาพ จึงไม่ปรากฏสัญญาณของอนุภาคนาโนทองรบกวนการวิเคราะห์ในแมสสเปกตรัมซึ่งแตกต่างจากการรายงานก่อนหน้าที่ใช้พอลิเมอร์ในรูปแบบของฟิล์มหรือพอลิเมอร์คอมโพสิต

นอกจากอนุภาคนาโนโลหะสามารถทำหน้าที่เป็นเมทริกซ์ได้แล้ว ยังมีรายงานถึงการทำหน้าที่ในการจับแยกสารตัวอย่างเพปไทด์ที่มีกรดแอมิโนซีสเตอีน (cysteine-containing peptide) ซึ่งมีหมู่ ไทออลเป็นองค์ประกอบอย่างจำเพาะเจาะจง เช่น กลูตาไธโอนและเพปไทด์ที่มีซีสเตอีนเป็นองค์ประกอบออกจากสารผสมที่มีหลากหลายชนิดได้อีกด้วย ดังตัวอย่างงานวิจัยของ Shrivas และคณะ ได้นำอนุภาคนาโนซิลเวอร์ (AgNPs) มาทำหน้าที่เป็นเมทริกซ์ช่วยในการวิเคราะห์ด้วยเทคนิคเซอร์เฟสแอสซิสเตดเลเซอร์ดีซอร์ปชันไอออไนเซชัน-แมสสเปกโทรเมตรี และทำหน้าที่เป็นโพรบ (probe) ในการจับกับสารชีวโมเลกุลที่มี ไทออล (biothiols) เป็นองค์ประกอบได้ เช่น เพปไทด์หรือโปรตีนที่มีกรดแอมิโนซีสเตอีนเป็นองค์ประกอบ โดยการมีระดับของโฮโมซีสเตอีน (homocysteine) ในเลือดในปริมาณสูงเป็นปัจจัยเสี่ยงหนึ่งที่นำไปสู่การเกิดโรคหัวใจและโรคอัลไซเมอร์ได้ จากการทดลองพบว่าความเข้มข้นต่ำสุดที่สามารถตรวจวัดได้ (limit of detection; LOD) ของซีสเตอีนและโฮโมซีสเตอีนในปัสสาวะตัวอย่างมีค่าเท่ากับ 7 และ 22 นาโนโมลาร์ ตามลำดับ ทั้งนี้จำเป็นต้องอาศัยการปั่นเหวี่ยงแยกอนุภาคนาโนซิลเวอร์ออกจากสารผสมก่อนนำมาทำการวิเคราะห์ (Rapid Commun. Mass Spectrom., Vol 22, p 2863-2872, 2008)

**ลักษณะและความมุ่งหมายของการประดิษฐ์**

การประดิษฐ์นี้เกี่ยวข้องกับแผ่นกระจกตรึงด้วยพอลิแอคริลิกแอซิดบรัชที่มีอนุภาคนาโนทองเป็นองค์ประกอบในลักษณะแพทเทิร์น สำหรับใช้ในการแยกและวิเคราะห์เพปไทด์ กรรมวิธีการผลิตและวิธีการวิเคราะห์ โดยการตรึงปลายข้างหนึ่งของโซ่พอลิแอคริลิกแอซิดบนแผ่นกระจกในลักษณะเป็นพอลิเมอร์บรัช ที่สามารถจับยึดและรีดิวซ์ออเรทไอออน (aurate ion: $Au^{3+}$) ที่เป็นประจุบวกทำให้เกิดเป็นอนุภาคนาโนทองอยู่ภายในเป็นวิธีการสังเคราะห์แบบภายใน (*in situ* synthesis) โดยไม่ต้องเติมตัวรีดิวซ์

จากภายนอก โดยอนุภาคนาโนทองที่เกิดขึ้นภายในนี้จะถูกกักไว้ภายในโซ่ของพอลิแอคริลิกแอซิดบรัชที่ตรึงบนกระจกไม่เกิดการหลุดออก จึงไม่เกิดสัญญาณรบกวนหรือเกิดการปนเปื้อนภายในเครื่องมือระหว่างการวิเคราะห์ด้วยเทคนิคเซอร์เฟสแอสซิสเตดเลเซอร์ดีซอร์ปชันไอออไนเซชัน-แมสสเปกโทรเมตรี และจากการที่หมู่คาร์บอกซิลในโครงสร้างของพอลิแอคริลิกแอซิดสามารถแตกตัวให้โปรตอนได้จึงสามารถทำหน้าที่เป็นแหล่งให้โปรตอน (proton source) กับสารตัวอย่างทำให้แตกตัวเป็นไอออนได้ง่ายขึ้นโดยไม่จำเป็นต้องเติมแหล่งให้โปรตอนจากภายนอก

ในส่วนการใช้อนุภาคนาโนทองทำหน้าที่เป็นโพรบสำหรับการจับแยกสารตัวอย่างเพปไทด์ที่มีกรดแอมิโนซีสเตอีน (cysteine-containing peptide) หรือสารประกอบที่มีหมู่ไทออลเป็นองค์ประกอบนั้นสามารถทำการแยกและวิเคราะห์สารตัวอย่างได้โดยตรงบนสับสเตรท โดยสามารถแยกเอาเฉพาะเพปไทด์ที่มีกรดแอมิโนซีสเตอีนและ/หรือสารประกอบที่มีหมู่ไทออลเป็นองค์ประกอบ นำไปวิเคราะห์ด้วยเทคนิคเซอร์เฟสแอสซิสเตดเลเซอร์ดีซอร์ปชันไอออไนเซชัน-แมสสเปกโทรเมตรีได้โดยตรง ไม่จำเป็นต้องใช้เครื่องปั่นเหวี่ยงเพื่อแยกอนุภาคซึ่งช่วยลดขั้นตอน ทำให้การแยกทำได้สะดวกและรวดเร็วกว่างานวิจัยที่ปรากฏอยู่ในภูมิหลังของศิลปะหรือวิทยาการที่เกี่ยวข้อง

ความมุ่งหมายของการประดิษฐ์นี้ คือ การพัฒนาสับสเตรทที่เตรียมได้มาใช้ในการแยกและตรวจวิเคราะห์เพปไทด์ด้วยเทคนิคเซอร์เฟสแอสซิสเตดเลเซอร์ดีซอร์ปชันไอออไนเซชัน-แมสสเปกโทรเมตรี โดยมีวิธีในการแยกและวิเคราะห์สารตัวอย่างได้โดยตรงบนสับสเตรท ช่วยให้การเตรียมสารตัวอย่างง่าย สะดวก รวดเร็ว และมีประสิทธิภาพในการวิเคราะห์

**คำอธิบายรูปเขียนโดยย่อ**

รูปที่ 1 แสดงแมสสเปกตรัมของกลูตาไธโอน (GSH) วิเคราะห์ด้วยเทคนิคเซอร์เฟสแอสซิสเตดเลเซอร์ดีซอร์ปชันไอออไนเซชัน-แมสสเปกโทรเมตรีบนแผ่นกระจกตรึงด้วยพอลิแอคริลิกแอซิดบรัชที่มีอนุภาคนาโนทองเป็นองค์ประกอบ

รูปที่ 2 แสดงขั้นตอนในการเตรียมพอลิแอคริลิกแอซิดบรัชในรูปแบบแพทเทิร์นที่มีอนุภาคนาโนทองเป็นองค์ประกอบ

**การเปิดเผยการประดิษฐ์โดยสมบูรณ์**

การประดิษฐ์นี้เกี่ยวข้องกับแผ่นกระจกตรึงด้วยพอลิแอคริลิกแอซิดบรัชที่มีอนุภาคนาโนทองเป็นองค์ประกอบในลักษณะแพทเทิร์น สำหรับใช้ในการแยกและวิเคราะห์เพปไทด์ เช่น บราดีไคนิน (bradykinin) กลูตาไธโอน (glutathione) เป็นต้น ประกอบด้วย แผ่นกระจกที่ด้านบนตรึงด้วยสับสเตรทซึ่งเตรียมได้จากพอลิแอคริลิกแอซิดบรัช ในปริมาณ 0.1 – 0.5 โซ่ต่อตารางนาโนเมตร (chains/nm$^2$) และอนุภาคนาโนทองในปริมาณ $3 \times 10^{-6}$ ถึง $3 \times 10^{-5}$ โมลต่อตารางเซนติเมตร เป็นองค์ประกอบในลักษณะแพทเทิร์น เพื่อทำหน้าที่ดูดซับและถ่ายโอนพลังงานจากแสงเลเซอร์ไปยังสารตัวอย่าง เพื่อทำให้สาร

ตัวอย่างเกิดการแตกตัวเป็นไอออน โดยสับสเตรทจะไม่แตกตัวเป็นไอออน จึงไม่ส่งสัญญาณรบกวนการวิเคราะห์สารตัวอย่างโดยเฉพาะอย่างยิ่งสารตัวอย่างที่มีน้ำหนักโมเลกุล < 500 มวลต่อประจุ

ในอีกลักษณะหนึ่ง การประดิษฐ์นี้เกี่ยวข้องกับกรรมวิธีการผลิตแผ่นกระจกตรึงด้วยพอลิแอคริลิกแอซิดบรัชที่มีอนุภาคนาโนโลหะเป็นองค์ประกอบในลักษณะแพทเทิร์น สำหรับใช้ในการแยกและวิเคราะห์เพปไทด์ ที่มีขั้นตอนประกอบด้วย

- การกราฟท์พอลิแอคริลิกแอซิดบรัชลงบนพื้นผิวกระจกที่ได้จากวิธีโฟโตลิโทกราฟี โดยใช้หน้ากาก (photomask) ที่มีแพทเทิร์นเป็นรูปวงกลมขนาดเส้นผ่าศูนย์กลางเท่ากับบริเวณสำหรับหยดสารตัวอย่างบน target plate ของเครื่องแมสสเปกโทรเมตรี ในขั้นตอนนี้จะทำให้แพทเทิร์นที่เตรียมได้มีพื้นผิวโดยรอบวงกลมมีสมบัติไม่ชอบน้ำสูง ซึ่งผ่านการตรึงด้วยสารประกอบฟลูออโรไซเลน (fluorosilane) และบริเวณวงกลมที่มีหมู่ไซลานอลจะนำไปใช้ในการติดสารริเริ่ม (initiator) บนพื้นผิวกระจก เพื่อทำปฏิกิริยาพอลิเมอไรเซชัน โดยเริ่มจากพื้นผิวของแพทเทิร์นบริเวณที่มีหมู่ริเริ่มของแอคริลิกแอซิด มอนอเมอร์ที่เป็นอนุพันธ์ของแอคริลิกแอซิด ที่ซึ่งมีหมู่ข้าง (side chain) ที่เปลี่ยนเป็นหมู่คาร์บอกซิลได้หลังจากเกิดเป็นพอลิเมอร์แล้ว เช่น เทอร์เทียรีบิวทิวแอคริเลต (tert-butyl acrylate) หรือแอคริลิกแอซิด/อนุพันธ์ของแอคริลิกแอซิดร่วมกับมอนอเมอร์ชนิดอื่น

- การสังเคราะห์อนุภาคนาโนโลหะด้วยวิธีการสังเคราะห์แบบภายในบนพอลิเมอร์บรัชของพอลิแอคริลิกแอซิดหรือโคพอลิเมอร์ที่มีหมู่คาร์บอกซิลเป็นองค์ประกอบ โดยการนำแผ่นกระจกที่มีแพทเทิร์นของพอลิเมอร์บรัชข้างต้น จุ่มในสารละลายไอออนโลหะที่เป็นประจุบวก เช่น คลอโรออริกแอซิด (chloroauric acid; $HAuCl_4$) ความเข้มข้น 1-10 มิลลิโมลาร์ สลับกับน้ำกลั่น เป็นจำนวน 5-15 รอบ เมื่อจุ่มสลับเป็นจำนวนรอบตามต้องการแล้ว นำแผ่นกระจกแช่ในน้ำกลั่นที่อุณหภูมิ 100-120 องศาเซลเซียส เป็นเวลา 1-3 ชั่วโมง จากนั้นนำไปแช่ในสารละลายไอออนโลหะที่เป็นประจุบวก เช่น สารละลายคลอโรออริกแอซิด ความเข้มข้นข้างต้นและให้ความร้อนที่อุณหภูมิ 100-120 องศาเซลเซียสในอ่างน้ำมันเป็นเวลา 1-4 ชั่วโมง จากนั้นล้างแผ่นกระจกด้วยน้ำกลั่นและทำให้แห้ง ในขั้นตอนนี้จะได้แผ่นกระจกเป็นแพทเทิร์นที่สังเกตเห็นเป็นจุดของอนุภาคนาโนโลหะที่เกิดขึ้นบริเวณที่มีพอลิแอคริลิกแอซิดบรัชหรือโคพอลิเมอร์ที่มีหมู่คาร์บอกซิลเป็นองค์ประกอบ

ในอีกลักษณะหนึ่ง การประดิษฐ์นี้เกี่ยวข้องกับวิธีการวิเคราะห์เพปไทด์ที่มีขั้นตอนประกอบด้วย

(1) ติดแผ่นกระจกที่มีแพทเทิร์นของพอลิเมอร์บรัชของพอลิแอคริลิกแอซิดหรือโคพอลิเมอร์ที่มีหมู่คาร์บอกซิลเป็นองค์ประกอบและมีอนุภาคนาโนโลหะเป็นองค์ประกอบบน target plate ของเครื่องแมสสเปกโทรเมตรี จากนั้นหยดสารตัวอย่างเพปไทด์ที่มีความเข้มข้นตามต้องการลงบนแผ่นกระจกบริเวณที่มีอนุภาคนาโนโลหะ ตั้งทิ้งไว้จนสารละลายระเหยแห้ง จากนั้นจึงนำไปวิเคราะห์ด้วยเครื่องแมสสเปกโทรมิเตอร์

(2) การแยกและวิเคราะห์สารตัวอย่างเพปไทด์ที่มีกรดแอมิโนซีสเตอีน และ/หรือสารประกอบที่มีหมู่ไทออลเป็นองค์ประกอบในสารละลายผสม ประกอบด้วย ติดแผ่นกระจกที่เป็นที่มีแพทเทิร์นของพอลิเมอร์บรัชของพอลิแอคริลิกแอซิดหรือโคพอลิเมอร์ที่มีหมู่คาร์บอกซิลเป็นองค์ประกอบและมีอนุภาคนาโนโลหะเป็นองค์ประกอบบน target plate ของเครื่องแมสสเปกโทรมิเตอร์ หยดสารละลายผสมที่มีสารตัวอย่างเพปไทด์ที่มีกรดแอมิโนซีสเตอีนและ/หรือสารประกอบที่มีหมู่ไทออลเป็นองค์ประกอบลงบนแผ่นกระจกบริเวณที่มีอนุภาคนาโนโลหะ ตั้งทิ้งไว้เป็นระยะเวลาตามต้องการ จากนั้นล้างบริเวณที่หยดสารตัวอย่างด้วยตัวทำละลายที่ต้องการ หลังจากสารละลายระเหยแห้งแล้วจึงนำไปวิเคราะห์ด้วยเครื่องแมสสเปกโทรมิเตอร์

ตัวอย่างต่อไปนี้แสดงให้เห็นเพิ่มเติมถึงการประดิษฐ์ มิได้มีวัตถุประสงค์ที่จะจำกัดขอบเขตการประดิษฐ์

<u>ตัวอย่างที่ 1</u> การผลิตแผ่นกระจกตรึงด้วยพอลิแอคริลิกแอซิดบรัชที่มีอนุภาคนาโนทองเป็นองค์ประกอบในลักษณะแพทเทิร์น สำหรับใช้ในการแยกและวิเคราะห์เพปไทด์ ตามรูปที่ 2 ที่มีขั้นตอนประกอบด้วย

(1) เตรียมแพทเทิร์นบนพื้นผิวของแผ่นกระจกด้วยวิธีโฟโตลิโทกราฟี นำแผ่นกระจกไปทำความสะอาดในเครื่องพลาสมาเป็นเวลา 5 นาที ก่อนนำไปใส่ในขวดแก้วที่บรรจุสาร 3-อะมิโนโพรพิลไตรเอทอกซีไซเลน ปิดฝาขวดแก้วแล้วนำไปอบที่อุณหภูมิ 80 องศาเซลเซียส เป็นเวลา 72 ชั่วโมง จากนั้นนำแผ่นกระจกไปล้างด้วยเอทานอล แอซิโตนและน้ำ ตามลำดับ นำแผ่นกระจกไปเคลือบด้วยสารโฟโตรีซิสชนิด positive UV-sensitive resist แล้วนำไปให้ความร้อนที่อุณหภูมิ 115 องศาเซลเซียส เป็นเวลา 1 นาที จากนั้นวางแผ่นหน้ากากที่เป็นแพทเทิร์นรูปวงกลมที่มีขนาดเส้นผ่าศูนย์กลางเท่ากับวงกลมที่เป็นตำแหน่งสำหรับหยดสารบน target plate ของเครื่องแมสสเปกโทรเมตรีลงบนแผ่นกระจก ฉายแสงยูวี 365 นาโนเมตร, 500 วัตต์ เป็นเวลา 15 วินาที นำหน้ากากบนแผ่นกระจกออกแล้วนำไปล้างด้วยสารละลายเดเวลอปเปอร์และล้างด้วยน้ำ ทำแผ่นกระจกให้แห้งด้วยการเป่าด้วยแก๊สไนโตรเจน และนำเข้าเครื่องพลาสมาเป็นเวลา 5 นาที นำแผ่นกระจกที่มีแพทเทิร์นของ $Si\text{-}NH_2/OH$ ใส่ในขวดแก้วที่บรรจุเปอร์ฟลูออโรเอทิลไทรคลอโรไซเลน 100 ไมโครลิตร ปิดฝาขวดแก้วแล้วนำไปอบที่อุณหภูมิ 80 องศาเซลเซียส เป็นเวลา 72 ชั่วโมง จากนั้นนำแผ่นกระจกไปล้างด้วยเอทานอล แอซิโตนและน้ำตามลำดับ ได้เป็นพื้นผิวที่เป็นแพทเทิร์นของ $Si\text{-}NH_2/O(CH_2)_2(CF_2)_5CF_3$ พร้อมที่จะนำไปใช้ในการติดสารริเริ่ม (initiator) ในขั้นการสังเคราะห์พอลิเมอร์ต่อไป

(2) ทำการกราฟต์พอลิแอคริลิกแอซิดบรัชบนพื้นผิวของกระจกที่เป็นแพทเทิร์น ละลาย 4,4-บิสไซยาโนวาเลอิกแอซิด 1 มิลลิโมล และ 4-ไดเมทิลแอมิโนไพริดีน 0.1 มิลลิโมล ในไดเมทิลฟอร์มาไมด์ 20 มิลลิลิตร คนเป็นเวลา 4 ชั่วโมง ที่อุณหภูมิห้องภายใต้บรรยากาศไนโตรเจน จากนั้นถ่ายสารละลายนี้ไปยัง ขวดแก้วที่บรรจุแผ่นกระจกที่เป็นแพทเทิร์นของ $Si\text{-}NH_2/O(CH_2)_2(CF_2)_5CF_3$ ที่เตรียมได้จาก (1) ทำ

การคน ที่อุณหภูมิห้องเป็นเวลา 20 ชั่วโมงภายใต้บรรยากาศไนโตรเจน จากนั้นนำแผ่นกระจกมาล้างด้วยเอทานอล และน้ำ ซึ่งในขั้นนี้จะได้แผ่นกระจกที่เป็นแพทเทิร์นที่ติดสารริเริ่ม ($Si\text{-}I/O(CH_2)_2(CF_2)_5CF_3$) จากนั้นละลาย 4,4-บิสไซยาโนวาเลอิกแอซิด 0.5 มิลลิโมล และ 4-ไซยาโน-4-ฟีนิลคาร์โบโนไทโออิลไทโอเพนทาโนอิก แอซิด 2 มิลลิโมล ในฟอสเฟตบัฟเฟอร์ที่มีพีเอช 7.4 (PBS buffer) 20 มิลลิลิตร และเติมแอคริลิกแอซิด 1.37 มิลลิลิตร ผสมสารละลายให้เข้ากันก่อนถ่ายโอนสารละลายนี้ไปยังขวดแก้วที่มีแผ่นกระจกที่เป็น แพทเทิร์นที่ติดสารริเริ่มแล้วทำปฏิกิริยาพอลิเมอไรเซชันที่อุณหภูมิ 70 องศาเซลเซียส ในอ่างน้ำมันเป็นเวลา 20 ชั่วโมง จากนั้นล้างแผ่นกระจกด้วยเอทานอลและน้ำ ทำแผ่นกระจกให้แห้งโดยการเป่าด้วยแก๊สไนโตรเจน

(3) สังเคราะห์อนุภาคนาโนทองด้วยวิธีการสังเคราะห์แบบภายในบนพอลิแอคริลิกแอซิดบรัช โดยการนำแผ่นกระจกที่มีแพทเทิร์นของพอลิแอคริลิกแอซิดบรัช ($Si\text{-}PAA/O(CH_2)_2(CF_2)_5CF_3$) จุ่มในสารละลายคลอโรออริกแอซิด ความเข้มข้น 1 มิลลิโมลาร์ ปริมาตร 5 มิลลิลิตร สลับกับน้ำกลั่น เป็นจำนวน 5 รอบ นำแผ่นกระจกแช่ในน้ำกลั่นที่อุณหภูมิ 100 องศาเซลเซียส เป็นเวลา 1 ชั่วโมง จากนั้นนำไปแช่ในสารละลายคลอโรออริกแอซิด และให้ความร้อนที่อุณหภูมิ 100 องศาเซลเซียสในอ่างน้ำมันเป็นเวลา 1 ชั่วโมง ล้างแผ่นกระจกด้วยน้ำกลั่นและทำให้แห้งด้วยการเป่าด้วยแก๊สไนโตรเจน จะได้แผ่นกระจกเป็นแพทเทิร์นที่สังเกตเห็นเป็นจุดสีม่วงของอนุภาคนาโนทองคำที่เกิดขึ้นบริเวณที่มีพอลิแอคริลิกแอซิดบรัช

(4) วิเคราะห์สารตัวอย่างเพปไทด์ ละลายสารตัวอย่างเพปไทด์แต่ละชนิดในน้ำกลั่น และปรับความเข้มข้นให้ได้ 500 นาโนโมลาร์ ติดแผ่นกระจกที่เป็นที่มีแพทเทิร์นของพอลิแอคริลิกแอซิดบรัชและมีอนุภาคนาโนทองเป็นองค์ประกอบบน target plate ของเครื่องแมสสเปกโทรเมตรีด้วยเทปคาร์บอนนำไฟฟ้า จากนั้นหยดสารละลายตัวอย่างปริมาตร 3 ไมโครลิตร ลงบนแผ่นกระจกบริเวณจุดสีม่วงที่มีอนุภาคนาโนทอง ตั้งทิ้งไว้จนสารละลายระเหยแห้ง จากนั้นจึงนำไปวิเคราะห์ด้วยเครื่องแมสสเปกโทรมิเตอร์ โดยยิงด้วยไนโตรเจนเลเซอร์ความยาวคลื่น 337 nm ความเข้ม 50 เปอร์เซ็นต์ เป็นจำนวน 100 ครั้ง

(5) แยกและวิเคราะห์สารตัวอย่างเพปไทด์ที่มีกรดแอมิโนซีสเตอีนในสารละลายผสม ติดแผ่นกระจกที่เป็นที่มีแพทเทิร์นของพอลิแอคริลิกแอซิดบรัชและมีอนุภาคนาโนทองเป็นองค์ประกอบบน target plate ของเครื่องแมสสเปกโทรมิเตอร์ ด้วยเทปคาร์บอนนำไฟฟ้า หยดสารละลายผสมปริมาตร 3 ไมโครลิตร ที่มีสารตัวอย่างเพปไทด์ที่มีกรดแอมิโนซีสเตอีนความเข้มข้น 500 นาโนโมลาร์ ลงบนแผ่นกระจกบริเวณจุดสีม่วงที่มีอนุภาคนาโนทองตั้งทิ้งไว้เป็นเวลา 10 นาที ที่อุณหภูมิห้อง จากนั้นล้างบริเวณที่หยดสารด้วยสารละลายพีบีเอชบัฟเฟอร์ พีเอช 7.4 และน้ำกลั่น หลังจากสารละลายระเหยแห้งแล้วจึงนำไปวิเคราะห์ด้วยเครื่องแมสสเปกโทรมิเตอร์ โดยยิงด้วยไนโตรเจนเลเซอร์ความยาวคลื่น 337 nm มีความเข้ม 50 เปอร์เซ็นต์ เป็นจำนวน 100 ครั้ง

ตามรูปที่ 1 แสดงแมสสเปกตรัมของกลูตาไธโอน (GSH) วิเคราะห์ด้วยเทคนิคเซอร์เฟสแอสซิสเตด เลเซอร์ดีซอร์ปชันไอออไนเซชัน-แมสสเปกโทรเมตรีบนแผ่นกระจกตรึงด้วยพอลิแอคริลิกแอซิด บรัชที่มีอนุภาคนาโนทองเป็นองค์ประกอบ โดยพบสัญญาณของกลูตาไธโอนและไดกลูตาไธโอน (2GSH) ที่ตำแหน่ง 308 มวลต่อประจุและ 615 มวลต่อประจุ ตามลำดับ และไม่พบสัญญาณของอนุภาคทองซึ่งเป็นเมทริกซ์ รบกวนการวิเคราะห์และให้อัตราส่วนสัญญาณของสารตัวอย่างต่อสัญญาณรบกวนสูง (S/N =6.36)

**วิธีการในการประดิษฐ์ที่ดีที่สุด**

เหมือนกับที่ได้กล่าวมาแล้วในหัวข้อการเปิดเผยการประดิษฐ์โดยสมบูรณ์

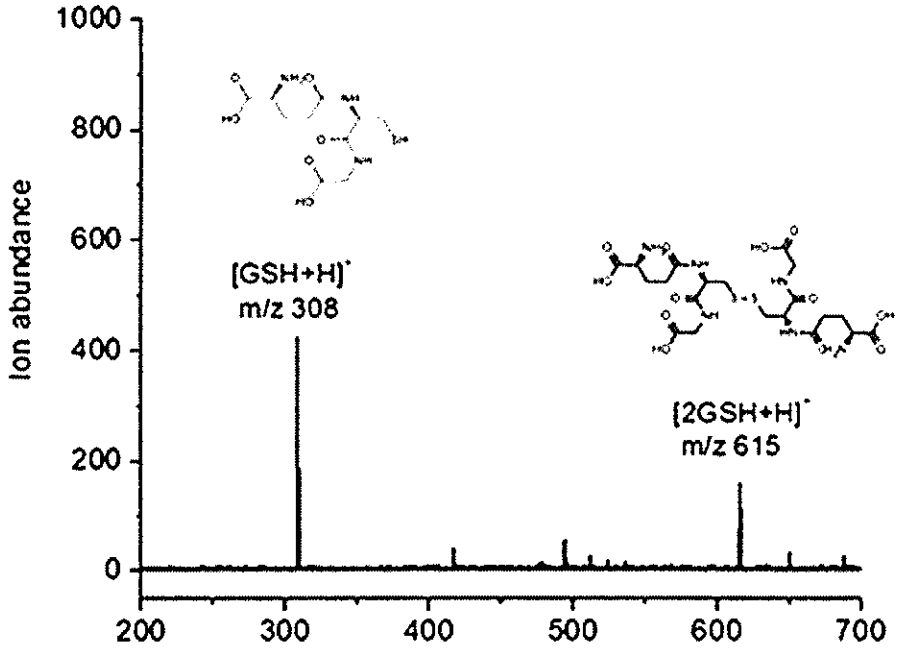
1000
800
600
400
200
0
Ion abundance
[GSH+H]+
m/z 308
[2GSH+H]+
m/z 615
200
300
400
500
600
700

รูปที่ 1

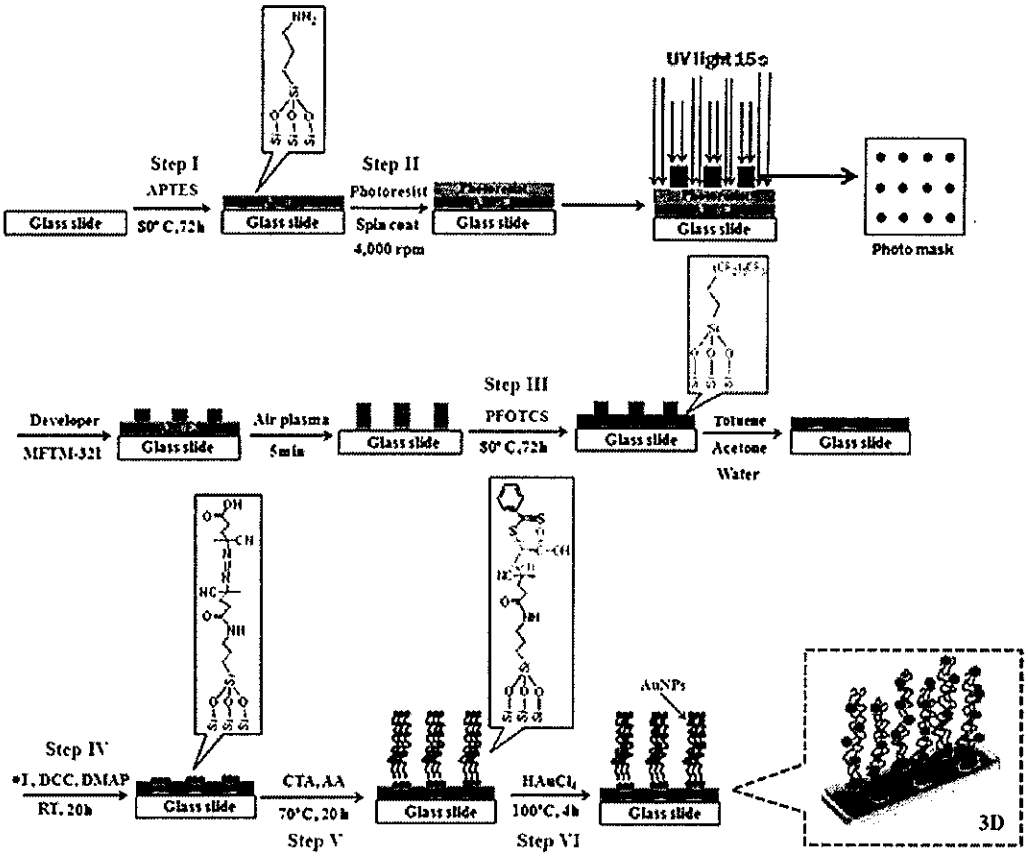
Step I
APTES
50° C,72h
Glass slide
Step II
Photoresist
Spin coat
4,000 rpm
UV light 15s
Photo mask
Developer
MFTM-321
Air plasma
5min
Step III
PFOTCS
50° C,72h
Toluene
Acetone
Water
Step IV
*I, DCC, DMAP
RT, 20h
CTA, AA
70°C, 20h
Step V
HAuCl4
100°C, 4h
Step VI
AuNPs
3D

รูปที่ 2

**ข้อถือสิทธิ**

1. แผ่นกระจกตรึงด้วยพอลิแอคริลิกแอซิดบรัชที่มีอนุภาคนาโนทองเป็นองค์ประกอบในลักษณะแพทเทิร์น สำหรับใช้ในการแยกและวิเคราะห์เพปไทด์ ซึ่งประกอบด้วย แผ่นกระจกที่ด้านบนตรึงด้วยสับสเตรท ซึ่งสับสเตรทเตรียมได้จากพอลิแอคริลิกแอซิดบรัช ในปริมาณ 0.1 – 0.5 โซ่ต่อตารางนาโนเมตร (chains/nm$^2$) และอนุภาคนาโนทองในปริมาณ 3 x $10^{-6}$ ถึง 3 x $10^{-5}$ โมลต่อตารางเซนติเมตร (mole/cm$^2$) เป็นองค์ประกอบในลักษณะแพทเทิร์น

2. กรรมวิธีการผลิตแผ่นกระจกตรึงด้วยพอลิแอคริลิกแอซิดบรัชที่มีอนุภาคนาโนทองเป็นองค์ประกอบในลักษณะแพทเทิร์น สำหรับใช้ในการแยกและวิเคราะห์เพปไทด์ ตามข้อถือสิทธิ 1 มีขั้นตอนประกอบด้วย

- การกราฟท์พอลิแอคริลิกแอซิดบรัชลงบนพื้นผิวกระจกที่ได้จากวิธีโฟโตลิโทกราฟี โดยทำปฏิกิริยาพอลิเมอไรเซชันจากพื้นผิวของแพทเทิร์นบริเวณที่มีหมู่ริเริ่มของแอคริลิกแอซิดมอนอเมอร์ที่เป็นอนุพันธ์ของแอคริลิกแอซิด ที่ซึ่งมีหมู่ข้าง (side chain) ที่เปลี่ยนเป็นหมู่คาร์บอกซิลได้หลังจากเกิดเป็นพอลิเมอร์แล้ว และ

- การสังเคราะห์อนุภาคนาโนโลหะด้วยวิธีการสังเคราะห์แบบภายในบนพอลิเมอร์บรัชของพอลิแอคริลิกแอซิดหรือโคพอลิเมอร์ที่มีหมู่คาร์บอกซิลเป็นองค์ประกอบ โดยการนำแผ่นกระจกที่มีแพทเทิร์นของพอลิเมอร์บรัช จุ่มในสารละลายไอออนโลหะที่เป็นประจุบวก

3. กรรมวิธีการผลิตแผ่นกระจกตรึงด้วยพอลิแอคริลิกแอซิดบรัชที่มีอนุภาคนาโนทองเป็นองค์ประกอบในลักษณะแพทเทิร์น สำหรับใช้ในการแยกและวิเคราะห์เพปไทด์ ตามข้อถือสิทธิ 2 ที่ซึ่ง การสังเคราะห์อนุภาคนาโนทองด้วยวิธีการสังเคราะห์แบบภายใน โดยอาศัยหมู่คาร์บอกซิลของพอลิแอคริลิกแอซิดบรัชในการรีดิวซ์ออเรทไอออนที่เป็นประจุบวก ซึ่งมีขั้นตอนประกอบด้วย

- การนำแผ่นกระจกที่มีแพทเทิร์นของพอลิเมอร์บรัช จุ่มในสารละลายไอออนโลหะที่เป็นประจุบวก ความเข้มข้น 1-10 มิลลิโมลาร์ สลับกับน้ำกลั่น เป็นจำนวน 5-15 รอบ

- นำแผ่นกระจกแช่ในน้ำกลั่นที่อุณหภูมิ 100-120 องศาเซลเซียส เป็นเวลา 1-3 ชั่วโมง

- แช่ในสารละลายไอออนโลหะที่เป็นประจุบวก และให้ความร้อนที่อุณหภูมิ 100-120 องศาเซลเซียส เป็นเวลา 1-4 ชั่วโมง

- ล้างแผ่นกระจกด้วยน้ำกลั่นและทำให้แห้ง

4. การแยกและวิเคราะห์สารตัวอย่างเพปไทด์ที่มีกรดแอมิโนซีสเตอีน สารประกอบที่มีหมู่ไทออลเป็นองค์ประกอบในสารละลายผสม ซึ่งประกอบด้วย การนำแผ่นกระจกที่ติดด้วยพอลิแอคริลิกแอซิดบรัชที่มี

อนุภาคนาโนทองไปติดบน target plate ด้วยเทปคาร์บอนนำไฟฟ้า หยดสารตัวอย่างลงบนแผ่นกระจก ล้างบริเวณที่หยดสารตัวอย่างด้วยตัวทำละลาย และนำไปวิเคราะห์ด้วยเครื่องแมสสเปกโทรมิเตอร์

## บทสรุปการประดิษฐ์

การประดิษฐ์นี้เกี่ยวกับการดัดแปรพื้นผิวของแผ่นกระจกเพื่อใช้เป็นสับสเตรทในการแยกและวิเคราะห์เพปไทด์ด้วยเทคนิคเซอร์เฟสแอสซิสเตดเลเซอร์ดีซอร์ปชันไอออไนเซชัน-แมสสเปกโทรเมตรี โดยการตรึงพอลิแอคริลิกแอซิดบรัชในรูปแบบแพทเทิร์นเพื่อทำหน้าที่ในการสังเคราะห์อนุภาคนาโนทองด้วยวิธีสังเคราะห์แบบภายใน และช่วยยึดจับไม่ให้อนุภาคนาโนทองหลุดออกไปเกิดสัญญาณรบกวนการวิเคราะห์และปนเปื้อนภายในเครื่องมือจึงทำให้สามารถวิเคราะห์เพปไทด์ที่มีโมเลกุลขนาดใหญ่ ($\geq$1000 มวลต่อประจุ) และขนาดเล็ก ($\leq$ 500 มวลต่อประจุ) ได้โดยไม่จำเป็นต้องมีการเติมสารให้โปรตอนจากภายนอก โดยอนุภาคนาโนทองนอกจากจะทำหน้าที่เป็นเมทริกซ์แล้ว ยังสามารถจับอย่างเลือกจำเพาะ (selective) กับสารตัวอย่างเพปไทด์ที่มีกรดแอมิโนซีสเตอีน สารประกอบที่มีหมู่ไทออลเป็นองค์ประกอบ ทำให้สามารถแยกสารดังกล่าวออกจากสารผสมได้ โดยมีขั้นตอนในการแยกที่สามารถทำได้สะดวก รวดเร็ว ประหยัดเวลา นอกจากนี้ลักษณะที่เป็นแพทเทิร์นทำให้สามารถทำการวิเคราะห์สารตัวอย่างหลายชนิดได้ในเวลาเดียวกัน

คำขอรับสิทธิบัตร/อนุสิทธิบัตร

☑ การประดิษฐ์
☐ การออกแบบผลิตภัณฑ์
☐ อนุสิทธิบัตร

ข้าพเจ้าผู้ลงลายมือชื่อในคำขอรับสิทธิบัตร/อนุสิทธิบัตรนี้ ขอรับสิทธิบัตร/อนุสิทธิบัตร ตามพระราชบัญญัติสิทธิบัตร พ.ศ. 2522 แก้ไขเพิ่มเติมโดยพระราชบัญญัติสิทธิบัตร (ฉบับที่ 2) พ.ศ 2535 และพระราชบัญญัติสิทธิบัตร (ฉบับที่ 3) พ.ศ 2542

**สำหรับเจ้าหน้าที่**

| วันรับคำขอ 16 ธ.ค. 2559 | เลขที่คำขอ 1601003554 |
|---|---|
| วันยื่นคำขอ 16 ธ.ค. 2559 | |

สัญลักษณ์จำแนกการประดิษฐ์ระหว่างประเทศ

ใช้กับแบบผลิตภัณฑ์
ประเภทผลิตภัณฑ์

| วันประกาศโฆษณา | เลขที่ประกาศโฆษณา |
|---|---|
| วันออกสิทธิบัตร/อนุสิทธิบัตร | เลขที่สิทธิบัตร/อนุสิทธิบัตร |

ลายมือชื่อเจ้าหน้าที่

1.ชื่อที่แสดงถึงการประดิษฐ์/การออกแบบผลิตภัณฑ์
กรรมวิธีการเตรียมสารประกอบอนุภาคที่สามารถจับกับเชื้อก่อโรคฟันผุได้อย่างจำเพาะสำหรับใช้ในการแยกและตรวจวัดเชื้อก่อโรคฟันผุเชิงกึ่งปริมาณได้ด้วยตาเปล่า



2.คำขอรับสิทธิบัตรการออกแบบผลิตภัณฑ์นี้เป็นคำขอสำหรับแบบผลิตภัณฑ์อย่างเดียวกันและเป็นคำขอลำดับที่
ในจำนวน คำขอ ที่ยื่นในคราวเดียวกัน

| 3.ผู้ขอรับสิทธิบัตร/อนุสิทธิบัตร และที่อยู่ (เลขที่ ถนน ประเทศ) ดูที่หน้า 3 | 3.1 สัญชาติ |
|---|---|
| | 3.2 โทรศัพท์ |
| | 3.3 โทรสาร |
| | 3.4 อีเมล์ |

4.สิทธิในการขอรับสิทธิบัตร/อนุสิทธิบัตร
☐ ผู้ประดิษฐ์/ผู้ออกแบบ ☑ ผู้รับโอน ☐ ผู้ขอรับสิทธิโดยเหตุอื่น

| 5.ตัวแทน(ถ้ามี)/ที่อยู่ (เลขที่ ถนน จังหวัด รหัสไปรษณีย์) ดูที่หน้า 3 | 5.1 ตัวแทนเลขที่ |
|---|---|
| | 5.2 โทรศัพท์ |
| | 5.3 โทรสาร |
| | 5.4 อีเมล์ |

6.ผู้ประดิษฐ์/ผู้ออกแบบผลิตภัณฑ์ และที่อยู่ ( เลขที่ ถนน ประเทศ )
ดูที่หน้า 3

7. คำขอรับสิทธิบัตร/อนุสิทธิบัตรนี้แยกจากหรือเกี่ยวข้องกับคำขอเดิม
ผู้ขอรับสิทธิบัตร/อนุสิทธิบัตร ขอให้ถือว่าได้ยื่นคำขอรับสิทธิบัตร/อนุสิทธิบัตรนี้ ในวันเดียวกับคำขอรับสิทธิบัตร
เลขที่ วันยื่น เพราะคำขอรับสิทธิบัตร/อนุสิทธิบัตรนี้แยกจากหรือเกี่ยวข้องกับคำขอเดิมเพราะ
☐ คำขอเดิมมีการประดิษฐ์หลายอย่าง ☐ ถูกคัดค้านเนื่องจากผู้ขอไม่มีสิทธิ ☐ ขอเปลี่ยนแปลงประเภทของสิทธิ

8.การยื่นคำขอนอกราชอาณาจักร

| วันยื่นคำขอ | เลขที่คำขอ | ประเทศ | สัญลักษณ์จำแนกการประดิษฐ์ระหว่างประเทศ | สถานะคำขอ |
|---|---|---|---|---|
| 8.1 | | | | |
| 8.2 | | | | |
| 8.3 | | | | |

8.4 ☐ ผู้ขอรับสิทธิบัตร/อนุสิทธิบัตรขอสิทธิให้ถือว่าได้ยื่นคำขอนี้ในวันที่ได้ยื่นคำขอรับสิทธิบัตร/อนุสิทธิบัตรในต่างประเทศเป็นครั้งแรกโดย
☐ ได้ยื่นเอกสารหลักฐานพร้อมคำขอนี้ ☐ ขอยื่นเอกสารหลักฐานหลังจากวันยื่นคำขอนี้

9.การแสดงการประดิษฐ์ หรือการออกแบบผลิตภัณฑ์ ผู้ขอรับสิทธิบัตร/อนุสิทธิบัตรได้แสดงการประดิษฐ์ที่หน่วยงานของรัฐเป็นผู้จัด
วันแสดง วันเปิดงานแสดง ผู้จัด

10.การประดิษฐ์เกี่ยวกับจุลชีพ

| 10.1 เลขทะเบียนฝากเก็บ | 10.2 วันที่ฝากเก็บ | 10.3 สถาบันฝากเก็บ/ประเทศ |
|---|---|---|
| | | |

11.ผู้ขอรับสิทธิบัตร/อนุสิทธิบัตร ขอยื่นเอกสารภาษาต่างประเทศก่อนในวันยื่นคำขอนี้ และจะจัดยื่นคำขอรับสิทธิบัตร/อนุสิทธิบัตรนี้ที่จัดทำเป็นภาษาไทยภายใน 90 วัน นับจากวันยื่นคำขอนี้ โดยขอยื่นเป็นภาษา
☐ อังกฤษ ☐ ฝรั่งเศส ☐ เยอรมัน ☐ ญี่ปุ่น ☐ อื่นๆ

12.ผู้ขอรับสิทธิบัตร/อนุสิทธิบัตร ขอให้อธิบดีประกาศโฆษณาคำขอรับสิทธิบัตร หรือรับจดทะเบียน และประกาศโฆษณาอนุสิทธิบัตรนี้ หลังจากวันที่ เดือน พ.ศ
☐ ผู้ขอรับสิทธิบัตร/อนุสิทธิบัตรขอให้ใช้รูปเขียนหมายเลข ในการประกาศโฆษณา

13.คำขอรับสิทธิบัตร/อนุสิทธิบัตรนี้ประกอบด้วย
ก. แบบพิมพ์คำขอ 3 หน้า
ข. รายละเอียดการประดิษฐ์ หรือคำพรรณนาแบบผลิตภัณฑ์ 8 หน้า
ค. ข้อถือสิทธิ 3 หน้า
ง. รูปเขียน 1 รูป 1 หน้า
จ. ภาพแสดงแบบผลิตภัณฑ์
☐ รูปเขียน รูป หน้า
☐ ภาพถ่าย รูป หน้า
ฉ. บทสรุปการประดิษฐ์ 1 หน้า

14.เอกสารประกอบคำขอ
☐ เอกสารแสดงสิทธิในการขอรับสิทธิบัตร/อนุสิทธิบัตร
☐ หนังสือรับรองการแสดงการประดิษฐ์/การออกแบบผลิตภัณฑ์
☐ หนังสือมอบอำนาจ
☐ เอกสารรายละเอียดเกี่ยวกับจุลชีพ
☐ เอกสารการขอนับวันยื่นคำขอในต่างประเทศเป็นวันยื่นคำขอในประเทศไทย
☐ เอกสารขอเปลี่ยนแปลงประเภทของสิทธิ
☐ เอกสารอื่น ๆ

15. ข้าพเจ้าขอรับรองว่า
☑ การประดิษฐ์นี้ไม่เคยยื่นขอรับสิทธิบัตร/ อนุสิทธิบัตรมาก่อน
☐ การประดิษฐ์นี้ได้พัฒนาปรับปรุงมาจาก.....

16.ลายมือชื่อ ( ☐ ผู้ขอรับสิทธิบัตร / อนุสิทธิบัตร; ☑ ตัวแทน )
นายบัญชา วงศ์ณัฐภัทร

3.ผู้ขอรับสิทธิบัตร/อนุสิทธิบัตร และที่อยู่ (เลขที่ ถนน ประเทศ)

จุฬาลงกรณ์มหาวิทยาลัย
อยู่ที่ 254 ถนนพญาไท แขวงวังใหม่ เขตปทุมวัน กรุงเทพฯ 10330
3.1 สัญชาติ ไทย 3.2 โทรศัพท์ 0-2218-4180 3.3 โทรสาร 0-2218-4181

สำนักงานกองทุนสนับสนุนการวิจัย
อยู่ที่ ชั้น 14 อาคาร เอส เอ็ม ทาวเวอร์ 979/17-21 ถนนพหลโยธิน แขวงสามเสนใน เขตพญาไท กรุงเทพฯ 10400
3.1 สัญชาติ ไทย 3.2 โทรศัพท์ 0-2278-8200 3.3 โทรสาร 0-2298-0476

5. ตัวแทน(ถ้ามี)/ที่อยู่ (เลขที่ ถนน จังหวัด รหัสไปรษณีย์)
นายมงคล แก้วมหา
อยู่ที่ สถาบันทรัพย์สินทางปัญญาแห่งจุฬาลงกรณ์มหาวิทยาลัย 254 อาคารวิจัยจุฬาลงกรณ์มหาวิทยาลัย ชั้น 14 ถนนพญาไท แขวงวังใหม่ เขตปทุมวัน กรุงเทพฯ 10330
5.1 ตัวแทนเลขที่ 1453 5.2 โทรศัพท์ 0-2218-4180 5.3 โทรสาร 0-2218-4181

และ/หรือ

นายบัญชา วงศ์ณัฐภัทร
อยู่ที่ สถาบันทรัพย์สินทางปัญญาแห่งจุฬาลงกรณ์มหาวิทยาลัย 254 อาคารวิจัยจุฬาลงกรณ์มหาวิทยาลัย ชั้น 14 ถนนพญาไท แขวงวังใหม่ เขตปทุมวัน กรุงเทพฯ 10330
5.1 ตัวแทนเลขที่ 2392 5.2 โทรศัพท์ 0-2218-4180 5.3 โทรสาร 0-2218-4181 5.4 อีเมล์ Bancha.V@chula.ac.th

6.ผู้ประดิษฐ์/ผู้ออกแบบผลิตภัณฑ์ และที่อยู่ ( เลขที่ ถนน ประเทศ )

นางสาวพนิดา ธัญญศรีสังข์
อยู่ที่ ภาควิชาจุลชีววิทยา คณะทันตแพทยศาสตร์ จุฬาลงกรณ์มหาวิทยาลัย ถนนพญาไท แขวงวังใหม่ เขตปทุมวัน กรุงเทพฯ 10330

นางสาวเอมวิกา วิทยาประสิทธิ์
อยู่ที่ หลักสูตรปิโตรเคมีและวิทยาศาสตร์พอลิเมอร์ คณะวิทยาศาสตร์ จุฬาลงกรณ์มหาวิทยาลัย ถนนพญาไท แขวงวังใหม่ เขตปทุมวัน กรุงเทพฯ 10330

นางวรวีร์ โฮเว่น
อยู่ที่ ภาควิชาเคมี คณะวิทยาศาสตร์ จุฬาลงกรณ์มหาวิทยาลัย ถนนพญาไท แขวงวังใหม่ เขตปทุมวัน กรุงเทพฯ 10330

นายโมโตยูกิ ซูไก
อยู่ที่ ภาควิชาแบคทีเรียวิทยา บัณฑิตวิทยาลัย วิทยาศาสตร์ชีวการแพทย์ และวิทยาศาสตร์สุขภาพ มหาวิทยาลัยฮิโรชิมา จังหวัดฮิโรชิมา ประเทศญี่ปุ่น

## รายละเอียดการประดิษฐ์

### ชื่อที่แสดงถึงการประดิษฐ์

กรรมวิธีการเตรียมสารประกอบอนุภาคที่สามารถจับกับเชื้อก่อโรคฟันผุได้อย่างจำเพาะสำหรับใช้ในการแยกและตรวจวัดเชื้อก่อโรคฟันผุเชิงกึ่งปริมาณได้ด้วยตาเปล่า

### สาขาวิทยาการที่เกี่ยวข้องกับการประดิษฐ์

สาขาเคมี และวิทยาศาสตร์ชีวการแพทย์ที่เกี่ยวข้องกับกรรมวิธีการผลิตสารประกอบอนุภาคที่สามารถจับกับเชื้อก่อโรคฟันผุได้อย่างจำเพาะสำหรับใช้ในการแยกและตรวจวัดเชื้อก่อโรคฟันผุเชิงกึ่งปริมาณได้ด้วยตาเปล่า

### ภูมิหลังของศิลปะหรือวิทยาการที่เกี่ยวข้อง

โรคฟันผุยังคงเป็นปัญหาสาธารณสุขที่สำคัญของประเทศไทย ดังจะเห็นได้จากรายงานผลการสำรวจทันตสาธารณสุขแห่งชาติครั้งที่ 7 พ.ศ. 2555 ที่ความชุกของโรคในกลุ่มเด็กก่อนวัยเรียนอายุ 3 และ 5 ปี และในกลุ่มเด็กวัยเรียน และเยาวชนอายุ 12 และ 15 ปีมีมากเกินกว่าครึ่งหนึ่งของประชากรที่ถูกสำรวจ ความชุกของโรคฟันผุในประชากรไทยอยู่ในระดับนี้มาตลอดระยะเวลาเกือบ 10 กว่าปีที่ผ่านมา สาเหตุหนึ่งอาจจะมาจากการให้การรักษา และป้องกันโรคฟันผุในคนไข้ทุกคนในระดับเดียวกัน ทั้ง ๆ ที่ความเสี่ยงของการเกิดโรคฟันผุเป็นเรื่องของแต่ละบุคคล ทำให้กลุ่มที่มีความเสี่ยงสูงได้รับการรักษา และป้องกันไม่เพียงพอที่จะทำให้หยุดการเกิดโรคขึ้นได้ การประเมินความเสี่ยงในการเกิดโรคฟันผุ เป็นกระบวนการประเมินว่าบุคคลนี้มีความเสี่ยงที่จะเกิดฟันผุอยู่ในระดับไหน ซึ่งค่าที่ประเมินได้นั้นจะช่วยให้ทันตแพทย์เลือกวิธีการรักษา และป้องกันได้อย่างเหมาะสม ความเสี่ยงของการเกิดโรคฟันผุนี้ประเมินโดยอาศัยหลายปัจจัยด้วยกัน เช่น พฤติกรรมการทานอาหาร การดูแลสุขภาพช่องปาก คุณลักษณะของน้ำลาย และปริมาณเชื้อก่อโรคฟันผุ เป็นต้น ปัจจัยที่นำมาประเมินนี้ส่วนใหญ่สามารถทำได้ทันทีข้างเก้าอี้ทำฟัน ยกเว้นการหาปริมาณเชื้อ ถึงแม้จะมีชุดตรวจเชื้อสำเร็จรูปออกมาจำหน่ายทำให้สะดวกมากขึ้น แต่ก็ยังต้องอาศัยเวลาในการอบเลี้ยงเชื้อ และต้องการอุปกรณ์ที่มีขนาดใหญ่เกินพกพา และมีราคาแพง ทำให้ไม่สะดวกที่จะนำมาใช้ในงานระดับชุมชน

มีเอกสารการยื่นขอสิทธิบัตรแสดงเครื่องมือตรวจเชื้อแบคทีเรียอย่างรวดเร็ว (rapid bacterial detection tool) โดยอาศัยหลักการอิมมูโนโครมาโทกราฟี และทองคอลลอยด์ (colloidal gold- based immunochromatography) โดยในชุดตรวจนี้ใช้แอนติบอดีที่จำเพาะกับเชื้อสเตรปโตคอคคัส มิวแทนส์เป็นเครื่องมือในการจับเชื้อ (probe) นำไปติดกับทองคอลลอยด์ (colloidal gold) ทำให้เห็นสีได้ด้วยตาเปล่า (เอกสารการยื่นขอสิทธิบัตรประเทศสหรัฐอเมริกาเลขที่ US 20080240993 A1) มีรายงานการวิจัยถึงประสิทธิภาพของ

เครื่องมือนี้ว่ามีความไวในการตรวจหาเชื้อ (sensitivity) อยู่ที่ร้อยละ 97.6 แต่มีความจำเพาะ (specificity) เพียงร้อยละ 90.6 เท่านั้นเมื่อเทียบกับการตรวจด้วยวิธีเรียลไทม์ พีซีอาร์ (real-time PCR) ซึ่งผู้วิจัยใช้เป็นวิธียืนยันจำนวนเชื้อ (Int J Paediatr Dent., Vol 22, p 363-368, 2012) ด้วยเหตุนี้ทำให้เกิดแนวคิดที่จะพัฒนาวิธีการตรวจที่มีความไว และความจำเพาะกับเชื้อมิวแทนส์ สเตรปโตคอคไค ที่มีประสิทธิภาพมากขึ้นและยังคงเห็นผลได้ด้วยตาเปล่า

เอนไซม์เปปทิโดไกลแคน ไฮโดรเลส (peptidoglycan hydrolase) เป็นเอนไซม์ที่พบได้ในแบคทีเรียเกือบทุกชนิด มีหน้าที่ในการย่อยสลายเปปทิโดไกลแคนซึ่งเป็นโครงสร้างที่พบได้ในผนังเซลล์ของแบคทีเรียทั่วไป โดยเฉพาะแบคทีเรียแกรมบวก (Gram positive bacteria) แต่เป็นโครงสร้างที่ไม่พบในเซลล์ของมนุษย์ เอนไซม์นี้มีบทบาทสำคัญต่อการแบ่งตัว และแยกตัวของเซลล์แบคทีเรีย จากรายงานสิทธิบัตร และจากงานวิจัยที่ผ่านมาพบว่าเชื้อสเตรปโตคอคคัส มิวแทนส์ (*Streptococcus mutans*) ผลิตเอนไซม์เปปทิโดไกลแคน ไฮโดรเลสซึ่งถูกตั้งชื่อว่า ออโตมิวตะโนไลซิน (automutanolysin) หรือเอเอ็มแอล (Aml) ที่มีความจำเพาะในการย่อยสลายเชื้อสเตรปโตคอคคัส มิวแทนส์ (*Streptococcus mutans*) และสเตรปโตคอคคัส ซอบรินัส (*Streptococcus sobrinus*) ซึ่งอยู่ในกลุ่มเชื้อมิวแทนส์ สเตรปโตคอคไค (mutans streptococci) อันเป็นเชื้อกลุ่มสำคัญกลุ่มหนึ่งต่อการเกิดโรคฟันผุ และเป็นตัวชี้วัดหนึ่งที่ใช้ในการประเมินความเสี่ยงในการเกิดโรคฟันผุ โครงสร้างของเอนไซม์นี้ประกอบขึ้นด้วยกรดอะมิโน 979 ตัว มีน้ำหนักโมเลกุลประมาณ 104 กิโลดาลตัน และมีสองโดเมนหลักได้แก่ คาตาไลติกโดเมนอยู่ทางฝั่งปลายด้านหมู่คาร์บอกซิล (C-terminal catalytic domain) ซึ่งมีบทบาทในการย่อยสลายผนังเซลล์ และอีกโดเมนอยู่ฝั่งปลายด้านหมู่อะมิโนทำหน้าที่ในการจับกับผนังเซลล์ (cell wall binding domain) ซึ่งมีความจำเพาะกับเชื้อมิวแทนส์ สเตรปโตคอคไค (Microbiol Immunol., Vol 50, p 729-42, 2006 และสิทธิบัตรประเทศสหรัฐอเมริกาเลขที่ US 7,776,325 B2 และ US 8,852,584 B2) ด้วยความจำเพาะนี้หากทำการตัดต่อยีนโดยเอาส่วนคาตาไลติกโดเมนที่ใช้ในการย่อยสลายเปปทิโดไกลแคนออกไป ก็จะสามารถใช้เอนไซม์ดังกล่าวนี้ในการจับกับผนังเซลล์ของเชื้อมิวแทนส์ สเตรปโตคอคไค (probe) เพื่อใช้ในการตรวจวัดปริมาณของเชื้อได้

ในการตรวจวัดปริมาณของเชื้อแบคทีเรียได้มีการพัฒนากรรมวิธีการผลิตของอนุภาคแม่เหล็กนาโนที่สามารถตรวจวัดปริมาณของเชื้อมิวแทนส์ สเตรปโตคอคไคที่สามารถเห็นผลได้ด้วยตาเปล่า ซึ่งทำได้โดยการยึดติดโดเมนจับกับผนังเซลล์ของเอนไซม์เอเอ็มแอลกับอนุภาคแม่เหล็กนาโน (magnetic nanoparticles, MNPs) ที่มีขนาดตั้งแต่ 5 ถึง 500 นาโนเมตร กลายเป็นสารประกอบอนุภาคที่มีความจำเพาะกับเชื้อมิวแทนส์ สเตรปโตคอคไค โดยทั่วไปอนุภาคแม่เหล็กนาโนที่นิยมใช้มักเป็นแบบแมกเนไทต์ ($Fe_3O_4$) หรือแมกฮีไมต์ ($\gamma$-$Fe_2O_3$) มีสมบัติที่สามารถตอบสนองต่อสนามแม่เหล็กภายนอกได้อย่างรวดเร็ว ด้วยสมบัติดังกล่าวจึงทำให้อนุภาคแม่เหล็กนาโนสามารถนำมาใช้ในการแยกเชื้อแบคทีเรียโดยการควบคุมผ่านสนามแม่เหล็กภายนอก เชื้อแบคทีเรียที่แยกมาได้จึง

มีความบริสุทธิ์ และง่ายต่อการตรวจวัดยิ่งขึ้น และเมื่อนำไปกรองแบบเลือกผ่าน (selective filtration) สารประกอบอนุภาคที่จับกับเชื้อแบคทีเรียจะติดอยู่บนแผ่นเมมเบรนไม่สามารถผ่านรูพรุนของแผ่นเมมเบรนมาได้ โดยปริมาณของสารประกอบอนุภาคที่จับกับเชื้อแบคทีเรียจะแปรผันตรงกับความเข้มของสีบนแผ่นเมมเบรน จึงสามารถวิเคราะห์หาเชื้อแบคทีเรียเชิงกึ่งปริมาณได้ด้วยตาเปล่า (semi-quantitative analysis)

มีสิทธิบัตรรายงานการผลิตอนุภาคแม่เหล็กนาโนตรึงแอนติบอดีมาใช้ในการจับกับเชื้อแบคทีเรีย โดยจากรายงานพบว่าจากกรรมวิธีการผลิตอนุภาคแม่เหล็กนาโนตรึงแอนติบอดีนี้ อนุภาคสามารถจับกับเชื้อแบคทีเรียได้ตามสิทธิบัตรประเทศสหรัฐอเมริกาเลขที่ 8,883,455 และเลขที่ 9,201,066 แต่ยังไม่มีงานวิจัยใดคิดค้นเกี่ยวกับกรรมวิธีการผลิตอนุภาคแม่เหล็กนาโนที่สามารถตรวจวัดปริมาณเชื้อมิวแทนส์ สเตรปโตคอคไค โดยใช้อนุภาคแม่เหล็กนาโนติดกับโดเมนที่จับกับผนังเซลล์ของเอนไซม์เอเอ็มแอล ซึ่งผลของการตรวจวัดปริมาณเชื้อนี้สามารถใช้ประกอบการประเมินความเสี่ยงการเกิดโรคฟันผุได้

มีงานวิจัยที่รายงานการตรวจวัดปริมาณของเชื้อซาลโมเนลลา ไทฟิมิวเรียม *(Salmonella typhimurium)* โดยมีกรรมวิธีการผลิตของอนุภาคแม่เหล็กนาโนตรึงด้วยแอนติบอดีที่มีความจำเพาะเจาะจงกับเชื้อ ผ่านการสร้างพันธะระหว่างหมู่คาร์บอกซิลบนพื้นผิวของอนุภาคนาโนแม่เหล็ก และหมู่อะมิโนของแอนติบอดี โดยใช้ 1-เอทิล-3-(3-ไดเมทิลลามีนโพรพิล) คาร์โบดิไอไมด์ไฮโดรคลอไรด์ (1-ethyl-3-(3-dimethylaminepropyl) carbodiimide hydrochloride; EDC) เป็นรีเอเจนต์คู่ควบ อย่างไรก็ตามงานวิจัยดังกล่าวยังประสบปัญหาการตรวจวัดเนื่องจากความเข้มข้นต่ำที่สุดของแบคทีเรียที่สามารถตรวจวัดได้ยังมีค่าสูง ดังนั้นจึงควรมีกรรมวิธีการตรึงพอลิเมอร์ลงไปบนพื้นผิวของอนุภาคเพื่อให้ได้อนุภาคแม่เหล็กนาโนที่สามารถตรวจวัดเชื้อในปริมาณต่ำได้และสามารถตรวจวัดเชื้อได้อย่างมีประสิทธิภาพ (Anal. Chem., Vol 406, p 406-866, 2014)

นอกจากนี้ยังมีรายงานการนำเอาพอลิเมอร์มาตรึงบนพื้นผิวของอนุภาคแม่เหล็กนาโน เพื่อช่วยทำให้อนุภาคมีความเสถียรมากขึ้น ไม่เกิดการเกาะกลุ่มของอนุภาคและสามารถกระจายตัวอยู่ในสารละลายได้ดียิ่งขึ้น มีงานวิจัยที่เปรียบเทียบสมบัติการกระจายตัว และความเสถียรของอนุภาคแม่เหล็กนาโนที่ตรึง และไม่ได้ตรึงพอลิเมอร์ โดยได้สังเคราะห์อนุภาคแม่เหล็กนาโนตรึงด้วยพอลิอะคริลิกแอซิด (poly(acrylic acid)) หรือพอลิสไตรีน (polystyrene) ลงบนพื้นผิว เริ่มจากนำอนุภาคนาโนแม่เหล็กมาทำปฏิกิริยากับโอโซน เพื่อเกิดหมู่เปอร์ออกไซด์ (peroxide group) บนพื้นผิว ซึ่งจะทำหน้าที่เป็นสารริเริ่มปฏิกิริยา และใช้ 1-เฟนิลเอทิลไดไทโอเบนโซเอท (1-phenylethyl dithiobenzoate; PVB) ทำหน้าที่เป็นสารถ่ายโอนโซ่ (chain transfer agent) นำไปทำปฏิกิริยาพอลิเมอไรเซชันแบบควบคุม (controlled polymerization) ด้วยกลไกแบบ reversible addition-fragmentation chain transfer (RAFT) จะได้อนุภาคแม่เหล็กนาโนที่ตรึงด้วยพอลิอะคริลิกแอซิดหรือพอลิสไต

รีน แล้วนำไปทดสอบสมบัติการกระจายตัวและความเสถียร พบว่าอนุภาคแม่เหล็กนาโนที่ตรึงพอลิเมอร์ลงบนพื้นผิวสามารถกระจายตัว และมีความเสถียรดีกว่าอนุภาคแม่เหล็กนาโนที่ไม่ได้ตรึงพอลิเมอร์ลงบนพื้นผิว (Macromolecules, Vol 27, p 1665-1669, 2006)

แนวทางหนึ่งที่น่าสนใจในการปรับปรุงพื้นผิวของวัสดุด้วยพอลิเมอร์คือ การเตรียมเป็นพอลิเมอร์บรัช (polymer brushes) ซึ่งเป็นพอลิเมอร์ที่มีปลายของโซ่ด้านหนึ่งยึดติดบนพื้นผิวด้วยพันธะโควาเลนต์ (covalent bond) ทำให้มีเสถียรภาพในการยึดติดบนพื้นผิวสูงกว่าการดูดซับทางกายภาพ (physical absorption) การเตรียมพอลิเมอร์บรัชนิยมเตรียมด้วยปฏิกิริยาพอลิเมอไรเซชันริเริ่มจากพื้นผิว (surface-initiated polymerization) ทั้งนี้ความยาวของโซ่พอลิเมอร์สามารถควบคุมได้หากใช้ปฏิกิริยาพอลิเมอไรเซชันแบบควบคุม (controlled polymerization) เช่น atom transfer radical polymerization (ATRP) และ reversible addition-fragmentation chain transfer (RAFT) (Prog. Polym. Sci., Vol 25, p 677-710, 2000 และ Chem. Rev., Vol 109, p 5437-5527, 2009) โดยสมบัติทางเคมีและกายภาพของพอลิเมอร์บรัชขึ้นกับชนิดของมอนอเมอร์ (monomer) ที่เลือกใช้ในการสังเคราะห์

การประดิษฐ์นี้สนใจที่จะตรึงพอลิเมอร์บรัชของพอลิอะคริลิกแอซิด (poly(acrylic acid); PAA) ลงบนพื้นผิวของอนุภาคแม่เหล็กนาโน ผ่านปฏิกิริยา และ reversible addition-fragmentation chain transfer polymerization โดยโครงสร้างของพอลิเมอร์บรัชมีหมู่คาร์บอกซิล (carboxyl group) ซึ่งสามารถยึดติดกับหมู่อะมิโน (amino group) ของโดเมนที่ทำหน้าที่จับกับผนังเซลล์ (cell wall binding domain; CWBD) ผ่านการเกิดพันธะเอไมด์ (amide bond) ได้ จึงสามารถติดโดเมนนี้ได้ปริมาณมาก ส่งผลให้สารประกอบอนุภาคมีประสิทธิภาพในการตรวจวัดเชื้อที่ดีขึ้น

**ลักษณะและความมุ่งหมายของการประดิษฐ์**

การประดิษฐ์นี้เกี่ยวข้องกับกรรมวิธีการผลิตสารประกอบอนุภาคที่สามารถจับกับเชื้อก่อโรคฟันผุได้อย่างจำเพาะสำหรับใช้ในการแยกและตรวจวัดเชื้อก่อโรคฟันผุเชิงกึ่งปริมาณได้ด้วยตาเปล่า ประกอบรวมด้วยกรรมวิธีการเตรียมโดเมนของเอนไซม์ที่ทำหน้าที่จับกับผนังเซลล์ของเชื้อก่อโรคฟันผุอย่างจำเพาะ และกรรมวิธีการผลิตอนุภาคแม่เหล็กนาโน เตรียมโดยการนำโดเมนของเอนไซม์ออโตมิวตะโนไลซินที่ทำหน้าที่จับกับผนังเซลล์ มายึดติดกับอนุภาคแม่เหล็กนาโนตรึงด้วยพอลิเมอร์ที่มีหมู่ฟังก์ชันเป็นหมู่คาร์บอกซิลหรือพอลิอะคริลิกแอซิดผ่านพันธะเอไมด์ เกิดเป็นสารประกอบอนุภาคที่มีความจำเพาะในการจับกับเชื้อมิวแทนส์ สเตรปโตคอคไค โดยโดเมนที่ทำหน้าที่จับกับผนังเซลล์นี้มีความจำเพาะต่อเชื้อมิวแทนส์ สเตรปโตคอคไค จึงสามารถเลือกจับเฉพาะเชื้อนี้ได้

ความมุ่งหมายของการประดิษฐ์นี้เพื่อผลิตสารประกอบอนุภาคที่ตรึงด้วยพอลิเมอร์และยึดติดโดเมนของเอนไซม์ออโตมิวตะโนไลซินซึ่งสามารถจับกับเชื้อก่อโรคฟันผุได้อย่างจำเพาะ โดยกรรมวิธีในการผลิตสารประกอบอนุภาคใช้วิธีการตรึงอนุภาคแม่เหล็กนาโนด้วยพอลิเมอร์ที่มีหมู่ฟังก์ชันเป็นหมู่คาร์บอกซิลหรือพอลิอะคริลิกแอซิด ทำให้สามารถยึดติดโดเมนที่ทำหน้าที่จับกับผนังเซลล์ได้เป็นจำนวนมาก ส่งผลให้เพิ่มประสิทธิภาพในการจับกับเชื้อได้ดียิ่งขึ้น

**คำอธิบายรูปเชียนโดยย่อ**

รูปที่ 1 แสดงพลาสมิดลูกผสมที่มียีนส่วนที่มีความจำเพาะในการจับผนังเซลล์ (cell wall binding domain; CWBD) จากเอนไซม์ออโตมิวตะโนไลซิน เชื่อมต่อกับเวคเตอร์ pColdIII

**การเปิดเผยการประดิษฐ์โดยสมบูรณ์**

การประดิษฐ์นี้เกี่ยวข้องกับกรรมวิธีการผลิตสารประกอบอนุภาคที่สามารถจับกับเชื้อก่อโรคฟันผุได้อย่างจำเพาะสำหรับใช้ในการแยกและตรวจวัดเชื้อก่อโรคฟันผุเชิงกึ่งปริมาณได้ด้วยตาเปล่า มีขั้นตอนประกอบด้วยการนำโดเมนของเอนไซม์ที่ทำหน้าที่จับกับผนังเซลล์ ซึ่งสามารถจับกับเชื้อก่อโรคฟันผุในกลุ่ม สเตรปโตคอคไคได้อย่างจำเพาะมายึดติดผ่านพันธะเอไมด์กับอนุภาคแม่เหล็กนาโนที่ตรึงด้วยพอลิเมอร์ที่มีหมู่ฟังก์ชันเป็นหมู่คาร์บอกซิล หรือพอลิอะคริลิกแอซิด (poly(acrylic acid)) เกิดเป็นสารประกอบอนุภาคที่มีความจำเพาะในการจับกับเชื้อก่อโรคฟันผุในกลุ่มสเตรปโตคอคไค โดยกรรมวิธีดังกล่าวประกอบรวมด้วยขั้นตอนย่อยดังนี้

<u>การเตรียมโดเมนของเอนไซม์ที่ทำหน้าที่จับกับผนังเซลล์ซึ่งสามารถจับกับเชื้อก่อโรคฟันผุในกลุ่ม สเตรปโตคอคไคได้อย่างจำเพาะ มีขั้นตอนประกอบด้วย</u>

(1) การสร้างพลาสมิดลูกผสม (recombinant plasmid) ที่มียีนของโดเมนที่ทำหน้าที่จับกับ ผนังเซลล์ (cell wall binding domain; CWBD) จากเอนไซม์ออโตมิวตะโนไลซิน โดยเริ่มจากการออกแบบไพรเมอร์ไปข้างหน้า และย้อนกลับ (forward and reward primers) จากลำดับนิวคลีโอไทด์ (nucleotide sequence) ของเอนไซม์ออโตมิวตะโนไลซินที่มีอยู่ในฐานข้อมูลของเจนแบงค์ รหัส เอบี253514 (GenBank accession AB253514) โดยดัดแปลงให้ทางปลาย 5' ของไพรเมอร์ไปข้างหน้ามีนิวคลีโอไทด์ซึ่งสามารถตัดได้ด้วยเอนไซม์ *Xho*I โดยมีลำดับนิวคลีโอไทด์ดังนี้ 5'AAAACTCGAGGATGAGCAAAAT3' และดัดแปลงให้ทางปลาย 5' ของไพรเมอร์ย้อนกลับมีนิวคลีโอไทด์ซึ่งสามารถตัดได้ด้วยเอนไซม์ *BamH*I โดยมีลำดับนิวคลีโอไทด์ดังนี้ 5'AAAAGGATCCTGGCAGAGCAACAGC3' จากนั้นเพิ่มจำนวนยีนโดยใช้โครโมโซมจากเชื้อสเตรปโตคอคคัสมิวแทนส์ เป็นดีเอ็นเอแม่แบบ (DNA template) ด้วยเทคนิคปฏิกิริยาลูกโซ่โพลิเมอเรส (polymerase chain reaction; PCR) แล้วเชื่อมชิ้นยีนนี้เข้ากับเวคเตอร์ pColdIII ที่ถูกดัดแปลงให้มีลำดับนิวคลีโอไทด์ของฮิสทิดีน

(histidine) อยู่ภายในลำดับดีเอ็นเอ (DNA sequence) เพื่อใช้ในขั้นตอนการทำให้โปรตีนบริสุทธิ์ และมียีนดื้อต่อยาปฏิชีวนะแอมพิซีลิน (ampicillin resistant gene) เพื่อใช้ในการคัดเลือกเชื้อที่รับพลาสมิดลูกผสมเข้าไปในเซลล์ได้สำเร็จ (รูปที่ 1) จากนั้นเคลื่อนย้ายพลาสมิดลูกผสมนี้เข้าสู่เชื้อเอสเชอริเชีย โคไล สายพันธุ์ BL-21 (*Escherichia coli* BL-21) (transformation) คัดเลือกเชื้อที่รับ พลาสมิดลูกผสมนี้เข้าไปได้สำเร็จโดยการเลี้ยงเชื้อบนอาหารเลี้ยงเชื้อชนิดแข็ง ลูเรีย-เบอร์ทานิ (Luria Bertani agar) ที่มียาปฏิชีวนะแอมพิซีลิน (ampicillin)

(2) การผลิตโปรตีนจากเชื้อเอสเชอริเชีย โคไล (*Escherichia coli*; *E. coli*) ที่รับพลาสมิดลูกผสมเข้าไปได้สำเร็จ และการทำให้โปรตีนบริสุทธิ์ โดยเริ่มจากการเลี้ยงเชื้อ *E. coli* สายพันธุ์ BL-21 ที่มีพลาสมิดลูกผสม (recombinant plasmid) ของยีนของโดเมนที่ทำหน้าที่จับกับผนังเซลล์ (cell wall binding domain; CWBD) จากเอนไซม์ออโตมิวตะโนไลซินในอาหารเลี้ยงเชื้อเหลวลูเรีย-เบอร์ทานิ (Luria Bertani; LB) ที่มียาปฏิชีวนะแอมพิซีลิน (ampicillin) นำไปอบที่อุณหภูมิ 37 องศาเซลเซียส เป็นเวลาข้ามคืน (12-16 ชั่วโมง) ถ่ายโอนหัวเชื้อที่ได้ในปริมาตร ที่เหมาะสมลงในอาหารเลี้ยงเชื้อเหลว LB ที่มียาปฏิชีวนะแอมพิซีลิน นำไปอบเลี้ยงต่อจนได้ค่าการดูดกลืนแสงที่ 600 นาโนเมตร อยู่ในช่วงระยะแบ่งตัวทวีคูณ (log phage; 0.4-0.6) จากนั้นนำไปอบที่อุณหภูมิ 15 องศาเซลเซียส เป็นเวลา 30-45 นาที แล้วจึงเติมสารละลายไอโซโพรพิล-เบต้า-ดี-ไทโอกาแลคโตไซด์ (isopropyl-β-D-thiogalactoside; IPTG) 0.5-1 มิลลิโมลาร์ เพื่อเหนี่ยวนำการสร้างโปรตีน จากนั้นนำไปอบที่อุณหภูมิ 15 องศาเซลเซียส เป็นเวลา 20-24 ชั่วโมง แล้วทำการเก็บเซลล์ด้วยการปั่นด้วยความเร็วสูง นำเซลล์ที่ได้ละลายในไลซิส บัฟเฟอร์ (lysis buffer) และนำไปทำให้เซลล์แตกโดยใช้เครื่องที่ให้คลื่นความถี่สูง (sonicator) เพื่อที่จะได้นำโปรตีนที่ถูกสร้างภายในเซลล์ไปทำให้บริสุทธิ์โดยผ่านคอลัมน์ที่แยกสารตามความจำเพาะ (affinity column) ล้างคอลัมน์ด้วยวอช บัฟเฟอร์ (wash buffer) และแยกโปรตีนออกจากคอลัมน์ด้วยอีลูชั่น บัฟเฟอร์ (elusion buffer) โดยแยกเก็บโปรตีนที่ได้ออกเป็นส่วนๆ (fractions) นำแต่ละส่วนแยกที่ได้ไปวิเคราะห์ด้วยเทคนิคพอลิอะคริลาไมด์เจลอิเลคโตรโฟรีซีส แบบเอสดีเอส-เพจ (polyacrylamide gel electrophoresis; SDS-PAGE) เพื่อเลือกส่วนแยกที่มี ปริมาณโปรตีนมากที่สุด (active fraction) มารวมกัน และนำไปไดอะไลซิส (dialysis) ในฟอสเฟตบัฟเฟอร์ซาลีน (phosphate buffer saline; PBS) หลังจากนั้นทำการวิเคราะห์หาปริมาณโปรตีนเปรียบเทียบกับความเข้มข้นของโปรตีนมาตรฐาน

<u>การเตรียมอนุภาคแม่เหล็กนาโนที่ตรึงด้วยพอลิเมอร์ที่มีหมู่ฟังก์ชันเป็นหมู่คาร์บอกซิล หรือพอลิอะคริลิกแอซิดบนพื้นผิว มีขั้นตอนประกอบด้วย</u>

(1) สังเคราะห์อนุภาคแม่เหล็กนาโนด้วยวิธีโซโวเทอร์มอล (solvothermal) โดยชั่งไอรอนคลอไรด์เฮกซาไฮเดรต (iron chloride hexahydrate) 0.01-0.05 โมลาร์ ละลายในเอทิลีน ไกลคอล (ethylene glycol) ผสมสารละลายให้เข้ากันโดยสารละลายจะเกิดการเปลี่ยนสีเป็นสีน้ำตาลเข้ม จากนั้นเติมโซเดียมอะซิเตต (sodium acetate) ความเข้มข้น 0.3-0.7 โมลาร์ ลงไปในขวดแก้วแล้วคนสารละลายให้เข้ากันเป็นเวลา 30-50 นาที แล้ว

จึงถ่ายสารละลายนี้ลงสู่ถ้วยสเตนเลสที่พื้นผิวเคลือบเทฟลอนเพื่อนำไปอบให้ความร้อนที่อุณหภูมิ 150-300 องศาเซลเซียส เป็นเวลา 14-18 ชั่วโมง หลังจากนั้นจึงนำไปแยกอนุภาคแม่เหล็กนาโนที่ต้องการออกจากสารละลายโดยใช้สนามแม่เหล็กภายนอก ล้างอนุภาคด้วยเอทานอลแล้วนำไปอบให้ความร้อนที่อุณหภูมิ 50-80 องศาเซลเซียส จะได้ผงอนุภาคแม่เหล็กนาโนตามที่ต้องการ

(2) นำอนุภาคแม่เหล็กนาโนที่สังเคราะห์ได้มาตรึงหมู่อะมิโนซึ่งเป็นหมู่ริเริ่มในการเกิดปฏิกิริยาโดยใส่อนุภาคแม่เหล็กนาโนที่เตรียมได้จาก (1) ในขวดก้นกลมที่บรรจุเอทานอล แล้วเติมด้วย 3-อะมิโนโพรพิลไทรเอทอกซีไซเลน (3-aminopropyltriethoxysilane; APTES) และสารละลายแอมโมเนีย เขย่าสารละลายให้เข้ากันที่อุณหภูมิห้อง เป็นเวลา 10-14 ชั่วโมง จากนั้นนำอนุภาคแม่เหล็กนาโนไปล้างด้วยเอทานอล ได้อนุภาคแม่เหล็กนาโนที่มีหมู่อะมิโนเป็นหมู่ริเริ่มในการเกิดปฏิกิริยาพร้อมจะนำไปใช้ในการติดสารริเริ่ม (initiator) ในขั้นการสังเคราะห์พอลิเมอร์ต่อไป

(3) ทำการกราฟต์พอลิอะคริลิกแอซิดบนพื้นผิวของอนุภาคแม่เหล็กนาโน โดยละลาย 4,4-บิสไซยาโนวาเลอิก แอซิด (4,4-bis(4-cyanovaleic acid; ACVA) 0.1-0.3 โมลาร์, ไดไซโคลเฮกซิลคาร์โบดิ ไอไมด์ 0.02-0.05 โมลาร์, (N,N'-dicyclohexylcarbodiimide; DCC) และ 4-ไดเมทิลแอมิโนไพริดีน (4-dimethylamino pyridine; DMAP) 0.01-0.04 โมลาร์ ในไดเมทิลฟอร์มาไมด์ (dimethyl formamide; DMF) คนให้สารละลายเข้ากันเป็นเวลา 3-6 ชั่วโมง ที่อุณหภูมิห้องภายใต้บรรยากาศไนโตรเจน จากนั้นถ่ายสารละลายนี้ไปยังขวดแก้วที่บรรจุอนุภาคแม่เหล็กนาโนที่มีหมู่อะมิโนที่เตรียมได้จาก (2) ทำการคนที่อุณหภูมิห้องเป็นเวลา 20-24 ชั่วโมง จากนั้นนำอนุภาคแม่เหล็กนาโนมาล้างด้วยไดเมทิลฟอร์มาไมด์และเอทานอล ตามลำดับ ซึ่งในขั้นนี้จะได้อนุภาคแม่เหล็กนาโนที่ติดสารริเริ่ม

(4) ละลาย 4,4-บิสไซยาโนวาเลอิก แอซิด (4,4-bis (4-cyanovaleic acid; ACVA) 0.03-0.06 โมลาร์ และ 4-ไซยาโน-4-เฟนิลคาร์โบโนไทโออิลไทโอเพนทาโนอิก แอซิด (4-cyano-4-phenyl carbonothioylthio) pentanoic acid) ซึ่งทำหน้าที่เป็นสารถ่ายโอนโซ่ (chain transfer agent; CTA) 0.3-0.7 โมลาร์ ในฟอสเฟตบัฟเฟอร์ซาลีนที่มีพีเอช 7.4 (PBS buffer) และเติมมอนอเมอร์ที่มีหมู่ฟังก์ชันเป็นหมู่คาร์บอกซิล หรือ อะคริลิกแอซิด 0.05-0.1 โมลาร์ ผสมสารละลายให้เข้ากันก่อนถ่ายโอนสารละลายนี้ไปยังขวดแก้วที่บรรจุอนุภาคแม่เหล็กนาโนที่ติดสารริเริ่มแล้วทำปฏิกิริยาพอลิเมอไรเซชันที่อุณหภูมิ 60-80 องศาเซลเซียส ในอ่างน้ำมันเป็นเวลา 20-24 ชั่วโมง นำอนุภาคแม่เหล็กนาโนที่ได้มาล้างด้วยเอทานอล และน้ำ ตามลำดับ ทำอนุภาคแม่เหล็กนาโนให้แห้ง ในขั้นนี้จะได้อนุภาคแม่เหล็กนาโนที่ตรึงด้วยพอลิเมอร์ที่มีหมู่คาร์บอกซิลหรือพอลิอะคริลิกแอซิด เพื่อนำไปใช้ในการติดกับโดเมนที่ทำหน้าที่จับกับผนังเซลล์

<u>กรรมวิธีการยึดติดโดเมนของเอนไซม์ที่ทำหน้าที่จับกับผนังเซลล์กับอนุภาคแม่เหล็กนาโนที่ตรึงด้วยพอลิเมอร์ที่มีหมู่ฟังก์ชันเป็นหมู่คาร์บอกซิล หรือพอลิอะคริลิกแอซิดขั้นตอนประกอบด้วย</u>

(1) ละลาย 1-เอทิล-3-(3-ไดเมทิลเอมีนโพรพิล) คาร์โบดิไอไมด์ไฮโดรคลอไรด์ (1-ethyl-3-(3-dimethyl aminepropyl) carbodiimide hydrochloride; EDC) ความเข้มข้น 0.1-0.3 โมลาร์ และเอ็นไฮดรอกซีซักซินิไมด์ (*N*-hydroxysuccinimide; NHS) ความเข้มข้น 0.3-0.6 โมลาร์ ในฟอสเฟตบัฟเฟอร์ซาลีนที่มีพีเอช 7.4 ตามลำดับ คนสารละลายให้เข้ากัน จากนั้นถ่ายสารละลายนี้ไปยังขวดแก้วที่บรรจุอนุภาคแม่เหล็กนาโนที่ตรึงด้วยพอลิเมอร์ที่มีหมู่คาร์บอกซิล หรือพอลิอะคริลิกแอซิดบนพื้นผิว ละลายในฟอสเฟตบัฟเฟอร์ซาลีนที่มีพีเอช 7.4 แล้วคนสารละลายให้เข้ากันที่อุณหภูมิห้องเป็นเวลา 20-50 นาที

(2) เติมโดเมนที่ทำหน้าที่จับกับผนังเซลล์ความเข้มข้น 0.1-0.3 มิลลิกรัม/มิลลิลิตร ปริมาณ 1-3 มิลลิลิตร ตั้งทิ้งไว้ที่อุณหภูมิ 2 - 10 องศาเซลเซียส เป็นเวลา 20-24 ชั่วโมง แล้วนำอนุภาคแม่เหล็กนาโนที่ได้ไปล้างด้วยฟอสเฟตบัฟเฟอร์ซาลีนที่มีพีเอช 7.4 และน้ำ ตามลำดับ ทำอนุภาคแม่เหล็กนาโนให้แห้ง จะได้อนุภาคแม่เหล็กนาโนตรึงด้วยพอลิเมอร์ที่มีหมู่คาร์บอกซิลหรือพอลิอะคริลิกแอซิดที่ยึดติดกับโดเมนที่ทำหน้าที่จับกับผนังเซลล์สำหรับนำไปใช้ในการจับกับเชื้อมิวแทนส์ สเตรปโตคอคไคต่อไป

**วิธีการในการประดิษฐ์ที่ดีที่สุด**

เหมือนกับที่ได้กล่าวไว้แล้วในหัวข้อการเปิดเผยการประดิษฐ์โดยสมบูรณ์

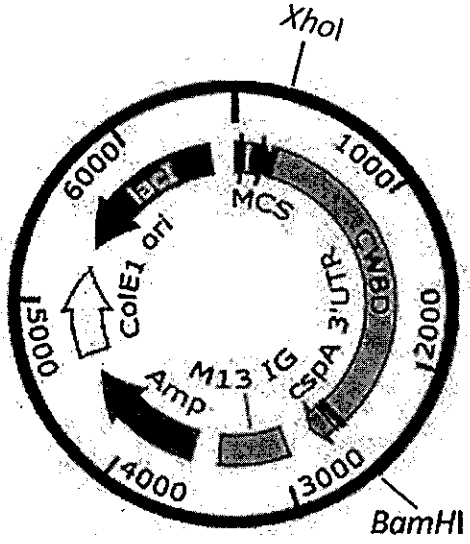
XhoI
1000
2000
3000
BamHI
4000
5000
6000
lacI
MCS
CMVIE
ori
ColE1
3'UTR
CspA
M13 IG
Amp

รูปที่ 1

**ข้อถือสิทธิ**

1. กรรมวิธีการผลิตสารประกอบอนุภาคที่สามารถจับกับเชื้อก่อโรคฟันผุได้อย่างจำเพาะสำหรับใช้ในการแยกและตรวจวัดเชื้อก่อโรคฟันผุเชิงกึ่งปริมาณได้ด้วยตาเปล่า มีขั้นตอนประกอบด้วยการนำโดเมนของเอนไซม์ที่ทำหน้าจับกับผนังเซลล์ซึ่งสามารถจับกับเชื้อก่อโรคฟันผุในกลุ่มสเตรปโตคอคไคได้อย่างจำเพาะมายึดติดกับอนุภาคแม่เหล็กนาโนตรึงด้วยพอลิเมอร์ที่มีหมู่ฟังก์ชันเป็นหมู่คาร์บอกซิล หรือพอลิอะคริลิกแอซิด เกิดเป็นสารประกอบอนุภาคที่มีความจำเพาะในการจับกับเชื้อก่อโรคฟันผุในกลุ่มสเตรปโตคอคไค
2. กรรมวิธีการเตรียมสารประกอบอนุภาคที่สามารถจับกับเชื้อก่อโรคฟันผุได้อย่างจำเพาะสำหรับใช้ในการแยกและตรวจวัดเชื้อก่อโรคฟันผุเชิงกึ่งปริมาณได้ด้วยตาเปล่า ตามข้อถือสิทธิ 1 ที่ซึ่งการเตรียมโดเมนของเอนไซม์ที่ทำหน้าที่จับกับผนังเซลล์ซึ่งสามารถจับกับเชื้อก่อโรคฟันผุในกลุ่ม สเตรปโตคอคไคได้อย่างจำเพาะ มีขั้นตอนประกอบด้วย

(1) การสร้างพลาสมิดลูกผสม (recombinant plasmid) ที่มียีนของโดเมนที่ทำหน้าที่จับกับผนังเซลล์ (cell wall binding domain; CWBD) จากเอนไซม์ออโตมิวตะโนไลซิน โดยเชื่อมชิ้นยีนนี้ เข้ากับเวคเตอร์ pColdIII ที่ถูกดัดแปลงให้มีลำดับนิวคลีโอไทด์ของฮิสทิดีน (histidine) อยู่ภายในลำดับดีเอ็นเอ (DNA sequence) เพื่อใช้ในขั้นตอนการทำให้โปรตีนบริสุทธิ์ และมียีนดื้อต่อยาปฏิชีวนะ (antibiotic resistant gene) เพื่อใช้ในการคัดเลือกเชื้อที่รับพลาสมิดลูกผสมเข้าไปในเซลล์ได้สำเร็จ จากนั้นเคลื่อนย้ายพลาสมิดลูกผสมนี้เข้าสู่เชื้อเอสเชอริเชีย โคไล (*Escherichia coli*) (transformation) หลังจากนั้นทำการคัดเลือกเชื้อที่รับพลาสมิดลูกผสมนี้เข้าไปได้ โดยเลี้ยงเชื้อในอาหารเลี้ยงเชื้อที่มียาปฏิชีวนะชนิดเดียวกับที่ในพลาสมิดมียีนดื้อต่อยานี้

(2) การผลิตโปรตีนจากเชื้อเอสเชอริเชีย โคไล (*Escherichia coli*; *E. coli*) ที่รับพลาสมิดลูกผสมเข้าไปได้สำเร็จ และการทำให้โปรตีนบริสุทธิ์ โดยเริ่มจากทำการเลี้ยงเชื้อเอสเชอริเชีย โคไล ให้ได้ค่าการดูดกลืนแสงที่ 600 นาโนเมตร อยู่ในช่วงระยะแบ่งตัวทวีคูณ (log phage) จากนั้นนำไปอบที่อุณหภูมิ 15 องศาเซลเซียส เป็นเวลา 30-45 นาที แล้วจึงเติมสารละลายไอโซโพรพิล-เบต้า-ดี-ไทโอกาแลคโตไซด์ (isopropyl-β-D-thiogalactoside; IPTG) เพื่อเหนี่ยวนำการสร้างโปรตีน จากนั้นนำไปอบที่อุณหภูมิ 15 องศาเซลเซียส เป็นเวลา 20-24 ชั่วโมง แล้วทำการเก็บเซลล์ด้วยการปั่นด้วยความเร็วสูง หลังจากนั้นสกัดโปรตีนภายในเซลล์ โดยการทำให้เซลล์แตก นำโปรตีนที่ได้ ไปทำให้บริสุทธิ์โดยผ่านคอลัมน์ที่แยกสารตามความจำเพาะ (affinity column) แยกเก็บโปรตีนที่ได้ออกเป็นส่วนๆ (fractions) นำแต่ละส่วนแยกที่ได้ไปวิเคราะห์ด้วยเทคนิคพอลิอะคริลาไมด์เจลอิเลคโตรโฟรีซีส แบบเอสดีเอส-เพจ (polyacrylamide gel electrophoresis; SDS-PAGE) เพื่อเลือกส่วนแยกที่มีปริมาณโปรตีนมากที่สุด (active fraction) มา

รวมกัน และนำไปไดอะไลซิส (dialysis) ในฟอสเฟตบัฟเฟอร์ซาลีน (phosphate buffer saline; PBS) หลังจากนั้นทำการวิเคราะห์หาปริมาณโปรตีน เปรียบเทียบกับความเข้มข้นของโปรตีนมาตรฐาน

3. กรรมวิธีการเตรียมสารประกอบอนุภาคที่สามารถจับกับเชื้อก่อโรคฟันผุได้อย่างจำเพาะสำหรับใช้ในการแยกและตรวจวัดเชื้อก่อโรคฟันผุเชิงกึ่งปริมาณได้ด้วยตาเปล่า ตามข้อถือสิทธิ 1 ที่ซึ่งการเตรียมอนุภาคแม่เหล็กนาโนที่ตรึงด้วยพอลิเมอร์ที่มีหมู่ฟังก์ชันเป็นหมู่คาร์บอกซิลหรือพอลิอะคริลิกแอซิดมีขั้นตอนประกอบด้วย

(1) เตรียมไอรอนคลอไรด์เฮกซาไฮเดรต ความเข้มข้น 0.01-0.05 โมลาร์ ในเอทิลีนไกลคอล แล้วเติมโซเดียมอะซิเตตความเข้มข้น 0.3-0.7 โมลาร์ คนสารละลายให้เข้ากันเป็นเวลา 30-50 นาที นำไปอบให้ความร้อนที่อุณหภูมิ 150-300 องสาเซลเซียส เป็นเวลา 14-18 ชั่วโมง หลังจากนั้นแยกอนุภาคแม่เหล็กนาโนที่ต้องการโดยใช้สนามแม่เหล็กภายนอก ล้างอนุภาคด้วยเอทานอลแล้วนำไปอบให้ความร้อนที่อุณหภูมิ 50-80 องศาเซลเซียส จะได้ผงอนุภาคแม่เหล็กนาโน

(2) เติมเอทานอล ลงไปในอนุภาคแม่เหล็กนาโนที่เตรียมได้จาก (1) แล้วเติมด้วย 3-อะมิโนโพรพิลไทรเอทอกซีไซเลน (3-aminopropyltriethoxysilane; APTES) และสารละลายแอมโมเนีย เขย่าสารละลายให้เข้ากันที่อุณหภูมิห้อง เป็นเวลา 10-14 ชั่วโมง จากนั้นนำอนุภาคแม่เหล็กนาโนไปล้างด้วย เอทานอล ได้อนุภาคแม่เหล็กนาโนที่มีหมู่อะมิโนเป็นหมู่ริเริ่มในการเกิดปฏิกิริยาพร้อมจะนำไปใช้ในการติดสารริเริ่ม (initiator) ในขั้นการสังเคราะห์พอลิเมอร์ต่อไป

(3) ละลาย 4,4-บิสไซยาโนวาเลอิกแอซิด 0.1-0.3 โมลาร์, ไดไซโคลเฮกซิลคาร์โบดิไอไมด์ 0.02-0.05 โมลาร์และ 4-ไดเมทิลแอมิโนไพริดีนในไดเมทิลฟอร์มาไมด์ 0.01-0.04 โมลาร์ คนให้สารละลายเข้ากันเป็นเวลา 3-6 ชั่วโมง ที่อุณหภูมิห้องภายใต้บรรยากาศไนโตรเจน ต่อมาผสมสารละลายกับอนุภาคแม่เหล็กนาโน ทำการคนที่อุณหภูมิห้องเป็นเวลา 20-24 ชั่วโมง จากนั้นนำอนุภาคแม่เหล็กนาโนมาล้างด้วยไดเมทิลฟอร์มาไมด์และเอทานอล ตามลำดับ ขั้นนี้จะได้อนุภาคแม่เหล็กนาโนที่ติดสารริเริ่ม

(4) ละลาย 4,4-บิสไซยาโนวาเลอิก แอซิด 0.03-0.06 โมลาร์ และ 4-ไซยาโน-4-เฟนิลคาร์โบโนไทโออิลไทโอเพนทาโนอิกแอซิด 0.3-0.7 โมลาร์ ในฟอสเฟตบัฟเฟอร์ซาลีนที่มีพีเอช 7.4 และเติมมอนอเมอร์ที่มีหมู่ฟังก์ชันเป็นหมู่คาร์บอกซิลหรืออะคริลิกแอซิด 0.05-0.1 โมลาร์ ผสมสารละลายให้เข้ากันแล้วถ่ายสารละลายนี้ไปผสมกับกับอนุภาคแม่เหล็กนาโนที่ติดสารริเริ่ม โดยทำปฏิกิริยาพอลิเมอไรเซชันที่อุณหภูมิ 60-80 องศาเซลเซียส ในอ่างน้ำมันเป็นเวลา 20-24 ชั่วโมง นำอนุภาคแม่เหล็กนาโนที่ได้มาล้างด้วยเอทานอลและน้ำ ตามลำดับ ทำอนุภาคนาโนแม่เหล็กให้แห้ง ขั้นนี้จะได้อนุภาคแม่เหล็กนาโนที่ตรึงด้วยพอลิเมอร์ที่มีหมู่ฟังก์ชันเป็นหมู่คาร์บอกซิลหรือพอลิอะคริลิกแอซิด

4. กรรมวิธีการเตรียมสารประกอบอนุภาคที่สามารถจับกับเชื้อก่อโรคฟันผุได้อย่างจำเพาะสำหรับใช้ในการแยกและตรวจวัดเชื้อก่อโรคฟันผุเชิงกึ่งปริมาณได้ด้วยตาเปล่า ตามข้อถือสิทธิ 1 ที่ซึ่งกรรมวิธีการยึดติดโดเมนของเอนไซม์ที่ทำหน้าที่จับกับผนังเซลล์กับอนุภาคแม่เหล็กนาโนที่ตรึงด้วยพอลิเมอร์ที่มีหมู่ฟังก์ชันเป็นหมู่คาร์บอกซิล หรือพอลิอะคริลิกแอซิด มีขั้นตอนประกอบด้วย

(1) ละลาย 1-เอทิล-3-(3-ไดเมทิลเอมีนโพรพิล) คาร์โบดิไอไมด์ไฮโดรคลอไรด์ ความเข้มข้น 0.1-0.3 โมลาร์ และเอ็นไฮดรอกซีซักซินิไมด์ ความเข้มข้น 0.3-0.6 โมลาร์ ในฟอสเฟตบัฟเฟอร์ซาลีนที่มีพีเอช 7.4 ตามลำดับ จากนั้นถ่ายสารละลายนี้ไปผสมกับอนุภาคแม่เหล็กนาโนที่ตรึงด้วยพอลิเมอร์ที่มีหมู่ฟังก์ชันเป็นหมู่คาร์บอกซิลหรือพอลิอะคริลิกแอซิดบนพื้นผิว ละลายในฟอสเฟตบัฟเฟอร์ซาลีนที่มีพีเอช 7.4 แล้วคนสารละลายให้เข้ากันที่อุณหภูมิห้องเป็นเวลา 20-50 นาที

(2) เติมโดเมนที่ทำหน้าที่จับกับผนังเซลล์ที่มีความเข้มข้น 0.1-0.3 มิลลิกรัม/มิลลิลิตร ปริมาณ 1-3 มิลลิลิตร ตั้งทิ้งไว้ที่อุณหภูมิ 2-10 องศาเซลเซียส เป็นเวลา 20-24 ชั่วโมง นำอนุภาคแม่เหล็กนาโนที่ได้ไปล้างด้วยฟอสเฟตบัฟเฟอร์ซาลีนที่มีพีเอช 7.4 และน้ำ ตามลำดับ แล้วทำอนุภาคแม่เหล็กนาโนให้แห้ง

**บทสรุปการประดิษฐ์**

การประดิษฐ์นี้เกี่ยวข้องกับกรรมวิธีการผลิตสารประกอบอนุภาคที่สามารถจับกับเชื้อก่อโรคฟันผุได้อย่างจำเพาะสำหรับใช้ในการแยกและตรวจวัดเชื้อก่อโรคฟันผุเชิงกึ่งปริมาณได้ด้วยตาเปล่า เตรียมโดยการนำโดเมนของเอนไซม์ออโตมิวตะโนไลซินที่ทำหน้าที่จับกับผนังเซลล์ ซึ่งสามารถจับกับเชื้อก่อโรคฟันผุในกลุ่ม สเตรปโตคอคไคได้อย่างจำเพาะมายึดติดผ่านพันธะเอไมด์กับอนุภาคแม่เหล็กนาโนที่ทำให้เสถียรด้วยพอลิเมอร์ที่มีหมู่ฟังก์ชันเป็นหมู่คาร์บอกซิลิก หรือพอลิอะคริลิกแอซิด (poly(acrylic acid)) ซึ่งการตรึงพอลิอะคริลิกแอซิดบนพื้นผิวอนุภาคแม่เหล็กนี้ ทำให้สามารถยึดติดโดเมนที่ทำหน้าที่จับกับผนังเซลล์ได้เป็นจำนวนมาก ส่งผลให้เพิ่มประสิทธิภาพในการจับกับเชื้อได้ดียิ่งขึ้น

**คำขอรับสิทธิบัตร/อนุสิทธิบัตร**

☐ การประดิษฐ์
☐ การออกแบบผลิตภัณฑ์
☑ อนุสิทธิบัตร

ข้าพเจ้าผู้ลงลายมือชื่อในคำขอรับสิทธิบัตร/อนุสิทธิบัตรนี้ ขอรับสิทธิบัตร/อนุสิทธิบัตร ตามพระราชบัญญัติสิทธิบัตร พ.ศ. 2522 แก้ไขเพิ่มเติมโดยพระราชบัญญัติสิทธิบัตร (ฉบับที่ 2) พ.ศ 2535 และ พระราชบัญญัติสิทธิบัตร (ฉบับที่ 3) พ.ศ 2542

| สำหรับเจ้าหน้าที่ | |
|---|---|
| วันรับคำขอ 16 ส.ค. 2559 | เลขที่คำขอ 1603001055 |
| วันยื่นคำขอ 16 ส.ค. 2559 | |
| สัญลักษณ์จำแนกการประดิษฐ์ระหว่างประเทศ | |
| ใช้กับแบบผลิตภัณฑ์ ประเภทผลิตภัณฑ์ | |
| วันประกาศโฆษณา | เลขที่ประกาศโฆษณา |
| วันออกสิทธิบัตร/อนุสิทธิบัตร | เลขที่สิทธิบัตร/อนุสิทธิบัตร |
| ลายมือชื่อเจ้าหน้าที่ | |

1.ชื่อที่แสดงถึงการประดิษฐ์/การออกแบบผลิตภัณฑ์
สารประกอบอนุภาคที่สามารถจับกับเชื้อก่อโรคฟันผุได้อย่างจำเพาะสำหรับใช้ในการแยกและตรวจวัดเชื้อก่อโรคฟันผุเชิงกึ่งปริมาณได้ด้วยตาเปล่า



2.คำขอรับสิทธิบัตรการออกแบบผลิตภัณฑ์นี้เป็นคำขอสำหรับแบบผลิตภัณฑ์อย่างเดียวกันและเป็นคำขอลำดับที่
ในจำนวน คำขอ ที่ยื่นในคราวเดียวกันนี้

| | |
|---|---|
| 3.ผู้ขอรับสิทธิบัตร/อนุสิทธิบัตร และที่อยู่ (เลขที่ ถนน ประเทศ) ดูที่หน้า 3 | 3.1 สัญชาติ |
| | 3.2 โทรศัพท์ |
| | 3.3 โทรสาร |
| | 3.4 อีเมล์ |
| 5.ตัวแทน(ถ้ามี)/ที่อยู่ (เลขที่ ถนน จังหวัด รหัสไปรษณีย์) ดูที่หน้า 3 | 5.1 ตัวแทนเลขที่ |
| | 5.2 โทรศัพท์ |
| | 5.3 โทรสาร |
| | 5.4 อีเมล์ |

4.สิทธิในการขอรับสิทธิบัตร/อนุสิทธิบัตร
☐ ผู้ประดิษฐ์/ผู้ออกแบบ ☑ ผู้รับโอน ☐ ผู้ขอรับสิทธิโดยเหตุอื่น

6.ผู้ประดิษฐ์/ผู้ออกแบบผลิตภัณฑ์ และที่อยู่ ( เลขที่ ถนน ประเทศ )
ดูที่หน้า 3

7. คำขอรับสิทธิบัตร/อนุสิทธิบัตรนี้แยกจากหรือเกี่ยวข้องกับคำขอเดิม
ผู้ขอรับสิทธิบัตร/อนุสิทธิบัตร ขอให้ถือว่าได้ยื่นคำขอรับสิทธิบัตร/อนุสิทธิบัตรนี้ ในวันเดียวกับคำขอรับสิทธิบัตร เลขที่ วันยื่น เพราะคำขอรับสิทธิบัตร/อนุสิทธิบัตรนี้แยกจากหรือเกี่ยวข้องกับคำขอเดิมเพราะ
☐ คำขอเดิมมีการประดิษฐ์หลายอย่าง ☐ ถูกคัดค้านเนื่องจากผู้ขอไม่มีสิทธิ ☐ ขอเปลี่ยนแปลงประเภทของสิทธิ

8.การยื่นคำขอนอกราชอาณาจักร

| วันยื่นคำขอ | เลขที่คำขอ | ประเทศ | สัญลักษณ์จำแนกการประดิษฐ์ระหว่างประเทศ | สถานะคำขอ |
|---|---|---|---|---|
| 8.1 | | | | |
| 8.2 | | | | |
| 8.3 | | | | |

8.4 ☐ ผู้ขอรับสิทธิบัตร/อนุสิทธิบัตรขอสิทธิให้ถือว่าได้ยื่นคำขอนี้ในวันที่ได้ยื่นคำขอรับสิทธิบัตร/อนุสิทธิบัตรในต่างประเทศเป็นครั้งแรกโดย
☐ ได้ยื่นเอกสารหลักฐานพร้อมคำขอนี้ ☐ ขอยื่นเอกสารหลักฐานหลังจากวันยื่นคำขอนี้

9.การแสดงการประดิษฐ์ หรือการออกแบบผลิตภัณฑ์ ผู้ขอรับสิทธิบัตร/อนุสิทธิบัตร ได้แสดงการประดิษฐ์ที่หน่วยงานของรัฐเป็นผู้จัด
วันแสดง วันเปิดงานแสดง ผู้จัด

10.การประดิษฐ์เกี่ยวกับจุลชีพ

| 10.1 เลขทะเบียนฝากเก็บ | 10.2 วันที่ฝากเก็บ | 10.3 สถาบันฝากเก็บ/ประเทศ |
|---|---|---|
| | | |

11.ผู้ขอรับสิทธิบัตร/อนุสิทธิบัตร ขอยื่นเอกสารภาษาต่างประเทศก่อนในวันยื่นคำขอนี้ และจะจัดยื่นคำขอรับสิทธิบัตร/อนุสิทธิบัตรนี้ที่จัดทำเป็นภาษาไทยภายใน 90 วัน นับจากวันยื่นคำขอนี้ โดยขอยื่นเป็นภาษา
☐ อังกฤษ ☐ ฝรั่งเศส ☐ เยอรมัน ☐ ญี่ปุ่น ☐ อื่นๆ

12.ผู้ขอรับสิทธิบัตร/อนุสิทธิบัตร ขอให้อธิบดีประกาศโฆษณาคำขอรับสิทธิบัตร หรือรับจดทะเบียน และประกาศโฆษณาอนุสิทธิบัตรนี้ หลังจากวันที่ เดือน พ.ศ
☐ ผู้ขอรับสิทธิบัตร/อนุสิทธิบัตรขอให้ใช้รูปเขียนหมายเลข ในการประกาศโฆษณา

13.คำขอรับสิทธิบัตร/อนุสิทธิบัตรนี้ประกอบด้วย
ก. แบบพิมพ์คำขอ 3 หน้า
ข. รายละเอียดการประดิษฐ์ หรือคำพรรณนาแบบผลิตภัณฑ์ 7 หน้า
ค. ข้อถือสิทธิ 1 หน้า
ง. รูปเขียน รูป หน้า
จ. ภาพแสดงแบบผลิตภัณฑ์
☐ รูปเขียน รูป หน้า
☐ ภาพถ่าย รูป หน้า
ฉ. บทสรุปการประดิษฐ์ 1 หน้า

14.เอกสารประกอบคำขอ
☐ เอกสารแสดงสิทธิในการขอรับสิทธิบัตร/อนุสิทธิบัตร
☐ หนังสือรับรองการแสดงการประดิษฐ์/การออกแบบผลิตภัณฑ์
☐ หนังสือมอบอำนาจ
☐ เอกสารรายละเอียดเกี่ยวกับจุลชีพ
☐ เอกสารการขอนับวันยื่นคำขอในต่างประเทศเป็นวันยื่นคำขอในประเทศไทย
☐ เอกสารขอเปลี่ยนแปลงประเภทของสิทธิ
☐ เอกสารอื่น ๆ

15. ข้าพเจ้าขอรับรองว่า
☑ การประดิษฐ์นี้ไม่เคยยื่นขอรับสิทธิบัตร/ อนุสิทธิบัตรมาก่อน
☐ การประดิษฐ์นี้ได้พัฒนาปรับปรุงมาจาก.....

16.ลายมือชื่อ ( ☐ ผู้ขอรับสิทธิบัตร / อนุสิทธิบัตร; ☑ ตัวแทน )
นายบัญชา วงศ์ณัฐภัทร

**หมายเหตุ** บุคคลใดยื่นขอรับสิทธิบัตรการประดิษฐ์หรือการออกแบบผลิตภัณฑ์ หรืออนุสิทธิบัตร โดยการแสดงข้อความอันเป็นเท็จแก่พนักงานเจ้าหน้าที่ เพื่อให้ได้ไปซึ่งสิทธิบัตรหรืออนุสิทธิบัตร ต้องระวางโทษจำคุกไม่เกินหกเดือน หรือปรับไม่เกินห้าพันบาท หรือทั้งจำทั้งปรับ

3.ผู้ขอรับสิทธิบัตร/อนุสิทธิบัตร และที่อยู่ (เลขที่ ถนน ประเทศ)

จุฬาลงกรณ์มหาวิทยาลัย
อยู่ที่ 254 ถนนพญาไท แขวงวังใหม่ เขตปทุมวัน กรุงเทพฯ 10330
3.1 สัญชาติ ไทย 3.2 โทรศัพท์ 0-2218-4180 3.3 โทรสาร 0-2218-4181

สำนักงานกองทุนสนับสนุนการวิจัย
อยู่ที่ ชั้น 14 อาคาร เอส เอ็ม ทาวเวอร์ 979/17-21 ถนนพหลโยธิน แขวงสามเสนใน เขตพญาไท กรุงเทพฯ 10400
3.1 สัญชาติ ไทย 3.2 โทรศัพท์ 0-2278-8200 3.3 โทรสาร 0-2298-0476

5. ตัวแทน(ถ้ามี)/ที่อยู่ (เลขที่ ถนน จังหวัด รหัสไปรษณีย์)
นายมงคล แก้วมหา
อยู่ที่ สถาบันทรัพย์สินทางปัญญาแห่งจุฬาลงกรณ์มหาวิทยาลัย 254 อาคารวิจัยจุฬาลงกรณ์มหาวิทยาลัย ชั้น 14 ถนนพญาไท แขวงวังใหม่ เขตปทุมวัน กรุงเทพฯ 10330
5.1 ตัวแทนเลขที่ 1453 5.2 โทรศัพท์ 0-2218-4180 5.3 โทรสาร 0-2218-4181

และ/หรือ

นายบัญชา วงศ์ณัฐภัทร
อยู่ที่ สถาบันทรัพย์สินทางปัญญาแห่งจุฬาลงกรณ์มหาวิทยาลัย 254 อาคารวิจัยจุฬาลงกรณ์มหาวิทยาลัย ชั้น 14 ถนนพญาไท แขวงวังใหม่ เขตปทุมวัน กรุงเทพฯ 10330
5.1 ตัวแทนเลขที่ 2392 5.2 โทรศัพท์ 0-2218-4180 5.3 โทรสาร 0-2218-4181 5.4 อีเมล์ Bancha.V@chula.ac.th

6.ผู้ประดิษฐ์/ผู้ออกแบบผลิตภัณฑ์ และที่อยู่ ( เลขที่ ถนน ประเทศ )

นางสาวพนิดา ธัญญศรีสังข์
อยู่ที่ ภาควิชาจุลชีววิทยา คณะทันตแพทยศาสตร์ จุฬาลงกรณ์มหาวิทยาลัย ถนนพญาไท แขวงวังใหม่ เขตปทุมวัน กรุงเทพฯ 10330

นางสาวเอมวิกา วิทยาประสิทธิ์
อยู่ที่ หลักสูตรปิโตรเคมีและวิทยาศาสตร์พอลิเมอร์ คณะวิทยาศาสตร์ จุฬาลงกรณ์มหาวิทยาลัย ถนนพญาไท แขวงวังใหม่ เขตปทุมวัน กรุงเทพฯ 10330

นางวรวีร์ โฮเว่น
อยู่ที่ ภาควิชาเคมี คณะวิทยาศาสตร์ จุฬาลงกรณ์มหาวิทยาลัย ถนนพญาไท แขวงวังใหม่ เขตปทุมวัน กรุงเทพฯ 10330

นายโมโตยูกิ ซูไก
อยู่ที่ ภาควิชาแบคทีเรียวิทยา บัณฑิตวิทยาลัย วิทยาศาสตร์ชีวการแพทย์ และวิทยาศาสตร์สุขภาพ มหาวิทยาลัยฮิโรชิมา จังหวัดฮิโรชิมา ประเทศญี่ปุ่น

# รายละเอียดการประดิษฐ์

## ชื่อที่แสดงถึงการประดิษฐ์

สารประกอบอนุภาคที่สามารถจับกับเชื้อก่อโรคฟันผุได้อย่างจำเพาะสำหรับใช้ในการแยกและตรวจวัดเชื้อก่อโรคฟันผุเชิงกึ่งปริมาณได้ด้วยตาเปล่า

## สาขาวิทยาการที่เกี่ยวข้องกับการประดิษฐ์

สาขาเคมี และวิทยาศาสตร์ชีวการแพทย์ที่เกี่ยวข้องกับสารประกอบอนุภาคที่สามารถจับกับเชื้อก่อโรคฟันผุได้อย่างจำเพาะสำหรับใช้ในการแยกและตรวจวัดเชื้อก่อโรคฟันผุเชิงกึ่งปริมาณได้ด้วยตาเปล่า

## ภูมิหลังของศิลปะหรือวิทยาการที่เกี่ยวข้อง

โรคฟันผุยังคงเป็นปัญหาสาธารณสุขที่สำคัญของประเทศไทย ดังจะเห็นได้จากรายงานผลการสำรวจทันตสาธารณสุขแห่งชาติครั้งที่ 7 พ.ศ. 2555 ที่ความชุกของโรคในกลุ่มเด็กก่อนวัยเรียนอายุ 3 และ 5 ปี และในกลุ่มเด็กวัยเรียน และเยาวชนอายุ 12 และ 15 ปีมีมากเกินกว่าครึ่งหนึ่งของประชากรที่ถูกสำรวจ ความชุกของโรคฟันผุในประชากรไทยอยู่ในระดับนี้มาตลอดระยะเวลาเกือบ 10 กว่าปีที่ผ่านมา สาเหตุหนึ่งอาจจะมาจากการให้การรักษา และป้องกันโรคฟันผุในคนไข้ทุกคนในระดับเดียวกัน ทั้ง ๆ ที่ความเสี่ยงของการเกิดโรคฟันผุเป็นเรื่องของแต่ละบุคคล ทำให้กลุ่มที่มีความเสี่ยงสูงได้รับการรักษา และป้องกันไม่เพียงพอที่จะทำให้หยุดการเกิดโรคขึ้นได้ การประเมินความเสี่ยงในการเกิดโรคฟันผุ เป็นกระบวนการประเมินว่าบุคคลนี้มีความเสี่ยงที่จะเกิดฟันผุอยู่ในระดับไหน ซึ่งค่าที่ประเมินได้นั้นจะช่วยให้ทันตแพทย์เลือกวิธีการรักษา และป้องกันได้อย่างเหมาะสม ความเสี่ยงของการเกิดโรคฟันผุนี้ประเมินโดยอาศัยหลายปัจจัยด้วยกัน เช่น พฤติกรรมการทานอาหาร การดูแลสุขภาพช่องปาก คุณลักษณะของน้ำลาย และปริมาณเชื้อก่อโรคฟันผุ เป็นต้น ปัจจัยที่นำมาประเมินนี้ส่วนใหญ่สามารถทำได้ทันทีข้างเก้าอี้ทำฟัน ยกเว้นการหาปริมาณเชื้อ ถึงแม้จะมีชุดตรวจเชื้อสำเร็จรูปออกมาจำหน่ายทำให้สะดวกมากขึ้น แต่ก็ยังต้องอาศัยเวลาในการอบเลี้ยงเชื้อ และต้องการอุปกรณ์ที่มีขนาดใหญ่เกินพกพา และมีราคาแพง ทำให้ไม่สะดวกที่จะนำมาใช้ในงานระดับชุมชน

มีเอกสารการยื่นขอสิทธิบัตรแสดงเครื่องมือตรวจเชื้อแบคทีเรียอย่างรวดเร็ว (rapid bacterial detection tool) โดยอาศัยหลักการอิมมูโนโครมาโทกราฟี และทองคอลลอยด์ (colloidal gold- based immunochromatography) โดยในชุดตรวจนี้ใช้แอนติบอดีที่จำเพาะกับเชื้อสเตรปโตคอคคัส มิวแทนส์เป็นเครื่องมือในการจับเชื้อ (probe) นำไปติดกับทองคอลลอยด์ (colloidal gold) ทำให้เห็นสีได้ด้วยตาเปล่า (เอกสารการยื่นขอสิทธิบัตรประเทศสหรัฐอเมริกาเลขที่ US 20080240993 A1) มีรายงานการวิจัยถึงประสิทธิภาพของ

เครื่องมือนี้ว่ามีความไวในการตรวจหาเชื้อ (sensitivity) อยู่ที่ร้อยละ 97.6 แต่มีความจำเพาะ (specificity) เพียงร้อยละ 90.6 เท่านั้นเมื่อเทียบกับการตรวจด้วยวิธีเรียลไทม์ พีซีอาร์ (real-time PCR) ซึ่งผู้วิจัยใช้เป็นวิธียืนยันจำนวนเชื้อ (Int J Paediatr Dent., Vol 22, p 363-368, 2012) ด้วยเหตุนี้ทำให้เกิดแนวคิดที่จะพัฒนาวิธีการตรวจที่มีความไว และความจำเพาะกับเชื้อมิวแทนส์ สเตรปโตคอคไค ที่มีประสิทธิภาพมากขึ้น และยังคงเห็นผลได้ด้วยตาเปล่า

เอนไซม์เปปทิโดไกลแคน ไฮโดรเลส (peptidoglycan hydrolase) เป็นเอนไซม์ที่พบได้ในแบคทีเรียเกือบทุกชนิด มีหน้าที่ในการย่อยสลายเปปทิโดไกลแคนซึ่งเป็นโครงสร้างที่พบได้ในผนังเซลล์ของแบคทีเรียทั่วไป โดยเฉพาะแบคทีเรียแกรมบวก (Gram positive bacteria) แต่เป็นโครงสร้างที่ไม่พบในเซลล์ของมนุษย์ เอนไซม์นี้มีบทบาทสำคัญต่อการแบ่งตัว และแยกตัวของเซลล์แบคทีเรีย จากรายงานสิทธิบัตร และจากงานวิจัยที่ผ่านมาพบว่าเชื้อสเตรปโตคอคคัส มิวแทนส์ (*Streptococcus mutans*) ผลิตเอนไซม์เปปทิโดไกลแคน ไฮโดรเลสซึ่งถูกตั้งชื่อว่า ออโตมิวตะโนไลซิน (automutanolysin) หรือเอเอ็มแอล (Aml) ที่มีความจำเพาะในการย่อยสลายเชื้อสเตรปโตคอคคัส มิวแทนส์ (*Streptococcus mutans*) และสเตรปโตคอคคัส ซอบรินัส (*Streptococcus sobrinus*) ซึ่งอยู่ในกลุ่มเชื้อมิวแทนส์ สเตรปโตคอคไค (mutans streptococci) อันเป็นเชื้อกลุ่มสำคัญกลุ่มหนึ่งต่อการเกิดโรคฟันผุ และเป็นตัวชี้วัดหนึ่งที่ใช้ในการประเมินความเสี่ยงในการเกิดโรคฟันผุ โครงสร้างของเอนไซม์นี้ประกอบขึ้นด้วยกรดอะมิโน 979 ตัว มีน้ำหนักโมเลกุลประมาณ 104 กิโลดาลตัน และมีสองโดเมนหลักได้แก่ คาตาไลติกโดเมนอยู่ทางฝั่งปลายด้านหมู่คาร์บอกซิล (C-terminal catalytic domain) ซึ่งมีบทบาทในการย่อยสลายผนังเซลล์ และอีกโดเมนอยู่ฝั่งปลายด้านหมู่อะมิโนทำหน้าที่ในการจับกับผนังเซลล์ (cell wall binding domain) ซึ่งมีความจำเพาะกับเชื้อมิวแทนส์ สเตรปโตคอคไค (Microbiol Immunol., Vol 50, p 729-42, 2006 และสิทธิบัตรประเทศสหรัฐอเมริกาเลขที่ US 7,776,325 B2 และ US 8,852,584 B2) ด้วยความจำเพาะนี้หากทำการตัดต่อยีนโดยเอาส่วนคาตาไลติกโดเมนที่ใช้ในการย่อยสลายเปปทิโดไกลแคนออกไป ก็จะสามารถใช้เอนไซม์ดังกล่าวนี้ในการจับกับผนังเซลล์ของเชื้อมิวแทนส์ สเตรปโตคอคไค (probe) เพื่อใช้ในการตรวจวัดปริมาณของเชื้อได้

ในการพัฒนาวิธีการตรวจวัดปริมาณของเชื้อมิวแทนส์ สเตรปโตคอคไคที่สามารถเห็นผลได้ด้วยตาเปล่านี้ นอกจากการนำโดเมนที่ทำหน้าที่จับกับผนังเซลล์มาใช้ในการตรวจจับเชื้อที่ต้องการแล้ว การแยกเชื้อออกจากเชื้ออื่น หรือสารเจือปนอื่นๆ และการนำเชื้อที่คัดแยกแล้วมาตรวจวัดปริมาณ และแสดงผลให้เห็นได้ด้วยตาเปล่านั้นทำได้โดยการยึดติดโดเมนดังกล่าวกับอนุภาคแม่เหล็กนาโน (magnetic nanoparticles, MNPs) ซึ่งมีขนาดตั้งแต่ 5 ถึง 500 นาโนเมตร กลายเป็นสารประกอบอนุภาคที่มีความจำเพาะกับเชื้อมิวแทนส์ สเตรปโตคอคไค โดยทั่วไปอนุภาคแม่เหล็กนาโนที่นิยมใช้มักเป็นแบบแมกเนไทต์ ($Fe_3O_4$) หรือแมกฮีไมต์ ($\gamma$-$Fe_2O_3$) มีสมบัติที่สามารถตอบสนองต่อสนามแม่เหล็กภายนอกได้อย่างรวดเร็ว ด้วยสมบัติดังกล่าวจึงทำให้อนุภาคแม่เหล็กนาโนสามารถ

นำมาใช้ในการแยกเชื้อแบคทีเรียโดยการควบคุมผ่านสนามแม่เหล็กภายนอก เชื้อแบคทีเรียที่แยกมาได้จึงมีความบริสุทธิ์ และง่ายต่อการตรวจวัดยิ่งขึ้น และเมื่อนำไปกรองแบบเลือกผ่าน (selective filtration) สารประกอบอนุภาคที่จับกับเชื้อแบคทีเรียจะติดอยู่บนแผ่นเมมเบรนไม่สามารถผ่านรูพรุนของแผ่นเมมเบรนมาได้ โดยปริมาณของสารประกอบอนุภาคที่จับกับเชื้อแบคทีเรียจะแปรผันตรงกับความเข้มของสีบนแผ่นเมมเบรน จึงสามารถวิเคราะห์หาเชื้อแบคทีเรียเชิงกึ่งปริมาณได้ด้วยตาเปล่า (semi-quantitative analysis)

มีสิทธิบัตรรายงานการนำอนุภาคแม่เหล็กนาโนตรึงแอนติบอดีมาใช้ในการจับกับเชื้อแบคทีเรีย และแยกเชื้อออกจากสารละลายโดยอาศัยสนามแม่เหล็กภายนอก แล้วนำมาตรวจวัดปริมาณของเชื้อแบคทีเรีย โดยจากรายงานพบว่าอนุภาคแม่เหล็กนาโนตรึงแอนติบอดีนี้สามารถจับกับเชื้อแบคทีเรีย และแยกเชื้อออกมาจากสารละลายโดยอาศัยสนามแม่เหล็กภายนอกได้จริง และสามารถตรวจวัดปริมาณเชื้อได้ตามสิทธิบัตรประเทศสหรัฐอเมริกาเลขที่ 8,883,455 และเลขที่ 9,201,066 แต่ยังไม่มีงานวิจัยใดคิดค้นเกี่ยวกับการแยก และตรวจวัดปริมาณเชื้อมิวแทนส์ สเตรปโตคอคไค โดยใช้อนุภาคแม่เหล็กนาโนติดกับโดเมนที่จับกับผนังเซลล์ของเอนไซม์เอเอ็มแอล ซึ่งผลของการตรวจวัดปริมาณเชื้อนี้สามารถใช้ประกอบการประเมินความเสี่ยงการเกิดโรคฟันผุได้

มีงานวิจัยที่รายงานการตรวจวัดปริมาณของเชื้อซาลโมเนลลา ไทฟิมิวเรียม *(Salmonella typhimurium)* โดยใช้อนุภาคแม่เหล็กนาโนตรึงด้วยแอนติบอดีที่มีความจำเพาะเจาะจงกับเชื้อ ผ่านการสร้างพันธะระหว่างหมู่คาร์บอกซิลบนพื้นผิวของอนุภาคนาโนแม่เหล็ก และหมู่อะมิโนของแอนติบอดี โดยใช้ 1-เอทิล-3-(3-ไดเมทิลลามีนโพรพิล) คาร์โบดีไอไมด์ไฮโดรคลอไรด์ (1-ethyl-3-(3-dimethylaminepropyl) carbodiimide hydrochloride; EDC) เป็นรีเอเจนต์คู่ควบ จากนั้นจึงแยกแบคทีเรียที่ต้องการตรวจวัดออกจากสารเจือปนอื่นๆ โดยอาศัยสนามแม่เหล็กภายนอก ตามด้วยการกรองด้วยกระดาษกรองแบบเลือกผ่านโดยใช้เมมเบรนเซลลูโลสแอซิเตต (cellulose acetate membrane) ที่รูพรุนมีขนาดเส้นผ่าศูนย์กลาง 0.8 ไมโครเมตร เพื่อแยกเชื้อที่ถูกจับด้วยอนุภาค และวิเคราะห์ปริมาณของเชื้อจากความเข้มสีที่ปรากฏบนแผ่นเมมเบรน โดยพบว่าความเข้มของสีบนแผ่นเมมเบรนแปรผันตรงกับปริมาณเชื้อ ทั้งนี้สามารถตรวจวัดปริมาณแบคทีเรียได้ความเข้มข้นต่ำสุด (Limit of detection; LOD) ที่ $2\times10^{1}$ โคโลนีต่อมิลลิลิตร อย่างไรก็ตามงานวิจัยดังกล่าวยังประสบปัญหาการตรวจวัดเนื่องจากความเข้มข้นต่ำที่สุดของแบคทีเรียที่สามารถตรวจวัดได้ยังมีค่าสูง ทำให้ไม่สามารถตรวจวัดเชื้อในปริมาณที่ต่ำได้ (Anal. Chem., Vol 406, p 406-866, 2014)

นอกจากนี้ยังมีรายงานการนำเอาพอลิเมอร์มาตรึงบนพื้นผิวของอนุภาคแม่เหล็กนาโน เพื่อช่วยทำให้อนุภาคมีความเสถียรมากขึ้น และสามารถกระจายตัวอยู่ในสารละลายได้ดียิ่งขึ้น มีงานวิจัยที่เปรียบเทียบสมบัติการกระจายตัว และความเสถียรของอนุภาคแม่เหล็กนาโนที่ตรึง และไม่ได้ตรึงพอลิเมอร์ โดยได้สังเคราะห์อนุภาคแม่เหล็กนาโนตรึงด้วยพอลิอะคริลิกแอซิด (poly(acrylic acid)) หรือพอลิสไตรีน (polystyrene) ลงบนพื้นผิว เริ่ม

จากนำอนุภาคนาโนแม่เหล็กมาทำปฏิกิริยากับโอโซน เพื่อเกิดหมู่เปอร์ออกไซด์ (peroxide group) บนพื้นผิว ซึ่งจะทำหน้าที่เป็นสารริเริ่มปฏิกิริยา และใช้ 1-เฟนิลเอทิลไดไทโอเบนโซเอท (1-phenylethyl dithiobenzoate; PVB) ทำหน้าที่เป็นสารถ่ายโอนโซ่ (chain transfer agent) นำไปทำปฏิกิริยาพอลิเมอไรเซชันแบบควบคุม (controlled polymerization) ด้วยกลไกแบบ reversible addition-fragmentation chain transfer (RAFT) จะได้อนุภาคแม่เหล็กนาโนที่ตรึงด้วยพอลิอะคริลิกแอซิดหรือพอลิสไตรีน แล้วนำไปทดสอบสมบัติการกระจายตัวและความเสถียร พบว่าอนุภาคแม่เหล็กนาโนที่ตรึงพอลิเมอร์ลงบนพื้นผิวสามารถกระจายตัว และมีความเสถียรดีกว่าอนุภาคแม่เหล็กนาโนที่ไม่ได้ตรึงพอลิเมอร์ลงบนพื้นผิว (Macromolecules, Vol 27, p 1665-1669, 2006)

แนวทางหนึ่งที่น่าสนใจในการปรับปรุงพื้นผิวของวัสดุด้วยพอลิเมอร์คือ การเตรียมเป็นพอลิเมอร์บรัช (polymer brushes) ซึ่งเป็นพอลิเมอร์ที่มีปลายของโซ่ด้านหนึ่งยึดติดบนพื้นผิวด้วยพันธะโควาเลนต์ (covalent bond) ทำให้มีเสถียรภาพในการยึดติดบนพื้นผิวสูงกว่าการดูดซับทางกายภาพ (physical absorption) การเตรียมพอลิเมอร์บรัชนิยมเตรียมด้วยปฏิกิริยาพอลิเมอไรเซชันริเริ่มจากพื้นผิว (surface-initiated polymerization) ทั้งนี้ความยาวของโซ่พอลิเมอร์สามารถควบคุมได้หากใช้ปฏิกิริยาพอลิเมอไรเซชันแบบควบคุม (controlled polymerization) เช่น atom transfer radical polymerization (ATRP) และ reversible addition-fragmentation chain transfer (RAFT) (Prog. Polym. Sci., Vol 25, p 677-710, 2000 และ Chem. Rev., Vol 109, p 5437-5527, 2009) โดยสมบัติทางเคมีและกายภาพของพอลิเมอร์บรัชขึ้นกับชนิดของมอนอเมอร์ (monomer) ที่เลือกใช้ในการสังเคราะห์

การประดิษฐ์นี้สนใจที่จะนำสารประกอบอนุภาคแม่เหล็กนาโนที่ตรึงด้วยพอลิเมอร์ที่มีหมู่ฟังก์ชันเป็นหมู่คาร์บอกซิล หรือพอลิอะคริลิกแอซิด และยึดติดโดเมนของเอนไซม์ออโตมิวตะโนไลซินซึ่งสามารถจับกับเชื้อ ก่อโรคฟันผุได้อย่างจำเพาะ มาใช้ในการแยก และตรวจวัดเชื้อก่อโรคฟันผุเชิงกึ่งปริมาณได้ด้วยตาเปล่า

โดยอนุภาคแม่เหล็กนาโนนอกจากจะทำหน้าที่ในการแยกเชื้อออกมาจากสารละลายโดยอาศัยสนามแม่เหล็กภายนอกแล้ว ยังสามารถทำหน้าที่เป็นตัวเร่งปฏิกิริยาการเกิดสีของซับสเตรทเททราเมทิลเบนซิดีน (3,3',5,5'-tetramethylbenzidine; TMB) และยูเรียไฮโดรเจนเปอร์ออกไซด์ (urea-hydrogen peroxide; $H_2O_2$) ได้มีประสิทธิภาพทัดเทียมกับเอนไซม์ฮอร์สเรดิชเปอร์ออกซิเดส (horseradish peroxidase; HRP) ดังตัวอย่างงานวิจัยของ Woo และคณะ ที่นำเอาอนุภาคแม่เหล็กนาโนมาใช้ในการหาปริมาณเชื้อไวรัสเอดส์ หรือเชื้อรีโทรไวรัส (retroviruses) และเซลล์มะเร็งเต้านม (breast cancer cells) โดยนำอนุภาคแม่เหล็กนาโนตรึงด้วยแอนติบอดีที่มีความจำเพาะเจาะจงกับเชื้อ แล้วใส่ลงไปในสารละลายที่มีเชื้อรีโทรไวรัส หรือเซลล์มะเร็งเต้านม วิเคราะห์ปริมาณของเชื้อไวรัสหรือเซลล์มะเร็งเต้านมที่พบได้โดยพิจารณาการเปลี่ยนสีของซับสเตรทเททราเมทิลเบนซิดีน และยูเรียไฮโดรเจนเปอร์ออกไซด์ ซึ่งใช้อนุภาคแม่เหล็กนาโนในการทำหน้าที่เป็นตัวเร่งการเกิดปฏิกิริยา

การเปลี่ยนสี จากการศึกษาพบว่าสีของสารละลายที่ปรากฏมีความเสถียรมากกว่าสีของสารละลายที่เกิดจากการใช้ฮอร์สเรดิชเปอร์ออกซิเดสเอนไซม์ในการขยายสัญญาณ และสามารถสังเกตเห็นผลได้ด้วยตาเปล่าเช่นกัน แต่จากงานวิจัยที่ผ่านมายังไม่พบงานวิจัยใดที่ทำการขยายสัญญาณบนแผ่นเมมเบรนจากปฏิกิริยาการเกิดสีของซับสเตรทเททราเมทิลเบนซิดีน และยูเรียไฮโดรเจนเปอร์ออกไซด์ ซึ่งใช้อนุภาคแม่เหล็กนาโนบนแผ่นเมมเบรนเป็นตัวเร่งปฏิกิริยาแทนฮอร์สเรดิชเปอร์ออกซิเดส (Int J Mol Sci., Vol 14, p 9999-10014, 2013)

**ลักษณะและความมุ่งหมายของการประดิษฐ์**

การประดิษฐ์นี้เกี่ยวข้องกับสารประกอบอนุภาคที่สามารถจับกับเชื้อก่อโรคฟันผุได้อย่างจำเพาะสำหรับใช้ในการแยกและตรวจวัดเชื้อก่อโรคฟันผุเชิงกึ่งปริมาณได้ด้วยตาเปล่า ประกอบรวมด้วย อนุภาคแม่เหล็กนาโน และโดเมนของเอนไซม์ที่ทำหน้าที่จับกับผนังเซลล์ของเชื้อก่อโรคฟันผุอย่างจำเพาะ เตรียมโดยการนำโดเมนของเอนไซม์ออโตมิวตะโนไลซินที่ทำหน้าที่จับกับผนังเซลล์ มายึดติดกับอนุภาคแม่เหล็กนาโนตรึงด้วยพอลิเมอร์ที่มีหมู่ฟังก์ชันเป็นหมู่คาร์บอกซิล หรือพอลิอะคริลิกแอซิดผ่านพันธะเอไมด์ เกิดเป็นสารประกอบอนุภาคที่มีความจำเพาะในการจับกับเชื้อมิวแทนส์ สเตรปโตคอคไค โดยโดเมนที่ทำหน้าที่จับกับผนังเซลล์นี้มีความจำเพาะต่อเชื้อมิวแทนส์ สเตรปโตคอคไค จึงสามารถเลือกจับเฉพาะเชื้อนี้ ในขณะที่อนุภาคแม่เหล็กนาโนตรึงด้วยพอลิเมอร์ที่มีหมู่ฟังก์ชันเป็นหมู่คาร์บอกซิล หรือพอลิอะคริลิกแอซิดที่ยึดติดกับโดเมนของเอนไซม์ข้างต้นก็จะทำหน้าที่แยกเชื้อที่ถูกจับอยู่กับโดเมนให้ออกมาจากสารละลายโดยอาศัยสนามแม่เหล็กภายนอก และยังสามารถวิเคราะห์ปริมาณของเชื้อที่แยกออกมาได้ โดยทำการกรองแบบเลือกผ่าน (selective filtration) ผ่านแผ่นเมมเบรนเพื่อแยกสารประกอบอนุภาคที่จับเชื้อมิวแทนส์ สเตรปโตคอคไค ออกจากสารประกอบอนุภาคที่ไม่จับกับเชื้อ ซึ่งสามารถวิเคราะห์จำนวนเชื้อเชิงกึ่งปริมาณ (semi-quantitative analysis) ได้ โดยพิจารณาจากความเข้มสีของสารประกอบอนุภาคที่ค้างอยู่บนแผ่นเมมเบรน นอกจากนี้เมื่อเติมเททราเมทิลเบนซิดีน และยูเรียไฮโดรเจนเปอร์ออกไซด์ลงบนเมมเบรน สามารถขยายสัญญาณจากปฏิกิริยาการเปลี่ยนสีโดยมีอนุภาคแม่เหล็กนาโนเป็นตัวเร่งปฏิกิริยา ช่วยเพิ่มประสิทธิภาพในการตรวจวัดทั้งในแง่ของความไว (sensitivity) และขีดจำกัด (detection limit)

ความมุ่งหมายของการประดิษฐ์นี้เพื่อพัฒนาผลิตภัณฑ์ที่ใช้ในการแยกและตรวจวัดเชื้อก่อโรคฟันผุเชิงกึ่งปริมาณได้ด้วยตาเปล่า โดยอาศัยการทำงานของสารประกอบอนุภาคแม่เหล็กนาโนที่ตรึงด้วยพอลิเมอร์ที่มีหมู่ฟังก์ชันเป็นหมู่คาร์บอกซิล หรือพอลิอะคริลิกแอซิด และยึดติดกับโดเมนของเอนไซม์ที่ทำหน้าที่จับกับผนังเซลล์ของเชื้อก่อโรคฟันผุอย่างจำเพาะ ซึ่งผลิตภัณฑ์นี้สามารถทำได้ข้างเก้าอี้คนไข้ โดยไม่ต้องใช้เครื่องมือที่มีความยุ่งยากซับซ้อน และประหยัดเวลา

**การเปิดเผยการประดิษฐ์โดยสมบูรณ์**

การประดิษฐ์นี้เกี่ยวข้องกับสารประกอบอนุภาคที่สามารถจับกับเชื้อก่อโรคฟันผุได้อย่างจำเพาะสำหรับใช้ในการแยกและตรวจวัดเชื้อก่อโรคฟันผุเชิงกึ่งปริมาณได้ด้วยตาเปล่า ประกอบรวมด้วย อนุภาคแม่เหล็กนาโน และโดเมนของเอนไซม์ที่ทำหน้าที่จับกับผนังเซลล์ของเชื้อก่อโรคฟันผุอย่างจำเพาะ เตรียมโดยการนำโดเมนของเอนไซม์ออโตมิวตะโนไลซินที่ทำหน้าที่จับกับผนังเซลล์ ซึ่งสามารถจับกับเชื้อก่อโรคฟันผุในกลุ่ม สเตรปโตคอคไคได้อย่างจำเพาะมายึดติดผ่านพันธะเอไมด์กับอนุภาคแม่เหล็กนาโนที่ทำให้เสถียรด้วยพอลิเมอร์ที่มีหมู่ฟังก์ชันเป็นหมู่คาร์บอกซิล หรือพอลิอะคริลิกแอซิด (poly(acrylic acid)) เกิดเป็นสารประกอบอนุภาคที่มีความจำเพาะในการจับกับเชื้อก่อโรคฟันผุในกลุ่มสเตรปโตคอคไค

โดเมนที่ทำหน้าที่จับกับผนังเซลล์นี้มีความจำเพาะต่อเชื้อมิวแทนส์ สเตรปโตคอคไค จึงสามารถเลือกจับเฉพาะเชื้อนี้ ในขณะที่อนุภาคแม่เหล็กนาโนตรึงด้วยพอลิเมอร์ที่มีหมู่ฟังก์ชันเป็นหมู่คาร์บอกซิล หรือพอลิอะคริลิกแอซิด ก็จะสามารถแยกเชื้อที่จับกับสารประกอบอนุภาคนี้ออกมาจากสารละลายโดยอาศัยสนามแม่เหล็กภายนอกและยังสามารถวิเคราะห์ปริมาณของเชื้อที่แยกออกมาได้

การแยกและตรวจวัดปริมาณเชื้อมิวแทนส์ สเตรปโตคอคไคเบื้องต้นแบ่งเป็น 3 ส่วน ดังนี้

(1) นำเอาสารประกอบอนุภาคที่มีความจำเพาะในการจับกับเชื้อมิวแทนส์ สเตรปโตคอคไค ใส่ลงไปในหลอดทดลองที่บรรจุเชื้อมิวแทนส์ สเตรปโตคอคไคที่มีความเข้มข้นของเชื้อตามต้องการ ตั้งทิ้งไว้เป็นเวลา 20-50 นาทีที่อุณหภูมิห้อง แล้วแยกสารประกอบอนุภาคที่มีความจำเพาะในการจับกับเชื้อมิวแทนส์ สเตรปโตคอคไคนี้ ออกจากอาหารเลี้ยงเชื้อ (culture media) โดยใช้สนามแม่เหล็กภายนอกเป็นเวลา 5-20 นาที ใช้หลอดดูดทำการดูดอาหารเลี้ยงเชื้อใส่ทิ้ง แล้วนำสารประกอบอนุภาคที่แยกออกมาไปวิเคราะห์ปริมาณเชื้อมิวแทนส์ สเตรปโตคอคไคที่พบ

(2) เตรียมสารประกอบอนุภาคที่แยกได้จาก (1) ความเข้มข้น 0.15 มิลลิกรัม/มิลลิลิตร ในฟอสเฟตบัฟเฟอร์ซาลีนที่มีพีเอช 7.4 จากนั้นใช้ไมโครปิเปตดูดสารละลายนี้ เพื่อนำไปกรองแบบสุญญากาศผ่านแผ่นเมมเบรนเซลลูโลสอะซิเตตที่มีรูพรุนขนาดขนาด 0.8-1.0 ไมครอน โดยสารประกอบอนุภาคที่จับกับเชื้อมิวแทนส์ สเตรปโตคอคไคได้จะมีขนาดใหญ่กว่าขนาดรูพรุนของแผ่นเมมเบรน ทำให้สารประกอบอนุภาคค้างอยู่บนแผ่นเมมเบรน ส่วนสารประกอบอนุภาคที่ไม่ได้จับกับเชื้อมิวแทนส์ สเตรปโตคอคไคจะมีขนาดเล็กกว่ารูพรุนของเมมเบรนจึงผ่านรูพรุนไปได้ ในขั้นนี้สามารถแยกสารประกอบอนุภาคที่จับกับเชื้อมิวแทนส์ สเตรปโตคอคไคออกมาวิเคราะห์เชื้อเชิงกึ่งปริมาณได้โดยพิจารณาจากความเข้มสีที่ปรากฏบนแผ่นเมมเบรน

(3) การขยายสัญญาณการตรวจวัดปริมาณเชื้อมิวแทนส์ สเตรปโตคอคไค ได้โดยการหยดเททราเมทิลเบนซิดีน, ยูเรียไฮโดรเจนเปอร์ออกไซด์ และบัฟเฟอร์โซเดียมอะซีเตตที่มีพีเอช 4-6 (sodium acetate; NaAc)

ความเข้มข้น 0.1-0.3 โมลาร์ ตามลำดับ ลงบนแผ่นเมมเบรน ทิ้งไว้ที่อุณหภูมิห้องเป็นเวลา 20-60 วินาที แผ่นเมมเบรนจะเกิดการเปลี่ยนจากสีน้ำตาลเป็นสีฟ้า ทำให้เห็นสีได้ชัดเจนขึ้น

**วิธีการในการประดิษฐ์ที่ดีที่สุด**

เหมือนกับที่ได้กล่าวไว้แล้วในหัวข้อการเปิดเผยการประดิษฐ์โดยสมบูรณ์

**ข้อถือสิทธิ**

1. สารประกอบอนุภาคที่สามารถจับกับเชื้อก่อโรคฟันผุได้อย่างจำเพาะสำหรับใช้ในการแยกและตรวจวัดเชื้อก่อโรคฟันผุเชิงกึ่งปริมาณได้ด้วยตาเปล่า ประกอบรวมด้วย อนุภาคแม่เหล็กนาโน และโดเมนของเอนไซม์ที่ทำหน้าที่จับกับผนังเซลล์ของเชื้อก่อโรคฟันผุอย่างจำเพาะ
2. สารประกอบอนุภาคที่สามารถจับกับเชื้อก่อโรคฟันผุได้อย่างจำเพาะสำหรับใช้ในการแยกและตรวจวัดเชื้อก่อโรคฟันผุเชิงกึ่งปริมาณได้ด้วยตาเปล่าตามข้อถือสิทธิ1ที่ซึ่งโดเมนของเอนไซม์สามารถจับกับผนังเซลล์ของเชื้อก่อโรคฟันผุในกลุ่มสเตร็ปโตคอคไคได้อย่างจำเพาะ
3. สารประกอบอนุภาคที่สามารถจับกับเชื้อก่อโรคฟันผุได้อย่างจำเพาะสำหรับใช้ในการแยกและตรวจวัดเชื้อก่อโรคฟันผุเชิงกึ่งปริมาณได้ด้วยตาเปล่าตามข้อถือสิทธิ 1 ที่ซึ่งอนุภาคแม่เหล็กนาโนเป็นอนุภาคที่ทำให้เสถียรด้วยพอลิเมอร์ที่มีหมู่ฟังก์ชันเป็นหมู่คาร์บอกซิล หรือพอลิอะคริลิกแอซิด (poly(acrylic acid))
4. สารประกอบอนุภาคที่สามารถจับกับเชื้อก่อโรคฟันผุได้อย่างจำเพาะสำหรับใช้ในการแยกและตรวจวัดเชื้อก่อโรคฟันผุเชิงกึ่งปริมาณได้ด้วยตาเปล่าตามข้อถือสิทธิ 1 ที่ซึ่งอนุภาคแม่เหล็กนาโน และโดเมนของเอนไซม์ที่ทำหน้าที่จับกับผนังเซลล์ยึดติดกันผ่านพันธะเคมี
5. การแยกและตรวจวัดปริมาณเชื้อในกลุ่มสเตร็ปโตคอคไคเชิงกึ่งปริมาณได้ด้วยตาเปล่าโดยใช้สารประกอบอนุภาคที่สามารถจับกับเชื้อก่อโรคฟันผุได้อย่างจำเพาะ มีขั้นตอนประกอบด้วย

(1) นำเอาสารประกอบอนุภาคที่สามารถจับกับเชื้อก่อโรคฟันผุได้อย่างจำเพาะผสมกับเชื้อตามความเข้มข้นที่กำหนดไว้ หลังจากนั้นแยกสารประกอบอนุภาคออกจากอาหารเลี้ยงเชื้อ (culture media) โดยใช้สนามแม่เหล็กภายนอกเป็นเวลา 5-20 นาทีที่อุณหภูมิห้อง แล้วดูดอาหารเลี้ยงเชื้อใสทิ้ง แล้วนำสารประกอบอนุภาคที่แยกออกมาไปวิเคราะห์ปริมาณเชื้อโดยการกรองผ่านเมมเบรนเซลลูโลสอะซิเตต

(2) เตรียมสารประกอบอนุภาคที่แยกได้จาก (1) ความเข้มข้น 0.15 มิลลิกรัม/มิลลิลิตร ในฟอสเฟตบัฟเฟอร์ซาลีนที่มีพีเอช 7.4 จากนั้นนำสารละลายไปกรองแบบสุญญากาศผ่านแผ่นเมมเบรนเซลลูโลสอะซิเตตที่มีรูพรุนขนาดขนาด 0.8-1.0 ไมครอน

(3) ทำการขยายสัญญาณการตรวจวัดปริมาณเชื้อก่อโรคฟันผุในกลุ่มสเตรปโตคอคไค โดยการหยดเททราเมทิลเบนซิดีน, ยูเรียไฮโดรเจนเปอรอกไซด์ และบัฟเฟอร์ โซเดียมอะซีเตต (sodium acetate; NaAc) ที่มีพีเอช 4 - 6 ความเข้มข้น 0.1-0.3 โมลาร์ ตามลำดับ ลงบนแผ่นเมมเบรน ทิ้งไว้ที่อุณหภูมิห้องเป็นเวลา 20-60 วินาที

**บทสรุปการประดิษฐ์**

การประดิษฐ์นี้เกี่ยวข้องกับสารประกอบอนุภาคที่สามารถจับกับเชื้อก่อโรคฟันผุได้อย่างจำเพาะสำหรับใช้ในการแยกและตรวจวัดเชื้อก่อโรคฟันผุเชิงกึ่งปริมาณได้ด้วยตาเปล่า ประกอบรวมด้วย อนุภาคแม่เหล็กระดับนาโนเมตร และโดเมนของเอนไซม์ที่ทำหน้าที่จับกับผนังเซลล์ของเชื้อก่อโรคฟันผุอย่างจำเพาะ เตรียมโดยการนำโดเมนของเอนไซม์ออโตมิวตะโนไลซินที่ทำหน้าที่จับกับผนังเซลล์ ซึ่งสามารถจับกับเชื้อก่อโรคฟันผุในกลุ่ม สเตรปโตคอคไคได้อย่างจำเพาะมายึดติดผ่านพันธะเอไมด์กับอนุภาคแม่เหล็กนาโนที่ทำให้เสถียรด้วยพอลิเมอร์ที่มีหมู่ฟังก์ชันเป็นหมู่คาร์บอกซิลิก หรือพอลิอะคริลิกแอซิด (poly(acrylic acid)) เกิดเป็นสารประกอบอนุภาคที่มีความจำเพาะในการจับกับเชื้อก่อโรคฟันผุในกลุ่มสเตรปโตคอคไค ซึ่งการตรึงพอลิอะคริลิกแอซิดบนพื้นผิวอนุภาคแม่เหล็กนี้ ทำให้สามารถยึดติดโดเมนที่ทำหน้าที่จับกับผนังเซลล์ได้เป็นจำนวนมาก ส่งผลให้เพิ่มประสิทธิภาพในการจับกับเชื้อได้ดียิ่งขึ้น และสามารถใช้สนามแม่เหล็กภายนอกดึงดูดสารประกอบอนุภาคที่จับกับเชื้อมิวแทนส์สเตรปโตคอคไคมารวมกัน แล้วแยกออกมาจากน้ำลายได้ แล้วนำมากรองแบบเลือกผ่านผ่านเมมเบรน โดยสารประกอบอนุภาคที่จับกับเชื้อจะมีขนาดใหญ่กว่าขนาดรูพรุนของเมมเบรนจึงค้างอยู่บนเมมเบรน ซึ่งสามารถวิเคราะห์จำนวนเชื้อเชิงกึ่งปริมาณ (semi-quantitative) ได้ด้วยตาเปล่า โดยพิจารณาจากความเข้มสีของสารประกอบอนุภาคที่ค้างอยู่บนแผ่นเมมเบรน นอกจากนี้เมื่อเติมเททราเมทิลเบนซิดีน และยูเรียไฮโดรเจนเปอร์ออกไซด์ลงบนเมมเบรน สามารถขยายสัญญาณจากปฏิกิริยาการเปลี่ยนสีโดยมีอนุภาคแม่เหล็กนาโนเป็นตัวเร่งปฏิกิริยา ดังนั้นการใช้สารประกอบอนุภาคนี้ทำให้การตรวจวัดเชื้อมิวแทนส์ สเตรปโตคอคไคซึ่งตัวชี้วัดหนึ่งของการประเมินความเสี่ยงต่อการเกิดโรคฟันผุสามารถทำได้ข้างเก้าอี้ได้ในเวลาอันรวดเร็ว สะดวก ไม่ต้องใช้เครื่องมือที่มีความยุ่งยากซับซ้อน